AD-A239 118

DTIC
ELECTE
JUL 31 1991
S
D
C

1

An International Journal of

BERICHTE DER BUNSEN-GESELLSCHAFT

DISCUSSION MEETING SEPTEMBER 10 – 13, 1990
"RATE PROCESSES IN DISSIPATIVE SYSTEMS:
50 YEARS AFTER KRAMERS"

23 91-06299

91 7 29 023

An International Journal of
Physical Chemistry
BERICHTE DER BUNSEN-GESELLSCHAFT

Volume 95, Number 3

NTIS GRA&I ☑
DTIC TAB ☐
Unannounced ☐
Justification
By
Distribution/
Availability Codes
Dist | Avail and/or Special
A-1

Papers

P. Hänggi, J. Troe	225	Rate Processes in Dissipative Systems: 50 Years after Kramers
N. G. van Kampen	225	Remembering Kramers (Dinner Speech)
J. Troe	228	On the Application of Kramers' Theory to Elementary Chemical Reactions
J. Schroeder	233	Photoisomerization in Dense Gases and Liquids
J. Jonas, X. Peng	243	High Pressure NMR Studies of the Kramers Turnover for Reactions in Liquid Solutions
S. T. Repinec, R. J. Sension, R. M. Hochstrasser	248	Femtosecond Studies of the Photoisomerization of *cis*-Stilbene in Solution
J. M. Jean, G. R. Fleming, R. A. Friesner	253	Classical and Quantum Models of Activationless Reaction Dynamics
W. Rettig	259	Solvent Polarity Dependent Formation Dynamics of TICT States. I. Differential Solvatokinetics
C. A. Chatzidimitriou-Dreismann, E. J. Brändas	263	Proton Delocalization and Thermally Activated Quantum Correlations in Water: Complex Scaling and New Experimental Results
H. Frauenfelder, G. U. Nienhaus, J. B. Johnson	272	Rate Processes in Proteins
N. Agmon and S. Rabinovich	278	Stiffness Effects in Multidimensional Diffusive Barrier Crossing
F. T. Arecchi	286	Rate Processes in Low Dimensional Chaotic Systems with Many Attractors
D. J. Russell, M. E. Paige, C. B. Harris	299	Energy Dissipation in Chemical Reactions on Ultrafast Timescales
F. Moss	303	Stochastic Resonance
P. Jung, P. Hänggi	311	Effect of Periodic Driving on the Escape in Periodic Potentials
B. Carmeli, V. Mujica, A. Nitzan	319	Dynamics of Multidimensional Barrier Crossing in the Overdamped Limit
P. Talkner	327	Interrelations of Different Methods for the Determination of Rates: Flux Over Population, Generalized Reactive Flux, the Lowest Eigenvalue and its Rayleigh Quotient
M. M. Klosek, B. J. Matkowsky, Z. Schuss	331	The Kramers Problem in the Turnover Regime: The Role of the Stochastic Separatrix
U. Behn, K. Schiele, R. Müller	337	Mean First Passage Times and Nonlinear Relaxation Time for Nonlinear Models Driven by Dichotomous Noise

C. Van den Broeck, V. Balakrishnan	342	First Passage Times and Transport in Systems with Disorder
L. Schimansky-Geier, J. J. Hesse, Ch. Zülicke	349	Harmonic Noise Driven Bistable Dynamics
F. Marchesoni	353	Pair Nucleation Rate in a Driven Sine-Gordon Chain
W. Ebeling, M. Jenssen	356	Soliton – Assisted Activation Processes
P. Reineker, J. Köhler	362	Hopping of Quantum Particles on Crystals with Energy Disorder: Influence on Spin Resonance
W. Schirmacher	368	Anomalous Diffusion in Disordered Systems: An Effective Medium Description
G. Careri, G. Consolini	376	Proton Quantum Tunneling in Hydrated Protein Surface
P. Hänggi, W. Hontscha	379	Periodic Orbit Approach to the Quantum-Kramers-Rate
P. S. Riseborough	385	Influence of Non-Linear Dissipation on Quantum Tunneling
W. H. Miller	389	Some New Approaches to Semiclassical and Quantum Transition State Theory
G. A. Voth	393	A Feynman Path Integral Approach for Calculating Quantum Rate Constants in Complex Systems
V. Ambegaokar	400	Quantum Brownian Motion and its Classical Limit
R. Landauer	404	Traversal Time in Tunneling
Yu. Kagan	411	The Role of Barrier Fluctuations in the Tunneling Problem
K. Kondo	422	Tunneling in Metals as a Dissipative Quantum Process
U. Weiss, M. Sassetti	427	Quantum Coherence in Rate Processes
S. Dattagupta, T. Qureshi	433	Dynamics of an Impurity Spin Coupled to a Spin-Boson Dissipative System
H. Wipf	438	Low-Temperature Tunneling of Hydrogen in $Nb(OH)_x$ and $Nb(NH)_x$
	443	Accepted Papers

Nachrichten/News Section

446	Personalia
447	Veranstaltungen
448	46. Bunsen-Kolloquium
448	Tagungsbericht
449	Verschiedenes
449	Bücher

Rate Processes in Dissipative Systems: 50 Years after Kramers

Discussion Meeting of the Deutsche Bunsen-Gesellschaft für Physikalische Chemie under the auspices of the Deutsche Physikalische Gesellschaft NATO Advanced Research Workshop (ARW. 890521)

Reactive processes often take place in the presence of random interactions of the reacting system with its environment. The article by H. A. Kramers, published in April 1940 in Physica, Vol. VII, pages 284–304, represented a milestone in the quantitative analysis. It provides a description for the "low damping" and the "high damping" range. It includes such important theories as the transition state theory or the Smoluchowski model of diffusion-controlled processes. Since phenomena of the considered kind are encountered in many places in physics, chemistry and molecular biology, it appeared most appropriate to bring together scientists from these different fields at the occasion of the fiftieth anniversary of Kramers' seminal paper. The goal of the endeavor was to compare the progress of formal solutions of the Kramers problem, to identify the common principles and the specific differences of the various fields of application.

By its multidisciplinary character, this discussion meeting brought together colleagues from such distant fields as photobiology, high pressure chemical kinetics, low temperature diffusion and Josephson junctions. The participation was really international, 15 countries being represented. The organizers are grateful to those organisations, which helped with financial support such as NATO, the DFG, and the Office of Naval Research (USA), the Evangelische Akademie at Tutzing, which provided the most beautiful facilities of Tutzing castle, good weather, and competent staff, their coworkers, who assured a smooth progress of the meeting, the musicians, who concluded the program with a heartening concert, and, last not least, all colleagues, who came and took part in the lively discussions.

B. J. Berne (New York), H. Grabert (Essen), P. Hänggi (Augsburg), E. Pollak (Rehovot), and J. Troe (Göttingen)

Obviously, the present discussion meeting should also remember the person of H. A. Kramers. We are grateful that Professor N. G. van Kampen, a former student of Kramers, undertook this task and presented the following dinner speech.

Peter Hänggi, Jürgen Troe

Remembering Kramers (Dinner Speech)

N. G. van Kampen

Instituut voor Theoretische Fysica, Rijksuniversiteit te Utrecht, Postbus 80006, 3508 TA Utrecht, The Netherlands

This dinner speech, presented at the Discussion Meeting "50 years after Kramers", describes personal memories to H. A. Kramers.

Ladies and gentlemen,

A good paper begins by formulating the problem. Let me tell you my problem. In a letter sent to me by the organizers of this conference I was asked, and I quote. "to present a dinner speech covering a historical overview of the life and impact of Kramers' work. In view of your connection with the family of Kramers the organizers feel that you would be the most appropriate person to present such a talk".

What I am supposed to do? To deal with his work – in historical perspective – would make it a very long dinner. Kramers was still one of those physicists who felt that the whole of physics was their field rather than succumbing to the modern pressure to specialize. To deal with his life would amount to reciting parts of the biography written by Max Dresden [1], who has made a thorough study of it. So what am I supposed to do? In this dilemma I have chosen the golden mean, and shall talk about myself.

When Kramers wrote his paper on Brownian motion in 1940 I did not know him yet. Only in 1945, after the war, was it possible for me to go to his lectures without risk of life and limb. Unfortunately I was not very assiduous, because the newly recovered freedom gave birth to an exu-

 © VCH Verlagsgesellschaft mbH, W-6940 Weinheim, 1991 0005-9021/91/0303-0225 $ 3.50+.25/0

berant student's life. Once I had a celebration that lasted all night and after I came home in the morning I dreamt that I was at a lecture, listening to Kramers. Unfortunately, when I woke up it turned out to be true. In an audience of six that cannot go unnoticed. But when I met Kramers later that day in the street he merely asked me mildly when I intended to begin studying seriously.

His own teacher Ehrenfest had been more drastic. He refused to accept Kramers as a Ph. D. student because Kramers had occasionally skipped a lecture. He told him to become a high-school teacher. Although in those days that was quite a respectable position, in the eyes of Ehrenfest it was the bottom rung of the scientific ladder. Kramers did become a teacher, but his mind was not in it. He often arrived late. When the rector of the school expressed his displeasure he answered: Don't forget that I teach them in half an hour as much as you do in an hour. Nonetheless the same rector helped him to get away and try his luck as a research physicist in Copenhagen.

The purpose of the anecdote about my falling asleep is to allow you to discount what I am now going to say. In my experience Kramers was not a good lecturer. He was thinking of too many aspects of his subject, and he would not simplify as a first approximation suitable for students. This became painfully clear in a series of popular lectures he gave in the fall of 1945. Also his book on quantum mechanics, on which he spent so much energy, failed as a textbook. It contains numerous treasures, but a beginning student can easily get drowned in it – I can tell you. A case in point is the way he treats field quantization. He conscientiously explains it as a change in representation, but then dismisses the by no means simple algebra as too trivial to bother about. That is a pity: if the book had been more pedagogical it might have prevented the prevailing misconception of second quantization among field theorists.

Kramers was not an argumentative debater, on the contrary. When you would bring up a point of discussion, either in physics or otherwise, he would listen attentively, think about it, and carefully formulate an answer. No wonder that he was universally liked and trusted – although it is true that sometimes his answer would be couched in rather sibylline terms and those who knew them could detect an ironic twinkling in his eyes. Once he told me that in his opinion one should give every person a religion that did not fit him. At the time I took it to mean that one should try to keep the balance, but later I realized that he may also have meant something entirely different. No wonder either, that his assistance was often requested when a difficult situation arose and feelings got excited. Unfortunately that sometimes meant a heavy toll on his time and energy, as in the following case.

In 1946 he was appointed by the government as a scientific advisor and alternate to the Dutch representative in the Atomic Energy Committee of the United Nations. While serving in that capacity he was elected as chairman of the Scientific and Technological Subcommittee, against the opposition of Gromyko. He managed to gently steer the subcommittee to a satisfactory conclusion in the form of a unanimous report. I am proud to know that the same mild way of remonstrating used earlier to get me back to work was also instrumental in subduing Gromyko. The subcommittee's report later disappeared in the political hassle, which goes to show that one should never waste one's time on committees set up by politicians.

Let me go back to the year 1916, when Kramers, not yet 22 years old, took the train to Copenhagen, to study with Niels Bohr. There he remained 10 years, wrote a Ph. D. thesis, married a Danish wife, and played a pivotal role in the development of quantum mechanics. In 1924 and 1925 he managed by means of an unparalleled tour de force to construct a quantum mechanical formula for the scattering of light by an atom, even though quantum mechanics did not yet exist. He did this by an inimitable combination of knowledge and insight; others might say by hook and by crook. It was published in a paper, which I am afraid few people have ever understood – but for the resulting formula. Although the paper carried the name of Heisenberg as joint author it was very much Kramers' work. The importance of this Kramers-Heisenberg dispersion formula was not confined to the special problem of light scattering. It served as a stepping stone from which Heisenberg arrived at the general formulation of quantum mechanics, and thereby stole the show. Kramers' role in the early development of quantum mechanics is often forgotten. I hope that Dresden's book will be instrumental in putting the record straight.

Yet Kramers was never satisfied by the way in which quantum mechanics treats the interaction between the electron and the electromagnetic field. Each electron, when considered as a point particle, is surrounded by a field of infinite strength and infinite energy, namely its own electrostatic field. This appeared already in the classical theory of Lorentz. Lorentz eliminated the infinite energy by adding it to the bare mass of the electron to give a combined mass – which is the mass observed in experiments. Kramers' aim was to eliminate the entire self field of the electron by treating it as part and parcel of the electron. He gave a talk about his idea at the Shelter Island conference in 1947 and thereby launched the idea of renormalization in quantum mechanics. This idea caught fire, and Bethe, on his way home, applied it in a rough calculation of the radiative correction of the energy levels of an atom. "He works so much faster than I", Kramers once ruefully said to me, but then his own aim was more ambitious and, moreover, he was overburdened by his duties in the AEC. And his health was beginning to fail.

He ended up by dumping his calculations into my lap as a subject for my thesis. At first I was rather overwhelmed by all these yellow pad sheets covered with calculations without text. At the time it was not customary to bother your professor and of course Kramers had many other obligations, so we talked about it roughly once every six weeks.

Nor should one expect to be encouraged by approbation or praise. I remember that once Kramers said to me that he had received some reprints from de Broglie, since he was going to visit Paris, he asked me to read them and tell him

the contents. After a week's struggle I gave up and told him that either I was a fool or de Broglie. He replied that he guessed that it was de Broglie. This was the only explicit expression of appreciation I received during my thesis work. Nonetheless he managed to convey the feeling of a shared effort and a common aim, which was more stimulating than words of praise, and did more to create ties of friendship.

In 1950 Kramers arranged for me to go to the Niels Bohr Institute. The international community of scientists was tremendously stimulating, but the contact with my thesis advisor was reduced to his occasional visits to Denmark. Once, while he spent a short vacation at Bohr's cottage at Tisvilde, he asked me to come there for the weekend to discuss my work. When I arrived on bicycle from Copenhagen, he said: you are tired and hot, let us first go for a swim. We went to the beach, walked into the sea, but by the time the water had reached my navel Kramers said: in your chapter IV about the Raman effect.... And so we stood there discussing for a long time. Although I never thought that scientific discussions should be confined to office hours and appropriate surroundings, it had not occurred to me that I would have to defend my thesis halfway submerged in the Kattegat.

In 1926 Kramers returned to the Netherlands to become a professor at Utrecht. He became more concerned with the applications of quantum mechanics to various fields, such as solid state and in particular magnetism. I cannot review these many and varied topics he dealt with, but let me mention as a few highlights: the Kramers-Kronig relations, the transfer matrix, and the work on polymers. The publications can all be found in the Collected Works.

It is a pity that Dresden's book had no room for all this, although a short account has appeared in Physics Today, September 1988. Allow me to insert here a word of criticism addressed at Dresden. He emphasizes that in many subjects Kramers did all the groundwork but failed to make the decisive step. There is a grain of truth in it, but to consider that as a basic flaw of Kramers as a physicist seems to me unfair. Does one blame Lorentz for not taking the final step to relativity? Einstein for not going on to discover quantum mechanics? Columbus for stopping half way on his voyage to India? Rather I think that it is in the nature of things that those who laboriously lay the foundations for the new development no longer have the freshness of mind needed to discern an entirely new approach.

When in 1934 Kramers was appointed in Leiden as the successor to Ehrenfest his interest in statistical mechanics was already fully developed. He admired the mathematical elegance of the Gibbs approach, but was equally conversant with the more physical ideas of Boltzmann and Ehrenfest. His views are reflected in the textbook that his student ter Haar wrote in 1954. It is in the vein of the Boltzmann approach that he wrote down the equation for the probability density in phase space of a Brownian particle in a field of force and formulated the escape problem. The motivation was that this might describe chemical dissociation, as suggested by Christiansen, and perhaps also the recently discovered nuclear fusion. But it is clear that these applications mainly serve as an excuse, and that Kramers is fascinated by the mathematical problem. Much is said about it during this meeting and I only want to make a few comments.

No potential having a well and a barrier is known for which the Kramers equation can be solved analytically. The game is therefore to disign an approximation method. The remarkable thing is that Kramers appears to have done almost everything that can be done. Although his results are not as complete as one might wish, the half century since his paper was published has taught us that it is very hard to find essential improvements. It is a typical Kramers paper, containing many gems, but as a whole somewhat confusing. It needs a careful perusal and that may well be the reason that it was not well known for many years.

The *first* gem is the discovery of the curious fact that it is sufficient to investigate the stationary case, even though one is interested in a decay rate. Note that this is not an approximation, but is precisely correct within the margin of uncertainty inherent in the very concept of escape time.

The *second* gem is that in *the limit of large friction* the equation reduces to a diffusion equation in coordinate space alone. This requires the elimination of the momentum of the particle, which Kramers achieved by means of an ingenious step. This has now become an industry under the title "adiabatic elimination of fast variables".

Thirdly, having obtained this one-dimensional diffusion equation Kramers found the mean first-passage time by deriving a formula for it, which is now common knowledge, although it is occasionally rediscovered.

In order to treat the case that *the friction is not large* he used a *fourth* ingredient: he decomposed the range of the coordinate into one region around the top of the potential barrier, and another region covering the potential well. This has now become a standard trick of singular perturbation theory. It enables one to apply different expansions in both regions, provided one can fit them smoothly together so as to get an approximation that covers the whole range.

The *fifth* ingredient is a real gem: the very ingenious construction of a solution in the barrier region. It is true that this is only one special solution, but it is precisely the one he needs: no incident particles from infinity, and thermal equilibrium on the side of the well. Hence it can be attached smoothly to the equilibrium distribution inside the well. Kramers also realized that *for very small friction* the fluctuations might not be able to maintain the equilibrium in the well; rather the leakage across the barrier would deplete the high energy tail of the distribution. For this case he introduced his *sixth* device. In the limit of low friction the particle in the well oscillates roughly with a constant energy. It is therefore possible to average out the phase. This leads to a one-dimensional diffusion equation in the energy scale, from which it is easy to compute the average time needed to reach the energy of the top of the barrier.

There are two difficulties with this low friction limit. First it is manifestly correct if the barrier is a sharp cusp, but if it has a smooth top the motion near the top is slow and phase averaging is problematic. The second difficulty is that there is no bridge between this result and the previous one for large and intermediate friction. Kramers confesses that

he has not found it. Many authors have tried, and it is the task of this conference to decide whether tris bridge now exists.

Kramers machte es alleine
Wir machen es zusammen,
Denn wir sind nur kleine!

Reference

[1] M. Dresden, "H. A. Kramers. Between Tradition and Revolution", Springer-Verlag, New York, Berlin, Heidelberg 1987.

On the Application of Kramers' Theory to Elementary Chemical Reactions

J. Troe

Max-Planck-Institut für biophysikalische Chemie, Am Faßberg, D-3400 Göttingen, Germany

Chemical Kinetics / Elementary Reactions / Energy Transfer / Statistical Mechanics

Kramers' diffusion model in the energy controlled low viscosity and the momentum controlled high viscosity range is confronted with reality for elementary unimolecular reactions and radical associations in dense media. Collisional energy transfer appears to be much more complicated than described by the idealized model. On the other hand, there are examples where the Kramers-Smoluchowski equation well describes the transition to high viscosity behavior. In other cases, solvent shifts of the reaction barriers are pronounced and superimposed on the transport effects described by Kramers' model.

1. Introduction

H. A. Kramers' article of 1940 [1], on Brownian motion in a force field and the diffusion model of chemical reactions, presents a milestone in studies of medium influences on rates of chemical reactions. In particular, our own program of studying elementary reactions over wide density ranges in the same solvent [2, 3], from low pressure gas via high pressure liquid phase into solid environments, has followed Kramers' concept very closely. For selected cases, experiments of this type are available now, such that one may ask to what extent the idealized Kramers model applies, or where more complicated situations are encountered in reality. Kramers' discussion clearly distinguishes between the small and large viscosity ranges, the former being characterized by a diffusion equation of the Fokker-Planck-type on the energy scale, the latter on the reaction coordinate. The following article briefly reviews which complications in reality arise in the low and high damping regimes which leave a lot of unsolved uncertainties beyond the formal solution of the Kramers problem.

2. Unsolved Problems in the Low Damping Range

In the gas phase low pressure limit of unimolecular isomerization, dissociation, and the reverse termolecular association reactions obviously the rate determining individual collisional energy transfer process is of central importance. Detailed experiments [4, 5] of this process have shown that it cannot be related to a macroscopic viscosity in the way initially suggested by Kramers. Trajectory calculations [6] have revealed its highly irregular character. Furthermore it has been shown that, although the diffusion theory [7–9] provides a useful limiting description for inefficient collisional energy transfer (average energy transfer $|\sqrt{\langle \Delta E^2 \rangle} \ll kT$), in reality more efficient collisions operate. Therefore, the diffusion treatment has to be generalized by solutions of the complete master equation. Sometimes, there are very strong and relatively weak energy transfer contributions which operate simultaneously in one system [10]. In addition, two-dimensional master equations have to be solved on the energy and angular momentum scales [9, 11–14], such that even the formal treatment of the diffusion problem on these two scales is nontrivial, apart from the difficulties of understanding state-to-state collisional energy transfer cross-sections. In this sense, the low damping-small viscosity treatment of Kramers in chemical applications has to be replaced by far more complicated considerations.

In the following we briefly review additional mechanistic complications which may occur in the combination of atoms with atoms and with small polyatomic molecules. In this case, there are activation-deactivation pathways which often dominate the low temperature reaction and which are not included in a diffusion model at all. The related problems deserve much more attention from the side of theory and are, therefore, emphasized in the following. The mechanisms considered probably involve major contributions from solvent-reactant van der Waals clusters. Furthermore, since the reactants are open shell species, larger numbers of electronic states may contribute with collision-induced and cluster-enhanced nonadiabatic transitions between these states. Because these effects vary over the low to high damping transition of the Kramers problem, they require careful attention besides the transport aspects discussed in the Kramers model.

As an example, we consider the ozone forming combination

$$O + O_2 + M \rightleftharpoons O_3 + M \qquad (1,-1)$$

and the reverse ozone dissociation. In the limiting low pressure range in the gas phase, the third order rate coefficient has a very strong temperature dependence [15] (see Figs.

 © VCH Verlagsgesellschaft mbH, W-6940 Weinheim, 1991 0005-9021/91/0303-0228 $ 3.50+.25/0

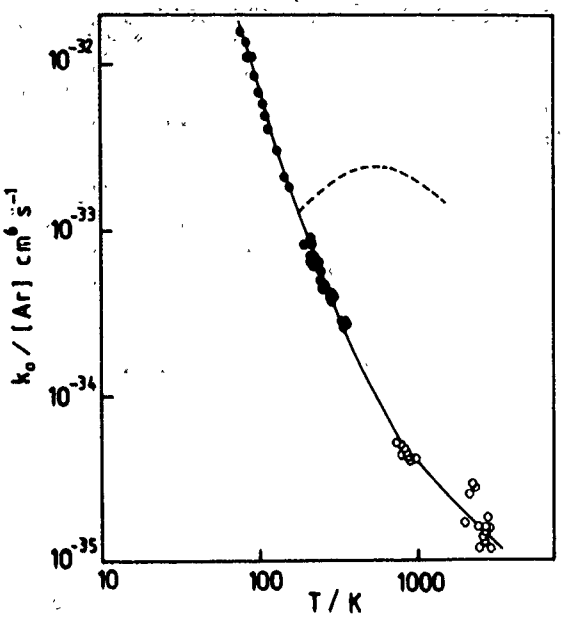


Fig. 1
Low pressure third order rate coefficients $k_0/[Ar]$ of the recombination O + O_2 + Ar → O_3 + Ar (closed circles: recombination experiments, see Ref. [15]; open circles: converted from dissociation experiments, see Ref. [15]; dashed line: from calculated strong collision unimolecular rate coefficients, see Ref. [16]

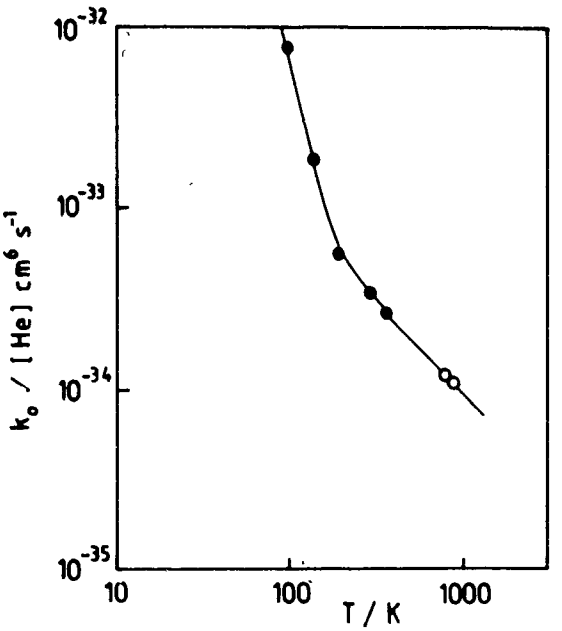


Fig. 2
As Fig. 1, for the recombination O + O_2 + He → O_3 + He (symbols as in Fig. 1, see Ref. [15])

1 and 2, for M = Ar and He respectively). Fig. 1 includes theoretical rate calculations [9,16] for the strong collision limit ($\sqrt{\langle \Delta E^2 \rangle} \gg kT$). At $T \geq 1000$ K, the experimental rate coefficients are about a factor of 100 below the strong collision calculation such that the diffusion limit of the energy transfer mechanism seems to apply. However, with decreasing temperature the rate coefficient rises much stronger than any collisional energy transfer model [4–6] would predict. At low temperatures it markedly exceeds the strong collison calculation. These observations suggest dominant contributions from the radical complex mechanism involving steps like

$$O + M \rightleftharpoons OM \qquad (2,-2)$$

$$OM + O_2 \rightleftharpoons O_3 + M \qquad (3,-3)$$

and/or contributions involving shallow excited electronic states of O_3, see below. Before the contributing species and states are well characterized by quantum-chemical calculations or separate experiments, the components of the reaction in addition to the energy transfer mechanism can hardly be understood.

The situation described for the ozone system is typical and known for atom recombination reactions [17]. The new experiments indicate that small polyatomic systems show similarly complicated mechanisms which also cannot be idealized by Kramers' model.

3. The Low-High Damping Transition Range

Investigations of the gas-liquid transition, from moderately high carrier gas pressures to low viscosity liquid solvents, provides an interesting access to the phenomena discussed in Kramers' model. At first, there is the typical falloff behavior of the standard energy transfer mechanism of unimolecular reactions which, because of its multi-dimensional-many coordinate formalism, supersedes the one-dimensional Kramers model. Narrow Kramers turn-overs from the low- to the high-damping regime, except for diatomic systems, are not expected within this theory [2,18]. The experimental results by Jonas and his coworkers (see. e.g. [19]) of narrow rate coefficient maxima on the pressure scale, therefore, probably cannot be interpreted by a low-high damping transition of a transport mechanism [20]. Besides the falloff pressure dependence of typical unimolecular reactions, there is ample experimental evidence now for a more complicated transition behavior, which can be attributed to mechanisms involving clusters and electronically nonadiabatic reactions. For instance, the recombination of iodine atoms [21,22] and bromine atoms [23] at high inert gas densities [M] show marked deviations from the reciprocal rate addition law

$$1/k \approx 1/k_0 + 1/k_{diff} \qquad (4)$$

(k_0 denotes the pressure-proportional low pressure second order rate coefficient and k_{diff} indicates second order rate coefficient of the diffusion controlled reaction). The transition between k_0 and k_{diff} can be much broader [21–23] than given by Eq. (4); for iodine recombination in gaseous propane [21], the reaction order exceeds 3; S-shaped curves are observed in the carrier gas He. More dramatic deviations for the recombination of chlorine atoms [24] in N_2 and CO_2 require further confirmation. Here one may think of the formation of relatively stable ClN_2 or $ClCO_2$ intermediates

which trap the halogen atoms. Similar effects where observed in the recombination of CH_3 radicals in N_2 as opposed to that in Ar [25] where N_2CH_3 radicals may play a role. These effects, which all take place in the gas pressure range 1–100 bar (at room temperature), suggest an important role of reactant-carrier gas clusters or even reactant-carrier gas chemical intermediates. The presence of large quantities of $I-C_2H_6$ clusters at C_2H_6 pressures near 1 bar has recently been confirmed by calculations [26].

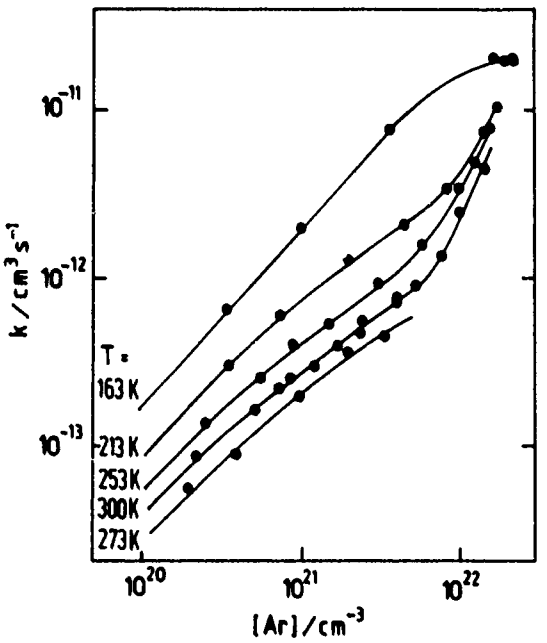


Fig. 3
Dependence of second order rate coefficients k of the recombination $O + O_2 + Ar \rightarrow O_3 + Ar$ on the bath gas concentration [Ar] (from Ref. [15])

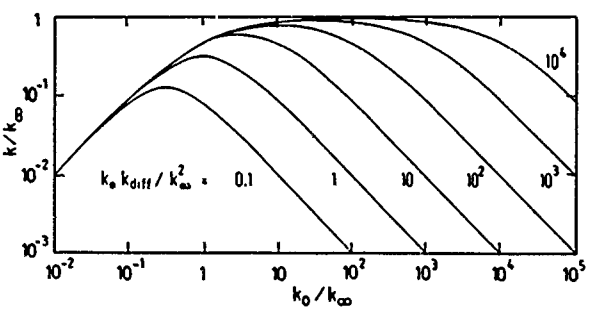


Fig. 4
Simplified model of the density dependence of rate coefficients of unimolecular reactions according to Eq. (5) (see Refs. [2, 18])

Mechanistic complications can lead to unexpected pressure and temperature dependences in the low-high damping transition range. As an example we again refer to the ozone system where Fig. 3 illustrates the corresponding experiments between 100 and 400 K at Ar pressures up to 1 kbar. The various changes in reaction order appear surprising and unexpected. The full analysis has to wait for better quantum-chemical calculations of excited electronic states and for a more elaborate theory of collision-induced nonadiabatic transitions (see, e.g., the work for I_2 in Ref. [27]). Fig. 3 is also in relation to the "feeling" of generations of kineticists about electronic degeneracy factors in atom recombination: at low pressures recombination was thought to proceed only via the electronic ground state whereas in liquid phase a contribution of all or at least a major part of the electronic states correlating two radicals was suggested. This problem is by no means solved. Fig. 3 shows how complicated the transition between the gas phase low pressure and the condensed phase range can be.

4. Elementary Chemical Reactions in the Kramers-Smoluchowski High Damping Range

In view of the many unsolved problems and the variety of different phenomena contributing to the low and intermediate density ranges such as discussed in sections 2 and 3, which have all not been considered in Kramers' treatment, it appears reasonable to completely separate the treatments in the low and high damping ranges of the Kramers model. For the low damping range, Kramers' approach has to be replaced by conventional unimolecular rate theory including adequate energy transfer models and accounting for the additional mechanisms discussed in section 2. The combination with the high damping Kramers-Smoluchowski treatment then can logically be achieved by modifying the boundary condition of the large-viscosity Kramers solution such as elaborated in Ref. [18]. In this way the low-viscosity limit of the large-viscosity Kramers solution is replaced by the general gas phase unimolecular rate expression. It is trivial to show [2, 18] that, in first approximation this again leads to a reciprocal rate addition law, see Fig. 4,

$$1/k \approx 1/k_0 + 1/k_\infty + 1/k_{diff} \qquad (5)$$

where k_0, and k_{diff} describe the low pressure gas phase, the high pressure gas phase and the diffusion control rate coefficients (being of first order for a unimolecular reaction, of second order for a bimolecular association reaction). The transition between the different ranges in the next approximation is corrected by suitable broadening factors [28].

In the present section we inspect some experimental studies of elementary chemical processes in the Kramers-Smoluchowski high damping range, in particular with respect to the viscosity dependence of the rate. We ask to what extent the effects of frequency dependent friction in the "turnover problem" (see e.g. Refs. [29, 30]) have become visible and/or which other phenomena may have manifested themselves. We only consider studies in single solvents where viscosities were varied by pressure (and temperature) changes. Halogen atom recombinations in the gas-liquid transition range in

all cases were found [21–23, 31] to approach a $k \propto 1/\eta$ relationship well characterized by Smoluchowski's equation for diffusion control. This behavior was confirmed up to 5–7 kbar in rare gases, small alkanes like ethane, but also larger liquid alkanes like n-heptane, methylcyclohexane and i-octane. Since no surprises were observed in these cases characterized by Morse-type potentials, similar experiments with energy barriers should be inspected.

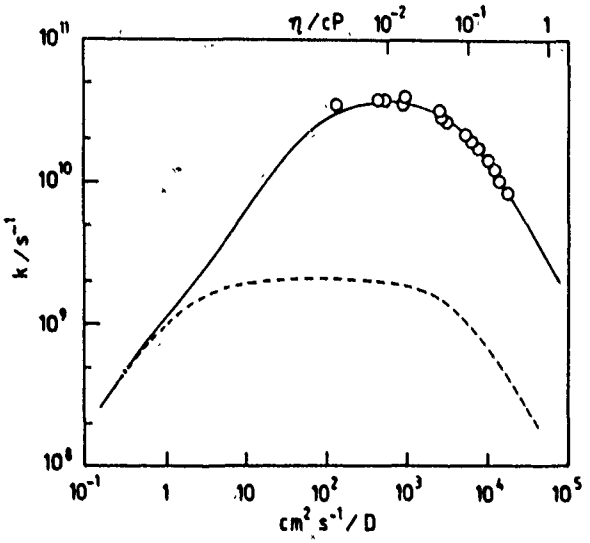


Fig. 5
First order rate coefficients of the photoisomerization of trans-stilbene in ethane (open circles: experiments from Ref. [32]; full line: representation by Eq. (5) with fitted threshold energy; dashed line: Eq. (5) with threshold energy from isolated molecule experiments)

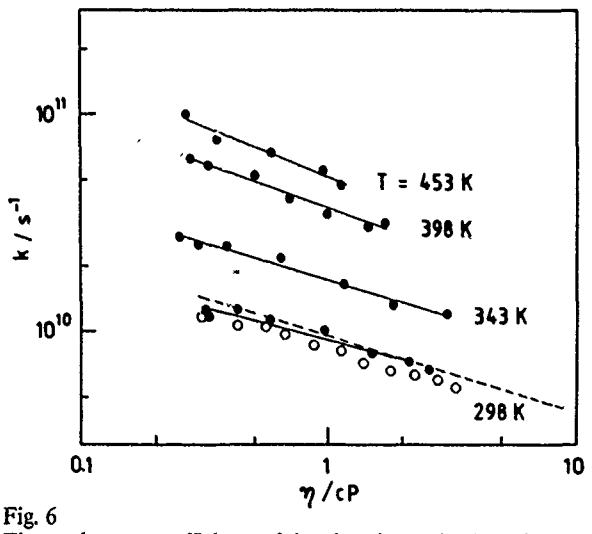


Fig. 6
First order rate coefficients of the photoisomerization of trans-stilbene in hexane (full circles and full lines from Ref. [35]; dashed line from Ref. [34], open circles: solvents = n-alkanes at 1 bar [33]

Association reactions of this type, for instance the addition of atoms to double bonds such as H + ethylene or H + benzene having small barriers in the 4–12 kJ mol^{-1} range, have not yet been studied in this way. However, unimolecular isomerization reactions with small barriers are ideal model systems for the considered problem. In particular, the isomerization of electronically excited trans-stilbene and diphenylbutadiene have provided a large amount of relevant data. Experiments in compressed ethane (see the last results [32] shown in Fig. 5) follow precisely the Kramers-Smoluchowski equation approaching $k \propto 1/\eta$ in the high damping limit (the $\log k - \log 1/D$ plot is chosen in Fig. 5 in order to represent the gas-liquid transition in the most reasonable way). While no signs of a frequency dependence of the friction are observed in this case, where viscosities of the solvent up to about 0.6 cP were applied, the situation changes with more complex solvent molecules. For instance, experiments in compressed n-hexane in the $\eta = 0.3-3$ cP range showed $k \propto \eta^{-a}$ dependences with $a = 0.3-0.5$ [33–35], see Fig. 6.

The comparison of Figs. 5 and 6 shows a striking difference. While the reaction in ethane at $\eta \approx 0.5$ cP accurately follows the $1/\eta$-dependence of the Smoluchowski limit of Kramers' theory, at the same viscosity strong deviations occur in n-hexane. First, this indicates that "isoviscosity plots" of reaction rates are not meaningful in this case. Doubts arise whether they are meaningful in other systems. Second, the temperature and pressure dependences as well as the dependences on the nature of the solvent [32, 36, 37] show such a complicated behavior that frequency dependent friction, if of importance at all, is only one of several factors influencing the reaction dynamics in dense media. Third, the comparison of isolated molecule isomerization data and the construction of transition curves into dense environments with the actual measurements (see Fig. 5) shows dramatic differences in stilbene and smaller but still marked differences in diphenylbutadiene [32, 37]. What looks like the transition state theory-low damping limit of Kramers theory in Fig. 6, apparently is already highly "contaminated" by reactant-solvent interactions compared to the isolated molecule reaction. We have attributed this to a modification of the potential energy surface in clusters which is typical for the 0.1–100 bar range, i.e. like for atom recombination we have postulated a "cluster mechanism" operating in the intermediate damping range. If the Kramers equation applies at higher densities, such as shown in Fig. 5, this apparently means that further solvation of the cluster here does not influence the potential. On the other hand, the η-dependence observed in n-hexane may indicate stronger interactions and modifications of the potential and/or microviscosity effects such as frequency dependent friction. The effects cannot be separated in a unique way such as emphasized before [28]. Apart from the difference between the "predicted" and measured curves in Fig. 5, shifts of the onset of a decay of k on the D^{-1}-scale between different low viscosity solvents [32, 37] clearly demonstrate the presence of solvent-specific reactant-solvent interactions in the cluster range. For this reason, studies of isomerization rates of energy-specifically excited isolated well-defined stilbene-solvent clusters are of great importance and should be done urgently.

There arise further complications in the analysis when the temperature dependences of the rates are investigated in addition to the pressure dependences. Recent work in this direction [32, 37] has emphasized the different role which

the multidimensionality of the potential plays in the Smoluchowski high damping and in the unimolecular reaction low damping regime. In the high damping range the shape of the potential near to the saddlepoint, i.e. anharmonicity in the reaction coordinate and nonlinear coupling with the perpendicular coordinates, can have a marked effect on the temperature dependence of k in the Smoluchowski limit. This aspect merits further attention.

5. On the Interpretation of Empirical "Activation Volumes"

Experimentalists working on high pressure liquid phase reaction kinetics traditionally represent their data in the language of conventional transition state theory, i.e. by deriving "activation volumes"

$$\Delta V^{+} = -RT(\partial \ln k/\partial p)_T . \qquad (6)$$

According to the foregoing discussions, the interpretation of ΔV^{+} is a complicated task being much more involved then done in the usual "naive" picture. Solvent-reactant interactions in clusters, solvent-reactant "shifts" of the barriers in solution, as well as pressure dependences of the transport processes all are included in the formal ΔV^{+} [18, 28, 38]. The picture of a "volume" obviously can be most misleading. Separating off the transport contribution, and relating the reactant-solvent modification of the potential with the "transition state activation volume" ΔV^{+}_{TST}, in the Smoluchowski range of Fig. 5 one would have $\Delta V^{+}_{TST} \approx 0$. A contribution $\Delta V^{+}_{TST} \neq 0$ may be present in Fig. 6, however, being nonseparable from transport contributions. Complicated pressure dependences of liquid phase reaction rates such as reported in Ref. [19] may as well be interpreted by a superposition of such static and dynamic reactant-solvent interactions. A modelling on the molecular dynamics level would require not only treatment of the transport effects [20] but also have to include quantum-chemical calculations of the modification of the potential by the solvent. More work in this direction is required.

Many helpful discussions with J. Schroeder as well as financial support by the Deutsche Forschungsgemeinschaft are gratefully acknowledged.

References

[1] H. A. Kramers, Physica *7*, 284 (1940).
[2] J. Troe, J. Phys. Chem. *90*, 357 (1986).
[3] J. Schroeder and J. Troe, Annu. Rev. Phys. Chem. *38*, 163 (1987).
[4] H. Hippler and J. Troe, in "Bimolecular Collisons", p. 209 eds. J. E. Baggott and M. N. Ashfold, The Royal Society of Chemistry, London 1989.
[5] I. Oref and D. C. Tardy, Chem. Rev., in press.
[6] K. F. Lim and R. G. Gilbert, J. Chem. Phys. *84*, 6129 (1986).
[7] J. C. Keck and G. Carrier, J. Chem. Phys. *43*, 2284 (1964).
[8] E. E. Nikitin, "Theory of Thermally Induced Gas Phase Reactions", Indiana University Press, Bloomington 1966.
[9] J. Troe, J. Chem. Phys. *66*, 4745, 4758 (1977).
[10] K. Luther and K. Reihs, J. Chem. Phys., in press.
[11] J. Troe, Z. Phys. Chem. Neue Folge *154*, 73 (1987).
[12] C. Knessl, M. Mangel, B. J. Matkowsky, Z. Schuss, and C. Tier, J. Chem. Phys. *81*, 1285 (1984).
[13] P. Hänggi, P. Talkner, and M. Borkovec, Rev. Mod. Phys. *62*, 250 (1990).
[14] N. Snider, J. Chem. Phys. *85*, 4207 (1986).
[15] H. Hippler, R. Rahn, and J. Troe, J. Chem. Phys. *93*, 6560 (1990).
[16] H. Endo, K. Glänzer, and J. Troe, J. Phys. Chem. *83*, 2083 (1979).
[17] J. Troe, Annu. Rev. Phys. Chem. *29*, 223 (1978).
[18] J. Troe, Habilitationsschrift, Göttingen 1968, in: "Physical Chemistry, Vol. VIB, Kinetics of Gas Reactions" p. 835, ed. W. Jost, Academic Press, New York 1975.
[19] J. Jonas and X. Peng, Ber. Bunsenges. Phys. Chem. *95*, 243 (1991).
[20] R. A. Kuharski, D. Chandler, J. Montgomery, F. Rabii, and S. J. Singer, J. Phys. Chem. *92*, 3261 (1988).
[21] H. Hippler, K. Luther, and J. Troe, Ber. Bunsenges. Phys. Chem. *77*, 1104 (1973).
[22] B. Otto, J. Schroeder, and J. Troe, J. Chem. Phys. *81*, 202 (1984).
[23] H. Hippler, V. Schubert, and J. Troe, J. Chem. Phys. *81*, 3931 (1984).
[24] H. Hippler and J. Troe, Int. J. Chem. Kinet. *8*, 501 (1976).
[25] H. Hippler, K. Luther, A. R. Ravishankara, and J. Troe, Z. Phys. Chem. Neue Folge *142*, 1 (1984).
[26] P. S. Pardi and J. S. Dahler, J. Chem. Phys. *93*, 242 (1990).
[27] M. G. Sceats, Chem. Phys. *96*, 299 (1985); J. M. Dawes and M. G. Sceats, Chem. Phys. *96*, 315 (1985).
[28] J. Schroeder and J. Troe, Chem. Phys. Lett. *116*, 453 (1985).
[29] E. Pollak, H. Grabert, and P. Hänggi, J. Chem. Phys. *91*, 4073 (1989).
[30] J. E. Straub, M. Borkovec, and B. J. Berne, J. Chem. Phys. *83*, 3127 (1985); *84*, 1788 (1986).
[31] K. Luther, J. Schroeder, J. Troe, and U. Unterberg, J. Phys. Chem. *84*, 3072 (1980).
[32] J. Schroeder, D. Schwarzer, J. Troe, and F. Voss, J. Chem. Phys. *93*, 2393 (1990).
[33] G. Rothenberger, D. K. Negus, and R. M. Hochstrasser, J. Chem. Phys. *79*, 5360 (1983).
[34] L. A. Brey, G. B. Schuster, and H. G. Drickamer, J. Am. Chem. Soc. *101*, 129 (1979).
[35] J. Schroeder, J. Troe, and P. Vöhringer, J. Phys. Chem., to be published.
[36] G. Maneke, J. Schroeder, J. Troe, and F. Voss, Ber. Bunsenges. Phys. Chem. *89*, 896 (1985).
[37] Ch. Gehrke, J. Schroeder, D. Schwarzer, and J. Troe, J. Chem. Phys. *92*, 4805 (1990).
[38] J. Troe, in: "High Pressure Chemistry" p. 489, ed. H. Kelm, D. Reidel Publ., Dordrecht, Boston and London 1978).

Presented at the Discussion Meeting of the Deutsche Bunsen-Gesellschaft für Physikalische Chemie "Rate Processes in Dissipative Systems: 50 Years after Kramers" in Tutzing, September 10–13, 1990 E 7519

Photoisomerization in Dense Gases and Liquids

Jörg Schroeder

Institut für Physikalische Chemie der Universität Göttingen, Tammannstraße 6, W-3400 Göttingen, Germany

Chemical Kinetics / High Pressure / Photochemistry

The pressure and temperature dependence of the rate coefficient for the singlet state photoisomerization of trans-stilbene and all-trans-diphenylbutadiene in supercritical and liquid alkane solvents reveal the importance of specific solvent effects modifying the reaction path on the potential energy surface. In the gas-liquid transition range the barrier height for the reaction seems to be lowered due to increasing solvation of the reactants in solute-solvent clusters. At higher pressures, the transition to the Smoluchowski-limit within each solvent is well described by Kramers' model. Differences between solvents can be attributed to a solvent-dependent barrier shape. Deviations from this description only appear for stilbene at higher viscosities. In part, they seem also be due to a specific influence of the compressed solvent on the reaction path and to a frequency dependence of the friction. Solvent-size dependent microfriction effects do not seem to be responsible for the observed solvent dependence of the reaction rates. Manifestations of multidimensional barrier crossing show up in the strong temperature dependence of the rate coefficient at constant solvent self-diffusion coefficient. Apparently, the reaction path on the energy surface changes with temperature leading to an effectively temperature dependent height and shape of the barrier for the reaction with increasing excitation of "perpendicular" modes. Possible reasons for the striking difference of the friction dependence of the rate coefficient between stilbene and diphenylbutadiene at intermediate to high friction are also discussed.

1. Introduction

The investigation of the influence of solvents on the rates of chemical reactions has been one of the main topics of chemical kinetics for several decades. The problem can be approached on different levels. Looking at the role of the solvent from the point of view of statistical mechanics in an abstract, "non-chemical" way, hypothetical "non-interacting" solvents simply act as a heat bath and may be considered as a continuous viscous medium at liquid phase densities. From this point of view, statistical theories are sufficient to describe solvent effects on reaction rates and enable us to predict, e.g., the entire pressure dependence of a unimolecular reaction from gas to liquid just from the microcanonical rate coefficients measured under isolated molecule conditions [1–3]. Such a prediction then has to be compared with experiments covering a pressure range as wide as possible in a single inert solvent. This approach opens the possibility to test the range of applicability of different theoretical models as well as – by comparing the pressure dependence in different solvents – to detect specific solvent-solute interactions that may obscure purely collisional or frictional effects in real solvents.

In this spirit [1,2], we have recently extended our earlier measurements [4] of the pressure and temperature dependence of two particularly well-studied reactions [5,6], the S_1-photoisomerization of trans-stilbene and E,E-1,3-diphenylbutadiene (1.3) (in the following referred to as stilbene and DPB, respectively) [7,9]. The dynamics of these two reactions has been investigated under isolated molecule conditions [10–16] as well as in numerous, mostly – with few exceptions [17–19] – liquid solvents with picosecond time resolution. Detailed systematic studies of the viscosity and polarity dependence of the rate coefficient in homologous series of nonpolar [20–23] and polar [19,24–29] solvents have been carried out, the temperature dependence in the low viscosity regime close to the so-called "Kramers-turnover" region [18,30–31] and the deuterium isotope effect have been investigated [12,19]. There have been also two studies of the pressure dependence in liquid solvents [23,32]. As a result of these experimental efforts, three phenomena have emerged that appear to be crucial to the understanding of the solvent influence on the photoisomerization dynamics in these systems:

(i) The turnover of the rate coefficient from the collisional activation into the diffusive regime is not observed in low viscosity liquids [30,31], as one would have expected on predictions based on Kramers' theory [33], but at even lower friction in supercritical solvents [4,17].

(ii) Assuming that statistical reaction rate theories are applicable, thermal averaging of the microcanonical rate coefficients obtained for isolated stilbene leads to a value of the high pressure limiting rate coefficient k_∞ which is an order of magnitude below the measured value in liquid solution [11,34]. For DPB, k_∞ is only about a factor of two below the measurement in liquid solvents [35,36].

(iii) In a series of n-alkane solvents, the observed nonradiative decay rate of the S_1-state, k_{nr}, does not show the expected inverse dependence on solvent viscosity η for neither stilbene [20] nor DPB [23].

No doubt remains that the first observation can be understood, if one includes multidimensionality in the theoretical description of the low-damping region, which is not taken into account by Kramers' original treatment [1, 2, 37–40]. The physical explanations offered for the other two phenomena, however, are still controversial and will be discussed here in the light of our recent results on the pressure and temperature dependence of k_{nr} for stilbene [7,41] and DPB [8,9] in nonpolar solvents.

 © VCH Verlagsgesellschaft mbH, W-6940 Weinheim, 1991 0005-9021/91/0303-0233 $ 3.50+.25/0

2. Experimental Technique

Decay rate coefficients of the S_1-state of stilbene in all solvents and of DPB in supercritical solvents, liquid ethane and propane were measured by picosecond pump-probe absorption spectroscopy as described in detail earlier [4, 8]. The were determined from the transient absorption decay at 616 nm after excitation at 308 nm. The FWHM of the UV-excitation pulse was approximately 5 ps, its value for the red probe pulse was 2.5 ps. the pump pulse energy hitting the sample was about 0.3 mJ at 308 nm, and the energy of the 616 nm probe pulse was about 0.05 mJ. The plane of polarization of the probe beam could be varied by means of a zero order halt-wave plate to eliminate the effects of overall rotational relaxation on the transient absorption signals. Samples of 200 mm thickness were used in high pressure gas phase experiments, and of 20 mm or 1.8 mm in liquid phase measurements.

The S_1-decay rates of DPB in liquid n-alkane solvents (pentane to dodecane) at room temperature were obtained from the fluorescence lifetimes measured by time-correlated single photon counting [9, 42]. Excitation light pulses at 308 nm from a frequency-doubled, synchronously-pumped dye laser (pulse autocorrelation FWHM 1.4 ps) were used at the full repetition rate of 76 MHz. Fluorescence from the 7 kbar high pressure cell was detected perpendicularly to the excitation beam in a "magic angle" arrangement. The FWHM of the instrument response function was 520 ps, its time resolution in conjunction with the high pressure fluorescence cell about 100 ps. For the analysis of the fluorescence decay histograms we used a convolution and fitting procedure in conjunction with a Fourier-transform method to take full advantage of the high repetition rate of the instrument. Fluorescence lifetimes measured at ambient pressure in a standard quartz fluorescence cell agreed to within 2% with literature data for the lifetime range from 150 ps to 2 ns, confirming the internal consistency of the fitting procedure. The data scatter obtained with the high pressure cell was slightly worse, amounting to at most 5%.

3. Results and Discussion

3.1. Solvation Effects at Low Friction

The comparison of the non-radiative rate coefficients k_{nr} of stilbene and DPB measured at low friction in different supercritical solvents with the corresponding calculated high pressure gas phase limiting rate coefficients k_∞ [7, 8] in Table 1 shows an order of magnitude discrepancy for stilbene and a systematic deviation for DPB of the order of two. The calculations are based on an optimized RRKM-fit [34, 35] to experimental specific rate constants $k(E)$ [10–16] which gives the reaction threshold $E_0([M] = 0)$ for the isolated molecule and an activated complex frequency scaling factor. Thermal averaging of $k(E)$ over a Boltzmann distribution then leads to k_∞. In this analysis, one makes – in addition to some minor approximations [7, 8] – the assumptions that

(i) k_{nr} is the rate coefficient for the twisting motion about the double bond, which is followed by rapid internal conversion to the ground state in a twisted geometry [5, 6], and that

(ii) This motion proceeds as a thermal adiabatic reaction on a singlet excited state potential energy surface.

Following this approach, we have proposed [4] that k_{nr} exceeds k_∞ for both molecules, because the effective barrier height for the reaction changes as a "solvation shell" gradually builds up around the reactants already at densities that are an order of magnitude below that of, e.g., liquid alkanes at ambient temperature. We model this increasing solvation in solvent clusters [8] simply by the equilibrium coverage Θ of the reactant "surface" due to "adsorption" of solvent molecules, which increases with solvent concentration [M]:

$$\Theta([M]) = K_s/(1 + K_s[M]) \tag{1}$$

where K_s is the adsorption equilibrium constant. We then propose a linear dependence of the barrier height on Θ, which allows us to calculate $k_\infty([M])$:

$$E_0([M]) = E_0([M] = 0) - \Theta([M]) \cdot \{E_0([M] = 0) - E_0(\text{solv})\} \tag{2}$$

$$k_\infty([M]) = \int_{E_0([M])}^{\infty} k(E) f(E)\, dE\,. \tag{3}$$

Here E_0(solv) denotes the reaction threshold energy for the reactant that is sufficiently solvated in solvent clusters. In

Table 1
Comparison of non-radiative rate coefficients k_{nr} of stilbene and DPB at low friction with the calculated high pressure limit k_∞. Estimates of degree of solvation Θ and barrier height E_0(solv) for solvated reactants

Solvent	T/K	$k_{nr}/10^9\ s^{-1}$	$k_\infty/10^9\ s^{-1}$	Θ ([M])[a]	E_0(solv)/ cm^{-1}	(kJ/mol)
		stilbene $E_0([M] = 0) = 1300\ cm^{-1}$ (15.5 kJ/mol)				
methane		(see text and Fig. 2)			725	(8.7)
ethane		(see text and Fig. 1)			675	(8.1)
propane	468	50	16	0.86	675	(8.1)
		DPB $E_0([M] = 0) = 1100\ cm^{-1}$ (13.2 kJ/mol)				
ethane	388	50	17.9	0.96	850	(10.2)
SF_6	388	32	17.5	0.96	930	(11.1)
	364	27	14.8	0.96	930	(11.1)
CO_2	384	50	17.5	0.97	810	(9.7)
Helium	429	40	25.9	0.92	955	(11.4)

[a] Taking $K_s \approx 10^4\ cm^3/mol$ (see text) for all solvents except Helium ($K_s = 2\ 10^3\ cm^3/mol$) and methane ($K_s = 4\ 10^3\ cm^3/mol$).

the following, we will continue to use the term "solvated" in this sense.

The gradually increasing solvation of stilbene and DPB in supercritical ethane is also visible in the spectral shift of the electronic ground state absorption spectra [7,8]. Plots of the redshift of the absorption maxima versus solvent polarizability show a steeper slope in low density supercritical solvents, where partial solvation in solvent clusters takes place, than at higher liquid phase densities. From the solvent density at which the fairly abrupt change in slope occurs, we can estimate the order of magnitude of K_s for ethane, $K_s \approx 10^4$ cm^3/mol. This value is in the same range as those estimated from the gas phase cage effect in iodine photolysis [43].

With this estimate of K_s we obtain from Eq. (1) the values for Θ listed in Table 1. Using Eqs. (2) and (3), we can then fit k_∞ ([M]) to the measured k_{nr} by choosing the appropriate value of E_0(solv). The results of this fitting procedure are listed in the last column of Table 1. Such an analysis of the rate coefficients of DPB shows that E_0(solv) definitely varies with the nature of the solvent. This indicates the presence of solvent-specific interactions that cause a decrease of the barrier height for the reaction in the solvated with respect to its magnitude in the isolated molecule. We would like to emphasize that in this low density range the friction is not sufficiently high to cause any barrier recrossing. It is, therefore, permitted to compare the measured k_{nr} directly with k_∞.

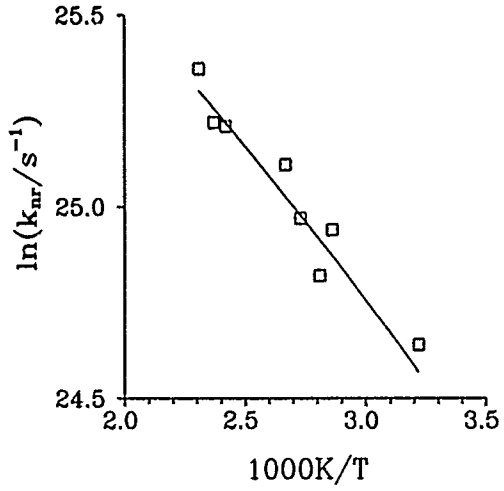


Fig. 1
Temperature dependence of the nonradiative rate coefficient k_{nr} of stilbene in ethane at low friction. The solid line represents the temperature dependence of the high pressure limit of the thermal rate coefficient, k_∞, calculated for an energy barrier E_0(solv) = 675 cm^{-1} (8.1 kJ/mol)

Fig. 1 shows an Arrhenius representation of the temperature dependence of k_{nr} for stilbene at such low densities in ethane. The dashed line represents the calculated temperature dependence of k_∞ for a barrier height E_0(solv) = 675 cm^{-1} (8.1 kJ/mol), corresponding to an activation energy $E_a \approx 530$ cm^{-1} (6.3 kJ/mol). The energy barrier is effectively lowered by a factor of about two in solvated stilbene. In DPB this effect is much less pronounced, amounting to approximately 25 percent in ethane.

Further support for a solvation-induced barrier shift comes from a corresponding analysis [8] of k_{nr}-values of stilbene measured in methane at room temperature [18] as shown in Fig. 2. The dashed curves represent the density dependence of the rate coefficient calculated according to the Lindemann-Hinshelwood expression

$$k = k_0[\mathrm{M}]\, k_\infty/(k_0[\mathrm{M}] + k_\infty) \qquad (4)$$

with the low-pressure limiting rate coefficient k_0[M] as given in Ref. [8] and k_∞ from Eq. (3) for E_0[M] = 0) = 1300 cm^{-1} (15.5 kJ/mol; lower curve) and E_0(solv) = 725 cm^{-1} (8.7 kJ/mol; upper curve). The experimental data demonstrate the transition between these two limits due to increasing solvation of stilbene in solvent clusters, which can be modelled (solid curve by Eqs. (1) to (3) with an equilibrium constant $K_S = 4 \cdot 10^3$ cm^3/mol.

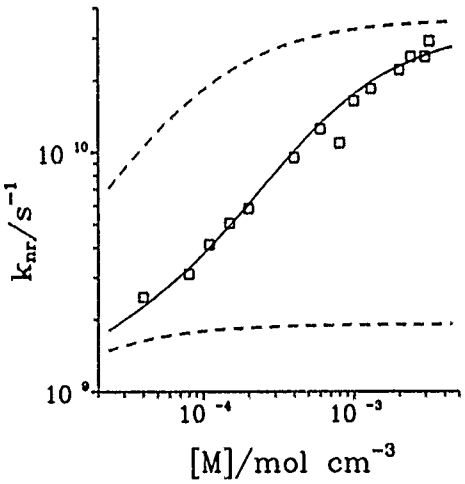


Fig. 2
Density dependence of the nonradiative rate coefficient k_{nr} of stilbene in methane (data from Ref. [18]). The upper and lower dashed curves represent calculations of the thermal rate coefficient for energy barriers E_0([M] = 0) = 1300 cm^{-1} (15.5 kJ/mol) and E_0(solv) = 725 cm^{-1} (8.7 kJ/mol), respectively. The solid curve is calculated from the solvation model (see section 3.1) using an equilibrium constant of $K_s = 2 \cdot 10^3$ cm^3/mol

The solvent dependence of K_S and E_0(solv) found for DPB is as one would intuitively expect: "less interacting" solvents give rise to smaller barrier shifts and also seem to have smaller values of K_S, though the latter are only rough estimates for all solvents but methane. As we do not know which of the electronic configurations contribute significantly to the excited state potential energy surface for the reaction and how solvent-solute interactions might affect the mixing of them, we can only speculate, why the solvation effects is much more pronounced for stilbene than for DPB photoisomerization. Evidently, the energy gap between the two lowest excited singlet state ^1A_g and ^1B_u is much smaller in DPB than in stilbene, and their order in the gas phase is reversed [14,15,44]. It seems, however, that the ^1B_u-state is the lower state for both molecules in solution [23,45]. How

this might affect the energy barrier for the twist around the double bond or its susceptibility to solvent interactions we do not know at present.

The solvation model should be tested experimentally by preparing stilbene-solvent clusters in a supersonic jet expansion and measuring k_{nr} at different excitation energies. If the cluster binding energy exceeds the height of the energy barrier, one can study the dependence of k_{nr} on cluster size, internal energy, and solvent. In this way solvent induced changes in the effective barrier height should become apparent that confirm the parameter values derived here.

The interpretation given here rests on the assumption that the photoisomerization can be treated as a thermal reaction on an adiabatic potential energy surface. In view of the deuteration effects on k_{nr} [12, 19], which seem to be in conflict with RRKM-calculations, it has been argued that these conditions might not be met, because of

(i) incomplete internal vibrational energy randomization (IVR) in the isolated molecule [18, 19, 36, 46], or

(ii) the non-adiabaticity of the reaction surface [11, 47], which concerns the question of the origin of the energy barrier in the lowest S_1-state of stilbene and DPB [5, 48–50].

In these alternative models, the apparent discrepancy between the nonradiative decay rates for isolated and solvated stilbene is then attributed to

(i) the reaction rate being controlled by slow IVR-processes in the isolated molecule [19, 51], or to

(ii) a transition from a diabatic to a adiabatic process with increasing friction due to a slowdown of the passage through the avoided curve crossing [12].

We have discussed these points in detail previously [7, 8, 38], and concluded that, as long as we do not have sufficient information on the potential energy surface for the reaction, we have no means to entirely reject any of the proposed explanations. The observation of solvent-specific effects, however, seems to support the view that the effective reaction barrier decreases due to solvent induced changes of the adiabatic potential energy surface.

If limited IVR alone would be responsible for the observation of an apparently higher barrier in the isolated molecule, then collisionally assisted IVR should eventually bring down the barrier height to its "real" intrinsic value, irrespective of the nature solvent. Also, one would not expect limited IVR to be of significance in a molecule of the size of DPB.

Specific solvent effects could be accounted for in the framework of the diabatic model, because differential solvent shifts of the two states involved could have an effect on the crossing point dynamics. But one would not expect an increase in the adiabaticity of the reaction already at methane densities where the transition of k_{nr} from isolated to solvated stilbene takes place (Fig. 2), because collision rates there would be far too low compared with the dwell time of the reactant in the crossing point region, as pointed out by Fleming et al. [18, 19].

An effect analogous to the shift of the reaction barrier induced by intermolecular interactions proposed here was observed as a consequence of intramolecular interactions in 4-alkyl-substituted stilbene, which shows a significantly lower reaction barrier under isolated molecule conditions upon substitution with ethyl and propyl [52].

3.2. Transition from Low to Intermediate Friction

We can now combine unimolecular rate theory – representing the pressure dependence of k_{nr} in the falloff regime, including the lowering of the reaction threshold with density as described above – with Kramers' expression [33] to describe the influence of increasing friction on the reaction [1, 37]:

$$k_{nr} = \frac{k_0[M]\,k_\infty}{k_0[M] + k_\infty} \cdot F_{Kr} \tag{5}$$

with

$$F_{Kr} = [\beta^2/4\omega_b^2 + 1]^{1/2} - \beta/2\omega_b\,. \tag{6}$$

The mass weighted friction coefficient β can be estimated from the molecular parameters of stilbene and DPB and the Stokes-Einstein relation [7, 8, 53] assuming that a hydrodynamic description is applicable. We use [4] the solvent self-diffusion coefficient D instead of solvent viscosity as the relevant parameter to describe solvent friction throughout the entire pressure range. The "imaginary barrier frequency" ω_b in Kramers' model describes the shape or curvature of the reaction path across the energy barrier. Without knowing the potential surface for the reaction, however, one should be careful not to a priori identify it with a unique physical quantity. Instead, it has to be considered as a fit parameter which essentially contains all pressure or friction induced variations of the prefactor that are not already taken care of by β and k_∞.

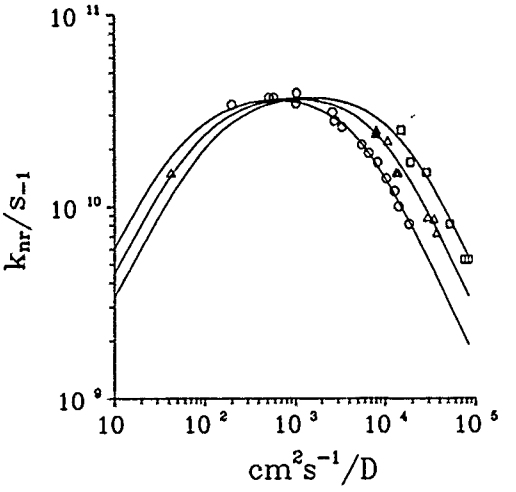


Fig. 3
Nonradiative rate coefficients k_{nr} of stilbene at $T = 298$ K in ethane (○), propane (△), and n-butane (□) versus D^{-1}. The solid lines represent model fits (see section 3.2) with E_0(solv) = 675 cm^{-1} (8.1 kJ/mol) and $\omega_b = 2.6\ 10^{12}$ s^{-1} for ethane, $\omega_b = 4.4\ 10^{12}$ s^{-1} for propane, and $\omega_b = 6.5\ 10^{12}$ s^{-1} for n-butane

Table 2
Solvent dependence of barrier heights E_0(solv) and imaginary barrier frequencies ω_b for stilbene and DPB

Solvent	T/K	E_0(solv)/ cm^{-1}	E_0(solv)/ (kJ/mol)	$\omega_b/10^{12}\ s^{-1}$	$\alpha/10^{-25}\ cm^{-3}$ a)
Stilbene					
ethane	298	675	(8.1)	2.6	42.6
propane	298	675	(8.1)	4.4	62.9
n-butane	298	675	(8.1)	6.5	81.2
CO_2	298	580	(6.9)	2.8	26.5
SF_6	298	590	(7.1)	6.0	
Xenon	298	600	(7.2)	10	41
DPB					
ethane	295	850	(10.2)	0.45	42.6
propane	295	850	(10.2)	0.65	62.9
n-butane	295	850	(10.2)	1.0	81.2

a) Molecular polarizability α, Ref. [55].

The result of modelling the isothermal pressure dependence of k_{nr} for stilbene at T = 298 K in ethane, propane and n-butane, using Eqs. (1)–(6) with E_0(solv) as determined independently at low pressures (Table 1) and fitting ω_b is shown by the solid curves in Fig. 3, a double logarithimic plot of k_{nr} versus $1/D$. There are two things to note:

(i) Kramers' expression, Eq. (6), perfectly describes the variation of k_{nr} with friction in each of the solvents (the maximum solvent viscosity in n-butane is 1.5 mPa·s).

(ii) There is a significant solvent dependence of k_{nr}, in addition to the purely frictional effect. (This appears as the successive shift of the curves in the region of higher friction. The shift in the falloff regime results from the proportionality between collision frequency and $1/D$ which contains the solvent-solute reduced mass as a constant). According to our model, this is a consequence of the solvent dependence of ω_b.

The variation of ω_b with solvent, which is found for both stilbene and DPB, is shown in Table 2. It appears that, to a first approximation, within the small alkane series at least, ω_b increases with the molecular polarizability α of the solvent. For the other solvents, ω_b is higher than expected by this correlation. Apparently specific solvent-solute interactions modify not only the barrier height, as in the low-density region, but also its shape.

An alternative explanation could be a variation of the proportionality constant linking β and the self-diffusion coefficient, i.e. a solvent dependent microfriction factor [22]. According to existing microviscosity models [54,55] this factor becomes increasingly important with decreasing solute to solvent size ratio. For a larger ratio, one would expext hydrodynamic models to give a better description than for a smaller ratio approaching unity. For the small size solvents listed in Table 2, therefore, ω_b should show a more pronounced variation for the smaller stilbene than for DPB. As ω_b increases by about a factor of three from ethane to n-butane for both stilbene and DPB, this expectation is not met. So either microfriction effects are not important or the hydrodynamic volume of the moving molecular group is about the same in both cases. In the latter case, this would throw doubts on the approach to use friction coefficients determined from the overall rotational relaxation of the molecule to describe the friction dependence of k_{nr} [22, 58, 59].

3.3 Beyond Intermediate Friction

Deviations from the inverse viscosity dependence of k_{nr} predicted by the Smoluchowski-limit of Kramers' expression,

$$k_{sm} \approx k_\infty\, \omega_b/\beta \qquad (7)$$

in nonpolar solvents for stilbene and DPB have been observed for viscosities $\eta \geq 2$ mPa·s in n-alkane solvents butane to hexadecane at atmospheric pressure [20–23]. In the past, the weak decrease of k_{nr} with $1/\eta$ – corresponding to a power law of about $\eta^{-0.5}$ – mostly has been associated with a breakdown of the standard hydrodynamic description of the frictional solvent forces contained in the parameter β in Eq. (7). It has been attributed to the frequency dependence of the friction [20–23, 57], i.e. to non-Markovian behaviour of the solvent, or, alternatively, to a breakdown of the Stokes-Einstein relation connecting friction and viscosity [22, 58–61], i.e. to microfriction effects. We have proposed that a variation of the barrier height with alkane could be responsible for the observed effect [4] – similar to those occurring in polar systems [26], – although it has been claimed [62] that available activation parameter data in liquid alkane solvents at atmospheric pressure preclude such an assumption.

Our recent study of the pressure dependence of k_{nr} for DPB in n-alkane solvents ranging from pentane to dodecane [9] demonstrates that restricting the experiments to just a variation of solvent may lead to a qualitatively different picture of the physical phenomena underlying the photoisomerization dynamics. Fig. 4 shows as one example a linear plot of k_{nr} for DPB versus $1/\eta$ in compressed pentane and dodecane at T = 298 K. The points to note are

(i) the linear correlation between k_{nr} and $1/\eta$,
(ii) the markedly different slope for the two solvents, and
(iii) the nonzero intercept for infinite viscosity.

The intercept was assigned to a second, viscosity independent nonradiative channel from the S_1-state of DPB, probably internal conversion to the E,E-ground state [9, 23]. Its rate coefficient k_{ic} varies slightly with solvent [9]. The slopes B_s increase with alkane chain length. (The variation in slope B_s with solvent is equivalent to the shift seen for the three solvents ethane to butane in Fig. 3 as expressed in a variable ω_b in Table 2). Fig. 5 shows a double logarithmic plot of $k_{iso}/B_s = (k_{nr} - k_{ic})/B_s$ versus demonstrating the perfect $1/\eta$-dependence.

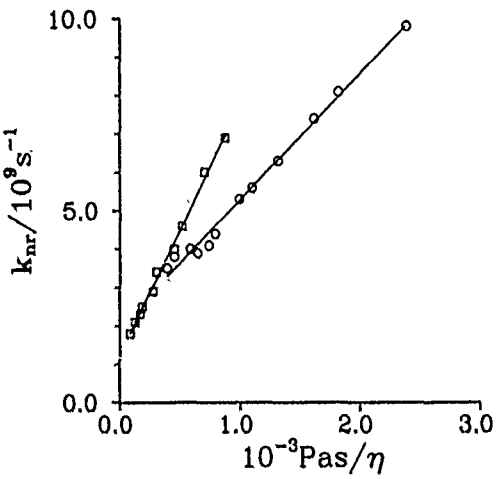


Fig. 4
Nonradiative rate coefficient k_{nr} of DPB in pentane (○) and dodecane (□) at T = 298 K versus $1/\eta$. Solid lines represent linear least squares fits to the experimental data

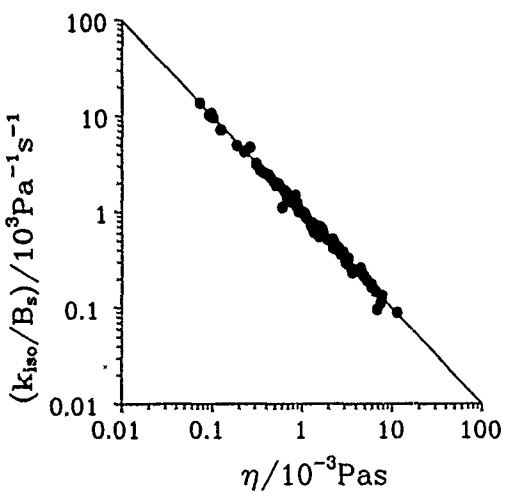


Fig. 5
Viscosity dependence of solvent scaled isomerization rate coefficient k_{iso}/B_s for DPB in n-alkane solvents from ethane to dodecane in the pressure range from 0.1 – 650 MPa. (B_s is the slope of the linear plot of k_{nr} versus $1/\eta$; see section 3.3)

A conclusion that can be drawn immediately from the observed linearity is that the reaction rates k_{iso} are not influenced by frequency dependent friction. Microfriction models that include available volume effects [55] and would predict a pressure dependence of microviscosity factors also do not apply.

There remain three possible explanations for the solvent dependence of B_s: (i) a solvent dependent microfriction factor, (ii) a variation of k_∞ with solvent, i.e. a solvent induced barrier shift of E_0(solv), and (iii) a change of the barrier shape ω_b with solvent.

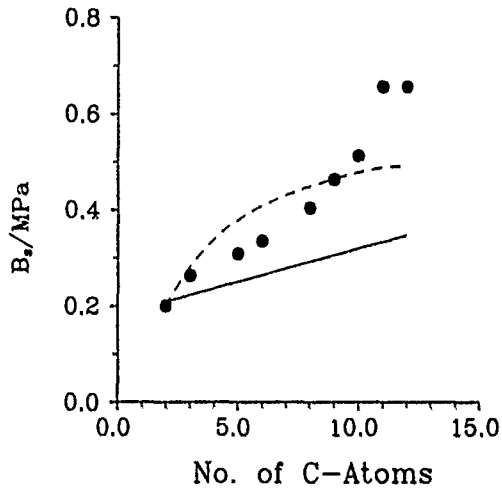


Fig. 6
Comparison of experimental slopes B_s (○) and slopes calculated from the Gierer-Wirtz microviscosity model (solid line) and from rotational relaxation via the Hubbard relation (dashed curve) (Ref. [9], see section 3.3)

In Fig. 6 we compare experimental B_s-values with estimates of microfriction factors calculated from the modified Gierer-Wirtz model [54, 55], which predicts a linear dependence of B_s on solvent size [9], and with friction coefficients β_R determined via the Hubbard relation [63, 64] from experimental molecular rotational relaxation times in the S_1-state [59, 65]. In both cases the calculated values increase with solvent size, but the observed dependece of B_s is qualitatively different, showing first an exponential rise followed by a turnover probably into saturation for the two largest solvents studied. From this apparent discrepancy we conclude that microfriction effects may contribute to some extent, but that existing models would predict a qualitatively different solvent dependence than observed [9]. This is in agreement with similar findings by Kim and Fleming for stilbene [22] and supports our interpretation that the different ω_b-values for ethane to butane in the intermediate friction regime indicate solvent-induced barrier shape changes and are not caused by changing microfriction factors.

As the hydrodynamic Kramers-Smoluchowski expression represents the variation of the rate coefficient of DPB with friction in longer chain alkane solvents, solvent-induced barrier height and shape variations remain as a possible cause for the strong solvent dependence of the slopes. As we find no variation of E_0(solv) for DPB from ethane to propane to butane, one can assume as a first approximation that there will probably be also little variation with further in-

creasing alkane chain length, and that changes of ω_b may be of greater importance.

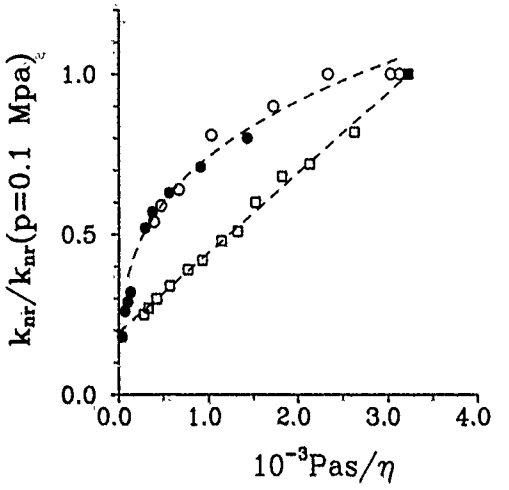


Fig. 7
Nonradiative rate coefficients $k_{nr}(p)/k_{nr}(p = 0.1\ MPa)$ of stilbene and DPB at $T = 298$ K in compressed n-hexane. (○) stilbene, Ref. [41]; (●) stilbene, Ref. [32] (calculated from fluorescence quantum yields); (□) DPB, Ref. [9]. The dashed line corresponds to a linear least squares fit, the dashed curve to a power law $\eta^{-0.29}$

Does the Kramers-Smoluchowski description also hold for stilbene photoisomerization in single solvents in the same friction regime? In Fig. 7 we compare the viscosity dependence of the rate coefficients for stilbene and DPB in compressed hexane relative to their respective values at atmospheric pressure. The strongly nonlinear behaviour of the stilbene rate coefficient corresponds to a fractional power of 0.29 [41] (indicated by the dashed curve), which is fairly close to the exponent 0.32 found for the alkane series [20,21,30,66]. This result agrees with a recent detailed study of Kim and Fleming [22], who conclude that the frequency dependence of the friction contributes significantly to the observed viscosity dependence rather than microviscosity effects. Since probably mainly the size ratio of twisting moiety to solvent molecule, which must be very similar for stilbene and DPB, determines to what extent the actual friction deviates from that measured by solvent viscosity, our results for DPB also rule out microfriction as a major contributor to the observed deviations.

Whether frequency dependent friction, pressure induced changes of the potential surface parameters or the multidimensionality of the barrier crossing process [68,74,78,79] are responsible for the observed phenomena, is still an open question. Further experiments on the pressure and temperature dependence of the rate coefficient at high friction are needed to answer it. It would be surprising, however, if the striking difference between stilbene and DPB would be caused by effects due to multidimensional barrier crossing in stilbene that would not appear in DPB. This would also contradict the experimental manifestations of multidimensionality we find in the temperature dependence of k_{nr} for stilbene and DPB (see section 3.4 below).

It might be that it is frequency dependent friction which is more important in stilbene than in DPB, because the time scale of the reaction in hexane at the same viscosity is more than one order of magnitude shorter for stilbene. An analysis of the pressure dependence of k_{nr} in hexane along different isotherms indicates, however, that possibly more than one effect is involved [41]. A comparison with corresponding measurements in methylcyclohexane again reveals the importance of specific solvent effects [41], although it remains difficult to decide whether the different viscoelastic response of the solvents or a potential energy surface effect is responsible. A comparative high pressure study of stilbene and DPB in alcohol solvents [67], where the reaction for both molecules is much faster due to a much lower barrier, however, reveals the same difference in viscosity dependence as in hexane: rate coefficients for DPB are linear in $1/\eta$ in each solvent, while for stilbene they show the power dependence found in solvent series experiments [24–27,66]. In the intermediate to high friction regime, independent of the nature of the solvent, there seems to be a basic difference between stilbene and DPB photoisomerization dynamics, the origin of which still has to be clarified in further experiments.

3.4. Multidimensional Barrier Crossing

The original Kramers model treats the diffusive barrier crossing as a one-dimensional process in which a single mode becomes the reaction coordinate. A multidimensional theory has only been fully developed fairly recently [68–73], and the importance of friction anisotropy [74,75] and the topology in the barrier region has been recognized [76,77]. Experimentally, the multidimensional barrier topology can manifest itself in the form of the temperature dependence of the rate coefficient [8,80], which – by high pressure techniques – can be measured in a single solvent at approximately constant self-diffusion coefficient or viscosity in the intermediate and high friction regimes [7,8]. Figs. 8 and 9 show Arrhenius plots of k_{nr} for stilbene and

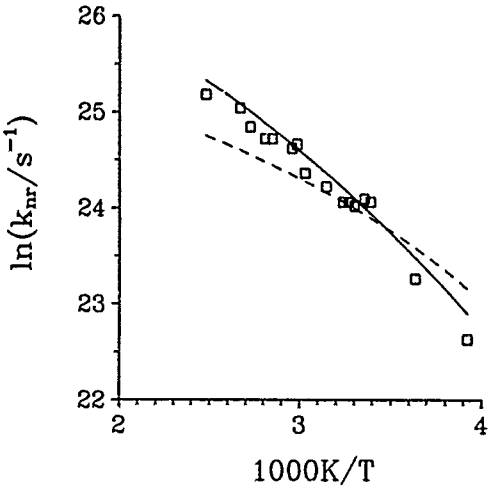


Fig. 8
Temperature dependence of the nonradiative rate coefficient k_{nr} of stilbene in ethane at constant friction ($D \approx 5 \cdot 10^{-1}$ cm^2/s): (○) experiment; dashed line: calculated from Eq. (5) with temperature-independent parameters ω_b and E(solv), solid line. calculated with temperature-dependent parameters (see section 3.4)

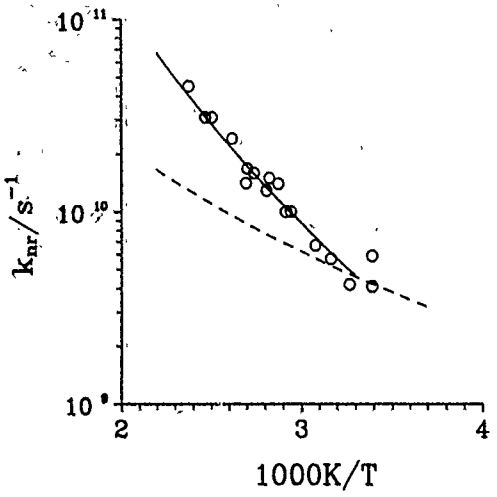


Fig. 9
Temperature dependence of the nonradiative rate coefficient k_{nr} of DPB in ethane at constant friction ($D \approx 4 \cdot 10^{-4}$ cm^2/s): (○) experiment; dashed line: calculated from Eq. (5) with temperature-independent parameters ω_b and E(solv); solid line: calculated with temperature-dependent parameters (see section 3.4)

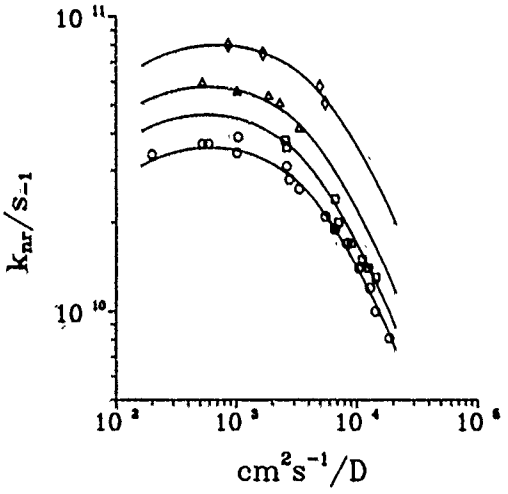


Fig. 10
Nonradiative rate coefficients k_{nr} of stilbene in ethane versus D^{-1} at different temperatures. The solid lines represent model calculations (see section 3.4).
(○) T = 298 K, E_0(solv) = 675 cm^{-1} (8.1 kJ/mol), ω_b = 2.6/ps;
(□) T = 330 K, E_0(solv) = 675 cm^{-1} (8.1 kJ/mol), ω_b = 2.6/ps;
(△) T = 356 K, E_0(solv) = 625 cm^{-1} (7.5 kJ/mol), ω_b = 3.0/ps;
(◇) T = 375 K, E_0(solv) = 590 cm^{-1} (7.1 kJ/mol), ω_b = 4.0/ps

DPB at intermediate friction in ethane for approximately constant D together with the temperature dependence predicted by Eqs. (5) and (6) (dashed curves) with input parameters from Table 2. The discrepancy between experiment and model is quite pronounced. Additional information comes from the pressure dependence of k_{nr} in ethane along different isotherms, Figs. 10 and 11. The solid curves in these plots correspond to fits obtained by allowing parameters E_0(solv) and ω_b to vary with temperature – the only way our model can account for the shift and increasing broadening of the isotherms with temperature. If we use the temperature variation of E_0(solv) and ω_b found from fitting the isotherms and recalculate the Arrhenius plot correspondingly, we obtain the solid curves in Figs. 8 and 9, which agree much better with the measured temperature dependence.

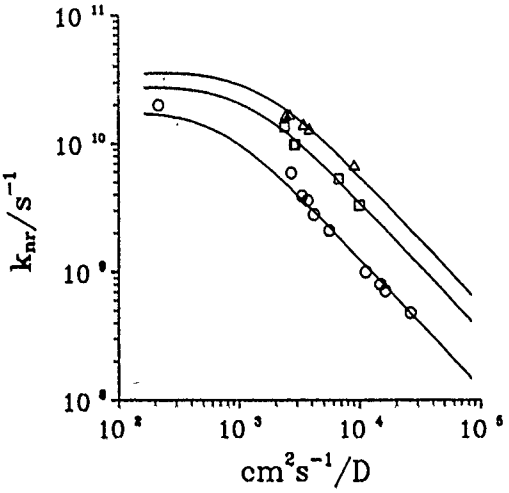


Fig. 11
Nonradiative rate coefficients k_{nr} of DPB in ethane versus D^{-1} at different temperatures. The solid lines represent model calculations (see section 3.4).
(○) T = 295 K, E_0(solv) = 850 cm^{-1} (10.2 kJ/mol), ω_b = 0.38/ps
(□) T = 340 K, E_0(solv) = 850 cm^{-1} (10.2 kJ/mol), ω_b = 0.80/ps
(△) T = 370 K, E_0(solv) = 850 cm^{-1} (10.2 kJ/mol), ω_b = 1.1/ps

Modelling $k_{nr}(T)$ in this way [7, 8] demonstrates that the higher activation energies in the intermediate friction regimes as compared to the values we find in the low friction region are caused predominantly by a significant increase of ω_b with temperature – in the case of stilbene the effective barrier height E_0(solv) actually seems to derease slightly as the temperature increases. The temperature dependence of ω_b for DPB and stilbene in ethane and propane can be represented by the expression

$$\omega_b(T_r) \approx \omega_b(T_r \leq 1) + a_T(T_r - 1)^2 ; \quad T_r = T/T_{ref} \qquad (8)$$

where the first term is the ω_b-value from Table 2, T_{ref} = 300 K, and a_T takes the values 13.6/ps K^2 for stilbene and 9.7/ps K^2 for DPB.

We have discussed this temperature effect in detail [7, 8] and inspected one-dimensional barrier anharmonicity (i.e. barrier shape effects) and multidimensional barrier crossing as possible explanations for this behavior. Anharmonicity effects are by far too small to account for the observed large temperature coefficients [7]. We concluded that these deviations from the one-dimensional Kramers-model are manifestations of multidimensional barrier crossing processes. We propose that with increasing thermal excitation of "perpendicular" low frequency modes the reaction path on the potential energy surface may change because the motion along the perpendicular coordinates has a much weaker friction dependence than the "main" reaction coordinate. (This is equivalent to the model proposed by Agmon and Kosloff [68] to explain the observed viscosity depend-

ence of stilbene at high friction). If the curvature of the barrier region increases with increasing perpendicular mode amplitude – as shown schematically in Fig. 12 – the system may cross the barrier at some distance from the saddle point, because the traversal time will be shorter and the probability of recrossing consequently lower. Because diffusion along the perpendicular coordinates is much faster, a Boltzmann distribution can be maintained in this mode whose high energy tail feeds the fast crossing channel. In a different terminology this means that the separatrix of the system due to anisotropic friction shifts away from the saddle point (73,74,80].

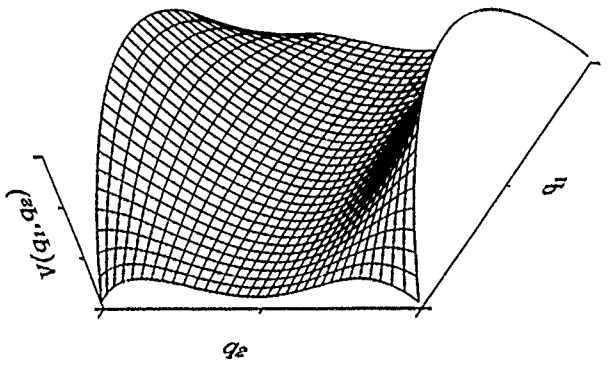


Fig. 12
Schematic representation of a potential energy surface $V(q_1, q_2)$ which shows a "sharpening" of the imaginary barrier frequency ω_b of the reaction coordinate q_1, when a perpendicular coordinate q_2 is excited (see section 3.4)

We have described a simple model [7], showing that the change of the effective curvature along the reaction path with the energy E_p in the perpendicular mode, e.g. $\omega_b \approx$ const. $\cdot E_p^n$, can lead to a corresponding temperature dependece $\omega_b \approx$ const. $\cdot T^n$. According to our model we find for both stilbene and DPB $n \approx 2$. This would imply that the degree of multidimensionality is similar for barrier crossing in stilbene and DPB.

In this picture, the activation energies observed in liquid solution [5,62] at intermediate or high friction do not correspond to the sum of an intrinsic and "viscous" barrier, but – in a formal sense – in addition reflect the temperature dependence of the prefactor due to the multidimensional dynamics at intermediate friction. Only in the low friction regime is the "intrinsic" barrier of the solvated molecule directly related to the activation energy. In this sense, it does not seem to be significant whether or not barrier heights determined under isolated molecule conditions agree with isoviscous activation energies measured in liquid solution.

Recently, Park and Waldeck [78] have inferred the multidimensional nature of the barrier crossing from a slight increase of isoviscous activation energies of ,,4'-dimethylstilbene with viscosity in a series of n-alkanes. The evidence is not very conclusive, however, as solvent size effects could also be involved and the general caveat concerning isoviscosity plots remains, as the authors note. They put forward further evidence for multidimensionality following their analysis of multiexponential fluorescence decays for 3,3'-dimethylstilbene [79], which they interpret as being caused by phenyl ring motion on the same timescale as isomerization. Photoisomerization of cis-stilbene also seems to exhibit multidimensional character [81].

Neglecting differences in emphasis and argument, it seems clear that experiments under a variety of conditions probe different details of the potential energy surface and begin to reveal its multidimensional character. Whether the excited electronic reaction surface is modified by solute-solvent interactions or whether one is probing different reactions paths on a solvent independent surface remains to be clarified. In view of the experimental information available, a simple one-dimensional picture is certainly no longer sufficient. Though we did not find pressure dependent intrinsic barriers for the smaller alkanes, which represent one of the effects behind formal "activation volumes", this does not necessarily mean that such effects may not be present in higher alkane solvents. A complete separation of the observed effects in terms of frequency dependent friction, pressure and solvent dependent barrier shifts, and multidimensional barrier crossing is a difficult task. It cannot be accomplished by the analysis of measurements at ambient pressure alone. Additional studies of the temperature and pressure dependence appear obligatory.

4. Conclusion

In the present article we have presented evidence for solvent-cluster induced modifications of the potential energy surface for photoisomerization of stilbene and DPB. Our anlysis allowed us to deduce the threshold energy for isomerization of solvated stilbene and DPB in a variety of solvents at low friction.

At intermediate friction, our analysis of the pressure dependence showed that the hydrodynamic form of Kramers equation is fully adequate to represent the observed dependence of the rate coefficient on friction for DPB in solvents up to dodecane. The observed solvent dependence can be reproduced neither by existing microfriction models nor by introducing rotational friction coefficients. By analogy we suggest that microfriction effects are also not important in stilbene photoisomerization. The hydrodynamic Kramers model also holds for stilbene in small solvents. In hexane, deviations occur which possibly can be attributed to frequency dependent friction effects.

The solvent dependence of the rate coefficient turns out to be a consequence of a variation of potential surface parameters. Their apparent variation with temperature is a manifestation of the multidimensional character of the barrier crossing process in both stilbene and DPB. Most probably, however, the multidimensionality is not responsible for deviations from an inverse viscosity dependence in higher alkane solvents, because DPB and stilbene behave differently under these conditions, whereas the pressure dependence of "stiff"-stilbene, where the phenyl rings are fixed in a five membered ring containing the ethylenic carbon

atoms, the nonradiative rate coefficients show a behaviour almost identical to that observed for stilbene [82].

The author is grateful to J. Troe for many stimulating discussions of the ideas put forward in this work. Contributions by Ch. Lienau, R. Mohrschladt, D. Schwarzer, and P. Vöhringer as well as financial support by the Deutsche Forschungsgemeinschaft (Sonderforschungsbereich 93 "Photochemie mit Lasern") are gratefully acknowledged.

References

[1] J. Troe in "High Pressure Chemistry", ed. H. Kelm, p. 489, Reidel, Dordrecht, 1978.
[2] J. Troe, J. Phys. Chem. *90*, 357 (1986); J. Schroeder and J. Troe, Annu. Rev. Phys. Chem. *38*, 163 (1987).
[3] For recent reviews see: J. T. Hynes in "The Theory of Chemical Reaction Dynamics", (ed. M. Baer) Vol. 4, p. 171, Chemical Rubber, Boca Raton 1985; J. T. Hynes, Annu. Rev. Phys. Chem. *36*, 573 (1985); J. Stat. Phys. *42*, 149 (1986); F. Marchesoni, Adv. Chem. Phys. *63*, 603 (1986); D. Chandler, J. Stat. Phys. *42*, 49 (1986); H. Frauenfelder and P. G. Wolynes, Science *229*, 337 (1985); B. J. Berne, M. Borkovec, and J. E. Straub, J. Phys. Chem. *92*, 3711 (1988); E. Pollak, H. Grabert, and P. Hänggi, J. Chem. Phys. *91*, 4073 (1989); P. Hänggi, P. Talkner, and M. Borkovec, Rev. Mod. Phys. *62*, 251 (1990).
[4] J. Schroeder and J. Troe, Chem. Phys. Lett. *116*, 453 (1985); G. Maneke, J. Schroeder, J. Troe, and F. Voß, Ber. Bunsenges. Phys. chem. *89*, 896 (1985); G. Maneke, J. Schroeder, J. Troe, and F. Voß, in: Time Resolved Vibrational Spectroscopy, eds. A. Laubereau and M. Stockburger, Springer Proc. Phys. *4*, 156 (1985).
[5] J. J. Saltiel and J. L. Charlton, in: Rearrangements in Ground and Excited States, ed. P. de Mayo, Vol. 3, p. *25*, Academic Press, New York 1980; J. Saltiel, J. D'Agostino, E. D. Megarity, L. Metts, K. R. Neuberger, M. Wrighton, and O. C. Zafiriou, Org. Photochem.*3*, 1 (1973); R. M. Hochstrasser, Int. J. Pure Appl. Chem. *52*, 2683 (1980).
[6] M. T. Allen and D. G. Whitten, Chem. Rev. *89*, 1691 (1989).
[7] J. Schroeder, D. Schwarzer, J. Troe, and F. Voß, J. Chem. Phys. *91*, 2393 (1990). (Due to a pressure scaling error of + 19%, the solvent parameters given in Tables 1 – 4 of this paper have to be corrected correspondingly).
[8] Ch. Gehrke, J. Schroeder, D. Schwarzer, J. Troe, and F. Voß, J. Chem. Phys. *92*, 4805 (1990). (Due to a pressure scaling error of + 19%, the solvent parameters given in Table 1 of this paper have to be corrected correspondingly).
[9] Ch. Gehrke, R. Mohrschladt, J. Schroeder, J. Troe, and P. Vöhringer, Chem. Phys. (1991).
[10] B. I. Greene, R. M. Hochstrasser, and R. B. Weismann, J. Chem. Phys. *71*, 544 (1979; Chem. Phys. *48*, 289 (1980).
[11] J. A. Syage, W. R. Lambert, P. M. Felker, A. H. Zewail, and R. M. Hochstrasser, Chem. Phys. Lett. *88*, 268 (1982); J. A. Syage, P. M. Felker, and A. H. Zewail, J. Chem. Phys. *81*, 4706 (1984).
[12] P. M. Felker and A. H. Zewail, J. Phys. Chem. *89*, 5402 (1985).
[13] A. Amirav and J. Jortner, Chem. Phys. Lett. *95*, 295 (1983); T. J. Majors, U. Even, and J. Jortner, J. Chem. Phys. *81*, 2330 (1984).
[14] L. A. Heimbrook, B. E. Kohler, and T. A. Spiglanin, Proc. Natl. Acad. Sci. USA *80*, 4580 (1983); J. S. Horwitz, B. E. Kohler, and T. A. Spiglanin, J. Chem. Phys. *83*, 2186 (1985).
[15] J. F. Shepanski, B. W. Keelan, and A. H. Zewail, Chem. Phys. Lett. *103*, 9 (1983).
[16] A. Amirav, M. Sonnenschein, and J. Jortner, Chem. Phys. *102*, 305 (1986).
[17] M. Lee, G. R. Holtom, and R. M. Hochstrasser, Chem. Phys. Lett. *118*, 359 (1985).
[18] M. W. Balk and G. R. Flemming, J. Phys. Chem. *90*, 3975 (1986).
[19] S. H. Courtney, M. W. Balk, L. A. Philips, S. P. Webb, D. Yang, D. H. Levy, and G. R. Fleming, J. Chem. Phys. *89*, 6697 (1988).
[20] G. Rothenberger, D. K. Negus, and R. M. Hochstrasser, J. Chem. Phys. *79*, 5360 (1983).
[21] V. Sundström and T. Gillbro, Ber. Bunsenges. Phys. Chem. *89*, 222 (1985).
[22] S. K. Kim and G. R. Fleming, J. Phys. Chem. *92*, 2168 (1988).
[23] S. P. Velsko and G. R. Fleming, J. Chem. Phys. *76*, 3553 (1982).
[24] V. Sundström and T. Gillbro, Chem. Phys. Lett. *109*, 538 (1984).
[25] E. Akesson, H. Bergström, V. Sundström, and T. Gillbro, Chem. Phys. Lett. *126*, 385 (1986).
[26] J. M. Hicks, M. T. Vandersall, E. V. Sitzmann, and K. B. Eisenthal, Chem. Phys. Lett. *135*, 413 (1987).
[27] S. K. Kim, S. H. Courtney, and G. R. Fleming, Chem. Phys. Lett. *159*, 543 (1989).
[28] N. Sivakumar, E. A. Hoburg, and D. H. Waldeck, J. Chem. Phys. *90*, 2305 (1989).
[29] K. M. Keery and G. R. Fleming, Chem. Phys. Lett. *93*, 322 (1982).
[30] S. F. Courtney and G. Fleming, J. Chem. Phys. *83*, 215 (1985).
[31] S. H. Courtney and G. R. Fleming, Chem. Phys. Lett. *103*, 433 (1984).
[32] L. A. Brey, G. B. Schuster, and H. G. Drickamer, J. Am. Chem. Soc. *101*, 129 (1979).
[33] H. A. Kramers, Physica *7*, 284 (1940).
[34] J. Troe, Chem. Phys. Lett. *114*, 241 (1985).
[35] J. Troe, A. Amirav, and J. Jortner, Chem. Phys. Lett. *115*, 245 (1985).
[36] S. H. Courtney, G. R. Fleming, L. R. Khundkar, and A. H. Zewail, J. Chem. Phys. *80*, 4559 (1984).
[37] J. Troe, Habilitationsschrift, Göttingen 1967; J. Troe in: "Physical Chemistry. An Advanced Treatise", ed. W. Jost, Vol. VIB, p. 835 Academic Press, New York 1975.
[38] J. Schroeder and J. Troe, J. Phys. Chem. *90*, 4215 (1986).
[39] A. Nitzan, J. Chem. Phys. *82*, 1614 (1985); J. Chem. Phys. *86*, 2734 (1987).
[40] M. Borkovec and B. J. Berne, J. Chem. Phys. *82*, 794 (1985); M. Borkovec and B. J. Berne, J. Chem. Phys. *86*, 2444 (1987).
[41] J. Schroeder, J. Troe, and P. Vöhringer, J. Phys. Chem., to be published.
[42] Ch. Lienau, Dissertation, Göttingen.
[43] B. Otto, J. Schroeder, and J. Troe, J. Chem. Phys. *81*, 202 (1984); H. Hippler, K. Luther, and J. Troe, Ber. Bunsenges. Phys. Chem. *77*, 1104 (1973).
[44] J. A. Bennet and R. R. Birge, J. Chem. Phys. *73*, 4243 (1980); B. M. Pierce and R. R. Birge, J. Phys. Chem. *86*, 2651 (1982).
[45] C.Rullière, A. Declemy, and Ph. Kottis, Laser Chem. *5*, 185 (1985).
[46] T. Urano, H. Hamaguchi, M. Tasumi, K. Yamanouchi, S. Tsuchiya, and T. L. Gustafson, J. Chem. Phys. *91*, 3884 (1989).
[47] F. Negri and G Orlandi, J. Phys. Chem. preprint.
[48] G. Orlandi and W. Siebrand, Chem. Phys. Lett. *30*, 352 (1975).
[49] G. Hohlneicher and B. Dick, J. Photochem. *27*, 215 (1984).
[50] J. Troe and K.-M. Weitzel, J. Chem. Phys. *88*, 7030 (1988).
[51] S. Nordholm, Chem. Phys. *137*, 109 (1989).
[52] K. Rademann, U. Even, and J. Jortner, Chem. Phys. Lett. *125*, 5 (1986).
[53] J. S. McCaskill and R. G. Gilbert, Chem. Phys. *44*, 389 (1979).
[54] A. Gierer and K. Wirtz, Z. Naturforsch. *8a*, 532 (1953).
[55] J. L. Dote, D. Kivelson, and R. Schwartz, J. Phys. Chem. *85*, 2169 (1981).
[56] J. Broz, V. Roskovec, and M. Valouch, Fyzikální a matematické tabulky, SNTL, Praha 1980.
[57] R. F. Grote and J. T. Hynes, J. Chem. Phys. *73*, 2715 (1980), ibid. *77*, 3736 (1982).
[58] S. H. Courtney, S. K. Kim, S. Canonica, and G. R. Fleming, J. Chem. Soc. Faraday 2, *82*, 2065 (1986).
[59] M. Lee, A. J. Bain, P. J. McCarthy, C. H. Han, J. N. Haseltine, A. B. Smith III, and R. M. Hochstrasser, J. Chem. Phys. *85*,

4341 (1986); M. Lee, J. N. Haseltine, A. B. Smith III, and R. M. Hochstrasser, J. Am. Chem. Soc. *111*, 5044 (1989).
[60] Y.-P. Sun and J. Saltiel, J. Phys. Chem. *93*, 8310 (1989).
[61] J. Lee, S.-B. Zhu, and G. W. Robinson, J. Phys. Chem. *91*, 4273 (1987).
[62] J. Saltiel and Y.-P. Sun, J. Phys. Chem. *93*, 6246 (1989).
[63] S. P. Velsko, D. H. Waldeck, and G. R. Fleming, J. Chem. Phys. *78*, 249 (1983).
[64] P. S. Hubbard, Phys. Rev. *131*, 1155 (1963).
[65] J. Schroeder, D. Schwarzer, and J. Troe, Ber. Bunsenges. Phys. Chem. *94*, 1249 (1990).
[66] G. R. Fleming, S. H. Courtney, and M. W. Balk, J. Stat. Phys. *42*, 83 (1986).
[67] J. Schroeder, D. Schwarzer, J. Troe, and F. Voß, Chem. Phys. Lett., to be published.
[68] N. Agmon and R. Kosloff, J. Phys. Chem. *91*, 1988 (1987).
[69] R. Landauer and J. A. Swanson, Phys. Rev. *121*, 1668 (1961).
[70] J. S. Langer, Ann. Phys. *54*, 258 (1969).
[71] Z. Schuss and B. J. Matkowsky, SIAM J. Appl. Math. *35*, 604 (1979).
[72] H. Weidenmüller and Zhang Jing-Shang, J. Stat. Phys. *34*, 191 (1984).
[73] M. M. Klosek-Dygas, B. M. Hoffmann, B. J. Mathowsky, A. Nitzan, M. A Ratner, and Z. Schuss, J. Chem. Phys. *90*, 1141 (1989).
[74] A. M. Berezhkovskii, L. M. Berezhkovskii, and V. Yu. Zitzerman, Chem. Phys. *130*, 55 (1989); A. M. Berezhkovskii and V. Yu. Zitzerman, Chem. Phys. Lett. *158*, 369 (1989); Physica A *166*, 585 (1990).
[75] S. Lee and M. Karplus, J. Phys. Chem. *92*, 1075 (1988).
[76] B. J. Matkowsky, A Nitzan, and Z. Schuss, J. Chem. Phys. *88*, 4765 (1988); *90*, 1292 (1989).
[77] R. S Larson and M. D. Kostin, J. Chem. Phys. *77*, 5017 (1982).
[78] N. S. Park and D. H. Waldeck, J. Chem. Phys. *91*, 943 (1989).
[79] N. S. Park and D. H. Waldeck, Chem. Phys. Lett. *168*, 379 (1990).
[80] A. M Berezhkovskii and V. Yu. Zitzermann, Chem. Phys. Lett. *172*, 235 (1990).
[81] S. Abrash, S. Repinec, and R. M. Hochstrasser, J. Chem. Phys. *93*, 1041 (1990).
[82] J. Schroeder, P. Vöhringer, and J. Troe, Chem. Phys. Lett., to be published.

Presented at the Discussion Meeting of the Deutsche Bunsen-Gesellschaft für Physikalische Chemie "Rate Processes in Dissipative Systems: 50 Years after Kramers" in Tutzing, September 10–13, 1990 E 7529

High Pressure NMR Studies of the Kramers Turnover for Reactions in Liquid Solutions

J. Jonas and X. Peng

Department of Chemistry, School of Chemical Sciences, University of Illinois, Urbana, Illinois 61801

Chemical Kinetics / High Pressure / Liquids / Solutions / Spectroscopy, Nuclear Magnetic Resonance

Advantages of NMR techniques to obtain the rate data for simple isomerizations in liquid solutions and advantages of using high pressure to change the viscosity of the solution are discussed. After a brief overview of our experiments on cyclohexane, 1,1-difluorocyclohexane, and N,N-dimethyltrichloroacetamide, the discussion focuses on the ethylene rotation in π-cyclopentadienylethylenetetrafluoroethylene-rhodium in several solvents. – The experimental data, as interpreted in terms of stochastic models of isomerization reactions, indicate a Kramers turnover for the pressure dependence of the rotation of coordinated ethylene in the Rh complex in solution. In fact, the observation of the energy-controlled regime in this system may be the consequence of the so-called heavy metal atom bottleneck effect which reduces the intramolecular energy transfer within the molecule. The experimental dependences of the rates upon solvent viscosity and/or Enskog collision frequency show that solvent shear viscosity represents only an approximative measure of the coupling of the reaction coordinate to the medium.

1. Introduction

It is quite remarkable to note the current level of activity [1–4] in both theoretical and experimental studies which can trace back their origin to the seminal Kramers work [5] published in 1940.

According to theoretical models [6–10] describing the dynamical solvent effects on reaction rates in liquid solutions, the reaction coordinate is coupled to the solvent, enabling the system to gain sufficient energy to cross the barrier, lose energy, and become trapped into the product well. In absence of electrostatic interactions, this coupling is produced by collisions between the solvent and solute molecules. In contrast to classical transition state theories for isomerization reactions, the stochastic models propose a dependence of the transmission coefficient κ upon so-called "collision frequency" α, which reflects the actual coupling of the reaction coordinate to the surrounding medium. According to theoretical models, the transmission coefficient κ is found to be a strong nonmonotonic function of α with two different limits. Activation due to collision rate is limiting and κ is proportional to α for the energy-controlled regime at low collision frequencies. At high collision frequencies in the diffusive regime, particles which have crossed but not yet cleared the barrier may suffer collisions and recross the barrier. The reaction in this limit is said to be diffusion controlled and the rate is inversely proportional

to α. Between these two regimes there is a nonmonotonic transition, Kramers turnover (crossover).

In our laboratory we observed such turnover behavior for the chair-chair inversion of cyclohexane in several solvents [11]. Hochstrasser et al. [12] have reported Kramers turnover region in the isomerization of trans-stilbene by using high pressure gaseous ethane. Troe et al. [13] have also observed Kramers turnover for trans-stilbene combining experiments performed both in liquid and in gas at high pressure. However, the great majority of systems [2,14] studied in dense liquid media show the high friction behavior.

It was not surprising that our results for isomerization of cyclohexane were met with a considerable degree of skepticism as the prevalent view was that the rapid internal energy flow would prevent observation of the low friction regime in dense liquid solvents. However, in their multidimensional molecular dynamics calculations, Chandler et al. [15] have reported that observation of the inertial behavior depends strongly on the relative strength between the intermolecular coupling and the intramolecular coupling. They concluded that the RRKM picture of unimolecular kinetics does not describe cyclohexane isomerization in liquid solutions as the energy exchange between the molecule and the stochastic bath occurs with similar ease as the energy rearrangement among intramolecular modes.

Clearly, the inefficient internal energy flow is the key ingredient in order to observe the energy controlled regime or the Kramers turnover for a system in dense solvent fluids. Therefore, we turned our attention to systems where we may expect an inefficient internal energy flow [16]. The theoretical predictions by Marcus et al. [17] and by Uzer and Hynes [18] about the heavy metal atom bottleneck effect on internal energy redistribution in a molecule provided the main motivation for our experiments dealing with Rh complexes in liquid solutions. Experimental studies on several organometallic compounds [19] have also suggested that a heavy metal atom acted as a barrier which reduced the rate of intramolecular vibrational energy transfer between the ligands, however, this effect was not observed for another system [20].

In our recent studies [21,22] we investigated the effects of temperature and pressure on the internal rotation rate of coordinated ethylene in π-cyclopentadienyldiethylenerhodium and π-cyclopentadienylethylenetetrafluoroethylenerhodium in several liquid solvents. Fig. 1 shows the molecular structure of the Rh complexes. It was found that the rotation of coordinated ethylene is initially accelerated by pressure, reaches a maximum and then decreases at high pressure. The experimental data, as interpreted in terms of stochastic models of isomerization reactions, indicate a Kramers turnover for the pressure dependence of the rotation of coordinated ethylene in the Rh complexes. The observation of the energy controlled regime in this system may be the consequence of the so-called heavy metal atom bottleneck effect which reduces the intramolecular energy transfer within the molecule. Table I summarizes the results of our experimental studies dealing with the dynamical solvent effects on reaction rates in dense liquid solvents.

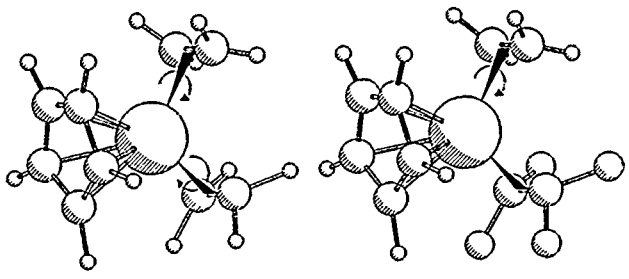
This contribution has several goals. First, we shall discuss the advantages of using pressure as an experimental variable together with an indication of relative merits of high resolution NMR techiques to investigate reaction rates in liquid solution. Second, the question of Kramers turnover for isomerization of cyclohexane and 1,1-difluorocyclohexane will be briefly revisited. Third, the study of temperature and pressure effects on ethylene rotation in π-cyclopentadienylethylenetetrafluoroethylenerhodium in several liquid solvents will be reviewed with the aim showing that viscosity represents only an approximate measure of the coupling of the reaction coordinate to the reaction medium.

Experimental

For studies listed in Table 1, the experimental procedures and equipment have been discussed in detail in the original references [11,21–24]. Thus, only a few comments about our experiments dealing with ethylene rotation in π-cyclopentadienylethylenetetrafluoroethylenerhodium will be made.

The high resolution FT NMR experiments were performed on the 300 MHz NMR spectrometer (GN-300) which was equipped with an Oxford Instruments, Inc. super-conducting 7.0 Tesla mag-

Molecular Structure of Rh Complexes



$(C_2H_5)Rh(C_2H_4)_2$ $(C_2H_5)Rh(C_2F_4)(C_2H_4)$

Fig. 1
Molecular structure of π-cyclopentadienyldiethylenerhodium and π-cyclopentadienylethylenetetrafluoroethylenerhodium

Table 1
Summary of recent results

System	Process	Result	Ref.
Cyclohexane	Conformational Isomerization	Kramers Turnover	[11]
1,1-difluorocyclohexane	Conformational Isomerization	?	[23]
N,N-Dimethyltrichloroacetamide	Hindered Rotation	Diffusive Regime	[24]
π-cyclopentadienyldiethylenerhodium	Ethylene Rotation	Inertial Regime	[21]
π-cyclopentadienylethylenetetrafluoroethylenerhodium	Ethylene Rotation	Kramers Turnover	[22]

net. A commercial GN-300 variable temperature probe was used for the temperature study and a homebuilt, high-resolution, high-pressure NMR probe was used for the pressure study. This probe has an exceptional resolution of 1 part in 10^8 for 8 mm sample without spinning, and allows one to achieve pressures up to 5000 bar. The rate constants were obtained from the NMR spectra by the complete lineshape analysis using the iterative lineshape analysis proposed by Jonas et al. [25].

Results and Discussion

In all our studies we used high-pressure, high-resolution NMR techniques to investigate the dynamical solvent effects on the reaction rates in liquid solutions. It is appropriate to comment on the importance of using pressure as an experimental variable in the studies of dynamical solvent effects on reaction rates, as the collision frequency which reflects the coupling of the reaction coordinate to the medium can be related through simple hydrodynamic arguments to shear viscosity η. The collision frequeny α in different solvents is given by the coefficient of friction ζ

$$\alpha = \zeta/m \tag{1}$$

and the molecular mass m of the solute. An estimate for ζ can be obtained by applying the Stokes law

$$\zeta = c\pi\eta(\sigma/2) \tag{2}$$

where σ is the hard-core diameter and the c is equal to 4 in the slipping boundary limit, whereas it is 6 for the sticking boundary limit. Both theoretical [26] and experimental [27] studies show that the slipping boundary conditions are appropriate for cases discussed in our experiments. Therefore, the collision frequency is given by

$$\alpha = \frac{2\pi}{m}\eta\sigma . \tag{3}$$

In most studies the shear viscosity η is changed by the use of different solvents but in the high pressure experiment, viscosity can be varied by changing pressure. One has to realize that viscosity represents only an approximative measure of the degree of coupling of the reaction coordinate to the reaction medium and consequently by changing solvents one may influence the reaction rate by different molecular shape, size, or strength of the intermolecular interactions of the solvent molecule used. Therefore, different solvents of the same shear viscosity may not have the same effect on the reaction rate measured. Clearly, using the same solvent and changing its viscosity by pressure represents a much cleaner experiment.

As most of the studies of simple isomerization reactions involve laser spectroscopic techniques, one should also comment on the relative merits of the NMR technique. There are several advantages of using NMR to study isomerization, and hindered rotation in liquid solutions. The system chosen can be very simple and the molecule can be studied in its ground state. For example, the chair-chair isomerization of cyclohexane is a relatively simple process which can be characterized by two degress of freedom.

However, there are some disadvantages connected with the use of the NMR line shape technique [25] to calculate the experimental rates. For this technique to be applicable, motions must fall within a narrow timescale and the restricted range of measurable rates leads to a relatively large error in determined activation parameters. This inherent weakness of the NMR lineshape analysis approach can be overcome in studies currently in progress in our laboratory using the NMR rotating frame technique [28] to measure rates. For example, for cyclohexane the highest measurable rate by the NMR lineshape technique is about $5\cdot10^3\ s^{-1}$, whereas the NMR rotating frame method allows one to measure rates up to $5\cdot10^5\ s^{-1}$.

In the following we shall discuss selected results obtained in our studies listed in Table 1. In order to clarify our discussion we have to mention several equations used in our analysis of the experimental data.

The stochastic models introduce a transmission coefficient to account for the collision effect on reaction rates as

$$k_{obs} = \kappa \cdot k_{TST} , \tag{4}$$

where k_{obs} is the observed isomerization rate and k_{TST} is that predicted by the classical transition state theory given by

$$k_{TST} = \frac{k_b T}{h}\exp\left(\frac{-\Delta G^*}{RT}\right) \tag{5}$$

with the symbols having their usual meaning.

The relationship between the transmission coefficient κ and the solvent viscosity provides a practical way to discuss the isomerization dynamics. Since κ and k_{TST} cannot be determined independently [11,23], we must evaluate the ratio of $\kappa(\eta)/\kappa(\eta_0)$. The normalized transmission coefficient can be obtained from

$$\frac{\kappa(\eta)}{\kappa(\eta_0)} = \frac{k(\eta)}{k(\eta_0)}\exp\left(\frac{(P-P_0)\,\Delta V^*_{TST}}{RT}\right) \tag{6}$$

where $\kappa(\eta_0)$ and $k(\eta_0)$ are the transmission coefficient and the observed rate constant at a chosen reference point. P_0 is pressure at the reference point.

Fig. 2 shows the schematic dependence of the normalized transmission coefficient upon viscosity η and ΔV^*_{TST} as generated from the experimental data for cyclohexane isomerization [11,23] in several dense solvents. In our original work we calculated the $\Delta V^*_{TST} = -1.5\ cm^3/mol$ which compares favorably with the value $\Delta V^*_{TST} = -1.9\ cm^3/mol$ given by Le Noble [11]. From Fig. 2, we see that the actual dependence of the normalized transmission coefficient is a sensitive function of the ΔV^*_{TST} value. In addition, we also discussed in detail why ΔV^*_{TST} should be pressure independent. Nevertheless, even if our estimate of ΔV^*_{TST} was off by 0.5 - 1.0 cm^3/mol, the experimental data will still exhibit inertial behavior for isomerization of cyclohexane in dense liquid solvents.

The situation is not that straightforward for isomerization of 1,1-difluorocyclohexane (DFCH) as shown in Fig. 3. For

DFCH isomerization we assumed $\Delta V^{\ddagger}_{TST} = -1.5$ cm^3/mol basing our estimate on analogy with cyclohexane. It is unlikely that $\Delta V^{\ddagger}_{TST}$ for DFCH isomerization is greatly different from that of cyclohexane. However, we cannot rule out the possibility that $\Delta V^{\ddagger}_{TST}$ may be -2.0 or -2.5 cm^3/mol which would bring the isomerization clearly in the diffusion controlled regime. Therefore, on the basis of the experimental data [23] obtained, we cannot determine with certainty whether DFCH isomerization exhibits inertial behavior.

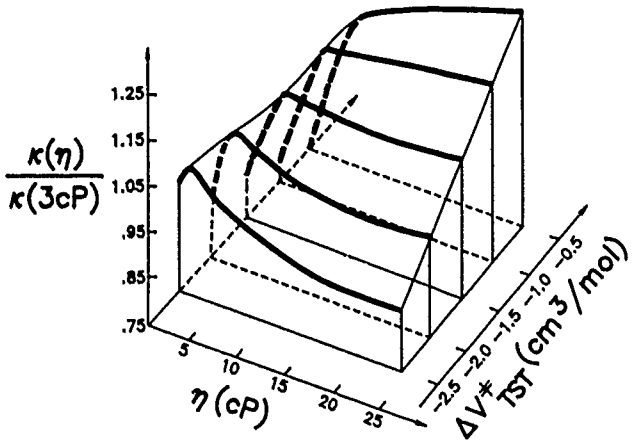


Fig. 2
Schematic dependence of normalized experimental transmission coefficient $\kappa(\eta)/\kappa(3cP)$ upon shear viscosity and $\Delta V^{\ddagger}_{TST}$ for conformational isomerization of cyclohexane at 228 K (for details, see Ref. [11])

SCS 0285-2

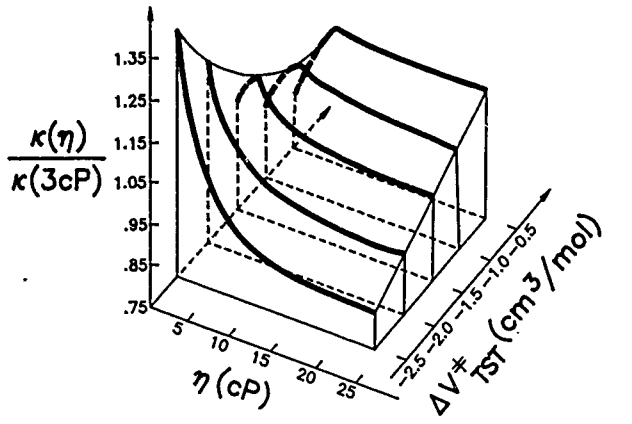


Fig. 3
Schematic dependence of normalized experimental transmission coefficient $\kappa(\eta)/\kappa(3cP)$ upon shear viscosity η and $\Delta V^{\ddagger}_{TST}$ for conformational isomerization of 1,2-difluorocyclohexane in the temperature range 218–253 K (for details, see Ref. [23])

In contrast to the results for cyclohexane and DFCH we found that the hindered rotation of N,N-dimethyltrichloroacetamide [24] falls into the diffusive regime. The pressure dependence of the hindered rotation about the amide C–N bond of N,N-dimethyltrichloroacetamide (DMTCA) has been studied at 282.3 K in n-pentane and methylcyclohexane solvents using the high-resolution, high-pressure nuclear magnetic resonance (NMR) technique. The experimental rotation rate k decreases with increasing pressure in both solvents and the correlation of the rates with solvent viscosity η shows that the rotation falls into the strongly coupled diffusive regime. Interpretation of the experimental k vs. η dependence in terms of the Kramers model fails to account for the leveling off of the rate constant at high viscosities. The Grote-Hynes theoretical model [29], which assumes frequency-dependent friction, reproduces well the observed rate behavior with viscosity of the solvent.

Another study [22] listed in Table 1 dealt with the effect of temperature and pressure on the internal rotation rate of coordinated ethylene in π-cyclopentadienylethylenetetrafluoroethylenerhodium in liquid solution. The solvents used in this study were n-pentane-d_{12}, carbon disulfide and methylcyclohexane-d_{14}. The activation energy (56.3 ± 0.84 kJ/mol) for the internal rotation of ethylene was independent of solvent and pressure as determined from conventional Arrhenius type plots and isoviscosity plots. It was found that the rotation of the coordinated ethylene is initially accelerated by pressure, reaches a maximum and then decreases at high pressure. The strong pressure dependence of the observed activation volume for the rotation suggested a strong collisional contribution to the activation volume and the presence of dynamical solvent effects. The experimental data, as interpreted in terms of stochastic models of isomerization reactions, indicated a Kramers turnover for the pressure dependence of the rotation of coordinated ethylene in the Rh complex in solution. In fact, the observation of the energy-controlled regime in this system may be the consequence of the so-called heavy metal atom bottleneck effect which reduces the intramolecular energy transfer within the molecule.

SCS 0212-9

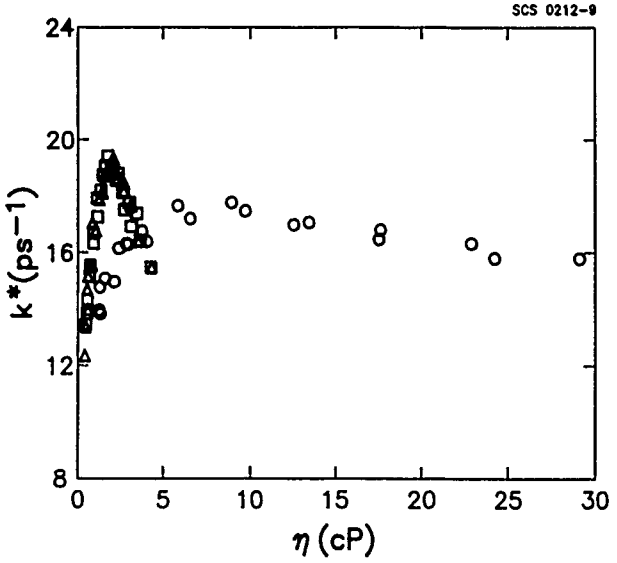


Fig. 4
The preexponential factor k^* as a function of solvent shear viscosity at 258.2 and 273.2 K for methylcyclohexane-d_{14} (○), n-pentane-d_{12} (△) and CS_2 (□)

In the following section, we shall focus on the experimental finding that the observed pressure dependence of ethylene rotation of the Rh complex studied was very different in the methylcyclohexane solvent than the dependence obtained for the CS_2 and n-pentane solvents. This striking difference in viscosity dependence for the solvents used is depicted in Fig. 4, which plots the preexpontential factor k^* as a function of solvent viscosity η for the ethylene rotation in π-cyclopentadienylethylenetetrafluoroethylenerhodium. The conventional definition of the preexponential factor [8] is used

$$k_{obs} = k^* \exp(-E_d/RT) . \qquad (7)$$

Fig. 4 shows that within experimental error, the preexponential factor is almost the same for CS_2 and n-pentane-d_{12} solvents. One should also mention that the Kramers turnover occurs at relatively high viscosity ~7 cP for methylcyclohexane-d_{14} while viscosity is 2 cP for the turnover point both for n-pentane-d_{12} and CS_2 solvents. The Skinner-Wolynes model [8] fits well the experimental data for CS_2 and n-pentane-d_{12} solvents but it does not fit the data for the most viscous solvent of methylcyclohexane-d_{14}. It is evident from Fig. 4 that the preexponential factor k^* is relatively insensitive to viscosity changes in methylcyclohexane solvent, particularly for high viscosity values.

In order to look for an explanation of this experimental finding, we follow the suggestion by Garrity and Skinner [30] that viscosity increases faster than the collision frequency for high packing fractions. Therefore we calculated the Enskog hard sphere collision frequency α_E for the solvents used and plotted α_E as a function of viscosity in Fig. 5. Indeed, this figure shows that the viscosity of methylcyclohexane-d_{14} solvent increases rapidly while the collision frequency α_E falls in the same range as the collision frequency for CS_2 and n-pentane-d_{12} solvents. If one plots the preexponential factor k^* versus the Enskog collision frequency α_E as shown in Fig. 6, one concludes that the results for the methylcyclohexane solvent are consistent with the other two solvents. In fact, the experimental k^* values span the same collisional frequency range, and the Kramers turnover occurred at 6–7 ps^{-1}. However, so far there is no explanation why k^* in methylcyclohexane solvent is consistently lower than its values in the other two solvents.

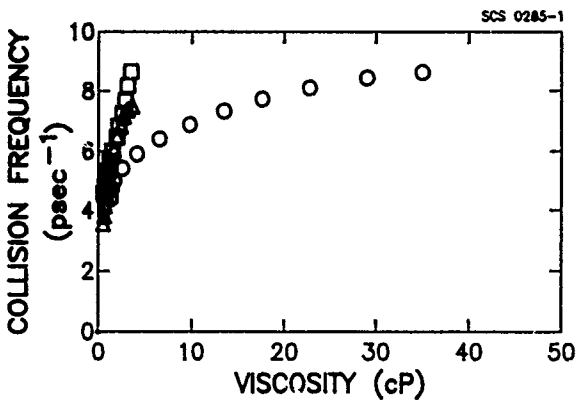


Fig. 5
Enskog collision frequency α_E as a function of shear viscosity for n-pentane (△); carbon disulfide (□) and methylcyclohexane (○)

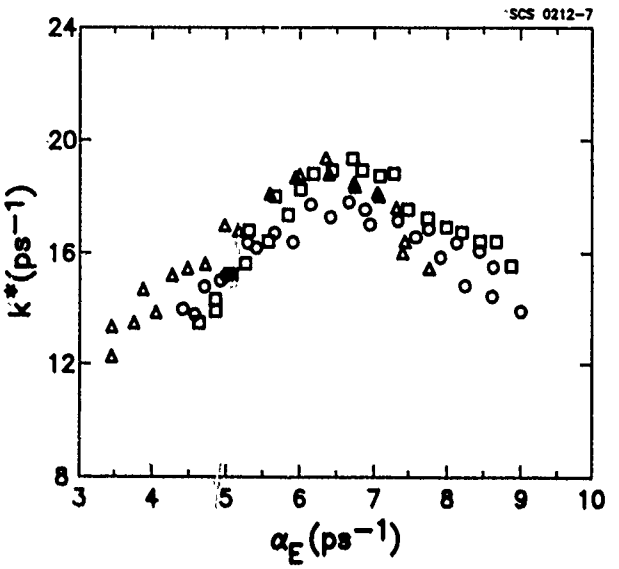


Fig. 6
The preexponential factor k^* as a function of Enskog collision frequency α_E for ethylene rotation in $(C_5H_5)Rh(C_2H_4)(C_2F_4)$ at 258.2 K and 283.2 K for methylcyclohexane-d_{14} (○); n-pentane-d_{12} (△) and CS_2 (□)

Naturally, there may be other reasons for this unusual behavior for the methylcyclohexane solvent. For example, in our earlier high-pressure studies [31] of self-diffusion and viscosity in liquid methylcyclohexane in the dense liquid region, we found that the rough hard sphere model is not strictly applicable for this liquid. In order to obtain an agreement between experiment and theory, we had to assume that the degree of coupling between the rotational and translational motions is strongly temperature dependent. One should also point out that it has been reported in the study of stilbene isomerization [32] that the data point for methylcyclohexane solvent deviated strongly from the relationship found for other solvents.

In spite of the phenomenological nature of our discussion, we can conclude that solvent viscosity represents only an approximative measure of the degree of coupling of the reactions coordinate to the reaction medium and the relationship between reaction rates and solvent shear viscosity may break down for high viscosity solvents at high packing fractions. Experiments aimed at improving our understanding of isomerization processes in highly viscous liquids are in progress in our laboratory by using the NMR rotating frame techniques and extension of the high pressure limit from 5 kbar to 10 kbar.

This work was supported in part by the National Science Foundation under grant NSF CHE 85-09870.

References

[1] J. T. Hynes, Annu. Rev. Phys. Chem. *36*, 573 (1985).
[2] J. Troe, J. Phys. Chem. *90*, 357 (1986).
[3] P. Hanggi, J. Stat. Phys. *42*, 105 (1986).

[4] G. R. Fleming and P. G. Wolynes, Phys. Today *36* May (1990).
[5] H. A. Kramers, Physica *7*, 284 (1940).
[6] J. L. Skinner and P. G. Wolynes, J. Chem. Phys. *69*, 2143 (1978).
[7] J. A. Montgomery, Jr., D. Chandler, and B. J. Berne, J. Chem. Phys. *70*, 405 (1979).
[8] J. L. Skinner and P. G. Wolynes, J. Chem. Phys. *72*, 4913 (1980).
[9] J. A. Montgomery, Jr., S. L. Holmgren, and D. Chandler, J. Chem. Phys. *73*, 3688 (1980).
[10] B. J. Berne, J. L. Skinner, and P. G. Wolynes, J. Chem. Phys. *73*, 4314 (1980).
[11] D. L. Hasha, T. Eguchi, and J. Jonas, J. Am. Chem. Soc. *104*, 2290 (1982).
[12] M. Lee, G. R. Holton, and R. M. Hochstrasser, Chem Phys. Lett. *118*, 359 (1985).
[13] J. Schroeder and J. Troe, Annu. Rev. Phys. Chem. *38*, 163 (1987).
[14] S. P. Velsko, H. Waldeck, and G. R. Fleming, J. Chem. Phys. *78*, 249 (1983).
[15] R. A. Kuharski, D. Chandler, J. A. Montgomery, Jr., F. Rabbi, and S. J. Singer, J. Phys. Chem. *92*, 3261 (1988).
[16] B. Hartke, J. Manz, and J. Mathis, Chem. Phys. *139*, 123 (1989).
[17] V. Lopez and R. A. Marcus, Chem. Phys. Lett. *93*, 232 (1982); S. M. Lederman, V. Lopez, V. Fairen, G. A. Voth, and R. A., Marcus, Chem. Phys. *139*, 171 (1989).
[18] T. Uzer and J. T. Hynes, J. Phys. Chem. *90*, 3524 (1986).
[19] P. J. Rogers, J. I. Selco, and F. S. Rowland, Chem. Phys. Lett. *97*, 313 (1983); P. J. Rogers, D. C. Montague, J. P. Frank, S. C. Tyler, and F. S. Rowland, ibid. *89*, 9 (1982).
[20] P. J. Rogers, J. I. Selco, and F. S. Rowland, Chem. Phys. Lett. *97*, 313 (1983); S. P. Wrigley and B. S. Rabinovitch, ibid. *98*, 386 (1984).
[21] C.-L. Xie, D. Campbell, and J. Jonas, J. Chem. Phys. *88*, 3396 (1988).
[22] X. Peng and J. Jonas, J. Chem. Phys. *93*, 2192 (1990).
[23] J. Ashcroft, C.-L. Xie, and J. Jonas, J. Chem. Phys. *90*, 5386 (1989).
[24] C.-L. Xie, D. Campbell, and J. Jonas, J. Chem. Phys. *92*, 3736 (1990).
[25] J. Jonas, A. Allerhand, and H. Gutowsky, J. Chem. Phys. *42*, 3396 (1965).
[26] C. Hu and R. Zwanzig, J. Chem. Phys. *60*, 4354 (1974).
[27] J. Jonas, Annu. Rev. Phys. Chem. *26*, 167 (1975).
[28] C. Deverell, R. E. Morgan, and J. H. Strange, Mol. Phys. *18*, 553 (1970).
[29] R. F. Grote and J. T. Hynes, J. Chem. Phys. *73*, 2715 (1980); *74*, 4465 (1981).
[30] D. K. Garrity and J. L. Skinner, Chem. Phys. Lett. *95*, 46 (1983).
[31] J. Jonas, D. Hasha, and S. G. Huang, J. Chem. Phys. *71*, 3996 (1979).
[32] J. Saltiel and J. T. D'Agostino, J. Am. Chem. Phys. *94*, 6445 (1972).

Presented at the Discussion Meeting of the Deutsche Bunsen-Gesellschaft für Physikalische Chemie "Rate Processes in Dissipative Systems: 50 Years after Kramers" in Tutzing, September 10–13, 1990 E 7489

Femtosecond Studies of the Photoisomerization of *cis*-Stilbene in Solution

S. T. Repinec, R. J. Sension, and R. M. Hochstrasser

Department of Chemistry, University of Pennsylvania, Philadelphia, PA 19104-6323

Fluorescence / Light, Absorption / Light, Emission / Liquids / Photochemistry / Ultrafast Spectroscopy, Visible and Ultraviolet

Femtosecond laser studies on cis-stilbene photoisomerization in alkane solvents show a weak friction dependence on the excited state lifetime. A possible barrier crossing process is indicated when these results are compared with various potential models. The anisotropy values of the transient absorptions allow the assignment of the various excited states to A type in C_2 symmetry. Anisotropy measurements in the regions of product ground state absorptions demonstrate a high alignment between reactant cis and product trans and a low alignment between cis and product dihydrophenanthrene (DHP) transition dipoles. These results indicate a significant angular displacement of the ethylene bond during isomerization. In addition, time resolved absorption studies detecting product trans fluorescence estimate an initial internal temperature of 725 ± 100 K which decays with ca. 14 ps time constant.

Introduction

The isomerization of stilbene has been extensively studied as a model for photoinduced molecular rearrangement and as a probe of solvent effects associated with isomerization and molecular rotation [1–5]. The isomerization of *trans*-stilbene in the first excited state involves a barrier crossing process which takes many tens of picoseconds depending on solvent [4]. Vibrational cooling of excited *trans*-stilbene molecules occurs in about 20 ps, which is shorter than the excited state lifetime [5]. Recent femtosecond experiments have allowed the study of the isomerization from the cis side of the potential surface which has long been assumed to be barrierless as shown in Fig. 1 [1, 2]. The cis-stilbene excited state decays in ca. 1 ps in alkane solvents, forming cis, trans, and dihydrophenanthrene (DHP) with quantum yields of 0.55, 0.35, and 0.1 respectively [6]. The rapid disappearance of the excited cis population makes possible the observation of spectra and dynamics of intermediates and product formed during the isomerization [2, 7]. Vibrational energy transfer may also be observed after the disappearance of cis population [8]. In this paper several results are discussed which were obtained by transient absorption experiments

 © VCH Verlagsgesellschaft mbH, W-6940 Weinheim, 1991 *0005-9021/91/0303-0248 $ 3.50+.25/0*

which probe optically excited *cis*-stilbene and fluorescence experiments which measure the appearance of *trans*-stilbene by exciting the trans molecules produced by the isomerization and observing their fluorescence.

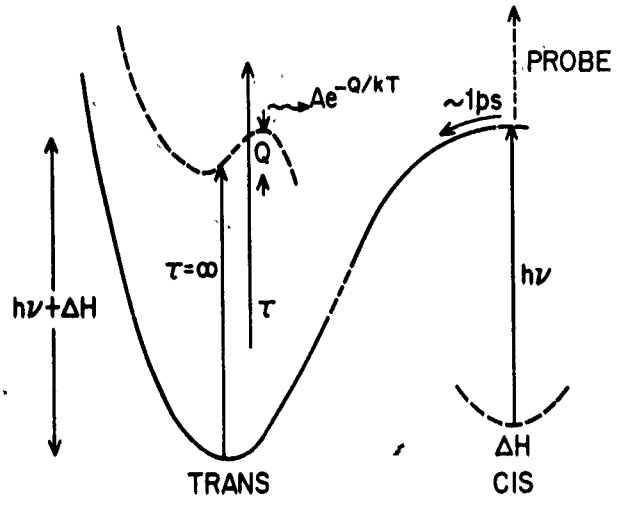


Fig. 1
Potential energy diagram for stilbene ground and excited states showing the transient absorption and fluorescence detection experiments

Experimental

The laser system, transient absorption, and fluorescence experiments have been described in detail elsewhere [2, 8]. Briefly, a CPM laser which is amplified in a four stage Nd:YAG pumped amplifier and then frequency doubled is used to excite *cis*-stilbene at 312 nm.

For the transient absorption experiments probe wavelengths in the visible are obtained by continuum generation in a cell of H_2O. Narrow slices of the continuum are selected with a set of interference filters. This probe can also be frequency doubled to obtain wavelengths in the ultraviolet.

In the fluorescence experiment a second pump beam at 312 nm is used to excite the *trans*-stilbene molecules created by the first pump pulse. The fluorescence from the excited trans molecules is collected by a photomultiplier tube perpendicular to the pump beams.

A half-wave plate in the pump arm of both experiments allows the rotation of the pump beam polarization to give the parallel and perpendicular polarization geometries for anisotropy studies.

Friction Dependence of Cis Relaxation

Transient absorption measurements carried out with *cis*-stilbene in a series of *n*-alkane solvents and at a number of probe wavelengths show a weak friction dependence [2]. The excited state lifetime ranges from about 1 ps in hexane to 1.4 ps in hexadecane. *Cis*-stilbene exhibits transient absorption spectra in the visible/IR and ultraviolet regions of the spectrum. The visible/IR transient has peaks at 650 nm and 450 nm. The ultraviolet transient spectrum starts around 390 nm increasing toward higher energy where it overlaps with the ground state spectra. The viscosity data were taken at 650 nm in the visible and at 350 nm in the ultraviolet. The friction dependence is similar for both the visible and the ultraviolet transients. In fact, across the entire spectrum the transient absorption rises with an instrument function limited rise and decays with a lifetime characteristic of a particular alkane solvent. This indicates that any spectral shift arising from the population moving along a barrierless potential energy surface does not occur within our time resolution.

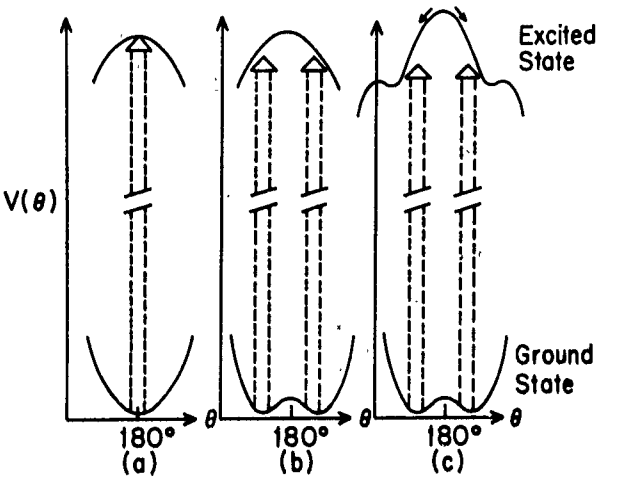


Fig. 2
Three possible models for the *cis*-stilbene ground and excited state surfaces

Models for *cis*-Stilbene Isomerization

The transient absorption data allow the comparison of the isomerization process with some simple models. Three models which could possibly describe the excited state surface are shown in Fig. 2. Because *cis*-stilbene is not planar due to the repulsion of the phenyl ring hydrogens there must exist a double minimum around the 180° (cis) configuration as is shown in b. and c. of Fig. 2. The first potential in Fig. 2 shows an inverted symmetric potential for the excited state. The Brownian motion of a particle in a harmonic force field was first considered by Chandrasekhar [9]. The motion of a particle on an inverted well follows as a straightforward extension of this form [2]. The decay curve for excited state *cis*-stilbene in hexane may be modeled as Brownian motion on an inverted well of frequency $\omega = 4 \times 10^{12}\ s^{-1}$. However, when the empirical angular friction factor β appropriate for hexane ($\beta = 1.18 \times 10^{13}\ s^{-1}$) is replaced by the value appropriate for hexadecane ($\beta = 5.88 \times 10^{13}\ s^{-1}$ [10]) the model predicts a much longer lifetime than is observed experimentally. This model also predicts the wrong functional form for the decay with the theoretical curves being highly nonexponential due to Brownian motion on top of the potential surface.

The second potential drawn in Fig. 2 is a displaced inverted harmonic well. Brownian motion on this model potential surface has many of the characteristics of the first surface in Fig. 2. It predicts a stronger friction dependence than observed experimentally. It also predicts improper functional forms for the decay of electronically excited *cis*-stilbene.

The third model in Fig. 2 is one in which *cis*-stilbene is excited into shallow wells displaced from 180 . A compari-

son of the data to a one dimensional Kramers equation gives a barrier on the order of $Q = 3kT$ [2]. With a barrier this size Kramers theory may not be valid but it does provide a qualitative prediction, along with the absence of excited cis-stilbene spectral shifts, that the region where *cis*-stilbene manifests its transient absorption at times in excess of a few hundred femtoseconds may be a shallow well on the potential surface.

These results in the non-polar alkane solvents indicate the possible existence of a small barrier to isomerization in the cis side of the excited potential surface. Recent experiments by Fleming and co-workers show an early spectral shift in alcohol solvents [11]. This indicates that the potential surface in these polar solvents is barrierless and confirms the notion that the shape of the *cis*-stilbene excited state surface is solvent dependent.

State Assignments

The measured anisotropy signal in a transient absorption experiment is:

$$r(t) = \frac{I_{\parallel}(t) - I_{\perp}(t)}{I_{\parallel}(t) + 2I_{\perp}(t)}$$

where $I_{\parallel}(t)$ and $I_{\perp}(t)$ are the signal intensity for parallel and perpendicular pump and probe beam polarization respectively. This anisotropy measures the quantity:

$$r(t) = 0.4\langle P_2[\cos\Phi(t)]\rangle$$

where $\Phi(t)$ is the instantaneous angle between the transition dipoles in the pumpprobe transitions. The absorption anisotropy provides information on the symmetry of the states involved in the two-photon pump probe process. The excitation of *cis*-stilbene at 312 nm involves an A→B type transition. The visible transients probed around 650 nm in both cis and *trans*-stilbene have anisotropies for the ground to excited state dipoles near 0.4. A value of $r = 0.4$ is the maximum for this type of experiment. This indicates that the transition dipole of the excited transition is nearly parallel to that for the transition dipole pumped at 312 nm. The *cis*-stilbene ultraviolet transient has $r = 0.15$ for a 350 nm probe. The ground state of stilbene is of A type and the first excited state is B therefore the positive anisotropies indicate the upper levels in these pump-probe experiments are of A type because excitations of A→B→B would give $r = -0.2$.

Reaction Coordinate

The ultraviolet absorption of *cis*-stilbene overlaps the ground state absorption of *trans*-stilbene in the region of 330 nm. Anisotropies in this region give information on the reaction coordinate by measuring the alignment between the reactant cis and product trans molecules. The transient absorption decay and anisotropy in hexadecane at 330 nm is shown in Fig. 3. In the region between 420 nm and 520 nm the spectrum of dihydrophenanthrene (DHP) is observable after the decay of the cis-population. The DHP is formed by a ring closing of the phenyl rings. In both spectral regions the excited cis signal decays in 1.4 ps in hexadecane to a long time product absorption as seen in Fig. 3. This longer time absorption partially decays due to vibrational cooling i.e. a spectral shift taking tens of picoseconds. The *cis*-stilbene isomerization allows the measurement of the reaction dipole for two separate reaction pathways. The product anisotropy at the earliest times remains high, $r = 0.20$ for cis to trans and is $r = 0.17$ for cis to DHP. At longer times the anisotropy decays due to rotational diffusion but in hexadecane the conventional rotational relaxation time is long enough that it does not influence the interpretation of the alignment of reactant and product.

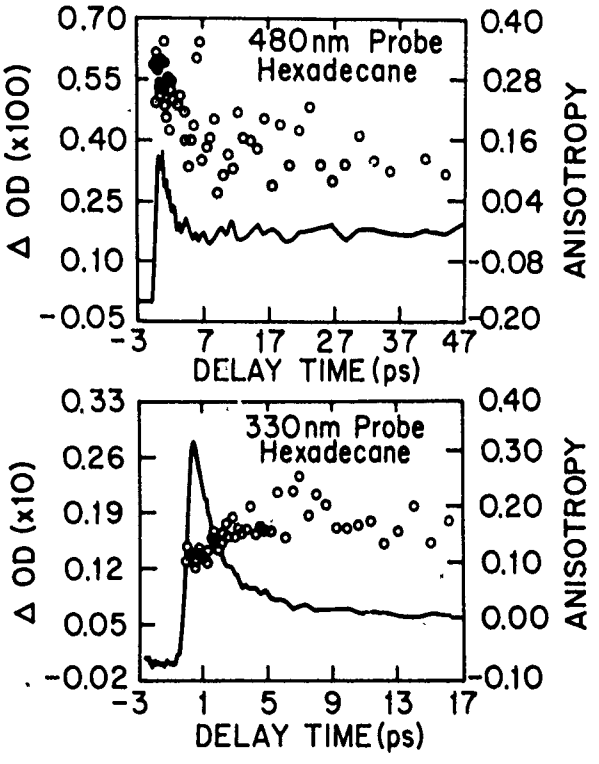


Fig. 3
Magic angle transient absorption decay curves (solid lines) and anisotropies (open circles) for excited *cis*-stilbene in hexadecane in the regions of *trans*-stilbene ground state (330 nm) and the dihydrophenanthrene absorption (480 nm)

The *trans*-stilbene $S_0 \rightarrow S_1$ transition dipole is known to lie along the longest axis of the molecule [12]. The transition dipole for *cis*-stilbene has not been measured but a recent calculation predicts the dipole to lie close to the ethylene bond [13]. The cis and trans transition dipoles for the ground to first excited state are shown in relation to the molecules in Fig. 4. A simple exiton model predicts the DHP ($S_1 \rightarrow S_1$) transition to be directed perpendicular to the C_2 symmetry axis and along the longest polyene axis [14]. The measured anisotropies at times after the decay of the excited cis population are quite high for both trans ($r = 0.2$) and DHP ($r = 0.17$). This indicates substantial alignment between the reactant and product transition dipoles.

One model to explain the high product anisotropies considers the reaction product dipoles to lie on the surface of a cone around a line along the reactant *cis*-stilbene ethylene bond. The data indicate a cone angle of about 35° for *trans*-stilbene product and 38° for DHP in such a model. If the isomerization to *trans*-stilbene proceeded as a simple rotation about the double bond, as shown in Fig. 4, a cone angle of 60° would be predicted from the trans and cis transition dipoles. This would lead to an anisotropy of $r = -0.05$. Since the measured anisotropy is much greater it is possible that the isomerization is not a simple rotation about the double as is usually assumed. The results require that the ethylene bond rotate by an angle of ca. 25° during the isomerization in order to produce this high anisotropy. The DHP product anisotropy of $r = 0.17$ indicates this reaction pathway also must involve a significant rotation of the ethylene bond being a lower value than is expected for a simple ring closing with the ethylene bond axis fixed in space.

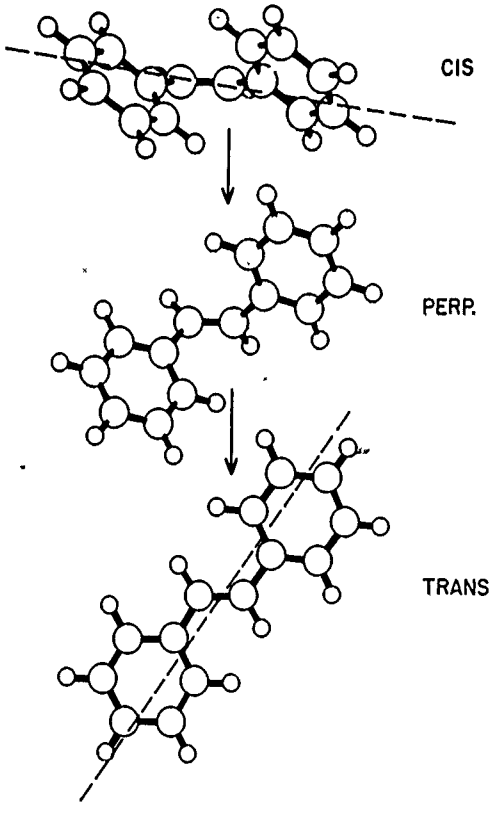


Fig. 4
Transition dipole directions for the isomerization of *cis*-stilbene. The simple rotation about the double bond relating these structures (cis, twisted, and trans) predicts a much lower anisotropy than is observed

A full interpretation of the anisotropy must consider overall rotations in the laboratory frame about a definite axis fixed in each molecule. To minimize the friction on the cis to trans isomerization, the whole molecule may be forced to rotate. Furthermore, the conrotatory motions of the phenyl rings of a cis-like structure must generate a torque that could lead to a reorientation of the whole molecule. Such effects involving the coupling of internal and overall motions have been considered by Moro for butane isomerization [16]. Our results indicate a reorientation of the ethylene bond in both the cis to trans *and* cis to DHP reactions suggesting that if the motion is dominated by the coupling of internal and overall rotations it is most likely to occur as a result of phenyl ring rotations common to both the DHP and trans reaction coordinates. Additional experimental and theoretical efforts are needed to separate these various angular motions.

Vibrational Cooling

Trans-stilbene molecules formed from the isomerization of cis can have excess internal energy. The ground state spectrum of the *trans*-stilbene product shifts with time constants on the order of 20 ± 10 ps [8]. The shift in the spectrum and the decay of the longtime absorption in the transient absorption curves results from the difference between the extinction coefficients of the hot and cold molecules. The decay is slightly longer toward the absorption peak and faster on the edges. These observations suggest that the internal energy resulting from the isomerization can be gauged by assuming a definite initial temperature achieved by distributing the excess energy over a substantial fraction of the internal modes.

The fluorescence experiment on *cis*-stilbene in solution was first done by Yoshihara and coworkers but with insufficient time resolution to measure the appearance of *trans*-stilbene [15]. The time resolution of the solution experiments presented here is able to detect the ground state *trans*-stilbene formation. The fluorescence experiment provides a good measure for the cooling of trans molecules. As seen in Fig. 1 after the formation of excited cis-stilbene by the pump beam hot trans molecules are formed in ca. 1 ps. The hot ground state trans molecules are excited after a time delay (τ) between the pulses and the integrated fluorescence signal

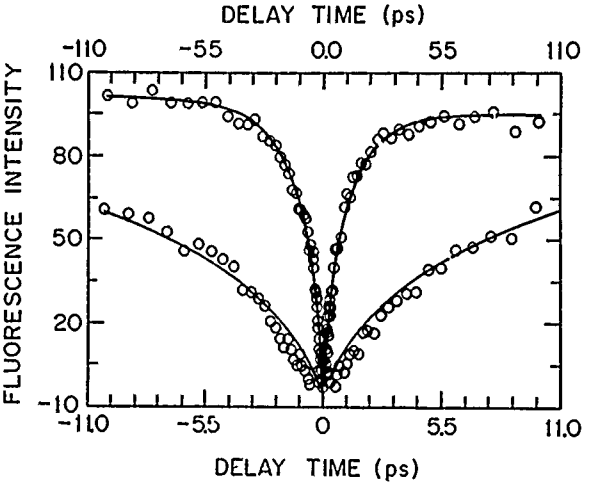


Fig. 5
Magic angle fluorescence intensity of *trans*-stilbene as a function of delay time between the excitation pulse which excites ground state *cis*-stilbene and the second pulse which excites the formed *trans*-stilbene product. The slow rise of the signal arises because the hot trans molecules generated initially do not fluoresce efficiently

is detected. For time delay $\tau = \infty$ the fluorescence excitation pulse probes the room temperature trans molecules. Because the pump and fluorescence excitation beams are of approximately equal energy the trans fluorescence signal will be at a minimum at time zero and rise nearly symmetrically on either side of zero delay as seen in Fig. 5. The data in Fig. 5 is for *cis*-stilbene in hexadecane. The solid line fit of the data is from a model that includes the variation of the fluorescence quantum yield with temperature [8]. The quantum yield changes as a result of the barrier to isomerization which renders the fluorescence temperature dependent. The fit models the temperature decay as a single exponential with a lifetime of 14 ps. The data for *cis*-stilbene in hexane is identical with that for hexadecane indicating that the cooling of the molecules is not noticeably solvent dependent for these alkane solvents.

Energy Partitioning

From the fluorescence experiment it is possible to obtain an estimate of the initial internal temperature of the hot trans molecules. Acceptable fits to the data are found for temperatures of 725 K ± 100 K [8]. A calculation assuming that the excess energy is distributed over all the internal modes of the molecule predicts an internal temperature of 1325 K following the absorption of one 32050 cm^{-1} photon. The ca. 600 K difference between the measured temperature and the maximum temperature suggests that the isomerizing stilbene molecule loses a significant portion (about 65%) of its energy into the solvent very rapidly i.e. before the appearance of trans. The rest of the photon energy is found in the internal modes of the trans molecule which cool with the above mentioned 14 ps time constant. This is the first time that energy partitioning between internal and external friction pathways has been identified experimentally and the result presents a significant challenge to theory.

Conclusions

The femtosecond experiments on *cis*-stilbene discussed here lead to a better understanding of the isomerization process. The cis molecules are excited onto a potential surface which may be barrierless or have shallow minima nearby depending on the solvent system. The isomerization to *trans*-stilbene and dihydrophenanthrene requires rotation of the ethylene bond in the laboratory frame. The *trans*-stilbene and DHP are formed with considerable internal energy. The rates of appearance of trans and DHP are not significantly different from the disappearance of excited cis. The hot trans molecules having already lost two-thirds of their excess energy when first detected cool with a characteristic time of about 14 ± 3 ps.

This research was supported by grants from NSF and NIH. We wish to thank Dr. G. Moro for helpful suggestions regarding the coupling of internal and external motions.

References

[1] F. E. Doany, R. M. Hochstrasser, B. I. Greene, and R. R. Millard, Chem. Phys. Lett. *118*, 1 (1985).
[2] S. Abrash, S. Repinec, and R. M. Hochstrasser, J. Chem. Phys. *93*, 1041 (1990).
[3] G. Rothenberger, D. K. Negus, and R. M. Hochstrasser, J. Chem. Phys. *79*, 5360 (1983).
[4] M. Lee, A. J. Bain, P. J. McCarthy, C. H. Han, J. N. Haseltine, A. B. Smith III, and R. M. Hochstrasser, J. Chem. Phys. *85*, 4341 (1986).
[5] B. I. Greene, R. M. Hochstrasser, and R. B. Weisman, Chem. Phys. Lett. *62*, 427 (1979).
[6] K. A. Muszkat and E. Fischer, J. Chem. Soc. (B) 662 (1967).
[7] R. J. Sension, S. T. Repinec, and R. M. Hochstrasser, manuscript in preparation.
[8] R. J. Sension, S. T. Repinec, and R. M. Hochstrasser, J. Chem. Phys. *93*, 9185 (1990).
[9] S. Chandrasekhar, Rev. Mod. Phys. *15*, 1 (1943).
[10] M. Lee, J. N. Haseltine, A. B. Smith III, and R. M. Hochstrasser, J. Am. Chem. Soc. *111*, 5044 (1989).
[11] J. M. Jean, D. C. Todd, A. J. Ruggiero, and G. R. Fleming, in: Ultrafast Phenomena VII, pp. 441–443, eds. C. B. Harris, E. P. Ippen, G. A. Mourou, and A. H. Zewail, Springer-Verlag, Berlin 1990.
[12] a) M. Traetteberg, E. B. Frantsen, F. C. Mijhoff, and A. Hoekstra, J. Mol. Struct. *26*, 56 (1975); b) M. Traetteberg and E. B. Frantsen, J. Mol. Struct. *26*, 69 (1975).
[13] B. Dick, private communication.
[14] K. A. Muszkat, Top. Curr. Chem. *88*, 89 (1980).
[15] M. Sumitani, N. Nakashima, and K. Yoshihara, Chem. Phys. Lett. *68*, 255 (1979).
[16] G. Moro, Chem. Phys. *118*, 167 (1987).

Presented at the Discussion Meeting of the Deutsche Bunsen-Gesellschaft für Physikalische Chemie "Rate Processes in Dissipative Systems: 50 Years after Kramers" in Tutzing, September 10–13, 1990 E 7497

Classical and Quantum Models of Activationless Reaction Dynamics

John M. Jean*), Graham R. Fleming

Department of Chemistry and the James Franck Institute, The University of Chicago, Chicago, IL 60637

Richard A. Friesner)**

Department of Chemistry, University of Texas, Austin, TX 78712

Chemical Kinetics / Energy Transfer / Photochemistry / Quantum Mechanics

Two aspects of barrierless processes are discussed. Adiabatic processes are discussed briefly in the context of diffusion to a sink. Second, a multi-level Redfield theory is developed as a model for rate processes where vibrational relaxation and dephasing occur on the time scale of the electronic process. The results of numerical calculations are presented and deviations from the Golden Rule predictions discussed.

Introduction

Kramers in his seminal 1940 paper [1] considered the problem of escape over a potential (or free energy) barrier. It is a natural extension of his ideas to include processes that have little or no intrinsic barrier. Because of the intrinsic time scale of nuclear motion, barrierless processes in chemistry and biology are very rapid and their study has advanced in parallel with developments in ultrafast laser spectroscopy. Examples of barrierless processes in chemistry include some isomerization reactions, a range of electron transfer reactions as well as many diffusion controlled reactions in solution. Barrierless reactions also seem to be common in biological processes. For example, the isomerization reaction triggering the visual process and the rebinding of CO to heme in myoglobin are believed to lack barriers. Perhaps the most striking barrierless reaction in nature is the primary charge separation step in photosynthesis. Here the ultrafast initial electron transfer step (~3 ps) actually speeds up 2–4 times as the temperature is lowered from 300 K to 10 K [2]. Electronic energy transfer between the prosthetic groups of the bacterial reaction center is even faster than the electron transfer; recent estimates from hole burning [3] and ultrafast [4] spectroscopy place the energy transfer rate in the 30–50 fs range. In this case the conventional separation between electronic and vibrational phase relaxation and energy relaxation time scales is unlikely to exist.

In descriptions of barrier crossing processes two types of approaches have been conventionally employed. For nonadiabatic processes the Golden Rule is used to calculate the rate, whereas for adiabatic processes in the presence of dissipation Kramers theory provides an appropriate description. In the following section we briefly sketch theoretical models appropriate to barrierless processes in these two limits. In fact the second approach we describe – multi-level Redfield theory – is applicable to both regimes and to systems with or without barriers. However, in the present paper we restrict ourselves to systems where the barrier is rather small.

Theory

1. Adiabatic Processes

In the adiabatic case, when the barrier is very small or lacking, Bagchi, Fleming and Oxtoby [5, 6] proposed a theory in which the reactive motion is modeled by the damped motion of a Brownian particle on a potential surface. The decay of population from the initial state occurs through a coordinate dependent sink. One of the most striking characteristics of such processes is the potential lack of time scale separation between reactive motion and the inverse "rate" of reaction. Clearly in this situation non-steady state dynamics might be rather common and the form of the population decay depends on the competition between diffusive motion toward the sink and removal of population from the sink region. Many aspects of the diffusion to a sink model have recently been discussed in detail [6] and here we restrict ourselves to some comments on the form of the population decay in various regimes.

In more quantitative terms the dynamics of the population decay can be described in terms of two rate constants, the time averaged rate, k_I, and the long time rate k_L. These are given by

$$k_I^{-1} = \int_0^\infty P(t)\,dt$$

and

$$k_L = -\lim_{t\to\infty} \frac{\partial}{\partial t} \ln P(t)$$

where $P(t)$ is the population at time t. The dynamics of adiabatic barrierless processes are controlled primarily by the dimensionless parameter $\tilde{k}_0 = k_0\zeta/\mu\omega^2$. Here k_0 is the decay rate at the sink, ζ is the friction coefficient, μ the reduced mass and ω the radial frequency of the potential surface. The parameter $\tilde{k}_0$ effectively determines how long it

*) Present address: Department of Chemistry, Washington University, St. Louis, MO 63130.

**) Present address: Department of Chemistry, Columbia University, New York, NY 10027.

 © VCH Verlagsgesellschaft mbH, W-6940 Weinheim, 1991 0005-9021/91/0303-0253 $ 3.50+.25/0

takes to attain a steady state condition, after which the population decay is exponential. A quantitative analysis can be made via an eigenvalue analysis of the Smoluchowski equation [6], where the eigenvalues correspond to the population decay rates. For small values of $\tilde{k}_0$ only the smallest eigenvalue contributes to the observed decay due to the large gap between the lowest and next to lowest eigenvalues. As $\tilde{k}_0$ is increased, the gap becomes smaller and more than one eigenvalue can fall within the dynamic range of the measurement. An interesting feature of this analysis is that in the region of large $\tilde{k}_0$, the density of the eigenvalue spectrum may be large enough that the observed dynamics will once again appear exponential due to the inability of the instrument to resolve the various decay components. Thus the appearance of exponential population decay does not necessarily invalidate the possibility of non-steady state dynamics. Recent experiments on the isomerization of cis-stilbene are consistent with this analysis [7] although the presence or absence of a small potential barrier is not fully established at present [7–9]. Fluorescence decays in the lowest viscosity solvents appear exponential, but in the most viscous solvent (largest $\tilde{k}_0$), decanol, as Fig. 1 shows the decay is clearly non-exponential consistent with this solvent lying in the intermeditate $\tilde{k}_0$ range.

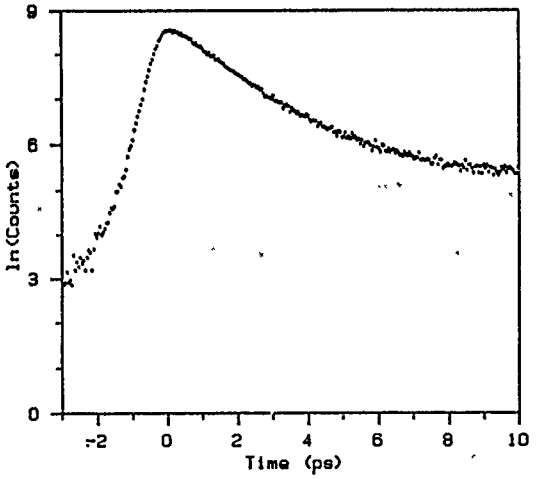


Fig. 1
Fluorescence decay of cis-stilbene in decanol detected at 430 ± 5 nm. The intensity scale is logarithmic and the decay is clearly non-exponential

An extensive review of barrierless dynamics in the context of a diffusional approach has recently appeared and interested readers are referred to that article for further details [6].

2. Nonadiabatic Processes

The diffusion to a sink model can roughly account for some effects of nonadiabiticity via finite decay rate models [6], but the approach is purely classical. In this section we sketch our initial efforts to develop a fully quantum mechanical model for such processes. Much effort has been expended over the past decade in attempting to take into account the role of nuclear motion, including collective solvent or lattice modes, in determining the details of the dynamics. Much of this work, especially in the field of electron transfer has taken a semi-classical path, in which the motion along a specific nuclear coordinate – the "reaction coordinate" – is treated classically incorporating the effects of friction provided by the very large number of orthogonal degrees of freedom. In such a description quantum mechanics enters only at the point of intersection between the diabatic reactant and product surfaces. At this configuration the Schroedinger equation is solved to compute the probability of making a transition from one surface to another. This standard surface hopping model has proved valuable in understanding the role of friction in non-adiabatic processes and in understanding the transition from non-adiabatic to adiabatic behavior in electron transfer [10]. In ultrafast processes, even in the condensed phase at high temperatures, the possibility exists that quantum interference effects play a role in the dynamics. The description of such effects does not fall in the realm of the standard surface hopping or Landau-Zener approach. Quantum effects will be important when there are strong resonances or when phase is preserved on the time scale of the electronic transition matrix element.

Onuchic and Wolynes [11] have recently presented a semi-quantitative discussion rooted in trajectory based arguments to describe quantum effects on dynamics. In this paper we introduce a density matrix formalism based on Redfield relaxation theory [12], appropriate to electron or electronic energy transfer in molecular systems and which enables quantitative exploration of many of the issues raised by Onuchic and Wolynes. Redfield's theory has been widely used in the field of magnetic resonance and to a lesser extent in optical spectroscopy [13]. By explicitly treating a subset of nuclear degrees of freedom quantum mechanically, and through a judicious choice of representations, we develop a multi-level theory that is valid for arbitrarily strong electronic coupling and properly takes account of the influence of finite vibrational and electronic dephasing rates and vibrational energy relaxation rates. Thus, the theory has the property that it interpolates between the coherent and incoherent limits of transport for sufficiently weak damping and between the adiabatic and nonadiabatic rate descriptions for over-damped systems. A significant feature of our approach is that parameters relating to vibrational relaxation and dephasing time scales are entered in the site representation where some experimentalist's intuition can be brought to bear in setting the magnitudes of the parameters. In addition, the light-matter interaction is included explicitly in the Hamiltonian so that in experiments involving optical preparation the initial state may be properly specified.

3. Formalism

A detailed description of the formalism will be given elsewhere [14]. Here we give some brief details of the approach and set up a simple model of electron transfer.

The effective Hamiltonian considered as a model for electron transfer between electronic states $|1\rangle$ and $|2\rangle$ is

$$H = [H_1(Q) + V_1(q,Q)]|1\rangle\langle 1| + [H_2(Q) + V_2(q,Q)]|2\rangle\langle 2| + J[|1\rangle\langle 2| + |2\rangle\langle 1|] + H_{SF}.$$

Q refers to the single system coordinate (i.e. "reaction coordinate") and q to the set of bath coordinates. In what follows, the reaction coordinate is treated quantum mechanically in order to properly incorporate the effect of finite vibrational relaxation and dephasing times. The remaining degrees of freedom (solvent or lattice modes) are assumed to relax quickly compared to motion along Q and are thus treated as a thermal reservoir. The operators $H_i (i = 1,2)$ are effective Hamiltonians for sites 1 and 2 and are averaged over the bath variables. $V_i(q,Q)$ is the operator coupling state (i) to the bath and represents fluctuations in the system energies from their canonical averages. $V_i(q,Q)$ is chosen so that both population relaxation and pure dephasing interactions are present. the exchange interaction giving rise to electron transfer is denoted by J. Finally, H_{SF} is the system field interaction which determines the nature of the initially photoexcited state.

In second quantized notation, the system Hamiltonian is

$$H_{sys} = \Delta\{|1\rangle\langle 1| - |2\rangle\langle 2|\} + g_1(b+b^+)|1\rangle\langle 1| + g_2(b+b^+)|2\rangle\langle 2| + J\{|1\rangle\langle 2| + J\{|1\rangle <2| + |2\rangle\langle 1|\}$$

where $\Delta = E_1 + g_1^2/\omega_1 - (E_2 + g_2^2/\omega_2)$ is the energy difference between the origins of the two excited electronic states and g_i is the displacement (in energy units) of excited state i. b^+ and b are the creation and annihilation operators for the system coordinate.

The system-bath interaction, $V(q,Q)$, is parametrized by matrix elements of the fluctuating bath variables between the system states. The rate constant for vibrational relaxation between states n and $n-1$ is given by $k_{n\to n-1} = n\gamma'^2$ where γ' is the off-diagonal fluctuation constant. Similarly the pure dephasing rate for levels m and n is given by $k^*_{m,n} = (m-n)\gamma^2$ where γ is the diagonal fluctuation constant.

The picture described by our model Hamiltonian is thus two displaced wells, each with a manifold of vibrational levels, undergoing relaxation and dephasing coupled by a purely electronic interaction that leads to a splitting of the surfaces in the crossing region. The multilevel nature of the model does not allow for an analytical solution for the dynamics, thus we rely on numerical procedures. However, the dynamics that emerge provide a realistic description of the competition between dissipative processes such as population relaxation and pure dephasing and coherent exchange. A detailed discussion of the strategy for solving for the dynamics of our model will be given elsewhere [14]. In brief, we choose to work in a basis that diagonalizes that part of the Hamiltonian that depends only on the system coordinate and the electronic exchange interaction. We call this representation the eigenstate representation and the original representation the site representation. By choosing an appropriate form for the fluctuation operators, $V_i(q,Q)$, we can calculate the appropriate energy and phase relaxation rates in the site representation. To properly describe the dissipative processes in the eigenstate representation, we perform the same canonical transformation on the fluctuation operators that we used to diagonalize the system Hamiltonian [15]. We thus transform the problem of two manifolds undergoing electron transfer and relaxation to a single manifold undergoing only relaxation processes.

The dynamics of the system are found by solving the Redfield equations for the reduced density operator in the eigenstate representation [12, 16]. This involves treating the system-bath interaction to secound-order. The appropriate equations are of the form

$$\dot{\varrho}_{ij} = -i\omega_{ij} + \sum_{kl} R_{ijkl}\varrho_{kl}.$$

The elements of the Redfield tensor (R_{ijkl}) describe the various relaxation processes involving the system eigenstates. It is important to note that the states labelled by i,j are admixtures of vibronic states belonging to states $|1\rangle$ and $|2\rangle$.

Once the dynamics are computed by finding the eigenvalues and eigenvectors of the Redfield tensor, we transform back to our original basis of site states and trace over the reactant manifold to obtain the population of state $|1\rangle$. In addition to correctly incorporating quantum effects, which arise from the persistence of phase coherence, the procedure described above is nonperturbative in the electronic coupling, J, and thus interpolates between the weak and strong coupling limits.

Numerical Results

Fig. 2 shows adiabatic potential surfaces for a typical system we have studied. Note that the diabatic surfaces cross close to the minimum of the reactant well and thus the electron transfer process is activationless (i.e. at the Marcus maximum).

The first set of calculations we describe uses a very short excitation pulse to prepare an initial state that can be written as a coherent superposition of vibronic states. The transition dipole operator is chosen such that only vibrational states in state $|1\rangle$ are initially excited. The pulse is short enough that the entire bandwidth is coherently prepared, leading to a wavepacket that is localized at the value of Q corresponding to the minimum of the ground state geometry ($Q = 0$). The populations and phase coherence are determined by the appropriate Franck-Condon factors, via

$$\dot{\varrho} = -[H_{SF}, \varrho]; \quad H_{SF} = -\mu \cdot E(t).$$

This is the appropriate form for the Liouville equation in the impulsive excitation limit (i.e. when the temporal width of the excitation pulse is short compared to any free motion of the system).

The population remaining in state $|1\rangle$ as a function of time was calculated as the electronic coupling, J, was pro-

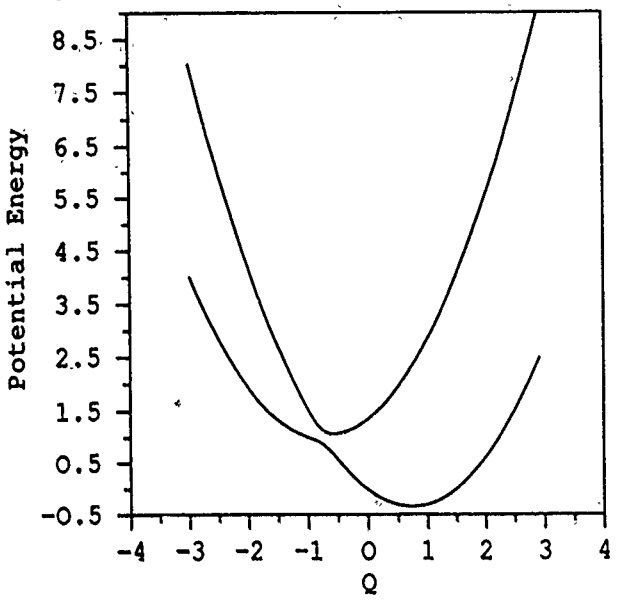


Fig. 2
Initial and final state potential surfaces for a typical activationless process. The minima of the two states are at $Q = \pm 0.72$. Here Q is a dimensionless coordinate defined by $Q = (M\omega/\hbar)^{1/2}q$ where M is the mass ω the frequency and q the actual coordinate

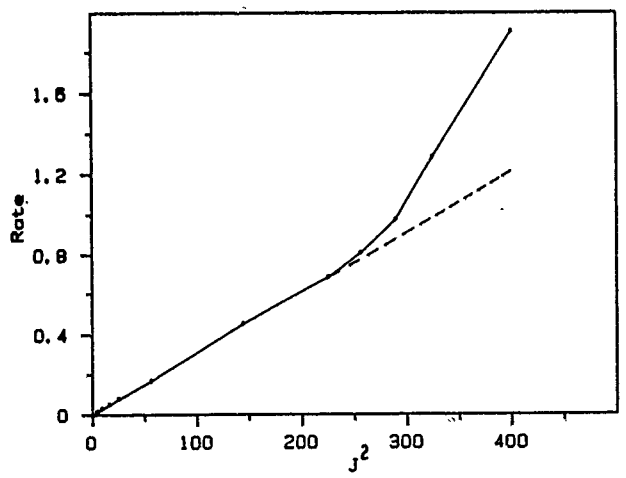


Fig. 3
1/e decay time vs. the square of the electronic coupling calculated from Redfield equations. The Golden Rule prediction is shown for comparison. Parameters are: $\omega_1 = \omega_2 = 190\ \text{cm}^{-1}$, $\Delta = 200\ \text{cm}^{-1}$, $g_1 = -95\ \text{cm}^{-1}$, $g_2 = 95\ \text{cm}^{-1}$, $T = 298$ K. The diagonal and off-diagonal fluctuation constants are $\gamma^2 = 9.0\ \text{cm}^{-1}\gamma'^2 = 4.0\ \text{cm}^{-1}$. $Q = \pm 0.72$ for states $|1\rangle$ and $|2\rangle$, respectively. The dashed line shows the extrapolation of the Golden Rule J^2 dependence

gressively increased. In a multilevel system, such as described here, the effective coupling strength will vary with each initial level due to varying Franck-Condon factors between states in different manifolds. If dephasing is much faster than the time scale of the electronic coupling then the Golden Rule expression should be valid, with the rate constant given by

$$k = \frac{2\pi}{\hbar} J^2(\text{FC}) \frac{\hbar\Gamma}{(\delta E)^2 + (\hbar\Gamma)^2}$$

where FC is the Franck-Condon factor, and δE the energy mismatch between initial and final vibronic levels, Γ is the level width and contains contributions from both T_1 and T_2^* processes. Thus the Golden Rule rate scales as J^2/Γ for small δE (near resonance case), however for finite δE the rate initially increases with increasing level width, then turns over. Fig. 3 shows how the Redfield rate, defined as the 1/e decay time, scales with J^2. In this particular system, the rate follows the Golden Rule up to about $J = 15\ \text{cm}^{-1}$. For higher J values the rate becomes progressively faster than the Golden Rule prediction. The vibrational frequency in this case is $\omega = 180\ \text{cm}^{-1}$. For calibration purposes, we note that the electronic coupling describing the primary charge separation in photosynthesis is estimated to be in the range $20-30\ \text{cm}^{-1}$ [2].

The Golden Rule breaks down when the effective electronic coupling strength gives rise to transfer on a time scale that is competitive with the population relaxation and dephasing processes that lead to equilibration in the reactant well. A particularly useful way of understanding the breakdown of the Golden Rule approximation may be obtained by looking at the ensemble averaged value of the coordinate operator as a function of time calculated from

$$\langle Q(t)\rangle = \text{Tr}[\varrho(t)Q]\,.$$

The initial excitation pulse is such that a number of vibrational levels are coherently prepared. This leads to an average value for Q that is initially displaced from the minimum of state $|1\rangle$. The subsequent ensemble averaged trajectory shows in a detailed way the competition between the electronic coupling which tends to take $\langle Q\rangle$ to values corresponding to state $|2\rangle$ and dephasing which leads to values of $\langle Q\rangle$ corresponding to the equilibrium configuration of the reactant state. Fig. 4 shows such a plot for $J = 0$. The oscillatory motion is due to the vibrational coherence which

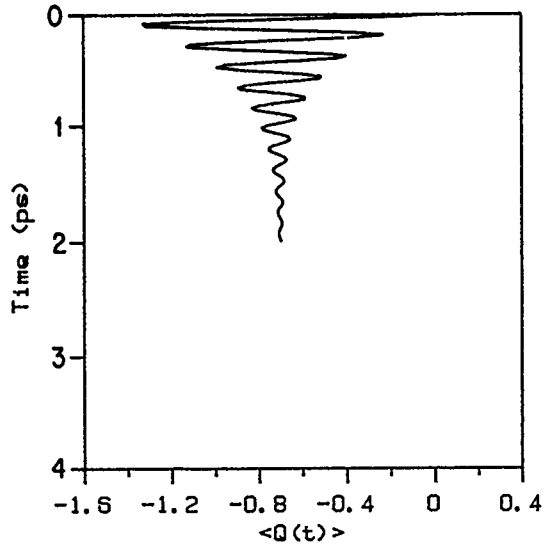


Fig. 4
Ensemble-averaged value for the reaction coordinate, $\langle Q(t)\rangle$, as a function of time for the parameters of Fig. 3. $J = 4.0\ \text{cm}^{-1}$

damps out due to the system-bath interaction. In this case the dephasing time is approximately 600 fs.

Fig. 5 shows a similar plot for $J = 4$ cm^{-1} The motion of population into the final state is revealed by the progressive increase in the value of $\langle Q \rangle$. All coherence has vanished before any significant increase in $\langle Q \rangle$ from the value $-Q_0$ has occurred. In this case the Golden Rule and Redfield rates are identical. By contrast, Fig. 6 shows results for $J = 12$ cm^{-1}, just at the point where the Golden Rule expression breaks down. Here, the vibrational coherence persists as population is depleted from the initial electronic state. The stutter seen in the oscillation at about 1.6 ps results from the interference between the electronic coherence, oscillating at a frequency of $2J$, and the vibrational coherence, oscillating at the vibrational frequency.

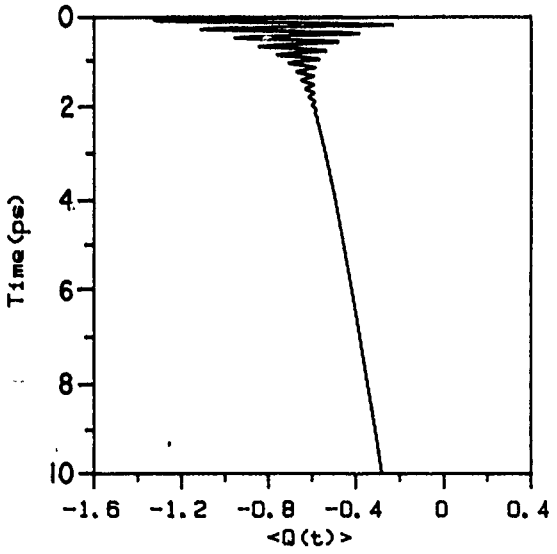


Fig. 5
Ensemble-averaged value for the reaction coordinate, $\langle Q(t) \rangle$, as a function of time for the parameters of Fig. 3. $J = 4.0$ cm^{-1}

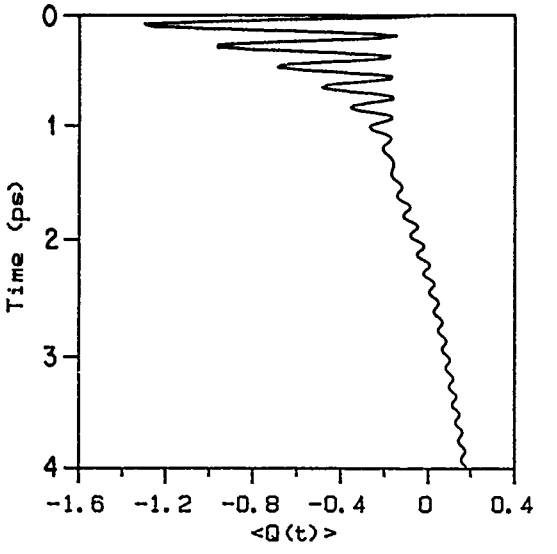


Fig. 6
Ensemble-averaged value for the reaction coordinate, $\langle Q(t) \rangle$, as a function of time for the parameters of Fig. 3. $J = 12.0$ cm^{-1}

The interaction between electronic and vibrational coherence is even more evident in Fig. 7 where the ensemble averaged energy $\langle H(t) \rangle$, is plotted against the ensemble averaged coordinate $\langle Q(t) \rangle$, for a somewhat different set of parameters (see figure caption). The corresponding population decay is shown in Fig. 8. Aside from a brief induction period during the first 100 fs, the decay is quite exponential and experimentally there would be little to indicate that phase coherence was playing a significant role. However, in this case the decay time of 1.7 ps is approximately three times faster than the Golden Rule prediction.

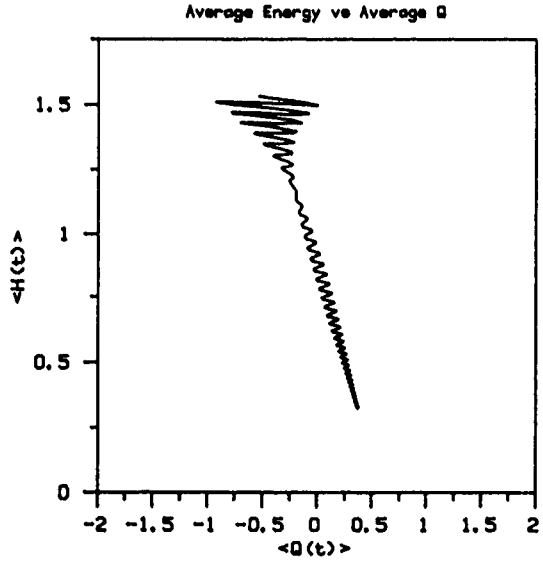


Fig. 7
Ensemble-averaged energy, $\langle H(t) \rangle$, vs. ensemble-averaged coordinate, $\langle Q(t) \rangle$, Parameters are: $\omega_1 = \omega_2 = 400$ cm^{-1}, $\Delta = 400$ cm^{-1}, $g_1 = -150$ cm^{-1}, $g_2 = 150$ cm^{-1}, $T = 298$ K, $J = 10.0$ cm^{-1}, $\gamma^2 = 4.0$ cm$^{-1}\gamma'^2 = 4.0$ cm^{-1}. The minima of the two states are at $Q = \pm 0.53$ in this calculation

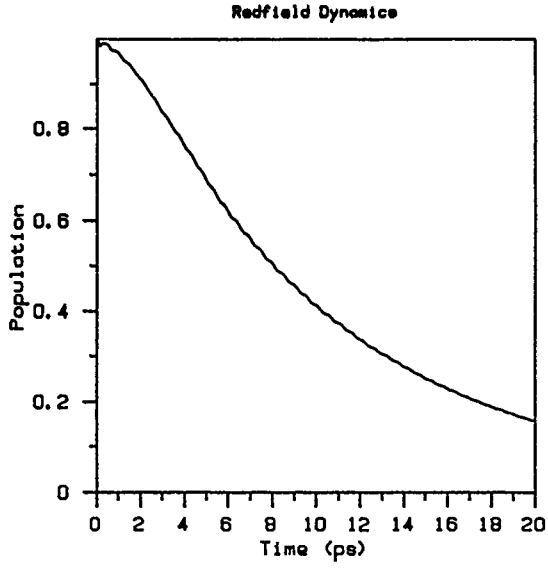


Fig. 8
Population of initial state as a function of time for the parameters of Fig. 7

In general, it is difficult to predict the range of validity of the Golden Rule formula or even the nature of deviations from the Golden Rule in multi-level systems. The increased complexity brought about by having many coupled levels with different dephasing times and effective J-values can lead to a wide range of behaviours depending on parameter values and even on the nature of the initial state. In the case just discussed, significant enhancement of the rate (above that predicted from the Golden Rule) was observed due to the presence of coherence. We surmise that because the levels in state $|1\rangle$ are essentially resonant with those of state $|2\rangle$, the relatively slow dephasing time allows the levels to remain resonant for a substantial period of time before fluctuations destroy the overlap. It is important to stress that the results shown above arise from the presence of many coupled levels and do not occur in an isolated three level system. Such a system is shown in Fig. 9 along with the 1/e decay time as a function of J^2. For small values of J/Γ the rate follows the Golden Rule prediction. At larger values, the rate starts to fall below the Golden Rule prediction. Of course, at sufficiently high values of J/Γ the concept of a rate is meaningless, and the population dynamics will have an oscillatory component.

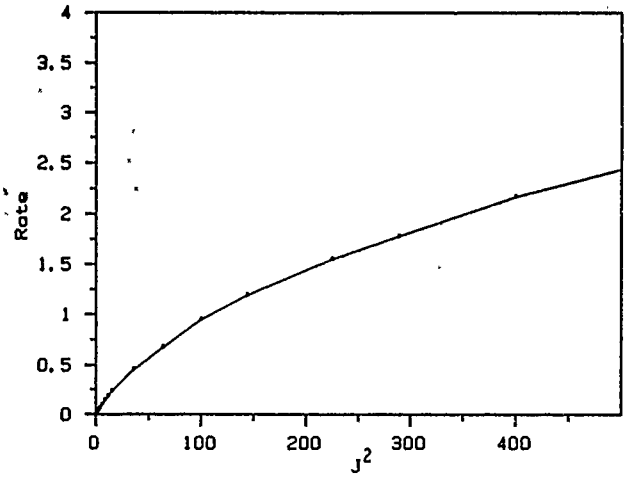


Fig. 9
1/e decay time vs. the square of the electronic coupling calculated from the Redfield equations. The Golden Rule prediction is shown for comparison. Parameters are $\omega_1 = \omega_2 = 800\ \text{cm}^{-1}$, $\Delta = 800\ \text{cm}^{-1}$, $g_1 = -400\ \text{cm}^{-1}$, $g_2 = 400\ \text{cm}^{-1}$, γ^2 0.0, $\gamma'^2 = 9.0\ \text{cm}^{-1}$

The method described above presents a realistic approach to understanding chemical rate processes when the dynamics are complicated by the presence of vibrational relaxation and dephasing on the time scale of the electronic transition.

Summary

We have discussed barrierless processes from two perspectives. A purely classical diffusive model was used to discuss some aspects of barrierless reactions involving large amplitude motion. Secondly, our initial studies of quantum effects in vibronic systems, where the vibrational structure and dynamics are included explicitly, was described. We plan to extend this latter work in studies of criteria for adiabaticity, and of energy transfer in moderately strongly coupled systems, for example, to investigate the influence of correlation in fluctuations at the two sites.

This work was supported by grants from the NSF. We thank David Todd for his help with the manuscript.

References

[1] H. A. Kramers, Physica *7*, 284 (1940).
[2] G. R. Fleming, J. L. Martin, and J. Breton, Nature *333*, 190 (1988).
[3] S. G. Johnson, D. Tang, R. Jankowiak, J. M. Hayes, G. J. Small, and D. M. Tiede, J. Phys. Chem. *94*, 5889 (1990).
[4] J. Breton, J. L. Martin, G. R. Fleming, and J. C. Lambry, Biochemistry *27*, 8276 (1988).
[5] B. Bagchi, G. R. Fleming and D. W. Oxtoby, J. Chem. Phys. *78*, 7375 (1983).
[6] B. Bagchi and G. R. Fleming, J. Phys. Chem. *94*, 9 (1990).
[7] D. C. Todd, J. M. Jean, S. J. Rosenthal, A. J. Ruggiero, D. Yang, and G. R. Fleming, J. Chem. Phys. *93*, 8658 (1990).
[8] S. Abrash, S. Repinec, and R. M. Hochstrasser, J. Chem. Phys. *93*, 1041 (1990).
[9] H. Petek, K. Yoshihara, Y. Fujiwara, Z. Lin, J. H. Penn, and J. H. Frederick, J. Phys. Chem. *94*, 7539 (1990).
[10] H. Frauenfelder and P. G. Wolynes, Science *229*, 337 (1985).
[11] J. N. Onuchic and P. G. Wolynes, J. Phys. Chem. *92*, 6495 (1988).
[12] A. G. Redfield, Adv. Mag. Reson. *1*, 1 (1965).
[13] D. A. Wiersma, Adv. Chem. Phys. *47* (part 2) 421 (1981).
[14] J. Jean, G. R. Fleming, and R. A. Friesner, in preparation.
[15] R. A. Friesner and R. Wertheimer, Proc. Natl. Acad. Sci. *79*, 2138 (1982).
[16] R. Wertheimer and R. Silbey, Chem. Phys. Lett. *75*, 243 (1980).

Presented at the Discussion Meeting of the Deutsche Bunsen-Gesellschaft für Physikalische Chemie "Rate Processes in Dissipative Systems: 50 Years after Kramers" in Tutzing, September 10–13, 1990 E 7492

Solvent Polarity Dependent Formation Dynamics of TICT States. I. Differential Solvatokinetics

Wolfgang Rettig

Iwan N.-Stranski-Institut, Technische Universität Berlin,
Straße des 17. Juni 112, W-1000 Berlin 12, Federal Republic of Germany

Chemical Kinetics / Fluorescence / Photochemistry / Polarity / Viscosity

Comparison of the fluorescence kinetics of two dialkylaminobenzonitriles with different hindrance to planarity is used to extract information on the polar-solvent induced shape changes of the excited-state potential surface for TICT formation. The conical intersection between B* and A* states is shown to move to smaller twist angles as solvent polarity increases.

Introduction

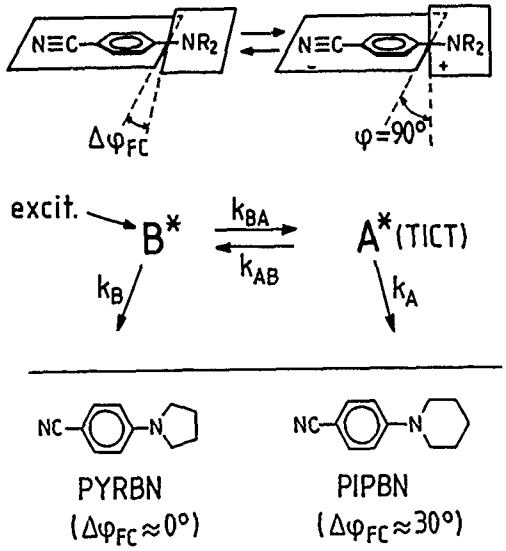
Just as the well-known technique of solvatochromic measurements is able to yield information on the dipole moment of excited states from the red- or blueshift of absorption and/or fluorescence spectra in solvents of different polarity [1–3], the measurement of the solvent polarity-dependence of reaction rates, called solvatokinetics here, can provide information on the electronic nature of the transition state and the dependence of barrier heights and barrier positions on solvent polarity. This field is relatively new, and only scarce data can be found in the literature. Regarding ground state reactions, examples for both retarding [4] and accelerating [5] influence of increasing solvent polarity have been observed. In excited-state reactions, too, cases of reaction rates increasing [6–8] and decreasing [9] with solvent polarity have recently been found.

The four examples cited refer to stilbene and related dyes which undergo trans-cis or cis-trans isomerization in the excited and/or ground state. In this case, the qualitatively different solvatokinetic dependences can directly be linked to the theoretical model of Biradicaloid Charge Transfer (BCT) states [10–13], and they result from the crossover of a polar and a nonpolar state for the conformation with a 90° twisted stilbenoid double bond, when donor and acceptor substituents are introduced [9].

The well-known Twisted Intramolecular Charge Transfer (TICT) state [12–15] can be viewed as a subclass of BCT states [10–13] where an essential single bond is twisted, and where the electronic structure is that of a radical cation/radical anion pair. Recent solvatokinetic measurements of the ps formation rate k_{BA} of the TICT state A* from its precursor state B* for dimethylaminobenzonitrile (DMABN) in isoviscous mixtures of alkylnitriles and alkanes, and in homologous series of alkylnitriles [8,16] established that the observed kinetics is accelerated when solvent polarity increases and everything else is kept constant. This lead to the notion of solvent-polarity dependent activation energies, similarly as observed in the stilbene examples [6–8]. In the case of DMABN, increasing solvent polarity lowers the activation energy for TICT formation [8,16] although the term "activation energy" should be handled with caution in view of the recent interpretations of TICT formation as a barrierless process [12,17,18].

This letter is intended to bring additional light into these questions and reports solvatokinetic measurements on two derivatives of DMABN which differ in initial conditions (twist angle). A large body of evidence is available indicating that substituted N-phenyl-piperidines are substantially twisted in the ground state ($\Delta\phi_{GS} = \Delta\phi_{FC} \simeq 30°$, see scheme 1) whereas N-phenyl-pyrrolidines are close to planar (see references cited in [19]). The corresponding 4-cyano-compounds, N-(4-cyanophenyl)-piperidine (PIPBN) and -pyrrolidine (PYRBN) also show this feature as evidenced by an analysis of their photoelectron spectra [20]. The TICT formation rates k_{BA} of these two compounds (see scheme 1) differ by a factor of more than 10 in n-butyl chloride, and the faster reaction of PIPBN was interpreted as being the result of pretwisting in the ground state [20]. Comparison of the solvatokinetics of these two dyes ("differential solvatokinetics") should thus allow to yield information on where along the excited state reaction potential the activation barrier is placed and how it moves upon changing the solvent polarity.

Scheme 1



 © VCH Verlagsgesellschaft mbH, W-6940 Weinheim, 1991 0005-9021/91/0303-0259 $ 3.50+.25/0

Experimental

The synthesis and purification of PYRBN and PIPBN have been described previously [19]. Solvents used were spectrograde or purified by repeated fractional chromatography and, where necessary, subsequent distillation. Fluorescence decay kinetics at low temperatures were measured using a time-correlated single photon counting setup and cooling equipment described in detail elsewhere [21,22]. Synchrotron radiation from BESSY was used as excitation source ($\lambda_{ex} = 300 \pm 10$ nm). The short wavelength fluorescence F_B was monitored at 350 ± 10 nm and its decay analysed by the iterative reconvolution technique [23] with a kinetic model according to Eq. 1 (sum of exponentials).

$$I_f(t) = \sum_i A_i \exp(-t/\tau_i) . \quad (1)$$

In all cases, three exponentials or less were sufficient for an acceptable fit ($\chi^2 \lesssim 1.2$). The nonexponential nature of the decays did not change when observed through a polarizer set at the magic angle (54.7°). Temperatures were kept far below T_1 the equilibration temperature around which the excited states equilibrium $B^* \rightleftarrows A^*$ can be established within the excited states lifetime [14,19,24], thus all kinetics belong to the "irreversible kinetic region" represented by simple $B^* \rightarrow A^*$ reaction. This is also evidenced by the fact that the long-time decay constants of the short (F_B) and the long-wavelength band (F_A) are significantly different [25,26].

Although a multiexponential model yields acceptable fits, other kinetic models, of a nonexponential nature, have equally ben discussed [12,17,25,27,28], especially to describe the kinetics observed in alcohols. In these solvents, plots of log $I(t)$ vs t are curved for F_B. A multiexponential model (according to Eq. (1)) can faithfully describe this curvature even though the (nonexponential) kinetics may have nothing to do with several independent species constituting the F_B-fluorescence. Therefore, the recovered time constants τ_i cannot directly be compared, and due care has to be taken to include the weights A_i associated with τ_i (Eq. 1) into the analysis.

One of the simplest ways to do this is to use the mean decay time $\bar{\tau}$ defined by Eq. 2 which is a measure for the time-integrated fluorescence (i.e. proportional to the fluorescence quantum yield [21]).

$$\bar{\tau} = \sum_i A_i \tau_i / \sum_i A_i . \quad (2)$$

Results

Fig. 1 shows examples of the F_B decays observed in different solvents. In all cases the decay of PYRBN (when measured by $\bar{\tau}$) is slower than the decay of PIPBN fluorescence. The results of the fits are presented in Table 1.

This table also contains the decay time τ_{77} measured at 77 K where the twisting motion is thought to be frozen. Then, TICT formation rates k_{BA} can be readily obtained by using Eq. 3. They are summarized in Table 2, together with the ratio of the rate constants for PIPBN and PYRBN as a function of solvent polarity (measured by $\Delta f = (\varepsilon-1)/(2\varepsilon+1) - (n^2-1)/(2n^2+1)$ [1]).

$$k_{BA} = (\bar{\tau})^{-1} - \tau_{77}^{-1} . \quad (3)$$

It is evident from Fig. 1 and Table 1 that nonexponential behaviour is mainly observed in the more polar solvents butyronitrile and propanol (larger values of A_2). But also in medium polar solvents like n-butyl chloride, a long decay component can be observed, although of very small weight ($A_2 < 1\%$) and negligibly affecting the value of $\bar{\tau}$. The nature of this long decay component is not yet completely clear but it could be indicative of a residual nonexponentiality. It is not linked to the $B^* \rightleftarrows A^*$ equilibration process and is observed for all the TICT forming compounds investigated so far [25]. It does not diminish upon repeated purification. The present results and conclusions, however, are not affected by it in any way.

Discussion

The above results can be understood using the simple model of a double-well S_1-potential with a barrier (or region with an approximately flat potential) separating B* and A* states, as schematically shown in Fig. 2. Due to the steric repulsions in PIPBN operative for near-planar conforma-

Table 1
Decay components τ_i(ns), relative weighty A_i (%) and derived mean relaxation times for the decay of F_B fluorescence of PYRBN and PIPBN in different solvents at low temperature

Solvent	Temp.	Compound	$\tau_1(A_1)$	$\tau_2(A_2)$	$\tau_3(A_3)$	$\bar{\tau}$
EOE[a]	−105°C	PYRBN	2.19 (1.0)	–	–	2.19
		PIPBN	0.32 (0.996)	3.45 (0.004)[g]	–	0.32[g]
EOE/I[b]	−120°C	PYRBN	2.02 (0.92)	4.8 (0.08)	–	2.24
		PIPBN	0.34 (0.99)	2.61 (0 01)	–	0.36
BCl[c]	−120°C	PYRBN	2.96	–	–	2.96
		PIPBN	0.315 (0.99)	3.9 (0.01)	–	0.35
BCN/I[d]	−120 C	PYRBN	1.00 (0.51)	2.32 (0.49)	–	1.65
		PIPBN	0.19 (0.85)	0.67 (0.14)	3.1 (0.01)[g]	0.26[g]
n-propanol	−105°C	PYRBN	0.91 (0.43)	3.6 (0.57)	–	2.46
		PIPBN	0.18 (0.47)	1.27 (0.35)	2.86 (0.18)	1.05
BCl[c]	77 K	PYRBN[e]	5.5 (1.0)	–	–	5.5
		PIPBN[f]				3.4

[a] diethylether, [b] diethylether/isopentane (9.1), [c] n-butyl chloride, [d] n-butyronitrile/isobutyronitrile (9.1), [e] solvent independent, [f] slightly nonexponential with curvature depending somewhat on solvent, [g] equilibration. longest time constant equal to decay time of F_A.

Table 2
TICT formation rate constants k_{BA} for PIPBN and PYRBN, and their ratio r, For solvent abbreviations, see Table 1. Low-temperature viscosity values η are also given

Solvent	Temperature	η (cP)	k_{BA} (PIPBN)/10^7 s^{-1}	k_{BA} (PYPBN)/10^7 s^{-1}	r
EOE	−105°C	2.1	283	27	10.5
EOE/I	−120°C		248	26	9.5
BCl	−120°C		280	15	19
BCN/I	−120°C		355	43	8.3
n-propanol	−105°C	900	66	20	3.3

tions, which are larger than for PYRBN, an additional steric potential is introduced (for both S_0 and S_1), but the rest of the potential, for larger twist angles, is thought to be roughly unaffected. Consequently, PIPBN starts its reactive motion on the S_1 surface much closer to the "critical twist angle" ϕ_{cr} where the downward slope of the TICT potential starts than PYRBN.

The potential depicted in Fig. 2 with the unbroken line is multidimensional in nature, i.e. it involves not only the twist angle ϕ as reaction coordinate but also an additional reactive mode of symmetry species B (in the point group C_2) of yet unknown nature [38]. The presence of an additional mode follows from considerations of fluorescence polarization measurements [29] and state correlations [30]. At the intersection at ϕ_{cr} of the zero-order B* and A* states (indicated by the broken lines), a conical intersection develops [30,31], and the system does not have to go over the top of that barrier but can follow the unbroken potential with reduced (or altogether absent) activation barrier.

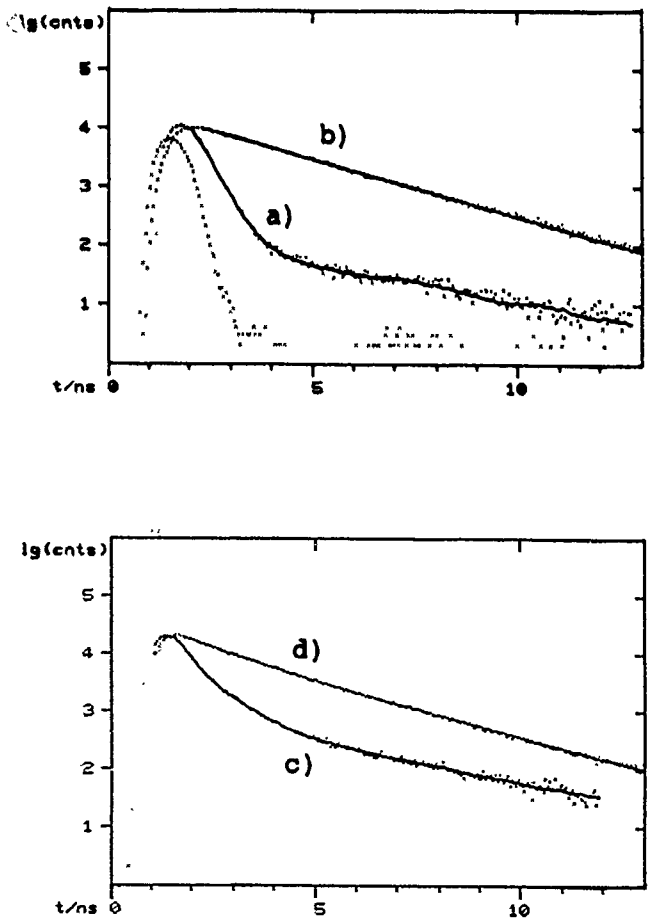


Fig. 1
Decay curves of the F_B fluorescence in diethylether at −105°C (a) PIPBN, b) PYRBN) and in n-butyronitrile/isobutyronitrile (9:1) at −120°C (c) PIPBN d) PYRBN). The figure also contains the fitted curves (unbroken line) and the experimental prompt response function. The longest decay components for a) and c) (with very small weight) are attributed to excited state equilibration

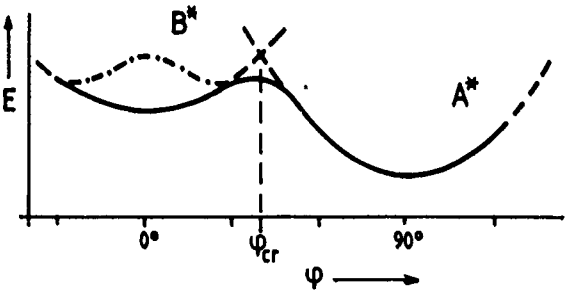


Fig. 2
Schematic S_1-potentials for PYRBN and PIPBN. PYRBN is assumed to possess a potential minimum at a twist angle $\phi = 0$ whereas steric repulsion (—·—·) leads to a twist angle of $\phi \simeq 30°$ for PIPBN. The zero order potential curves for B* and A* states (— — —) cross at the critical twist angle ϕ_{cr} where a conical intersection develops providing a potential (———) with strongly lowered or absent activation energy from B* to A*

As the TICT (A*) state is considerably more polar than the B* state [14,15], an increase of solvent polarity will preferentially lower the A* with respect to the B* state thus shifting ϕ_{cr} to lower twist angles (and lowering any activation barrier which might be present) as indicated in Fig. 3a). If the solvent polarity is high such that the initial twist angle of PIPBN (~30°) exceeds ϕ_{cr} then the reactive motion starts off with a nonzero gradient and corresponds to driven diffusion which is faster than diffusion over a barrier or along a flat potential (applicable to PYRBN for twist angles between 0° and ϕ_{cr}).

The diffusion along the flat portion of the potential ($0° < \phi < \phi_{cr}$) can be modelled by the "staircase model", leading to a stochastic differential equation the solution of which has recently been presented [32,33]. In this model (Fig. 3b), the reactive system can emit (F_B) fluorescence as

long as it diffuses along the flat portion of the potential. The diffusion starts at $x = x_0$; at $x = 0$, it is reflected; and at $x = a$ (corresponding to ϕ_{cr} in our case) the system reacts and thus instantaneously stops to emit.

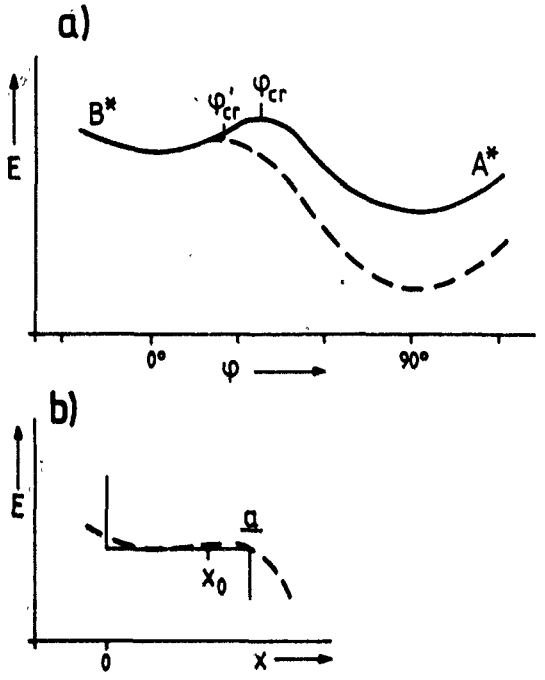


Fig. 3
a) Schematic S_1 potential for PYRBN (see Fig. 2) under the influence of varying solvent polarity. For weakly polar solvents (——), ϕ_{cr} is situated at larger twist angles than for strongly polar ones (—·—·—, ϕ'_{cr}). b) Staircase model (——) for calculating the survival probability on the flat part of a potential (— — —) similar to that of a). For the significance of a and x_0, see text

The time-dependent fluorescence intensity $I_f(t)$ is proportional to the survival probability $P(t)$ on the surface the average decay rate of which is given, under simplifying assumptions, by Eq. (4) [33],

$$k_{av} = \frac{2kT}{\xi} \frac{1}{(a - x_0)(a + x_0)} \tag{4}$$

where kT has the usual meaning, ξ is the solvent friction, a the location of the sink or step, and x_0 the initial condition (starting twist angle in our case).

Eq. (4) predicts that, as a (or ϕ_{cr}) decreases the survival time gets shorter, and thus the reaction rate increases (for all other conditions being equal). The isoviscous experiments by Hicks et al. [8,16] showing a positive solvatokinetic behaviour i.e. increased reaction rate with increased solvent polarity can thus be interpreted in two ways: i) variation of the barrier height [8,16] or ii) variation of the barrier position, or of ϕ_{cr} defining the edge of a flat portion of the surface. On the basis of recent discussions of kinetics on barrierless and low-barrier potentials and from the comparison of measured activation energies with those of the solvent viscous flow [12,17,18] the second possibility seems to be more likely although reality may also well correspond to a mixture of both cases.

The kinetic data presented here are not isoviscous. Due to the lack of low-temperature viscosity data of most of the solvents used only few values for η [34] could be included into Table 2.

These values make evident, that at temperatures around −105 °C, propanol possesses a considerably higher viscosity than the nonhydroxylic solvents used. For these low viscosity solvents, an overall acceleration in rate is observed especially for the strongly polar butyronitrile.

Comparison of the two dyes PYRBN and PIPBN, however, in a way eliminates the conditions of different viscosity, and the rate ratio r yields evidence for the change of the position of ϕ_{cr}.

By application of Eq. (4) to the present problem, Eq. (5) is derived, where the initial conditions x_0 have been set 0° and 30° for PYRBN and PIPBN, respectively, and where a has been identified with ϕ_{cr}.

$$r = \frac{k_{BA}(\text{PIPBN})}{k_{BA}(\text{PYRBN})} = \frac{\phi_{cr}^2}{(\phi_{cr} - 30)(\phi_{cr} + 30)} . \tag{5}$$

From Eq. (5), r is expected to increase and to approach infinity as ϕ_{cr} tends towards 30°. In reality, a maximum but finite value for r may be expected. Eq. (5) is not applicable to cases with $\phi_{cr} < 30°$ (more polar solvents), and an appropriate stochastic model would have to include both a flat and a curved potential region. It can, however, easily be seen that, as ϕ_{cr} decreases below 30°, the relaxation of PIPBN starts off with driven diffusion whereas for PYRBN a flat potential region remains which has to be crossed. We therefore expect r to decrease for ϕ_{cr} decreasing below 30° and to reach its lowest value for ϕ_{cr} approaching 0° (which is, of course, a somewhat unphysical case). Thus, the observed r-dependence on solvent polarity (Table 2) with its maximum reached for n-butyl chloride can be interpreted to signify $\phi_{cr} \simeq 30°$ in this solvent, with $\phi_{cr} > 30°$ in diethylether, and $\phi_{cr} < 30°$ in n-butyronitrile and propanol.

The very low value of r in propanol is probably related to an additional source, namely the competition between the reactive motion along ϕ (k_{BA}) and that of the more or less concerted solvent relaxation, k_{solv}. In alcohols, k_{solv} is especially slow such that k_{BA} and k_{solv} have the same time scale, and a two-dimensional diffusion model should be used in this case. This problem is dealt with in a separate paper [35] and can account both for the nonexponentialities observed (Table 1) and the observation of A*-rise times being shorter than B*-decay time [12,17,36]. Additionally, H-bond formation may play a role in alcohols [8,37].

Finally, it should be mentioned that nonexponentialities are inherent in the staircase model [32,33], and that the theoretical long-time decay constant given by Eq. (6) [33] does not depend any more on the initial condition x_0, (different to the average decay rate constant, Eq. (4))

$$k_{long} = \frac{1}{4} \frac{\pi^2 kT}{a^2 \xi} \tag{6}$$

but only on a, on temperature and on solvent friction ξ. The long decay components observed in Table 1, with their

weight increasing with solvent polarity, could well be due to this latter source.

This work has been supported by the Bundesministerium für Forschung und Technologie (project 05314 FAI5). W. R. wishes to thank the Deutsche Forschungsgemeinschaft for a Heisenberg Fellowship.

References

[1] E. Lippert, Z. Naturforsch. *A10*, 541 (1955).
[2] N. Mataga, Y. Kaifu and M. Koizumi, Bull. Chem. Soc. Jpn. *29*, 465 (1956).
[3] W. Liptay, Z. Naturforsch. *A20*, 272 (1965).
[4] D.-M. Shin and D. G. Whitten, J. Am. Chem. Soc. *110*, 5206 (1988).
[5] S. T. Abdel-Halim, M. H. Abdel-Kader, and U. E. Steiner, J. Phys. Chem *92*, 4324 (1988).
[6] V. Sundström and T. Gillbro, Chem. Phys. Lett *109*, 538 (1984).
[7] V. Sundström and T. Gillbro, Ber. Bunsenges. Phys. Chem. *89*, 222 (1985).
[8] J. M. Hicks, M. T. Vandersall, E. V. Sitzmann, and K. B. Eisenthal, Chem. Phys. Lett. *135*, 413 (1987).
[9] W. Rettig and W. Majenz, Chem. Phys. Lett. *154*, 335 (1989).
[10] V. Bonačić-Koutecký and J. Michl, J. Am. Chem. Soc. *107*, 1765 (1985).
[11] V. Bonačić-Koutecký, J. Koutecký, and J. Michl, Angew. Chem. Int. Ed. Engl. *26*, 170 (1987).
[12] E. Lippert, W. Rettig, V. Bonačić-Koutecký, F. Heisel, and J. A. Miehé, Adv. Chem. Phys. *68*, 1 (1987).
[13] W. Rettig, in "Modern Models of Bonding and Delocalization" (Molecular Structure and Energetics, Vol., chapter 5, p. 229), J. W. Liebman and A. Greenberg, ed., VCH Publishers, New York, 1988.
[14] Z. R. Grabowski, K. Rotkiewicz, A. Siemiarczuk, D. J. Cowley, and W. Baumann, Nouv. J. Chim. *3*, 443 (1979).
[15] W. Rettig, Angew. Chem. *98*, 969 (1986); Angew. Chem. Int. Ed. Engl. *25*, 971 (1986).
[16] J. Hicks, M. Vandersall, Z. Babarogic, and K. B. Eisenthal, Chem. Phys. Lett. *116*, 18 (1985).
[17] F. Heisel and J. A. Miehé, Chem. Phys. *98*, 233 (1985).
[18] F. Heisel, J. A. Miehé, and J. M. G. Martinho, Chem. Phys. *98*, 243 (1985).
[19] W. Rettig, J. Lumin. *26*, 21 (1981).
[20] W. Rettig and R. Gleiter, J. Phys. Chem. *89*, 4676 (1985).
[21] M. Vogel and W. Rettig, Ber. Bunsenges. Phys. Chem. *91*, 1241 (1987).
[22] W. Rettig, M. Vogel, and A. Klock, Eur. Photochem. Associat. Newslett. *27*, 41 (1986).
[23] D. V. O'Connor and D. Phillips, "Time-correlated Single Photon Counting", Academic Press, London, 1984.
[24] W. Rettig and E. Lippert, J. Mol. Struct. *61*, 17 (1980).
[25] W. Rettig, M. Vogel, E. Lippert, and H. Otto, Chem. Phys. *103*, 381 (1986).
[26] W. Rettig, in preparation.
[27] S. R. Meech and D. Phillips, Chem. Phys. Lett. *116*, 262 (1985).
[28] S. R. Meech and D. Phillips, J. Chem. Soc., Faraday Trans. 2, *83*, 1941 (1987).
[29] W. Rettig, G. Wermuth, and E. Lippert, Ber. Bunsenges. Phys. Chem. *83*, 692 (1979).
[30] W. Rettig and G. Wermuth, J. Photochem. *28*, 351 (1985).
[31] H. Köppel, W. Domke, and L. S. Cederbaum, Adv. Chem. Phys. *57*, 59 (1984).
[32] B. Bagchi, Chem. Phys. Lett. *135*, 558 (1987).
[33] B. Bagchi, and G. R. Fleming, J. Phys. Chem. *94*, 9 (1990).
[34] Landolt-Börnstein "Zahlenwerte und Funktionen aus Physik, Chemie, Astronomie, Geophysik und Technik", ed. K. H. Hellwege (Springer, Berlin) Vol. I, Part 2, p. 190 (1967) and Vol. II, Part 5, p. 215 (1969).
[35] W. Rettig, Z. R. Grabowski, and G. R. Fleming, to be published.
[36] F. Heisel and J. A. Miehé, Chem. Phys. Lett. *100*, 183 (1983) and Chem. Phys. *98*, 233 (1985).
[37] Y. Wang and K. B. Eisenthal, J. Chem. Phys. *77*, 6076 (1982).
[38] Note added in proof: A likely candidate for this additional mode is the umbrella motion at the amino nitrogen, see: S. Kato and Y. Amatatsu, J. Chem. Phys. *92*, 7241 (1990).

Presented at the Discussion Meeting of the Deutsche Bunsen-Gesellschaft für Physikalische Chemie "Rate Processes in Dissipative Systems: 50 Years after Kramers" in Tutzing, September 10–13, 1990 E 7487

Proton Delocalization and Thermally Activated Quantum Correlations in Water: Complex Scaling and New Experimental Results

C. A. Chatzidimitriou-Dreismann

Iwan-N.-Stranski-Institut für Physikalische und Theoretische Chemie, Technische Universität Berlin, Straße des 17 Juni 112, D-1000 Berlin 12, Federal Republic of Germany

E. J. Brändas

Quantum Chemistry Group for Research in Atomic, Molecular and Solid State Physics, Uppsala University, Box 518, S-751 20 Uppsala, Sweden

Electrochemistry / Isotope Effects / Quantum Mechanics / Spectroscopy, Nuclear Magnetic Resonance / Statistical Mechanics

Recently we applied, for the first time, the general theory of dilation analyticity (or: Complex Scaling Method, CSM) to quantum statistics of nonequilibrium. A novel kind of (universal) coherence was revealed from first quantum theoretical principles. The corresponding irreducible structures we called coherent-dissipative structures, since they represent a short-lived and spatially restricted cooperative phenomenon. The crucial points of the theory are stressed. Similarities as well as differences with (i) the BCS-states of

superconductivity, (ii) the dissipative structures of the Brussels school, and (iii) Yang's concept of ODLRO are mentioned. Very recently the general theory was applied to different dynamical processes in amorphous condensed matter, and specific and quantitative predictions were made. In connection with current work, we discuss here in some detail two new predicted effects concerning protonic delocalization in water (and other materials) and proper experiments to test them. These effects are: (1) a novel relation between proton transfer rates and proton mobility in water; (2) an anomalous decrease of proton mobility in H_2O/D_2O mixtures. Both effects are shown to contradict the predictions of all thus far existing theories or models. Current experimental results verify undoubtedly our theoretical predictions.

1. Introduction

Recently we studied the possibilities for an extension of the theory of dilation analytic operators of quantum mechanics [1,2] (also called Complex Scaling Method, CSM) into the Liouville (or: superoperator) level [4,3]. The starting point of this work was the conjecture that an intrinsic physical connection between the CSM and the conceptual basis of Prigogine's novel theory of microscopic irreversibility [5–11] may exist. Our corresponding theoretical investigations, which are based on

(i) the CSM of ordinary quantum mechanics and
(ii) Coleman's density matrix theory for fermionic systems [12,13],
led us to the first "extension" of the CSM into the canonical ensemble formalism of quantum statistics [4].

An unexpected theoretical result is that the fermionic second-order density matrix $\Gamma^{(2)}$, after proper CSM-transformation and "thermalization", may contain submatrices γ that have no diagonal representation.

The physical meaning of this surprising finding is that the quantities γ, which are associated with quantum correlations, represent a new kind of "undivisible units" (or: structures), due to the fact that the well-known probabilistic interpretation for the diagonal elements γ_{ii} ($i = 1, \ldots s$) of γ is now impossible.

These units we called coherent-dissipative structures, because they are short-lived, short-ranged, and exhibit a finite minimal dimension $s_{\min}$ in the space of state functions (i.e., the corresponding Hilbert space after the application of CSM); additionally, and most surprisingly, increasing temperature seems to support their extension. These structures represent a new cooperative (or synergetic) phenomenon that may be of significance for dynamical processes in condensed matter. As their existence follows "from first principles" of quantum theory, we also studied [4] their connection with (and difference to) (i) the "standard" coherent states of quantum theory (like the BCS states of superconductivity [14]), (ii) Prigogine's dissipative structures of phenomenological irreversible thermodynamics [15,16], and (iii) Yang's concept of off-diagonal long-range order (ODLRO) [17].

Very recently we succeeded with the application of the above general CSM-theory of quantum correlations to different and concrete dynamical processes in condensed amorphous matter [18–25]. The predictive power of our theory was recently demonstrated by its different experimental applications [18,19, 22–26], and its quantitative predictions [20] concerning certain new experiments [22,26], which have been motivated by the theory, cf. Sections 3 and 4.

Thus far the existing theoretical and experimental results strongly indicate that quantum correlations (as revealed by our general CSM-theory) play a fundamental role in the dynamics of condensed matter and – this being a crucial point – they can explicitly be associated with concrete experimental results.

In Section 2 a short outline of the general theory is given. Section 3 contains the application of the theory to the physical context of proton transfer reactions and proton mobility in water, a predicted novel relation between these quantities [20] and certain very recent experimental results [26]. Section 4 presents the predicted "anomalous" decrease of protonic conductance in H_2O/D_2O mixtures [20] and the experimental confirmation of this effect [22].

2. A Short Outline of the CSM-Theory of Coherent-Dissipative Structures

Trying to make the paper as self-contained as possible, a short outline of our general CSM-theory of thermally activated (or: supported) quantum correlations in condensed matter is given in this section. For the full proofs, see Ref. [4].

(A) We start with the presentation of the crucial formal-mathematical ingredients of the theory and its main result.

There is an algebraic corollary due to Reid and Brändas (for the proof, see [27]) which states the following:

The $s \times s$ Jordan block $C_s(0)$ represented by the matrix

$$C_s(0) = \begin{pmatrix} 0 & 1 & 0 & \ldots & 0 \\ \vdots & \ddots & \ddots & \ddots & \vdots \\ & & \ddots & \ddots & 0 \\ \vdots & & & \ddots & 1 \\ 0 & \ldots & & \ldots & 0 \end{pmatrix} \tag{1}$$

is similar to the $s \times s$ matrix q with matrix elements

$$q_{kl} = \left(\delta_{kl} - \frac{1}{s}\right) \cdot \exp\left(i\pi \frac{k+l-2}{s}\right), \tag{2}$$

where

$$1 \leq k,l \leq s\,. \tag{3}$$

From this corrolary it follows that there does not exist any similarity transformation (unitary or not) which can diagonalize q.

(B) The proper theoretical entity for the description of the quantum entanglement between physical states in the level

of "two-particle-" (better: two-states-) correlations is the second order reduced density operator (or: matrix) $\Gamma^{(2)}$. For fermionic systems, many fundamental results concerning $\Gamma^{(2)}$ have been achieved, a considerable part of them being proved by Coleman [12, 13].

Coleman considered the $\Gamma^{(2)}$ defined with respect to the AGP function $|g^{(N/2)}\rangle$, where $N/2$ is the number of "paired fermions". This function is constructed with the aid of the geminal

$$|g(1,2)\rangle = \sum_{k=1}^{s} g_k |k, k+s\rangle \tag{4}$$

of rank s, with $s > N/2$, where $|k\rangle$ and $k+s\rangle$ are "one-particle" functions, and the AGP ("antisymmetrized geminal power"), which is defined by

$$|g^{N/2}\rangle = A_N \{g(1,2)g(3,4) \ldots g(N-1, N)\}, \tag{5}$$

A_N being the conventional antisymmetrization operator. In the specially important case where the eigenvalues of the corresponding first order reduced matrix $\Gamma^{(1)}(g)$ are all equal, the AGP function is called extreme. In this case, all the wave amplitutes g_l in (4) are equal.

It was proved by Coleman that $\Gamma^{(2)}(g^{N/2})$ exhibits a simple "box and tail" matrix form, if it is represented in the basis

$$\{\{|i, i+s\rangle, 1 \le i \le s\}, \{|i,j\rangle, j \ne i+s, \ 1 \le i,j \le 2s\}\}. \tag{6}$$

In the following we consider extreme AGP's exclusively. In this case $|g\rangle$ is an eigenfunction of the matrix $\Gamma^{(2)}(g^{N/2})$ corresponding to the large eigenvalue $\lambda_L^{(2)}$ of the matrix $\Gamma^{(2)}(g^{N/2})$. The remaining eigenvalues are equal and consitute a $(2s+1)$ $(s-1)$ degenerate eigenvalue $\Gamma_S^{(2)}$, which is very small, if $2s/N \gg 1$. The matrix $\Gamma^{(2)}(g^{N/2})$ can therefore be decomposed as follows:

$$\begin{aligned} \Gamma^{(2)} &= \Gamma^{(2)}(g^{N/2}) \\ &= \Gamma^{(2)}_{\text{Box}} + \Gamma^{(2)}_{\text{Tail}} \\ &= (\Gamma^{(2)}_L + \Gamma^{(2)}_S) + \Gamma^{(2)}_{\text{Tail}}, \end{aligned} \tag{7}$$

where the "large box part" is given by

$$\Gamma^{(2)}_L = |g\rangle \lambda^{(2)}_L \langle g|, \tag{8}$$

with

$$|g\rangle = \frac{1}{\sqrt{s}} \sum_k |k, k+s\rangle,$$

the "small box part" is defined by

$$\Gamma^{(2)}_S = \lambda^{(2)}_S \sum_{k,l} |k, k+s\rangle \left(\delta_{k,l} - \frac{1}{s}\right) |l, l+s\rangle, \tag{9}$$

and the completely uncorrelated "tail part" is given by

$$\Gamma^{(2)}_{\text{Tail}} = \lambda^{(2)}_S \sum_{\substack{k<l \\ k+s \ne l}} |k,l\rangle\langle k,l|. \tag{10}$$

The "coherent" part $\Gamma^{(2)}_L$, which is representable by a wave function, is intrinsically connected with the BCS-function of superconductivity; see below. Our theoretical work showed however that – for the description of thermally activated quantum correlations – the relevant part of the density operator $\Gamma^{(2)}$ is the small box part $\Gamma^{(2)}_S$, Eq. (9), where the constant $\lambda^{(2)}_S$ depends on the (finite) number of particles N and the accompanying (finite number of) fermionic degrees of freedom s,

$$\lambda^{(2)}_S = \frac{N(N-2)}{4s(s-1)}, \tag{11}$$

where $s > N$. (Full details are given in [12, 13] and also in [4]).

(C) In order to apply the above density matrix formalism to a physical microdynamical process exhibiting irreversibility, the focus is on the resonance picture of unstable states [4]. Here enters the CSM into the formalism. The "part of the ensemble"-correlations represented by the quantum correlated density operator (9) is then subjected to the "thermalization transformation"

$$\gamma \equiv \frac{1}{Z} e^{-\frac{\beta}{2}H^c} \Gamma^{(2)}_S e^{-\frac{\beta}{2}H^c}, \tag{12}$$

with the standard abbreviation $\beta = 1/k_B T$. This transformation makes the connection with the canonical ensemble formalism of statistical mechanics. The notation $(\ldots)^c$ refers to complex scaled quantities. Here, e.g., H^c represents the appropriate complex scaled second order reduced Hamiltonian, and Z is the appropriate normalization factor.

Further straightforward derivations within our general CSM-theory showed that, in the important special case where all the paired states $|(k, k+s)^c\rangle$ have the same (real) energy, i.e.

$$E_k = E, \quad (k = 1, 2, \ldots s), \tag{13}$$

the considered density operator, Eq. (12), takes the form

$$\gamma \equiv \sum_{k,l} \gamma_{k,l} |(k, k+s)^c\rangle\langle(l, l+s)^{c*}| \tag{14}$$

with

$$\gamma_{kl} = \frac{1}{Z} e^{-\beta E} \lambda^{(2)}_S \left(\delta_{kl} - \frac{1}{s}\right) e^{i\frac{\beta}{2}(\varepsilon_k + \varepsilon_l)}. \tag{15}$$

Here, the familiar Boltzmann factor, $\exp(-\beta E)$, appears explicitly. Parenthetically, the general CSM formalism associates with the "widths" ε_k the "lifetimes" τ_k in the standard way, i.e.

$$\varepsilon_k = \frac{\hbar}{2\tau_k}. \tag{16}$$

The following crucial point should now be observed. The matrix elements γ_{kl}, Eq. (15), of the operator γ become pro-

portional to the matrix elements of the matrix q, Eq. (2), if the restrictive quantization conditions

$$\pi \frac{k}{s} = \frac{1}{2k_B T} \varepsilon_k, \quad (k = 1, 2, \ldots s), \tag{17}$$

are fulfilled. In this specific case the equality

$$\gamma_{kl} = \frac{1}{Z} e^{-\beta E} \lambda_S^{(2)} q_{kl} \equiv \text{const} \cdot q_{kl} \tag{18}$$

holds true.

In more physical terms, if the "widths" ε_k and the energies E_k of the complex scaled pairs $|(k, k+s)^c\rangle$ fulfill the conditions (13) and (17), then the matrix elements, Eq. (15), of the density operator γ constitute a Jordan block similar to $C_s(0)$, Eq. (1). This is a very important result, because it means that in this case the operator γ has no diagonal representation. Furthermore this implies that all the "paired" states constituting γ coalesce and act "cooperatively" as an undivisible unit. Thus the well-known probabilistic interpretation of the diagonal elements γ_{kk} is completely lost here.

It should be pointed out that this surprising finding is intrinsically connected with the application of the CSM into the formalism, since the proved Jordan block structure of γ is necessarily connected with the complex factors

$$e^{i\frac{\beta}{2}(\varepsilon_k + \varepsilon_l)}$$

appearing in (15). The density operator γ, Eq. (14), gives the mathematical representation of the coherent-dissipative structures, i.e., the synergetic phenomenon of interest.

(D) From the quantization conditions (17) and further physical reasoning, we finally derived the result that the minimal "dimension" $s_{\min}$ of γ is given by

$$s_{\min} = \frac{4\pi k_B T}{\hbar} \tau_{\text{rel}}. \tag{19}$$

τ_{rel} represents the relaxation time (or lifetime) characterizing the specific microdynamical process of a microsystem. Thus $s_{\min}$ determines the minimal "size" (in the space of CSM-transformed state functions) that the Jordan block at least must have, and at the same time it defines the new "unit", i.e. a coherent-dissapative structure. As $s_{\min}$ is direct proportional to T, one may conclude that the thermal motion supports the extension of these structures.

In this context it is also interesting to observed that the trace of γ representing coherent-dissipative structures vanishes identically, as e.g. one immediately sees from Eq. (1). Our current investigations indicate that this result may be of considerable importance in the physical context of laser light scattering on water, because it can be connected – under specific conditions – with an additional light scattering component from "strongly" H-bonded regimes; cf. [20, 21].

(E) The above structures we have called coherent-dissipative due to (i) the new kind of coherence associated with the appearance of Jordan blocks in the CSM-transformed density matrix γ, and (ii) the finite lifetime τ_{rel} of these structures.

The physical context of the above formalism as well as the physical meaning of different restrictive conditions appearing therein have been discussed in detail [4, 21]. Here let us mention three important points which are related to the fundamentals of our general CSM-theory of quantum correlations in condensed matter.

(i) It has been proved by Blatt [28] and repeatedly pointed out by Coleman [12, 13] that the BCS ground state ansatz is "equivalent" to an AGP ansatz, Eq. (5). More specifically, the superconducting state is here represented by the large box part $\Gamma_{\square}^{(2)}$, Eq. (8), which is representable by a wave function. Also it should be pointed out that the coherent-dissipative structures always have finite lifetime and extension (in Hilbert space). In contrast to this, a superconducting state has an infinite lifetime and may contain all particles of the system (at $T = 0$K).

(ii) The following similarity exists between the coherent-dissipative structures and the well known dissipative structures [15, 16] of Prigogine and coworkers: Both cannot have a "size" smaller than a critical one; and both cannot exist, if they are not in contact with the environment. On the other hand, it should be stressed that the dissipative structures are concepts of phenomenological thermodynamics, whereas the coherent-dissipative structures are concepts of microscopic theory. These remarks support the following speculation: The formalism of coherent-dissipative structures may represent the framework in which the phenomenological dissipative structures could be established "from first principles".

(iii) It has been pointed out [4] that the aforementioned extreme condition on the AGP is a necessary condition for the appearance of Yang's concept of off-diagonal long-range order (ODLRO) [17]. As shown above, the appearance of coherent-dissipative structures is intrinsically connected with the existence of off-diagonal terms in the thermalized and complex dilated $\Gamma_S^{(2)}$. Therefore, and in order to prevent possible confusion and misunderstanding, it should be stressed that coherent-dissipative structures are intimately (although not in the "BCS sense") connected with Yang's ODLRO, the connection being even strengthend by the fact that the corresponding density operator γ has no diagonal representation. In this context, one should also observe that no intuitively appealing explanation (i.e., an explanation in classical mechanical terms) of the emergence of coherent-dissipative structures is possible. Namely, as Yang points out: "Since off-diagonal elements [of the density matrix] have no classical analog, the off-diagonal long-range order ... is a quantum phenomenon not describable in classical mechanical terms" [17].

(F) The different applications [18–25] of the above general CSM-theory make use of the following ansatz [21] concerning the actual delocalization (in coordinate space) of coherent-dissipative structures:

$$\Xi_X = F_X(\hat{H}_{\text{eff}} \ldots) \cdot W_X^{\text{dB}} \cdot s_{\min,X}. \tag{20}$$

The symbols have the following meanings: Ξ may represent – depending on the specific application – (i) a transport coefficient, or (ii) the geometrical size of a coherent-dissipative structure; X the specific microscopic quantum system; $s_{\min,X}$ the "size" (in the space of state functions) of the structure as given by the main formula (19); W_X^{dB} the conventional thermal de Broglie wavelength of one quantum system X; and, finally, $F_X(\hat{H}_{eff}, \ldots)$ a functional of the "effective" or "relevant" Hamiltonian $\hat{H}_{eff}$ being proper to the dynamics of X in the condensed system. F may depend on some external parameters, too.

One should observe that the specific "mechanism", $\hat{H}_{eff}$, being responsible for the microdynamics of the system appears explicitly in this ansatz. However, its actual form is often not needed, as the different successful applications [18–25] demonstrate.

3. Coherent-Dissipative Structures and Proton Transfer in Water

One of the oldest and most fundamental problems in the physical chemistry of water is the evaluation of the rate constants characterizing the following processes [29]:

$$H_3O^+ + H_2O \overset{k_1, E_1}{\rightleftharpoons} H_2O + H_3O^+ \qquad (21a)$$

$$OH^- + H_2O \overset{k_2, E_2}{\rightleftharpoons} H_2O + OH^- . \qquad (21b)$$

These processes play an important role in many biological processes, too. With the pioneering work of Meiboom [30] it has been proved that one can measure these reaction rates, k_i, and activation energies, E_i, (with i = 1,2) by NMR spectroscopic methods; see below. The study of proton transfer reactions in water is also of importance to the understanding of the excess (or: anomalous) conductivities (or: mobilities) of the hydronium (H_3O^+) and hydroxyl ions in water and aqueous solutions. Furthermore, in aqueous solutions of acids and bases, fast proton transfer in the water is often considered to be involved as part of the actual reaction scheme; see the classic work of Eigen [31].

Recently Hertz [32] presented a detailed analysis of a series of different experimental methods (NMR, X-ray and neutron scattering, etc.) used to detect the H^+ (or the H_3O^+) ion in aqueous solutions directly. This analysis, together with an extensive discussion of some corresponding experimental results, revealed that, thus far, none of the considered experimental investigations was able to detect directly the so-called H^+ particle (or the H_3O^+) in aqueous solutions [32].

In all the traditional (and well-established) theories of the ionic solutions, however, the entity H^+ is postulated to exist – at least for sufficient short times – and to correspond to some fast "moving" (or "jumping", or "tunnelling") particle (a proton). In this context let us just mention the well-known Grotthus mechanism, a traditional model that is believed to explain classically the high excess conductivity of H^+ (and OH^-) in aqueous solutions; see Ref. [33] for a detailed discussion. Nevertheless, the aforementioned exhaustive analysis [32] led to the surprising conclusion that the physical object usually defined to be the H^+ (or H_3O^+) cannot be considered – thus far – to represent a particle in the conventional sense. This finding led Hertz to the conclusion: "... what we call H^+ ion in aqueous solutions is really a dynamical property of the solution" [32]. At this stage, it is important to point out that the analysis of reference [32] is carried out entirely within classical mechanics. In this framework, of course, there are no delocalization effects like those being typical for quantum mechanical processes, and therefore the aforementioned conclusion is clearly remarkable.

Motivated by the above remarks, it appeared worthwhile to investigate some of the main aspects of the microdynamical behaviour of the system "H^+/water", in the light of our general CSM-theory of quantum correlations [18]. An important point of these investigations may be illustrated by the following. From the quantum mechanical viewpoint it appears that the H-constituents forming the H^+ ions are indistinguishable from those belonging to the water molecules and being in the vicinity of the ions. This "unconventional" consideration may be motivated by the fact that the thermal de Broglie wavelength of a "quasi-free" proton, $W_{H^+}^{dB}$, is about 1 Å at room temperature (cf. [21,29]). This is large enough to find (in most cases) water protons in a distance of the order of $W_{H^+}^{dB}$ around each H^+. This fact may – even in the present case – lead to the typical delocalization and/or interference effects being characteristic for the quantum theory. The assumption of quantum effects between protons "belonging" to ions and water molecules, of course, represents a hypothesis. Nevertheless it appears that two important predictions, which follow straightforwardly from this assumption, are in contradiction to all known conventional theories (or models); see the present and the next section. Fortunately, these predictions are capable of experimental testing, so that the question concerning the validity and/or physical significance of the assumed protonic delocalization can be decided and/or clarified.

The first of these two predictions is given by a novel form [18,20,21] of the connection of

(i) the proton transfer rates, k_i, of Eqs. (21a, b)

with

(ii) the excess ionic conductivities of H^+ and OH^-, $\lambda^e_{H^+}$ and $\lambda^e_{OH^-}$, in water.

The latter quantities are conventionally defined as

$$\lambda^e_{H^+} = \lambda_{H^+} - \lambda_{X^+} , \qquad (22)$$

with $X^+ = K^+$ or Na^+, and

$$\lambda^e_{OH^-} = \lambda_{OH^-} - \lambda_{Cl^-} , \qquad (23)$$

where λ_X represents the experimentally measured ionic conductance of the ion X in water [34].

The conventional treatment of the connection under consideration (see e.g. Refs. [30,35] for a derivation) is based on the well established equations of Nernst

$$\lambda^e = \frac{qD}{k_B T} \tag{24}$$

and Einstein

$$D = \frac{\langle x^2 \rangle}{6\tau_{rel}}. \tag{25}$$

The notations are as follows: q is the elementary charge, D the diffusion coefficient describing charge transport due to proton transfers, τ_{rel} the average lifetime of a H_3O^+ (or OH^-) ion, and $\langle x^2 \rangle$ the average of the square of the charge displacement accompanying a proton transfer. In a simple model, one may identify $\langle x \rangle$ with the mean distance between two oxygen atoms of water molecules [30].

From these equations and the standard relation [30] for the "relaxation times" associated with the reaction (21 a),

$$\frac{1}{\tau_{rel,H^+}} = k_1 \cdot [H_2O], \tag{26}$$

one obtains

$$\lambda^e_{H^+} T = C \cdot k_1, \tag{27}$$

where C is a temperature independent constant. A corresponding equation holds true with respect to OH^-, and finally one obtains

$$\frac{\lambda^e_{H^+}}{\lambda^e_{OH^-}} = \frac{k_1}{k_2}, \tag{28}$$

which represents the desired connection. A useful reformulation of this result is given by using the standard Arrhenius-type ansatz for the rate constants of Eqs. (21 a, b),

$$k_i = C_i \cdot e^{-E_i/RT} \quad (i = 1,2), \tag{29}$$

in which case it follows immediately

$$\log\left(\frac{\lambda^e_{H^+}}{\lambda^e_{OH^-}}\right) = C - \frac{E_1 - E_2}{RT}. \tag{30}$$

It will be show that the result (28), or equivalently (30), is definitely in disagreement with the corresponding prediction of our CSM-theory of quantum correlations.

The aforementioned precise data of Ref. [34] for the ionic conductances in water yield the classically predicted value

$$\frac{k_1}{k_2} \approx 2.35 \quad \text{at } T = 25°C, \tag{31}$$

which follows from Eq. (28), and

$$E_1 - E_2 \approx -2.0 \text{ kJ/mol} \quad \text{for } T = 15° \ldots 55°C, \tag{32}$$

which follows from Eq. (30), for the considered difference of the activation energies; cf. [35].

We proceed now to the presentation of the predictions of the CSM-theory [18, 20]. Starting with the application of the general ansatz (20) to the transport coefficients $\lambda^e_{H^+}$ and $\lambda^e_{OH^-}$, i,e.

$$\lambda_X = F_X(\hat{H}_{eff}, T) \cdot W_X^{dB} \cdot s_{min,X} \quad (X = H^+, OH^-), \tag{33}$$

and formula (19), one immediately obtains

$$\frac{\lambda^e_{H^+}}{\lambda^e_{OH^-}} = \frac{F_{H^+}}{F_{OH^-}} \cdot \frac{W^{dB}_{H^+}}{W^{dB}_{OH^-}} \cdot \frac{\tau_{rel,H^+}}{\tau_{rel,OH^-}}. \tag{34}$$

Further insertion of the explicit form of the thermal de Broglie wavelength

$$W_X^{dB} = \hbar \sqrt{\frac{2\pi}{m_X k_B T}} \tag{35}$$

and the standard relation (26) in Eq. (34) yields the result

$$\frac{\lambda^e_{H^+}}{\lambda^e_{OH^-}} = \frac{F_{H^+}}{F_{OH^-}} \cdot \sqrt{\frac{m_{OH^-}}{m_{H^+}}} \cdot \frac{k_2}{k_1}. \tag{36}$$

This formula is the main result of the CSM-Theory. To make it capable of experimental testing, we considered [18, 20] the following slight simplification: In the present context we may assume on physical grounds that

$$F_{H^+} = F_{OH^-}, \tag{37}$$

because, in both cases (21 a, b), the larger part of the system with Hamiltonian $\hat{H}_{eff}$ consists of water molecules, i.e. of the same compound. It should be pointed out that Eq. (37) represents a physical assumption, which is based on reasonable considerations concerning the extension and the dynamics of quantum correlations around each "relaxing center" (classically described by Eqs. (21 a, b)), and thus it is probably of approximative character. Nevertheless its validity and/or physical significance is supported by the experiment; see Eq. (37a) below.

Thus, with the assumption (37) we obtain

$$\frac{\lambda^e_{H^+}}{\lambda^e_{OH^-}} = \sqrt{\frac{m_{OH^-}}{m_{H^+}}} \cdot \frac{k_2}{k_1}. \tag{38}$$

As in the above classical treatment, one can make use of the Arrhenius form of the reaction rates k_i, Eq. (29), converting Eq. (38) to the form

$$\log\left(\frac{\lambda^e_{H^+}}{\lambda^e_{OH^-}}\right) = C' + \frac{E_1 - E_2}{RT}. \tag{39}$$

With the aid of the aforementioned precise data of Ref. [34] for the ionic conductivities, we predicted [20] the values

$$\frac{k_1}{k_2} \approx 1.75 \quad \text{at } T = 25°C \tag{40}$$

and

$$E_1 - E_2 = \begin{cases} +2.1 \text{ kJ/mol for } X^+ = K^+ \\ +1.9 \text{ kJ/mol for } X^+ = Na^+ \end{cases} \tag{41}$$

in the aforementioned temperature range $T = 15° \ldots 55°C$.

It is important to observe that the result of the CSM-theory, Eqs. (38,39), is fundamentally different from the result of the conventional theory, Eqs. (28,30). E.g., $\lambda^c_{H^+}$ is proportional to k_1 in the "classical" case, cf. Eq. (28), whereas quite the opposite is predicted in the "quantal" case, cf. Eq. (38). As a consequence, the classically predicted numerical value of $E_1 - E_2$, Eq. (32), differs even by sign (!) from the CSM-predicted value of this quantity, Eq. (41).

Thus far the existing experimental data for the difference $E_1 - E_2$ exhibit a considerable scattering: -8.8 kJ/mol in Ref. [36]; -0.4 kJ/mol in Ref. [37]; $+1.25$ kJ/mol in Ref. [35].

To test the above theoretical predictions, new high precision experiments (utilizing the ^{1}H-NMR spin-echo technique) for the correct measurement of the difference $E_1 - E_2$ have been carried out in the laboratory of H. G. Hertz (Karlsruhe). The NMR-experimental data [26] are graphically presented in Fig. 1, together with the classical and CSM-theoretical predictions based on the same high precision conductivity data [34]. In our treatment of these data, we prefer to omit the experimental values of k_1 and k_2 at $T = 5.3°C$, since – to our knowledge – no experimental value of λ_{OH^-} around 5°C exists in the literature, and due to the well-known "anomaly" that water exhibits at 4°C. For the temperature range $T = 10.7° \ldots 58.8°C$ we obtain the experimental value

$$E_1 - E_2 = + (1.9 \pm 0.5) \text{ kJ/mol} \tag{42}$$

Including the data point at $T = 5.3°C$ one obtains $E_1 - E_2 \approx +1.3$ kJ/mol [26]. In any case, however, the above experimental result confirm the positive sign of $E_1 - E_2$ definitely, thus being in clear disagreement with the prediction of the classical theory.

In this context, it is interesting to point out that the well-known "traditional" treatment of the reactions (21a, b) by Gierer and Wirtz [38] predicts – in accordance with the aforementioned classical treatment – a negative sign for $E_1 - E_2$; cf. also [29].

The above results allow us also to test the relation (37), which was justified by physical considerations and was assumed to be approximately valid. From the data of Fig. 1 one obtains the relation.

$$F_{H^+} \approx 1.16 \cdot F_{OH^-} . \tag{37a}$$

The physical interpretation of this interesting finding is subject to current investigations, in connection with our very recent work [23–25] (which concerns the determination of the "effective mass" of a coherent-dissipative structure).

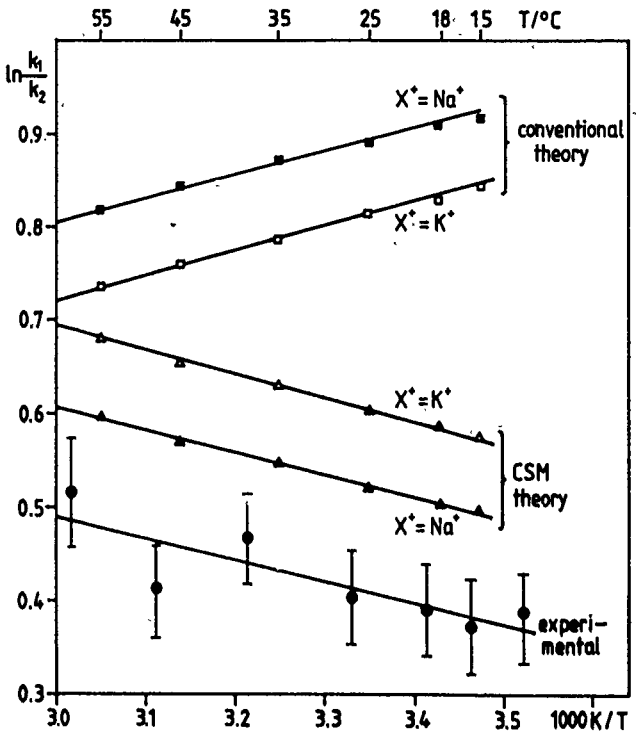


Fig. 1
Graphical representation of the quantity log k_1/k_2 as a function of the inverse temperature. Shown are (i) the predictions of conventional theory and CSM-theory, and (ii) the experimentally (NMR) determined values of Ref. [26] for the temperature range $T = 10.7° \ldots 58.8°C$. The data points for the two theoretical predictions were calculated with the aid of the high-precision conductivity data of Ref. [34] and Eqs. (28) and (38). The reference cation (K^+ and Na^+) used by the calculation of the H^+-excess conductivity, Eq. (22), is shown on the graphs

As mentioned in Sec. 2, the general theory of coherent-dissipative structures applies directly to fermionic systems. Current investigations being in progress now, however, seem to indicate that the theory could be extended, under specific conditions, to the case of bosonic systes, too. Thus it would be very interesting to have knowledge of the experimental values of the two corresponding activation energies (in analogy to Eqs. (21a, b)) characterizing D^+ transfer in D_2O. This knowledge would also greatly support the further development of the present theory.

4. Further Evidence for Proton Delocalization: Anomalous Decrease of H^+ Mobility in H_2O/D_2O Mixtures

The above experimental findings clearly support the aforementioned assumption of "proton delocalization" in water. Further investigations based on this physical idea permitted one of us to derive a new prediction [20] and to conceive a corresponding experiment for its testing. That work predicted an "anomalous" decrease of the H^+ (and probably also D^+) conductance, in H_2O/D_2O mixtures.

The physical considerations leading to this prediction are as follows. As already mentioned above, quantum correlations between "protons" in aqueous H^+ solutions may be expected even within conventional quantum theory, viz. due

to the large thermal de Broglie wavelength of a quasi-free H^+ that is about 1 Å at room temperature. In more modern physical terms, one can then say that the underlying physical idea is that H^+ is delocalized and correlated through Einstein-Podolsky-Rosen (EPR) correlations [39–41] with water protons of its surroundings "belonging" to H_2O or HDO molecules. This physical picture is obviously in clear contrast to the viewpoint taken by quantum chemistry and molecular dynamics, where protons are considered as classical particles being subject to the Born-Oppenheimer approximation.

The following point is now crucial. If the well-known high H^+ conductance, λ_{H^+}, in liquid water is caused by the assumed quantum interference effects, then there must be an anomalous decrease of λ_{H^+} in H_2O/D_2O mixtures due to the so-called mass and spin superselection rules (cf. [40]). In these mixtures, viz., the possible quantum interference between appropriate protonic states becomes disrupted by deuterons ("belonging" to D_2O, HDO, or D^+ ions and) being "near" or "between" the considered protons. For exactly the same reasons we also might expect an anomalous decrease of the D^+ conductance in H_2O/D_2O; cf., however, the corresponding remarks at the end of the previous section.

(A crude estimate of the decrease of λ_{H^+} in a equimolar H_2O/D_2O mixture may be based on the model that coherent-dissipative structures, in water, extend over the partial volumina being "occupied" by protons or deuterons (and not by oxygen atoms). A rough calculation in these lines shows that the considered decrease would then be of the order of 10%; cf. [20, 21].

In order to test this prediction experimentally, molar conductances, Λ, of different HCl/DCl and KCl solutions in H_2O/D_2O mixtures were measured [22]. The experimental results are summarized in Figs. 2 and 3.

Firstly, let us consider the conductivity of KCl solutions. The conductances of KCl solutions in H_2O/D_2O mixtures are found to depend almost linearly on the D-atom fraction, X_D, of the solvent, cf. Fig. 2. This "linearity" appears to be independent of the concentration of the measured solutions ($C = 0.01 \ldots 0.1$ mol/l); see [22] for details. This result is as expected from standard (or: classical) electrochemical theory, cf. e.g. [34], because

(i) it is experimentally well established [42] that the fluidity (i.e., the inverse of viscosity) of the considered mixtures depends almost linearly on X_D and

(ii) ionic conductances are, to a very good approximation, direct proportional to the fluidity of the solvent (Walden's rule).

Secondly, let us consider the conductivity data for HCl/DCl in the considered H_2O/D_2O-mixtures. Figure 2 shows the resulting conductances at infinite dilution, Λ^0, plotted against the mole fraction X_D. It is seen that at intermediate solvent compositions the curve lies distinctly below the straight line connecting the limiting values in pure H_2O, where $X_D = 0$, and D_2O, where $X_D = 1$.

To be able to formulate the experimental results in more quantitative terms, we define the deviation of the measured

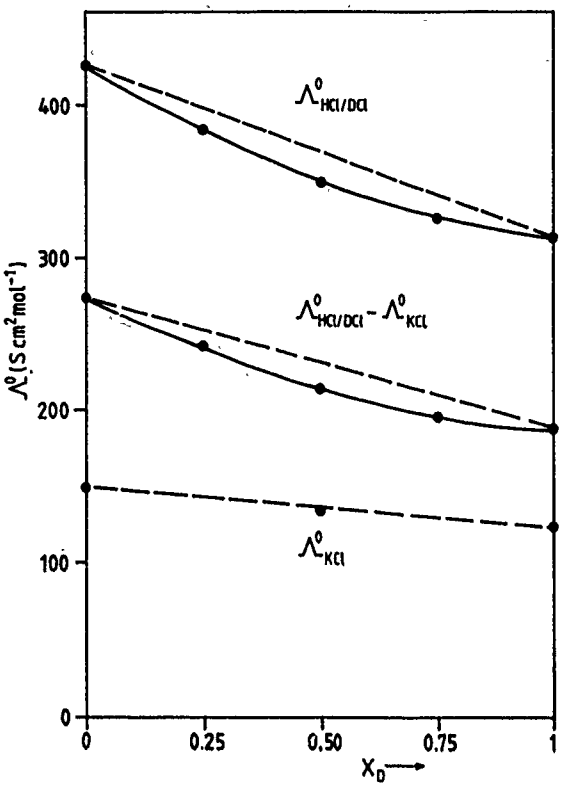


Fig. 2
Molar conductances of HCl/DCl, $\Lambda^0_{HCl/DCl}$, and of KCl, Λ^0_{KCl}, in H_2O/D_2O mixtures at infinite dilution and $T = 25°C$ as a function of the mole fraction X_D of deuterium. Also shown is the "excess conductance", determined from the difference between the data for HCl/DCl and KCl. Solid and brocken lines are guides to the eye. Error bars are smaller than the size of each data point. (Reproduced from Nature, Ref. [22])

conductance of a mixture, of concentration C, $\Lambda(X_D, C)$, from that determined by linear interpolation between the values of the two pure solutions ($X_D = 0$ and 1), $\Lambda_{lin}(X_D, C)$, as

$$\Delta\Lambda(X_D, C) = \Lambda(X_D, C) - \Lambda_{lin}(X_D, C)$$
$$= \Lambda(X_D, C) - [(1 - X_D) \cdot \Lambda(0, C) + X_D \cdot \Lambda(1, C)] \quad (43)$$

and the corresponding relative deviation in per cent by

$$\Delta^{rel}(X_D, C) \equiv 100 \cdot \Delta\Lambda(x_D, C)/\Lambda_{lin}(X_D, C). \quad (44)$$

The relative deviation at the equimolar solvent composition is $\Delta^{rel}(0.5, C \to 0) \approx -5.1\%$.

Furthermore, and as already stated in the previous section, the quantum effects of interest are expected to be reflected by the excess conductance, which is defined by the difference of the data obtained for HCl/DCl and KCl. (This definition is based on the fact that the main thermodynamic data of these two solutions are very similar [34]). The corresponding "anomalous decrease" of the excess conductance at $X_D = 0.5$ is now -7.7%, cf. Fig. 2.

For illustration, the following point may also be observed. The aforementioned "disrupted quantum interference" is

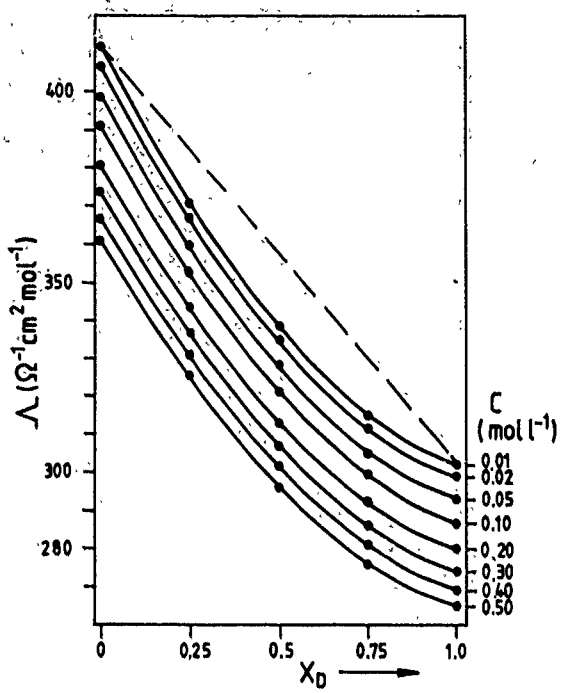


Fig. 3
Graphical representation of the experimentally determined molar conductances of HCl/DCl in H_2O/D_2O mixtures at 25°C as a function of solvent composition (expressed by the atom fraction X_D of deuterium) and of acid concentration C. (Data were taken from Ref. [22])

easily seen to become most effective at $X_D = 0.5$, thus leading to a maximum of the predicted anomalous decrease of the H^+/D^+ conductance at $X_D = 0.5$. The experimental data confirm this expectation, too.

The analysis of the experimental results shows also that the magnitude of the anomalous decrease under consideration is independent of the acid concentration ($C = 0.01 \ldots 0.5$ mol/l), cf. Fig. 3. The small experimental error of $\pm 0.1\%$ strongly supports the significance of these results. For full details, see [22].

In conclusion, we found that the conductances of KCl solutions in H_2O/D_2O mixtures are completely in accord with standard electrochemical theory. But, at the same time, it is the almost linear dependence of Λ^0_{KCl} on the mole fraction X_D in connection with linear dependence of the fluidity of H_2O/D_2O on X_D that proves that the observed "anomalous" decrease $\Delta\Lambda^0$ of the (excess) molar conductance of HCl/DCl is – plainly speaking – a specific property of the H^+ and D^+ ions and the H_2O/D_2O solvent.

Therefore it is hardly conceivable how the considered effect could be interpreted in terms of standard (or conventional) electrochemistry. At the same time, the presented experimental results are in line with the underlying physical picture of H^+ delocalization in water and clearly confirm the prediction [20] of the "anomalous" decrease of the H^+/D^+ conductance in H_2O/D_2O mixtures.

5. Concluding Remarks

As the short outline of Sec. 2 shows, our CSM-theory of (thermally activated) quantum correlations in condensed matter [4] is based on the first principles of quantum theory. Thus the cooperative phenomenon being described by coherent-dissipative structures appears to represent a new form of "selforganization" of matter in the microscopic level of physical description.

Recent applications of the general theory to thus far five different physical contexts (i.e., the two applications considered above [18, 20, 22], ionic conductivity of molten alkali chlorides [19], spin waves in magnetic systems above T_c [23, 24], and quantum correlation effects in high-T_c superconductors [25]) demonstrated the predictive power of the theory and the – more or less – universal character of quantum correlations in condensed matter. In this paper, we discussed two surprising predictions of the CSM-theory concerning proton mobility and proton transfer reactions in water, and also the results of two very recent experiments which clearly verified these predictions [22, 26].

The above theoretical investigations and experimental findings indicate that coherent-dissipative structures may play an important role in the dynamics of H^+-transport and H-bond formation (cf. [43, 44]) in further physical, chemical and biological systems. Further work is in progress.

We thank H. G. Hertz and H. Weingärtner (Karlsruhe) for fruitful cooperation and many insightful discussions. H. G. Hertz and R. Pfeifer are thanked for communicating to us their experimental NMR-data prior to publication. This work was supported by the Commission of the European Communities (SCIENCE-plan), the Deutsche Forschungsgemeinschaft, and the Fonds der Chemischen Industrie.

References

[1] (a) E. Balslev and J. M. Combes, Commun. Math. Phys. *22*, 280 (1971); (b) J. Aguilar and J. M. Combes, Commun. Math. Phys. *22*, 269 (1971).
[2] (a) B. Simon, Commun. Math. Phys. *27*, 1 (1972); (b) B. Simon, Ann. Math. *97*, 247 (1973).
[3] C. A. Chatzidimitriou-Dreismann and E. J. Brändas, Ber. Bunsenges. Phys. Chem. *92*, 549 (1988).
[4] E. J. Brändas and C. A. Chatzidimitriou-Dreismann, in: Resonances, Lecture Notes in Physics, Vol. *325*, pp. 485–540, Springer, Berlin 1989.
[5] I. Prigogine, From Being To Becoming, Freeman, San Francisco 1980.
[6] I. Prigogine, C. George, F. Henin, and L. Rosenfeld, Chem. Scr. *4*, 5 (1973).
[7] I. Prigogine, Nature *246*, 67 (1973).
[8] C. George, F. Henin, F. Mayné, and I. Prigogine, Hadronic J. *1*, 520 (1978).
[9] C. George, F. Mayné, and I. Prigogine, Adv. Chem. Phys. *61*, 223 (1985).
[10] Ch. Obcemea and E. Brändas, Ann. Phys. *151*, 383 (1983).
[11] C. A. Chatzidimitriou-Dreismann, Int. J. Quantum Chem. Symp. *19*, 369 (1986).
[12] A. J. Coleman, Rev. Mod. Phys. *35*, 668 (1963).
[13] A. J. Coleman, J. Math. Phys. *6*, 1425 (1965).
[14] J. Bardeen, L. N. Cooper, and J. R. Schrieffer, Phys. Rev. *108*, 1175 (1957).
[15] P. Glansdorff and I. Prigogine, Thermodynamic Theory of Structure, Stability, and Fluctuations, Wiley, New York 1971.
[16] G. Nicolis and I. Prigogine, Self-Organization in Nonequilibrium Systems, Wiley, New York 1977.
[17] C. N. Yang, Rev. Mod. Phys. *34*, 694 (1962).
[18] C. A. Chatzidimitriou-Dreismann and E. J. Brändas, Int. J. Quantum Chem. *37*, 155 (1990).

[19] C. A. Chatzidimitriou-Dreismann and E. J. Brändas, Ber. Bunsenges. Phys. Chem. *93*, 1065 (1989).
[20] C. A. Chatzidimitriou-Dreismann, Int. J. Quantum Chem. Symp. *23*, 153 (1989).
[21] C. A. Chatzidimitriou-Dreismann, Ber. Bunsenges. Phys. Chem. *94*, 234 (1990); Adv. Chem. Phys., Vol. *80* (eds.: S. A. Rice and I. Prigogine), 1991, in the press.
[22] H. Weingärtner and C. A. Chatzidimitriou-Dreismann, Nature *346*, 548 (1990).
[23] C. A. Chatzidimitriou-Dreismann, E. J. Brändas, and E. Karlsson, Phys. Rev. B: Rapid Commun. *42*, 2704 (1990).
[24] E. Karlsson, C. A. Chatzidimitriou-Dreismann, and E. J. Brändas, Hyperfine Interactions (1991), in the press.
[25] E. Karlsson, E. J. Brändas, and C. A. Chatzidimitriou-Dreismann, Phys. Scri. (1991), in the press.
[26] R, Pfeifer and H. G. Hertz, Ber. Bunsenges. Phys. Chem. *94*, 1349 (1990).
[27] C. E. Reid and E. J. Brändas, in: Resonances – The Unifying Route towards the Formulation of Dynamical Processes, (eds.: E. J. Brändas and N. Elander) Lecture Notes in Physics, Vol. *352*, pp. 475–483, Springer, Berlin 1989.
[28] J. M. Blatt, Prog. Theor. Phys. (Kyoto) *23*, 447 (1960).
[29] M. Eigen and L. de Maeyer, Proc. R. Soc. (London) *A247*, 505 (1958).
[30] S. Meiboom, J. Chem. Phys. *34*, 375 (1961).
[31] M. Eigen, Angew. Chem. *75*, 489 (1963); Angew. Chem. Int. Ed. Engl. *3*, 1 (1964).
[32] H. G. Hertz, Chem. Scr. *27*, 479 (1987).
[33] H. G. Hertz, B. M. Braun, K. J. Müller, and R Maurer, J. Chem. Educ. *64*, 777 (1987); and references cited therein.
[34] R. A. Robinson and R. H. Stokes, Electrolyte Solutions, Butterworths, London 1970.
[35] Z. Luz and S. Meiboom, J. Am. Chem. Soc. *86*, 4768 (1964).
[36] A. Loewenstein and A. Szöke, J. Am. Chem. Soc. *84*, 1151 (1962).
[37] R. E. Glick and K. C. Tewari, J. Chem. Phys. *44*, 546 (1966).
[38] A. Gierer and K. Wirtz, Ann. Phys. Lpz. (6) *6*, 257 (1949).
[39] A. Einstein, B. Podolsky, and N. Rosen, Phys. Rev. *47*, 777 (1935).
[40] H. Primas, Chemistry, Quantum Mechanics, and Reductionism, Springer, Berlin 1983.
[41] B. d'Espagnat, Conceptual Foundations of Quantum Mechanics (2nd ed.), Benjamin, London 1976.
[42] G. Jones and H. Fornwald, J. Chem. Phys. *4*, 30 (1936).
[43] G. Zunder and M. Eckert, J. Mol. Struct. (Theochem) *200*, 73 (1989).
[44] M. Eigen, Naturwissenschaften *58*, 465 (1971).

Presented at the Discussion Meeting of the Deutsche Bunsen-Gesellschaft für Physikalische Chemie "Rate Processes in Dissipative Systems: 50 Years after Kramers" in Tutzing, September 10–13, 1990 E 7488

Rate Processes in Proteins

Hans Frauenfelder, G. Ulrich Nienhaus, and J. Bruce Johnson

Department of Physics, University of Illinois at Urbana-Champaign, 1110 West Green Street, Urbana, Il 61801 USA

Chemical Kinetics / Conformational Substrates / Flash Photolysis / Nonequilibrium Phenomena / Protein Dynamics

Flash photolysis experiments on carbonmonoxymyoglobin over wide ranges in time and temperature provide information about the rate processes involved in the rebinding reaction. The non-exponential rebinding at low temperatures shows that the myoglobin molecules are frozen into a large number of conformational substates with different enthalpic barriers. Above 160 K we observe a relaxation process that shifts the peak of the barrier distribution from ~ 10 kJ/mol to ~ 21 kJ/mol. This process is non-exponential in time and does not obey the Arrhenius law. Above 220 K equilibrium fluctuations between the conformational substates lead to an averaging of the binding rate distribution and to the opening of pathways for the ligands to escape from the protein molecules.

1. Proteins as Laboratories for Rate Processes

Proteins form excellent laboratories for the study of rate processes. Nearly every aspect of rate theories is important for the elucidation and explanation of the function of proteins. In turn such investigations may shed light on rate theories. A partial list of keywords includes: Kramers theory [1, 2, 3], Landau-Zener-Stückelberg theory [4, 5, 6], tunnel effect [7, 8, 9], stochastic approach [10, 11], non-exponential processes and distributed barriers [12], gating [2, 13], and pressure effects [14]. In the present contribution we select some other aspect, namely the relaxation and fluctuation processes in proteins. These processes are crucial for the function of proteins, but they are also of considerable interest to the study of rate theories. The relaxation processes in proteins display characteristic similarities to those in glasses [15]. Since the corresponding theory is still in a state of flux, detailed studies of the dynamics of protein reactions may add to an understanding of rate processes in all complex systems.

Our approach to studying rate processes in proteins is straightforward: We select a "simple" protein, explore a "simple" reaction experimentally in great detail, and construct the simplest model that fits the data. The binding of a small ligand like CO or O_2 to the dioxygen-storage protein myoglobin (Mb) satisfies our selection criteria. The first step in the exploration of the dynamics of such an apparently simple process is the construction of the reaction energy landscape, the second the examination of the conforma

tional energy landscape. Finally, the two landscapes are joined to describe the reaction in terms of the dynamic features of the protein.

2. The Reaction Energy Landscape

Myoglobin is a small globular protein with a size of $45 \times 35 \times 25$ A^3 and a molecular weight of 17,800 daltons. It consists of a polypeptide chain of 153 amino acids enclosing the disk-shaped heme group. The CO molecule binds to the central heme iron in the reaction

$$\mathrm{Mb} + \mathrm{CO} \rightleftharpoons \mathrm{MbCO}\,. \tag{1}$$

While this reaction was first described as a simple one-step process [16], a long series of experiments has revealed an increasingly complex picture [12, 17, 18]. The most detailed information about ligand binding has been obtained from flash photolysis experiments performed over a wide temperature range. Fig. 1 shows the flash photolysis kinetics of MbCO between 60 and 300 K. These data can be explained with the reaction landscape for the binding of CO to myoglobin as shown in Fig. 2b. The effective enthalpy is plotted as a function of the reaction coordinate. Two barriers are involved in the binding process. The inner barrier is associated with the final binding step close to the iron, the outer one with the gate between the heme pocket and the solvent. The system Mb + CO is initially in state A, where the ligand is bound to the heme iron. A short laser pulse cleaves the bond and the system moves to state B where the ligand is in the heme pocket. Below 200 K, the ligand cannot escape from the pocket because the barrier between B and S is too high. Therefore, it rebinds internally (Process I, B → A). The internal process should be exponential for a well-defined barrier heigth H_{BA}. The observed non-exponential behavior is explained with an inhomogeneous population of myoglobin molecules that possess different activation enthalpies H_{BA} and consequently rebind ligands with different rates. The rebinding is described by

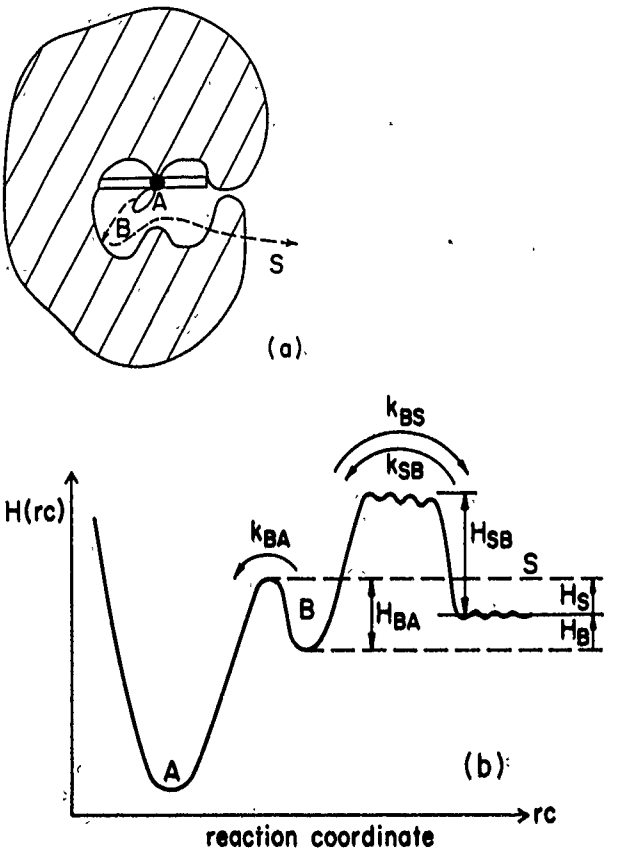


Fig. 2
(a) Schematic cross-section through a myoglobin molecule showing a hypothetical ligand pathway.
(b) The effective enthalpy H of the system Mb + CO is given as a function of the reaction coordinate rc

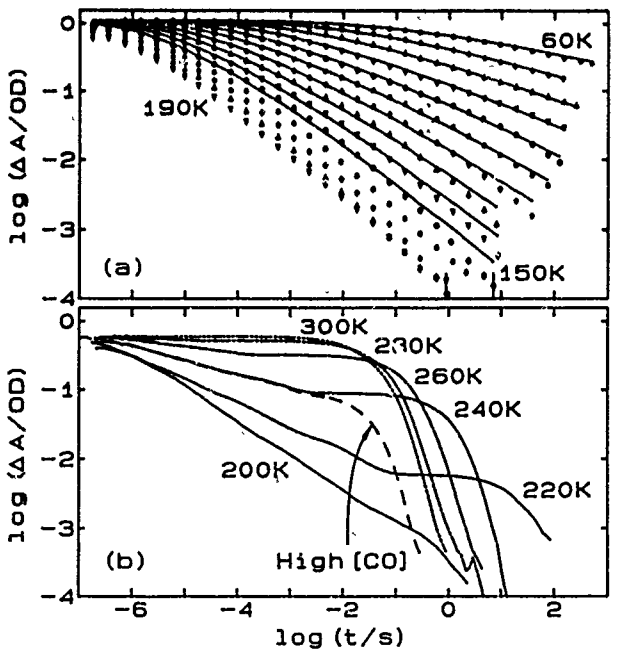


Fig. 1
Flash photolysis kinetics of MbCO in 75% (v/v) glycerol/phosphate buffer (pH 7). The absorbance change ΔA at 440 nm is given as a function of log t. The sample was prepared with a partial pressure of CO of 0.05 atm (except for the trace denoted by "High [CO]", where it was 1 atm)

$$N_I(t) = \int_0^\infty \mathrm{d}H_{BA}\, g(H_{BA})\, \mathrm{e}^{-k(H_{BA},T)t}\,. \tag{2}$$

$N_I(t)$ is the fraction of molecules that have not yet rebound a ligand at time t after the photolyzing flash. $g(H_{BA})$ is the probability density of finding an Mb molecule with enthalpic barrier H_{BA} in the ensemble. For MbCO $g(H_{BA})$ has a maximum at about 10 kJ/mol. The rate coefficient $k(H_{BA}, T)$ above about 60 K is given by the transition-state expression [19]

$$k(H_{BA}, T) = A_{BA}(T/T_0)\, \mathrm{e}^{-H_{BA}/RT}\,. \tag{3}$$

At lower temperatures, the rate $k(H_{BA}, T)$ is influenced by quantum-mechanical tunneling effects [8].

A second, slower process is observed in the flash photolysis kinetics above 200 K. This process is exponential and

dependent on the CO concentration. It is due to those molecules that lose their ligands to the solvent. Subsequently, other ligands will diffuse from the solvent toward the protein, enter the heme pocket through the protein matrix and bind to the iron (Process S, S→B→A).

The description of ligand binding with the reaction energy landscape sketched in Fig. 2b corresponds to the motion of a particle in a fixed potential. This single-particle model reflects the general features of the reaction well. Nevertheless, it oversimplifies the picture, because it does not account for the influence of protein motions. It will be shown in Section 4 that a more realistic description of the binding process has to incorporate time- and temperature-dependent barriers which arise from protein relaxations and fluctuations. These are strongly influenced by the dynamics of the surrounding solvent [2, 20].

3. The Conformational Energy Landscape

To understand the influence of protein motions on the ligand binding reaction we must take a closer look at the states in which these molecules exist and at the laws that govern the transitions between the states. Most proteins perform some kind of function such as transport of matter or enzymatic activity. Therefore they must have at least two different conformations which generally differ in structure and properties. Myoglobin for example has a ligated and an unligated conformation. Within a given conformation, a protein molecule does not possess a unique ground state, but a large number of nearly isoenergetic states which we call conformational substates (CS) [21, 22]. The phenomenon CS is also found in other complex systems like glasses [23] and spin glasses [24]. Transitions between conformational substates involve two different types of motions. Equilibrium fluctuations (EF) occur between the different conformational substates at sufficiently high temperatures. Transitions between different conformations (states) are due to nonequilibrium motions. We call those functionally important motions (FIM). Both types of motions are not independent of each other, but related by fluctuation-dissipation theorems [25].

First evidence for the existence of conformational substates came from the nonexponential rebinding observed with flash photolysis experiments at low temperatures [12]. Over the past 15 years, information about conformational substates has been continuously accumulated. Experiments on MbCO give evidence that the conformational substates are arranged in a hierarchy [17] as depicted in Fig. 3. The diagram gives a one-dimensional cross-section through the multidimensional conformational energy landscape of MbCO. The substates are grouped into a number of tiers, three of which are shown in the figure. The substates of tier 0 (CS0) are separated by the highest energy barriers. Within each of the CS0 the molecule can assume a large number of substates of tier 1 (CS1), separated by smaller barriers than the CS0. Each CS1 is again subdivided into substates CS2 and so on.

Evidence for substates of tier 0 is derived from infrared absorption experiments on MbCO [20]. They reveal three

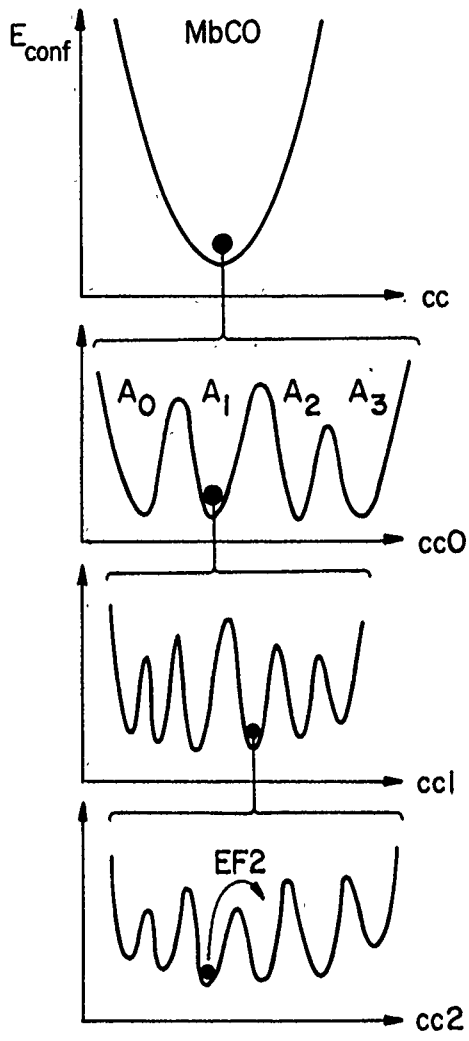


Fig. 3
The hierarchical arrangement of conformational substates (CS) in MbCO. A one-dimensional cross-section through the multidimensional conformational energy landscape is sketched as a function of the conformational coordinates of tier i (cc i)

major stretch bands for the CO ligands, which we denote by A_0, A_1, A_3, corresponding to three different substates. Slight differences in their structure have been proven by measurements of the tilt angles of the CO molecules against the heme normal [26] and by the x-ray structure analysis [27]. The rebinding kinetics of these substates is markedly different. Within each CS0 substate the ligand rebinding is non-exponential at low temperatures [20]. Therefore we conclude that each CS0 contains a large number of CS1 substates. Lower tiers are less well explored. Rebinding experiments after extended illumination give evidence for CS2. The existence of even lower tiers of substates is implied by specific heat measurements on proteins at temperatures below 10 K [28].

The hierarchical arrangement implies that the system is only ergodic at sufficiently high temperatures where fluctuations within all tiers occur. As the temperature is lowered, fluctuations will gradually freeze out, first among the substates of the highest tier, then successively in the lower tiers. The degree of nonergodicity is thus dependent on time and

temperature. The freezing of the EF0 and EF1 occurs very smoothly with temperature and is similar to a glass transition. The transition temperature depends on the glass transition temperature T_g of the surrounding solvent. Therefore, we call the transition a "slaved glass transition".

The hierarchical arrangement poses restrictions on the dynamics of the system. A transition between two arbitrary substates depends on the way in which the two are connected in this hierarchical space. The connection may be ultrametric. Remarkable analogies between the dynamics of ultrametric systems and proteins have been found [29].

4. Relaxation Phenomena and Equilibrium Fluctuations

4.1 The Relaxation Mb* → Mb

Below 160 K proteins are frozen in their particular substates. Therefore, the rebinding is characterized by a barrier distribution $g(H_{BA})$. Process I speeds up with increasing temperature as expected from the Arrhenius law for the rate coefficient $k(H_{BA}, T)$. Between 160 and 180 K this increase slows; above 180 K a reversal sets in so that Process I slows down with increasing temperature (see. Fig. 4).

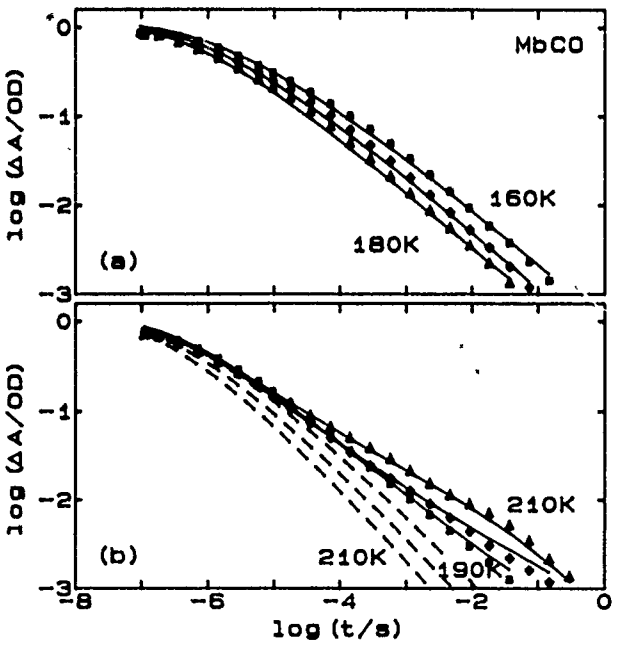


Fig. 4
Rebinding data and fits to the relaxation model for MbCO. (a) Process I at 160–180 K. (b) Process I at 190–210 K. Dashed lines: Prediction for Process I if no relaxation Mb* → Mb occurs. Solid lines: The relaxation Mb* → Mb was taken into account to fit the data (see Eq. (6))

An explanation for this – at a first glance – surprising behavior can be found by taking a closer look at the molecular structure of myoglobin. The room temperature x-ray coordinates tell us that the iron atom is about 0.35 Å away from the heme plane in deoxy Mb [30]. On binding a ligand, the iron has to move closer to the heme. In MbCO, the iron has been reported to be completely in the plane of the heme disk [27]. At temperatures below 160 K, the globin matrix is frozen. Thus, after photodissociation the iron cannot move fully out of the plane. The structure of this low temperature photoproduct is denoted by Mb*. Above 160 K the iron is able to relax into the deoxy position on the time scale of a photolysis experiment. The motion of the iron is accompanied by an increase of the enthalpy barrier H_{BA} for rebinding. Consequently, a slowing of the kinetics is observed.

Evidence for this scenario comes from kinetic experiments with Band III, a weak absorption band in the near infrared (~760 nm) that is only present in unligated myoglobin, either deoxy Mb or Mb*. Band III arises from a charge transfer transition involving iron d- and porphyrin π-orbitals [31] and is therefore sensitive to structural details near the heme iron. We studied this band in photolyzed Mb* (CO) in the temperature range between 10 and 160 K. As ligands rebind, the area of this band decreases while its position shifts to higher wave numbers. The explanation for this shift is as follows: Band III is inhomogeneously broadened. Different substates give different contributions to Band III so that it is approximately a Gaussian superposition of Lorentzians with peak positions ν. Our experiments show that the position ν and the barrier height H_{BA} are linearly related [18]. Such a relation is expected if both the enthalpy barrier and the charge-transfer transition depend in a similar way on the out-of-plane distance of the iron. From the difference of 116 cm^{-1} between the position of Band III in deoxy Mb and Mb* (CO) at 10 K and the measured relation between H_{BA} and ν we estimate an increase of the barrier for rebinding of about 12 kJ/mol as the iron shifts from the position in Mb* to the fully relaxed position.

This relaxation Mb*→Mb can be introduced into the kinetic equations that describe the rebinding process after flash photolysis. The increase of the rebinding barrier is modelled by

$$H_{BA}(t,T) = H_0 + \Delta H^* [1 - \Phi^*(t,T)]. \tag{4}$$

Immediately after photodissociation the barrier height equals H_0. It approaches the value $H_0 + \Delta H^*$ with a time dependence given by the relaxation function $\Phi^*(t,T)$ as the iron moves further away from the heme plane. Consequently, the rate coefficient for rebinding $k(H_{BA}(k,T),T)$ becomes time-dependent. For a single barrier the differential equation $dN_I(t,T) = -k(H_{BA}(t,T),T) \times N_I(t,T)$ leads to

$$N_I(t,T) = \exp\left[-\int_0^t k(H_{BA}(t',T))\,dt'\right]. \tag{5}$$

The rebinding data show that the entire barrier distribution shifts without markedly changing its shape. Therefore, the fraction of molecules $N_I(t,T)$ in the ensemble that have not yet rebound a ligand within the time t after the flash is given by

$$N_I(t,T) = \int_0^\infty dH_0\, g(H_0) \exp\left[-\int_0^t k(H_{BA}(t',T))\,dt'\right]. \tag{6}$$

The experiments show that the relaxation function is strongly nonexponential in time as we also observe when studying protein relaxations after pressure jumps [14]. A stretched exponential fits our data well

$$\Phi^*(t,T) = \exp[-\kappa^*(T)t]^\beta . \quad (7)$$

If the temperature dependence of the rate coefficient $\kappa^*(T)$ is described by an Arrhenius relation, the pre-exponential factor becomes unphysically large. We consequently use a relation that is known to describe relaxation phenomena in glasses and synthetic polymers,

$$\kappa^*(T) = A^* \exp[-(E^*/RT)^2] . \quad (8)$$

This relation has been derived for a random walk of an excitation within a Gaussian density of states [32, 33, 34, 35]. In Fig. 4 we show the rebinding of MbCO together with fitted curves. The reversal of the kinetics with temperature near 180 K is very well described by a barrier distribution $g(H_{BA})$ that shifts as a whole to higher values without changing its shape. The value ΔH^* of 11 kJ/mol is in good agreement with the estimate of 12 kJ/mol from the kinetic experiments on Band III. The other parameters obtained from the fit are $A^* = 10^{18}\ s^{-1}$, $E^* = 10$ kJ/mol, $\beta = 0.24$.

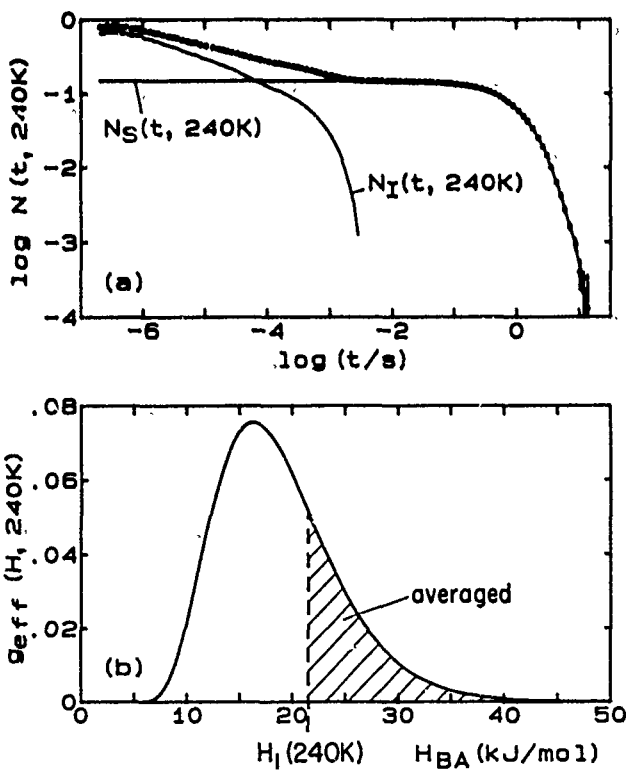


Fig. 5
(a) The measured survival probability $N(t, 240\ K)$ is plotted as a function of log t and decomposed into the exponential solvent process $N_S(t, 240\ K)$ and the internal process $N_I(t, 240\ K)$.
(b) The distribution function $g_{eff}(H_{BA}, T)$ at 240 K. Protein molecules in substates with $H_{BA} < H_I$ have rebinding rates faster than τ^{-1}. They rebind before hopping to another substate. Proteins in the hatched part have $H_{BA} > H_I$ and therefore $k_{BA} < \tau^{-1}$. They fluctuate from CS to CS; their ligands can either rebind internally or move into the solvent

4.2 Equilibrium Fluctuations

Molecular dynamics simulations show that the protein structure has to fluctuate in order to open pathways for the ligand to escape [36]. These motions set in at about 200 K [15, 37]. Our flash photolysis experiments confirm these results: Above 200 K some photodissociated CO molecules escape into the solvent, and the subsequent rebinding is approximately exponential in time (see Fig. 1):

$$N_S(t,T) = N_S(t,T) \exp[-\langle\lambda_S\rangle t] . \quad (9)$$

We decompose the rebinding curves into the solvent process $N_S(t,T)$ and the internal process $N_I(t,T)$ as shown in Fig. 5a. At early time $N_I(t,T)$ decreases slowly and non-exponentially. From a certain time τ_I on a nearly exponential drop-off is observed leading to a rapid depletion of the internally rebinding molecules. It is caused by two effects: (i) CO molecules migrate into the solvent and rebind from there. (ii) The distribution of rate coefficients $k(H_{BA}, T)$ collapses into an average value. We assume that both effects are due to equilibrium fluctuations in tier 1 (EF1), characterized by an average rate coefficient $\langle\kappa_1\rangle$. The inverse of the time τ_I gives an estimate for the fluctuation rate $\langle\kappa_1\rangle$.

The influence of the equilibrium fluctuations can be explained with an effective enthalpy distribution, $g_{eff}(H_{BA}, T)$, as sketched in Fig. 5b for $T = 240$ K. It is much broader than the low temperature distribution because of the relaxation Mb* → Mb: Molecules with small barriers rebind ligands at early times without having shifted significantly, molecules with high barriers rebind more slowly and therefore shift to even higher barriers before rebinding. The distribution $g_{eff}(H_{BA}, T)$ is divided into two parts separated by the enthalpy $H_I(T)$ given by

$$H_I(T) = RT \ln[A_{BA} T/\langle\kappa_1\rangle T_0) . \quad (10)$$

Proteins in the shaded area experience equilibrium fluctuations. They rebind the ligand with an average rate $\langle k_{BA}\rangle < \langle k_1\rangle$ either from the pocket (Process I) or from the solvent (Process S).

4.3 The Viscosity Dependence of Protein Motions

The relaxation Mb* → Mb and the equilibrium fluctuations (EF1) appear to have their origin in quite different types of motions because the distribution of barriers $g(H_{BA})$ shifts without narrowing at temperatures around 180 K. We tentatively assign the relaxation Mb* → Mb to the second tier of the substate hierarchy and call it FIM2.

Another difference between the two dynamic processes becomes obvious when looking at rebinding curves that were obtained using samples with different solvents. In principle, both the relaxation Mb* → Mb and the equilibrium fluctuations could be influenced by the viscosity of the solvent around the protein molecules. Fig. 6 shows the kinetics of Process I for MbCO in three solvents with different viscosities. All three sets of data were taken at 250 K. The nonexponential part of the rebinding curves is almost iden-

tical for the three cases. Therefore, the solvent viscosity η has little or no effect on the relaxation Mb* → Mb. This observation is also supported by measurements with MbCO embedded in ice or solid poly- (vinyl alcohol) [12]. In a rigid matrix ($\eta \to \infty$), no solvent process appears, but Process I is still influenced by the relaxation Mb* → Mb. We conclude that the shift of the iron out of the heme plane is a process that is controlled close to the heme. It involves correlated motions of only a small part of the protein. In contrast, the equilibrium fluctuations (EF1) depend strongly on viscosity and must involve larger parts including the interface between protein and solvent.

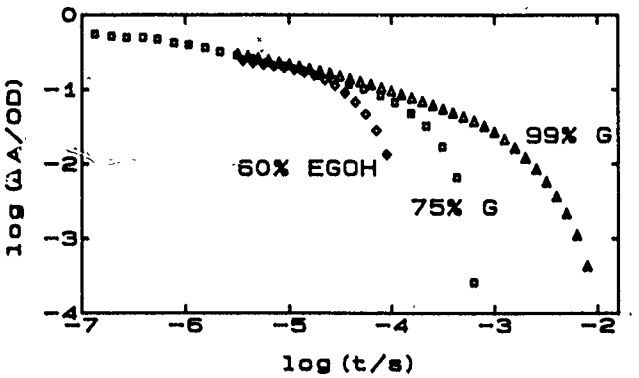


Fig. 6
The viscosity dependence of the rebinding of CO to Mb at 250 K. The rebinding function $N_I(t)$ for Process I is shown for the solvents 60% ethylene glycol/buffer, 75% glycerol/buffer, 99% glycerol/buffer

5. Beyond Kramers

The study of a biological process like the binding of a ligand to a small heme protein reveals exciting phenomena that influence the kinetics of the reaction. At low temperatures the enthalpic barriers are distributed within the ensemble. Glass-like, non-exponential relaxations are observed which lead to an increase of the rebinding barriers with time. At sufficiently high temperatures the proteins perform fluctuations between a large number ($>10^3$) of conformational substates. As a consequence, the heights of the activation barriers fluctuate with time.

Proteins are exceedingly complex systems. Nevertheless, they establish a highly organized environment in which fundamental aspects of rate processes can be investigated. A deep understanding of biological processes will only be possible if the reaction theory of the underlying chemical processes is developed. Therefore, the study of rate processes in proteins offers a challenge to both experiment and theory.

We thank our collaborators at the University of Illinois for their contributions and many illuminating discussions. GUN thanks the Alexander von Humboldt Foundation for a Feodor Lynen Fellowship. This work was supported in part by the National Science Foundation (Grant DMB87-16476), the National Institutes of Health (Grants GM 18051 and 32455), and the Office of Naval Research (N00014-89-R-1300).

References

[1] B. Gavish, and M. M. Werber, Biochemistry *18*, 1269 (1979).
[2] D. Beece, L. Eisenstein, H. Frauenfelder, D. Good, M.C. Marden, L. Reinisch, A. H. Reynolds, L. B. Sorensen, and K. T. Yue, Biochemistry *19*, 5147 (1980).
[3] W. Doster, Biophys. Chem. *17*, 97 (1988).
[4] M. H. Redi, B. S. Gerstman, and J. J. Hopfield, Biophys. J. *35*, 471 (1981).
[5] J. Jortner, J. Ulstrup J. Am. Chem. Soc. *101*, 3744 (1979).
[6] H. Frauenfelder, and P. G. Wolynes, Science *229*, 337 (1985).
[7] J. O. Alben, D. Beece, S. F. Bowne, L. Eisenstein, H. Frauenfelder, D. Good, M. C. Marden, P. P. Moh, L. Reinisch, A. H. Reynolds, and K. T. Yue, Phys. Rev. Lett. *44*, 1157 (1980).
[8] H. Frauenfelder in: Tunneling in Biological Systems, eds. B. Chance, H. Frauenfelder, R. A. Marcus, J. R. Schrieffer, and N. Sutin, pp 627, Academic, New York, 1979.
[9] P. Hänggi, P. Talkner, and M. Borkovec, Rev. Mod. Phys. *62*, 251 (1990).
[10] N. Alberding, R. H. Austin, K. W. Beeson, S. S. Chan, L. Eisenstein, H. Frauenfelder, and T. M. Nordlund, Science *192*, 1002 (1976).
[11] P. Hänggi, J. Theor. Biol. *74*, 337 (1978).
[12] R. H. Austin, K. W. Beeson, L. Eisenstein, H. Frauenfelder, and I. C. Gunsalus, Biochemistry *14*, 5355 (1975).
[13] A. Szabo, D. Shoup, S. H. Northrup, and J. A. McCammon, J. Chem. Phys. *77*, 4484 (1982).
[14] H. Frauenfelder, N. A. Alberding, A. Ansari, D. Braunstein, B. R. Cowen, M. K. Hong, I. E. T. Iben, J. B. Johnson, S. Luck, M. C. Marden, J. R. Mourant, P. Ormos, L. Reinisch, R. Scholl, A. Schulte, E. Shyamsunder, L. B. Sorensen, P. J. Steinbach, A. Xie, R. D. Young, and K. T. Yue, J. Phys. Chem. *94*, 1024 (1990).
[15] I. E. T. Iben, D. Braunstein, W. Doster, H. Frauenfelder, M. K. Hong, J. B. Johnson, S. Luck, P. Ormos, A. Schulte, P. J. Steinbach, A. H. Xie, and R. D. Young, Phys. Rev. Lett. *62*, 1916 (1989).
[16] E. Antonini and M. Brunori, Hemoglobin and Myoglobin in Their Reactions with Ligands, North-Holland, Amsterdam, 1971.
[17] A. Ansari, J. Berendzen, S. F. Bowne, H. Frauenfelder, I. E. T. Iben, T. B. Sauke, E. Shyamsunder, and R. D. Young, Proc. Nat. Acad. Sci. USA *82*, 5000 (1985).
[18] P. J. Steinbach, A. Ansari, J. Berendzen, D. Braunstein, K. Chu, B. J. Cowen, D. Ehrenstein, H. Frauenfelder, J. B. Johnson, D. C. Lamb, S. Luck, J. R. Mourant, G. U. Nienhaus, P. Ormos, R. Philipp, A. Xie, and R. D. Young, submitted to Biochemistry.
[19] D. D. Dlott, H. Frauenfelder, P. Langer, H. Roder, and E. Dilorio, Proc. Nat. Acad. Sci. USA *80*, 6239 (1983).
[20] A. Ansari, J. Berendzen, D. Braunstein, B. R. Cowen, H. Frauenfelder, M. K. Hong, I. E. T. Iben, J. B. Johnson, P. Ormos, T. B. Sauke, R. Scholl, A. Schulte, P. J. Steinbach, J. Vittitow, and R. D. Young, Biophys. Chem. *26*, 337 (1987).
[21] H. Frauenfelder, G. Petsko, and D. Tsernoglou, Nature (London) *280*, 558 (1979).
[22] H. Frauenfelder, F. Parak, and R. D. Young, Annu. Rev. Biophys. Biophys. Chem. *17*, 451 (1988).
[23] M. Goldstein, J. Chem. Phys. *51*, 3728 (1969).
[24] P. W. Anderson, Phys. Today *41* No. 9, 9 (1988).
[25] R. Kubo, Rep. Prog. Phys. *29*, 255 (1966).
[26] P. Ormos, D. Braunstein, H. Frauenfelder, M. K. Hong, S.-L. Lin, T. S. Sauke, and R. D. Young, Proc. Nat. Acad Sci. USA *85*, 8492 (1988).
[27] J. Kuriyan, S. Wilz, M. Karplus, and G. Petsko, J. Mol. Biol. *192*, 133 (1986).
[28] G. P. Singh, H. J. Schink, H. v. Löhneysen, F. Parak, and S. Z. Hunklinger, Phys. *B55*, 23 (1984).
[29] A. T. Ogielski and D. L. Stein, Phys. Rev. Lett. *55*, 1634 (1985).
[30] S. E. V. Phillips (1981) Brookhaven Protein Data Bank.
[31] W. A. Eaton and J. Hofrichter, Meth. Enzymol. *76*, 175 (1981).

[32] F. Richert and H. Bässler, J. Phys.: Condens. Matter *2*, 2273 (1990).
[33] J. Bryngelson and P. G. Wolynes, J. Phys. Chem. *93*, 6902 (1981).
[34] R. Zwanzig, Proc. Nat. Acad. Sci. USA *85*, 2029 (1988).
[35] H. Bässler, Phys. Rev. Lett. *58*, 767 (1987).
[36] D. A. Case and M. Karplus, J. Mol. Biol. *132*, 343 (1979).
[37] G. U. Nienhaus, J. Heinzl, E. Huenges, and F. Parak, Nature *338*, 669 (1989).

Presented at the Discussion Meeting of the Deutsche Bunsen-Gesellschaft für Physikalische Chemie "Rate Processes in Dissipative Systems: 50 Years after Kramers" in Tutzing, September 10–13, 1990 E 7539

Stiffness Effects in Multidimensional Diffusive Barrier Crossing

Noam Agmon and Savely Rabinovich

Department of Physical Chemistry and the Fritz Haber Research Center, The Hebrew University, Jerusalem 91904, Israel

Chemical Kinetics / Diffusion / Liquids / Photo Isomerization / Viscosity

The model of Agmon and Kosloff for two-dimensional diffusive barrier crossing is extended. We demonstrate how an increase in stiffness of the potential perpendicular to the reaction coordinate leads to viscosity dependent rates which are closer to the one-dimensional Kramers result. The range over which the dynamics are truly two dimensional is characterized by a fractional viscosity dependence of reaction rates and viscosity dependent activation energies. It is a transition region between Kramers behaviors observed in the two extreme limits. A simple kinetic approximation rationalizes these observations as arising from two competing pathways. It shows surprisingly good agreement with the full calculation.

1. Introduction

In the last decade the Kramers [1] model of diffusive barrier crossing has been revived and extended as part of an effort to understand molcular chemical transformations in solution. Some of the review articles published in the last few years are listed below [2–6]. Until recently much of the theoretical research focused on non-Markovian (memory) effects and frequency dependent friction [2–8]. In this approach other degrees of freedom are usually represented as a harmonic bath. It seems that presently attention is directed towards the understanding of truly multidimensional barrier crossing phenomena [9–13].

Advances in theory are motivated by parallel progress in experiment, especially in the study of photochemical isomerization following ultrafast laser excitation [14]. One model system that has been extensively studied is the isomerization of stilbene, both in solution and pressurized gasses [14–23]. Focusing on the high friction limit, it is often found [15–17] that the dependence of the isomerization rate coefficient, k, on the solvent's macroscopic (shear) viscosity, η, is weaker than predicted by the Kramers theory [1]: Instead of an inverse viscosity dependence, one has

$$k = b/\eta^a, \quad 0 < a \leq 1 \tag{1}$$

with constant a and b. A similar viscosity dependence is also observed in ligand binding to myoglobin [24].

The above deviation from Kramers' prediction can be explained in several ways: (i) Non-Markovian theories [2,5,7,8] can predict slower than $1/\eta$ viscosity dependence, though often with non-realistic potential parameters [15,17,20a]. (ii) Macroscopic viscosity may be a poor approximation to the microscopic friction. Indeed, better agreement with experiments showing the fractional viscosity dependence, Eq. (1), can sometimes be obtained [16] using the conventional Kramers theory with microscopic friction assumed proportional to the rotational diffusion lifetime. (iii) Potentials may vary systematically with solvent composition [18,19]. (iv) Multidimensional effects may be dominant [10–13]. While we concentrate below on multidimensional effects, this by no means implies that we believe other effects listed above to be unimportant in explaining the experimental results.

To our knowledge, Agmon and Kosloff [11] were the first to consider the explicit solution for diffusional barrier crossing dynamics in more than one degree of freedom, with anisotropic diffusion and a potential more general than a channel connecting reactants and products [10]. Their model was motivated by earlier work on hemeprotein dynamics [9] and by the experimental observation [15] that, while *trans*-stilbene shows a fractional viscosity dependence ($a < 1$), its stiff counterpart (*trans*-"stiff" stilbene, see Fig. 1) conforms to Kramers kinetics ($a = 1$). The evident difference between these two molecules is that "stiff" stilbene has only one active degree of freedom in its isomerization process (rotation around the double-bond, dihedral angle θ), whereas stilbene has an additional rotational motion available (around the phenyl-carbon bond, dihedral angle ϕ). The effect of the perpendicular degree of freedom, ϕ, is manifested in two ways. First, the barrier for θ-isomerization is expected to decrease as the phenyl rings are rotated out of planarity, due to a decrease of π-orbital coupling. Such an effect still awaits verification by quantum chemistry calculations [25]. Second, the diffusion tensor in these two coordinates is expected to be anisotropic. The phenyl ring rotation displaces much less solvent than the isomerization

 © VCH Verlagsgesellschaft mbH, W-6940 Weinheim, 1991 0005-9021/91/0303-0278 $ 3.50+.25/0

motion and is therefore less sensitive to macroscopic viscosity. In addition, the θ-motion might be less viscosity sensitive when the phenyl rings cut through the solvent with their narrow side i.e., the diffusion coefficient in θ decreases as the phenyl rings are rotated out of plane [26]. This last effect has not yet been incorporated in the model.

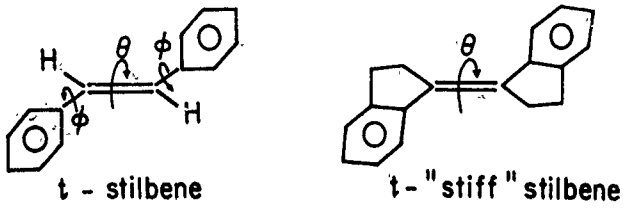


Fig. 1
Chemical structure of stilbene and biindanylidene ("stiff"-stilbene)

By solving numerically the time-dependent Smoluchowski equation in two dimensions for a potential surface and diffusion tensor with the above mentioned properties, it was shown [11] that viscosity dependences of the form [1] arise. However, it was never explicitly demonstrated that the kinetics become more Kramers-like as the potential along the perpendicular coordinate ϕ becomes stiffer as, for example, one expects for "stiff"-stilbene. In the present contribution, we extend the results of Ref. [11] by adding to the potential surface a parabola in ϕ and investigating the viscosity dependence as a function of its stiffness. The investigation involes a wide range of viscosity and temperature. A deeper investigation of two dimensional models is timely, especially because in the last year or so several experimental results have been interpreted with the aid of similar ideas [20b–22].

2. Theoretical Procedures

We investigate below a simple extension of the Agmon-Kosloff hypothetical stilbene potential [11], namely

$$V(\theta,\phi) = V_0(\theta,\phi) + V_\phi(\theta,\phi) + \beta\phi^2 \tag{2}$$

with the functions V_0 and V_ϕ given in Ref. [11]

$$V_0(\theta,\phi) = Q_0[3\cos(2\theta) - 6\cos(4\theta) + \cos(6\theta) - 4\cos(\theta)][1 + \alpha\cos^2(\phi)]/[8(\alpha+1)] \tag{3a}$$

$$V_\phi(\theta,\phi) = Q_\phi[3\cos(2\phi) - 4\cos(4\phi) + \cos(6\phi)]/8 \tag{3b}$$

with $Q_0 = 3$ and $Q_\phi = 2$ energy units (these units were chosen such that the barrier resembles that of stilbene in alkanes, ca. 14.7 kJ/mol) and $\alpha = 4$. For $\beta = 0$ the potential in Eq. (2) reduces exactly to that of Ref. [11]. Increasing values of β mimic increasing stiffness of the phenyl ring rotation (ϕ-coordinate). Experimentally, such increased stiffness can be obtained by a series of aliphatic rings of decreasing size e.g., 7–5 membered rings [16b, 22]. We stress that the stiffness parameters, β, never modifies the energy profile along the one-dimensional projection of the reaction coordinate ($\phi = 0$). A comparison of a "normal" ($\beta = 0$) and "stiff" ($\beta > 0$) potential is shown in Fig. 2: The initial *trans* configuration with in-plane phenyl rings is at the origin of the coordinates ($\theta = 0$, $\phi = 0$) while the final "perpendicular" conformation is at $\theta = \pi/2$ and $\phi = 0$.

The diffusion tensor, $\boldsymbol{D}$, is assumed diagonal and the diagonal elements are denoted by D_{00} and $D_{\phi\phi}$. As in Ref. [11], we assume that

$$D_{\phi\phi} = \text{const} = 1 \tag{4}$$

in units of radian^2/time, while D_{00} varies. This represents an extreme idealization of a situation where the smaller amplitude motion of the phenyl ring is less sensitive to solvent viscosity compared with the larger amplitude isomerization. The rate coefficients are considered a function of D_{00}^{-1}, which is assumed proportional to the macroscopic viscosity, η. In relation to interpretations [16] stressing the role of deviations from the Stokes-Einstein hydrodynamic relation, we note that here the reaction coordinate θ strictly conforms to such a relation, while the assumed (large) deviations from classical hydrodynamics are only in the perpendicular coordinate, ϕ.

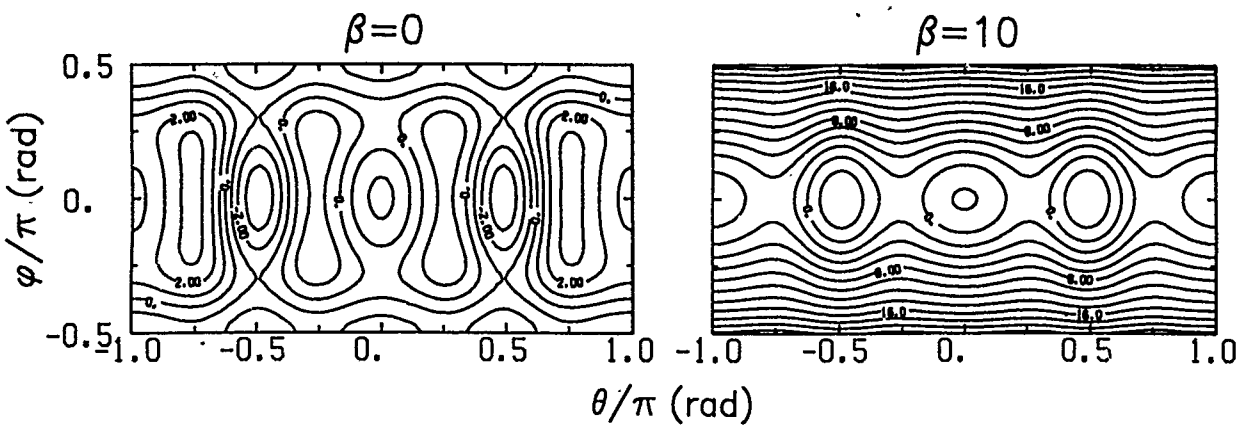


Fig. 2
Effect of the stiffness parameters, β, on the potential surface, Eqs. (2) and (3). Equipotential contour spacings are 1 and 2 energy unit for $\beta = 0$ and 10, respectively

The dynamics on the potential surface are assumed [11] to obey the Smoluchowski (diffusion-in-a-potential-field) equation

$$\partial p(\theta,\phi,t)/\partial t = \nabla \cdot \boldsymbol{D} \cdot [\nabla + \nabla V(\theta,\phi)/k_B T]\, p(\theta,\phi,t) \qquad (5)$$

for the time evolution of the probability density distribution, $p(\theta,\phi,t)$, in the two dimensional space (θ,ϕ). In Eq. (5), T is the absolute temperature and k_B is Boltzmann's constant. The initial distribution is a delta function at the origin of the coordinates,

$$p(\theta,\phi,0) = \delta(\theta)\,\delta(\phi)\,. \qquad (6)$$

This differs from the initial distribution in Ref. [11], which was like a Gaussian centered at the origin. This difference, however, persists only for the first few time steps during which the initial distribution thermalizes in the reactant's well. As long as the isomerization barriers are high, the barrier crossing process evolves on a considerably slower time scale.

A detailed description of the computational procedures is given in Ref. [11], where the spatial operator was evaluated by a fast Fourier transform (FFT) routine, and time evolution obtained by Chebyshev propagation. The Chebyshev expansion [27] allows us to take comparably large time steps. Unfortunately, the FFT algorithm may be tricky to implement, and does not easily handle delta function distributions or complicated boundary conditions. In the present calculation we have replaced the FFT procedure by a Master operator. This amounts to discretizing the (θ,ϕ) plane and assigning transition probabilities among nearest-

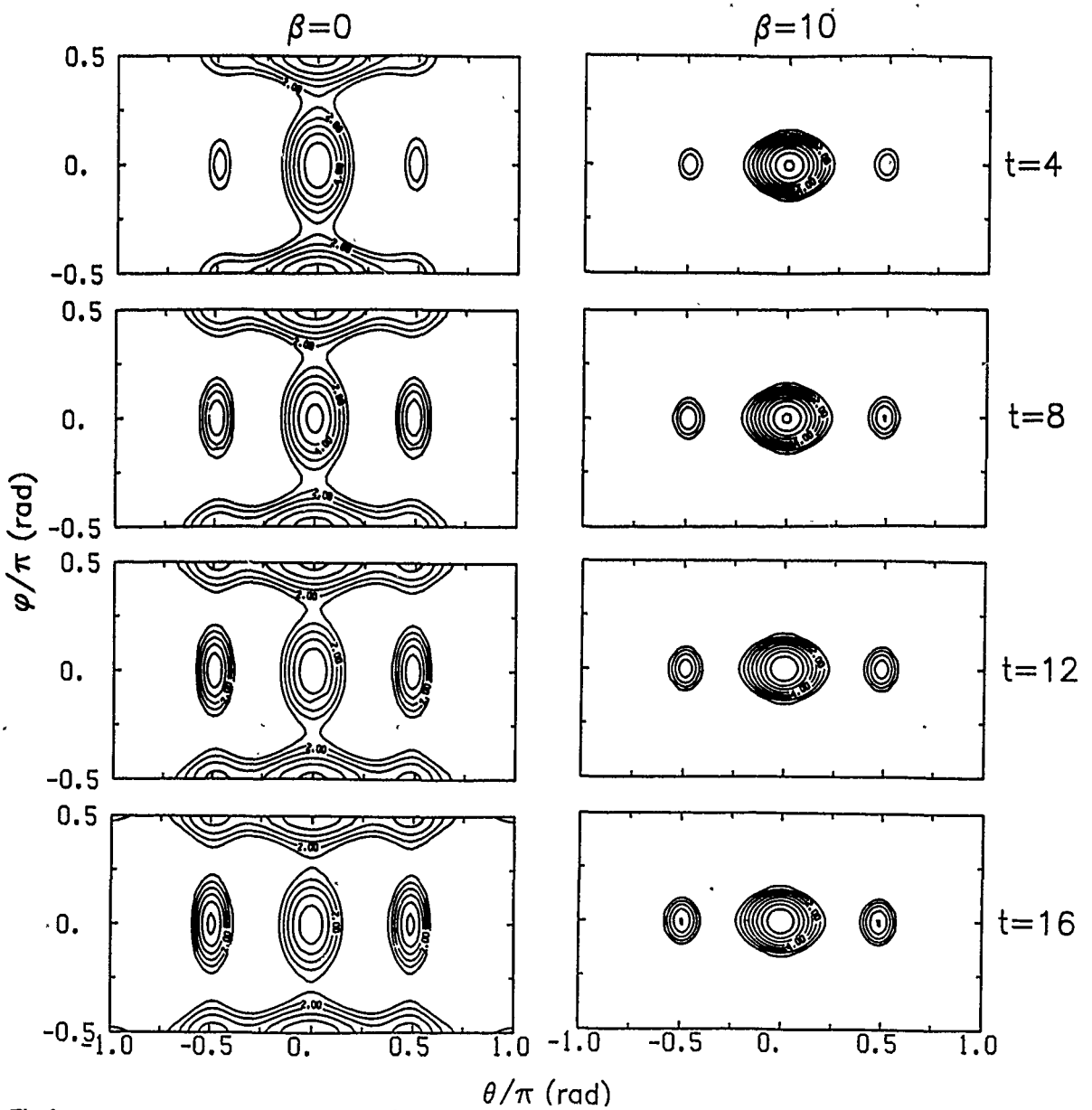


Fig. 3
Effect of stiffness on the density distribution, $p(\theta,\varphi,t)$, propagated on the potential surfaces of Fig. 2. Logarithmic contours for $p = 2^n$, 100, $n = 1,2,...$

neighboring points along θ or ϕ (no diagonal transitions are allowed) in such a way that Eq. (5) becomes a Master equation with detailed balancing. While additional details may be found in Refs. [9, 28, 29], we stress that implementing finite-differencing in space via a prescription in which detailed-balancing is rigorously obeyed, ensures that as $t \to \infty$ we obtain the exact equilibrium distribution namely, $\exp[-V(\theta,\phi)/k_B T]$ properly normalized. The Master operator is one line of computer code, compared with the large software package needed to implement the FFT routine.

To obtain the reaction rate, we first integrate the density distribution, $p(\theta,\phi,t)$, over the reactants' region to obtain the reactants "survival probability", $S(t)$. This quantity is denoted by $Q(t)$ in Ref. [11]. The reactants' region is assumed to be separated from the products' region by the ridge line on the potential surface. For a potential with the simple shape shown in Fig. 2, these ridges are straight lines parallel to ϕ, at $\theta \approx \pm 0.26\pi$. Next, we fit $S(t)$ to the solution of a 2-state kinetic scheme, reactants $\leftrightarrows$ products, which is

$$S(t) = S_\infty + (1 - S_\infty)\exp(-t/\tau) \tag{7a}$$

$$\tau^{-1} = k_f + k_r\,, \quad S_\infty = k_r \tau\,. \tag{7b}$$

Here k_f is the forward (reactants $\to$ products) rate coefficient, while k_r is a similar quantity for the reverse direction. The ultimate equilibrium survival probability, S_∞, can be calculated analytically from the potential as the integral of $\exp[-V(\theta,\phi)/k_B T]$ over the reactants' region divided by its integral over the whole space. With the knowledge of S_∞, we fit our $S(t)$ data to Eq. (7a) to determine τ and then evaluate (say) the forward rate coefficient as $k_f = (1 - S_\infty)/\tau$. This procedure differs from that of Ref. [11], which used both S_∞ and τ as fitting parameters.

3. Results

We have propagated the Smoluchowski equation (5), starting from a delta-function initial distribution, for several values of $D_{\theta\theta}$ ($D_{\phi\phi} = 1$ rad^2/time) and three values of the stiffness parameter, β, in the potential function of Eq. (2). The probability density was subsequently integrated and analyzed via Eq. (7) to yield rate coefficients. These calculations were carried out on a Convex computer with single precision accuracy and a grid of 64×32. This grid represents the rectangle $-\pi \le \theta \le \pi$, $-\pi/2 \le \phi \le \pi/2$, with periodic boundary conditions at its edges. Propagations on a doubled grid (128×64) yielded rate coefficients that differed by 5% at most. In several cases, we have propagated to extremely long times so that the final distribution was very close to the equilibrium density. We verified in these cases that the analytic values of S_∞

Table 1
Parameters used in the propagation of Eq. (5) on a 64×32 grid and parameters obtained from the kinetic analysis via Eq. (7). $D_{\phi\phi} = 1$ rad^2/time. n_B, Δt and n_t are number of Bessel coefficients, time step and total number of time steps, cf. Ref. [11]. Note the general agreement of k_f for $\beta = 0$ and $k_B T = 0.6$ with data in Table 1, runs 1 and 2, of Ref. [11]

$k_B T$	β	S_∞	$D_{\theta\theta}$	n_B	Δt	n_t	$1000/\tau$	$1000\ k_f$
0.4	0	0.0676	10	229	0.1	100	131.7	123
			1	217	0.5	100	69.8	65.2
			0.1	226	1.0	100	35.0	32.7
	1	0.0205	10	229	0.1	500	66.3	64.9
			1	217	0.5	400	10.7	10.5
			0.1	226	1.0	1000	1.46	1.43
0.6	0	0.1514	100	219	0.01	200	7451	6323
			10	229	0.1	30	1006	854
			1	139	0.2	30	249	210
			0.1	226	1.0	60	62.6	53.0
			0.01	216	1.0	200	7.25	6.17
			0.001	215	1.0	200	0.755	0.640
	1	0.0733	100	219	0.01	200	6307	5844
			10	229	0.1	50	688	638
			1	217	0.5	80	97.4	90.3
			0.1	226	1.0	200	12.4	11.5
			0.01	216	1.0	2000	1.39	1.28
			0.001	215	1.0	20000	0.148	0.137
	10	0.0639	100	219	0.01	200	5100	4773
			10	229	0.1	100	516	481
			1	217	0.5	200	51.3	48.1
			0.1	219	0.5	600	5.13	4.81
1	0	0.2385	10	229	0.1	200	5416	4221
			1	100	0.1	200	668	509
			0.1	226	1.0	200	91.6	69.8
	1	0.1881	10	229	0.1	200	4276	3470
			1	139	0.2	200	486	394
			0.1	226	1.0	300	55.7	45.1
	10	0.1589	10	229	0.1	200	3127	2630
			1	139	0.2	300	313	265
			0.1	226	1.0	500	31.8	26.7

are reproduced to 3–4 digit accuracy. Propagation parameters and rate coefficients obtained are collected in Table 1.

Fig. 3 compares the time dependence of the probability density, $p(\theta,\phi,t)$, for two values of β. When $D_{00}=0.1$ and $\beta=0$, a considerable fraction of the flux bypasses the $\phi=0$ barrier and proceeds via the "indirect" route that combines isomerization (θ-motion) with phenyl ring rotation (ϕ-motion). This agrees with the results in Fig. 4 of Ref. [11]. As β increases, the indirect route becomes higher in energy (see Fig. 2), so most of the flux flows via the direct barrier crossing route, and the reaction becomes more "one-dimensional".

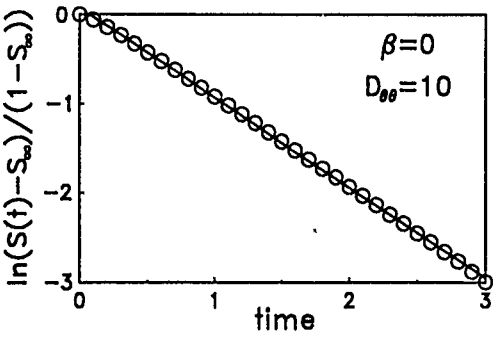


Fig. 4
An example of the kinetic analysis of the calculated density distribution by Eq. (7). Open circles represent the density, $p(\theta,\phi,t)$, integrated over the reactants' region $= 0.26\pi \le \theta \le 0.26\pi$, $-\pi/2 \le \phi \le \pi/2$, for every fifth time step

Fig. 4 shows a typical kinetic analysis by the two-state kinetic model, Eq. (7). We usually exclude from the analysis the first few time steps, during which the initial distribution reaches quasi-equilibrium in the reactants' well, and very long times for which the difference $S(t) - S_\infty$ becomes smaller than the numerical accuracy of our calculation. Occasionally, we found that the decay of $S(t) - S_\infty$ was not well represented by a single exponential over the whole time range. In these cases we used the initial decade of the decay in the analysis.

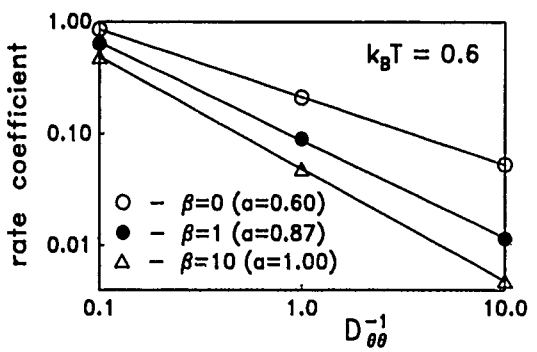


Fig. 5
Viscosity dependence of the reaction rate coefficient (Table 1) for intermediate anisotropy variations. Lines represent a fit to Eq. (1) yielding the parameters collected in Table 2

Table 2
Fitting parameters of the $k_BT = 0.6$ data (Table 1, Fig. 5) to the fractional viscosity dependence, Eq. (1)

β	0	1	10
a	0.603	0.873	1.000
b	0.212	0.0870	0.0481

Fig. 5 shows the forward rate coefficient, k_f, obtained from the above kinetic analysis, as a function of viscosity, $\eta \propto D_{00}^{-1}$. Over the anisotropy range in the diffusion tensor considered in Ref. [11], namely $0.1 \le D_{\phi\phi}/D_{00} \le 10$, we obtain straight lines on a log-log scale (Fig. 5). The slope of these lines yields the parameter a. The parameters a and b of Eq. (1) are collected in Table 2. For $\beta = 0$, we find $a = 0.60$, in excellent agreement with Ref. [11]. As β is increased, the indirect path becomes less probable (see Fig. 3) and a increases smoothly to unity. This qualitatively agrees with the experimental observation for stilbenes, whose behavior becomes more Kramers-like when phenyl-ring rotation is restricted e.g., in "stiff" stilbene [15,16]. As the dynamics become more one-dimensional, the magnitude of the rate coefficients decrease due to the elimination of alternate pathways. We note that experimental rate coefficients for stiffened stilbene derivatives are typically larger than for the unbridged molecule [22]. Within the present model, this is not a consequence of reduced dimensionality. It could be attributed [16] to a decrease in the one-dimensional barrier heigth, perhaps due to electronic interactions with the bridging atoms.

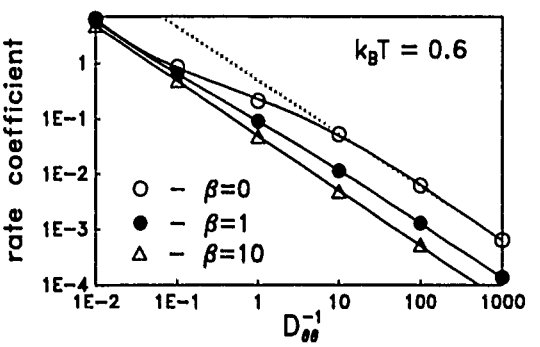


Fig. 6a
Viscosity dependence over an extended range. Full curves are interpolation by 4'th order polynomials. Dotted line is a fit to the high viscosity end of the $\beta = 0$ data, showing the convergence to a Kramers behavior in this limit. Data from Table 1

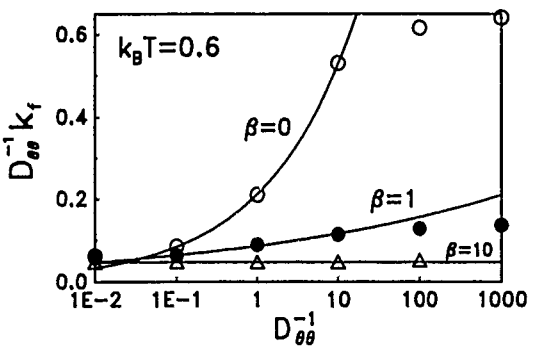


Fig. 6b
A different representation of the data in Fig. 6a, showing the viscosity dependence of the rate coefficient times the viscosity. Full curves are the fractional viscosity fit (Fig. 5) utilizing the parameters from Table 2

In Fig. 6 we have considerably extended the anisotropy range. A propagation for the largest anisotropy value $D_{\phi\phi}/D_{00} = 1000$, required some 100 hrs of Convex time. The results show that, for the present model, the power law behavior depicted by Eq. (1) actually represents a transition region between the two asymptotic limits of large and small anisotropy. In both of these limits one has a Kramers $1/\eta$ behavior, though with a different prefactor. This agrees with Eq. (16) of Ref. [11]. The reason why the dynamics become effectively one dimensional in these two limits is physically clear: For large D_{00} the density has no time to develop in the orthogonal,

ϕ direction. The dynamics then represents direct over the barrier evolution of a "frozen" (in ϕ) initial distribution. In the opposite limit of small D_{00}, the initial density rapidly equilibrates in the perpendicular direction. Thereafter, it retains its shape and diminishes in amplitude, as an increasing fraction of the population in the reactants' region crosses the ridgeline into the products' region. The rate of this process is governed by the magnitude of D_{00} at various ϕ values. Since we have assumed that D_{00} scales as $1/\eta$ for all values of ϕ, we regain the Kramers behavior in this limit too. Most of the photoisomerization experiments [14–22] have not explored such huge viscosity variations in the diffusive regime.

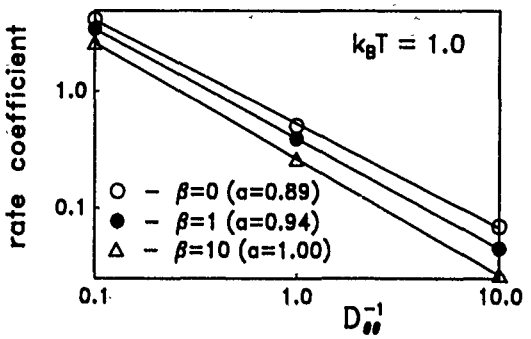


Fig. 7
Viscosity dependence at a higher temperature. Lines are a fit to Eq. (1)

Returning to more moderate variations in anisotropy, we have investigated temperature effects on the observed fractional viscosity behavior, Eq. (1). Fig. 7 shows the viscocity dependence of the reaction rate for a higher temperature, again for the three values of the stiffness parameter, β. As expected, increasing temperature results in increasing reactivity and decreasing selectivity, as depicted by the increase in the slope, a. The increase in a is more prominent for smaller a values. Since increasing T is equivalent to a scaling-down of the potential surface, it leads to a decrease in the variation of the barrier height along the perpendicular coordinate and hence to a more Kramers-like behavior [11].

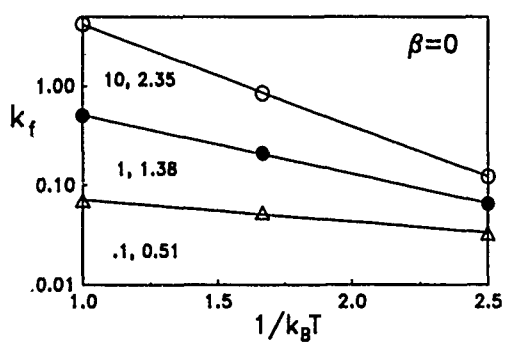


Fig. 8
Temperature dependence of the reaction rate coefficient. Lines are a fit to the Arrhenius expression, $\ln k_f = -E_A/k_BT$ + const. The two numbers next to each line denote the values of D_{00} and E_A, respectively

In Ref. [19b] the photoisomerization of *trans*-stilbene was studied as a function of temperature in isoviscous alcohols. A dependence of the activation energy, E_A, on viscosity was interpreted as a failure of the fractional viscosity behavior, Eq. (1). It is more appropriate to interpret the observed behavior as a temperature dependence of a. In Fig. 8 we have rearranged the data of Figs. 6 and 7 to yield Arrhenius plots at different D_{00} values. To these we have

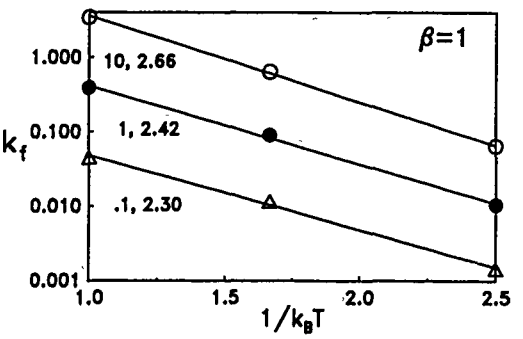


Fig. 9
Temperature dependence of the reaction rate coefficient for a "stiffened" potential surface. See caption of Fig. 8 for details

added data $k_BT = 0.4$. For large D_{00} (small viscosity) the activation energy is large, since the majority of the reactive flux proceeds directly over the relatively large barrier pertaining to the θ motion at $\phi = 0$. For small D_{00}, much of the flux goes via the indirect path which involves lower isomerization barriers, resulting in a considerably smaller activation energy. This behavior is in qualitative agreement with the experimental data shown in Fig. 3 of Ref. [19b].

The effect of stiffness on the viscosity dependence of the activation energy is shown in Fig. 9. As observed above (see Figs. 5 and 7), the variation of a with T diminishes as, with increasing stiffness, $a \to 1$. Indeed we find (Fig. 9) that for $\beta = 1$ the variations in E_A with viscosity are smaller than for $\beta = 0$. One might say that such variations [19b] are an indication of truly multidimensional dynamics. It is therefore expected that "stiff"-stilbene will show a viscosity independent E_A.

Table 3
Minima analysis on the potential surface of Fig. 2, Eqs. (2)–(3)

Minima	A	B	C	D
Relative energy[a]	0	−0.20	−0.504	−1.52
Coordinates[b]	(0, 0)	(0, 0.5)	(0.49, 0.5)	(0.49, 0)
Force-constants[c]	(19.5, 7.6)	(3.9, 24.4)	(10.7, 22.0)	(53.6, 10.0)

[a] Energies relative to the origin of the coordinates.
[b] θ and ϕ values in units of radian/π.
[c] $f_{\theta\theta}$ and $f_{\phi\phi}$ in units of energy/radian^2.

4. A Kinetic Model

In order to qualitatively understand the physics behind the effects demonstrated in Figs. 5–7, it is instructive to construct a simple kinetic model. We apply the model to the case where $\beta = 0$. The model involves four states, A, B, C and D, corresponding to the four distinct wells in the potential surface of Fig. 2. The coordinates (θ, ϕ), energies and force-constants $(f_{\theta\theta}, f_{\phi\phi})$ of the four states, as evaluated from the potential surface, Eqs. (2)–(3), are collected in Table 3. Between the four states one has transitions according to the following kinetic scheme

$$\begin{array}{ccc} B & \xrightarrow{k_3} & C \\ {\scriptstyle k_2}\uparrow\downarrow{\scriptstyle k_{-2}} & & \\ A & \xrightarrow[k_1]{} & D \end{array} \qquad (8)$$

In this scheme state A represents the initial state, A and B are the reactants while C and D are the products. This corresponds most closely to the dividing surface employed in our full calculation, with an absorbing boundary condition at the product states (C and D). There are two paths leading from initial state to products: The direct path with $k_{dir} \equiv k_1$ and the indirect path, involving the intermediate state B.

The effective rate coefficient for the indirect path, k_{ind}, is evaluated under steady-state conditions, assuming $d[B]/dt = 0$. This gives

$$k_{ind} = \frac{k_2 k_3}{k_3 + k_{-2}}. \tag{9}$$

The overall forward rate coefficient for the conversion of A to products (C ∪ D) is

$$k_f = k_{dir} + k_{ind}. \tag{10}$$

Since k_3 and k_1 will be proportional to D_{00}, hence to $1/\eta$, while k_2 and k_{-2} will be proportional to $D_{\phi\phi}$ and are hence constants, the overall viscosity dependence has the form

$$k_f = \frac{a}{1 + b\eta} + \frac{c}{\eta} \tag{11}$$

with a, b and c constants. This form indeed shows a $1/\eta$ behavior in the two extreme limits of $\eta \to 0$ and $\eta \to \infty$ (cf. Eq. (16) in Ref. [11]), with a transition region in between.

To evaluate k_f from Eqs. (9) and (10), we need to know the rate coefficients for the various steps in the reaction scheme, Eq. (8). We estimate these from the one-dimensional Kramers expression [1] which, in the diffusive regime for parabolic well and barrier, becomes [13]

$$2\pi k_B T k_i = (-f_{\varrho\varrho} f^{\dagger}_{\varrho\varrho} f_{\sigma\sigma} | f^{\dagger}_{\sigma\sigma})^{1/2} D_{\varrho\varrho} \exp[-\Delta V^{\dagger}/k_B T]. \tag{12}$$

Here $f_{\varrho\varrho}$ and $f^{\dagger}_{\varrho\varrho}$ are the force-constants at the reactants' well and the barrier, respectively. Both are evaluated along some one dimensional coordinate, ϱ ($\varrho = \theta$ or ϕ in the present case). In other words, the potential near the reactants (ϱ_0) and transition state ($\varrho^{\dagger}$) is approximated (up to a constant) as $\frac{1}{2} f_{\varrho\varrho}(\varrho - \varrho_0)^2$ and $\frac{1}{2} f^{\dagger}_{\varrho\varrho}(\varrho - \varrho^{\dagger})^2$, respectively. $\Delta V^{\dagger} \equiv V(\varrho^{\dagger}) - V(\varrho_0)$ is the classical barrier height along ϱ. $f_{\sigma\sigma}$ and $f^{\dagger}_{\sigma\sigma}$ are the corresponding well and barrier force-constants along the direction σ perpendicular to ϱ. Using the data in Tables 3 and 4, one can evaluate the rate coefficients k_i, i = 1, 2, −2 and 3, to be used in Eq. (9). These coefficients were multiplied by a statistical factor of 2, to account for the fact that each well in Fig. 2 leads to two equivalent wells, and collected in Table 5.

Table 4
Saddle point analysis on the potential surface of Fig. 2, Eqs. (2)–(3)

Saddle-point.	AD	BB	BC	CD
Relative energy[a]	3.46	1.99	0.49	1.23
Coordinates[b]	(0.26, 0)	(0, 0.28)	(0.26, 0.50)	(0.49, 0.30)
Force-constants[c]	(−36.8, 2.1)	(10.2, −19.9)	(−7.34, 29.9)	(25.6, −21.2)

[a] Energies relative to the origin of the coordinates.
[b] θ and ϕ values in units of radian, π for the saddle-point located in between the two indicated wells.
[c] f_{00} and $f_{\phi\phi}$ in units of energy/radian^2. Negative value indicates a maximum in the given direction.

Table 5
Rate parameters for the reaction scheme in Eq. (8)

Rate coefficient Transition	k_1/D_{00} A → D	$k_2/D_{\phi\phi}$ A → B	$k_{-2}/D_{\phi\phi}$ B → A	k_3/D_{00} B → C
Magnitude	0.0846	0.326	0.808	0.812

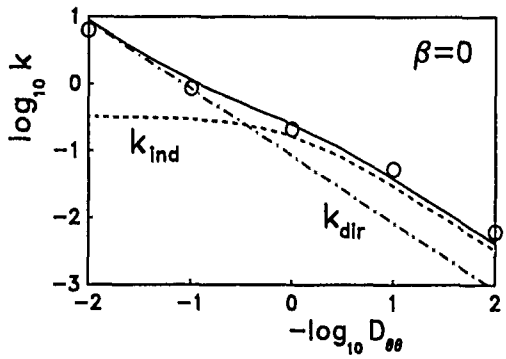


Fig. 10
Viscosity dependence of the reaction rate coefficient as calculated from the kinetic model, Eqs. (9) and (10). The overall rate coefficient (full curve) is the sum of the contributions from the direct and indirect pathways (dashed curves). Circles denote results from exact propagation, Table 1

The outcome of the kinetic approximation is shown in Fig. 10. While the direct rate coefficient is a straight line on a log-log plot, the indirect rate coefficient is constant at small viscosities and Kramers-like at large viscosities, see Eq. (11). When these two curves intersect, they give rise to the full curve, which shows the above mentioned transition between the two asymptotic limits. In simple chemical language, increasing viscosity induces a change of mechanism, from a direct to an indirect pathway. As the stiffness, β, is increased, the direct pathway dominates: The curve for k_{ind} drops until eventually is does not intersect the k_{dir} curve at all. Hence as $\beta \to \infty$ we get that $k_f \to k_{dir}$, with a pure Kramers behavior over the whole viscosity range.

5. Conclusion

We have extended the two dimensional diffusive barrier crossing model of Agmon and Kosloff [11] in several directions, with the following conclusions:

(a) Over an extended anisotropy range in the diffusion tensor, the rate coefficient shows a Kramers-like behavior in the two extreme limits with a transition region, which can be described by a fractional viscosity dependence, Eq. (1).

(b) As the stiffness of the potential in the perpendicular coordinate is increased, the transition region decreases until the dynamics become Kramers-like over the whole anisotropy range.

(c) In the regime where two dimensional dynamics is important, the power a in Eq. (1) increases with temperature. This is manifested by an Arrhenius activation energy which varies with anisotropy. As the stiffness of the potential increases, this temperature effect diminishes.

(d) A simple kinetic scheme, employing four states with transition rates evaluated from the two dimensional potential surface by the one-dimensional Kramers expression, produces a qualitatively good agreement with the exact solution of the two-dimensional Smoluchowski equation. Within this framework, the observed behavior is a consequence of a viscosity dependent change in mechanism.

It is interesting to note that, for anisotropy, $D_{\phi\phi}/D_{00}$, which is proportional to the macroscopic viscosity, all of the above conclusions are borne out by photochemical isomerization experiments:

(a) Experimental rate coefficients conform to fractional viscosity dependences over a limited viscosity range [15–17].

(b) "Stiff"-stilbene shows a $1/\eta$ viscosity dependence, as opposed to stilbene which shows the fractional viscosity dependence [15, 16].

(c) Stilbene has a viscosity dependent activation energy for its isomerization, the larger the viscosity the smaller the activation energy [19b].

(d) Isomerization of substituted stilbenes can be interpreted [22] with the aid of kinetic schemes which are similar to Eq. (8).

Although this qualitative agreement between model and experiment does not necessarily imply that the model is the correct description of experiment, it will be interesting to check its predictions experimentally. For example, one could check whether the activation energy for isomerization of "stiff" stilbene is viscosity independent. It would also be interesting to initiate measurements at extremely high viscosities in an effort to determine the asymptotic form of the viscosity dependence.

We thank Ronnie Kosloff, Abraham Nitzan and Wolfgang Rettig for fruitful discussions. Work supported by grant numer 86-00197 from the US-Israel Binational Science Foundation (BSF), Jerusalem, Israel. The Fritz Haber Research Center is supported by the Minerva Gesellschaft für die Forschung, Munich, FRG.

References

[1] H. A. Kramers, Physica *7*, 284 (1940); S. Chandrasekhar, Rev. Mod. Phys. *1*, 1 (1943).
[2] A. Nitzan, Adv. Chem. Phys. *70*, 489 (1988).
[3] B. J. Berne, M. Borkovec, and J. E. Straub, J. Phys. Chem. *92*, 3711 (1988).
[4] B. Bagchi, Int. Rev. Phys. Chem. *6*, 1 (1987).
[5] J. T. Hynes, Annu. Rev. Phys. Chem. *36*, 573 (1985); J. Stat. Phys. *42*, 149 (1986).
[6] P. Hänggi, J. Stat. Phys. *42*, 105 (1986); *44*, 1003 (1986).
[7] R. F. Grote and J. T. Hynes, J. Chem. Phys. *77*, 3736 (1982).
[8] E. Pollak, J. Chem. Phys. *86*, 3944 (1987).
[9] N. Agmon and J. J. Hopfield, J. Chem. Phys. *79*, 2042 (1983).
[10] M. Berkowitz, J. D. Morgan, J. A. McCammon, and S. H. Northrup, J. Chem. Phys. *79*, 5563 (1983); R. S. Larson, Physica *137A*, 295 (1986).
[11] N. Agmon and R. Kosloff, J. Phys. Chem. *91*, 1988 (1987). See also: A. D. Kaufman and K. B. Whaley, J. Chem. Phys. *90*, 2758 (1989).
[12] A. M. Berezhkovskii, L. M. Berezhkovskii, and V. Yu. Zitserman, Chem. Phys. *130*, 55 (1989); A. M. Berezhkovskii and V. Yu. Zitserman, Chem. Phys. Lett. *172*, 235 (1990); Physica *A166*, 585 (1990).
[13] M. M. Klosek-Dygas, B. M. Hoffman, B. J. Matkowsky, A. Nitzan, M. A. Ratner, and Z. Schuss, J. Chem. Phys. *90*, 1141 (1989).
[14] P. F. Barbara and G. C. Walker, Rev. Chem. Intermediates *10*, 1 (1988) and references therein.
[15] G. Rothenberger, D. K. Negus, and R. M. Hochstrasser, J. Chem. Phys. *79*, 5360 (1983).
[16] (a) M. Lee, A. J. Bain, P. J. McCarthy, C. H. Han, J. N. Haseltine, A. B. Smith III, and R. M. Hochstrasser, J. Chem. Phys. *85*, 4341 (1986); (b) M. Lee, J. N. Haseltine, A. B. Smith III, and R. M. Hochstrasser, J. Am. Chem. Soc. *111*, 5044 (1989).
[17] S. H. Courtney and G. R. Fleming, J. Chem. Phys. *83*, 215 (1985); S. K. Kim and G. R. Fleming, J. Phys. Chem. *92*, 2168 (1988); G. R. Fleming, S. H. Courtney and M. W. Balk, J. Stat. Phys. *42*, 83 (1986).
[18] V. Sundström and T. Gillbro, Chem. Phys. Lett. *109*, 538 (1984); Ber. Bunsenges. Phys. Chem. *89*, 222 (1985).
[19] (a) J. M. Hicks, M. Vandersall, Z. Babarogic, and K. B. Eisenthal, Chem. Phys. Lett. *116*, 18 (1985); (b) J. M. Hicks, M. T. Vandersall, E. V. Sitzmann, and K. B. Eisenthal, Chem. Phys. Lett. *135*, 413 (1987).
[20] (a) N. Sivakumar, E. A. Hoburg and D. H. Waldeck, J. Chem. Phys. *90*, 2305 (1989); (b) N. S. Park and D. H. Waldeck, J. Chem. Phys. *91*, 943 (1989); Chem. Phys. Lett. *168*, 379 (1990).
[21] (a) Ch. Gehrke, J. Schroeder, D. Schwarzer, J. Troe, and F. Voß, J. Chem. Phys. *92*, 4805 (1990); (b) J. Schroeder, D. Schwarzer, J. Troe, and F. Voß, J. Chem. Phys. *93*, 2393 (1990).
[22] W. Rettig and W. Majenz, Chem. Phys. Lett. *154*, 335 (1989); R. Lapouyade, K. Czeschka, W. Majenz, W. Rettig, E. Gilabert, and C. Rullière, to be published.
[23] P. M. Felker and A. H. Zewail, J. Phys. Chem. *89*, 5402 (1985).
[24] D. Beece, L. Eisenstein, H. Frauenfelder, D. Good, M. C. Marden, L. Reinisch, A. H. Reynolds, L. B. Sorensen, and K. T. Yue, Biochemistry *19*, 5147 (1980).
[25] J. Troe and K.-M. Weitzel, J. Chem. Phys. *88*, 7030 (1988).
[26] N. Agmon in "Tunneling", ed. J. Jortner and B. Pullman, Jerusalem Symposia on Quantum Chemistry and Biochemistry *19*, 373 (Reidel, Dordrecht, 1986).
[27] R. Kosloff and H. Tal-Ezer, Chem. Phys. Lett. *127*, 223 (1986).
[28] E. Pines, D. Huppert and N. Agmon, J. Chem. Phys. *88*, 5620 (1988).
[29] W. Nadler and K. Schulten, J. Chem. Phys. *84*, 4015 (1986).

Presented at the Discussion Meeting of the Deutsche Bunsen-Gesellschaft für Physikalische Chemie "Rate Processes in Dissipative Systems: 50 Years after Kramers" in Tutzing, September 10–13, 1990 E 7496

Rate Processes in Low Dimensional Chaotic Systems with Many Attractors

F. T. Arecchi

Phys. Dept. of the University and Istituto Nazionale di Ottica. Firenze

Chaotic Dynamics / Nonequilibrium Phenomena / Nonlinear Phenomena

Kramers' paper and its successive elaborations up to the last decade have considered the transition rate between two stable situations. In the language of system dynamics, we say that the process consists in the transition between the basins of attraction of two fixed point attractors. – Here I present four situations of transitions in non equilibrium systems explored experimentally, and which await a formal treatment in terms of a generalized Kramers transition rate theory.

I) Since 1967, with reference to Q-switched lasers, we have studied the decay out of an unstable state, exploring the passage time statistics in its first and higher order moments.
II) In the '80s we have been exploring situations of low dimensional chaos where two or more strange attractors coexist. The jumps from one to another are either noise induced jumps, or they are induced by a change in a control parameter which lowers the energy barrier separating the two attractors (crises).
III) Investigating a dynamics with competing unstable points we have shown evidence of Shil'nikov chaos. The identification is done in terms of the iteration map of the successive return times to a given surface of section. This may be considered as an extension of the passage time method to the case of multiple passages.
IV) We have given experimental evidence of "chaotic itinerancy", that is, of jump processes self triggered by the same dynamics. So far, the corresponding understanding is based only on numerical simulations. Since chaotic itinerancy has been observed in optical systems displaying space-time chaos, a short survey of these phenomena is presented for sake of completeness.

1. Introduction

At variance with the other contributions of this Discussion meeting, I do not present the calculations for an already established rate process, but rather I introduce novel rate processes whose theoretical understanding required a generalization of Kramers' approach.

Precisely I present four situations of transitions in non-equilibrium systems which have been explored experimentally by my research group, and which await a formal treatment in terms of a generalized Kramers transition rate theory.

I) Since 1967, with reference to Q-switched lasers, we have studied the decay out of an unstable state, exploring the passage time statistics in its first and higher order moments. This investigation is reviewed in Sec. 2.

II) In the '80s we have been exploring situations of low dimensional chaos where two or more strange attractors coexist. The jumps from one to another are either noise induced jumps, or they are induced by a change in a control parameter which lowers the energy barrier separating the two attractors (crises).

In both cases the power spectrum has a low freuency part (jump spectrum) independent from the chaotic spectrum which accounts for the decay of correlations within a single attractor. This is discussed in Sec. 3.

III) Investigating a dynamics with competing unstable points we have shown evidence of homoclinic and heteroclinic orbits and Shil'nikov chaos. The identification is done in terms of the iteration map of the successive return times to a given surface of section. This may be considered as an extension of the passage time method to the case of multiple passages. Shil'nikov chaos and its representation in terms of time maps is discussed in Sec. 4.

IV) Sec. 6 is devoted to describe the recent experimental evidence of "chaotic itinerancy", that is, of jump processes self triggered by the same dynamics, without external noise or parameter modulation. So far, the corresponding theoretical understanding is based only on numerical simulations. Since chaotic itinerancy has been observed in optical systems displaying space-time chaos, a short survey of these phenomena is presented for sake of completeness in Sec. 5.

What is common to cases II to IV, is that they refer to cases of deterministic chaos in dissipative systems, characterized by two features, namely, i) the dynamics is low-dimensional, that is, the corresponding attractors can be embedded in low-dimensional ($d < 10$) phase space and ii) many attractors coexist for the same parameter values.

Feature i) means that the system can be modelled by a small number of non-linearly coupled O.D.E.'s (ordinary differential equations). Even if the physics refers to a distributed field ruled by P.D.E.'s (partial differential equations), that means that the relevant motion can be confined to low-dimensional manifolds. Feature ii) means that repeated preparations of the physical system do not lead to the same attractor, since in general an ensemble of initial conditions is spread over many basins of attraction. As said in Sec 3, even in the evolution from a fixed initial condition, the trajectory can belong successively to different attractors, either because activation by external noise has violated the uniqueness theorem, allowing a jump across a basin boundary, or because external modulation of a control parameter has induced a "crisis" whereby the attractor hits the basin

 © VCH Verlagsgesellschaft mbH, W-6940 Weinheim, 1991 0005-9021/91/0303-0286 $ 3.50+ 25/0

boundary and can go across it without an activation (this would be the equivalent of barrier-less transitions).

A new phenomenon, recently introduced theoretically and just observed is that of "chaotic itinerancy". It consists in the successive visit of different slow manifolds with a chaotic dynamics within each of them, persisting for a time much longer than the transition time from one to another. This stems form the interplay of a rather small number of degrees of freedom, without any added noise.

In conclusion this communication addresses the question whether a suitable extension of Kramers' theory might yield the transition rates from one to another slow manifold and the persistence time within each of them.

Due to the novelty of the phenomena here reported and to the lack of a formalized, Kramers type, rate treatment, the presentation is rather sketchy and introductory. I sincerely hope that it will stimulate the theoretical investigation.

2. Rate Processes in Optical Non-equilibrium Systems

In Sec. XI of their comprehensive review on "Reaction rate theory", Hänggi, Talkner and Borkovec [1] devote a short remark to rate theory in non-equilibrium systems, and particularly to mean first passage time in the decay of initially unstable states. Motivated by my old time acquaintance with such a problem [2], in the late seventies I addressed the problem of rate processes in terms of first passage time statistics, extending the acquisition not only to the mean, but also to higher order moments [3, 4]. Such a tool was applied by my group to electronic nonlinear circuits [4] and later used to explore transitions in class A lasers [5] by Roy et al. [6] and then by Mecozzi et al to semiconductor lasers [7] and by my group to CO_2 lasers [8]. In these two latter cases, dealing with class B lasers, the corresponding dynamics was no longer simply modeled as a one dimensional motion within a potential well.

Let me summarize the main results.

The first observation of a statistical spread in the leading edge of a Q-switched laser pulse was associated with the appearence of a large peak in the variance of the transient photon distribution [2]. This fact was explained in terms of an approximately deterministic decay out of macroscopic unstable state, to be averaged over the statistical distribution of the initial states. Such behavior was later shown to be peculiar of quenching phenomena in macroscopic systems, such as spinodal decomposition in thermodynamic systems [9].

As stressed by Haake [10], the phnomenon is the transient counterpart of the stationary fluctuations at the critical point of a thermodynamic phase transition (or more generally at the bifurcation points in a nonlinear dynamics which display the same formal features of asecond-order phase transition). Precisely, if we call N the number of degrees of freedom of a macroscopic system decaying out of an unstable state, the initial fluctuations are of the order of $1/N[0(1/N)]$, however, in the linear part of the decay they are amplified by $0(N)$, hence the relative fluctuations are of $0(1)$.

The assumption of deterministic evolution out of a spread initial state neglected the role of fluctuations along the build up with respect to the initial ones. The relation between the two types of noise were explored in a series of papers by Suzuki, summarized at the XVII Solvay Conference on Physics [11a]. In that conference, a remark by P. Martin to Arecchi [11b] reopened the question of the nature of these large fluctuations.

Upon Martin's remark a quest for a discrimination between fluctuations on the initial condition and those along the path led a new observation method, based on the statistics of passage times at a given threshold [3, 4]. From this method it resulted clearly that, when a laser is suddenly switched far above threshold, the fluctuations are mainly due to the initial spread, as already guessed in Ref. [2]. This method of passage time provided an important difference between gas and dye lasers, since in the latter case it permitted detection of the role of pump fluctuations as "noise along the path" [6].

Both the He–Ne and the dye laser have in common a population decay rate large with respect to the photon decay rate (so called class-A lasers [5]). Hence the population adiabatically follows the intensity changes, with a consequent reduction of inversion as the cavity losses are lowered. This adiabatic following forbids any overshoot in the laser intensity. Indeed, Q-switching in class-A lasers is characterized by an intensity monotonically increasing up to an asymptotic value. In contrast, when the population decay is lower than the photon decay (class-B lasers) the initially large population storage provides a large intensity pulse by stimulated emission, and only later the population feels the slower depletion channels (either spontaneous emission in ruby and semiconductors, or collisional deexcitations in CO_2). This explains why, after a sudden loss reduction, class-B lasers release giant intensity pulses well above the asymptotic value, whereas class-A lasers do not.

We generate transient dynamics in a single-mode CO_2 laser by switching an intracavity modulator from absorption to transparency in a time shorter than the build up time of the giant pulse. We summarize below the main results [8].

(i) The average buildup time is around 3 μs. The average spread of the δt leading front (jitter) is around 0.2 μs.

(ii) If we consider the time t_1 necessary to reach a photon number n_1 still below the saturation value n_s, the laser dynamics up to t_1 can be taken as linear. In this linear regime, a simplified version of pasage time statistics leads to a very powerful relation which permits evaluation of the effective seeding photon number at the onset of the dynamics in terms of the threshold photon number n_1 and of the ratio of the average $\bar{t}_1$ the spread δt. Our method [8] is self-calibrating, in the sense that the second moment of the observed statistics provides the amplification gain without any previous calibration, and the higher-order cumulants provide the error bars of the experimental points.

(iii) We can detect a few initial photons in a laser cavity by linear optical amplification. The reported amplification factors are of the order of 10^8, but in principle they could be larger. The linearity of the amplification process is pre-

served up to the saturation photon number, which is over 11 decades in our case.

(iv) While in a class-A laser the photon population reaches a maximum and remains clamped to that value, in a class-B laser the photon-population inversion is practically decoupled from its thermal reservoir, and its evolution depends only on the coupling with the radiation field.

3. Chaos with Many Attractors: Noise Induced Jumps and Crises

3a. Noise Induced Jumps and 1/f Spectra

In the pioneering work on chaos in a single mode laser [12] we show that modulating the losses of a class B, ruled by two equations, at a frequency close to a nonlinear resonance intrinsic of the system (around 60 kHz) chaos is reached via a sub-harmonic route.

Furthermore at $f = 63.85$ kHz a new feature appears, namely the coexistence of two independent stable attractors, one of period 4 ($f/4$) and the other of period 3 ($f/3$) (Fig. 1). This bistable situation has nothing to do with the common optical bistability where to dc output amplitude values appear for a single dc driving amplitude. We call this coexistence of two attractors "generalized bistability". More generally, $1/f$ type low-frequency spectra, that is, power spectra as $f^{-\alpha}(\alpha = 0.6-1.2)$, appear when the following conditions are fulfilled: (i) There are at least two basins of attraction; (ii) the attractors have become strange and any random noise (always present in a macroscopic system) acts as a bridge, triggering jumps between them. These jumps have the f feature. In the region of bistability (see Fig. 1) we have increased the modulation amplitude up to the point where the two attractors have become strange. Fig. 2 shows the sudden increase in the low-frequency spectrum. The divergent part has a power-law behavior $f^{-\alpha}$ with $\alpha \simeq 0.6$.

Let us show how addition of random noise in a nonlinear dynamical system with more than one attractor may lead to $1/f$ spectra, provided that the basin boundary be fractal. This shows that combining the features leading to deterministic chaos with a random noise is somewhat equivalent to a double randomness and we call "hyperchaos" such a situation. Indeed random-random walks in ordinary space,

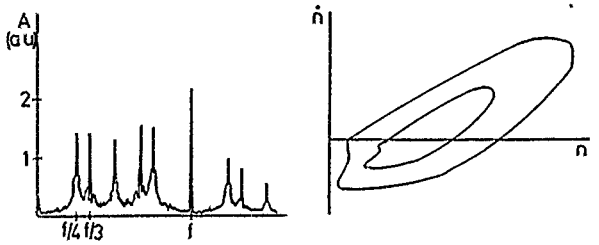


Fig. 1
Modulated CO_2 laser: power spectra and phase portrait $(n, \dot{n})$ where n is the photon number. $f = 63.85$ kHz. Experimental evidence of generalized multistability (coexistence of two independent attractors). The power spectrum shows that those attractors correspond to $f/3$ and $f/4$ subharmonic bifurcations, respectively; in phase space we see independent loop. The multiple winding (corresponding to period 3 and 4, respectively) is masked by the particular projection.

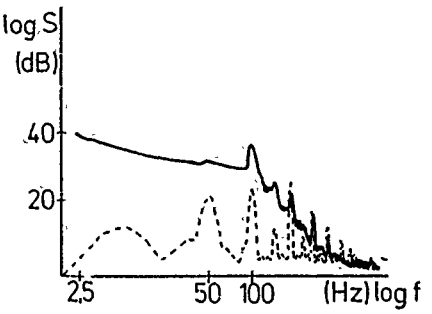


Fig. 2
Experimental power spectra in the case of two attractors, without noise (dashed line), and with noise (solid line). Notice that this low frequency range is two decades below the high frequency spectra of Fig. 1. The solid spectrum (noise activated) shows a power law component from 20 to 40 dB above the dashed (jump free) spectrum

as diffusion in disordered systems, have shown a $1/f$ behavior [13]. Thus, hyperchaos here introduced is a random-random walk in phase space, where in fact one of the two sources of complex behavior is due to the fractal structure arising from deterministic dynamics.

To evaluate the impact of the following arguments, we premise some historical remarks on $1/f$ spectra in nonlinear dynamics.

Some years ago we discovered [14] that in a nonlinear dynamical system with more than one attractor, introduction of random noise induces a hopping between different basins of attraction, giving rise to a low frequency spectral divergence, resembling the $1/f$ noise well known in many areas of physics. Such a discovery was confirmed by the laser experiment implying two coexisting attractors already reported and later the effect was observed in other areas as e.g., Josephson tunnel junctions [15].

The effect was questioned with two objections:

a) a noise induced jump across a boundary leads to a telegraph signal, hence to a single Lorentzian spectrum [16a].

b) a computer experiment yielded a power law only over a limited spectral range [16b].

The questions were answered [16c] with a statement of the empirical conditions under which the $1/f$ spectra appeared, namely:

(i) coexistence of a least two attractors,
(ii) presence of noise,
(iii) some "strangeness" in the attractors.

As a matter of fact this third condition was rather vague. To make it more precise, two theoretical models were explored, namely, a one dimensional cubic iteration map with noise [17] and a forced Duffing equation with noise [18].

The numerical evaluation of Ref. [18] showed that for some control parameters the boundary between basins of attraction was an intricated set of points, through which it was impossible to draw a simple line. In such cases the noise was most effective in yielding low frequency spectra $1/f$-like.

On the other hand a fundamental logical approach to the $1/f$ problem was based on the composition of a large number

of Lorentzians (or elementary Markov processes with exponential decay) whose weights are log-normally distributed [19], thus fulfilling the relation

$$\int_{\gamma_1}^{\gamma_2} \frac{\gamma}{\omega^2+\gamma^2}\, p(\gamma)\, d\gamma \simeq \text{cost.} \times \frac{1}{\omega} \tag{1}$$

provided $p(\gamma) \sim 1/\gamma$, and for the frequency range $\gamma_1 \ll \omega \ll \gamma_2$. Thus, this suggested that the boundary structure was the real responsible for a large number of decay constants (possibly log-normally distributed).

In the meantime, the fractal, structure of a basin boundary for chaotic dynamics was investigated [20]. This means the following. As the phase point wanders within one basin of attraction, if we draw a sphere around the point defining its distance from the other basin of attraction, the radii of these spheres are distributed with all scale lengths, according to the self similar structure of the fractal boundary.

Based on the above considerations, we have built an elementary model for the motion of the phase point within a fractal basin boundary under the presence of random noise [21]. We model the boundary region of two basins of attraction A and B as two adjacent one-dimensional lattices of sites. Suppose we start from site i. At each discrete time step, if i belongs to A ($i = i_A$) it moves one step forward on the same lattice [$i_A \rightarrow (i_A + 1)$] and if it belongs to B it goes one step beckward [$i_B \rightarrow (i_B - 1)$]. In the absence of noise, one the motion has started on one basin, it will remain on it forever. In the presence of noise, at each time step there is a finite probability of a "cross" jump at the same lattice site, from stripe A to B: $i_A \rightarrow i_B$.

We call L the maximum size of the boundary region (distance between the two lattices A, B) and $l_i \leq L$ any of the possible sizes of the fractal set. At each time step, the probabilities of permanence and jump are respectively

$$\begin{aligned} P_{AA}\, P_{BB} &= l_i/L \\ P_{AB}\, P_{BA} &= 1 - l_i/L\,. \end{aligned} \tag{2}$$

To build a self-similar structure we allow l_{i_k} to sacale as $l_{i_k}/L = (1/2)^{V(i_k)}$ where $V(i_k)$ is a natural number sorted randomly for each site ($i = -\infty$ to ∞, k = A, B). To deal with a real numerical experiment we consider finite sequences of N sites (e.g., $N = 10^3$) and we truncate the fractality by imposing $0 \leq V(i_k) < F$. Here, F is a finite integer denoting the maximum partitioning $(1/2)^{F-1}$, that is, the ultimate resolution of the measuring device in appreacing the fractal structure of our set. With all this in mind, for each evolution we extract a double sequence of N integers randomly distributed between 0 and $F-1$, and denote each site i_k by the corresponding number $V(i_k)$. This means that we have attributed to each site an "area of respect", that is, a specific separation l_{i_k} from the other attractor, with l_{i_k} depending on $V(i_k)$ as shown above. We start, e.g. on the basin A from $i_A = N/2$.

At this step, to account for a suitable noise yielding the permanence and jump probabilities (2), we generate a random number γ uniformly distributed between 0 and 1. If $\gamma \leq (1/2)^{V(i_A)}$, then at the next time the point goes to $i_A + 1$ on attractor A; if $\gamma > (1/2)^{V(i_A)}$, then the point jumps instantaneously to site i_B and at the next time it goes to $i_B - 1$ on attractor B.

By measuring the position coordinate, taking the Fourier transform and squaring it, we can build the power spectra, that is, the transforms of the position correlation functions.

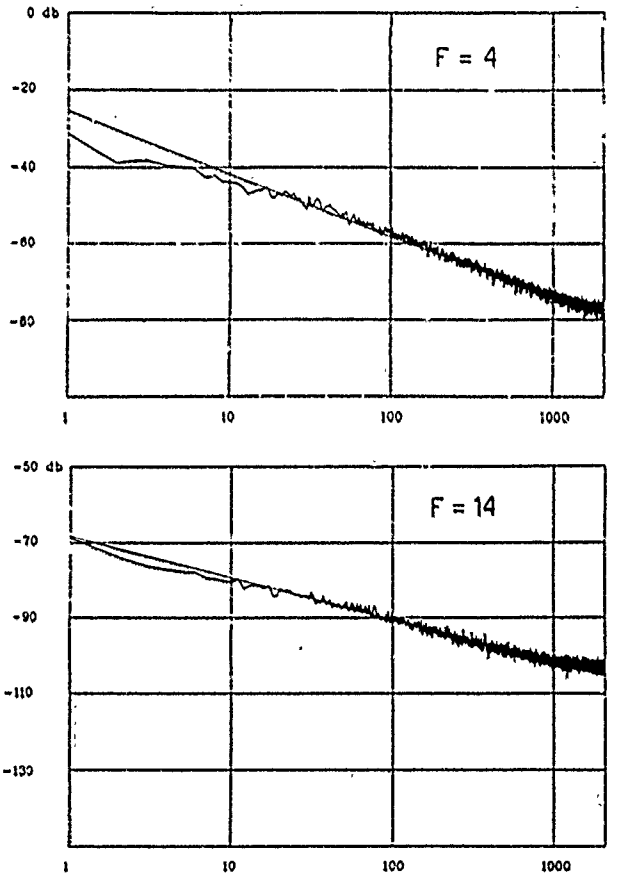


Fig. 3
Deterministic motion on two one dimensional lattices with random mutual separations and each site, at with possible noise induced jumps. Power spectra (vertical) vs. frequency (horizontal) in log-log scale. Wavy lines: measured spectra, straight lines: best fits, whose slopes α are 1.7 ($F = 4$), and 1.1 ($F = 14$)

In Fig. 3 we show two power spectra for $F = 4$, and 14 respectively. In fact, we have measured spectra for all integer values of F between 4 and 14, but we just report two samples over slightly more than three frequency decades. The sequence shows that, as the fractality increases, the slope of the log-log plot goes from about 2 (single Lorentzian) to about 1 ($1/f$ spectrum). The Lorentzian ($\alpha = 2$) of the random telegraph model is easily recovered for $F = 1$, thus showing that noise induced jumps across a regular line boundary fulfill the intuitive expectation of a single decay rate. An analogy with the random-random walk [13] is easily drawn. Indeed our motion is bound with an r.m.s. deviation going from about $\sqrt{t}$ to $|\log t|^2$ as the fractality F increases from 4 to 14, according to Sinai.

3b) Spontaneous Inter-attractor Transitions (Crises)

In nonlinear dynamics it is generally possible to have collisions between unstable orbits and chaotic attractors, leading to interior, boundary and external crises [22,23]. The former one preserves the chaotic attractor enlarging monotonically its basin, the second one destroys the attractor by sweeping off its basin of attraction, while the latter one enlarges discontinuously its basin of attraction. The presence of those different crises in the system depend on the amount of dissipation [22]. Such crises have been observed experimentally in a variety of systems [24]. Boundary crises in the modulated laser have been observed by Glorieux et al. [25].

Working on the modulated CO_2 laser [12] we have given experimental evidence of the three types of crises which are due to collisions among strange attractors and unstable periodic orbits created in saddle node bifurcations [26]. These collisions are also responsible for the existence of isles that can be reached only by hard mode excitation and for periodic windows that separate different regions.

Furthermore, from the shape and size of the multistable region as a function of the modulation amplitude, m, we draw a connection between the amount of attractor overlap in parameter space and the volume contraction rate in phase space, that is, the dissipativity of a dynamical system.

4. Shil'nikov Chaos: How to Characterize Homoclinic and Heteroclinic Behavior by Return Time Maps

Shil'nikov dynamics [27] corresponds to orbits asymptotic to an unstable saddle focus in at least a 3D space. Limiting to a 3D space let us call $\alpha \pm i\omega$ the pair of complex eigenvalues on the stable ($\alpha < 0$) manifold and $\gamma > 0$ the eigenvalue in the unstable direction orthogonal to the plane.

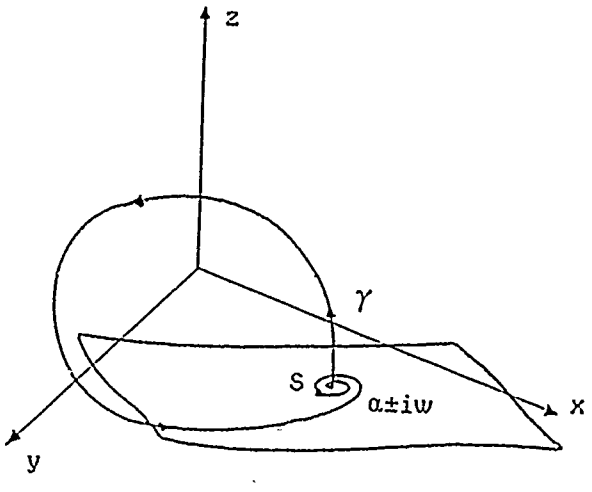


Fig. 4
Schematic representation of a trajectory in Shil'nikov dynamics

Let us consider a dynamics where all fixed points are unstable, within a given range of control parameters. We call such situation a regime of competing instabilities [28]. In physical implementations we can adjust [29] the control parameter in order to isolate a non zero set of initial conditions such that trajectories departing from there approach asymptotically the unstable saddle focus and remain at a finite distance from all other fixed points. In such a case, under the Shil'nikov condition [27]

$$|\alpha/\gamma| < 1 \tag{3}$$

the motion becomes chaotic.

A single orbit of this type spiralling around an unstable saddle focus S is qualitatively sketched in Fig. 4.

With the understanding that the only interesting dynamical features occur around point S we obtain a global description by just studying the linearized dynamics within a small box around S (Fig. 5).

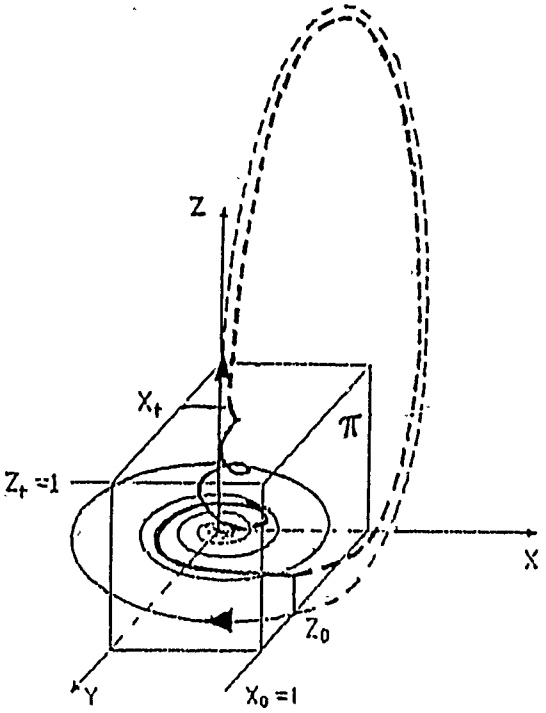


Fig. 5
Construction of unit box leading to the unidimensional map (6) through the linearization of the flow around the saddle focus

In Fig. 5, we orient the three axes along the eigenvectors with $x-y$ coinciding with the stable plane and z being the expanding direction. We take the π plane (vertical plane of equation $x = 1$ containing a face of the cube) as the Poincaré section and we calculate the return map for the coordinate z. Starting at $t = 0$ at $z = 0$ on $x = 1$ (y is irrelevant for the following considerations) the phase point leaves the upper cube side $z = 1$ at time τ such that

$$1 = z_0 e^{\gamma\tau}$$

from which it results

$$\tau = -\frac{1}{\gamma}\log z_0 . \tag{4}$$

The horizontal coordinate x evolves over the same time as

$$x(\tau) = e^{-\alpha\tau}\cos\gamma\tau \tag{5}$$

since the initial condition is $x(0) = 1$. Neglecting a phase shift due to the y position, we constrain the motion external to the box to a rigid translation (see dashed trajectories).

$$y(\tau) \rightarrow z_1$$

besides an offset ε added at each turn and which may be considered as a second control parameter, the first one being the ratio $|\alpha/\gamma|$. Using relation (4) and writing z as z_{n+1} and z_0 as z_n we obtain the return map

$$z_{n+1} = z_n^{\alpha/\gamma}\cos\left(\frac{\omega}{\gamma}\log z_n\right) + \varepsilon \tag{6}$$

which describes the homoclinic orbits.

The map (6), even though representing a sensible global description, may provide a poor experimental criterion whenever the z coordinates on the π plane are clustered in a small region. A lack of experimental sensitivity appears in experimental return maps which do not display the nice features that Eq. (6) provides for the theory. Such was the case for the Belouzov Zabotinski reaction [3]. On the other hand, the above behavior appears rather universal whenever one can isolate a spiral type orbit, as it occurs in Lorenz or Roessler chaos [31].

In dealing with a quantum optical experiment we introduced a more sensitive dynamical indicator [32, 33]. Based on the logarithmic relation between position z on the π plane and times τ that the orbits take to return to that plane, and assuming that the relevant time is that spent in the box of Fig. 5, map (6) transforms via relation (4) into a return map for orbital times. We rescale τ as $T = \gamma\tau = -\log z$ and obtain

$$\begin{aligned} T_{+1} &= -\ln[\exp(-\lambda/\gamma T_n)\cos(\omega/\gamma T_n) + \varepsilon] \\ &= -\ln[\phi(T) + \varepsilon]\,. \end{aligned} \tag{7}$$

Comparison of Eqs. (6) and (7) shows the enhanced sensitivity to fluctuations of the T map with respect to the z map. Indeed, suppose that the offset ε from homoclinicity is affected by a small amount of noise. The sensitivies of the two maps to such a noise are given, respectively, by $\partial z/\partial\varepsilon = 1$ and

$$\partial T/\partial\varepsilon = [\phi(T) + \varepsilon]^{-1}\,. \tag{8}$$

This sensitivity factor acts as a level arm whenever $\phi(T) + \varepsilon$ becomes very small. Note the following: (1) This is not deterministic chaos; in fact, large fluctuations can be expected even for a regular dynamics, implying a fixed point T^*, (2) It is not associated with the homoclinicity condition $\varepsilon = 0$; in fact, for finite ε there may be a T^* such that $\phi(T^*) + \varepsilon = 0$.

Since a homoclinic orbit is the dynamic counterpart of repeated decays out of an unstable state, the result is like repositioning the initial condition in an experiment on a single decay. Here the repetition is automatically provided by the contracting motion asymptotic to the stable manifold. As a consequence, superposed upon the deterministic dynamics (either regular or chaotic), the high sensitivity (Eq. (8)) may provide a broadening of the T maps not de-

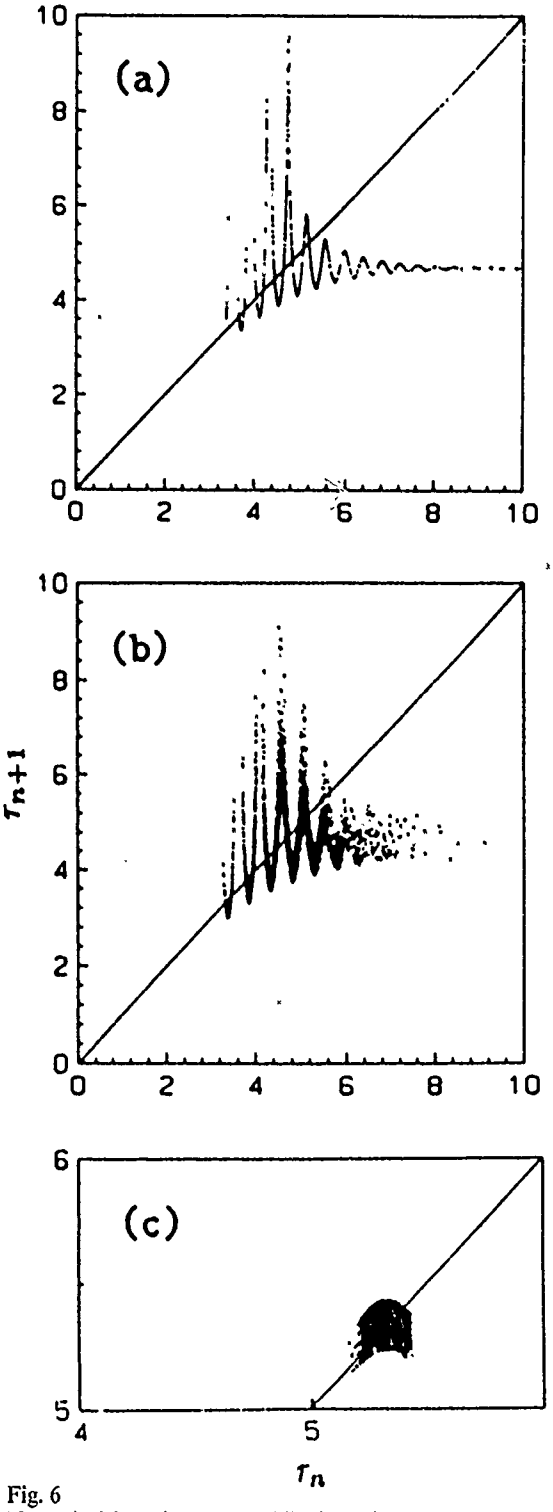


Fig. 6
Numerical iteration maps Shil'nikov chaos. Parameter values: $\omega/\gamma = 13.0$, $\alpha/\gamma = 0.986$, $\varepsilon = 0.01$. (a) and (b), T maps without and with noise $\delta\varepsilon = 10^{-2}$, respectively. (c) Stable fixed point of the regular dynamics, broadened by a noise $\delta\varepsilon = 10^{-2}$

tectable in the z maps whenever noise in the offset ε is present.

In fact, the model description $\dot{x} = F(x)$ of a large system in terms of a low-dimensional dynamic variable x is just an ensemble-averaged description, and residual fluctuations on position x must be considered at some initial time, even though the successive evolution is accounted for by a deterministic law. In our case such a fluctuation is a stochastic spread $\delta\varepsilon$ on the offset ε of the position z.

As shown in Fig. 6, the same amount of $\delta\varepsilon$ in Eqs. (6) and (7) leaves the z maps unaltered, while it strongly affects the T maps. If we specialize the map parameters α, γ, ω, and ε to a regular orbit (fixed points both in z and T spaces), introduction of $\delta\varepsilon$ does not broaden the z point, while the T point broadens.

For example, the values $\alpha/\gamma = 0.98$, and $\varepsilon = 0.01$ yield one fixed point $T^* = 5.327$, with a sensitivity $\delta T^*/\delta\varepsilon = 182$ (Fig. 6 (c)), Note that the noise effect reported here has nothing to with additive noise effects on return maps [34]. Indeed, the latter effects refer to the scaling behavior near stationary bifurcations, whereas our data refer to transient fluctuation enhancement, and they do not leave a permanent mark (such as an orbital shift or broadening).

Thus, while Shil'nikov chaos is a deterministic effect described on average by the backbone of the z or T maps, the superposed thickening is a noise effect peculiar to T maps undetectable in z maps. This new effect is a specific indicator of intrinsic fluctuations, and it permits a demarcation line to be drawn between a real-life experiment and a model simulation, from which this second feature is absent.

In order to explore the regular behavior of these closed orbits, we take the fixed point of map (7).

$$T^* = \ln[\exp(-\lambda/\gamma T^*)\cos(\omega/\gamma T^*) + \varepsilon]\,. \tag{9}$$

Eq. (9) gives a stable fixed point, provided Shil'nikov condition is violated. Solving transcendental Eq. (9) and plotting the Poincaré frequency $1/T$ versus the control parameter ε, yields two different items, namely

i) a staircase region implying histeresis cycles
ii) a logarithmic divergence for small ε

After having summarized the main features of Shil'nikov chaos we describe the corresponding experiments. As a matter of fact, things have gone in the reverse order: we first found evidence of spiral type orbits, including large time fluctuations, or regular periods scaling with the control parameter as i), ii) above; then we looked in the theoretical literature and found that, using the orbital period as a dynamical indicator more sensitive than Poincaré position, we could nicely describe what had been previously treated only at a qualitative level, in terms of a symbolic dynamics coding the number of spirals around the saddle focus [30].

Our experimental setup consists of a single mode CO_2 laser with an intracavity electro-optic modulator. A signal proportional to the laser output intensity is sent back to the electro-optic modulator [35]. Single mode CO_2 lasers have a dynamic behavior described by two coupled differential equations, one for the field amplitude and the order for the

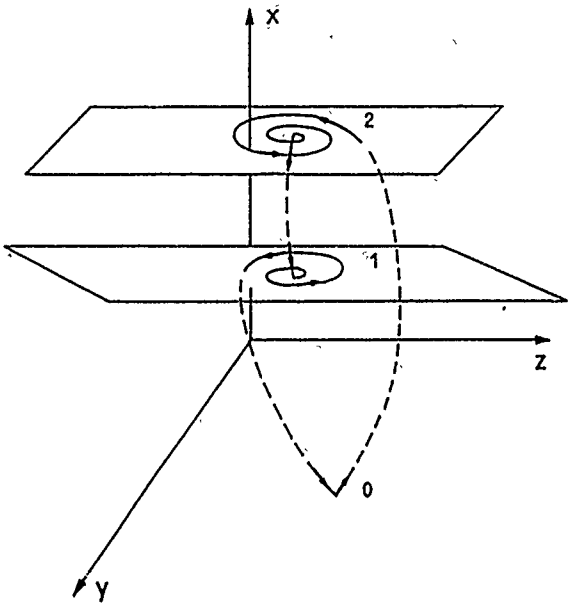


Fig. 7
Schematic view of a trajectory in the phase space when the dynamics is affected by all three unstable stationary points.

population inversion, the fast polarization being adiabatically eliminated from the complete set of Maxwell-Bloch equations. Thus, the presence of feedback introduces a third degree of freedom. With suitable normalizations such a system is described by three first-order differential equations for the laser intensity $x(t)$, the population inversion $y(t)$, and the modulation voltage $z(t)$. Keeping all other parameters fixed, the dynamics is controlled by varying a bias voltage B in the feedback loop. In Fig. 7 we present a schematic view of the trajectory in the three-dimensional space, obtained by a linear stability analysis of the motion around the stationary points, and qualitative connections between the linear manifolds (dashed lines).

From an experimental point of view we are able to visualize $(x - z)$ phase-space projections, obtained by feeding onto a scope the photodetector signal proportional to the laser output intensity $x(t)$ and the feedback voltage $z(t)$. This phase-space projection consists of closed orbits visiting successively the neighborhoods of the three unstable stationary points 0, 1, and 2.

The local chaos around point 1, established at the end of a subharmonic sequence, has been characterized by standard methods as power spectra and correlation dimension measurements [35]. The competition of the three instabilities in controlling the global features of the motion was described in Ref. [29]. There $|\alpha/\gamma|$ was adjusted major then one showing regular behavior and experimental evidence of items i) and ii) above. Here we adjust the control parameters in order to have a dominance of the saddle focus, so that the motion consits of a quasi homoclinic orbit asymptotic to it.

In Fig. 8 we report experimental plots of the laser intensity vs. time for two slightly different conditions. Fig. 8b) shows clear evidence of a homoclinic orbit in the two long transients, which provide a lengthy permanence in a phase space

region of almost constant intensity. This appears more clearly in the corresponding phase space projections (Fig. 9 and b)). For comparison we give in Fig. 9c) a photographic exposure (over 1 s) of 30000 orbits as that of Fig. 9a), to show the stability of shape.

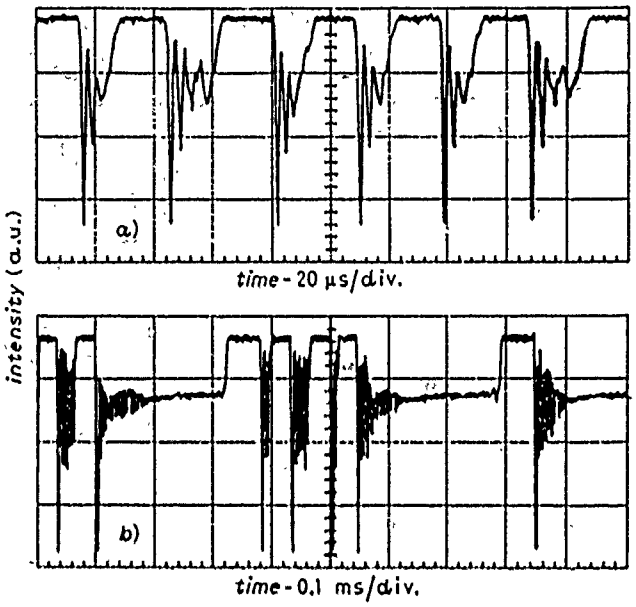


Fig. 8
Time plots of the laser intensity in the regime of Shil'nikov chaos. a) and b) refer to two different gains of the feedback loop. b) shows two long transients corresponding to a large number of small spirals around the saddle focus

Before we discuss comparison with Shil'nikov theory, a crucial question arises: how much of the spread in the return times has to be attributed to point 2 or 0? Indeed, we have quasi-heteroclinic orbits visiting the surroundings of the two unstable points 2 and 0. But in our experimental situation the dynamics can be assimilated to a quasi-homoclinic orbit around point 2, which is thus mainly responsible for the spread in return times. This is easily proved my measuring the spread T in the residence times T_0 around 0 (zero intensity stripes) and the spread T_2 in the residence times T_2 around 2 (complementary stripes, such that $T_0 + T_2$ is the total orbital time). In Fig. 8, which shows typical time sequences used to build the two averaged relative spreads are approximately

$$(\Delta T_0)/(T_0) \sim 14\%, \quad (\Delta T_2)/(T_2) \sim 80\%,$$

$$(\Delta T_0)/(T_0) \sim 40\%, \quad (\Delta T_2)/(T_2) \sim 250\%.$$

The comparison shows that point 0 introduces a perturbation around 14% with respect to pure homoclinicity, that is, the orbital regularity is ruled mainly by point 2. Thus a theoretical approach to our experiment in terms of homoclinic chaos appears justified.

We measure the time spacings by setting a threshold circuit near the top of the largest peak of the intensity signal.

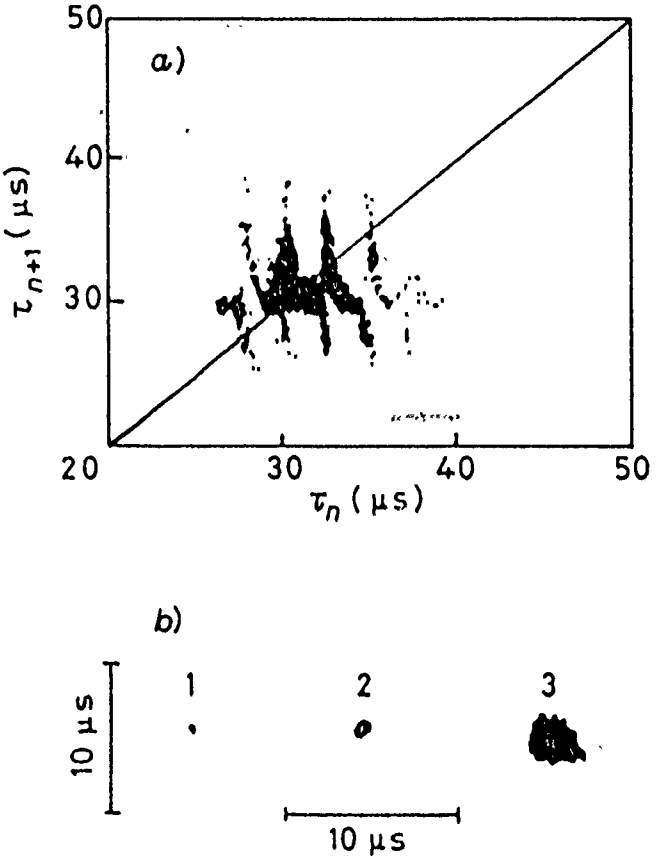


Fig. 10
Experimental iteration maps of the return times. a) refers to Fig. 8a). b) shows the maps corresponding to regular periodic situations, namely, 1) an electronic oscillator, 2) the laser in a regular periodic regime and 3) the laser just at the onset of the instability but still with a regular period

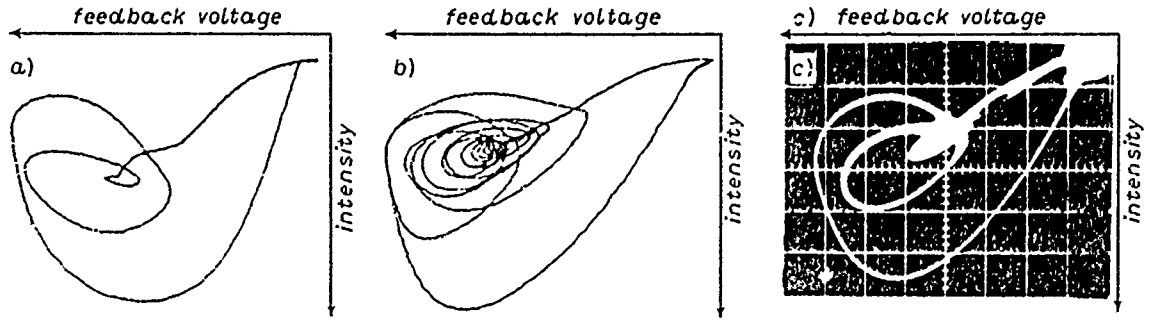


Fig. 9
Phase space projections $x - z$ (laser intensity - feedback voltage). a) and b) are single orbits obtained by a digitizer, referring to the same parameters of Fig. 8a) and b), respectively. c) is the superposition of 30000 orbits of type a)

A time-to-amplitude converted (TAC) yields the sequence T_i of successive time spacings, which is then classified as a statistical distribution by a multichannel pulse height analyser, or stored in a digitizer, so that correlation functions or iteration maps can be sorted out.

The statistical distribution of return times is a broad featureless curve which does not offer curves on the ordering of T_i. On the contrary, the iteration map (T_{i+1} vs. T_i) displays a regular structure (Fig. 10a)). To check whether we are in the presence of one-dimensional (1D) iteration map, and the remaining thickness is due to the observation technique, or the map is more that 1D, we report in Fig. 10b) the iteration maps corresponding to three regular situations.

In the absence of fluctuations in T_i they should be point-like (the image of a stable fixed point). In fact 1) corresponds to an electronic oscillator and it just shows the resolution of the TAC, 2) corresponds to the laser in a regular periodic regime away from the Shil'nikov instability, and 3) corresponds to the laser on the verge of the instability but still with a regular period. In this last case, the fluctuation associated with the nearby transition shows that, even without chaos in the return time, the close approach to an instability point introduces a fluctuation enhancement, which has no theoretical counterpart in the current treatment of deterministic chaos. To deal with this broadening, the dynamical equations should include a statistical spread in the injection coordinate at the Poincaré section near the saddle focus, to account for the macroscopic character of the experimental system. As it was shown in Refs. [2,3], even though this spread has no relevance on the average dynamics, it contributes a large transient fluctuation whenever the system decays from an unstable point.

5. Space Complexity in Nonlinear Optics

In chemical relations and in fluids it is straightforward to scale up the system size from small to large cells, thus making it possible to explore in many ways the passage from systems coherent (fully correlated) in space to systems made up of many uncorrelated, or weakly correlated, domains.

Crucial questions such as: i) the passage from order to chaos within a single domain and ii) possible synchronizations of time behaviors at different space domains, have been addressed in the past years, with the general idea in mind that space-time organization is what makes a large scale object complex.

Thus far, such an investigation was not possible in the optical field, because all coherent optics is based on Schawlow-Townes original idea of a drastic mode selection.

Here I show very recent evidence of space-time complexity in optics. The experimental configurations which have made possible to fulfill this twenty-year long search appear so promising that we can foresee an extensive investigation of space phenomena in optics along the coming decade. Let me call this area of investigation "dry hydrodynamics".

Here I anticipate and explain what we are going to see in the experiments reported in Sec. 6. To appreciate the role of space coupling let me summarize the present status of affairs in quantum optics. Since all coherent phenomena take place in a cavity mainly extended in a z-direction (as e.g. the Fabry-Perot cavity), we expand the field $e(r,t)$, which obeys the wave equation

$$\Box^2 e = -\mu \ddot{p} \tag{10}$$

(where $p(r,t)$ is the induced polarization), as

$$e(r,t) = E(x,y,z,t)\, e^{-i(\omega t - kz)}. \tag{11}$$

If the longitudinal variations are mainly accounted for by the plane wave, then we can take the envelope E as slowly varying in t and z with respect to the variation rates ω and k in the plane wave exponential. Furthermore we cll P the projection of p on the plane wave. By neglecting second

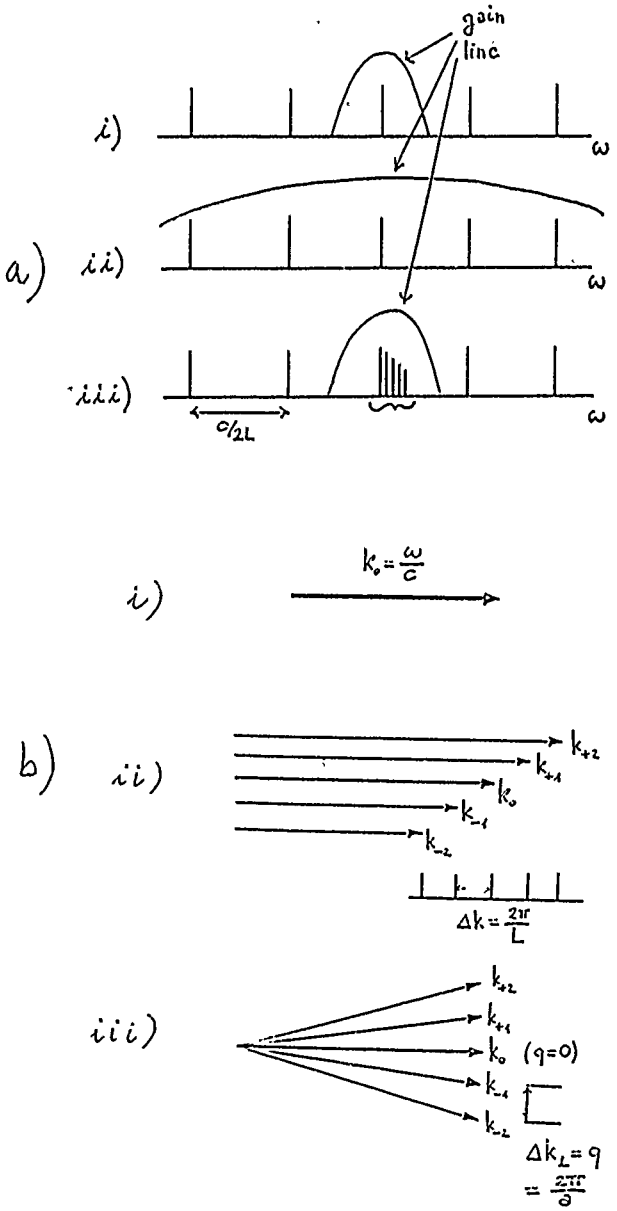


Fig. 11
ω-space (a) and K-space (b) pictures of the lasing modes in the i) (1 + 0), ii) (1 + 1), and iii) (1 + 2)-dimensional cases

order envelope derivatives it is easy to approximate the operator on $\hat{E}$ as

$$\Box^2 \to 2ik\left(\partial_z + \frac{1}{c}\partial_t\right) + \partial_x^2 + \partial_y^2 \tag{12}$$

as is usually done in the eikonal approximation of wave optics. This further suggests three relevant physical situations.

5.1. (1 + 0)-Dimensional Optics

In such a case there is only a time dependence and no space derivatives, that is, $\Box^2 \to 2i\omega d_t$. Assuming that the laser cavity is a cylinder of length L, with two mirrors of radius a at the two ends, the cavity resonance spectrum is made of discrete lines separated by $c/2L$ in frequency, each one corresponding to an integer number of half wavelengths contained in L, plus a crown of quasi-degenerate transverse modes at the same longitudinal wavenumber, with their propagation vectors separated from each-other by a diffraction angle λ/α (Fig. 11b).

This case corresponds to a gain line narrower than the longitudinal frequency separation (so called free spectral range) and to a Fresnel number

$$F \equiv \frac{a^2}{\lambda L}$$

of the order of unity, so that the first off axis mode already escapes out of the mirror. Intuitively F is the ratio between the geometric angle α/L of view of one mirror from the other and the diffractive angle λ/α.

In such a case, the resulting ODE replacing the wave PDE has to be coupled to the matter equations giving the evolution of P. In the simple case of a cavity mode resonant with the atomic line, we obtain the so called Maxwell-Bloch equations.

A comprehensive review of experiment and theory for these single-domain, (1 + 0)-dimensional systems is given in the book cited in Ref. 5, covering the period 1982–1987 over which these space invariant instabilities have been studied.

5.2. (1 + 1)-Dimensional Optics

Here, we have a cavity thin enough to reject off axis modes, but fed by a gain line wide enough to overlap many longitudinal modes. The superposition of many longitudinal modes means that one must retain the z gradient. Thus the wave equation reduces to

$$(\partial_t + c\partial_z)\, E = GP \tag{13}$$

where G is a scaled coupling constant.

Having a PDE, any mode expansion with reasonable wavenumber cut offs provides a large number of coupled ODE's, thus it is immaterial whether P and N are adiabatically eliminated, as in class A and B lasers, or whether they keep their dynamical character as in class C laser. Anyway, we have enough equations to see space time chaos.

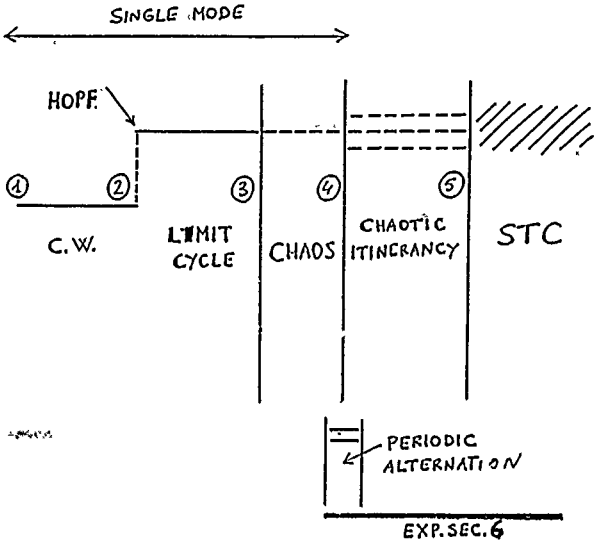


Fig. 12
Space-time complexity in optics. Qualitative plots of different behaviors observed in laboratory experiments and in numerical solutions of model equations

Equations as (13) have been solved numerically in the sixties, to explain space variations on a length scale much smaller than L, as seen in regular or erratic mode locking. Fig. 12 collects a sequence of possible behaviors as one increases an intensive control parameter (the pump to loss ratio) for a cavity long enough to provide a high ratio of gain linewidth to free spectral range, or alternatively, as one increases an extensive parameter, that is, the latter ratio for a fixed pump-to-loss ratio. Since the free spectral range is given by $c/2L$, increasing the extensive parameter amounts to increasing the cavity length L.

The circled numbers 1 to 5 denote the transition points.

Threshold n. 1 is the usual laser threshold, whereby uncorrelated spontaneous emission selforganizes into single mode coherent laser action. Mathematically it is a pitchfork bifurcation, with critical divergence of the fluctuation amplitude and correlation time (critical slowing down). These transition phenomena have been experimentally demonstrated in the middle sixties in a series of experiments reported by me at the 1978 Solvay Conference [11b].

In order to consider space variations, one must couple Eq. (13) with the matter equations. This was done by a mode expansion of Eq. (13), and a second threshold, n.2, which is a Hopf bifurcation toward an oscillatory regime, was introduced [36].

A third threshold marks the onset of deterministic chaos in a single mode laser. In fact it is a cascade of bifurcations depending on the specific route to chaos, which is influenced by possible laboratory perturbations, as modulations or feedback. The isomorphism of the single mode laser equations with Lorenz equations was first pointed out by Haken [37]. After that, a large amount of experimental and theo-

retical investigation has been devoted to chaos in a single mode laser.

Recent consideration of a space extended optical system [38] by a model made up of Eq. (13) plus material equations has shown evidence of a further behavior, called "chaotic itinerancy". It consits in the jump from one slow manifold to another, i.e., from one quasi-attractor to another. At any time, a single mode with a chaotic behavior is present, but after a while it is replaced by another mode, and so on. Alternatively, in Sec. 6 we will show experimental evidence of a non chaotic, but periodic alternation of modes, schematized in the lower part of Fig. 12. The main indicator of chaotic itinerancy is that, while a local measurement provides a chaotic signal, measurement of the space correlations provides a highly correlated signal.

Above the threshold n.5 we enter a new regime, called spatio-temporal chaos (STC) where a large number of modes coexist. This regime has been characterized on very general grounds by Hohenberg and Shraiman [39]. STC is characterized by some statistical features observed in the experiment reported in Sec. 6. Such features however play no role for the scope of this paper and will not be covered here.

5.3. (1 + 2)-Dimensional Optics

As shown in Fig. 11 iii), let us consider a gain line allowing for a single longitudinal mode, but take a Fresnel number high enough to allow for many transverse modes.

We rescale the transverse coordinates x,y with respect to the cross cavity size α, and the time t to the longitudinal photon lifetime $L/(cT)$, where T is the mirror transmittivity. The new variables are

$$x' = x/a\,, \quad y' = y/a$$

$$t' = \frac{t}{L/cT}\,.$$

Furthermore we neglect the longitudinal gradient. Then the wave equation reduces to

$$(\partial_{t'} - i\alpha\nabla_\perp^2)\, E = GP \tag{14}$$

where $\nabla_\perp^2$ is the transverse Laplacian and

$$\alpha = \frac{1}{4\pi FT}\,.$$

As in the (1 + 1) case, Eq. (14) must be coupled with the material equation. If P has a fast relaxation toward a local equilibrium with the field, and if we expand its dependence to the lowest orders, we have a relation as

$$P = aE - b|E|^2 E\,.$$

Introducing this into Eq. (14), one has a nonlinear Schrodinger equation (NLS) which has been recently considered in many theoretical investigations [40].

On the other hand, important considerations have been developed for the complex Ginzburg-Landau equation (CGL) [41]. This can be written as

$$\partial_t \mu = (\alpha_l + i\alpha_2)\nabla^2 u - \mu u - (1 - i\beta)|u|^2 u\,. \tag{15}$$

The CGL includes NLS (for $\alpha_1 = 0$) the chemical reaction-diffusion equation (for $\alpha_2 = 0$) and the single mode laser equation (for $\alpha_1 = \alpha_2 = 0$). Otsuka and Ikeda [41] used a discretized version of CGL on $N = 5$ sites with a space coupling which mimics the second derivative i.e.:

$$\nabla^2 u \to u_{l+1} + u_{l-1} - 2u_l \quad (i = 1, \ldots N)$$

and give solutions for $\mu = 1, \alpha_1 = \alpha_2 = 0.1$, and β increasint for 10 to 30.

For increasing β the system displays a variety of dynamical behaviors as shown in Fig. 12.

6. Chaotic Itinerancy in Optics [42]

In this Section I report the first experimental evidence of (1 + 2)-dimensional physics in an extended optical medium. Precisely, we seed ring cavity with a photorefractive gain medium pumped by an Argon laser and study the time and space features of the generated field. By varying the size of the cavity pupil, we control the number of transverse modes which can oscillate. We report two different regimes, namely one of a low dimensional chaos, where a single mode at a time is oscillating, and a small number of modes alternates in a fashion with displays close similarities and one of STC where many modes oscillate simultaneously yielding a very small transverse correlation length and spectral fluctuations with Gaussian statistics.

The experimental set up, consits of a ring cavity with photorefractive gain. The gain medium is a BSO (Bismuth Silicon Oxide) crystal to which a dc electric field is applied. The crystal is pumped by a CW Argon laser.

The Fresnel number of the cavity is controlled by a variable aperture. F can be varied in the range from 0 to 100 approximately. This corresponds roughly to the variation of the number of transverse modes that can oscillate. The mechanical and thermal stability are ensured on time intervals longer those of the measurements (half an hour).

Fig. 13 shows the transverse (x,y) intensity pattern recorded by the video camera (left) and its spatial autocorrelation function (right). For low F ($F = 5$) one single mode at a time oscillates and the wavefront is wholly correlated, indeed the correlation length ξ is of the same order as the cross size D of the beam (Fig. 13a). For high F ($F = 70$) many modes oscillate simultaneously, yielding a speckle-like pattern (Fig. 13c) whose correlation length is very small ($\xi/D < 0.1$). The correlation test is crucial, otherwise one might suppose that the intensity pattern at left refers to a pure mode with a large mode number. Between these two asymptotic limits, we have a smooth variation of the ratio ξ/D, with intermediate situations as shown in Fig. 13b.

The low F limit corresponds to a periodic alternation of a few modes of the diffraction limited propagation followed

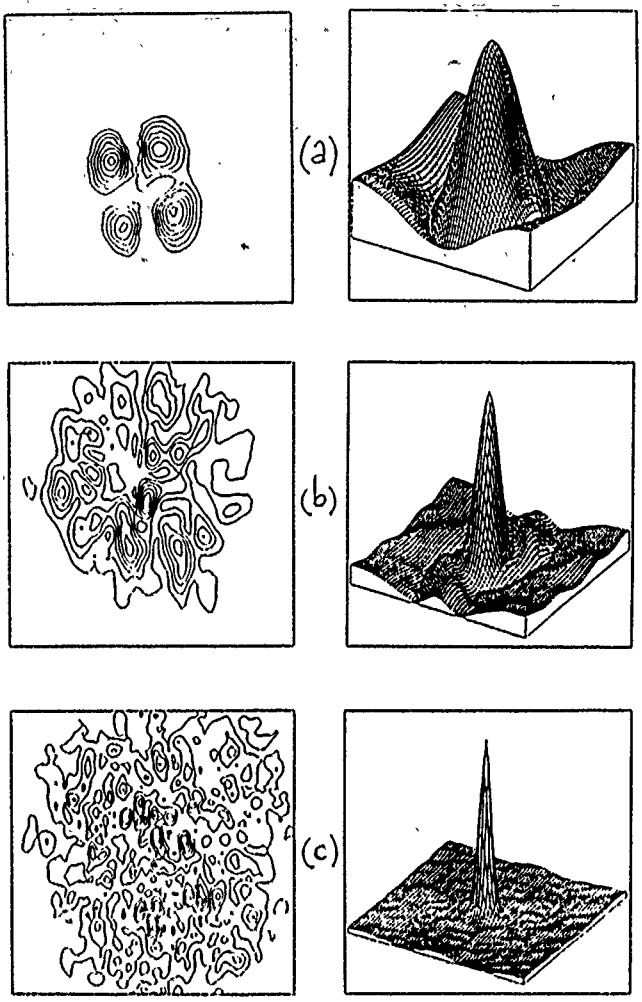


Fig. 13
Intensity distribution on the wavefront (left) and space autocorrelation function (right) for increasing Fresnel number,
a) $F = 5$, one single mode at a time is present, ratio between coherence length ξ and frame size D is $\xi/D \simeq 1$
b) $F = 20$, $\xi/D \simeq 0.25$
c) $F = 70$, $\xi/D \simeq 0.1$

by a dark period. The radial quantum number is always 0 and the azimuthal quantum number changes from $q = 0$ to q around 10. (From now on, we identify the modes by their azimuthal quantum number).

To study the time behavior, the input of an optical fiber picks up the intensity at a generic point on the wavefront (the signal level is a suitable code of each mode). The time plot shows fine details on a time scale of seconds, corresponding to the dielectric relaxation time of BSO. This time scale is typical of the fluctuations in a pure mode and of the intermode switches. Each mode persist for a time of the order of a few minutes. The mode pattern (e.g. 7,6,5,4,3,2 in Fig. 14b) repeats almost periodically. To improve the selectivity we commute from the pinhole (low pass filter) to the pinhole plus an axial stop (band pass filter). For the same aperture size, introduction of the axial stop cuts off the lowest modes (1 and 0) and produces the regularization shown in going from Fig. 14a) to b).

At the minimum Fresnel number for which some signal is observed (F around 2) still 4 different modes oscillate one at a time, followed by a dark interval, in a very regular periodic sequence. We call such a behavior "periodic alternation". Increasing the pump intensity, the frequency of the alternation increases but it remains regular. For a slight increase of F above 5 the regularity is lost, that is, the duration of each mode is no longer repeatable. This is an experimental evidence of "chaotic itinerancy".

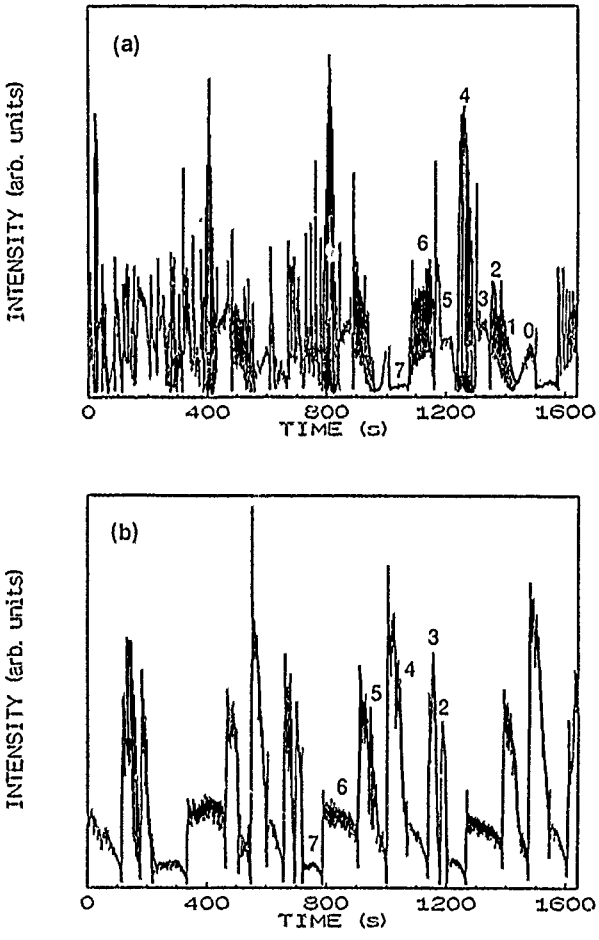


Fig. 14
Time records of the local intensity (samples collected at 10 Hz rate) at $F = 8$
a) with the low pass filter (chaotic itinerancy)
b) with the band pass filter (periodic alternation)

In the high F limit, when $\xi/D \ll 1$, we expect spatio-temporal chaos (STC) and indeed we have given evidence [42] of Gaussian spectral fluctuations.

In conclusion, we have reported experimental evidence of periodic alternation and STC as two asymptotic limits for very small and large Fresnel numbers in a $(1+2)$-dimensional optical system. At the lower edge of the intermediate region we have observed chaotic itinerancy. For still larger F we should expect transition phenomena which are not simply a mathematical bifurcation as the usual laser threshold but which display the scaling properties of phase transitions in extended media.

References

[1] P. Hänggi, P. Talkner, and M. Borkovec, Rev. Mod. Phys. *62*, 251 (1990).

[2] F. T. Arecchi, V. Degiorgio, and B. Querzola, Phys. Rev. Lett. *19*, 1168 (1967); F. T. Arecchi, and V. Degiorgio, Phys. Rev. *A3*, 1108 (1971).

[3] F. T. Arecchi, and A. Politi, Phys. Rev. Lett. *45*, 1219 (1990).

[4] F. T. Arecchi, A. Politi, and L. Ulivi, Nuovo Cimento *71B*, 119 (1982).

[5] By now it has become of general use a classification of laser dynamical types, depending on the number of coupled equations which describe the single mode dynamics, namely, Class A, B, C when the number of equations is 1, 2 or 3, respectively. See: F. T. Arecchi, in Instabilities and Chaos in Quantum Optics, p. 9, ed. by F. T. Arecchi and R. G. Harrison, Springer-Verlag, New York 1987.

[6] R. Roy, A. W. Yu, and S. Zhu, Phys. Rev. Lett. *55*, 2794 (1985).

[7] P. Spano, A. D'Ottavi, A. Mecozzi, and B. Daino, Appl. Phys. Lett. *52*, 2203 (1988); A. Mecozzi, S. Piazzolla, A. D'Ottavi, and P. Spano, Phys. Rev. *A38*, 3136 (1988).

[8] a) F. T. Arecchi, R.Meucci, and J. A. Roversi, Europhys. Lett. *8*, 225 (1989); b) F. T. Arecchi, W. Gadomski, R. Meucci, and J. A. Roversi, Phys. Rev. *A39*, 4004 (1989).

[9] R. Kubo, in Synergetics, pp. 28–44, ed. H. Haken, Teubner, Stuttgart 1973.

[10] F. Haake, Phys. Rev. Lett. *41*, 1685 (1978).

[11] a) M. Suzuki, in: Order and Fluctuations in Equilibrium and Nonequilibrium Statistical Mechanics, XVII International Solvay Conference in Physics, pp. 299–365, eds. G. Nicolis, G. G. Dewel, and J. W. Turner, Wiley, New York 1981; b) F. T. Arecchi, as above, pp. 107–157.

[12] F. T. Arecchi, R. Meucci, G. P. Puccioni, and J. R. Tredicce, Phys. Rev. Lett. *49*, 1217 (1982).

[13] Ia. G. Sinai, Proc. Berlin Conf. on Math. Problems in Theoretical Physics p. 12, eds. R. S. Schrader et al., Springer 1982; E. Marinari, G. Parisi, D. Ruelle, and P. Windey, Phys. Rev. Lett. *50*, 1223 (1983).

[14] F. T. Arecchi, and F. Lisi, Phys. Rev. Lett. *49*, 94 (1982).

[15] R. F. Miracky, J. Clarke, and R. H. Koch, Phys. Rev. Lett. *50*, 1856 (1983).

[16] a) M. R. Beasley, D. D. Humieres, and B. A. Huberman, Phys. Rev. Lett. *50*, 1328 (1983); b) R. Voss, Phys. Rev. Lett. *50*, 1329 (1983); c) F. T. Arecchi, and F. Lisi, Phys. Rev. Lett. *50*, 1330 (1983).

[17] F. T. Arecchi, R. Badii, and A. Politi, Phys. Rev. *A29*, 1006 (1984).

[18] F. T. Arecchi, R. Badii, and A. Politi, Phys. Lett. *A103*, 3 (1984); b) F. T. Arecchi, R. Badii, and A. Politi, Phys. Rev. *A32*, 402 (1985).

[19] E. W. Montroll, and M. F. Shlesinger, Proc. Nat. Acad. Sci. USA *79*, 3380 (1982).

[20] G. Grebogi, E. Ott, and J. A. Yorke, Phys. Rev. Lett. *50*, 935 (1983); S. M. McDonald, C. Grebogi, E. Ott, and J. A. Yorke, Physica *17D*, 125 (1985).

[21] F. T. Arecchi and S. Califano, Europhys. Lett. *3*, 5 (1987).

[22] C. Grebogi, E. Ott, and J. A. Yorke, Physica *7D*, 181 (1983).

[23] C. Grebogi, E. Ott, and J. A. Yorke, Phys. Rev. Lett. *57*, 1284 (1986).

[24] C. Jeffries and J. Perez, Phys. Rev. *A27*, 601 (1983); S. K. Brorson, D. Dewey, and P. S. Linsay, Phys. Rev. *A28*, 1201 (1983); M. Iansiti, Q. Hu, R. M. Westervelt, and M. Tinkham, Phys. Rev. Lett. *55*, 746 (1985).

[25] D. Hennequin, P. Glorieux, and Dangoisse, Phys. Rev. Lett. *57*, 2657 (1986).

[26] R. Meucci, A. Poggi, F. T. Arecchi, and J. R. Tredicce, Optics Commun. *65*, 151 (1988).

[27] L. P. Shil'nikov, Dokl. Akad. Nauk SSSR *160*, 558 (1965); L. P. Shil'nikov, Mat. Sb. *77*, 119, 461 (1968); *81*, 92, 123 (1979).

[28] A. Arneodo, P. H. Coullet, E. A. Spiegel, and C. Tresser, Physica *14D*, 327 (1985).

[29] F. T. Arecchi, R. Meucci, and W. Gadomski, Phys. Rev. Lett. *58*, 2205 (1987).

[30] F. Argoul, A. Arneodo, and P. Richetti, Phys. Lett. *A120*, 269 (1987).

[31] P. Glendinning and C. Sparrow, J. Stat. Phys. *35*, 645 (1984); P. Gaspard, R. Kapral, and G. Nicolis, J. Stat. Phys. *35*, 697 (1984).

[32] F. T. Arecchi, A. Lapucci, R. Meucci, J. A. Roversi, and P, Coullet,
i) ELITE Meeting, Torino, Italy, March 1987.
ii) International Workshop on Instabilities and Chaos in Nonlinear Optical systems, Il Ciocco, Italy, July 1987 paper WC 13-2
iii) Europhys. Lett. *6*, 677 (1988).

[33] F. T. Arecchi, W. Gadomski, A. Lapucci, R. Meucci, H. Mancini, and J. A. Roversi, JOSA *B5*, 1153 (1988).

[34] J. P. Crutchfield, D. Farmer, and B. A. Hubermann, Phys. Rev. *92*, 45 (1982).

[35] F. T. Arecchi, W. Gadomski, and R. Meucci, Phys. Rev. *A34*, 1617 (1986).

[36] H. Risken and K. Nummedal, J. Appl. Phys. *39*, 4662 (1968).

[37] H. Haken, Phys. Lett. *53A*, 77 (1975).

[38] K. Ikeda, K. Otsuka, and K. Matsumoto Prog. Theor. Phys. Suppl. N. 99, 295 (1989); K. Otsuka, Phys. Rev. Lett. *65*, 329 (1990).

[39] P. C. Hohenberg and B. I. Shraiman, Physica *D37*, 109 (1989).

[40] J. V. Moloney, F. A. Hopf, and H. M. Gibbs, Phys. Rev. *A25*, 3442 (1982); D. W. Laughlin, J. V. Moloney, and A. C. Newell, Phys. Rev. Lett. *51*, 75 (1983) W. J. Firth and E. M. Wright, Phys. Lett. *92A*, 211 (1982).

[41] L. D. Landau and V. L. Ginzburg, On the theory of Superconductivity, in Collected papers of L. D. Landau p. 217, ed. D. Ter Haar, Pergamon Press 1965, K. Otsuka and K. Ikeda, Global chaos in a discrete time-dependent CGL Equation, Preprint 1990.

[42] F. T. Arecchi, G. Giacomelli, P. L. Ramazza, and S. Residori, Phys. Rev. Lett. *65*, 2531 (1990).

Presented at the Discussion Meeting of the Deutsche Bunsen-Gesellschaft für Physikalische Chemie "Rate Processes in Dissipative Systems: 50 Years after Kramers" in Tutzing, September 10–13, 1990 E 7561

Energy Dissipation in Chemical Reactions on Ultrafast Timescales

Daniel J. Russell, Mark E. Paige, and Charles B. Harris

Department of Chemistry, University of California, Berkeley, CA 94720, USA

Elementary Reactions / Energy Transfer / Liquids / Nonequilibrium Phenomena / Statistical Mechanics

A series of picosecond experiments and computer simulations will be presented that test collisional and hydrodynamic models for vibrational relaxation in liquids. The relationships between isolated binary collision models (IBC) and stochastic dynamics will be presented. The appropriateness of IBC theory in describing vibrational relaxation in liquids will also be discussed.

A proper description of vibrational energy transfer is essential to the development of chemical reaction theory. In liquids, progress in this area is far behind that which has been made in other phases because of the complexity inherent to this phase. Generally, two approaches have been taken in attempting to model the vibrational relaxation of an excited oscillator in solution. One approach takes the perspective of the excited molecule being solvated in a continuous viscoelastic media which exerts a frictional force on the molecule. The most general form of this interaction is described by the generalized Langevin equation:

$$ma(t) = -\int_{t_0}^{t} dt' m\gamma(t')\, v(t-t') + R(t) \qquad (1)$$

where m is the mass of the particle, $R(t)$ is the random force, and $\gamma(t)$ is the memory function which provides the friction. In this description, the noninstantaneous response of the media to the motions of the oscillator are included. The difficulty with this method has been in developing a model of determining the form of $\gamma(t)$ [the frequency dependence of the friction]. Very early during the theoretical development of vibrational relaxation in liquids, prior to use of the generalized Langevin model, a simpler form of this model known as the Langevin equation was used to describe vibrational relaxation in solution [1]. According to the Langevin equation,

$$ma(t) = -\gamma v(t) + R(t)\,. \qquad (2)$$

In the Langevin model, γ, the friction coefficient, is a constant and thus, the solvent is assumed to respond instantaneously to all oscillator motions. While this model has been successful in describing some phenomenon where the solute moves slowly in relation to the solvent molecules, it has failed in the modeling of vibrational relaxation where the oscillator motions can be quite fast in comparison to that of the solvent [2].

An alternative perspective adapted to describing vibrational relaxation in solution is that based on the molecular nature of the solvent-solute interactions. In this framework, the interactions which are important to vibrational relaxation are assumed to be dominated by isolated binary collisions between the solvent molecules and the oscillator, just as they occur in the gas phase. This model known as the Isolated Binary Collision Model (IBC) states that $K_{i\to j}(\varrho, T)$, the relaxation rate of vibrational level i to j, is:

$$K_{i\to j}(\varrho, T) = P_{i\to j} \cdot Z(\varrho, T) \qquad (3)$$

where $P_{i\to j}(T)$ is the probability of $i \to j$ per collision, $Z(\varrho, T)$ is the oscillator-solvent collision frequency, ϱ is the solvent density, and T is the solvent temperature. Since $P_{i\to j}$ is independent of density, the difference between relaxation in the liquid and gas phases at constant T is solely given by $Z(\varrho)$. Thus, multibody effects (i.e., correlations between collisions) are considered to be inconsequential in this model. The validity of this assumption has been the subject of a longstanding debate in the literature.

As a test system for IBC theory, we have examined its applicability to experimental measurements and computer simulations of the ground state vibrational relaxation of geminately recombined I_2 in liquid Xe. Following photodissociation and recombination on the ground state surface, the I_2 has an excess of 12500 cm^{-1} of vibrational energy which it then dissipates to the solvent. This relaxation process occurs over 100 I_2 vibrational levels with the vibrational spacing varying from 0 to 214 cm^{-1}. Since I_2 contains only one vibrational degree of freedom, the role of the solvent in dissipating the excess vibrational energy of the excited I_2 can be studied with this system without competition from intramolecular vibrational energy transfer. Furthermore, Xe is an ideal choice as the solvent because of its spherical geometry which makes computations on this system easier and eliminates all but the translational degrees of freedom as the solvent energy accepting modes.

IBC theory is not expected to be valid for this system for two reasons. Frist, the low vibrational frequencies involved are comparable to the expected collision frequencies. Thus, interference between collisions would be expected to occur. Second, IBC theory should not be applicable to a highly excited oscillator in solution as the collisions will be driven by the large amplitude motions of the oscillator rather than occurring at random intervals resulting from the solvent motion. In contrast, previous studies of the IBC theory's validity at liquid density have focussed on the density de-

 © VCH Verlagsgesellschaft mbH, W-6940 Weinheim, 1991 0005-9021/91/0303-0299 $ 3.50+.25/0

pendence of the $v = 1 \rightarrow 0$ time of high frequency oscillators such as H_2 and N_2 where the above conditions do not exist and IBC theory may be valid [3].

Additionally, study of the multilevel relaxation process of I_2 offers a unique perspective on the validity of the IBC model as compared to these other experiments. The difficulty with interpreting the results of the $v = 1 \rightarrow 0$ studies is that a calculation of $Z(\varrho)$ is necessary in order to ascertain the validity of the IBC model since the relative change in relaxation rates between two densities ϱ_1 and ϱ_2 according to the IBC model is given by

$$\frac{K_{i-j}(\varrho_1)}{K_{i-j}(\varrho_2)} = \frac{Z(\varrho_1)}{Z(\varrho_2)}. \tag{4}$$

In solution, a collision is a nebulous concept and calculations of Z vary widely in magnitude with model and are very sensitive to parameters such as molecular size. Thus, studies in which the relaxation rate between two levels is measured as a function of density do not test the underlying assumption of the density independence of $P_{i \rightarrow j}$ separately from the model of $Z(\varrho)$ employed. In the experiments on I_2, the relaxation has been experimentally measured over approximately 30 vibrational levels (we could not directly observe the relaxation over the upper half of the ground state surface). Following the relaxation over a large number of vibrational levels as a function of solvent density eliminates the need of calculating Z in testing the density dependence of the $P_{i \rightarrow j}$.

To understand this distinction, consider the relaxation process over many vibrational levels in the IBC framework. After $Z(\varrho) \cdot t$ binary collisions, the vibrational population distribution vector, $N(t)$, would be

$$N(t) = P \cdot P \cdot P \ldots \cdot P \cdot N(t=0) = P^{z \cdot t} \cdot N(t=0) \tag{5}$$

where P is the matrix of relaxation probabilities per collision for transitions between all levels of the system. The role of $Z(\varrho)$ in this description of the relaxation is to control the timescale of the relaxation process. If the time were normalized by $Z(\varrho)$, i.e., $t' = t/Z(\varrho)$, then the resulting $N(t')$ would be identical for all ϱ. Hence, plots of the average energy of the system as a function of time for different density should show the same functional form, differing only by a linear scaling of the time axis which accounts for the change in $Z(\varrho)$. Provided $Z(\varrho)$ does not vary with vibrational energy, any deviation from linear scaling would be an indication of nonbinary behavior. The timescaling factor S necessary to overlap the energy decay curve at ϱ_2 to that of ϱ_1 can be determined from

$$Z(\varrho_1) \cdot t = S \cdot Z(\varrho_2) \cdot t \tag{6}$$

which leads to

$$S = \frac{Z(\varrho_1)}{Z(\varrho_2)}. \tag{7}$$

The I_2 vibrational energy as a function of time is determined experimentally through picosecond transient absorption spectroscopy. Due to the change of the Franck-Condon factors with vibrational energy, the transient absorption shifts from the near infrared at high vibrational energies to approximately 520 nm at $v = 0$. With the transient absorptions in this wavelength region and by calculating the extinction coefficients for the ground state absorption, the vibrational population distribution can be determined as a function of time by applying Beer's law. This analysis has been performed for the lower 6000 cm^{-1} of the I_2 ground state potential surface. The density range of Xe in which the experiment was performed was 1.8 to 3.4 g/cc at 280 K which corresponds to a Lennard-Jones reduced density ($\varrho\sigma^3$) range of 0.57 to 1.07 at a Lennard-Jones reduced temperature (kT/ε) of 1.26. A sample plot of vibrational energy vs. time for the 1.8 g/cc and the time scaled 3.0 g/cc is shown in the Fig. 1. *The functional form of the relaxation at all densities is the same.* Thus, the $P_{i \rightarrow j}$ are density independent over the entire liquid density portion of the Xe phase diagram as is assumed in the IBC model.

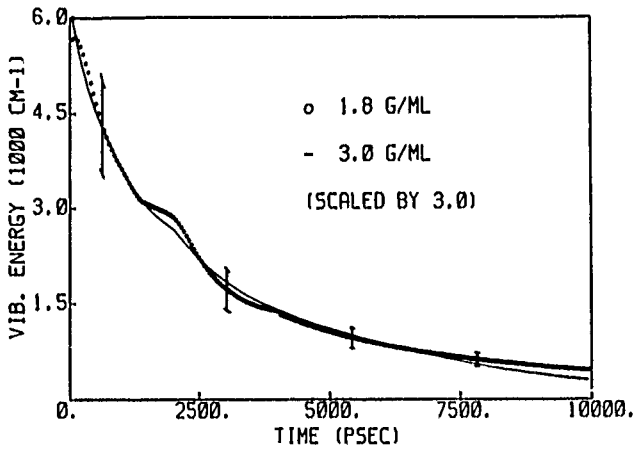


Fig. 1
The I_2's average vibrational energy as a function of time in 1.8 g/cc Xe (circles) and in 3.0 g/cc Xe (line) where the time base of the 3.0 g/cc data has been multiplied by 3.0. The functional form of the relaxation is identical for the two solvent densities. The error bars represent one standard deviation of the average energy for the 1.8 g/cc Xe solution

Concurrent with the experiments, a theoretical model of the I_2/Xe system was constructed. In order to provide a reference system for comparison of IBC and continuum theories, a molecular dynamics simulation of I_2/Xe was performed. Comparisons of the predictions of these theories with the simulation results will therefore not depend upon differences in the potentials assumed (in contrast to comparisons with the experimental results) [4]. The system was a classical molecular dynamics simulation using periodic boundary conditions. The potentials used were a Lennard-Jones potential between the iodine atoms and Xe atoms and a RKR potential for I_2. There were 255 xenon atoms and one iodine molecule in the system, these numbers were chosen because they minimized the effects of heating of the

liquid after dissociation due to the small number of particles and it was still a small enough system to allow a reasonable number of trajectories to calculated on a Cray X-MP. The functional forms of the vibrational energy vs. time for all the densities performed were the same. This would seem to indicate as described above that the $P_{i\to j}$ are density independent. Also, the functional form found from the molecular dynamics simulations was seemingly the same functional form found in the experiments. The only difference was that the molecular dynamics relaxed about 12.4 times faster than the experiment. This may be due in part to the finite volume of Xe heating up from the dissociation energy of the iodine. Also, the Lennard-Jones potential may be steeper than the real I_2-Xe potential. Qualitatively, the density dependence of the relaxation was the same for both the molecular dynamics and the experiment. There was some discrepancy in the actual numbers. Over the liquid range studied by the experiment, from 1.8 g/cc to 3.4 g/cc, the vibrational relaxation was 4 times faster. The molecular dynamics was also 4 times faster for the range of 1.8 g/cc to 3.0 g/cc. The molecular dynamics could not be run at 3.4 g/cc because that is Lennard-Jones solid while real Xe is a fluid. This shows that the molecular dynamics seems to be a fairly realistic representation of the vibrational relaxation in the liquid and only fails mainly to lack of exact potentials.

Given the success of reproducing experimental results by the molecular dynamics and the evidence that IBC theory may provide a valid model for explaining the experimental results, an IBC calculation was performed. The calculation of $P_{i\to j}$ performed for I_2 and Xe is a one dimensional classical calculation of energy loss. Studies have shown that the one dimensional calculation is a reasonable substitute for three dimensions if the constraints described in a paper by McKenzie are realized [5]. The I-I potential used is the same RKR surface as used in the molecular dynamics simulations. The potential between I and Xe is a Weeks Chandler Anderson (WCA) decomposition of the Lennard-Jones potential [6]. Note that the WCA decomposition was originally intended to explain liquid structures for reduced densities greater that 0.6. Even though most of the comparisons to molecular dynamics will be in this range, WCA was not chosen for this reason.

$$V(r) = 4\varepsilon\left[\left(\frac{\sigma}{r}\right)^{12} - \left(\frac{\sigma}{r}\right)^{6}\right] + C \quad \text{where } r < r_c$$

$$C = 4\varepsilon\left[\left(\frac{\sigma}{r_c}\right)^{12} - \left(\frac{\sigma}{r_c}\right)^{6}\right] \quad \text{where } r_c = 2^{(1/6)}\sigma \qquad (8)$$

$$V(r) = 0 \quad \text{where } r > r_c.$$

The WCA decomposition was chosen for three reasons. When a gas liquifies, energy (the heat of vaporization) is released due to the solvent atoms spending most of their time in the bottom of the well where the potential is repulsive. The attractive part of the potential is defined as the part of the potential where the accelerations are negative. Note that in the Lennard-Jones potential, the potential energy may be negative for $r < \sigma 2^{1/6}$, but the accelerations are not negative. Since the liquid rarely samples the attractive part of the potential, it was thought that the IBC simulation would be more realistic if it also did not sample that part of the potential. The turning point in the gas phase will also be on average at a smaller radius than in the liquid due to the heat of vaporization, however, the one dimensional model's turning point should be comparable to the molecular dynamics simulation due to the use of the WCA potential. Secondly, not having an attractive section of the potential makes the integration of the trajectory much quicker since there is less distance to integrate over and there is no possibility of forming a long lived complex. Thirdly, the molecular dynamics simulation that the one dimensional trajectories would be compared to used a Lennard-Jones potential and the WCA decomposition is the closest approximation to the Lennard-Jones potential within the above constraints.

The trajectories show qualitatively what you would expect keeping in mind I_2's anharmonicity. Vibrational energy transfer increases non linearly as a function of v, the vibrational quantum number. This at variance to Landau Teller theory, which predicts a linear increases with v. Of course, Landau Teller theory is based on a harmonic oscillator and I_2 is most definitely not a harmonic oscillator. A calculation of I_2's average vibrational energy vs. time was performed using data provided by the one dimensional calculations and it was found that the functional form of the energy loss was the same as both the molecular dynamics simulations and the experiments.

In order for IBC theory to be a useful theory it must also be able to make quantitative predictions of the relaxation for a particular density and predictions of the density dependence. The collision rate of 4.5 per ps., which was required to fit the molecular dynamics simulation, is a quite reasonable first order guess of what the collision rate should be for Xe at. 1.8 g/cc. Since the trajectory calculations were one dimensional, there must be some steric weighting factor to take into account that some collisions are not collinear. It is not clear what that factor should be, the value for the steric factor could range from one to less than 1/3 [7,8]. Nevertheless, the fact that $P_{i\to j}$ seems to be constant as a function of density demonstrates that the steric factor is also a constant of density. An estimate of the scale factor can be found using

$$\frac{K_1}{K_2} = \left(\frac{\varrho_1}{\varrho_2}\right)\frac{g_1(R^*)}{g_2(R^*)} \qquad (9)$$

K_1 is the rate for the liquid at density ϱ_1, where the $i\to j$ subscript has been dropped, K_2 is rate at liquid density ϱ_2, $g_1(R^*)$ is the radial distribution function for that liquid density evaluated at some R^*, and $g_2(R^*)$ is the radial distribution function evaluated at R^* for density 2. R^* is the turning point for the most effective collisions and it is assumed that this region is small. In 1971, Davis and Oppenheim derived this equation, using a master equation approach to describe vibrational relaxation in the weak coupling limit in a liquid [9,10]. Their theory was thought at

the time to apply only to high frequency oscillators, although work by Chesnoy seems to indicate otherwise [11].

This presents the problem of calculating the $g(R^*)$ for the oscillator. One approach to this problem was to use the attractive hard spheres pair distribution model by Delalande and Gale [12]. This model assumes that the collision rate should be calculated at the hard sphere radius. One then assumes the radial distribution function at R^* can be approximated by the Carnahan and Starling approximation, [13]

$$g(R^*) \simeq g_{\mathrm{HS}}(\mathrm{sig}) = \frac{\left(1-\frac{\eta}{2}\right)}{(1-\eta)^3}; \quad \eta = \frac{\pi}{6}\varrho\sigma^3 \tag{10}$$

where σ is the hard sphere contact distance and ϱ is the number density. The problem with this approximation is that the hard sphere radius which provides the best model for the radial distribution is not necessarily the correct radius at which to evaluate R^*. A more sophisticated version of this theory was employed by Madden and van Swol [14]. They used WCA theory to calculate the cavity distribution function which was then related to the ratio of vibrational relaxation rates in a dilute gas to a dense liquid. This assumed that $g(R)$ could be approximated by a properly chosen hard sphere fluid of the same density. They did not equate R^* with the hard sphere diameter used to calculate the radial distribution function. We calculated the radial distribution of an iodine atom in liquid Xe directly. Using the R^* calculated from the one dimensional trajectories, 3.7–3.8 Å, good agreement was found for the scale factors given by equation nine for the different densities.

The scale factors could also have been calculated using continuum theories. It has been shown that the vibrational relaxation rate is affected by [15,16]

$$F(t) = \left\langle \sum_b f(r_b(t)) \sum_c f(r_c(0)) \right\rangle \tag{11}$$

$$F_b(t) = \left\langle \sum_b f(r_b(t)) f(r_b(0)) \right\rangle . \tag{12}$$

Where $F(t)$ is the total force autocorrelation, $F_b(t)$ is the binary force autocorrelation and $f(t)$ is the coupling from the liquid to the oscillator at time t. Oxtoby has also considered this type of division of the forces [17]. From these correlation functions and the Golden Rule, the relaxation rate is

$$\frac{1}{T_1} \approx \int \mathrm{d}t\, \mathrm{e}^{\mathrm{i}\omega t} F(t) . \tag{13}$$

Basically, the component of the force autocorrelation spectrum at the oscillator frequency determines the relaxation rate. Figs. 2 and 3 show the force autocorrelations and the frequency spectrum for an I atom in liquid Xe at 1.8 g/cc. It has been found that the binary force autocorrelation function frequency spectrum was very similar to the total force autocorrelation function frequency spectrum, down to frequencies of $\approx 50\ \mathrm{cm}^{-1}$. This is evidence for the appropriateness for using IBC theory to model the vibrational relaxation even though I_2 has such a low vibrational frequency. This implies that the coupling to the bath is weak and could be treated as linear. Accordingly, stochastic theories should also be appropriate for this system. A stochastic approach should work due to the linearity of the system and its ability to take into account the many body forces through the total force autocorrelation. Smith and Harris have applied a generalized Langevin equation technique to this problem and also found results that agree with the molecular dynamics simulations [18,19].

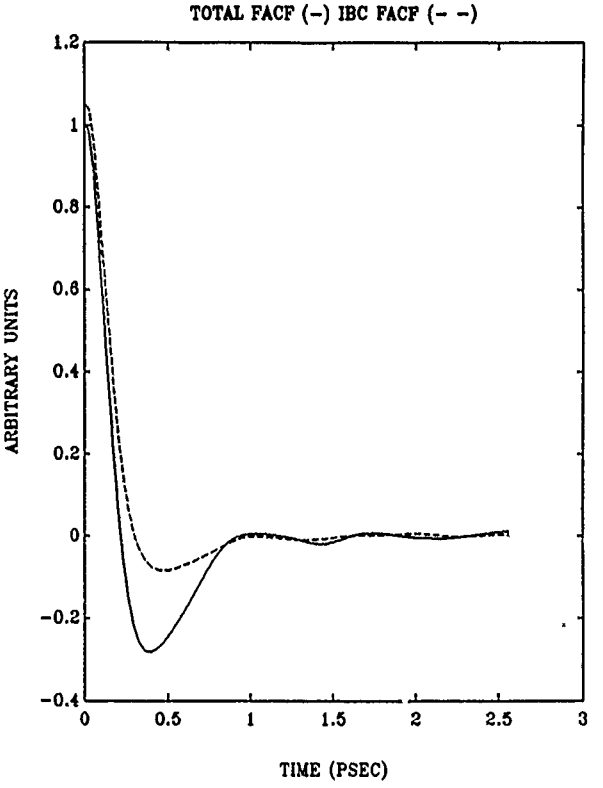


Fig. 2
The total force autocorrelation and the binary force autocorrelation described in Eqs. (11) and (12) are calculated for an I atom in 1.8 g/cc Xe. The early time components are very similar

Both of the above approaches will fail if the coupling between the bath and oscillator is strong. IBC theory will also fail if the binary force autocorrelation function power spectrum at the appropriate frequency is not the same as the total force autocorrelation. The most probable reason for the two force autocorrelation functions not being the same is if many body effects become more important and provide damping at the oscillators frequency.

Thus we have shown through experiments and calculations that IBC theory and continuum theories seem to model well the vibrational relaxation of I_2 in a simple liquid. This is somewhat surprising given that I_2 is such a low frequency oscillator and the I_2 vibrational amplitude is quite large in the upper part of the well. Further experiments in

a simple Lennard-Jones fluid such as Ar are required to test the above theories in a more quantitative fashion.

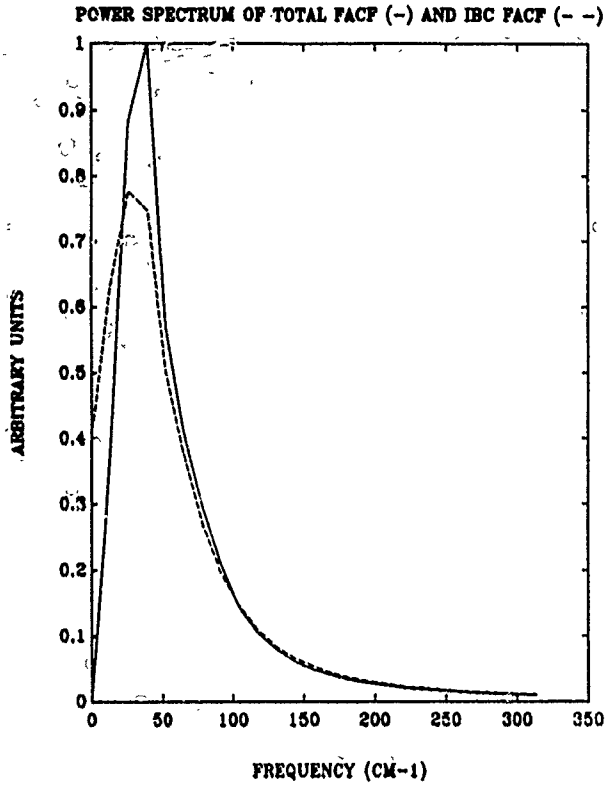


Fig. 3
The power spectrum of the total and binary force autocorrelation from Fig. 4. The magnitudes are about the same for vibrational frequencies above 50 cm^{-1}, which suggests that IBC theory may be appropriate for I_2 in Xe

This work was supported in part by a grant by the National Science Foundation and in part by the Office of Naval Research. Molecular Dynamics Simulations were performed at the San Diego Supercomputer Center. We also acknowledge the U.S. Department of Energy, Office of Basic Energy Sciences, Chemical Sciences Division, under Contract No. DE-AC03-76SF00098 for some specialized equipment used in these experiments.

References

[1] M. Fixman, J. Chem. Phys. *34*, 369 (1961).
[2] K. F. Herzfeld, J. Chem. Phys. *36*, 3305 (1962).
[3] M. Chatelet, J. Kieffer, and B. Oksengorn, Chem. Phys. *79*, 411 (1983).
[4] J. K. Brown, C. B. Harris, and J. C. Tully, J. Chem. Phys. *89*, 6687 (1988).
[5] R. L. McKenzie, J. Chem. Phys. *66*, 1457 (1975).
[6] D. Chandler, J. D. Weeks, and H. C. Anderson, Science *220*, 778.
[7] J. T. Yardley, *Introduction to Molecular Energy Transfer*, Academic, New York 1980.
[8] H. K. Shin, *Dynamics of Molecular Collisions Part A*, ed. W. H. Miller, Plenum, New York 1967.
[9] P. K. Davis and I. Oppenheim, J. Chem. Phys. *57*, 505 (1972).
[10] P. K. Davis and I. Oppenheim, J. Chem. Phys. *56*, 86 (1972).
[11] J. Chesnoy and J. J. Weis, J. Chem. Phys. *84*, 5378 (1986).
[12] C. Delalande and G. M. Gale, J. Chem. Phys. *71*, 4531 (1979).
[13] N. F. Carnahan and K. E. Starling, J. Chem. Phys. *51*, 635 (1969).
[14] P. A. Madden and F. van Swol, Chem. Phys. *112*, 43 (1987).
[15] R. Zwanzig, J. Chem. Phys. *34*, 1931 (1961).
[16] J. Chesnoy and J. J. Weis, J. Chem. Phys. *84*, 5378 (1986).
[17] D. W. Oxtoby, Mol. Phys. *34*, 987 (1977).
[18] D. E. Smith and C. B. Harris, J. Chem. Phys. *92*, 1304 (1990).
[19] D. E. Smith and C. B. Harris, J. Chem. Phys. *92*, 1312 (1990).

Presented at the Discussion Meeting of the Deutsche Bunsen-Gesellschaft für Physikalische Chemie "Rate Processes in Dissipative Systems: 50 Years after Kramers" in Tutzing, September 10–13, 1990 E 7491

Stochastic Resonance

Frank Moss

Department of Physics, University of Missouri at St. Louis, St. Louis, MO 63121, USA

Computer Experiments / Diffusion / Nonlinear Phenomena / Statistical Mechanics

Stochastic Resonance (SR) is a term given to an effect which is manifest in multi stable nonlinear systems driven simultaneously by noise and a weak periodic function, whereby the information flow through the system, in the form of the frequency of the periodic function, is assisted by the noise. For every frequency of the modulation, the information flow is optimum for a specific noise intensity, that is for a specific Kramers transition rate, hence the term *resonance*. Two physical quantities which characterize the response of such a system have been the objects of a flurry of recent experimental and theoretical activity: the Fourier transform, or auto correlation function of the appropriate state variable, and the probability density of the residence or escape times. The former have been used to obtain the power spectra and hence the signal-to-noise ratios of the response, while the latter directly reflect the rates and symmetry properties of the system. Calculation of these quantities pose specific problems for theorists characteristic of non stationary Fokker-Planck systems. In this paper, I will briefly review the recent activity and include some remarks on the historical foundations of SR.

1. Introduction

In recent years, interest in time modulated, stochastic, nonlinear systems has been increasing. Such systems are important in studies on dynamical bifurcation phenomena, for example, phase transitions occuring under the simultaneous influence of noise and time dependent parameters as well as

various transport and phase locking properties of multistable systems [1–6]. Stochastic resonance (SR) is an example with an interesting history as well as a number of modern applications. The physical phenomenon of SR is simply explained. Consider, for example, an over damped particle moving in a double well potential subject to a random force. The system may be in contact with a heat bath, so that the random forces result from thermal fluctuations. This simple construction is the starting point for many molecular dynamical models which form the microscopic basis of modern chemical rate theory, as well as a variety of other physical applications [7].

In the presence of noise, assumed to be Gaussian distributed, the particle can make transitions. SR arises because of an interplay between the modulation frequency and the famous Kramers rate [8], which in the unmodulated system is given by

$$r_0 = \frac{1}{2\pi}[|U''(0)|U''(c)]^{1/2}\exp(-\Delta U_0/D), \tag{1}$$

where $U''(0)$ is the curvature of the potential barrier located (at $x = 0$) between the two wells. $U''(c)$ is the curvature of the bottom of the wells (at $x = \pm c$), ΔU_0 is the height of the barrier of the unmodulated potential, and D is the noise (or thermal fluctuation) intensity, defined by the correlation function.

$$\langle \xi(t)\xi(s)\rangle = 2D\delta(t-s), \tag{2}$$

with $\langle \xi(t)\rangle = 0$. In the absence of modulation, the particle makes transitions over the barrier at random times and resides in one or the other well for a random length of time. The response is similar to the random telegraph signal. The probability density of the residence times is a decreasing exponential function, and the power spectrum is a Lorentzian.

Now we can further imagine that the particle is subject to an additional force: a weak periodic modulation of frequency ω. Here, "weak" means that the periodic force *alone* is not sufficiently strong to induce the particle to undergo a transition from one potential well to the other. However, in the additional presence of the noise, the particle makes transitions, which are now, however, to some extent coherent with the modulation. The potential is time dependent

$$U(x,t) = U_0(x) + \varepsilon x \sin\omega_0 t, \tag{3}$$

and if $\varepsilon \ll \Delta U_0$, and $\omega_0 \ll r_0$ (the latter is known as the adiabatic approximation) the time dependent Kramers rate is approximately given by

$$r(t) = \frac{1}{2\pi}[|U''(0)|U''(c)]\exp[(-\Delta U_0 + \varepsilon\sin\omega_0 t)/D]. \tag{4}$$

It is this modulation of the rate which accounts for the coherence between the response and the modulation functions.

For vanishingly small noise intensity, $D \to 0$, the switching rate approaches zero, and consequently the coherence vanishes. For indefinitely large noise, the coherence again becomes vanishingly small as the system response becomes completely randomized. Between these two limits, there is an optimum noise intensity which maximizes the coherence. Early theorists unfortunately called this a "resonance", though the phenomenon is clearly distinct from true resonances, for example resonance activation which occurs when under damped systems with inertia are driven by an external frequency comparable to a natural frequency [1,2].

A number of characteristics of SR have been observed experimentally and satisfactorily explained by modern theory, as I will outline in Section 2. The dynamics of SR can be approached, both in theory and experiment, on two levels. One can look at a reduced, or "two state", dynamics wherein the only information required is which well the particle resides in at a given moment. Alternatively, one can observe the complete dynamics which, in addition to the switching events, includes the stochastic and regular motions within the individual wells.

The most frequently observed physical quantity in SR experiments is the power spectrum $P(\omega)$. In measurements on real physical systems with symmetric potentials $U(x)$, the power spectrum shows a sequence of sharp peaks (in theory they are delta functions) of decreasing amplitude located at odd integer multiples of the modulation frequency riding on a broad Lorentzian noise background. If the symmetry of $U(x)$ is destroyed, weaker peaks at the even integer multiples of ω appear. The signal-to-noise ratio (SNR) is the ratio of the amplitude of the signal peak to the amplitude of the noise background, both determined at the fundamental frequency. The signal peaks represent the coherent part of the response. SR is demonstrated by observing that the SNR increases from zero and passes through a maximum with noise intensity in the two state dynamics. (For the complete dynamics, in addition, the SNR $\to \infty$ in the limit $D \to 0$, due to the coherent motion within a single well.)

The total power contained in the noise and the signal can be determined by integration of the power spectra. In the two state dynamics, it is observed that the total power is a constant, i.e. as the power of the modulation is increased the power in the signal peak increases while the noise power decreases to maintain the total constant. For the complete dynamics, the relation between these two powers is more complicated, but generally, the signal power grows at the expense of the noise power in the response.

An alternative quantity, which also clearly demonstrates the coherence of the stochastic response with the modulation, is the probability density of residence times. This quantity shows a sequence of strong, Gaussian-like peaks centered at odd integer multiple of the modulation half period, $T/2 = \pi/\omega$, characterized by exponentially decaying maximum amplitudes. There are no corresponding features at sub harmonics of ω in the power spectra.

In Section 2 of this paper, I will sketch the historical development of SR theory and outline the modern theories. In Section 3, I will discuss the two experiments which have

been done and summarize their results. In Section 4 the technique of physical measurements on analog simulators of SR systems will be introduced. Some representative data is presented in this section and compared with the theory. Finally, a summary and some speculation on future possibilities are presented in Section 5.

2. Historical Background and Modern Theory

A. Historical Background

The mechanism of SR was first propounded and investigated by Vulpiani and his co workers [9] as an interesting stochastic effect in nonlinear dynamics which might have useful applications in a variety of fields. The chief theoretical difficulty in SR problems is that in the presence of an external temporal modulation, the corresponding Fokker-Planck (F-P) equation is not solvable for the probability density exactly. These early authors, therefore, concentrated on estimates of the mean residence or "sojourn time", demonstrating that this time became closely comparable to the half period of the external periodic modulation for the optimum value of the noise intensity. Residence time theory for periodically modulated stochastic systems, which avoided the problems posed by the non stationary F-P equation, had been earlier developed by Eckmann, Thomas and Wittwer and was successfully applied to SR early on [10]. It can be mentioned at this point that residence time measurements have only recently been made on experimental SR systems, as I shall discuss in Section 3. The first study of SR in a partial differential system was carried out on the stochastically perturbed Ginzburg-Landau equation also by Vulpiani and company [11]. Finally, these same authors, together with Parisi, proposed SR, in 1982, as a possible explanation of the observed periodicities in the recurrences of the earth's ice ages [12]. In this view, the earth's climate is represented by a one dimensional bistable potential, one (meta) stable state of which represents a largely ice covered earth [13]. The external noise is assumed to come from short term fluctuations in the balance between radiative and transport processes, and the periodic modulation is most often supposed to originate from variations in the insolation resulting from a small observed oscillation in the eccentricity of earth's orbit having a period of 100,000 years. Moreover, the power spectrum of the dynamical coordinate of the system was introduced here for the first time in SR systems in numerical simulations of the climate model.

In 1983, Fauve and Heslot made detailed measurements on a noise driven, periodically modulated, bistable electronic system (a Schmitt trigger) [14]. They measured the power spectrum of the output from which they extracted the SNR, and observed that this quantity passed through a maximum with increasing noise intensity, thus demonstrating SR for the first time in a laboratory experiment. The location of the maximum in the SNR was identified (roughly) with the specific value of the noise intensity for which the Kramers rate in the unperturbed potential becomes comparable to the modulation frequency. No theory was put forth by these authors. Instead, their experiment served to clearly demonstrate the observable, physical aspects of SR.

Interest in SR seems then to have waned until 1988 when McNamara, Wiesenfeld and Roy demonstrated it in an ingenious experiment with a ring laser [15] which I will briefly discuss in Section 2. This experiment immediately stimulated a rash of theoretical activity [16–23] as well as two analog simulations [22–25] which I will discuss further in Section 2.

B. Outline of the Recent Theory

Two models have been considered, as mentioned before: the two state and the complete dynamics models. Considering these models, contemporary theories fit into two categories: the adiabatic approximations [16, 17, 20, 22], and the non adiabatic calculations [18, 21]. Though originally the means by which F-P systems could be treated within adiabatic approximations was put forth by Carolli et. al. [26], and more recently by Bryant, Wiesenfeld and McNamara [27], the first contemporary use of this approximation for SR theory was due to McNamara and Wiesenfeld [16] (MW).

The object is to calculate the power spectrum of the motion of a particle moving in a generic bistable potential within the framework of the two state model. Following MW, discrete variables $x_\pm$ are chosen to denote the location of the particle in either the right (+) or left (−) potential well with corresponding probabilities $n_\pm$, for which $n_+ = 1 - n_-$. A rate equation can then be written in terms of $W_\pm$, the transition rates out of the $\pm$ states:

$$\frac{dn_+}{dt} = -\frac{dn_-}{dt} = W_- n_- - W_+ n_+ . \tag{5}$$

The probability density is effectively reduced to a pair of delta functions located at the minima of the two potential wells and weighted by n_+ and n_- respectively, and from this density the moments can be computed. Specifically the second moment $\langle x^2 \rangle$, is needed. In order to solve (5), some approximate form for $W_\pm$ is required, and MW use an expansion in terms of a small parameter $\eta_0 \cos\omega_0 t$, where $\eta_0 = \varepsilon/D$:

$$W_\pm = \frac{1}{2}(\alpha_0 \pm \alpha_1 \eta_0 \cos\omega_0 t + \ldots), \tag{6}$$

where α_0 and the product $\alpha_1 \eta_0$ are treated as parameters of the system. From Eq. (5), a solution for n_+ can be obtained, and from that the autocorrelation function $\langle x(t)x(t+\tau)|x_0, t_0\rangle$ and its $t_0 \to \infty$ asymptotic limit $\langle x(t)x(t+\tau)\rangle$. This quantity leads directly to the power spectrum through the Wiener-Khintchine theorem:

$$S(\omega) = \left[1 - \frac{\alpha_1^2 \eta_0^2}{2(\alpha_0^2 + \omega_0^2)}\right]\left[\frac{4\langle x^2\rangle \alpha_0}{\alpha_0^2 + \omega^2}\right] + \frac{\pi \langle x^2\rangle \alpha_1^2 \eta_0^2}{\alpha_0^2 \omega_0^2}\delta(\omega - \omega_0). \tag{7}$$

This result makes two notable predictions, both born out by experiment, as shown in Section 3. first, the shape of the

power spectrum is a delta function contributed by the modulation riding on a Lorentzian noise background; and second, the total power, signal plus noise, is a constant. This latter remarkable property means that the power in the signal part of the response grows at the precise expense of the noise power: a property which is true only of the two state model. MW have generalized their theory to include the complete dynamics of an over damped particle in the standard quartic potential:

$$U(x,t) = -\frac{a}{2}x^2 + \frac{b}{4}x^4 - \varepsilon x \cos\omega_0 t\,, \tag{8}$$

where, for the unperturbed ($\varepsilon = 0$) potential, $\Delta U_0 = a^2/4b$ and the minima are located at $\pm c = \pm\sqrt{a/b}$. The Langevin equation therefore reads,

$$\dot{x} = -\partial U_x(x,t) = ax - bx^3 + \varepsilon\cos\omega_0 t + \sqrt{2D}\xi(t)\,. \tag{9}$$

In this case, the parameters are known: $\alpha_0 = (\sqrt{2}a/\pi)\exp(-\Delta U_0/D)$; $\alpha_1 = 2\alpha_0$ and $\eta_0 = \varepsilon c/2D$, which can be substituted into Eq. (7) in order to obtain the power spectrum. For the complete solution, I refer the reader to Ref. [16], and quote here instead only an approximate expression for the SNR, valid for small modulation strength

$$\mathrm{SNR} \cong \frac{a\varepsilon^2 c^2}{D^2}\exp(-\Delta U_0/D)\,. \tag{10}$$

It only remains to summarize briefly the approximations used by MW. First, the adiabatic approximation in the MW theory is $\omega_0 \ll U''(\pm c)$ rather than the more stringent condition (at least for small D) that $\omega_0 \ll r_0$. The retention of only the first two terms in the expansion of Eq. (6) requires that $\alpha_1\eta_0 \ll \alpha_0$, or in the model using the quartic potential, that $\eta_0 \ll 1$. This means that $\varepsilon \ll D$ and that $\varepsilon \ll \Delta U_0$.

I mention here that the adiabatic approximation has also been used for construction of a contemporary theory of the residence times in SR systems. For the details of that theory, I refer the reader to Ref. [22] and to the paper by P. Jung and P. Hänggi in this Proceedings. Suffice it to say here that the theory predicts a sequence of peaks in the probability density of residence times, of exponentially decreasing amplitude, located at the odd integer multiples of the modulation half period π/ω_0. Some examples measured on the analog simulator experiments are shown in Section 3.

The MW theory has also been used to calculate the SNRs of a noisy neuron [25] using the Hopfield potential [28],

$$U(x,t) = \frac{x^2}{2} - \eta(t)\ln(\cosh x) - \varepsilon x\cos\omega_0 t - x\xi_a(t)\,, \tag{11}$$

where the one dimensional state variable x, represents the firing rate. Moreover, for this model the MW theory has been generalized to include multiplicative noise.

$$\eta(t) = \eta_0 + \xi_m(t)\,, \tag{12}$$

where ξ_a and ξ_m are the additive and multiplicative noises respectively. For the details of this calculation and for the results of an analog simulation of this neuron potential for both over damped and inertial dynamics, the reader is referred to Ref. [25].

Turning now to the non adiabatic theory of Hänggi and Jung [18], the generic Langevin equation used in the development reads

$$\dot{x} = x - x^3 + \varepsilon\cos(\omega_0 t + \phi) + \xi(t)\,, \tag{13}$$

where ϕ is a random phase uniformly distributed over one cycle $[0, 2\pi]$, and where $\xi(t)$ is the usual Gaussian, white noise. The periodicity of the resulting, non stationary F-P equation is used in analogy with procedures used in periodically forced quantum mechanical systems to write down a solution in terms of a Floquet characteristic exponent μ

$$p_t^\mu(x) = e^{\mu t}\sum_{n=-\infty}^{\infty} p_n^\mu(x)^{in\omega_0 t}\,. \tag{14}$$

The Floquet exponents are identified with the eigenvalues of an analogous two dimensional F-P process which are purely imaginary. This implies that the autocorrelation function $x(t)$ is a non decaying periodic function. This function is calculated explicitly from the asymptotic probability density obtained as the solution of the non stationary F-P equation. It is shown that the very same autocorrelation function can be obtained from the non stationary F-P equation by averaging over the random phase ϕ. It is important to note that *all* SR experiments, using both the laser and analog simulators, are performed by inherently averaging over the (random) phase of the periodic modulation. This is discussed further in Section 3. The predictions of this theory for the real one-sided (i.e. measurable) power spectrum are twofold: first, the predicted signal features in the power spectrum are a sequence of delta functions, and second, for symmetric potentials like the standard quartic, they occur only at odd multiples of the modulation frequency. These predictions have been born out by both the laser experiment [15] and most especially by measurements on analog simulators [24] where the measured line widths in the signal are completely accounted for by the instrumental resolution and bandwidth (i.e. the signal features in a system with infinite resolution and bandwidth would be ideally delta functions). Moreover, the sequence of peaks at odd multiples of ω_0 are readily observed.

Finally, I conclude this section with a brief outline of the theory developed by Marchesoni and coworkers [20, 23]. They have treated first the case of an over damped particle in the standard quartic potential within the framework of perturbation theory also in analogy to techniques developed for treating periodically forced quantum mechanical systems. Thus they also avoid the limitations of the adiabatic approximation, but are instead confined by the limitations of perturbation theory. While the results of these calculations are in qualitative agreement with analog simulations performed by the same group, the theory does not predict

the delta function form for the signal function nor does it predict the sequence of features at odd harmonics of ω_0. A major contribution by this group has been to treat the case of inertial motion within the adiabatic approximation, and to show that the same approximation can be used to obtain some predictions about the behavior of SR systems in the presence of colored noise. the relevant Langevin equation is

$$\ddot{x} + \gamma\dot{x} = x - x^3 + \xi(t)\,, \tag{15}$$

where γ is the damping constant, and $\xi(t)$ is now a colored noise defined by

$$\langle \xi(t)\xi(s)\rangle = \frac{D}{\tau}\exp[-|t-s|/\tau]\,, \tag{16}$$

with τ the noise correlation time. The results of this theory are in quite good agreement with SNR measurements made on an analog simulator of Eqs. (15) and (16) for various values of both γ and τ considered as parameters.

3. Experiments and Simulations

An early electronic experiment on SR was done by Fauve and Heslot [14] using a Schmitt trigger. This experiment was repeated more recently also by McNamara and Wiesenfeld [16]. The dynamics of the Schmitt trigger are represented by the two state model. An elementary diagram and the input-output voltage characteristic of this device are shown in Fig. 1. When operated such that $\langle V_{in}\rangle = 0$, i.e. in the middle of the bistable region, the output voltage V_0, can assume either of the two values, $V_{out} = \pm V_1$. With noise alone as the input, the trigger randomly switches between these states, and the output is the random telegraph signal. When the periodic modulation is added to the noise, the switching events become to some degree coherent, and the measured power spectrum of the output shows the characteristic sequence of delta-like peaks riding on the Lorentzian noise background as discussed in Section 2. The SNR can be measured in the usual way using the amplitudes of the signal peak and the noise at the fundamental modulation frequency. MW find good agreement between their SNR measurements and the two state theory.

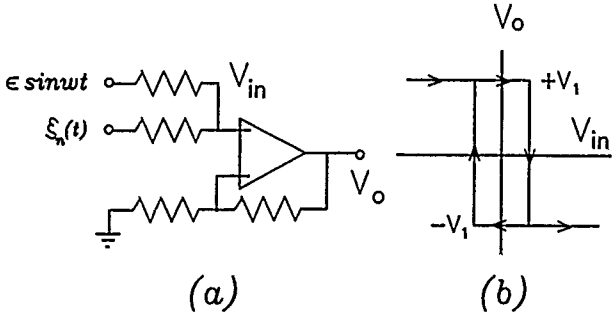


Fig. 1
(a) A schematic diagram of a Schmitt trigger using an operational amplifier driven by noise and a periodic function. (b) The transfer characteristic of the Schmitt trigger. The circuit operates as the two state model within the bistable region

It was the observation of SR in a dye, ring laser [15] by McNamara, Wiesenfeld and Roy, however, which triggered the modern burst of theoretical activity. These authors described an experiment wherein the bistability is represented by the direction of travel of the light within the ring. An acousto-optic modulator is inserted in the ring. This device creates a potential having a weak barrier separating two stable states which correspond to the two directions of light travel. The potential can be modulated with the acoustic frequency which is in turn controlled by the external noise and periodic signal voltages. A fraction of the light traveling in one direction was extracted from the ring and passed to a photo diode. The output of the photo diode was amplified, stored in a digital oscilloscope and then Fourier analyzed to obtain the power spectrum. This experiment provided the first evidence for SR in a physical system other than electronic.

Though some early authors and MW as well performed digital simulations by integrating an appropriate stochastic differential equation, the most recent tests of the modern theory have been provided by analog simulators. These are electronic circuit models, designed following a particular stochastic differential equation using modern analog components, for example, voltage multipliers, dividers, logarithmic and antilogarithmic amplifiers etc. [29,30]. Addition of voltages is performed in the usual way with operational amplifiers. The circuit integrates the mimicked differential equation by collecting charge on a capacitor in the feedback path of an operational amplifier. An example electronic simulator of over damped motion in the standard quartic potential is shown schematically in Fig. 2. The two components shown with crosses represent voltage multipliers. The minus sign indicates an inverting operational amplifier, and the summer adds all the inputs to form the voltage equivalent of the right hand side of the differential equation shown. Integration in time then computes $x(t)$, which closes the loop on the circuit. The feedback capacitor and the input resistor of the integrator define the integrator time constant τ_i, which establishes the time scale on which the simulator operates. As shown in Fig. 2, the circuit is driven by a signal generator which provides the periodic modulation, and a noise generator [31] which provides wide band Gaussian noise. A linear filter between the noise generator and the circuit model (not shown) produces time correlated noise with correlation function given by Eq. (16) [32]. The mean square noise voltage $\xi(t)$, $\langle \xi^2(t)\rangle$ at the output of the filter is measured with a wide band voltmeter, and the noise intensity is obtained from $\langle \xi^2(t)\rangle = D/\tau_n$.

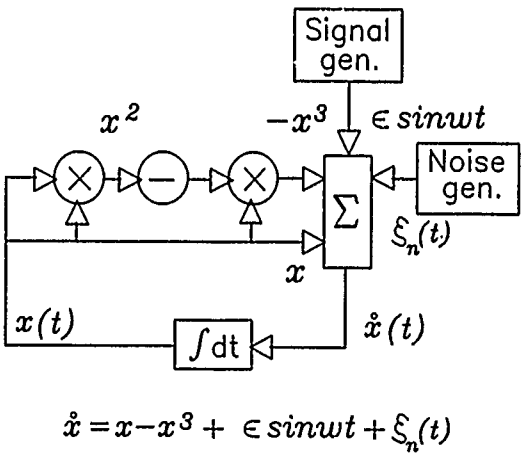


Fig. 2
A schematic diagram of the analog simulator of the standard quartic potential. The × symbols represent multipliers, the − is an inverting amplifier, Σ is an operational amplifier summing circuit, and the integrator, shown by $\int dt$, is an operational amplifier with an input resistor R and a feedback capacitor C which result in a time constant $\tau_i = RC$. The stochastic differential equation of the motion is shown below

The time dependent voltages $x(t)$, and in some cases $\dot{x}(t)$, are then passed to an analog-to-digital convertor (ADC). After digitizing, these time series are then stored in a computer and processed. A number of quantities, and their ensemble averages, can be obtained

from these data, only two of which are discussed here: the power spectrum and the residence time probability density.

Typically, 2000 digitized points are obtained in a single time series by opening the gate on the ADC at a random phase of the periodic modulation. The power spectrum and/or probability density are computed and stored for averaging. Perhaps 10.000 such operations are performed, each time opening the ADC gate at a random phase. In this way the final result is obtained as an average over the phase of the modulation. Example data are shown in Fig. 3. In Fig. 3(a), an example time series, $x(t)$, is shown as digitized directly from the circuit model. Note that this represents the complete dynamics. The switching behavior between the two wells is evident as well as the intra well motion. A sample of the periodic modulation is shown in Fig. 3(b), and the final, averaged power spectrum is shown in (c). Note the Lorentzian noise background, the delta-like peak at the modulation frequency and the small 3ed harmonic peak.

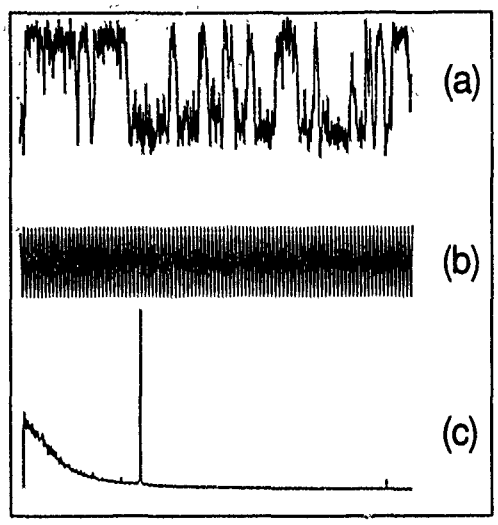


Fig. 3
Example data from the analog simulator, showing (a) a digitized time series $x(t)$; (b) the periodic modulation; and (c) the power spectrum averaged from many samples of time series. The width of the signal peak is determined completely by the bandwidth and frequency resolution of the measuring and Fourier transforming systems

In order to study the two state model or to measure the probability density of residence times, it is necessary to eliminate the intra well motion by replacing it with a constant, say one volt. This is accomplished by connecting the output if the circuit to a voltage comparator whose output voltage obeys the following logic:

$$x_{\text{twostate}} = \begin{matrix} +1 & \text{if} \quad x(t) > 0 \\ -1 & \text{if} \quad x(t) < 0\,. \end{matrix} \tag{17}$$

An example of the comparator output is shown in Fig. 4 (a). The residence times, T_i, for the right well ($x_{\text{twostate}} = +1$) are shown. Fig. 4 (b) shows an example of the measured probability density of residence times for a modulation frequency of $f_0 = 2$ kHz. Note the first maximum located at $T_0/2 = 1$ ms and the successive peaks at odd multiples of $T_0/2$. We note in passing that, while the power spectrum is the almost universally accepted tool of choice for harmonic analysis, the residence time probability density certainly exhibits a distinctive characteristic structure and in some applications may be more suitable. Indeed, Fletcher, Havlin and Weiss [33] have found this quantity most useful in studies on random walk problems. Further, we note that if converted to frequencies, these peaks, except for the first one, would be subharmonics of the fundamental frequency. Yet, in spite of careful, precision searches, no such subharmonics are observable in the measured power spectra. We conclude that the sequences of peaks in the residence time probability density and in the power spectrum are unrelated except that they both reflect the inherent symmetry of the standard quartic potential.

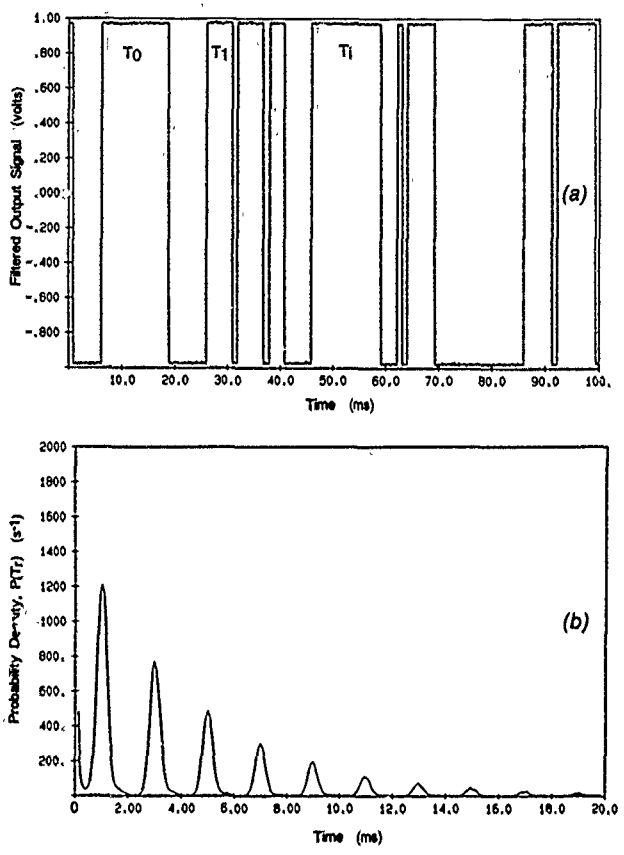


Fig. 4
(a) A time series measured after connecting a voltage comparator at the output of the analog simulator. The simulator dynamics thus mimic the two state model. The sequence of residence times, $T_0, T_1 \ldots T_i$, are determined for one well only, in this example the well located near + 1 volt. (b) An example of a measured probability density of residence times assembled from many samples of the time series. In this example the modulating frequency was 500 Hz so that the half period, $T_0/2 = 1$ ms. Note the sequence at odd multiples of $T_0/2$

The particular circuit shown in Fig. 2, and the example results of Figs. 3 and 4, are for over damped motion in the standard quartic potential, many other models are possible as discussed in Ref. [29] including also cases of inertial motion with arbitrary damping. A recent example is the noisy Hopfield neuron as discussed in Ref. [25]. In every case, the simulators were constructed following the principles outlined here.

4. Some Results

In this section, I will present some further data for comparison with the theoretical predictions. First, the SNR data for the case of $\epsilon = 0.4$ and $f_0 = 50$ Hz using the standard quartic, over damped dynamics specified by Eqs. (8) and (9) are shown in Fig. 5. The asterisks are the measured SNRs and the solid curve is the calculated result from Eq. (10). The plus signs show the behavior of the noise background amplitude measured from the power spectrum at the modulation frequency. These are plotted on the vertical scale in decibels using the standard definition, amplitude in db = 10 logSNR. We see that the location of the maximum is predicted by the approximate relation with reasonable accuracy. Since Eq. (10) is valid only for small D, it is not surprising that the agreement seems to break down at larger noise intensity. An inaccuracy in the

plotting routine accounts for the apparent discrepancy near the origin.

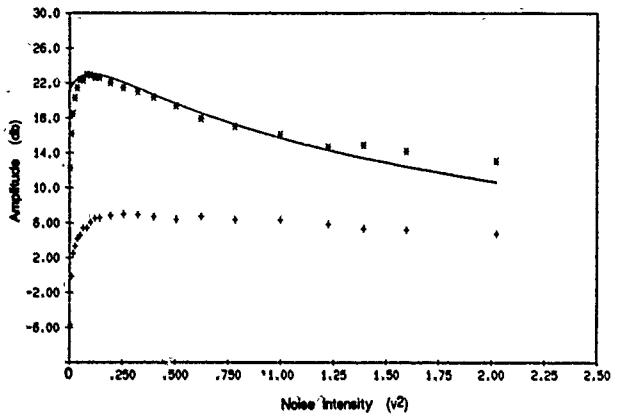


Fig. 5
An example of stochastic resonance. The vertical scale is the SNR in decibels. The asterisks are the measured results, the curve is an approximate theory and the plus signs are the values of the noise background measured at the modulation frequency

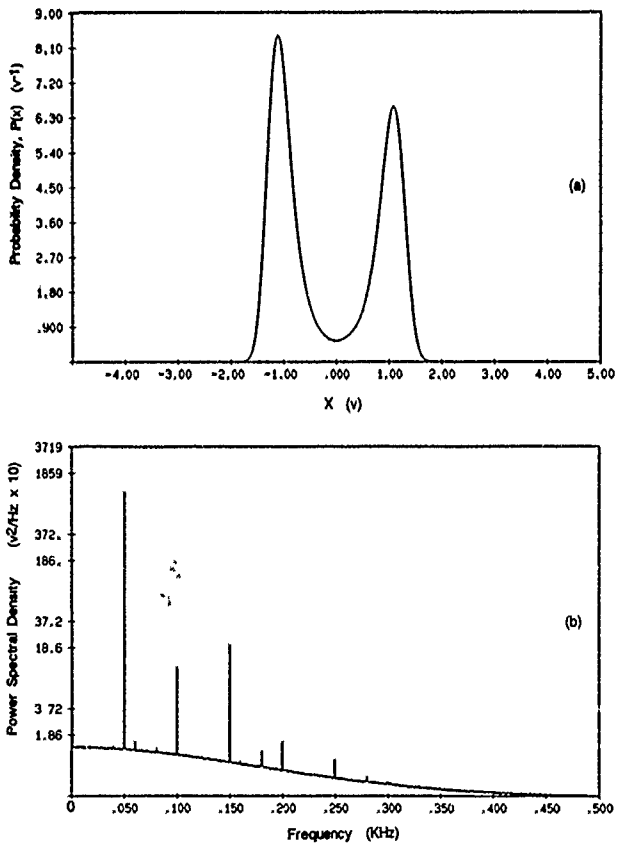


Fig. 6
(a) A measured probility density $P(x)$, in the absence of modulation for the asymmetric potential. The well near -1 volt is the more stable. (b) The power spectrum measured for the asymmetric potential, showing the usual sequence of peaks at the odd harmonics as well as a weaker set of peaks at the even harmonics

Next, the effect of the symmetry of the potential on the sequence of peaks in the power spectrum can be investigated. The symmetry of the standard quartic can be destroyed by adding a small constant force q:

$$U(x,t) = -\frac{a}{2}x^2 + \frac{b}{4}x^4 - \varepsilon \cos\omega_0 t + qx. \tag{18}$$

The effect of q can be illustrated by setting $\varepsilon = 0$, applying the noise and simply measuring the stationary probability density $P(x)$. An example is shown in Fig. 6(a) which shows that we have lowered the left well at $x = -1$ V and raised the right hand well. If the modulation is now switched on ($\varepsilon \neq 0$), then a power spectrum as shown in Fig. 6(b) is obtained. We note the usual sequence of stronger peaks at $f_0 = 50$ Hz and its odd multiples. In addition, there are now weaker peaks at the even harmonics. This clearly demonstrates the symmetry arguments made by Hänggi and Jung [18].

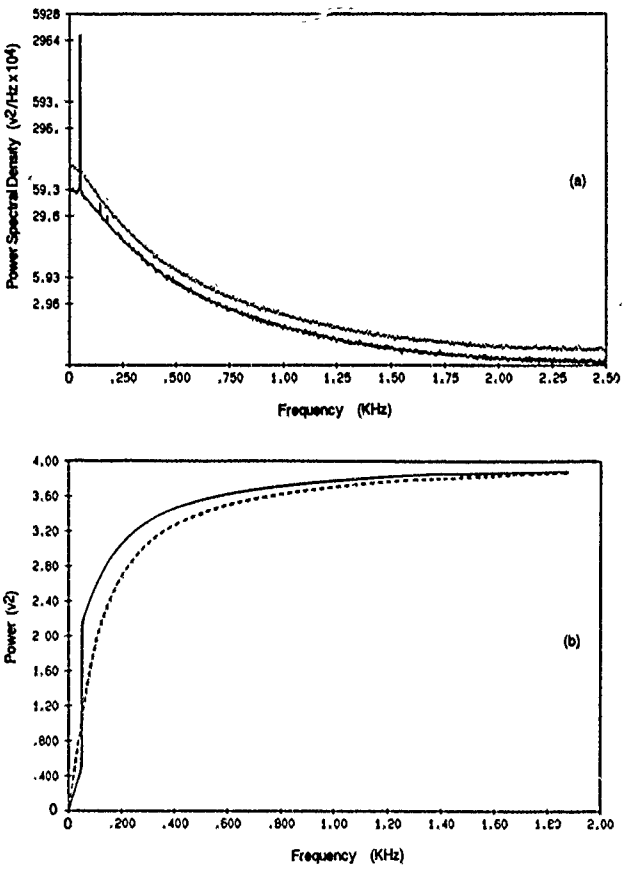
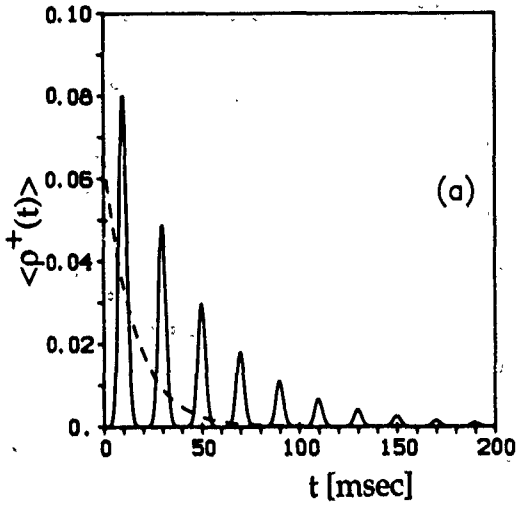


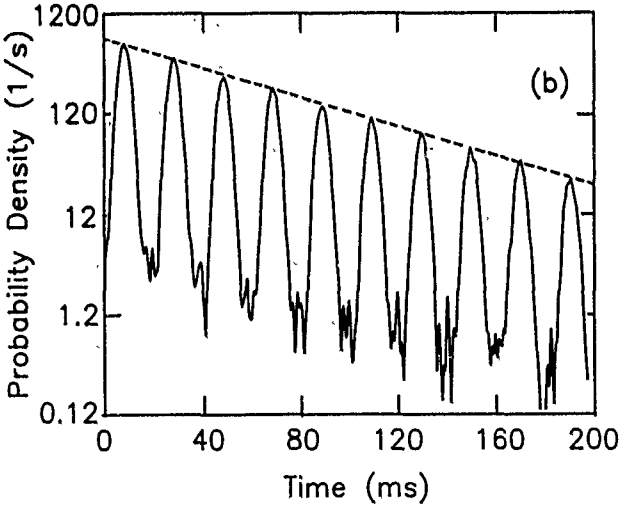
Fig. 7
(a) Two power spectra, one of the noise alone (dotted curve) and the other of the modulation plus the noise (solid curve). Note the decreased noise background when the modulation is present. (b) The integrals of the data shown in (a), where the dashed curve is the noise alone and the solid curve is the noise plus the modulation. The two curves converge at high frequency indicating that the total power in each spectrum is a constant

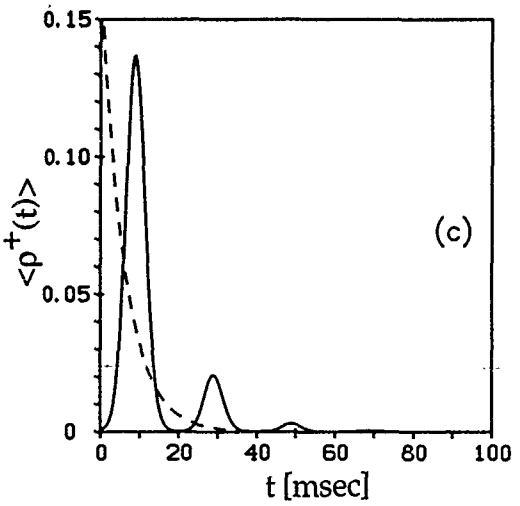
Finally, the constancy of total power in the noise and signal spectra can be demonstrated as shown in Fig. 7. First the noise spectrum alone is measured by setting $\varepsilon = 0$. This is shown by the dotted curve in Fig. 7(a). For all the same experimental conditions, the modulation is now switched on as shown by the solid curve with the familiar signal peak. Note that the noise background has been suppressed by the modulation. The magnitudes of the total powers can be displayed by digitally integrating the data of Fig. 7(a). These curves are shown in (b), where the solid curve is the result with the modulation present and the dashed curve is the noise alone. The two curves converge at high frequency indicating the same total power. This result clearly demonstrates the total power prediction of MW in Ref. [16]. It is, however, true only for the two

state model, and can only be obtained from the simulator with the voltage comparator on the output.

We now turn to the probability density of residence times, the adiabatic theory of which was developed in Ref. [22]. This probability density was assembled in the usual way from the T_i obtained from measured time series as shown, for example, in Fig. 4. A result calculated from the theory of Ref. [22] is shown in Fig. 8(a), where







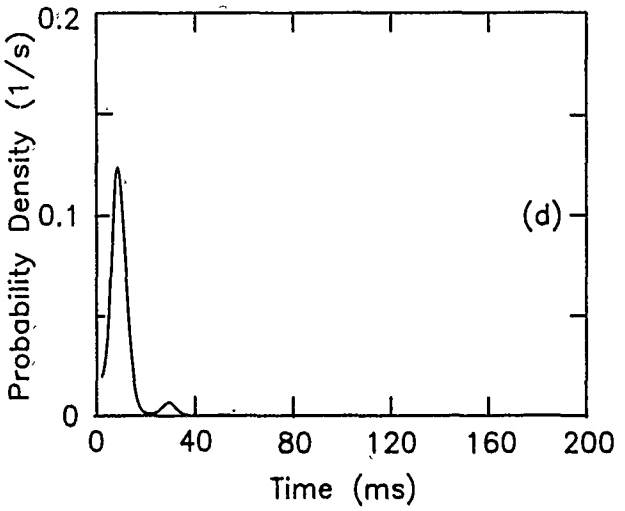


Fig. 8
(a) A $P(T)$ curve and its mean (dashed curve) calculated from the theory of Ref. [22] for $D = 0.03$ and $\varepsilon = 0.2$. (b) a measured $P(T)$ curve for the same conditions from the analog simulator. The data are plotted on a semi logarithmic scale in order to illustrate the near exponential decay of amplitudes. (c) Calculated results for $D = 0.05$, and (d) measured for the same conditions

the dashed curve is a calculation of the average density and is a near exponential. This property is further illustrated by the data, measured for the same parameter values, shown in Fig. 8(b), where $P(T)$ is plotted on a semi logarithmic scale. The straight dashed line illustrates the near exponential decay of the amplitudes as measured on the analog simulator. The slope of the dashed line is a strong function of D. Fig. 8(c) shows the theoretical results for a larger value of D, and the corresponding measured result is shown in (d). There is a small discrepancy between the calculated and measured slopes. This derives from an inherent uncertainty in determinations of D from the analog simulator near the white noise limit.

5. Discussion

In this paper, I have reviewed the development of the theory of SR and summarized the modern results. In particular, the striking predictions related to the symmetry properties of the potential have been clearly demonstrated by the analog simulations both in the frequency domain, by measurements of the power spectra, and in the time domain by measurements of the residence time probability densities. Moreover, the constant total power property of the two state model was also demonstrated by direct measurements. It should be noted that SR can occur in any bi- or multi-stable potential, possibly in more than one spatial dimension as well. It has only been demonstrated, however, for the standard, one dimensional quartic and for a single Hopfield neuron potential. It is likely that SR will find further applications if the theory can be generalized to networks.

It is a pleasure to thank Peter Hänggi and Peter Jung for incisive discussions and a continuing collaboration. Moreover, I have benefited from conversations with Kurt Wiesenfeld, Bruce McNamara, Rajarshi Roy, and Fabio Marchesoni, and I am indebted to Ting Zhou for his continuing help with the simulations. This work was supported by the U. S. Office of Naval Research grant no. N00014-90-J-1327 and from N. A. T. O. grant no. 0770/85.

References

[1] (a) M. H. Devoret, J. M. Martinis, D. Esteve, and J. Clarke, Phys. Rev. Lett. *53*, 1260 (1984); (b) H. M. Devoret, D. Esteve, J. M. Martinis, A. Cleland, and J. Clarke, Phys. Rev. *B36*, 58 (1987).

[2] (a) T. Munakata and T. Kawakatsu, Prog. Theor. Phys. *74*, 262 (1985); (b) T. Munakata, Prog. Theor. Phys. *75*, 747 (1986).

[3] S. Martin and W. Martienssen, Phys, Rev. Lett. *56*, 1522 (1986).

[4] (a) W. W. Chow, J. Gea-Banacloche, L. M. Pedrotti, V. E. Sanders, W. Schleich, and M. O. Scully, Rev. Mod. Phys. *57*, 61 (1985); (b) M. O. Scully, Phys. Rev. *A 35*, 752 (1987); (c) J. Krause and M. O. Scully, Phys. Rev. *A 36*, 1771 (1987).

[5] (a) M. James and F. Moss, J. Opt. Soc. Am. *B5*, 1121 (1988); (b) J. Y. Gao and L. M. Narducci, Opt. Commun., *58*, 360 (1986).

[6] R. G. K. Habiger, H. Risken, M. James, F. Moss, and W. Schleich, Phys. Rev. *A 41*, 3950 (1990).

[7] (a) H. Risken, The Fokker-Planck Equation: Methods of Solution and Applications, 2nd edition, Springer-Verlag, Berlin 1989; (b) N. G. Van Kampen, Stochastic Processes in Physics and Chemistry, North-Holland, Amsterdam 1981; (c) W. Horsthemke and R. Lefever, Noise Induced Transitions, Theory and Applications in Physics, Chemistry and Biology, Springer-Verlag, Berlin 1984; (d) P. Hänggi and H. Thomas, Phys. Rep. *88C*, 207 (1982).

[8] H. A. Kramers, Physica, *7*, 284 (1940); for a review see: P. Hänggi, P. Talkner, and M. Borkovec, Rev. Mod. Phys. *62*, 251 (1990).

[9] R. Benzi, S. Sutera, and A. Vulpiani, J. Phys. *A 14*, L 453 (1981).

[10] (a) J.-P. Eckmann, L. Thomas, and P. Wittwer, J. Phys. *A 14*, 3153 (1981); (b) J.-P. Eckmann and L. E. Thomas, J. Phys. *A 15*, L 261 (1982).

[11] R. Benzi, A. Sutera, and A. Vulpiani, J. Phys. *A 18*, 2239 (1985).

[12] (a) R. Benzi, G. Parisi, A. Sutera, and A Vulpiani, Tellus *34*, 10 (1982); (b) R. Benzi, G. Parisi, A. Sutera, and A. Vulpiani, SIAM, J. Appl. Math. *43*, 565 (1983); (c) A. Sutera, Quart. J. R. Meterol. Soc. *107*, 137 (1981).

[13] See for example, M. Ghil and S. Childress, Topics in Geophysical Fluid Dynamics: Atmospheric Dynamics, Dynamo Theory and Climate Dynamics Part IV. Springer-Verlag, Berlin 1987.

[14] S. Fauve and F. Heslot, Phys. Lett. *97 A*, 5 (1983).

[15] (a) B. McNamara, K. Wiesenfeld, and R. Roy, Phys. Rev. Lett. *60*, 2626 (1988); (b) G. Vermuri and R. Roy, Phys. Rev. *A 39*, 4668 (1989).

[16] B. McNamara and K. Wiesenfeld, Phys. Rev. *A 39*, 4854 (1989).

[17] R. F. Fox, Phys. Rev. *A 39*, 4148 (1989).

[18] (a) P. Jung, Z. Phys. *B 16*, 521 (1989); (b) P. Jung and P. Hänggi, Europhys. Lett. *8*, 505 (1989).

[19] P. Jung, this volume.

[20] C. Presilla, F. Marchesoni, and L. Gammaitoni, Phys. Rev. *A 40*, 2105 (1989).

[21] P. Jung and P. Hänggi, Phys. Rev. *A 41*, 2977 (1990).

[22] T. Zhou, F. Moss, and P. Jung, Phys. Rev. *A*, *42*, 3161 (1990).

[23] (a) L. Gammaitoni, F. Marchesoni, E. Menichella-Saetta, and S. Santucci, Phys. Rev. Lett. *62*, 349 (1989); (b) L. Gammaitoni, E. Menichella-Saetta, S. Santucci, F. Marchesoni, and C. Presilla, Phys. Rev. *A 40*, 2114 (1989).

[24] (a) G. Debnath, T. Zhou, and F. Moss. Phys. Rev. *A 39*, 4323 (1989); (b) T. Zhou and F. Moss, Phys. Rev. *A 41*, 4255 (1990).

[25] A. Bulsara, E. Jacobs, T. Zhou, F. Moss, and L. Kiss, in press, J. Theor. Biol.

[26] B. Carolli, C. Carolli, B. Roulet, and D. Saint-James, Physica *A 108*, 233 (1981).

[27] P. Bryant, K. Wiesenfeld, and B. McNamara, J. Appl. Phys. *62*, 2898 (1987).

[28] J. J. Hopfield, Proc. Nat. Acad. Sci. USA *81*, 3088 (1984), and references therein.

[29] For a review, see Noise in Nonlinear Dynamical Systems, Vol. 3, p. 243, edited by F. Moss and P. E. V. McClintock, Cambridge University Press, Cambridge 1989.

[30] These specialized electronic components can be obtained from Analog Devices, Inc., Box 9106, Norwood, MA 02062, USA or Burr-Brown, Inc., Box 11400, Tucson, AZ 85734, USA.

[31] Quan-Tech model 420.

[32] In the simulations described here, filtered real noise, having a non zero correlation time τ_n, is applied to the electronic model. However, we wish to compare our results to a white noise ($\tau_n \to 0$) theory. In the simulations we therefore keep the ratio $\tau_n/\tau_i = 0.1$, which is a reasonable approximation to white noise within the limits of accuracy of the analog simulator. The integrator time constant τ_i is the system characteristic time by which all other times are scaled. See Ref. [29] for further details.

[33] J. E Fletcher, S. Havlin, and G. W. Weiss, J. Stat. Phys. *51*, 215 (1988).

Presented at the Discussion Meeting of the Deutsche Bunsen-Gesellschaft für Physikalische Chemie "Rate Processes in Dissipative Systems: 50 Years after Kramers" in Tutzing, September 10–13, 1990 E 7500

Effect of Periodic Driving on the Escape in Periodic Potentials

Peter Jung and Peter Hänggi

Lehrstuhl für Theoretische Physik, Universität Augsburg, Memminger Straße 6, D-8900 Augsburg, Germany

Chemical Kinetics / Diffusion / Nonequilibrium Phenomena / Statistical Mechanics

We consider activation processes in multistable systems exposed to external fluctuations and periodic modulation. The concept of defining escape rates out of a basin of attraction as the ratio of total flux over the basin boundary and the population inside the basin of attraction is generalized for periodically driven systems. Thereby, the escape rate is connected with the Floquet-spectrum of the time inhomogeneous Fokker-Planck operator. Our formalism is demonstrated for the particular case of a multistable washboard potential. Numerical results are compared with theoretical results in the limits of small and large driving frequencies, respectively.

1. Introduction

Activation processes in bi- and multistable systems play an important role in many fields of physics and chemistry such as optical bistability [1], tunnel junctions [2] and chemical reaction kinetics [3] to quote but a few. The common situation is a dynamical system with at least two basins of attraction. Fluctuations provide the possibility of crossing a basin boundary and thus give rise to escape events. The statistics of barrier crossings has been discussed in terms of escape rates in the celebrated paper by Kramers [4], and subsequently in a large number of publications [5]. More recently, the role of additional periodic driving, modeling the influence of periodic external fields, has been considered in a number of experimental and theoretical investigations [6]. In the low friction regime, the dynamical system has been transformed to action angle variables, yielding under the assumption of regular deterministic motion a time homogeneous Fokker-Planck equation in action or equivalently in energy space [6a,f]. The overdamped limit has been considered recently by one of us for a quartic double well potential [7]. In the regime of small and large driving frequencies, approximation schemes have been derived [7] while, thus far, in the intermediate regime only numerical results are yet available.

In section 2 of this paper a general concept for escape rates in periodically driven systems is presented. In section 3 the particular model, Brownian motion in a washboard potential, is introduced and the equations of motion are discussed. The connections between escape rates, mobility and the diffusion coefficient in the overdamped limit are derived within a jump model in section 4. In section 5, the enhancement of the escape rate due to periodic forcing is computed as a function of the driving amplitude and frequency in the overdamped limit.

The static current voltage characteristics, i.e. the averaged velocity as a function of the bias, is known to exhibit Shapiro steps. In section 6, the dynamical current voltage characteristic, i.e. the averaged velocity as a function of the driving amplitude, is evaluated. The observed dynamical behavior is surprisingly rich and includes besides steps, which are closely related to Shapiro steps, also oscillatory behavior. One main difference to the static current-voltage characteristic is that the averaged velocity can also decrease with increasing driving amplitude.

2. Basic Concept

In this section a general concept for escape rates in systems with periodic forcing is presented. For the following discussion we assume that our problem is stated in terms of a set of Langevin equations

$$\dot{x}_i = h_i(x_1,x_2,\ldots,x_n) + \xi_i(t) \quad i = 1,2,\ldots,n\,, \tag{2.1}$$

where the set $\{x_i\}$ denotes macrovariables, $h_i(x_1,\ldots,x_n)$ are the force fields acting on x_i and ξ_i are Gaussian white noise forces, i.e.

$$\begin{aligned} &\langle \xi_i(t)\rangle = 0 \\ &\langle \xi_i(t)\,\xi_j(t')\rangle = 2D\delta_{ij}\delta(t-t')\,. \end{aligned} \tag{2.2}$$

The dynamical system without noise is assumed to have two coexisting basins of attraction, A_1 and A_2. Under the influence of noise, the systems can cross the basin boundary and can thus escape from one basin of attraction to the other. Injecting particles in A_1 and absorbing them in the neighboring attractor A_2 (by appropriate use of reflecting and absorbing boundary conditions [3]) a stationary flux $S_{12}(x)$ over the basin boundary $\partial(A_1,A_2)$ between A_1 and A_2 builds up. The escape rate from A_1 to A_2 is then given by the ratio of the total flux over the basin boundary and the total population in A_1, i.e. [8]

$$r^{12} = \int\limits_{\partial(A_1,A_2)} \mathrm{d}x^{n-1}\, n(x)\, S_{12}(x) \Big/ \int\limits_{A_1} \mathrm{d}x^n\, p(x)\,. \tag{2.3}$$

In the weak noise limit, i.e. $D\to 0$, the rates are connected to the smallest non-vanishing eigenvalue $\lambda_{\min}$ of the Fokker-Planck equation, corresponding to (2.1, 2.2), by

$$\lambda_{\min} = r^{12} + r^{21}\,. \tag{2.4}$$

In periodically driven systems, e.g.

$$\begin{aligned} &\dot{x}_i = h_i(x_1,x_2,\ldots,x_n) + \delta_{ik} A \sin\Omega t + \xi_i(t)\,, \\ &\quad i = 1,2,\ldots,n \text{ and } k\in[1,n]\,, \end{aligned} \tag{2.5}$$

there is no stationary structure of attractors in the phase space, spanned up by the variables x_i. Thus, the flux-over-population method cannot immediately be applied. Time dependent escape rates, defined as momentary rates have been discussed in the literature [9]. As a consequence, the decay of the population is non-exponential [10]. The latter conception is therefore questionable. In the following we introduce a concept which results in time independent escape rates and in exponentially decaying populations.

In a first step we extend the phase space to $n+1$ dimensions by introducing the additional variable $\Theta \equiv \Omega t + \varphi$. Escape rates are now defined in the same way just as in the stationary case, but now in the extended phase space. Particles have to be injected into and absorbed out of the relevant attractors in the extended phase space. The resulting stationary flux has to be integrated along the basin boundary of the extended phase space. Since the integration of the flux along the basin boundary involves also an integration over the additional variable Θ, the total flux and thus also the rate is time-independent [7, 11]. The smallest non-vanishing eigenvalue $\lambda^{(2)}_{\min}$ of the Fokker-Planck equation in the extended phase space is connected in the limit of weak noise to the escape rates $\hat{r}^{12}$ and $\hat{r}^{21}$ evaluated via flux over population method in the extended phase space by

$$\lambda^{(2)}_{\min} = \hat{r}^{12} + \hat{r}^{21}\,. \tag{2.6}$$

The eigenvalues of the Fokker-Planck equation in the extended phase space are indentical with the Floquet-coefficients of the non-stationary stochastic process in n dimensions [7, 11, 12] (described by the Fokker-Planck equation corresponding to (2.1) without extending the phase space).

Thus, the escape rate of the periodically driven stochastic process (2.5) is also given by the smallest non-vanishing Floquet-coefficient of the corresponding time inhomogeneous Fokker-Planck equation.

In one dimensional bistable systems, i.e. $n=1$, the extended phase space is the two-dimensional $x-\Theta$-space. The basin boundary is the unstable periodic orbit, i.e. $\partial(A_1, A_2)$ is a one-dimensional object in $x-\theta$-space. In two-dimensional problems, such as the Kramers' problem with periodic driving, $\dot{x}=v$, $\dot{v}=-\gamma v+f(x)+A\sin\Omega t+\xi(t)$, the extended phase space becomes three-dimensional and the basin boundary is an object which is two dimensional below homoclinic threshold (regular motion), and a fractal above homoclinic threshold (irregular motion). The escape in the latter case is connected with the flux through a fractal basin boundary. While the regular regime has been treated in the weak damping limit within an energy diffusion equation as mentioned in the introduction, the irregular regime is not yet solved.

3. The Model: Equations of Motion

The (tilted) one dimensional washboard potential

$$V(x) = -d\cos x - \hat{F}x \tag{3.1}$$

is a multistable potential for $\hat{F} < d$ with minima and maxima given by

$$x_n^{\min} = \arcsin\frac{\hat{F}}{d} + 2\pi n \qquad n = 0, \pm 1, \pm 2, \ldots \tag{3.2}$$

$$x_n^{\max} = \pi - \arcsin\frac{\hat{F}}{d} + 2\pi n \qquad n = 0, \pm 1, \pm 2, \ldots . \tag{3.3}$$

The variable x is dimensionless and can thus be interpreted as an angle variable (but not necessarily modulo 2π). The Newtonian equation of motion supplemented by a noise term, i.e. the Langevin equation, reads:

$$\ddot{x} + \hat{\gamma}\dot{x} - V'(x) = \hat{A}\sin(\omega\hat{t}) + \xi(\hat{t}), \tag{3.4}$$

where dots indicate differentiation with respect to the time $\hat{t}$. The fluctuation-dissipation-theorem of the second kind [13] is fulfilled without periodic driving, i.e.

$$\langle \xi(\hat{t})\,\xi(\hat{t}')\rangle = 2\hat{\gamma}kT\,\delta(\hat{t}-\hat{t}'). \tag{3.5}$$

In dimensionless variables, i.e.

$$\begin{aligned}
\bar{t} &\equiv \sqrt{d}\hat{t}\\
\gamma &\equiv \hat{\gamma}/\sqrt{d}\\
A &\equiv \hat{A}/\sqrt{d}\\
\bar{\Omega} &\equiv \omega/\sqrt{d}\\
D &\equiv kT/d\\
F &\equiv \hat{F}/d
\end{aligned}$$

the Langevin equation (3.4) reads

$$\ddot{x} + \gamma\dot{x} + \sin x = F + A\sin(\bar{\Omega}\bar{t}) + \xi(\bar{t}) \tag{3.6}$$

with

$$\langle \xi(\bar{t})\,\xi(\bar{t}')\rangle = 2\bar{\gamma}D\,\delta(\bar{t}-\bar{t}'). \tag{3.7}$$

Here, the dots denote differentiation with respect to $\bar{t}$. For large damping, i.e. $\gamma \gg \sqrt{d}$, the first term on the l.h.s. of (3.6) or equivalently (3.4) can be neglected, and we obtain

$$\frac{dx}{dt} = -\sin x + F + A\sin\Omega t + \sqrt{D}\,\xi(t), \tag{3.8}$$

with the scaled time $t \equiv (d/\hat{\gamma})\bar{t} = \gamma^{-1}\bar{t}$ and the scaled frequency $\Omega = \gamma\bar{\Omega} = (\hat{\gamma}/d)\omega$.

4. Escape Rates, Mobility and Diffusion Constant in the Overdamped Limit

The stochastic dynamics in the multiwell potential (3.1) may be modelled by a hopping dynamics between the wells. In the overdamped case there is only hopping between neighboring wells, i.e.

$$\dot{P}_n = r^+ P_{n-1} + r^- P_{n+1} - (r^+ + r^-)P_n, \tag{4.1}$$

where P_n denotes the probability that the system is in the p-th well and $r^{\pm}$ are the escape rates from the n-th to the $(n\pm 1)$-th well. The rates r^+ and r^- are assumed to be independent of the site n. In periodically modulated systems the rates and populations above are understood as those defined in the extended phase space. The stationary solution for k-fold periodic boundary conditions, i.e.

$$P_{n+2\pi k} = P_n \tag{4.2}$$

is the uniform distribution

$$P_n^{(\mathrm{st})} = 1/k. \tag{4.3}$$

The mean velocity is given by the product of the stationary flux $(r^+ - r^-)P^{(\mathrm{st})}$ and the length $2\pi k$, i.e.

$$\langle v\rangle = 2\pi(r^+ - r^-). \tag{4.4a}$$

The mobility, defined by the ratio of the mean velocity $\langle v\rangle$ and force F then reads

$$\mu = \frac{\langle v\rangle}{F} = \frac{2\pi}{F}(r^+ - r^-). \tag{4.4b}$$

The diffusion coefficient can be obtained from the first and second-order moments $\langle n(t)\rangle$ and $\langle n^2(t)\rangle$ of the master equation (4.1)

$$\begin{aligned}
\langle n^2(t)\rangle &= (r^+ + r^-)t + (r^+ - r^-)^2 t^2\\
\langle n(t)\rangle &= (r^+ - r^-)t.
\end{aligned} \tag{4.5}$$

The second term on the r.h.s. of the first equation of (4.5) is a transport term and vanishes for zero bias, while the first term on the r.h.s. of (4.5) is a diffusive term. The diffusion coefficient D_{eff}, defined by

$$D_{\text{eff}} = \frac{1}{2}\frac{\mathrm{d}}{\mathrm{d}t}\langle(x(t)-\langle x(t)\rangle)^2\rangle \tag{4.6}$$

is given by

$$D_{\text{eff}} = \frac{1}{2}(2\pi)^2\frac{\mathrm{d}}{\mathrm{d}t}(\langle n^2(t)\rangle - \langle n(t)\rangle^2) = 2\pi^2(r^+ + r^-). \tag{4.7}$$

In the weak noise limit, the escape rate is connected with the smallest non-vanishing eigenvalue of the Fokker-Planck operator corresponding to (3.8) in the extended phase space.

A delicate problem, however, is the choice of the boundary conditions for the Fokker-Planck equation. Using simple periodic boundary conditions, i.e. $P(x,\theta,t) = P(x+2\pi,\theta,t)$, the potential is not bistable in the interval $[0,2\pi]$. The outgoing flux at one boundary is identical with the incoming flux at the other boundary. Thus, the population in the well is not decaying and the smallest non-vanishing eigenvalue has not the meaning of an escape rate. Using two-fold periodic boundary conditions, i.e. $P(x,\theta,t) = P(x+4\pi,\theta,t)$, the potential is bistable in $[0,4\pi]$. Thus, the population in one of the wells may decay, and the smallest non-vanishing eigenvalue $\lambda_{\min}$ is connected with the escape rates $r^{\pm}$ by

$$\lambda_{\min} = 2(r^+ + r^-). \tag{4.8}$$

Using n-fold periodic boundary conditions, i.e. $P(x,\theta,t) = P(x+2\pi n,\theta,t)$, additional branches of eigenvalues emerge, being connected with relaxation processes between not-adjacent potential wells. The situation can be understood in terms of a Bloch theory. A periodic force field in space x provides eigen-solutions of the Bloch-type,

$$\psi_\sigma^k(x,\theta) = \exp(\mathrm{i}kx)\,u_\sigma^k(x,\theta) \tag{4.9a}$$

with

$$u_\sigma^k(x+2\pi,\theta) = u_\sigma^k(x,\theta), \tag{4.9b}$$

where the quasi continuous index k may be restricted to the first Brillouin zone (Bz), i.e. $-1/2 < k < 1/2$ (in the symmetric choice). In Fig. 1 a typical band structure is sketched for illustration. The other index σ numbers the eigenvalues for a given value of k, i.e. is the analogue to the band index in solid state theory. Simple periodic boundary conditions restrict the possible values for k to $k=0$, while two-fold periodic boundary conditions allow for $k=0,\pm 1/2$. n-fold periodic boundary conditions select as possible values $k_n = 0, \pm 1/n, \pm 2/n, \ldots$ with $|k_n| < 1/2$. The relevant eigenvalue for the rate, however, is only the smallest non-vanishing eigenvalue at one of the boundaries of the first Bz, although there are smaller eigenvalues within the first Bz. Note, that for $(2n+1)$-fold periodic boundary conditions, the Bz boundaries $k = \pm 1/2$ are not allowed values. Therefore, for this choice of boundary conditions the rates are not connected via (4.8) to eigenvalues!

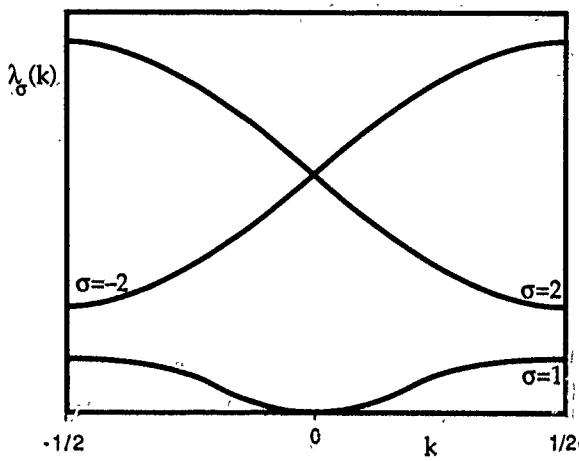


Fig. 1
A typical reduced band structure for the eigenvalues of a Fokker-Planck equation with a periodic potential is shown. Two bands $\sigma=1$ and $\sigma=\pm 2$ are plotted within the first Brillouin zone $k\in[-1/2,1/2]$

The individual rates $r^{\pm}$ may be obtained by using (4.4b) and (4.8), i.e.

$$r^{\pm} = \frac{\lambda_{\min}}{4} \pm \frac{\mu F}{4\pi}. \tag{4.10}$$

For symmetric potentials ($F=0$) the rates $r^{\pm}$ are obtained from the eigenvalue $\lambda_{\min}$ only, while for tilted potentials ($F\neq 0$) it is necessary to compute also the mobility.

Finally we note that the diffusion coefficient D_{eff} in (4.6) is connected to the eigenvalue $\lambda_{\min}$ by

$$D_{\text{eff}} = \pi^2\lambda_{\min}. \tag{4.11}$$

4.1. Results for the Unperturbed System ($A = 0$)

Here we briefly review on the results without periodic driving. In Gaussian approximation the rates are given by [14]

$$r^{\pm} = \frac{1}{2\pi}\sqrt{1-F^2}\exp\left[-\frac{1}{D}(\mp F + 2F\arcsin F + 2\sqrt{1-F^2})\right]. \tag{4.12}$$

The total rate out of a potential well is then given by

$$\begin{aligned} r_0 &= r^+ + r^- \\ &= \frac{1}{\pi}\sqrt{1-F^2}\exp\left[-\frac{2}{D}F\arcsin F\right. \\ &\quad \left. -\frac{2}{D}\sqrt{1-F^2}\right]\cosh\left(\frac{F\pi}{D}\right). \end{aligned} \tag{4.13}$$

In (4.12) and (4.13) the normalization of (3.8) has been used. The mobility is obtained from (4.4b), i.e.

$$\mu = \frac{2}{F}\sqrt{1-F^2}\exp\left[-\frac{2}{D}F\arcsin F - \frac{2}{D}\sqrt{1-F^2}\right]\sinh\left(\frac{F\pi}{D}\right), \tag{4.14}$$

while the diffusion coefficient D_{eff} is given by

$$D_{\text{eff}} = 2\pi\sqrt{1-F^2}\exp\left[-\frac{2}{D}F\arcsin F - \frac{2}{D}\sqrt{1-F^2}\right]\cosh\left(\frac{F\pi}{D}\right). \tag{4.15}$$

5. Escape Rates for the Periodically Forced System in the Overdamped Limit

The Langevin equation (3.8) in the extended phase space reads

$$\dot{x} = -\sin x + F + A\sin\theta + \xi(t)$$
$$\dot{\theta} = \Omega. \tag{5.1}$$

Without noise, the unstable periodic orbits for small A/Ω^2 may be obtained by linearization around the unstable fixed points, i.e.

$$x^n_{\text{un}}(\theta) = \pi(2n+1) - \arcsin F + \frac{A}{\sqrt{1-F^2+\Omega^2}}\sin\left[\theta - \arctan\left(\frac{\Omega}{\sqrt{1-F^2}}\right)\right], \tag{5.2}$$

where $n = 0, \pm 1, \pm 2, \ldots$ The stable periodic orbits for small A/Ω^2 are obtained similarly and are given by

$$x^n_{\text{st}}(\theta) = 2n\pi + \arcsin F + \frac{A}{\sqrt{1-F^2+\Omega^2}}\sin\left(\theta - \arctan\left(\frac{\Omega}{\sqrt{1-F^2}}\right)\right). \tag{5.3}$$

In Fig. 2, the $x-\theta$ phase space ($x \in [-\pi, 3\pi]$, $\theta \in [0, 2\pi]$ is shown with numerically evaluated stable and unstable periodic orbits without bias ($F = 0$) for $A = 0.5$. The unstable periodic orbit divides the phase space into two basins of attraction. The basin boundary becomes for large frequencies Ω or small driving amplitudes A a straight line. The escape rate is given in terms of the smallest non-vanishing real eigenvalue $\lambda_{\min}(A,\Omega,D)$ of the Fokker-Planck equation

$$\frac{\partial}{\partial t}P(x,\theta,t) = \frac{\partial}{\partial x}(\sin x + A\sin\theta)\,P(x,\theta,t) - \Omega\frac{\partial}{\partial\theta}P(x,\theta,t) + D\frac{\partial}{\partial x^2}P(x,\theta,t) \equiv L_{\text{FP}}P(x,\theta,t) \tag{5.4}$$

for periodic boundary conditions in θ, i.e. $P(x,\theta,t) = P(x,\theta+2\pi,t)$ and two-fold periodic boundary conditions in x, i.e. $P(x,\theta,t) = P(x+4\pi,\theta,t)$. More generally, the full band-scheme for the eigenvalues $\lambda_\sigma(k)$ is obtained from the boundary value problem

$$[\lambda_\sigma(k) + Dk^2]\,u^k_\sigma(x,\theta) = \left[L_{\text{FP}} + ik(\sin x + A\sin\theta) + 2iDk\frac{\partial}{\partial x}\right]u^k_\sigma(x;\theta) \tag{5.5}$$

with simple periodic boundary conditions for $u^k_\sigma(x,\theta)$ in θ and x and $k \in [-1/2, 1/2]$. As already mentioned earlier, $\lambda_{\min}$ is identical with $\lambda_{\sigma=1}(k = 1/2)$.

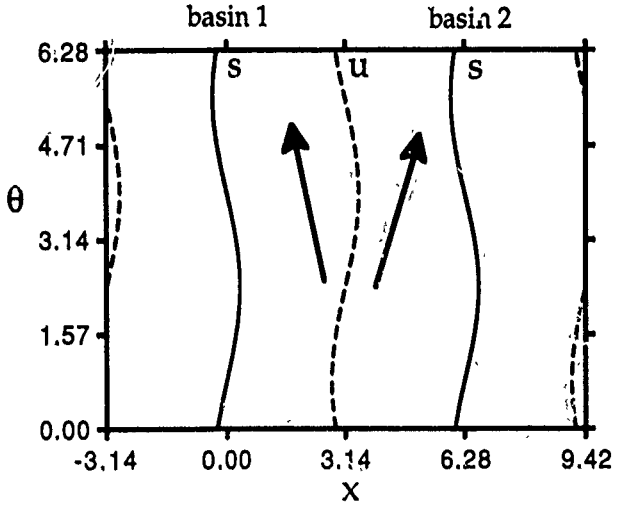


Fig. 2
The stable (full lines) and unstable (dashed lines) periodic orbits are shown in the $x-\theta$ phase space. The unstable periodic orbit close to $x = \pi$ separates the phase space $x \in [-\pi, 3\pi]$ into two basins of attraction. The attractors are the stable periodic orbits (limit cycles) in the $x-\theta$ phase space

The numerically evaluated rate enhancement $\eta(A,\Omega,D)$ due to the periodic driving, i.e.

$$\eta(A,\Omega,D) = \frac{\lambda(A,\Omega,D)}{\lambda(A=0,D)} - 1 \tag{5.6}$$

is plotted in Fig. 3 as a function of the amplitude A for different values of the driving frequency in a double logarithmic plot. The straight lines for small A with a slope of 2 clearly indicate the law

$$\eta(A,\Omega,D) = \kappa(\Omega,D)\,A^2 \tag{5.7}$$

being valid for small driving amplitudes A. In Fig. 4, the rate enhancement factor $\kappa(\Omega,D)$ is shown as a function of the driving frequency Ω for various values of the noise strength D in a double logarithmic plot. For small Ω, the factor κ reaches a certain plateau, while for large Ω the rate enhancement factor exhibits a decrease $\propto \Omega^{-2}$.

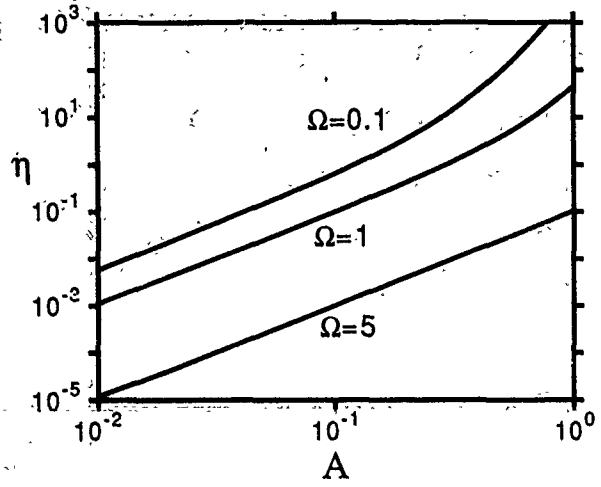


Fig. 3
The rate enhancement $\eta(A,\Omega)$ is shown as a function of A in a double logarithmic plot for $\Omega = 0.1$, $\Omega = 1$ and $\Omega = 5$. The power law for small A is evident

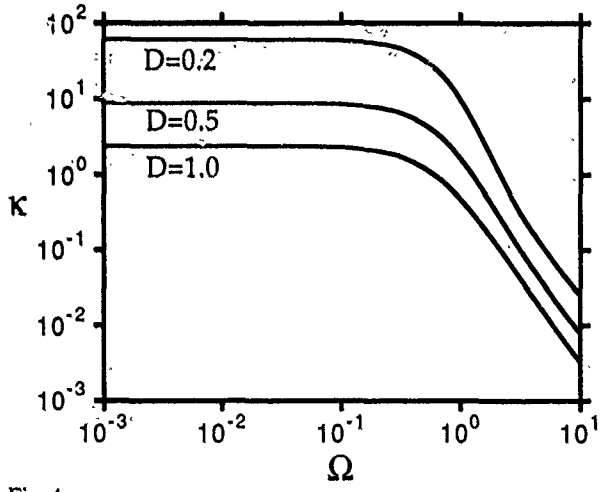


Fig. 4
The rate enhancement factor κ is shown as a function of the driving frequency Ω for $D = 0.2$, $D = 0.5$ and $D = 1$

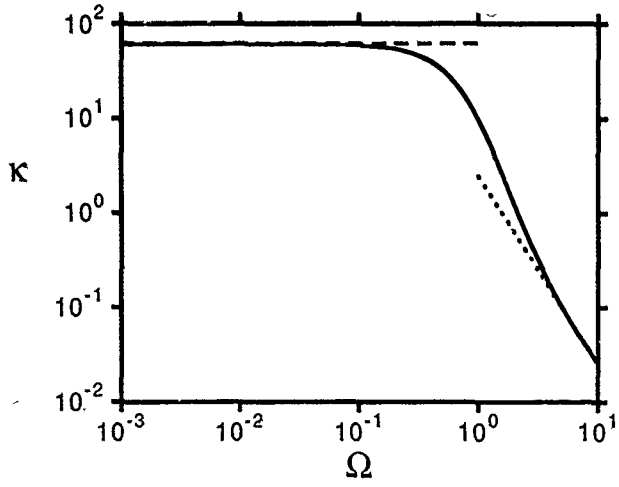


Fig. 5
The rate enhancement factor κ is compared with the theoretical results (5.9) and (5.10) at $D = 0.2$ for small and large driving frequencies.

Both limits, Ω small and Ω large, can be described approximately. For small frequencies $\Omega \ll \omega_{\text{hopping}}$ an adiabatic approximation [7] yields

$$\eta(A,\Omega,D) \approx I_0(A\pi/D) - 1\,, \tag{5.8}$$

where $I_0(x)$ is a modified Bessel function [15]. For $A/D \to 0$ one finds approximately

$$\kappa(\Omega,D) = \frac{\eta}{A^2} \approx \frac{\pi^2}{4D^2}\,. \tag{5.9}$$

The crux with the adiabatic approximation is that with small noise strength it is valid only for exponentially small driving frequencies.

In the high frequency limit the averaging method of Ref. 7 yields for the rate enhancement

$$\eta(A,\Omega,D) \approx \frac{1}{2D\Omega^2}A^2 \text{ or } \kappa \approx \frac{1}{2D\Omega^2}\,. \tag{5.10}$$

Both limits (5.9) and (5.10) are compared with the numerical results for $D = 0.2$ in Fig. 5.

We do not discuss individual rate r^+ or r^- in the presence of bias ($F \neq 0$), since the effect of periodic driving is the same as in the symmetric case ($F = 0$). We want to point out, however, that they can be obtained by computing the averaged mobility μ and the relevant eigenvalue $\lambda_{\min}$ and by using (4.10). The effective diffusion coefficient D_{eff} (4.6) is connected with the relevant eigenvalue $\lambda_{\min}$ by Eq. (4.11) and thus exhibits the same dependence on the driving frequency and amplitude.

6. The Dynamical Current-Voltage Characteristic

The current-voltage characteristics of the model (3.8), i.e. $\langle \dot{x} \rangle$ (≡ voltage) as a function of the bias F (≡ current) has been discussed in the context of Josephson junctions [16], phase locking in electric circuits [17] and mode locking in ring laser gyroscopes [18]. The periodic driving gives rise to steps which have been observed first by Shapiro [19] in Josephson junctions. In terms of the model (3.8) without noise, these steps occur when the periodic output $x_p(t)$ "locks" into the phase of the periodic driving. The locking condition is fulfilled when the period $T = 2\pi/\Omega$ of the driving is a multiple of the time T_S, the system needs for running down the tilted potential one period $L = 2\pi$, i.e. when

$$\langle \dot{x} \rangle = n\Omega\,, \tag{6.1}$$

where $\langle \dot{x} \rangle$ is the averaged velocity along one spatial period 2π. The influence of noise consists in rounding the steps or destroying them if the noise strength is sufficiently large. Characteristic is the stepwise but monotonous increase of the voltage with increasing current F.

The dynamical current-voltage characteristic will be defined as the voltage $\langle \dot{x} \rangle$ as a function of the driving amplitude A. Without noise, such a dynamical current-voltage

characteristic is shown in Fig. 6a for $F=0.8$ and $\Omega=1$ (dashed line). The voltage vanishes for $A<A^{(1)}$, since the system cannot overcome the barrier. At $A=A^{(1)}$ the system jumps into a running state, and is locked into the phase of the periodic driving in the locking regime $n=1$ (see Eq. (6.1)). For $A^{(3)}>A>A^{(2)}$ the locking conditions cannot be fulfilled (for an explanation see below) and the voltage drops down. The locking conditions are fulfilled only on disconnected intervals of the A-axis, and the width of the locked regions decreases for increasing driving amplitudes A. For very large values of A, i.e. $A\to\infty$, the locking condition cannot be fulfilled any more and the voltage relaxes oscillatory to its asymptotic value $\langle\dot{x}\rangle = F$. The influence of noise (full line in Fig. 6a) results in rounding off the plateaus in the phase locked regions and finally in destroying the phase locking for large driving amplitudes.

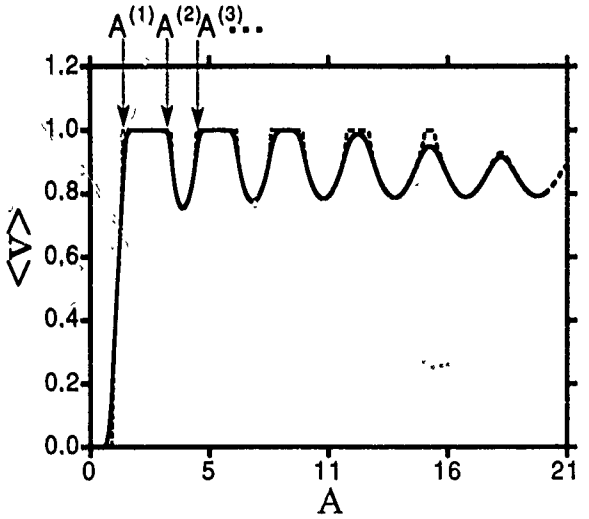


Fig. 6a:
The dynamical current-voltage characteristic ($\langle v\rangle \equiv \langle\dot{x}\rangle$) is shown for $F=0.8$ and $\Omega=1$ without noise (dashed line) and with the noise strength $D=0.01$ (full line)

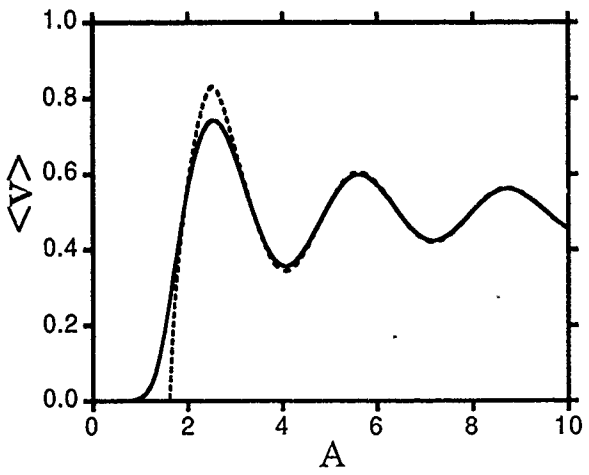


Fig. 6b:
The dynamical current-voltage characteristic ($\langle v\rangle \equiv \langle\dot{x}\rangle$) is shown for $F=0.5$ and $\Omega=1$ without noise (dashed line) and with the noise strength $D=0.01$ (full line)

In Fig. 6b the dynamical current voltage characteristics is shown for the smaller bias $F=05$. Here are no phase locked regions at all. The locked regions are estimated without noise in the following [20]. For convenience we choose a cos-driving in the equation of motion, i.e.

$$\dot{x} = -\sin x + A\cos\Omega t + F\,. \tag{6.2}$$

Inserting the ansatz

$$x(t) = x_0 + \frac{A}{\Omega}\sin\Omega t + \langle\dot{x}\rangle t \tag{6.3}$$

into (6.2) we obtain

$$\langle\dot{x}\rangle = F - \sum_{k=-\infty}^{\infty} J_k(A/\Omega)\sin(x_0 + (k\Omega + \langle\dot{x}\rangle)t) \tag{6.4}$$

from which $\langle\dot{x}\rangle$ follows self consistently. In (6.4) $J_k(x)$ are Bessel functions [15], and x_0 is an arbitrary phase. In the phase locked regions we find by using (6.1) and averaging over one period the conditions for locking into the n-th region, i.e.

$$F - n\Omega = J_n(A/\Omega)\,(-1)^n \sin x_0\,. \tag{6.5}$$

For the 0-th region ($\langle\dot{x}\rangle = 0$) the condition $F = J_0(A/W)\sin x_0$ has to be fulfilled. The solution is discussed graphically in Fig. 7 for $F=0.8$. It follows from Fig. 7 that for $A>A^{(1)}$ there is no x_0 which makes the locking condition for $n=0$ fulfilled. For $A>A^{(1)}$, however, the condition (6.5) for $n=1$ can be fulfilled and the system locks into the $n=1$ region. At a certain value of $A=A^{(2)}$ the condition (6.5) for $n=1$ can not be fulfilled any more and the locked regime $\langle\dot{x}\rangle = 2\Omega (n=2)$ cannot be reached for $\Omega=1$. Thus, the system cannot lock to the external signal and the voltage $\langle\dot{x}\rangle$ shows oscillatory behavior as a function of the driving am-

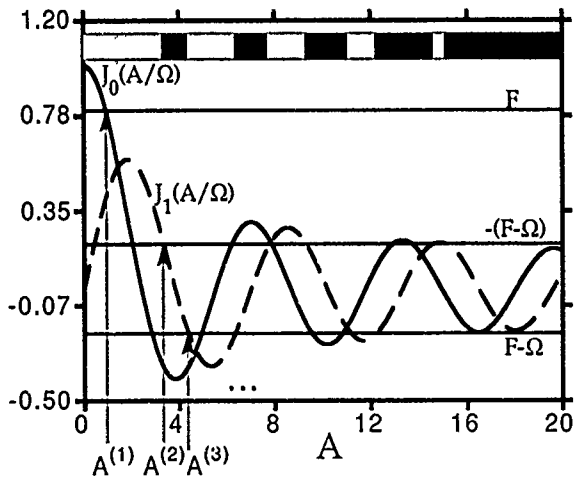


Fig. 7
The functions $J_0(A/\Omega)$ (full line) and $J_1(A/\Omega)$ (dashed line) are plotted together with the straight lines F, $F-\Omega$ and $\Omega-F$. The light regions of the stripe on top of the curves indicate phase locked regions

plitude. Due to the oscillatory behavior of the Bessel functions, the locking condition for $n = 1$ can be fulfilled again in a number of intervals of larger A. It is obvious from Fig. 7 that the width of the locked intervals decrease for increasing values of the driving amplitude A until the Bessel functions, which decay asymptotically proportional to $A^{-1/2}$, are too small for locking. Note, that the agreement of the numerical values $A^{(i)}$ (Fig. 6a) with those obtained from the theory becomes better for increasing driving amplitudes.

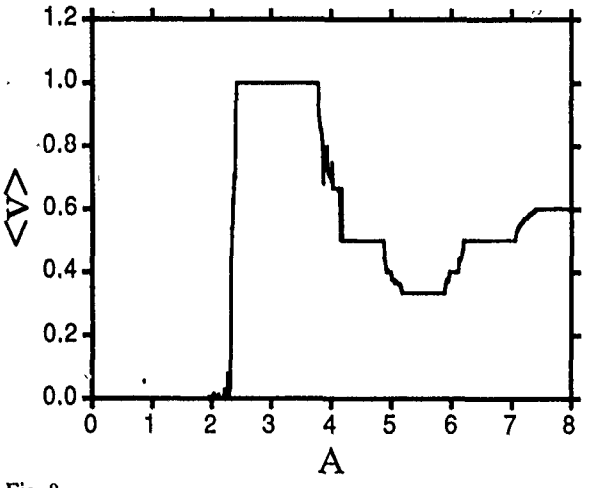


Fig. 8
The dynamical current voltage characteristic with an inertia term (model (3.4)) is shown for $F = 0.5$, $\bar{\Omega} = 1$ and $\gamma = 1$.

The dynamical current-voltage characteristics for systems with inertia (the model 3.4)) is even more rich, since it allows also for subharmonic phase locking, i.e.

$$\langle v \rangle = \frac{m}{n}\Omega \qquad m, n \in \mathbb{N}\,. \tag{6.7}$$

The numerical results for $F = 0.5$, $\bar{\Omega} = 1$ and $\gamma = 1$ are shown in Fig. 8 for vanishing noise. The voltage $\langle \dot{x} \rangle$ as a function of the driving amplitude shows besides the steps also regions with wild oscillations. These oscillations occur with chaotic solutions.

7. Conclusions

In this paper we have presented a concept for escape rates in periodically driven systems. For a periodic (multistable) potential we have derived explicit results for the escape rate as a function of the driving frequency and amplitude. The relations between rates, mobilitiy and diffusion coefficients have been discussed as well as the role of boundary conditions. In addition we have presented dynamical current-voltage characteristics, i.e. $\langle \dot{x} \rangle$ as a function of the driving amplitude A. The observed rich dynamical behavior has been explained in terms of phase locking.

We are grateful for the financial support by the Stiftung Volkswagenwerk. We wish to thank Peter Talkner for helpful discussions on rate theory.

References

[1] In "Optical Bistability III", edited by H. M. Gibbs, P. Mandel, N. Peyghambarian and S. D. Smith, Springer Verlag Berlin, Heidelberg, New-York, Tokyo.
[2] For an overview, see A. Barone and G. Paterno, Physics and Applications of the Josephson Effect, John Wiley & Sons, New York 1982.
[3] For an overview see P. Hänggi, P. Talkner, and M. Borkovec, Rev. Mod. Phys. *62*, 251 (1990).
[4] K. H. Kramers, Physica *7*, 284 (1940).
[5] See references in Ref. [3].
[6] a) B. Carmeli and A. Nitzan, Phys. Rev. *A32*, 2435 (1985); b) H. M. Devoret, D. Esteve, J. M. Martinis, and J. Clarke, Phys. Rev. *B36*, 58 (1987); c) M. H. Devoret, J. M. Martinis, D. Esteve, and J. Clark, Phys. Rev. Lett. *53*, 1260 (1984); d) A. I. Larkin and Yu. N. Ovchinikov, Low Temp. Phys. *36*, 317 (1986); e) K. S. Chow and V. Ambegaokar, Phys. Rev. *B 38*, 11168 (1988); f) S. Linkwitz, Ph. D. thesis, University of Stuttgart (1990); A. L. Gerasimov, Phys. Lett. *A135*, 29 (1989); A. L. Gerasimov, J. Stat. Phys. *60*, 485 (1990); J. F. Schonfeld, Ann. Phys. (N.Y.) *160*, 149–263 (1985).
[7] P. Jung, Z. Phys. *B 76*, 521 (1989).
[8] L. Farkas, Z. Phys. Chem. (Leipzig) *125*, 236 (1927).
[9] a) B. Caroli, C. Caroli, B. Roulet, and D Saint-James, Physica *108 A*, 233 (1981); b) W. Weidlich and G. Haag, Z. Phys. *B 39*, 81 (1980).
[10] T. Zhou, F. Moss and P. Jung, Phys. Rev. *A 42*, 3161 (1990).
[11] P. Jung and P. Hänggi, Europhys. Lett. *8*, 505 (1989).
[12] P. Jung and P. Hänggi, Phys. Rev. *A 41*, 2977 (1990).
[13] R. Kubo and Toda, "Statistical Physics II", Springer Series in Solid-State Sciences, eds. M. Cardona. P. Fulde, H.-J. Queisser, Springer Verlag, Berlin, Heidelberg, New-York.
[14] R. L. Stratonovich, "Theory of Random Noise", Vol II, p. 254, Gordon & Breach, New York 1967.
[15] M. Abramowitz and I. A. Stegun, Handbook of Mathematical Functions, Dover Publications, Inc., New York 1972.
[16] R. L. Kautz, J. Appl. Phys. *52*, 3528 (1981).
[17] a) A. J. Viterbi: "Principles of coherent communication", McGraw-Hill, New York 1966; b) W. C. Lindsay: "Synchronization Systems in Communication and Control", Prentice Hall, Englewood Cliffs, New York 1972.
[18] W. Schleich, C.-S. Cha, and J. D. Cresser, Phys. Rev. *A 29*, 230 (1984).
[19] S. Shapiro, Phys. Rev. Lett. *11*, 80 (1963).
[20] In large parts we follow the calculations in Ref. [16].

Presented at the Discussion Meeting of the Deutsche Bunsen-Gesellschaft für Physikalische Chemie "Rate Processes in Dissipative Systems. 50 Years after Kramers" in Tutzing, September 10–13, 1990 E 7501

Dynamics of Multidimensional Barrier Crossing in the Overdamped Limit

Benny Carmeli[1], Vladimiro Mujica[2], and Abraham Nitzan[3]

School of Chemistry, Tel-Aviv University, Tel-Aviv 69978, Israel

Chemical Kinetics / Diffusion / Nonequilibrium Phenomena / Transport Properties

Two methods for numerical solution of multidimensional diffusion problems are presented and applied to the two dimensional barrier crossing problem in the overdamped limit. One of these methods is based on evaluating the smallest non-vanishing eigenvalue of the Smoluchowski equation, and the other is based on an adaption of Chandler's steady state correlation function approach. Both methods make use of the fast Fourier transform algorithm for solving a transformed version of the Smoluchowski equation. The numerical solutions are compared to results based on the Kramers theory and some observations concerning effects of the dynamics of barrier crossing problems are made.

1. Introduction

The concept of activated processes provides a common reference framework for the description of numerous important phenomena in chemistry and physics, such as chemical reactions in gaseous and condensed phases, desorption from and diffusion on surfaces, diffusion of atoms and ions inside solids, dynamics of Josephson junctions and others [1]. The Smoluchowski equation has been widely used for describing these and other kind of relaxation processes [2] in the overdamped (high friction) regime. In the one dimensional case it takes the following form

$$\frac{\partial}{\partial t} P(x,t|x') = D \frac{\partial}{\partial x}\left[\frac{\partial}{\partial x} + \beta \frac{\mathrm{d}V(x)}{\mathrm{d}x}\right] P(x,t|x') \qquad (1)$$

where $P(x,t|x')$ is the probability density for finding the system at position x at time t given that it has been initially at x', $D = k_B T/\gamma M$ is the diffusion constant (k_B is the Boltzman constant, T is the absolute temperature, γ denotes the friction coefficient and M is the mass of the diffusing particle), β is the inverse of $k_B T$ and $V(x)$ is the potential of mean force. While one dimensional models are frequently useful to describe the evolution of a system along the reaction coordinate (namely the minimum energy path between the initial and final states) motion in directions normal to the reaction coordinate may have significant dynamic consequences [2–13].

In this paper we discuss methods for the numerical solution of the multidimensional analog of Eq. (1), and apply two such methods to a two dimensional barrier crossing problem. Multidimensional effects on the dynamics of barrier crossing processes have been subjects of several studies lately [2–12]. Several issues, such as the effect of diffusion in directions other then the reaction coordinate, the effect of curvature of the reaction coordinate and the effect of non-isotropic diffusion, are of interest. A numerical algorithm based on the use of fast Fourier transform (FFT) for solving the diffusion equation was recently presented by Agmon and Kosloff [12]. Approximate methods based on time dependent self consistent field approximations were investigated by Kaufman and Whaley [14]. In the present work we describe an improved FFT method, where by transforming the original Smoluchowski equation to a Schrödinger-like equation (eliminating the first order spatial derivatives) we are able to use the analog of the Fleck and Feit split order propagation scheme [15] rather than the finite difference method of Kosloff and Kosloff [16]. Moreover, we focus on the barrier crossing rate, and apply the numerical technique to directly evaluate theoretically based expressions for this rate rather than trying to extract it from the resulting time evolution. Finally we use our results to discuss several issues associated with barrier crossing problems as mentioned above.

Section (2) of this paper describes the numerical method. Section (3) describes the application of the numerical approach to the calculation of the rate by solving for the smallest non-vanishing eigenvalue of the Smoluchowski equation and by evaluating the saturation-plateau value of $\langle N(0)\dot{N}(t)\rangle$ where $N(t)$ is the population in the reactant well at time t. Application to a particular two dimensional model is described in Section (4). Section (5) presents and discusses the numerical results for a model two dimensional system. We conclude in Section (6).

2. Numerical Solution of the Diffusion Equation

The multidimensional version of the diffusion equation (Eq. (1)) is

$$\frac{\partial}{\partial t} P(x,t|x') = \nabla^T \cdot \mathbf{D} \cdot [\nabla + \nabla(\beta V(x))]\, P(x,t|x') \qquad (2)$$

where x denotes a vector in the multidimensional configuration space and $\mathbf{D}$ is the multidimensional diffusion tensor.

---

[1] Present address: Department of Physics, Nuclear Research Centre – Negev, P.O. Box 9001, Beer-Sheva 84190, Israel.

[2] Present address: Escula de Quimica, Facultad de Ciencias, Universidad Central de Venezuela, Apartado 47102, Caracas 1051, Venezuela.

[3] Present address: Chemical Physics Department, Weizmann Institute of Science, Rehovot 76100, Israel.

 © VCH Verlagsgesellschaft mbH, W-6940 Weinheim, 1991 0005-9021/91/0303-0319 $ 3.50+.25/0

$\mathbf{D}$ is assumed to be constant (namely independent of position) but not necessarily isotropic.

A formal solution to Eq. (2) is

$$P(x,t|x') = \exp(\mathbf{L}t)\cdot P(x,t=0|x') \tag{3}$$

where

$$\mathbf{L} = \nabla^T\cdot\mathbf{D}\cdot[\nabla+\nabla(\beta V(x))]\,. \tag{4}$$

An exact solution to Eq. (2) cannot be obtained in the general case. The FFT method for solving time dependent problems associated with linear partial differential equations has been recently shown by Agmon and Kosloff [12] to be very useful for solving the Smoluchowski equation. The simplest time propagation procedure is based on a first order difference scheme, namely

$$P(x,t+\Delta t|x') = P(x,t|x')+\Delta t\mathbf{L}P(x,t|x')+O(\Delta t^2). \tag{5}$$

The 2nd order scheme used for Schrödinger equation is not stable in the present case. Agmon and Kosloff [12] have used an expansion of the evolution operator in Chebychev polinomials [16b]. Another convenient algorithm can be obtained in principle by working with the exponential propagator defined in Eq. (3), in the spirit of the split operator method of Feit and Fleck [15]. However since the operator $\mathbf{L}$ contains coupling between x and ∇ it is not possible to split $\exp(\mathbf{L}\Delta t)$ (for small Δt) into a product of exponentials which depend either on x or on $\partial/\partial x$ as is done in the quantum mechanical case.

There exist a transformation [17], which allows to decouple the position from the gradient operators, thus making it possible to use the exponential propagator without the need to linearize it. Let $P_e(x)$ denote the equilibrium solution of Eq. (2) and define

$$\Phi(x,t|x') = \frac{P(x,t|x')}{\sqrt{P_e(x)}}\,. \tag{6}$$

Then it is easy to show that the function Φ satisfies a Schrödinger like equation

$$\frac{\partial}{\partial t}\Phi = -\mathbf{H}\Phi \tag{7}$$

where the "Hamiltonian" H is

$$\mathbf{H} = -\nabla^T\cdot\mathbf{D}\cdot\nabla + U(x) \tag{8}$$

and the "effective potential" U is

$$U(x) = \nabla^T(\beta V/2)\cdot\mathbf{D}\cdot\nabla(\beta V/2)-\nabla^T\cdot\mathbf{D}\cdot\nabla(\beta V/2)\,. \tag{9}$$

To obtain these results it has been assumed that the diffusion tensor is symmetric (i.e., $\mathbf{D} = \mathbf{D}^T$).

Let $\{\varphi_n(x)\}$ and $\{\lambda_n\}$ respectively denote the sets of (normalized) eigenfunctions and eigenvalues of $\mathbf{H}$. The Green's function associated with Eq. (7) is given by

$$\Phi(x,t|x') = \sum_{n=0}^{\infty}\varphi_n(x)\cdot\exp(-\lambda_n t)\cdot\varphi_n(x')\,. \tag{10}$$

Since $\mathbf{H}$ is real and symmetric its left eigenfunctions are identical to its right eigenfunctions $\varphi_n(x)\equiv\langle n|x\rangle = \langle x|n\rangle$. This is in contrast to the operator $\mathbf{L}$ whose right and left eigenfunctions are not identical. Denoting the latter by $\psi_n(x)$ and $\psi_n^+(x)$ we have

$$\psi_n(x) = \varphi_n(x)\cdot\sqrt{P_e(x)} \tag{11a}$$

$$\psi_n^+(x) = \varphi_n(x)/\sqrt{P_e(x)}\,. \tag{11b}$$

The corresponding eigenvalues are identical to those of $\mathbf{H}$ and satisfy

$$\lambda_n = \langle\varphi_n(x)|\mathbf{H}|\varphi_n(x)\rangle = \langle\psi_n(x)|\mathbf{L}|\psi_n(x)\rangle \geq 0\,. \tag{12}$$

Assuming that the "ground state" $\varphi_0(x)$ is nondegenerate, only one of the eigenvalues, λ_0, is zero and all the others are positive. The normalization condition implies

$$\int_{-\infty}^{\infty} dx^{(N)}\varphi_0(x)\cdot\Phi(x,t|x') = \int_{-\infty}^{\infty} dx^{(N)}\Phi(x,t|x')\cdot\varphi_0(x') = 1 \tag{13}$$

where N is the dimensionality.

The problem of solving Eq. (2) has thus been transformed into that of solving Eq. (7) where the "momentum" terms (the terms containing ∇) and those depending on position are separated. Note that this simple form for the "Hamiltonian" (Eq. (8)) is obtained only for position-independent diffusion tensors.

The time evolution associated with Eq. (7) is obtained from

$$\Phi(x,t) = \langle x|\exp(-\mathbf{H}t)|\Phi(t=0)\rangle \approx \langle x|\prod_1^n\exp(-\mathbf{T}\Delta t)\cdot\exp(-\mathbf{U}\Delta t)|\Phi(t=0)\rangle \tag{14}$$

where the "kinetic energy" operator $\mathbf{T}$ denotes the term $-\nabla^T\cdot\mathbf{D}\cdot\nabla$ appearing in Eq. (8) and where $\Delta t = t/n$. In practice, the function Φ is defined on a grid in configuration space. The $\exp(-\mathbf{T}\Delta t)$ operator is carried out by the FFT technique.

$$\Phi(x,\Delta t)\approx F_{x\leftarrow k}[e^{-\mathbf{T}\Delta t}F_{k\leftarrow x}(e^{-\mathbf{U}\Delta t}\Phi(x,0))] \tag{15}$$

where the two exponential operators appear in their diagonal representations in the appropriate space, and where $F_{x\leftarrow k}$ denotes a Fourier transform from k-space to x-space

$$f(x) = F_{x\leftarrow k}\hat{f}(k) = \left(\frac{1}{2\pi}\right)^N\int_0^{2\pi} dk^{(N)}\exp(-ik\cdot x)\hat{f}(k)\,. \tag{16}$$

The choice of the initial distribution requires some attention. In principle it is possible to make an arbitrary selection but

it is advantageous to do it in such a way that the calculation of the specific observable of interest, e.g., transition rate, is easier. This point is discussed below.

3. The Transition Rate and the Reactive Flux

The type of processes which are considered in this section involve classical diffusion over a barrier, from a potential well to another region of the configuration space. In particular we are interested in the transition rate and in the condition for it to exist as a meaningful measure of the reaction dynamics [17–21].

It is convenient to write Eq. (2) as a continuity equation

$$\partial_t P(x,t) + \nabla^T \cdot J(x,t) = 0 \tag{17}$$

where the probability flux vector, $J(x,t)$ is given by

$$J(x,t) = -\mathbf{D}\cdot[\nabla + \nabla(\beta V(x))]\,P(x,t)\,. \tag{18}$$

At a stationary state $J(x,t) = J_s$, is a constant, and $P(x,t) = P_s(x)$ does not evolve in time. For closed systems the only stationary state is the equilibrium distribution $P_e(x)$, for which $J_e = 0$. The barrier crossing process is characterized by a single rate (for practical purposes) if, following a short transient period after the initiation of the process, the system developes a quasi steady state whose time evolution is governed by the smallest non-vanishing eigenvalue of the Smoluchowski equation and by a nearly constant flux from the reactant to the product well. Several approximate methods to evaluate this steady state rate are available:

(a) The Smallest Non-Vanishing Eigenvalue (SNVE) Method [18, 20]

The existence of a well defined rate implies that λ_1, the smallest non-vanishing eigenvalue of $\mathbf{L}$, is well separated from the higher eigenvalues (i.e., $\lambda_1 \ll (\lambda_2 - \lambda_1) \equiv \tau^{-1}$) and that this eigenvalue is not degenerate. With this in mind and for times t such that $\lambda_2^{-1} \ll t < \infty$ the relaxation to equilibrium is governed by λ_1 which is then equal to the transition rate $K(\beta)$.

These well recognized facts can be used within the numerical scheme described in Sect. (2) as follows: Using an arbitrary initial distribution $\varphi(x,0)$ the distribution at time t is obtained by performing the evolution $\varphi(x,t) = e^{-\mathbf{H}t}\varphi(x,0)$ numerically. Observing that

$$\theta(x,t) = \varphi(x,t) - \varphi_0(x) \tag{19}$$

($\varphi_0(x)$ is the state corresponding to the eigenvalue $\lambda_0 = 0$) satisfies

$$\|\theta(t)\|^2 \equiv \int_{\infty}^{\infty} dx\,|\theta(x,t)|^2 = \|\varphi(t)\|^2 - 1 \tag{20}$$

the transition rate $K(\beta)$ is obtained from

$$K(\beta) = -\frac{1}{2}\lim_{t\gg\tau}\frac{d}{dt}\ln[\|\varphi(t)\|^2 - 1]\,. \tag{21}$$

Alternatively, if the initial "wave function" $\varphi(x,0)$ does not contain the "ground state" $\varphi_0(x)$ i.e., $\langle\varphi_0|\varphi(0)\rangle = 0$, (this may be achieved, since $\varphi_0(x)$ is the known equilibrium distribution, by the projection $\varphi(x,0) \to \varphi(x,0) - \langle\varphi_0(x)|\varphi(x,0)\rangle$ followed by renormalization) then

$$K(\beta) = \lambda_1 = \lim_{t\gg\tau}\frac{d}{dt}\ln[\|\varphi(t)\|)\,. \tag{22}$$

(b) Chandler's Method [21]

A different treatment for the calculation of the transition rate is based on the fluctuation dissipation theorem. Close to equilibrium the relaxation process of an observable $A(t)$ obeys the following relation

$$\frac{\langle\delta A(t)\rangle_{ne}}{\langle\delta A(0)\rangle_{ne}} = \frac{\langle\delta A(0)\,\delta A(t)\rangle}{\langle\delta A(0)^2\rangle}\,. \tag{23}$$

Where $\langle\cdots\rangle$ and $\langle\cdots\rangle_{ne}$ respectively represent an equilibrium ensemble average (over initial conditions) and a non-equilibrium one, and $\delta A(t) = A(t) - \langle A\rangle$.

The observable of interest is

$$N(t) = \int_{\Omega} dx\,P(x,t|x_0) \tag{24}$$

where Ω is the domain defining the reactant state and $P(x,t|x_0)$ is the distribution at time t given that initially it was

$$P(x,t=0|x_0) = \delta(x - x_0)\,; \quad x_0 \in \Omega \tag{25}$$

where x_i is the i-th component of the N-dimensional vector x and x_{i0} is the initial location of the distribution on the i-th coordinate axis. The reaction coordinate is the minimum energy path between the reactants and the products potential wells. However dynamical effects may create situations in which the maximum reactive flux does not go along the minimum energy path. This aspect of the problem will be discussed below in the specific application to two-dimensional diffusion. Define

$$\delta N(t) = \int_{\Omega} dx\,[P(x,t|x_0) - e^{-\beta V(x)}/Q] \tag{26a}$$

where

$$Q = \int_{-\infty}^{\infty} dx\,e^{-\beta V(x)}\,. \tag{26b}$$

Assuming that the relaxation of $\langle\delta N(t)\rangle$ to its equilibrium value (i.e., zero) is given by the chemical rate $K(\beta)$, we find from Eq. (23)

$$\langle\delta N(0)\,\delta N(t)\rangle = \langle[\delta N(0)]^2\rangle\exp(-K(\beta)t) \tag{27}$$

and consequently

$$\langle\delta N(0)\,\delta\dot{N}(t)\rangle = -K(\beta)\,\langle[\delta N(0)]^2\rangle\exp(-K(\beta)t)\,. \tag{28}$$

As discussed above (see also Ref. [21]) for the process at hand to have a uniquely defined rate constant one must consider times such that $\tau \ll t \ll K^{-1}$. Then Eq. (28) implies

$$K(\beta) = \xrightarrow[\tau \ll t \ll K^{-1}]{} - \frac{\langle \delta N(0)\, \delta \dot{N}(t) \rangle}{\langle [\delta N(0)]^2 \rangle}. \tag{29}$$

Thus, evaluating the saturation or plateau value of the r.h.s. of Eq. (29) (using the numerical procedure of Sect. (2) for the numerator) yields $K(\beta)$. It is obvious that apart from reasons of numerical accuracy, the procedures based on Eqs. (20), (21) and (29) should yield identical results.

(c) Kramer's Formula [22]

Kramers has derived an expression for the escape rate out of a one dimensional potential well in several limits associated with the magnitude of the friction. For the overdamped limit governed by the Smoluchowski equation (1) and for high barriers ($E_B \gg k_B T$) his result for the rate is

$$K_{KR}^{(1D)} = \frac{\omega_r^{(B)}\, \omega_r^{(W)}}{2\pi\gamma} \exp\left(-\frac{E_B}{k_B T}\right) \tag{30}$$

where $\omega_r^{(B)}$ and $\omega_r^{(W)}$ are the vibrational frequencies corresponding to the top of the barrier and to the bottom of the well respectively and where the potential in these two regions has been approximated by its expansion up to quadratic terms about these points. For a multidimensional system, Eq. (30) can be generalized by assuming that the nonreactive modes are in thermal equilibrium. Under this assumption the rate takes the form [23]

$$K_{KR}^{(ND)} = \frac{\omega_r^{(B)}}{\gamma} K_{TST}^{(ND)} \tag{31}$$

where ND stands for "N-Dimensional" and where K_{TST} is the rate obtained from transition state theory

$$K_{TST} = \sqrt{\frac{2k_B T}{\pi M}} \frac{\int dx_{nr}\, e^{-\beta V(x_r = x_b)}}{\int dx_r \int d\dot{x}_{nr}\, e^{-\beta V(x)}}. \tag{32}$$

In Eqs. (31) and (32) the subscripts r and nr stand for reactive and nonreactive coordinates respectively.

4. A Two Dimensional Model

The method described in Sect. (2) has been applied to solve numerically the diffusion equation in two dimensions, to compare the Kramers expression (31)) to different numerical ways of evaluating the rate and to examine effects of multidimensionality on the reaction rates other ther. these incorporated in Eqs. (31) and (32). The potential surface used in this study may be written in the form

$$V(x,y) = V_0 \cdot f_R(x,y)\, f_L(x,y) \tag{33}$$

where $f(x,y)$ is a quadratic form in x and in y such that $f(x,y) = 0$ describes the locus of an ellipse. In terms of the geometrical parameters defined in Fig. 1, $f(x,y)$ is

$$\begin{aligned} f(x,y) = &\left(\frac{x-x_0}{a}\right)^2 [\cos^2(\theta) + \alpha \sin^2(\theta)] \\ &+ \frac{x-x_0}{a} \cdot \frac{y-y_0}{a} (1-\alpha) \sin(2\theta) \\ &+ \left(\frac{y-y_0}{a}\right)^2 [\sin^2(\theta) + \alpha \cos^2(\theta)] - 1 \end{aligned} \tag{34}$$

where $(x_0; y_0)$, a, θ and α represent the parameters of any of the two ellipses $f(x,y) = 0$. The subscripts R and L (Right and Left) represent different choices of the parameters. These parameters are chosen for the two ellipses such that the saddle point of the potential is at the origin. For the sake of simplicity we have considered in this article only potentials which are symmetric with respect to the y axis. The parameter V_0 is the hight of the potential barrier and the reaction coordinate i.e., the minimum energy path, goes from one well to the other through the origin. In all the calculations described below we have taken $a_R = a_L = a$, and have chosen the units of time and length such that $a = D_x + D_y = 1$.

In the numerical evaluation of the rate Eq. (22) can be used as written, but Eqs. (28) and (29) may be simplified for the model considered. The dividing surface s, where the flux is calculated, is taken as the y axis. By using the symmetry of the potential $V(x,y)$ with respect to this axis, Eqs. (24), (25) and (2) lead to

$$\begin{aligned} \delta N(t=0) &= \int_0^\infty dx \int_{-\infty}^\infty dy [\delta(x-x_0) \cdot \delta(y-y_0) - e^{-\beta V(x)}/Q] \\ &= \Theta(x_0) - \frac{1}{2} \end{aligned} \tag{35}$$

where $\Theta(x)$ is the Heaviside function. Also from Eq. (2)

$$\begin{aligned} \delta \dot{N}(t) = &-D_x \int_{-\infty}^\infty dy \left(\frac{\partial}{\partial x} + \beta \frac{\partial V(x,y)}{\partial x}\right) \\ &\cdot P(x,y,t|x_0,y_0) \end{aligned} \tag{36}$$

$$\begin{aligned} -\langle \delta N\, \delta \dot{N}(t) \rangle = &\frac{D_x}{Q} \int_{-\infty}^\infty dy e^{-\beta V(0,y)} \frac{\partial}{\partial x} \\ &\cdot \int_{-\infty}^\infty dx_0 \int_{-\infty}^\infty dy_0 e^{\beta V(x,y)} \\ &\cdot P(x,y,t|x_0,y_0) e^{-\beta V(x_0,y_0)} \left[\Theta(x_0) - \frac{1}{2}\right]\Big|_{x=0}. \end{aligned} \tag{37}$$

Defining

$$\hat{P}(x,y) = e^{-\beta V(x,y)} \left[\Theta(x) - \frac{1}{2}\right]/Q. \tag{38}$$

Eq. (37) takes the form

$$\begin{aligned} -\langle \delta N\, \delta \dot{N}(t) \rangle = &D_x \int_{-\infty}^\infty dy\, e^{-\beta V(0,y)} \frac{\partial}{\partial x} \\ &\cdot e^{+\beta V(x,y)} P(x,y,t|\hat{P})]|_{x=0} \end{aligned} \tag{39}$$

where

$$P(x,y,t|\hat{P}) = \int_{-\infty}^{\infty} dx_0 \int_{-\infty}^{\infty} dy_0 \, P x,y,t|x_0,y_0) \cdot \hat{P}(x_0,y_0) = e^{\mathbf{L}t}\hat{P}. \tag{40}$$

Eqs. (39) and (40) imply that the calculation of $\langle \delta N \delta \dot{N}(t) \rangle$ (hence of the escape rate, Eq. (29)) can be done by simply propagating the initial "distribution" $\hat{P}(x,y)$ of Eq. (38). This propagation is performed using the FFT algorithm and the equivalent Schrödinger equation (see below). A final FFT procedure is then used to get the derivative with respect to x in Eq. (39). The evaluation of Eq. (29) is facilitated by noting that the symmetry of the potential implies

$$\langle [\delta N(0)]^2 \rangle = \frac{1}{4}. \tag{41}$$

Note that $\hat{P}(x,y)$ can be negative (in fact $\int dx \hat{P}(x,y) = 0$) hence it is not a real distribution. An initial real normalized distribution can be constructed as

$$P(x,y,t=0) = P_e(x,y) + \hat{P}(x,y) \tag{42}$$

where $P_e(x,y)$ is the equilibrium distribution. Note that P_e is orthogonal to $\hat{P}$, $\langle P_e|\hat{P}\rangle = 0$; ($\langle P_e| =$ constant). If this choice of initial distribution is made than $\hat{P}$ can be interpreted as the deviation of the initial distribution from equilibrium. In fact it is easy to see that $P(x_0,y_0,t=0)$ can be used in the r.h.s. of Eq. (40) instead of $\hat{P}(x_0,x_0)$ without changing the results for $\langle \delta N \delta \dot{N}(t) \rangle$ in Eq. (37).

In actual calculation we use the language of the equivalent Schrödinger equation to compute the r.h.s. of Eq. (39). The rate Eq. (29) is the given by

$$K = \lim_{\tau \ll t \ll K^{-1}} \frac{4D_x}{Q^{1/2}} \int_{-\infty}^{\infty} dy \, e^{-\beta V(0,y)} \frac{\partial}{\partial x} \cdot [e^{+\beta V(x,y)} \Phi(x,y,t|\hat{\Phi})|_{x=0}] \tag{43}$$

where $\Phi(x,y,t|\hat{\Phi})$ is defined in analogy with Eq. (40) as the "wave function" at time t, given that at $t=0$ it was

$$\hat{\Phi}(x_0,y_0) = \varphi_0(x_0,y_0)\left[\Theta(x_0) - \frac{1}{2}\right]. \tag{44}$$

It is evaluated as $\Phi(x,y,t|\hat{\Phi}) = e^{-\mathbf{H}t}\hat{\Phi}$. Note that by symmetry it is orthogonal to the "ground state" $\varphi_0(x,y)$ at all time.

Next consider the Kramers result in two dimensions. Eq. (31) takes the form

$$K_{KR}^{(2D)} = \frac{\omega_r^{(B)}}{\gamma} K_{TST}^{(2D)} \tag{45}$$

where γ is given by

$$\gamma = \frac{k_B T}{D_x M} \tag{46}$$

and where

$$K_{TST}^{(2D)} = A\sqrt{\frac{2k_B T}{\pi M}} \tag{47}$$

with

$$A = \frac{\int_{-\infty}^{\infty} dy \, e^{-\beta V(0,y)}}{\int_{-\infty}^{\infty} dx \int_{-\infty}^{\infty} dy \, e^{-\beta V(x,y)}}. \tag{48}$$

Since the origin is at the saddle point the barrier frequency is obtained from

$$\left.\frac{\partial^2 V}{\partial x^2}\right|_{x=0,\,y=0} = -M(\omega_r^{(B)})^2. \tag{49}$$

Substitution of Eqs. (47) and (48) in (45) then leads to

$$K_{TST}^{(2D)} = D_x A \sqrt{-\frac{2\beta}{\pi}\left.\frac{\partial^2 V}{\partial x^2}\right|_{x=0,\,y=0}}. \tag{50}$$

5. Results and Discussion

The initial "distribution" used in our calculation is given by Eq. (38). This corresponds to the actual distribution Eq. (42), leading to

$$P_R = \int_0^{\infty} dx \int_{-\infty}^{\infty} dx \, P(x,y,0) = \frac{3}{4} \tag{51a}$$

and

$$P_L = \int_{\infty}^{0} dx \int_{-\infty}^{\infty} dx \, P(x,y,0) = \frac{1}{4}. \tag{51b}$$

Eqs. (51a) and (51b) imply that the diffusion process following the preparation of this initial state proceeds from right to left.

In Table 2 we present results obtained from the different methods described in the previous sections: The smallest eigenvalue (SNVE) method (Eq. (22)), Chandler's steady state relaxation rate (CSSR) method (Eqs. (29) and (43)) and the Kramers' steady state rate (KSSR Eq. (50)). These results are given for different choices of the model parameters given in Table 1. All the calculations where performed on a $2^7 \times 2^7$ grid covering the physical dimensions $x = (-1.5;1.5)$, $y = (-1.0,1.0)$ (hence the spacings are $\Delta x = 1.5 \times 2^{-6}$ $\Delta y = 1.0 \times 2^{-6}$). The parameters in Table 1 characterize the potential surface and the diffusion rates. The last colomn in Table 2 gives the number of timesteps used in the numerical time evolution.

Two of the potential surfaces used in the calculations described here are shown in Figs. 2 and 3. These figures display the potential surfaces corresponding to cases 1 (also 3 and 4) and 9 (also 11 and 12) of Table 1 respectively. Cases 1–4

Table 1
Description of cases

Potential parameters*)	D_x/D_y	βV_0	Case
$\theta_L = 0$	1.0	6	1
$\theta_R = 0$	1.0	2	2
$\theta_S = \pi/2$	5.0	6	3
$\alpha_L = 5.0$	0.2	6	4
$\alpha_R = 5.0$			
$\tau = 1$			
$\theta_L = \pi/3$	1.0	6	5
$\theta_R = \pi/6$	1.0	2	6
$\theta_S = \pi/2$	5.0	6	7
$\alpha_L = 0.2$	0.2	6	8
$\alpha_R = 5.0$			
$\tau = 1$			
$\theta_L = \pi/4$	1.0	6	9
$\theta_R = \pi/4$	1.0	2	10
$\theta_S = \pi/2$	5.0	6	11
$\alpha_L = 0.2$	0.2	6	12
$\alpha_R = 5.0$			
$\tau = 1$			

*) See Fig. 1.

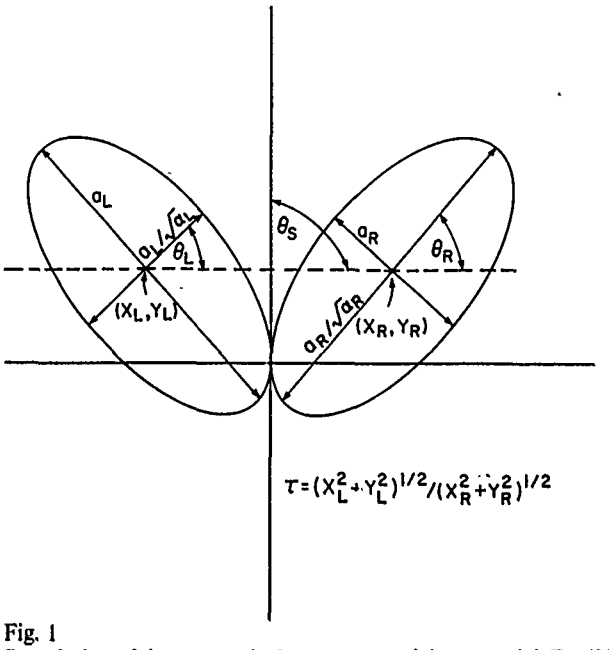


Fig. 1
Description of the geometrical parameters of the potential, Eq. (33). θ_S is the angle between the two principal axes of the diffusion tensor. In all the present calculations $\theta_S = \pi/2$ and these two principal axes are taken as the cartesian axes x and y

Table 2
Transition rates

Case	SNVE[1]	CSSR[1]	KSSR[3]	Time
1	0.05007	0.05027	0.05658	2000
2	0.70500	0.69150	0.69950	2000
3	0.08379	0.08260	–	2000
4	0.01449	0.01775	–	2000
5	0.05123	0.05156	0.05616	2000
6	0.70290	0.60090	0.59740	2000
7	0.07191	0.07252	–	2000
8	0.01774	0.02086	–	2000
9	0.04751	0.04853	0.05677	2000
	0.04742	0.04712	–	3000
10	0.69200	0.59080	0.57210	2000
	0.67330	0.50260	–	3000
11	0.06221	0.06521	–	2000
	0.06170	0.06214	–	3000
12	0.01870	0.02101	–	2000
	0.01833	0.01942	–	3000

[1] SNVE: Smallest Non-Vanishing Eigenvalue method, Eq. (22).
[2] CSSR: Chandler's Steady State relaxation Rate, Eq. (43).
[3] KSSR: Kramer's Steady State relaxation Rate, Eq. (45).

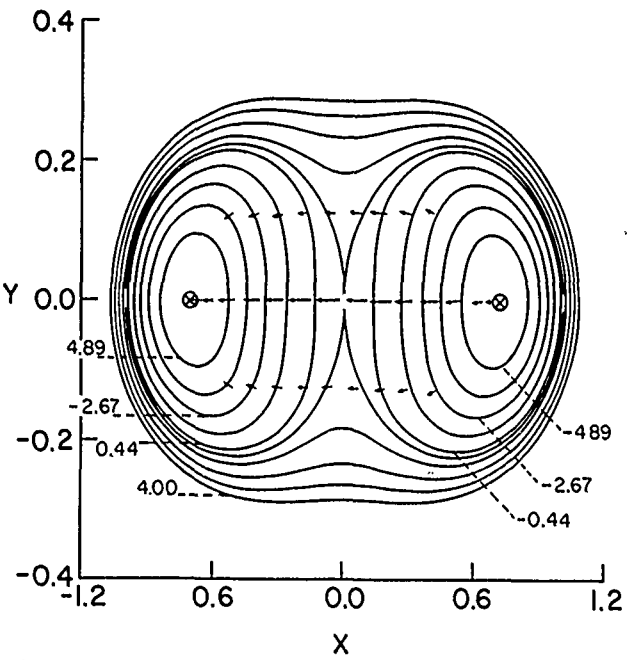


Fig. 2
Contour plot of the potential energy surface of case 3 with arrows indicating the direction and magnitude of the steady state reactive flux

correspond to a linear reaction coordinate while cases 5–8 and 9–12 represent two groups of situations with curved reaction coordinate. Some of the cases (2,6 and 10) correspond to a small barrier hight ($\beta V_0 = 2$) where the experimental reaction rate is not well defined. For the other cases $\beta V_0 = 6$. Finally in cases 1,2,5,6, and 9,10 the diffusion tensor is isotropic while the other cases correspond to non isotropic diffusion.

From Table 2 we see that good agreement between the two numerical procedures considered in this paper exists in all cases where the rate is well defined (discrepancies are of the same order as the numerical accuracy of the results). It should be noted that the numerical accuracy is also considerably better for the high potential barrier cases where the smallest non-vanishing eigenvalue is well separated from the higher eigenvalues (or where the saturation region in Eq. (29) is well defined). In these cases we have found that at time 2000 (time units correspond to $a = D_x + D_y = 1$)

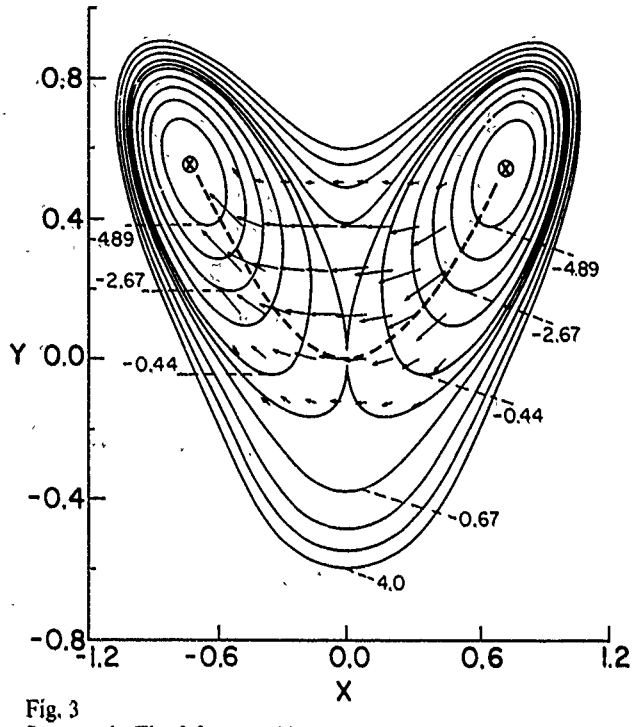


Fig. 3
Same as in Fig. 2 for case 11

the error was less than 3%. The Kramers result also works reasonably well when applied to the isotropic cases (in fact its success for cases 2,6 and 10 ($\beta V_0 = 2$) is surprising, and is probably fortuitous.

Consider now the effect of curvature on the reaction coordinate and of anisotropy on the diffusion tensor. These issues have been recently subjects of several studies. A recent study [6] of the effect of the reaction path curvature in the overdamped (Smoluchowski) limit of the Kramers problem has shown that for isotropic diffusion (and isotropic potential wells) the curvature of the reaction coordinate plays no direct role in the reaction kinetics, as is intuitively clear since this kinetics is dominated by the flux across the saddle point. Still Matkowsky et al. [6] have shown that the pre-exponential factor in the reaction rate may be modified by the diffusion in direction(s) normal to the reaction coordinate, and thus may account for part of the difference between the result based on the (essentially one dimensional) Kramers expression and the numerical work. (Note that the Kramers result is the lowest order term in an expansion in powers of $(\beta V_0)^{-1}$, so corrections are expected even in one dimension).

Of more interest is the effect of non isotropic diffusion, particularly when the reaction coordinate does not coincide with a principal axis of the diffusion tensor. (Cases 3 and 4 correspond to situations when it does). Kłosek et al. [8,9], as well Berezhkovskii and Zitserman [10,11] have shown that a qualitative difference exists between the cases where the second derivative A of the potential at the saddle point in the direction of fast diffusion is larger or smaller than zero. When $A > 0$ the large potential barrier and large diffusion anisotropy are interchangable, and a trivial generalization of the Kramers problem applies. When $A < 0$ the situation is much more complicated. We defer a detailed

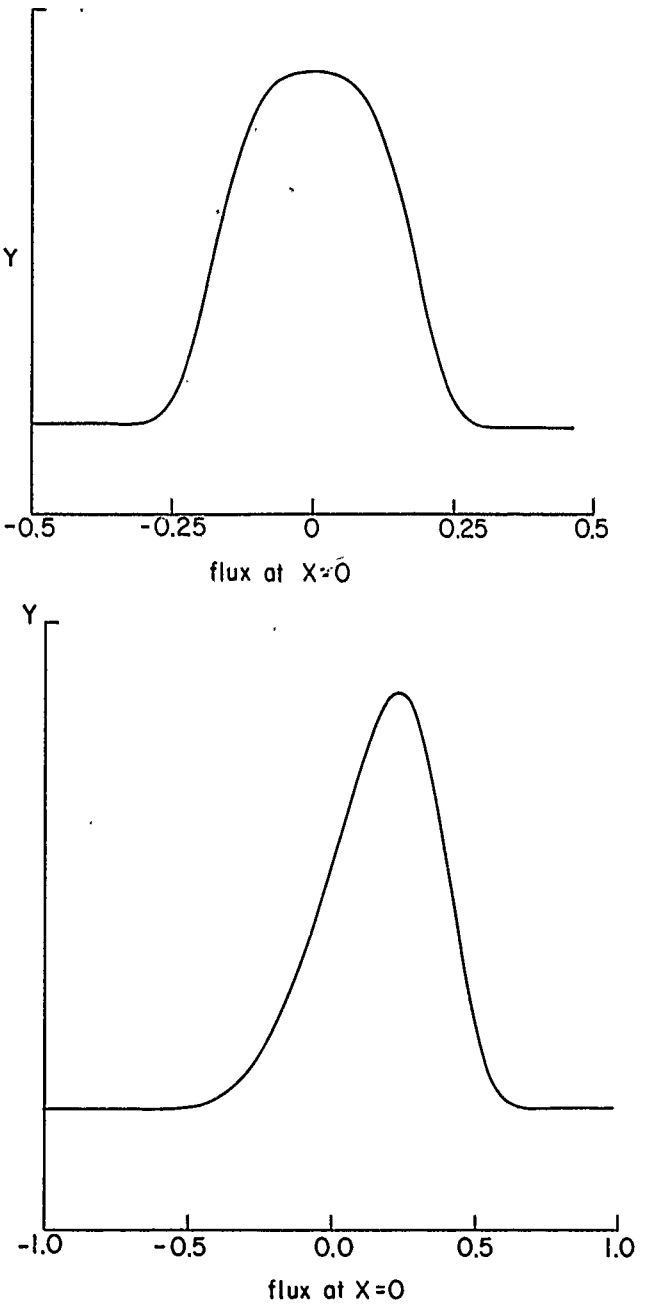


Fig. 4
The reactive flux along the y axis, at $\lambda = 0$ vs. position.
(a) case 3; (b) case 11

comparison between the analysis of this situation and the numerical work to a later publication. Here we note that this case correspond to $D_x > D_y$ (cases 3, 7 and 11) and is characterized here by the fact that the reactive flux across the ridge ($\upsilon = 0$) between the two wells is not necessarily the largest at the saddle point. To see this we have plotted in Figs. 2 and 3, superimposed on the potential surfaces corresponding to cases 1(3,4) and 9(11,12) respectively, arrows whose direction and length represent the direction and magnitude of the reaction flux. The latter is obtained from

$$J_x(x,y,t) = -D_x\left[\frac{\partial}{\partial x} + \beta\frac{\partial V(x,y)}{\partial x}\right]P(x,y,t) \qquad (52)$$

$$J_y(x,y,t) = -D_y\left[\frac{\partial}{\partial y} + \beta\frac{\partial V(x,y)}{\partial y}\right]P(x,y,t) \tag{53}$$

where $P(x,y,t)$ is taken at the quasi-stationary state for which the transition rate is calculated. The flux arrows in Fig. 2 correspond to case 3 and the flux arrows in Fig. 3 – to case 11. The length $l(x,y)$ of an arrow at location (x,y) is taken as

$$l(x,y) = p\cdot\left[\left(\frac{\partial J}{\partial x}\right)^2 + \left(\frac{\partial J}{\partial y}\right)^2\right]^{1/2} \tag{54}$$

where p is an arbitrary scale factor.Fig. 3 clearly shows the deviation of the maximal flux from the geometrical saddle point. This deviation depends on the geometry of the potential surface, on the diffusion anisotropy and on the temperature, and may lead to non-Arrhenius temperature dependence of the reaction rate. Another view of the same effect is shown in Fig. 4, where we plotted the x component of the reactive flux as a function of the position y along the y axis ($x = 0$). Shown are plots for case 3 (Fig. 4a) and for case 11 (Fig. 4b). The fact that for the latter case the flux peaks at $y = 0$ (position of the saddle point) clearly demonstrates the effect discussed above.

6. Conclusion

In this paper we have described numerical methods for solving multidimensional diffusion equations and have applied these methods to a model chemical reaction where curved reaction coordinates and anisotropic diffusion play non-trivial role in determining the reaction rate. The appearence of such multidimensional effects even in the relatively simple overdamped situation emphasizes the shortcomings of analyzing reaction rates from equilibrium and dynamical considerations purely at the transition state.

This work has been supported in part by the U.S-Israel Binational Science Foundation and by the Israel Academy of Science. We thank N. Agmon for helpful comments.

References

[1] For a very recent review see P. Hänggi, P. Talkner, and M. Borkovec, Rev. Mod. Phys. *62*, 251 (1990).
[2] N. Agmon and J. J. Hopfield, J. Chem. Phys. *78*, 6947 (1983); ibid. *70*, 2042 (1983); N. Agmon, Biochemistry *27*, 3507 (1988).
[3] R. S. Larson and D. Kostin, J. Chem. Phys. *77*, 5017 (1982).
[4] R. S. Larson, Physica *A 137*, 295 (1986).
[5] R. S. Larson, J. Chem. Phys. *89*, 1291 (1989).
[6] B. J. Matkowsky, A. Nitzan, and Z. Schuss, J. Chem. Phys. *88*, 4765 (1988).
[7] B. J. Matkowsky, A. Nitzan, and Z. Schuss, J. Chem. Phys. *90*, 1292 (1989).
[8] M. M. Kłosek-Dygas, B. M. Hoffman, B. J. Matkowsky, A. Nitzan, M. A. Ratner, and Z. Schuss, J. Chem. Phys. *90*, 1141 (1989).
[9] M. M. Kłosek-Dygas, B. J. Matkowsky, and Z. Schuss, to be published.
[10] A. M. Berezhkovskii, L. M. Berezhkovskii, and V. Yu. Zitserman, Chem. Phys. *30*, 55 (1989); Chem. Phys. Lett. *158*, 369 (1989).
[11] A. M. Berezhkovskii and V. Yu. Zitserman, to be published.
[12] N. Agmon and R. Kosloff, J. Phys. Chem. *91*, 1988 (1987). Further numerical work on this model is presented in the paper by Agmon and Rabinovich in this volume.
[13] C. Gehrke, J. Schröder, D. Schwartzer, J. Troe, and F. Voss, J. Chem. Phys. *92*, 4805 (1990).
[14] A. D. Kaufman and K. B. Whaley, J. Chem. Phys. *90*, 2758 (1989).
[15] M. D. Feit, J. A. Fleck, Jr., and Steiger, J. Comput. Phys. *47*, 412 (1982); M. D. Feit and J. A. Fleck, Jr., J. Chem. Phys. *78*, 301 (1983).
[16] a) D. Kosloff and R. Kosloff, J. Comput. Phys. *53*, 35 (1983); b) H. Tal Ezer and R. Kosloff, J. Chem. Phys. *81*, 3967 (1984). c) Review see: R. Kosloff, J. Phys. Chem. *68*, 2959 (1978).
[17] N. G. van Kampen, J. Stat. Phys. *17*, 71 (1977).
[18] N. G. van Kampen, Stochastic Processes in Physics and Chemistry, North Holland, Amsterdam 1981.
[19] D. Chandler, Introduction to Modern Statistical Mechanics, Oxford University Press, Oxford 1987.
[20] H. Risken, The Fokker-Planck Equation, Springer-Verlag, Berlin 1984.
[21] D. Chandler, J. Chem. Phys. *68*, 2959 (1978).
[22] H. A. Kramers, Physica *7*, 284 (1940).
[23] H. C. Brinkman, Physica *22*, 149 (1956); G. H. Vineyard, J. Phys. Chem. Solid *3*, 121 (1957); R. Landauer and J. A. Swanson, Phys. Rev. *121*, 1668 (1961); H. R. Glyde, Rev. Mod. Phys. *39*, 373 (1967); J. S. Langer, Phys. Rev. Lett. *21*, 973 (1968) and A.. Phys. (NY) *54*, 258 (1979); Z. Schuss, Theory and Application of Stochastic Differential Equations, Wiley, New York 1980; R. F. Grote and J. T. Hynes, J. Chem. Phys. *74*, 4465 (1981) and ibid. *75*, 2191 (1981).

Presented at the Discussion Meeting of the Deutsche Bunsen-Gesellschaft für Physikalische Chemie "Rate Processes in Dissipative Systems: 50 Years after Kramers" in Tutzing, September 10–13, 1990

E 7490

Interrelations of Different Methods for the Determination of Rates: Flux Over Population, Generalized Reactive Flux, the Lowest Eigenvalue and Its Rayleigh Quotient

Peter Talkner

Paul Scherrer Institute, CH-5232 Villigen

Nonequilibrium Phenomena / Reaction Rates / Reactive Flux

The ratio of Kramers' current carrying stationary probability density and the equilibrium probability density is utilized as smoothed characteristic function in the generalized reactive flux method recently proposed by Borkovec and Talkner [J. Chem. Phys. *92*, 5307 (1990)]. Under a certain condition on the potential, as generalized transition state rate Kramers' phase space diffusion limited rate is obtained. It then represents an upper bound for the true rate. An approximate expression for the plateau value of the generalized reactive flux yields a Rayleigh quotient for the lowest eigenvalue of the considered Fokker Planck process.

1. Introduction

The generalized reactive flux method [1] primarily aims at the effective numerical simulation of rate constants [2] for those classes of dynamics as e.g. Smoluchowski or jump processes that cannot be tackled by the original reactive flux idea [3]. This goal was achieved by the use of a smoothed characteristic function from which the reactive flux is derived in contrast to a discontinuous one for the original reactive flux method [1]. In this note it will be demonstrated that the same idea may lead to an important improvement of the initial reactive flux rate compared with the transition state rate. For the sake of simplicity this discussion is restricted to the original, one dimensional Kramers' model [4]. The generalization to higher dimensional models is straightforward. From Kramers' solution for a current carrying probability density one finds a smoothed characteristic function for which the initial reactive flux rate already yields Kramers' phase space diffusion limited rate. The initial conditions for the individual transmission factors that lead to the time dependent reactive flux rate, are given by the sources and sinks that render Kramers' current carrying solution stationary [1, 5]. In order that these initial conditions follow from proper nonnegative probability densities, the nonlinear potential which is obtained from the original potential by subtracting the barrier part must be convex. Under this condition it is sure that Kramers' rate is an upper bound for the true rate. In an appropriate limit an exact expression for the plateau value is obtained that deviates from the smallest eigenvalue of the considered Fokker-Planck process only by an exponentially small amount. An approximate calculation of the plateau value leads to a Rayleigh quotient for the smallest eigenvalue which is different from previously used ones [5].

2. Kramers' Model

As a model of a chemical reaction Kramers [4] considered a Brownian particle of mass M moving in a potential $U(x)$ with local minima corresponding to an initial reactant and a final product state. The reactant state $x_r < 0$ is separated from the product states $x_p > 0$ by a barrier located at $x_b = 0$. The vicinity of the barrier is assumed to be parabolic with curvature $-\omega_b^2$:

$$U(x) \simeq -\frac{1}{2} M \omega_b^2 x^2 + U(0) \quad \text{for } x \text{ near the barrier} \tag{2.1}$$

Under these conditions Kramers could construct a stationary Fokker Planck equation in the parabolic vicinity of the barrier:

$$\dot{L} p(x,v) = 0 \qquad \text{for } x \text{ near the barrier} \tag{2.2}$$

where the Fokker Planck operator is given by

$$L = -\frac{\partial}{\partial x} v + \frac{\partial}{\partial v}\left(\frac{U'(x)}{M} + \gamma v\right) + \frac{\gamma k_B T}{M} \frac{\partial^2}{\partial v^2} \tag{2.3}$$

and where γ denotes the friction rate and T the temperature of the heat bath causing fluctuations and dissipation.

The solution p is given by the product of a form-function $\zeta(x,v)$ and the equilibrium Boltzmann distribution $p_{eq}(x,v)$

$$p(x,v) = \zeta(x,v)\, p_{eq}(x,v) \tag{2.4}$$

where

$$p_{eq}(x,v) = Z^{-1} e^{-(\frac{1}{2}Mv^2 + U(x))/k_B T}. \tag{2.5}$$

The form function matches smoothly the equilibrium distribution in the initial well with a vanishing probability density at the product state. It is given by [4]

$$\zeta(x,v) = \omega_b^2 (M/2\pi\gamma k_B T \lambda_+)^{1/2} \cdot \int_{x-\lambda_+ v/\omega_b^2}^{\infty} e^{-\frac{M\omega_b^2 u^2}{2\gamma k_B T \lambda_+}} du \tag{2.6}$$

 © VCH Verlagsgesellschaft mbH, W-6940 Weinheim, 1991 0005-9021/91/0303-0327 $ 3.50+.25/0

where

$$\lambda_+ = -\frac{\gamma}{2} + \left(\omega_b^2 + \left(\frac{\gamma}{2}\right)^2\right)^{1/2}. \tag{2.7}$$

The stationary solution $p(x,y)$ carries a probability current over the barrier that follows from

$$j = \int_{-\infty}^{\infty} \mathrm{d}v\, v\, p(x=0,v). \tag{2.8}$$

This flux is maintained by sources and sinks which are given by [1,5]

$$S(x,v) = -Lp(x,v) \tag{2.9a}$$

$$= \left(\frac{\lambda_+}{2\pi\gamma M k_B T}\right)^{1/2} V'(x)\, \mathrm{e}^{-\frac{M\omega_b^4}{2\gamma\lambda_+ k_B T}\left(x - \frac{\lambda_+ v}{\omega_b^2}\right)^2} \tag{2.9b}$$

where $V(x)$ denotes the nonlinear part of the potential resulting from the full potential $U(x)$ subtracted by its parabolic contribution (2.1)

$$V(x) = U(x) + \frac{1}{2} M\omega_b^2 x^2 - U(0). \tag{2.10}$$

Kramers' phase space diffusion limited rate k_{kr} is then readily obtained from the ratio of the flux given by Eq. (2.8) and the population n of the well

$$k_{kr} = \frac{j}{n} \tag{2.11}$$

$$= \frac{\lambda_+}{\omega_b}\frac{\omega_0}{2\pi}\mathrm{e}^{-E_b/k_B T} \tag{2.12}$$

where $E_b = U(0) - U(x_0)$ denotes the barrier height and

$$n = \int_{-\infty}^{0} \mathrm{d}x \int_{-\infty}^{\infty} \mathrm{d}v\, p(x,v). \tag{2.13}$$

This result represents a reasonable estimate of the true rate, if all trajectories ejected by the source properly thermalize before eventual thermal fluctuations drive them out of the initial well [1,5].

We conclude this section by noting that the action of the Fokker Planck operator L on a product of a function $f(x,v)$ and the equilibrium distribution can be expressed by another operator L^* acting solely on f:

$$Lfp_{eq} = p_{eq} L^* f. \tag{2.14}$$

The operator L^* coincides with the backward operator of the time reserved process [7,8]

$$L^* = -v\frac{\partial}{\partial x} + \left(\frac{U'(x)}{M} - \gamma v\right)\frac{\partial}{\partial v} + \frac{\gamma k_B T}{M}\frac{\partial^2}{\partial v^2}. \tag{2.15}$$

Moreover, we note that the operator L^* is just the adjoint operator of the backward operator L^+ of the original process with respect of the scalar product defined by the equilibrium expectation value

$$\langle f L^+ g\rangle = \langle g L^* f\rangle \tag{2.16}$$

where

$$\langle f\rangle = \int_{-\infty}^{\infty} \mathrm{d}x \int_{-\infty}^{\infty} \mathrm{d}v\, f(x,v)\, p_{eq}(x,v) \tag{2.17}$$

and

$$L^+ = v\frac{\partial}{\partial x} - \left(\frac{U'(x)}{M} + \gamma v\right)\frac{\partial}{\partial v} + \frac{\gamma k_B T}{M}\frac{\partial^2}{\partial v^2}. \tag{2.18}$$

In the next Sect. we shall discuss the generalized reactive flux method for this classical model.

3. The Generalized Reactive Flux Method

After a transient on a microscopic time scale τ_m, the reaction rate governs the time behavior of the correlation function

$$C(t) = \frac{\langle f(x,v)\,\theta(-x(t))\rangle}{\langle f(x,v)\,\theta(-x)\rangle} \simeq \mathrm{e}^{-kt} \tag{3.1}$$

where $\langle\cdot\rangle$ again denotes the equilibrium average. $\theta(-x)$ is the step function being unity for negative and zero for positive values of x. In contrast, $f(x,v)$ is a function that smoothly interpolates from unity in the phase space region of reactants to zero in that of products. In order to avoid back reactions, phase space regions of products must be absorbing.

The time derivative of Eq. (3.1) yields a time-dependent expression:

$$k(t) = -\frac{\mathrm{d}C(t)}{\mathrm{d}t} = -\frac{\langle\theta(-x(t))\, L^* f(x,v)\rangle}{\langle f(x,v)\,\theta(-x)\rangle}. \tag{3.2}$$

In order to obtain this result, one expresses the time dependent part $\theta(-x(t))$ formally by

$$\theta(-x(t)) = \mathrm{e}^{L^+ t}\theta(-x) \tag{3.3}$$

and, after differentiation with respect to t, uses Eq. (2.16).

In a standard way the generalized transition state $k(0)$ and the transmission coefficient $\kappa(t)$ are introduced:

$$k(t) = k(0)\,\kappa(t) \tag{3.4}$$

where

$$k(0) = -\frac{\langle\theta(-x)\, L^* f(x,v)\rangle}{\langle f(x,v)\,\theta(-x)\rangle} \tag{3.5}$$

and

$$\kappa(t) = \langle\theta(-x(t))\rangle_+ - \langle\theta(-x(t))\rangle_-. \tag{3.6}$$

The nonequilibrium initial states $p_\pm$ by which the expectation values $\langle\theta(-x(t))\rangle_\pm$ are determined, read

$$p_\pm = \frac{\theta(\mp x)\, p_{eq}(x,v)\, L^* f(x,v)}{\langle\theta(\mp x)\, L^* f(x,v)\rangle}. \tag{3.7}$$

In order that $p_\pm$ are nonnegative probability densities, the function $f(x,v)$ has to be properly chosen. The best choice would be the eigenfunction $\tilde{h}(x,v)$ of L^* with the smallest eigenvalue $-\lambda$:

$$L^* \tilde{h}(x,v) = -\lambda \tilde{h}(x,v). \tag{3.8}$$

With this choice, the time dependent rate $k(t)$ varies exclusively on the long time scale, determined by the inverse rate

$$k(t) = \lambda\, e^{-\lambda t}. \tag{3.9}$$

Hence, the generalized transition state rate already coincides with the true rate λ

$$k(0) = \lambda. \tag{3.10}$$

However, the eigenfunction $\tilde{h}$ and the corresponding eigenvalue $-\lambda$ are not known exactly.

As an approximation Kramers' function $\zeta(x,v)$ suggests itself because first, it shows the desired qualitative behavior and second, approximates the eigenvalue Eq. (3.8) in the important barrier region [cf. Eqs. (2.2), (2.4) and (2.14)]

$$L^* \zeta(x,v) = 0 \qquad \text{for } x \text{ near the barrier}. \tag{3.11}$$

With Eqs. (2.5), (2.6), (2.15) and (3.5) we obtain for the generalized transition state rate $k(0)$ Kramers' phase space diffusion rate (2.12)

$$k(0) = k_{kr}. \tag{3.12}$$

Combining Eqs. (2.5), (2.9), (2.14) with Eq. (3.7) we obtain for the initial distributions p_+ and p_- the normalized projection of the source and sink density (2.9) on the reactant and product phase space regions, respectively:

$$p_\pm = \frac{\theta(\mp x)\, S(x,v)}{\int_{-\infty}^{\infty} dx \int_{-\infty}^{\infty} dv\, \theta(\mp x)\, S(x,v)}. \tag{3.13}$$

From (2.9b) we immediately find that the functions $p_\pm$ are nonnegative if the nonlinear potential $V(x)$ defined by Eq. (2.10) is a convex function

$$V''(x) \geq 0. \tag{3.14}$$

Under this condition, the Kramers' form function $\zeta(x,v)$ is an admissible choice for the reactive flux function $f(x,v)$.

Since, as for the original reactive flux, for proper nonnegative $p_\pm$ the expectation values fulfill the obvious inequalities

$$0 \leq \langle\theta(-x(t))\rangle_- \leq \langle\theta(-x(t))\rangle_+ \leq 1 \tag{3.15}$$

for any admissible choice of $f(x,v)$ the generalized reactive flux rate is an upper bound for the true rate

$$k(0) \geq k. \tag{3.16}$$

From the above consideration we find that a sufficient condition for the Kramers rate to be a bound for the true rate, is the convexity of the nonlinear potential. This is certainly too strong a condition. For example, for a cubic potential $U(x) = M\omega_b^2 x^2/2 - ax^3/3$, $a > 0$ one can modify Kramers' form function for positive values of x such that one obtains proper probability densities $p_\pm$ without a change of Kramers rate. Consequently, still in cases where $V(x)$ is not convex, the Kramers rate may be an upper bound.

Recently, Pollak et al. [9] obtained the weaker condition that $V(x)$ must be nonnegative in order that k_{kr} be an upper bound.

4. The Plateau Value

The time dependence of the reactive flux rate is determined by the propagator $e^{L^+ t}$ see Eqs. (3.2), (3.3), and results finally in an exponential decay proportional to $e^{-\lambda t}$; where $-\lambda$ is the smallest eigenvalue of L^* and, with Eq. (2.16) also of L^+. In order to compensate for this decay, one may multiply the reactive flux rate (3.5) by $e^{\lambda t}$. Then, in the limit $t \to \infty$, one obtains for the plateau value k_{pl} of the reactive flux rate

$$k_{pl} = \lim_{t\to\infty} k(t)\, e^{\lambda t} = -\frac{\langle h(x,v)\, L^* f(x,v)\rangle \langle \tilde{h}(x,v)\, \theta(-x)\rangle}{\langle f(x,v)\, \theta(-x)\rangle} \tag{4.1}$$

where the fact is used that $e^{(L^+ + \lambda)t}$ in the limit $t \to \infty$ projects onto the eigenspace of L^+ belonging to the smallest eigenvalue $-\lambda$:

$$\lim_{t\to\infty} e^{(L^+ + \lambda)t} = P_\lambda. \tag{4.2}$$

The projection operator P_λ may in the usual way be constructed from the right – and left – eigenvectors of L^+:

$$L^+ h(x,v) = -\lambda h(x,v) \tag{4.3a}$$

$$L^* \tilde{h}(x,v) = -\lambda \tilde{h}(x,v) \tag{4.3b}$$

where

$$\langle h(x,v)\, \tilde{h}(x,v)\rangle = 1 \tag{4.3c}$$

and where we have used that L^+ and L^* are adjoint to each other [see Eq. (2.16)]. Since L^+ and L^* are further connected by time reversal [compare Eqs. (2.15), (2.18)] h and $\tilde{h}$ are also connected by the time reversal transformation:

$$\tilde{h}(x,v) = h(x,-v). \tag{4.4}$$

Using Eqs. (2.16) and (4.3a) one obtains from Eq. (4.1) for the plateau value k_{pl}

$$k_{pl} = \lambda \frac{\langle f(x,v)\, h(x,v)\rangle \langle \tilde{h}(x,v)\, \theta(-\lambda)\rangle}{\langle f(x,v)\, \theta(-x)\rangle}. \tag{4.5}$$

All three factors $\langle f(x,v)h(x,v)\rangle$, $\langle \tilde{h}(x,v)\theta(-x)\rangle$, and $\langle f(x,v)\theta(-x)\rangle$ deviate from the population of the well only by factors of order $1-e^{-E_b/k_BT}$. Hence, as one expects, the plateau value of the reactive flux rate coincides up to exponentially small corrections with the smallest eigenvalue of the Fokker Planck operator.

Since, however, the exact eigenfunctions h and $\tilde{h}$ are unknown, one can try to evaluate the expression (4.1) for the plateau value of the reactive flux with the help of an appropriate pair of test functions $h_0(x,v)$ and $\tilde{h}_0(x,v)$, that one may choose consistently with the reactive flux function $f(x,v)$:

$$h_0(x,v) = \frac{\tilde{f}(x,v)}{\langle f(x,v)\tilde{f}(x,v)\rangle^{1/2}} \tag{4.6}$$

where [see Eq. (4.4)]

$$\tilde{f}(x,v) = f(x,-v) \tag{4.7}$$

and where the normalization is given by Eq. (4.3c). $\tilde{h}(x,v)$ follows immediately with Eq. (4.4). For the plateau value k_{pl} one then obtains a Rayleigh quotient for the smallest eigenvalue of L^*:

$$k_{pl} = \frac{\langle f(x,v)\, L^*\tilde{f}(x,v)\rangle}{\langle f(x,v)\tilde{f}(x,v)\rangle}. \tag{4.8}$$

This expression is different from previously suggested forms of the Rayleigh quotient [6], as it contains two different test functions for the left and right eigenvectors which are related by time reversal, rather than only one of these. Only in cases with strict detailed balance [7,10] where the operators L^+ and L^* coincide the classical Rayleigh quotient for a selfadjoint eigenvalue problem is recovered from Eq. (4.8).

If one chooses for $f(x,v)$ again Kramers' function $\zeta(x,v)$ one finds from Eqs. (2.6), (4.6) and (4.8) for a symmetric potential for the plateau value

$$k_{pl} = k_{kr}\left\{1 - \frac{l_{th}^2}{8M\omega_b^2}\, U^{(4)}(0) + O(l_{th}^4)\right\} \tag{4.9}$$

where

$$l_{th}^2 = \frac{k_BT}{M\omega_b^2}\,\frac{\gamma^2}{\gamma^2 + (2\omega_b)^2}. \tag{4.10}$$

Possible temperature corrections to the Gaussian approximation of the well population are neglected. For $\gamma \to \infty$ k_{pl} goes over to the Smoluchowski rate with its leading temperature corrections [11], whereas the expression (4.9) fails to give the correct behavior for small friction constants γ, because then the Kramers form function does not adequately approximate the eigenfunction $\tilde{h}(x,v)$.

Conclusions

In this note the generalized reactive flux method is applied to the original Kramers' model. It is shown that under the condition of a convex nonlinear potential Kramers' phase space diffusion rate may be obtained as a generalized transition state rate. It is then an upper bound for the exact rate. Further, it is demonstrated that the crucial modification of the reactive flux function from a discontinuous to a smooth characteristic function does not change the plateau value of the time dependent reactive flux rate which is given by the lowest eigenvalues of the Fokker Planck operator. The Rayleigh quotient that follows from the expression for the plateau value allows for the nonselfadjointness of the backward operator as it contains two different test functions.

The generalization of the demonstrated method to higher dimensional systems with detailed balance is straightforward. In principle, the generalized reactive flux method may also be applied to problems without detailed balance. The main problem then consists in the determination of a stationary state corresponding to the thermal equilibrium state.

The author gratefully acknowledges valuable discussions with Mischa Borkovec, Peter Hänggi, and Eli Pollak.

References

[1] M. Borkovec and P. Talkner, J. Chem. Phys. *92*, 5307 (1990).
[2] For a recent review on transition rates from metastable states see P. Hänggi, P. Talkner, and M. Borkovec, Rev. Mod. Phys. *62*, 251 (1990).
[3] B. J. Berne, in: "Multiple Time Scales", eds. J. V. Brackbill and B. I. Cohen, Academic, New York 1985; D. Chandler, "Introduction to Modern Statistical Mechanics", Oxford University, New York 1988.
[4] H. A. Kramers, Physica *7*, 284 (1940).
[5] P. Talkner, Helv. Phys. Acta *62*, 932 (1989).
[6] R. S. Larson and M. D. Kostin, J. Chem. Phys. *72*, 1392 (1980); D. Dekker, Phys. Lett. *112A*, 197 (1985).
[7] H. Risken, "The Fokker Planck equation", Springer Series in Synergetics, Vol. 18, Springer, Berlin.
[8] D. Ryter, J. Stat. Phys. *49*, 751 (1987); there extensive use of the duality between L^* and L^+ is made in order to calculate rates in the regime of weak and moderate noise by means of eigenvalues.
[9] E. Pollak, S. C. Tucker, and B. J. Berne, Phys. Rev. Lett. *65*, 1399 (1990); E. Pollack, J. Chem. Phys., *93*, 1116 (1990).
[10] P. Hänggi and H. Thomas, Phys. Rep. *88*, 207 (1982).
[11] R. S. Larson and M. D. Kostin, J. Chem. Phys. *69*, 4821 (1978); O. Edholm and O. Leimar, Physica *98A*, 313 (1979); W. Bez and P. Talkner, Phys. Lett. *A82*, 313 (1981).

Presented at the Discussion Meeting of the Deutsche Bunsen-Gesellschaft für Physikalische Chemie "Rate Processes in Dissipative Systems. 50 Years after Kramers" in Tutzing, September 10–13, 1990

E 7502

The Kramers Problem in the Turnover Regime: The Role of the Stochastic Separatrix

M. M. Klosek[1], B. J. Matkowsky[2], and Z. Schuss[2,3]

Department of Engineering Sciences and Applied Mathematics, Northwestern University, Evanston, Illinois 60208, USA

Activated Rate Processes / Diffusion / Nonequilibrium Phenomena / Statistical Mechanics

We consider the problem of activated escape of a Brownian particle from a potential well. We find the stochastic separatrix S (the locus of starting points of the phase space trajectories which have equal probabilities of ending up inside or outside the well) for (i) the extremely anisotropic overdamped motion of a two-dimensional Brownian particle in a bistable potential, and (ii) the damped and underdamped motion of a one-dimensional Brownian particle in a single metastable state. The significance of S is that (1) it defines the reactant and product wells in a natural though not necessarily intuitive way, and (2) it reduces the calculation of the escape rate to the solution of the stationary Fokker-Planck equation inside S, with absorbing boundary conditions on S. Finally, employing this approach we derive an expression for the Kramers escape rate which bridges uniformly between Kramers weak damping regime and transition state theory.

1. Introduction

The correct description of the transition state (TS) of a diffusive activated rate process with a (single) metastable state, and of the stochastic dynamics in the neighborhood of the TS, is crucial for the understanding of the activation process. However, descriptions of this behavior for diffusion processes (see e.g. [1–16]) do not seem to be complete. Indeed, the behavior of the stochastic trajectories near the TS has often been assumed, rather than derived from analysis of the underlying diffusion model. For example, a frequently used assumption in Kramer's problem [1] is that trajectories do not return from the TS (see e.g. [2]). When applied to the stochastic trajectories of the Langevin equation, although correct in the extremely underdamped regime, as shown below, it does not hold for higher values of the damping coefficient γ [1]. Analyses of stochastic trajectories near the TS (see e.g. [6,7,10–12]) also do not provide a complete picture. In particular, an adequate theory of the return probability in the transition region between the underdamped and the transition state theory range of γ, which must be taken into account in the calculation of the escape rate, has not been developed. This issue did not arise in [3] and [4], where the Langevin description was replaced by one based on a Hamiltonian of a particle in a bath of harmonic oscillators, thus changing the formulation of the diffusion problem posed by Kramers. In addition, because of the choice of normal mode coordinates in [3,4], the stochastic phase space trajectory of the particle near the TS was not described.

The purpose of this paper is to clarify the behavior of the random trajectories near the TS and to calculate the activation rate in several problems described by the Langevin equation. We describe analytically the *stochastic separatrix* S, the locus of starting points of the phase space trajectories which have equal probabilities of ending up inside or outside the potential well. Thus S is taken as the definition of the TS.

There are several important applications for S. Obviously, the escape rate κ_{esc} from the domain bounded by S is twice the absorption rate κ_{abs} in S, which explains the factor 1/2 in the relation between κ_{esc} and the mean first passage time to S [8]. The analytical and numerical calculation of κ_{esc} can thus be reduced to that of calculating the first non-zero eigenvalue of the forward or backward Fokker-Planck operator inside S, with absorption in S. It also defines the reactant and product wells for bistable damped models in a natural, though not necessarily intutitive way, independently of the ridge R of the potential (see Fig. 1), and so on. Therefore the determination of S is of considerable importance.

We determine S in two classical examples. In Section 2 we consider the case of a two dimensional anisotropic bistable Smoluchowski system. We show that depending on the relative sizes of the anisotropy parameter δ and the dimensionless temperature ε (measured in units of the well depth), either $S = \Gamma$ (e.g., if $\delta \gg \varepsilon$), or S is an altogether different curve (if $\delta \ll \varepsilon$), depending on the geometry of the potential near the saddle point M. While in the first instance S passes through M, in the latter it may not. This explains the non-saddle point activation energy predicted in [9–12]. It also shows that S is not always close to Γ when ε is small, as implied in [6]. If however $\delta = O(1)$ and $\varepsilon \ll 1$, then $S = \Gamma$, as asserted in [6] and [8]. The proof that $S = \Gamma$ for $\varepsilon \ll \delta$ is the same as that for the classical Kramers' problem of activated escape of a Brownian particle from a metastable state for $\varepsilon \ll \gamma$. The Langevin equation in this case is given in dimensionless variables by

$$\ddot{x} + \gamma\dot{x} + V'(x) = \sqrt{2\gamma\varepsilon}\,\dot{w}. \tag{1.1}$$

[1] Department of Mathematical Sciences, University of Wisconsin-Milwaukee, Milwaukee, WI 53201.
[2] Department of Engineering Sciences and Applied Mathematics, Northwestern University, Evanston, IL 60208.
[3] Department of Mathematics, Tel-Aviv University, Ramat-Aviv, Tel-Aviv 69978. Israel.

where $\dot{w}$ is standard Gaussian white noise. We assume that $V(x)$ has a single local minimum (maximum) at $x_A (< x_C)$. The domain of attraction D of the stable point $x = x_A, \dot{x} = 0$ in phase space is bounded by a separatrix Γ, which in this example is determined by the solution of

$$\dot{x} = y\,, \quad \dot{y} = -\gamma y - V'(x)\,, \tag{1.2}$$

which converges to the saddle point $x = x_C$, $y = 0$ as $t \to \infty$. We set $\omega_A^2 \equiv V''(x_A)$ and $\omega_C^2 \equiv -V''(x_C)$. Kramers' expressions for the escape rate from D are:

$$\kappa_{ud} = \frac{\gamma \omega_A I_C}{2\pi\varepsilon} e^{-\Delta V/\varepsilon} \quad \text{for} \quad \gamma \ll \varepsilon \ll 1\,, \tag{1.3}$$

where I_C is the action of the motion on the critical energy contour $E = E_c \equiv V(x_C)$ and $\Delta V \equiv V(x_C) - V(x_A)$, and

$$\kappa_{kr.} = \Omega \kappa_{tst} \quad \text{for} \quad \varepsilon \gg \gamma\,, \tag{1.4}$$

where

$$\Omega \equiv \frac{\sqrt{\gamma^2 + 4\omega_C^2} - \gamma}{2\omega_C}\,, \tag{1.5}$$

and where the transition state theory rate κ_{tst} is given by

$$\kappa_{tst} = \frac{\omega_A}{2\pi} e^{-\Delta V/\varepsilon}\,. \tag{1.6}$$

Obviously $\Omega \sim 1$ if $\gamma \ll \omega_C$, so that κ_{kr} reduces to κ_{tst} in this limit, rather than to κ_{ud}, as it should. This leaves a gap between the expansion of the escape rate in the extremely underdamped region $\gamma \ll \varepsilon \ll 1$ and the TST region $\varepsilon \ll \gamma \ll \omega_C$.

In Section 3 we show that for $\varepsilon \ll \delta$ in a two-dimensional anisotropic Smoluchowski problem, as well as in Kramers' problem in the limit (1) $\varepsilon \to 0$, $\gamma = O(1)$, the stochastic separatrix is the deterministic separatrix $S = \Gamma$. In Section 4 we show that in the limit (2) $\gamma \to 0$, S is the constant energy contour $E = E_c - \varepsilon \log 2$, thus solving the problem cited in [7]. In Section 5 we find an asymptotic expansion of S in the range of parameters (3) $\varepsilon \ll 1$, $\gamma \ll \omega_C$, which includes the range where ε and γ are comparable, and which bridges between (1) and (2). Finally, in Section 6 we derive an expression for the escape rate in the region (3), which bridges between Kramers' expression (1.3) in the limit (1) and the TST expression (1.6) in region (3).

2. The Stochastic Separatrix for an Extremely Anisotropic System

We first consider the extremely anisotropic overdamped motion of a two dimensional Brownian particle in a bistable potential $V(x_1, x_2)$ [10,13]. In dimensionless variables the dynamics is given by the Smoluchowski equations

$$\begin{aligned} \dot{x}_1 &= -\frac{\partial V}{\partial x_1} + \sqrt{2\varepsilon}\,\dot{w}_1 \\ \dot{x}_2 &= -\delta \frac{\partial V}{\partial x_2} + \sqrt{2\varepsilon\delta}\,\dot{w}_2\,, \end{aligned} \tag{2.1}$$

where δ is the anisotropy parameter, and $\dot{w}_1$, $\dot{w}_2$ are independent standard white noises. The bottom of the reactant (product) well is at $a = (x_{1a}, x_{2a})$ ($b = (x_{1b}, x_{2b})$). The domains of attraction D_a and D_b of the wells a and b, are separated by a separatrix Γ, which is the curve determined by the noiseless dynamics ((2.1) with $\varepsilon = 0$) which converges to M as $t \to \infty$. In the isotropic case $\delta = 1$, $\Gamma = R$, where R is the ridge of the potential surface (see Fig. 1).

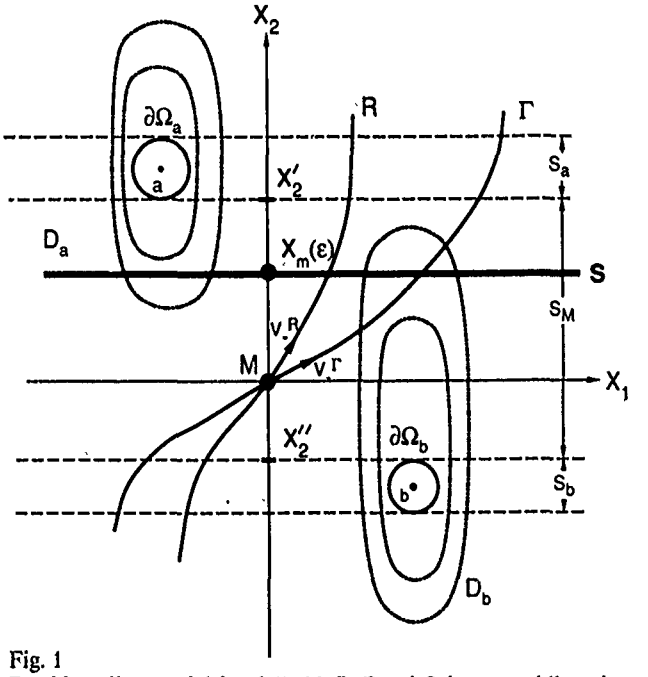


Fig. 1
Double well potential for (2.1). M, R, Γ and S denote saddle point, the ridge, the deterministic and stochastic separatrices respectively. The dashed curves represent level curves of V

If however $\delta \ll 1$, Γ differs considerably from R. The directions of R and Γ at M are shown in Fig. 1. If the local expansion of V near M is given by

$$V(x_1, x_2) \sim \frac{1}{2} A x_1^2 + B x_1 x_2 + \frac{1}{2} C x_2^2 + \ldots\,, \tag{2.2}$$

the scenario depicted in Fig. 1 corresponds to $A < 0$.

Let $\Omega_{a(b)}$ be a neighborhood of $a(b)$, deep inside the reactant (product) well and let $p(x_1, x_2)$ be the probability that a trajectory of (2.1), starting at (x_1, x_2), will hit Ω_a before it hits Ω_b. For a trajectory that starts in the reactant well and reaches the point (x_1, x_2), $p(x_1, x_2)$ is the probability of return from (x_1, x_2). The curve defined by $p(x_1, x_2) = 1/2$ is the

stochastic separatrix S. The function $p(x_1, x_2)$ is the solution of [14]

$$L_0 p + \delta L_1 p \equiv -\frac{\partial V}{\partial x_1}\frac{\partial p}{\partial x_1} + \varepsilon\frac{\partial^2 p}{\partial x_1^2} + \delta\left[-\frac{\partial V}{\partial x_2}\frac{\partial p}{\partial x_2} + \varepsilon\frac{\partial^2 p}{\partial x_2^2}\right] = 0, \tag{2.3}$$

with the boundary conditions

$$p(x_1, x_2) = 1 \quad \text{if} \quad (x_1, x_2) \in \partial\Omega_a, \qquad p(x_1, x_2) = 0 \quad \text{if} \quad (x_1, x_2) \in \partial\Omega_b, \tag{2.4}$$

where $\partial\Omega_a$ and $\partial\Omega_b$ are the boundaries of Ω_a and Ω_b, respectively. If $\delta \ll \varepsilon$, we expand

$$p \sim p^0 + \delta p^1 + \ldots \tag{2.5}$$

and obtain

$$L_0 p^0 = 0 \tag{2.6}$$

$$L_0 p^1 = -L_1 p^0, \tag{2.7}$$

and so on. From (2.6) we obtain that p^0 is independent of x_1, and from (2.4) we obtain that $p^0 = 1$ (0) in the strip $S_a(S_b)$. Next we determine p^0 in the strip S_M (see Fig. 1). The solvability condition for (2.7) is that the right hand side is orthogonal to the solution $\exp(-V/\varepsilon)$ of the homogeneous problem for L_0^* (the one-dimensional Fokker-Planck operator). Thus

$$\varepsilon\frac{d^2 p^0}{dx_2^2} - \frac{dV^{\text{eff}}(x_2, \varepsilon)}{dx_2}\frac{dp^0}{dx_2} = 0 \text{ for } x_2' < x_2 < x_2'', \tag{2.8}$$

(see Fig. 1) with the boundary conditions

$$p^0(x_2') = 0, \quad p^0(x_2'') = 1, \tag{2.9}$$

where

$$V^{\text{eff}}(x_2, \varepsilon) \equiv -\varepsilon \log \int_{-\infty}^{+\infty} e^{-V(x_1, x_2)/\varepsilon}\, dx_1. \tag{2.10}$$

We consider the case that V^{eff} has two minima, and achieves its local maximum at a point $x_m(\varepsilon)$ in the interval (x_2', x_2''). The solution of (2.8) and (2.9) is given by

$$p^0 = \frac{\int_{x_2'}^{x_2} e^{-V^{\text{eff}}(x_2, \varepsilon)/\varepsilon}\, dx_2}{\int_{x_2'}^{x_2''} e^{-V^{\text{eff}}(x_2, \varepsilon)/\varepsilon}\, dx_2}. \tag{2.11}$$

Clearly, $\lim_{\varepsilon \to 0} p^0 = 1(0)$ for $x_2 > (<) x_m(0)$. Thus S, the locus of points (x_1, x_2) such that $p(x_1, x_2) = 1/2$, is given to leading order in δ and ε by $x_2 = x_m(0)$ (see Fig. 1). Note that S differs considerably from both Γ and R. The reactant and the product wells for an extremely anisotropic ($\delta \ll \varepsilon$) chemical reaction described by (2.1) [13] are naturally defined as the domains on either side of S, rather than the domains on either side of R or Γ [9–13]. Thus the physically meaningful separatrix is neither Γ nor R [9–13], but rather S. Other cases will be discussed elsewhere.

3. The Stochastic Separatrix for $\varepsilon \to 0$

We now consider (2.1) in the limit $\varepsilon \to 0$ with $\delta = O(1)$ as well as (1.1) in the limit $\varepsilon \to 0$ with $\gamma = O(1)$ and prove that in these limits $S = \Gamma$. These problems were considered in [6] [7] and [17], however the argument in [6] does not cover all cases, as may be seen, e.g., from the simple example of a drift which vanishes on Γ (constant ridge height). For definiteness we present the proof for the Langevin equation (1.1). The proof for (2.1) is exactly the same. Let Ω_a be a neighborhood of the stable point $(x_A, 0)$, and Ω_b be the half plane $x > x_B$, where x_B is chosen so that $x_B > x_C$. The probability $p(x, y)$ that the particle, initially located at (x, y) will hit $\partial\Omega_a$ before it his $\partial\Omega_b$, is the solution of

$$Lp \equiv \varepsilon\gamma\frac{\partial^2 p}{\partial y^2} + y\frac{\partial p}{\partial x} - (\gamma y + V'(x))\frac{\partial p}{\partial y} = 0 \tag{3.1}$$

outside Ω_a and Ω_b, with the boundary conditions

$$p = 1 \text{ on } \partial\Omega_a, \quad p = 0 \text{ on } \partial\Omega_b. \tag{3.2}$$

The outer expansion

$$p = p^0 + o(1) \text{ as } \varepsilon \to 0, \tag{3.3}$$

implies that on the trajectories $(x(t), y(t))$ of (1.2) we have

$$\frac{p^0(x(t), y(t))}{dt} = 0, \tag{3.4}$$

so that $p^0(x(t), y(t)) = \text{const.}$ on each such trajectory. Since trajectories that start inside (outside) Γ reach $\partial\Omega_a$ (the line x_B), we have by (3.2)

$$p^0 = 1 \text{ inside } \Gamma, \quad p^0 = 0 \text{ outside } \Gamma. \tag{3.5}$$

The outer solution p^0 is discontinuous across Γ. Therefore we construct an asymptotic solution in a layer about Γ, to smoothly connect the solutions (3.5). We change variables in (3.1) to (x, μ), where

$$\mu \equiv \frac{\chi(x)\varrho}{\sqrt{\gamma\varepsilon}}, \quad \varrho \equiv \text{dist}((x, y), \Gamma), \tag{3.6}$$

and $\chi(x)$ is a solution of the Bernoulli equation

$$y_\Gamma(x)\chi'(x) + b_0(x)\chi(x) = \gamma(\partial\varrho(x, y_\Gamma(x))/\partial y)^2\chi^3, \tag{3.7}$$

that satisfies the initial condition

$$\chi(x_C) = \sqrt{\frac{b_0(x_C)}{\dot{\gamma}(\partial\varrho(x_C,0)/\partial y)^2}}. \tag{3.8}$$

Here

$$b_0(x_C) = \frac{\lambda\omega_C^2 + \lambda - \gamma}{1+\lambda^2}, \tag{3.9}$$

where

$$\lambda = \frac{\gamma + \sqrt{\gamma^2 + 4\omega_C^2}}{2} \tag{3.10}$$

(see [5], Eqs. (2.23)–(2.29) or [15], Eqs. (5.26)–(5.45)). Setting $p(x,y) \equiv P(x,\mu)$ and expanding

$$P(x,\mu) = P^0(x,\mu) + o(1) \text{ for } \varepsilon \ll 1, \tag{3.11}$$

we obtain the leading order boundary layer equation

$$\frac{\partial^2 P^0}{\partial\mu^2} + \mu\frac{\partial P^0}{\partial\mu} + \frac{y_\Gamma(x)}{\varrho_y^2(x,0)\chi^2(x)}\frac{\partial P^0}{\partial x} = 0, \tag{3.12}$$

with the boundary and matching conditions

$$\lim_{\mu\to\infty} P^0(x,\mu) = 1, \quad \lim_{\mu\to-\infty} P^0(x,\mu) = 0. \tag{3.13}$$

Here $\varrho_y \equiv \partial\varrho/\partial y$. The solution of (3.12), (3.13) is [17]

$$P^0(x,\mu) = \sqrt{\frac{1}{2\pi}}\int_{-\infty}^{\mu} e^{-s^2/2}\,ds. \tag{3.14}$$

Thus if $(x,y) \in \Gamma$, then $\varrho(x,y) = 0$, so that $\mu = 0$, and

$$P^0(x,0) = \sqrt{\frac{1}{2\pi}}\int_{-\infty}^{0} e^{-s^2/2}\,ds = \frac{1}{2}. \tag{3.15}$$

It follows that $S = \Gamma$ in the limit $\varepsilon \to 0$ for $\gamma = O(1)$ [6–8, 17].

4. The Stochastic Separatrix in the Extremely Underdamped Kramers' Problem

Next we consider (3.1) for $\gamma \ll \varepsilon \ll 1$. We expand

$$p(x,y) \sim p^0(x,y) + o(1) \text{ as } \gamma \to 0, \tag{4.1}$$

and obtain that $p^0(x,y)$ is constant on constant energy contours. Thus for every (x,y) such that $E \equiv y^2/2 + V(x) > E_c$, the outer solution is

$$p^0(x,y) = 0. \tag{4.2}$$

For $E < E_c$ we average (3.1) over constant energy contours, to obtain

$$\varepsilon\left(I(E)\frac{\partial^2 p^0}{\partial E^2} + T(E)\frac{\partial p^0}{\partial E}\right) - I(E)\frac{\partial p^0}{\partial E} = 0, \tag{4.3}$$

where the action $I(E)$ and the period $T(E)$ of the undamped noiseless motion on the constant energy contour E, are given by

$$I(E) = \oint_E y\,dx, \text{ and } T(E) = I'(E) = \oint_E \frac{dx}{y}. \tag{4.4}$$

We choose $\partial\Omega_a$ to be the contour $E = E_1 < E_c$. The boundary condition for p^0 is given by

$$p^0(x,y) = 1 \quad \text{on} \quad E = E_1, \tag{4.5}$$

and the matching condition is that the solution of (4.3) matches with the outer solution (4.2) as $E \to E_c$, which implies that

$$p^0(x,y) = 0 \quad \text{on} \quad E = E_c. \tag{4.6}$$

The solution of (4.3), (4.5), and (4.6) is

$$p^0(x,y) = \left\{\int_E^{E_c} \frac{e^{s/\varepsilon}}{I(s)}\,ds\right\} \Big/ \left\{\int_{E_1}^{E_c} \frac{e^{s/\varepsilon}}{I(s)}\,ds\right\} \text{ for } (x,y) \in E. \tag{4.7}$$

Note that the matching condition (4.6) implies that trajectories which reach E_c are unlikely to reach $\partial\Omega_a$ before $\partial\Omega_b$, i.e., are unlikely to return.

Now we use (4.7) to find S, by finding the value $E_{1/2}$ of E, for which

$$p^0(x,y) = \frac{1}{2}. \tag{4.8}$$

Since for small ε the main contribution to the integrals in (4.7) come from $E = E_c$, we obtain to leading order in ε

$$E_S \equiv E_{1/2} \sim E_c - \varepsilon\log 2 \quad \text{for} \quad \varepsilon \ll 1. \tag{4.9}$$

Thus in the limit $\gamma \to 0$, S is the contour $E = E_{1/2}$. Obviously, for $\gamma \neq 0$, S lies between the $E_{1/2}$ and Γ. Particles whose energy is higher than $E_c - \varepsilon\log 2$ have a probability of at least 1/2 not to return to the well, contrary to commonly held beliefs. Obviously as γ increases, the probability of returning from the barrier top to the well increases continuously from 0 to 1/2.

Note that for E close to E_c, $I(s)$ is close to I_c, the action of the motion on the critical energy contour $E = E_c$, so that (4.7) implies that

$$p^0(x,y) \sim 1 - e^{-\zeta}, \tag{4.10}$$

where

$$\zeta \equiv \frac{E_c - E}{\varepsilon}. \tag{4.11}$$

Thus, in a layer near E_c, the probability $p^0(x,y)$ as a function of ζ, satisfies

$$p^0_{\zeta\zeta} + p^0_{\zeta} = 0. \tag{4.12}$$

This fact is used in the next section.

5. A Uniform Expansion of the Stochastic Separatrix in Kramers' Problem

In Sections 3 and 4 we found S for $\varepsilon \ll \gamma$ and for $\gamma \ll \varepsilon$, respectively. Here we determine S in the range where γ and ε are comparable. Comparing (3.14) with (4.7) we see that neither is uniform in ε and γ, since they do not reduce to one another in the appropriate limits. Therefore we now construct a boundary layer to connect the outer solutions (3.5) in the parameter range where ε and γ are comparable. We introduce in (3.1) the variables

$$\zeta \equiv \frac{E_c - E}{\varepsilon}, \quad \xi \equiv -\frac{\gamma}{\varepsilon} I_\Gamma(x), \tag{5.1}$$

where

$$I_\Gamma(x) \equiv \int_{x_c}^{x} y_\Gamma(x)\,dx \tag{5.2}$$

is the (negative) action of the motion on Γ between the points x_c and x. Setting $p(x,y) = Q(\xi,\zeta)$ in (3.1) we obtain

$$Q_{\zeta\zeta} + Q_\zeta\left(1 - \frac{\varepsilon}{y^2}\right) = Q_\xi \sqrt{1 + \frac{2\varepsilon(\zeta+\xi)}{y^2}}. \tag{5.3}$$

Matching to the outer expansion implies that

$$Q(\xi,\zeta) = 0 \quad \text{for} \quad \zeta + \xi = 0, \quad \zeta < 0 \tag{5.4}$$

and

$$Q(\xi,\zeta) \to 1 \quad \text{as} \quad \zeta \to \infty. \tag{5.5}$$

The initial condition at $\xi = 0$ is obtained as follows. The limit $\xi \to 0$ corresponds to $\gamma \to 0$, so that in this limit $Q(0,\zeta)$ must agree with (4.10). Thus (4.12) implies the initial condition

$$Q_{\zeta\zeta} + Q_\zeta\left(1 - \frac{\varepsilon}{y^2}\right) = 0 \quad \text{for} \quad \xi = 0. \tag{5.6}$$

Setting $\eta \equiv \zeta + \xi$ and expanding $Q = Q^0 + o(1)$ we obtain

$$Q^0_{\eta\eta} = Q^0_\xi \quad \text{for} \quad \eta > 0, \ \xi > 0 \tag{5.7}$$

with the initial and boundary conditions

$$Q^0_{\eta\eta}(0,\eta) + Q^0_\eta(0,\eta) = 0 \quad \text{for} \quad \eta > 0 \tag{5.8}$$

and

$$Q^0(\xi,0) = 0, \quad \text{and} \quad Q^0(\xi,\eta) \to 1 \quad \text{as} \quad \eta \to \infty. \tag{5.9}$$

The solution is given by

$$\begin{aligned} Q^0(\xi,\eta) = {} & \sqrt{\frac{2}{\pi}} \int_0^{\eta/\sqrt{2\xi}} e^{-z^2/2}\,dz \\ & + \frac{e^{\eta+\xi}}{\sqrt{2\pi}} \int_{\sqrt{2\xi}+\eta/\sqrt{2\xi}}^{\infty} e^{-z^2/2}\,dz \\ & - \frac{e^{-\eta+\xi}}{\sqrt{2\pi}} \int_{\sqrt{2\xi}-\eta/\sqrt{2\xi}}^{\infty} e^{-z^2/2}\,dz \equiv R^1(\xi,\eta) \\ & + R^2(\xi,\eta) - R^3(\xi,\eta). \end{aligned} \tag{5.10}$$

Next we show that in the limits $\gamma \ll \varepsilon \ll 1$ and $\varepsilon \ll \gamma \ll \omega_C$, (5.10) reduces to the results obtained in sections 3 and 4, so that (5.10) provides a uniform expansion of the probability $p(x,y)$.

First we consider $\gamma \ll \varepsilon$, which corresponds to $\xi \to 0$ in (5.10). Obviously, in this limit the initial condition (5.8) is recovered, so that

$$Q^0(\xi,\eta) \sim Q^0(0,\eta) = 1 - e^{-\eta} = 1 - e^{-(E_\Gamma - E)/\varepsilon}. \tag{5.11}$$

Setting

$$Q^0(\xi,\eta) = \frac{1}{2} \tag{5.12}$$

we obtain

$$E_S = E_\Gamma - \varepsilon \log 2 = E_c - \gamma I_\Gamma(x) - \varepsilon \log 2. \tag{5.13}$$

Clearly, (4.10) is recovered as $\gamma \to 0$, and (5.13) also provides a first correction term to (4.10).

Next we consider $\varepsilon \ll \gamma$, which corresponds to $\xi \to \infty$. It is easily seen that $R^2(\xi,\eta)$ and $R^3(\xi,\eta)$ in (5.10) vanish, so that $R^1(\xi,\eta)$ determines the asymptotic behavior of $Q^0(\xi,\eta)$, which agrees with (3.14). To determine S in this limit, we set $R^1(\xi,\eta) = 1/2$. There exists a value $z_{1/2}$ such that

$$\sqrt{\frac{2}{\pi}} \int_0^{z_{1/2}} e^{-z^2/2}\,dz = \frac{1}{2}. \tag{5.14}$$

Therefore S is determined from the equation

$$\frac{\eta}{\sqrt{2\xi}} = z_{1/2}, \tag{5.15}$$

or equivalently

$$E_S \sim E_\Gamma - \sqrt{2\varepsilon\gamma |I_\Gamma(x)|}\, z_{1/2}. \tag{5.16}$$

Clearly, (5.16) reduces to $S = \Gamma$ in the limit $\varepsilon \to 0$, and also provides a first-correction term in the expansion of S.

We note that in the two limits considered, we obtain different correction terms in the expansion of S, so that neither one can be separately used as a uniform expansion of S.

6. A Uniform Expansion of the Activation Rate in Kramers' Problem

Next we calculate the escape rate from the relation

$$\kappa_{\rm esc} = \frac{1}{2}\kappa_{\rm abs}\,, \tag{6.1}$$

where $\kappa_{\rm abs}$ is the absorption rate in S. To this end we calculate the stationary probability density function $f(x,y)$ inside S (in phase space), with a source at $(x_A,0)$ and absorption in S. Thus $f(x,y)$ is Green's function for the Fokker-Planck operator with absorption in S. Then

$$\kappa_{\rm abs} = \frac{F}{N}\,, \tag{6.2}$$

where F is the total probability current on S and N is the total population inside S. The Fokker-Planck equation is given by

$$\gamma\varepsilon f_{yy} - y f_x + [(\gamma y + V'(x))f]_y = -\delta(x-x_A,y)\,, \tag{6.3}$$

with the boundary condition

$$f(x,y)|_S = 0\,. \tag{6.4}$$

The asymptotic structure of $f(x,y)$ for small ε is given by [15]

$$f(x,y) = \mathrm{e}^{-E/\varepsilon} q(x,y)\,, \tag{6.5}$$

where $q(x,y)$ is the solution of (3.1) with the absorbing boundary condition (6.4) and the matching condition

$$q \sim \text{const. as } \varepsilon \to 0,\ (x,y) \text{ inside } S - \{(x_A,0)\}\,, \tag{6.6}$$

The function $q(x,y)$ has an integrable singularity at the source. We note that although $q(x,y)$ and $Q(\xi,\eta)$ satisfy the same equation $Lq = 0$ (see (3.1)) and the same matching conditions (6.6), the absorbing boundary condition for $q(x,y)$ is assigned on S, whereas that for $Q(\xi,\eta)$ is assigned on Γ. However, since to leading order in ε we have $Q(\xi,\eta) = 1/2$ on S, the function $2Q(\xi,\eta) - 1$ vanishes on S, matches to 1 away from S, and satisfies (6.4). It follows that to leading order in ε

$$q(x,y) \sim 2Q^0(\xi,\eta) - 1\,, \tag{6.7}$$

so that by (6.5)

$$f(x,y) \sim \mathrm{e}^{-E/\varepsilon}(2Q^0(\xi,\eta) - 1)\,. \tag{6.8}$$

By definition, the probability current F and the total population N are given by [15, 16]

$$F \equiv -\int_S \gamma\varepsilon f_y\,\mathrm{d}x \sim -2\varepsilon\gamma\int_S \mathrm{e}^{-E/\varepsilon}\frac{\partial Q^0(\xi,\eta)}{\partial y}\,\mathrm{d}x \tag{6.9}$$

and

$$N \equiv \iint_D f\,\mathrm{d}x\,\mathrm{d}y \approx \frac{2\pi\varepsilon}{\omega_A}\mathrm{e}^{-E_A/\varepsilon}\,, \tag{6.10}$$

where D denotes the reactant well. Hence, by (6.1),

$$\kappa_{\rm esc} \sim \frac{-\gamma\omega_A\int_S \mathrm{e}^{-E/\varepsilon}\frac{\partial Q^0(\xi,\eta)}{\partial y}\,\mathrm{d}x}{2\pi}\,\mathrm{e}^{V(x_A,x_A)/\varepsilon}\,. \tag{6.11}$$

Next we consider (6.11) in the two limits, $\gamma \ll \varepsilon$ and $\varepsilon \ll \gamma$, From (5.10) we have

$$\begin{aligned} Q^0_\eta(\xi,\eta) = {} & \frac{\mathrm{e}^{\eta+\xi}}{\sqrt{2\pi}}\int_{\sqrt{2\xi}+\eta/\sqrt{2\xi}}^{\infty}\mathrm{e}^{-z^2/2}\,\mathrm{d}z \\ & + \frac{\mathrm{e}^{-\eta+\xi}}{\sqrt{2\pi}}\int_{\sqrt{2\xi}+\eta/\sqrt{2\xi}}^{\infty}\mathrm{e}^{-z^2/2}\,\mathrm{d}z\,. \end{aligned} \tag{6.12}$$

The limit $\gamma \ll \varepsilon$ corresponds to $\xi \to 0$ so that by (5.13), $E_S \sim E_c - \varepsilon\log 2$, the first integral in (6.12) vanishes, the second integral tends to 1, and $-\eta + \xi \to -\log 2$. Therefore (6.11) reduces to

$$\begin{aligned} \kappa_{\rm esc} &\sim \frac{\gamma\omega_A\int_S \mathrm{e}^{-E_c/\varepsilon}y_S(x)\,\mathrm{d}x}{2\pi\varepsilon}\,\mathrm{e}^{V(x_A,y_A)/\varepsilon} \\ &\sim \frac{\gamma\omega_A I_C}{2\pi\varepsilon}\,\mathrm{e}^{-\Delta V/\varepsilon} \quad \text{for} \quad \gamma \ll \varepsilon \ll 1\,, \end{aligned} \tag{6.13}$$

which is Kramers' result (1.3) in this limit.

The limit $\varepsilon \ll \gamma$ corresponds to $\xi \to \infty$. As noted in Section 5,

$$Q^0(\xi,\eta) \sim R^1(\xi,\eta) \quad \text{as} \quad \xi \to \infty\,, \tag{6.14}$$

and it can be easily seen from (6.12) that

$$Q^0_\eta(\xi,\eta) \sim R^1_\eta(\xi,\eta) \quad \text{as} \quad \xi \to \infty\,. \tag{6.15}$$

The boundary layer function $R^1(\xi,\eta)$ is similar to $P^0(x,\mu)$ in (3.14). It has been shown in [5, 15] that if $Q^0(\xi,\eta)$ is replaced by $P^0(x,\mu)$ in (6.11), then

$$\frac{\kappa_{\rm esc}}{\kappa_{\rm tst}} \longrightarrow \Omega \quad \text{as} \quad \varepsilon \to 0\,, \tag{6.16}$$

which is equivalent to $\kappa_{\rm esc} \sim \kappa_{\rm kr}$ for $\varepsilon \ll 1$. In particular $\Omega \sim 1$ if $\gamma \ll \omega_C$, that is,

$$\kappa_{\rm esc} \sim \kappa_{\rm tst} \quad \text{for} \quad \varepsilon \ll \gamma \ll \omega_C\,. \tag{6.17}$$

Therefore in order to show that (6.17) holds for κ_{esc} defined by (6.11), it suffices to show that

$$I \equiv \left\{\frac{\eta}{\sqrt{2\xi}}\right\} \Big/ \left\{\frac{\chi(x)\varrho}{\sqrt{\varepsilon\gamma}}\right\} \sim 1, \quad \text{for} \quad \varepsilon \ll \gamma \ll \omega_C \tag{6.18}$$

for (x,y) in a boundary layer near the saddle point $(x_C,0)$ (in particular for $(x,y) \in S$, near $(x_C,0)$). According to [5, 15]

$$\chi(x_C) = \frac{\sqrt{\lambda_+}}{\varrho_y(x_C,0)}, \tag{6.19}$$

where λ_+ and λ_- are the positive and negative roots of

$$\lambda^2 + \lambda\gamma - \omega_C^2 = 0, \tag{6.20}$$

respectively. On the other hand, for (x,y) in the boundary layer near $(x_C,0)$

$$\frac{\eta}{\sqrt{2\xi}} = \frac{y_I^2(x) - y^2}{2\sqrt{-2\varepsilon\gamma I_I(x)}} \sim \frac{(y_I(x) - y)\, y_I(x)}{\sqrt{-2\varepsilon\gamma I_I(x)}}. \tag{6.21}$$

Since near $(x_C,0)$

$$y_I(x) = \lambda_-(x - x_C) + O((x - y_C)^2), \tag{6.22}$$

we have by (5.2)

$$I_I(x) = \frac{\lambda_-(x - x_C)^2}{2} + O((x - x_C)^3) \text{ near } (x_C,0), \tag{6.23}$$

and

$$y_I(x) - y \sim \frac{\varrho(x,y)}{\varrho_y(x_C,0)} \text{ for } \varepsilon \ll 1 \text{ and } (x,y) \text{ near } (x_C,0). \tag{6.24}$$

It follows that

$$\frac{\eta}{\sqrt{2\xi}} \sim \frac{\sqrt{-\lambda_-}}{\varrho_y(x_C,0)\sqrt{\varepsilon\gamma}}, \tag{6.25}$$

so that the limit (6.18) is

$$I = \sqrt{\frac{\lambda_+}{\lambda_-}} \sim 1 \quad \text{for} \quad \varepsilon \ll \gamma \ll \omega_C, \tag{6.16}$$

hence (6.17). Thus (6.11) bridges between the extremely underdamped regime $\gamma \ll \varepsilon \ll 1$ and the TST regime $\varepsilon \ll \gamma \ll \omega_C$. A uniform approximation to the rate constant is given by

$$\kappa_{unif} = \Omega\kappa_{esc} \tag{6.27}$$

(see [2]), where Ω is Karmers' factor given by (1.5).

References

[1] H. A. Kramers, Physica (Utrecht) *7*, 284 (1940).
[2] V. I. Melnikov and S. V. Meshkov, J. Chem. Phys. *85*, 1018 (1986).
[3] H. Grabert, Phys. Rev. Lett. *61*, 1683–1686 (1988).
[4] E. Pollak, H. Grabert, and P. Hänggi, J. Chem. Phys. *91*, 4073 (1989).
[5] B. J. Matkowsky, Z. Schuss, and C. Tier, J. Stat. Phys. *35* (3/4), 443–456 (1984).
[6] D. Ryter, Physica *142A*, 103 (1987).
[7] D. Ryter, J. Stat. Phys. *49* (3/4), 751 (1987).
[8] Z. Schuss and B. J. Matkowsky, SIAM J. Appl. Math. *35*, 604 (1979).
[9] S. H. Northrup and J. A. McCammon, J. Chem. Phys. *78*, 987 (1983).
[10] A. M. Berezhkovskii and V. Yu. Zitserman, Chem. Phys. Lett. *158*, 369 (1989).
[11] A. M. Berezhkovskii, L. M. Berezhkovskii, and V. Yu. Zitserman, Teor. Eksp. Khim.
[12] A. M. Berezhkovskii, L. M. Berezhkovskii, and V. Yu. Zitserman, Chem. Phys. *130*, 55 (1989).
[13] M. M. Kłosek-Dygas, B. M. Hoffman, B. J. Matkowsky, A. Nitzan, M. A. Ratner, and Z. Schuss, J. Chem. Phys. *90*, 1141 (1989).
[14] Z. Schuss, Theory and Applications of Stochastic Differential Equations, Wiley, New York 1980.
[15] T. Naeh, M. M. Kłosek, B. J. Matkowsky, and Z. Schuss, SIAM J. Appl. Math. *50* (2), 595 (1990).
[16] W. C. Gardiner, Handbook of Stochastic Methods, Springer-Verlag, Berlin 1985.
[17] M. Mangel and D. Ludwig, SIAM J. Appl. Math. *33* (2), 256 (1977).

Presented at the Discussion Meeting of the Deutsche Bunsen-Gesellschaft für Physikalische Chemie "Rate Processes in Dissipative Systems: 50 Years after Kramers" in Tutzing, September 10–13, 1990 E 7503

Mean First Passage Times and Nonlinear Relaxation Time for Nonlinear Models Driven by Dichotomous Noise

Ulrich Behn[1], Konrad Schiele[1], and Reinhard Müller[2]

[1] Sektion Physik, Universität Leipzig, Augustusplatz 10/11, O-7010 Leipzig, Germany

[2] Zentralinstitut für Isotopen- und Strahlenforschung, Permoserstr. 15, O-7050 Leipzig, Germany

Dichotomous Markov Process / Mean First Passage Time / Nonequilibrium Phenomena / Nonlinear Phenomena / Nonlinear Relaxation Time

The mean first passage time to reach a noise induced state starting from a local minimum of the stationary probability density is calculated analytically for the Stratonovich model exploiting a natural reflecting boundary condition. Furthermore, the nonlinear relaxation time is calculated and compared with the mean first passage time. The results are checked by digital simulation for typical values of the parameters.

1. Introduction

The problem of dynamical properties of nonlinear systems driven by colored noise is subject of considerable interest [1]. In this paper we consider the general nonlinear flow

$$\dot{x}_t = f(x_t) + g(x_t) I_t = F_\sigma(x_t),\ I_t = \sigma\Delta,\ \sigma = \pm \tag{1}$$

driven by the dichotomous Markovian process (DMP) I_t which jumps between the two values $\pm\Delta$ with the mean frequency α. To be specific we investigate the Stratonovich model [2]

$$\dot{x}_t = a x_t - x_t^3 + x_t I_t \tag{2}$$

where a is the control parameter which (in the absence of noise) describes a bifurcation of the stable stationary state when changing its sign. A variety of physical phenomena (some of them are listed in [3]), where stochastic fluctuations of the control parameter around the mean value occur, is modelled by (2).

The full information about the dynamical properties contains of course the time dependent probability density which, however, can be hardly calculated for nontrivial problems. For the Stratonovich model, e.g., only the asymptotics is known [3].

There are, however, characteristic times which can be calculated without explicit knowledge of the time dependent probability density, the mean first passage time (MFPT) and the nonlinear relaxation time (NLRT). Whereas the MFPT is the average of stochastic first passage times which are needed in a representative number of realizations to leave a given interval, the NLRT describes the relaxation of the *mean* trajectory starting far from equilibrium to its stationary value. The concept of MFPT remains even meaningfull if no stationary state of the system exists.

MFPT's of non-Markovian processes driven by dichotomous noise are investigated starting from the Kolmogorov-backward equation [4–14] or, alternatively, enumerating the stochastic trajectories [15–19]. In the former approach boundary conditions characterizing the end points of the interval have to be posed. The exit point is *absorbing*, the other end point may be *reflecting* [13] or absorbing, if it coincides with the natural boundary of the support it is *natural reflecting* [14]. With these boundary conditions the MFPT can be calulated up to quadratures [11–14, 17]. These quadratures can be evaluated analytically in terms of hypergeometric functions of multiple arguments if the flow $F_\sigma(x)$ is polynomial in x [14].

The NLRT generalizes the formalism of linear relaxation times (LRT) which describes the relaxation of correlation functions in the steady state. For the LRT there exist exact results for Gaussian white noise (GWN) [20] as well as for the DMP [21, 22]. For the NLRT exact results are known for GWN [23]. For the Ornstein-Uhlenbeck process (OUP) approximative methods are available [24–27], only very recently an exact result for the Verhulst model was obtained via the calculation of time dependent moments [28]. In this paper we give an exact calculation of the NLRT for systems driven by the DMP generalizing previous results for the LRT [20–22].

We consider the Stratonovich model in a parameter region where the stationary probability density

$$P_s(x) = N|x|^{-1} \prod_{\sigma=\pm} |x|^{-2\lambda\sigma} |x^2 - x_\sigma^2|^{\lambda\sigma - 1}$$
$$2\lambda_\sigma = \alpha/(a + \sigma\Delta),\quad x_\sigma^2 = a + \sigma\Delta, \tag{3}$$

(N is a normalizing factor) exhibits a noise induced local maximum, i.e. for $\max\{a/\Delta - 1, (\Delta/a - a/\Delta)/4\} < \alpha/(2\Delta) < a/\Delta + 1$ [3, 4]. We investigate in Section 2 the MFPT to reach the local maximum x_{max} of P_s injecting the system at the local minimum x_{min},

$$x^2_{max/min} = \{\alpha + 3a \mp [(\alpha - 2a)^2 + 5\Delta^2]^{1/2}\}/5. \tag{4}$$

In Section 3 we calculate the NLRT characterizing the relaxation of the system starting from x_{min}, i.e. the decay of an unstable state (see also [29] and references therein) and compare the result with a MFPT.

2. Mean First Passage Time

The MFPT $T_\sigma(x_0)$ to leave the first time a given interval $\mathcal{J}$ starting at $t = 0$ with realization $I_{t=0} = \sigma\Delta$ from x_0 is governed by

$$-1 = F_\sigma T'_\sigma - \alpha(T_\sigma - T_{-\sigma}),\ \sigma = \pm, \tag{5}$$

where T'_σ is the shorthand for $\partial/\partial x_0\ T_\sigma$.

Eq. (5) is obtained in the simplest way by integrating the Kolmogorov backward equations over the interval $\mathcal{J}$ and over the time span from 0 to ∞ [4–14].

The boundary conditions depend on the nature of the end points of the interval $\mathcal{J}$ under consideration. At an *exit point* x_E one imposes an *absorbing* boundary condition, i.e. if the flow for the realization $\sigma_E\Delta$ of the driving process leaves the interval at x_E we have

$$T_{\sigma_E}(x_E) = 0. \tag{6}$$

If the interval is bounded by two exit points we simply have two absorbing boundary conditions. A different situation appears if the other end point coincides with one of the natural boundaries x_B of the support. There the flow for the realization $\sigma_B\Delta$ of the driving process vanishes, $F_{\sigma_B}(x_B) = 0$. Putting the system with $I_{t=0} = \sigma_B\Delta$ at x_B it remains there until the driving process jumps to $-\sigma_B\Delta$ which needs in average the time $1/\alpha$. Then due to the nonvanishing flow $F_{-\sigma_B}(x_B)$ the system is reflected into support. We call this type of boundary condition *natural reflecting* [14],

$$T_{\sigma_B}(x_B) = 1/\alpha + T_{-\sigma_B}(x_B). \tag{7}$$

In Fig 1. both types of boundary conditions are illustrated. Most of the previous work deals with absorbing boundary

conditions, only very recently the case of *immediate reflection* was considered in some detail [13]. There, in the appendix, a reflection with finite rates but of different nature than considered here was also discussed.

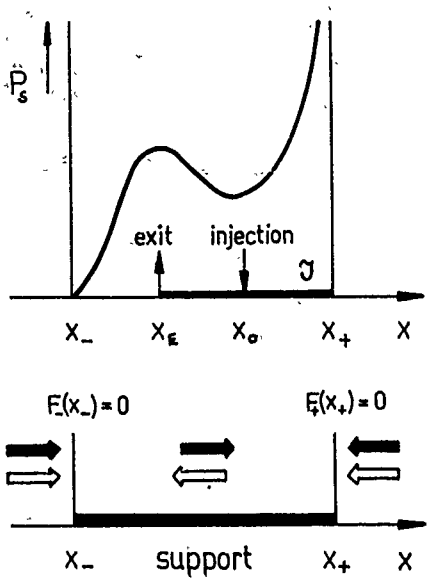


Fig. 1
Typical shape of the probability density in the considered parameter region. The system is injected at x_0. We ask for the mean time the system needs to reach x_E. The boundary conditions at the end points of the Interval $\mathcal{I}$ become obvious looking at the flow $\dot{x}_t = F_\sigma(x_t)$ which is shown in the lower part for the realizations $I_t = \Delta$ (solid arrow) and $I_t = -\Delta$ (opon arrow)

From (1) an equivalent first order equation for T'_σ is readily obtained

$$F_\sigma F_{-\sigma} T''_\sigma + (F'_\sigma F_{-\sigma} - 2\alpha f) T'_\sigma = 2\alpha . \tag{8}$$

The natural reflecting boundary conditions transform to

$$T'_{-\sigma_B}(x_B) = -2/F_{-\sigma_B}(x_B),\ T'_{\sigma_B}(x_B) = 0 . \tag{9}$$

Obviously, Eq. (4) can be immediately integrated up to quadratures [4–14]. For $F_\sigma(x)$ polynomial in x of order n these quadratures can be evaluated analytically in terms of hypergeometric functions of $n-1$ arguments [14].

To be specific we now consider the Stratonovich model (2) choosing a starting point x_0 and an exit point $x_E < x_0$ so that the other end point of the interval is the natural right boundary $x_B = x_+$ (cf. Fig. 1). Then one obtains after straightforward but length calculations [14]

$$T_+(x_0) = \alpha[2(\lambda_+ + 1)x_+^4]^{-1} \cdot \sum_{m,n=0}^{\infty} \frac{(\lambda_+ + 1)_{m+n}(1+\lambda_+ + \lambda_-)_m (1-\lambda_-)_n}{(\lambda_+ + 2)_{m+n}(1+m+n)\,m!\,n!} \cdot z_1^m(x_0) z_2^{n+1}(x_0) F_1[1+m+n, 1-\lambda_+ - \lambda_-, \lambda_+ + 2, 2 + m + n, z_1(x_0), z_2(x_0)] + 1/\alpha + T_-(x_+), \tag{10}$$

where

$$z_1(x) = (x_+^2 - x^2)/x_+^2, z_2(x) = (x_+^2 - x^2)/(x_+^2 - x_-^2), \tag{11}$$

and

$$T_-(x_+) = \alpha[2\lambda_+ \cdot x_+^4]^{-1} \cdot \sum_{m,n=0}^{\infty} \frac{(\lambda_+)_{m+n}(1+\lambda_+ + \lambda_-)_m (-\lambda_-)_n}{(\lambda_+ + 1)_{m+n}(1+m+n)\,m!\,n!} \cdot z_1^m(x_E) z_2^{n+1}(x_E) \cdot F_1[1+m+n, 1-\lambda_+ - \lambda_-, \lambda_+ + 1, 2 + m + n, z_1(x_E), z_2(x_E)] . \tag{12}$$

In Fig. 2 the MFPT to reach the local noise induced maximum of $P_s(x)$, starting from the local minimum of $P_s(x)$, i.e. $x_E = x_{max}$ and $x_0 = x_{min}$, is shown as function of the mean frequency α of the driving DMP. The dominant effect seems to be that the MFPT diverges as x_{max} reaches the left boundary of the support x_- (cf. lower part of Fig. 2). This is clear since the flow for $I_t = -\Delta$ vanishes near the boundary x_- as $\dot{x}_t = -(x_t - x_-)\,x_-^2$. Here, both initial and exit points depend on parameters. Introducing $(x_0 - x_E)/T_+$ one finds that this quantity systematically increases with increasing α, i.e. the noise induced state is reached as "faster" as faster the driving processes is [14]. This agrees with the tendency that the MFPT to reach a preassigned value increases with increasing correlation time observed for different models driven by several types of colored noise [6, 30].

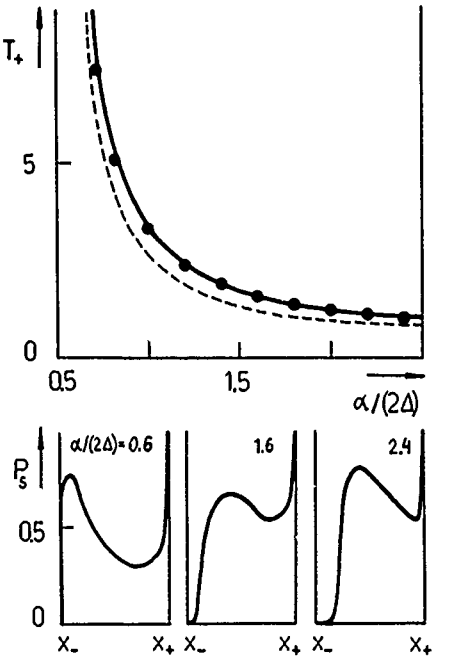


Fig. 2
MFPT $T_+(x_{min})$ for the Stratonovich model to reach the noise induced local maximum of P_s starting with $\sigma = +$ in the local minimum. For $a = 1.5$, $\Delta = 1$ we compare the exact result (solid line) against the noise parameters $\alpha/(2\Delta)$ with a digital simulation from 10^3 realizations (full circles) and the simple approximation (13) (broken line). The lower part exhibits $P_s(x)$ for characteristic parameter values

The finite support (which results from the multiplicative coupling of the noise and its finite space of states) and the peculiar behaviour near its boundaries make a steepest descent approximation unfeasible where the finite boundaries are replaced by infinite ones. Instead, a simple approximation is obtained from the rigorous result (10) as [14]

$$T_+(x_0) \approx \frac{1}{x_+^2}\left[-\frac{\alpha}{\alpha+2x_+^2}\frac{x_+^2-x_0^2}{x_0^2-x_-^2} + \frac{x_+^2-x_E^2}{x_E^2-x_-^2}\right] + 1/\alpha. \tag{13}$$

The problem to calculate the MFPT to reach the local minimum $x_{\min}$ starting from the local maximum $x_{\max}$ of $P_s(x)$ which is more close to Kramers' escape problem [31] (for a recent review see [32]) can be treated in a similar way. The calculations slightly modify since then $x_B = x_-$ and $x_0 = x_{\max} < x_E$.

We furthermore mention that a superposition of N independent realizations of the DMP scaled in an appropriate way gives in the limit $N \to \infty$ the Ornstein-Uhlenbeck process. Already a finite sum DMP's (pregaussian noise [33]) models some characteristics of the Ornstein-Uhlenbeck process. In this case the support is finite too, and stratified into regions which cannot be left for a given realization of the pregaussian noise. At the boundaries of these regions similar conditions as developed in this paper hold.

In the next Section we consider the NLRT which characterizes the relaxation of the mean trajectory $\langle x_t^2\rangle$ to its stationary value a starting from $x_{\min}^2$. We compare the result with the MFPT to reach $x_E = a^{1/2}$ starting from $x_0 = x_{\min}$, $T_{\mathrm{MFPT}}(x_0) = [T_+(x_0) + T_-(x_0)]/2$.

3. Nonlinear Relaxation Time

The NLRT of a function $\phi(x_t)$ of a stochastic process x_t is defined as [34]

$$T_{\mathrm{NLRT}}^{\phi} = \frac{\int_0^\infty \mathrm{d}t\,(\langle\phi\rangle_t - \langle\phi\rangle_s)}{\langle\phi\rangle_0 - \langle\phi\rangle_s} = \frac{\int_{\mathrm{supp}} \mathrm{d}x\,\varrho_1(x)\,\phi(x)}{\langle\phi\rangle_0 - \langle\phi\rangle_s}, \tag{14}$$

where $\langle\phi\rangle_t = \int_{\mathrm{supp}} \mathrm{d}x\,P_t(x)\,\phi(x)$ and $P_t(x) = \langle\delta(x-x_t)\rangle^{\mathrm{DMP}}$ is the time dependent probability density, and $P_0(x)$ and $P_s(x)$ are the initial and stationary densities, repectively. The quantity

$$\varrho_1(x) = \int_0^\infty \mathrm{d}t\,[P_t(x) - P_s(x)] \tag{15}$$

can be determined without explicit knowledge of $P_t(x)$ as follows.

Introducing $P_t = (P_t, Q_t)^T$ where $Q_t(x) = \langle I_t\,\delta(x-x_t)\rangle$ DMP the Kolmogorov forward equation reads

$$\dot{P}_t = \hat{L}(P_t - P_s),\ \hat{L} = -\begin{pmatrix} \partial_x f & \partial_x g \\ \Delta^2\partial_x g & 2\alpha + \partial_x f\end{pmatrix}. \tag{16}$$

After time integration we obtain

$$P_s - P_0 = \hat{L}\varrho, \tag{17}$$

where $\varrho = (\varrho_1, \varrho_2)^T$, ϱ_1 given by (15) and $\varrho_2(x) = \int_0^\infty \mathrm{d}t\,[Q_t(x) - Q_s(x)]$. We proceed integrating the first component of (17) between one boundary of the support, say x_-, and x with the result

$$G(x) = \int_{x_-}^{x} \mathrm{d}y\,(P_s - P_0) = -f(x)\,\varrho_1(x) - g(x)\,\varrho_2(x). \tag{18}$$

In (18) we have imposed that the probability flux

$$J_t(x) = f(x)P_t(x) + g(x)Q_t(x) \tag{19}$$

vanishes at the boundaries $x_B = x_\pm$. Eq. (19) can be used to eliminate $\varrho_2(x)$ in the second component of (17). We further impose that in the stationary state the probability flux vanishes everywhere, $J_s(x) \equiv 0$, and that there are no initial correlations $Q_0(x) \equiv 0$. Thus we obtain a closed first order equation for $\varrho_1(x)$,

$$2\alpha f\cdot g^{-1}\varrho_1 + \partial_x(F_+ F_- g^{-1}\cdot\varrho_1) = -H(x), \tag{20}$$

where $H = 2\alpha G/g + \partial_x(Gf/g) + P_s f/g$. Eq. (20) is readily solved up to quadratures as

$$\varrho_1(x) = P_s(x)\left[\int_{x_-}^{x} \mathrm{d}y\,H(y)/E(y) - \int_{x_-}^{x_+} \mathrm{d}z\,P_s(z)\int_{x_-}^{z} \mathrm{d}y\,H(y)/E(y)\right], \tag{21}$$

the integration constant was determined by the normalization condition $\int_{\mathrm{supp}} \mathrm{d}x\,\varrho_1(x) = 0$. Note, that the stationary probability density [35]

$$P_s(x) = N\frac{-g}{F_+F_-}\exp\left(-2\alpha\int_{x_-}^{x}\mathrm{d}y\frac{f}{F_+F_-}\right) = \frac{-g}{F_+F_-}E(x) \tag{22}$$

solves the homogeneous part of (20) and that the normalization factor N cancels out in (21).

We finally write the NLRT as

$$T_{\mathrm{NLRT}}^{\phi} = \frac{1}{\langle\phi\rangle_0 - \langle\phi\rangle_s}\int_{x_-}^{x_+}\mathrm{d}x(\phi(x) - \langle\phi\rangle_s) \cdot P_s(x)\int_{x_-}^{x}\mathrm{d}y\,H(y)/E(y). \tag{23}$$

In the limit of the Gaussian white noise the result [23] is reproduced.

Similar to the MFPT, the integrals in (23) can be evaluated in terms of generalized hypergeometric functions of multiple arguments if ϕ and F are polynomial in x.

The choice $\phi(x) = f(x)/g(x)$ makes the integrals in (23) especially simple. For the Stratonovich model we investigate therefore the relaxation of the second moments $\langle x^2\rangle_t$ to the stationary value $\langle x^2\rangle_s = a$ from the initial value $x_0^2 = x_{\min}^2$ in the parameter region considered above.

After some algebra we obtain

$$T^{x^2}_{\mathrm{NLRT}} = \frac{1}{x_0^2 - a}\left[\ln x_0 - \int_{x_-}^{x_+} \mathrm{d}x\, P_s(x) \ln x\right]. \tag{24}$$

The evaluation of the integral yields

$$\int_{x_-}^{x_+} \mathrm{d}x\, P_s(x) \ln x = \ln x_- + \frac{a\, x_-^{2\lambda_+}\, (2\Delta)^{1-2\lambda_-}}{x_+^{2(\lambda_+ + 1)} \cdot B(\lambda_+, \lambda_-)}$$

$$\cdot \sum_{l,m,n=0}^{\infty} \frac{(\lambda_+ + \lambda_-)_m \cdot (1-\lambda_-)_n}{(\lambda_+ + l + m + n + 1) \cdot (\lambda_+ + m + n)\, m!\, n!} \tag{25}$$

$$\cdot z_1 (x_-)^{l+m}.$$

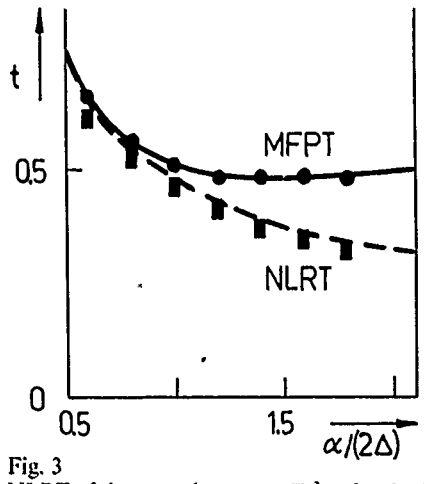


Fig. 3
NLRT of the second moment $T^{x^2}_{\mathrm{NLRT}}$ for the Stratonovich model to reach the stationary value a starting from $x_{\min}$ for $a = 1.5$, $\Delta = 1$ (broken line) against the noise parameters $\alpha/(2\Delta)$. We compare the NLRT with MFPT $T_{\mathrm{MFPT}} = (T_+ + T_-)/2$ to reach first the value $a^{1/2}$ starting from $x_{\min}$ (solid line). The results of a digital simulation from $10^3 - 10^5$ realizations are indicated by the full rectangles and full circles, repectively

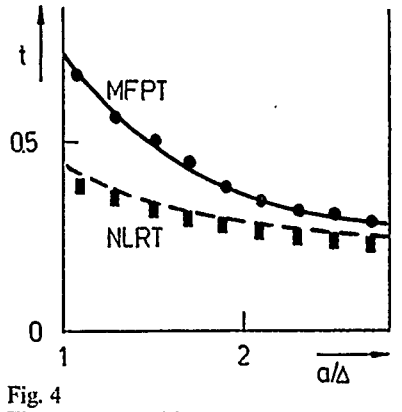


Fig. 4
The same quantities as in Fig. 3 against the control parameter a for $\alpha = 3.6$, $\Delta = 1$

In Figs. 3 and 4 we compare the NLRT given by (24) with the MFPT to reach $x_E = a^{1/2}$ starting from $x_0 = x_{\min}$. The analytic results for both NLRT and MFPT are checked by a digital simulation.

Both characteristic times have the same order of magnitude, and show a similar behaviour in dependence on system's and noise parameters. For slow processes MFPT and NLRT come very close, the difference enlarges however if the driving process becomes faster and the control parameter reaches the critical point.

A more detailed derivation and thorough discussion will be published elsewhere [36].

Valuable discussions with Peter Hänggi, Frank Moss, and Peter Jung are gratefully acknowledged.

References

[1] F. Moss and P. V. E. McClintock, Noise in Nonlinear Dynamical Systems, Cambridge University Press, Cambridge 1989.
[2] R. L. Stratonovich, Topics in the Theory of Random Noise, Vols. 1 and 2, Gordon and Breach, New York 1963 and 1967.
[3] A. Teubel, U. Behn, and A. Kühnel, Z. Phys. *B71*, 393 (1987).
[4] P. Hänggi, Phys. Rev. *A26*, 2996 (1982).
[5] P. Hänggi and Ph. Talkner, Phys. Rev. Lett. *51*, 2242 (1983).
[6] P. Hänggi and P. Riseborough, Phys. Rev. *A27*, 3379 (1983).
[7] C. van den Broeck and P. Hänggi, Phys. Rev. *A30*, 2730 (1984).
[8] P. Hänggi and P. Talkner, Phys. Rev. *A32*, 1934 (1985).
[9] J. M. Sancho, Phys. Rev. *A31*, 3523 (1985).
[10] F. Sagues, Physica *A132*, 489 (1985).
[11] M. A. Rodriguez and L. Pesquera, Phys. Rev. *A34*, 4532 (1986).
[12] K. Schiele and U. Behn, Wiss. Z. KMU Leipzig, Math.-Nat. R. *36*, 409 (1987).
[13] V. Balakrishnan, C. van den Broeck, and P. Hänggi, Phys. Rev. *A38*, 4213 (1988).
[14] U. Behn and K. Schiele, Z. Phys. *B77*, 485 (1989).
[15] J. Masoliver, K. Lindenberg, and B. J. West, Phys. Rev. *A33*, 2177 (1986); ibid *34*, 1481 (1986); ibid *34*, 2351 (1986).
[16] J. Masoliver, K. Lindenberg, and B. J. West, in Transport and relaxation in random materials, ed. by J. Klafter, R. Rubin, and M. F. Shlesinger, World Scientific, Singapore 1987.
[17] C. R. Doering, Phys. Rev. *A35*, 3166 (1987).
[18] G. H. Weiss, J. Masoliver, K. Lindenberg, and B. J. West, Phys. Rev. *A36*, 1435 (1987).
[19] G. P. Tsironis and C. van den Broeck, Phys. Rev. *A38*, 4362 (1988); K. Lindenberg, B. J. West, and J. Masoliver, in Noise in Nonlinear Dynamical Systems, ed. by F. Moss and P. V. E. McClintock, Cambridge University Press, Cambridge 1989.
[20] P. Jung and H. Risken, Z. Phys. *B59*, 469 (1985).
[21] J. Casademunt, and J. M. Sancho, Phys. Lett. *A123*, 271 (1987).
[22] J. Casademunt and J. M. Sancho, J. Stat. Phys. *56*, 911 (1989).
[23] J. I. Jimenez-Aquino, J. Casademunt, and J. M. Sancho, Phys. Lett. *A133*, A, 3641 (1988).
[24] J. Casademunt and J. M. Sancho, Phys. Rev. *A39*, 4915 (1989).
[25] J. Casademunt, J. I. Jimenez-Aquino, and J. M. Sancho, Physica *A156*, 628 (1989).
[26] J. Casademunt, J. I. Jimenez-Aquino, and J. M. Sancho, Phys. Rev. *A40*, 5905 (1989).
[27] J. Casademunt, J. I. Jimenez-Aquino, J. M. Sancho, C. J. Lambert, R. Manella, P. Martano, P. V. E. McClintock, and N. G. Stocks, Phys. Rev. *A40*, 5915 (1989).
[28] R. Manella, C. J. Lambert, N. G. Stocks, and P. V. E. McClintock, Phys. Rev. *A41*, 3016 (1990).

[29] M. James, F. Moss, P. Hänggi, and C. van den Broeck, Phys. Rev. *A38*, 4690 (1989); J. M. Sancho and M. San Miguel, Phys. Rev. *A39*, 2722 (1989).
[30] P. Hänggi, F. Marchesoni, and P. Grigolini, Z. Phys. *B56*, 333 (1984).
[31] H. A. Kramers, Physica *7*, 284 (1940).
[32] P. Hänggi, P. Talkner, and M. Borkovec, Rev. Mod. Phys. *62*, 251 (1990).
[33] K. Wodkiewicz, B. W. Shore, and J. H. Eberly, J. Opt. Soc. Am. *B1*, 398 (1984).
[34] K. Binder, Phys. Rev. *B8*, 3423 (1973).
[35] The stationary probability density for general dichotomous flows has been obtained first by Klyatskin, Radiophys. Quantum Electr. *20*, 382 (1977). For a more complete list of references see [3].
[36] R. Müller, U. Behn, and K. Schiele, in preparation.

Presented at the Discussion Meeting of the Deutsche Bunsen-Gesellschaft für Physikalische Chemie "Rate Processes in Dissipative Systems: 50 Years after Kramers" in Tutzing, September 10–13, 1990 E 7504

First Passage Times and Transport in Systems with Disorder

C. Van den Broeck*)

Department of Chemistry, B-040, University of California at San Diego, La Jolla, CA 92093

V. Balakrishnan

Department of Physics, Indian Institute of Technology, Madras 600036, India

Diffusion / Statistical Mechanics / Transport Properties

We illustrate how first passage times can be calculated in systems with disorder. We use a renormalization approach to discuss first passage times in one-dimensional continuous time random walks and on deterministic fractals. We discuss the phenomenon of field-induced trapping on a random comb. Finally, we calculate mean first-passage times for one-dimensional random random walks, and discuss, in particular, the case of Sinai disorder. In a short Appendix, we show how mean first-passage times can be calculated for an arbitrary inhomogeneous continuous time random walk in one dimension, using a recursion relation similar in spirit to the renormalization approach.

1. Introduction

We are celebrating the 50th anniversary of Kramers' seminal paper [1] on thermal escape over a potential barrier. As is indicated by the vast literature on the subject, there has been a great deal of effort in trying to improve and generalize the results of Kramers [2]. One of the challenges has been to obtain results for thermal escape in higher-dimensional systems. Another challenge, the one that we will address here, is to study transport and escape phenomena in systems with disorder. The paper by Kramers is known, among physicists, mainly in relation to the result for the transition rate in a bistable system in the high-friction or Smoluchowski limit. This result, however, was anticipated by earlier results on first passage time in a one-dimensional diffusion process (and by the "flux-over-population" calculation for the transition rate) [2]. There has also been a lot of progress in the calculation of first passage time properties, especially in one-dimensional systems [3]. Here we will briefly review how first passage time densities and their moments can be calculated in an elegant way, using renormalization procedures, and how these results can be applied to study transport properties in systems with disorder [4].

We will discuss four types of models that have been introduced to study the properties of systems with disorder. One of the simplest approaches is based on a description in terms of a continuous time random walk on a regular lattice with an effective waiting time density that captures the essential features of the disorder. This approach was adopted with success by Montroll and Scher [5] in their paper on anomalous transport in amorphous semiconductors. In Sections 2 of this paper, we will illustrate how first passage time densities can be obtained for biased random walks on the line, using the above mentioned renormalization procedure.

Systems with disorder lack translational invariance. In many cases, however, it is found that they are characterized by scale invariance. This suggests that the study of transport on simple scale invariant structures, such as deterministic fractals, is relevant to the understanding of transport in systems with disorder. In Section 3, we illustrate how the renormalization approach, applied to continuous time random walks in one dimension, can also be formulated for deterministic fractals.

A third way to model disorder is to consider a simplified random model, which hopefully displays transport properties similar to that of the physical system. An example is the random comb, which is discussed in Section 4. This model is of interest because it displays a transition between field-induced convection to field-induced trapping.

Finally, in Section 5, we calculate the mean first passage time in a so-called random random walk (in one dimension). We discuss in particular the case of Sinai disorder, which corresponds to the case of a random walk with symmetric disorder.

*) Permanent address: LUC, B-3610 Diepenbeek, Belgium.

 © VCH Verlagsgesellschaft mbH, W-6940 Weinheim, 1991 0005-9021/91/0303-0342 $ 3.50+.25/0

A typical feature of all these models is that disorder can give rise to anomalous transport. By this, one usually means that the dispersive motion is subdiffusive (cf. Sections 2 and 3), or that the convective motion is sub-ballistic (in the presence of a field, cf. Section 4). In the context of Kramers escape, the density of escape times may be non-exponential (cf. Section 5 for an example).

2. Renormalization of Biased Continuous Time Random Walks

We consider a continuous time, nearest-neighbour random walk on the set of natural numbers $i = 0,1,2,\ldots$. The walk is characterized by the waiting time densities $\psi_+^{(0)}(\tau)$ and $\psi_-^{(0)}(\tau)$ for the walker at any site $i > 0$ to step to the sites $i+1$ and $i-1$ respectively, after a residence time at i equal to τ. The waiting time density for the walker, located at the origin, to step to site $+1$ after a total time τ is denoted $\psi_*^{(0)}(\tau)$. For simplicity, we will assume that these are also the waiting time densities for the occurrence of the first jump, which is the appropriate choice for a so-called ordinary renewal process.

Since

$$p^{(0)} = \int_0^\infty \psi_+^{(0)}(\tau)\,d\tau, \quad q^{(0)} = \int_0^\infty \psi_-^{(0)}(\tau)\,d\tau \tag{2.1}$$

are the probabilities for stepping to the right or left at any site $i > 0 (p^{(0)} + q^{(0)} = 1)$, we see that the case $q^{(0)} > p^{(0)}$ corresponds to the situation of a particle trapped at the origin by a bias field equal to $q^{(0)} - p^{(0)}$. Our purpose is to calculate the probability density for the escape time from this trap by using a renormalization procedure. Apart from giving a new and elegant solution to this problem, the renormalization procedure has also the advantage that it can be applied to deterministic fractals (cf. Section 3).

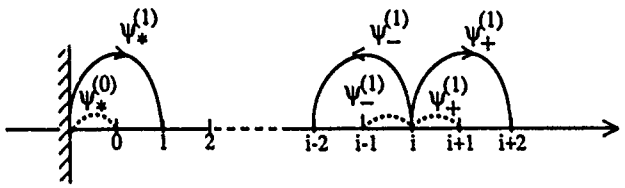


Fig. 1
Renormalization of a biased continuous time random walk in one dimension, with a reflecting boundary at the origin

The procedure is as follows (see Fig. 1). Starting from site 1, we decimate every other site on the lattice. The decimated lattice has the same structure as the original one, but the renormalized waiting time density, e.g. $\psi_+^{(1)}(\tau)$, gives the probability density for the waiting time to go from a site (say i) to the appropriate next nearest neighbour $(i+2)$. This transition can be realized by an arbitrary number of excursions to the nearest neighbours, $i+1$ or $i-1$, and returns to i, followed by the final excursion to the next nearest neighbour $i+2$. Moreover, the partial times spent in these various excursions have to add up to τ. In terms of Laplace transforms, a convolution becomes a product, and we get the following simple result:

$$\tilde\psi_-^{(1)}(s) = [\tilde\psi_+^{(0)}(s)]^2 + 2\tilde\psi_+^{(0)}(s)\tilde\psi_-^{(0)}(s)[\tilde\psi_+^{(0)}(s)]^2 + [2\tilde\psi_+^{(0)}(s)\tilde\psi_-^{(0)}(s)]^2[\tilde\psi_+^{(0)}(s)]^2 + \ldots \tag{2.2}$$

or

$$\tilde\psi_+^{(1)}(s) = \frac{[\tilde\psi_+^{(0)}(s)]^2}{1-2\tilde\psi_+^{(0)}(s)\,\tilde\psi_-^{(0)}(s)}. \tag{2.3}$$

Here, the superscript $\sim$ denotes the Laplace transformed function,

$$\tilde f(s) = \int_0^\infty e^{-st} f(t)\,dt. \tag{2.4}$$

Since the decimated lattice has a structure identical to the original lattice, the renormalization equation will have a form identical to the one above, at any stage of the decimation. Similar equations are easily derived for the other two waiting time densities, and we find (dropping for brevity, the s-dependence):

$$\tilde\psi_+^{(n)} = \frac{[\tilde\psi_+^{(n-1)}]^2}{1-2\tilde\psi_+^{(n-1)}\,\tilde\psi_-^{(n-1)}} \tag{2.5a}$$

$$\tilde\psi_-^{(n)} = \frac{[\tilde\psi_-^{(n-1)}]^2}{1-2\tilde\psi_+^{(n-1)}\,\tilde\psi_-^{(n-1)}} \tag{2.5b}$$

$$\tilde\psi_*^{(n)} = \frac{\tilde\psi_+^{(n-1)}\,\tilde\psi_*^{(n-1)}}{1-\tilde\psi_-^{(n-1)}\,\tilde\psi_*^{(n-1)}}. \tag{2.5c}$$

Before we give the solution to these recursion relations, we make a few comments. First, the waiting time densities $\psi_+^{(n)}$ and $\psi_-^{(n)}$ are, in fact, the first passage time densities to the sites at a distance $+2^n$ and -2^n of the considered site on the original lattice (assuming, of course, that the initial site i is situated sufficiently far from the boundary at 0, i.e., assuming that $i > 2^n$). $\psi_*^{(n)}$ is the first passage time or escape time density from site 0 to the site at the position 2^n on the original lattice. Second, normalization implies that $\tilde\psi_+^{(0)}(0) + \tilde\psi_-^{(0)}(0) = 1$ and $\tilde\psi_*^{(0)}(0) = 1$. This normalization property is preserved under renormalization. Finally, a remarkable feature of the renormalization equations is that the s-dependence of the functions $\tilde\psi$ plays no role in the solution of these recursion relations.

To solve the renormalization Eqs. (2.5) we first notice that Eqs. (2.5a) and (2.5b) are closed in $\tilde\psi_+$ and $\tilde\psi_-$, and can be rewritten in the following convenient form:

$$\frac{\tilde\psi_+^{(n)}}{\tilde\psi_-^{(n)}} = \left[\frac{\tilde\psi_+^{(n-1)}}{\tilde\psi_-^{(n-1)}}\right]^2 \tag{2.6a}$$

and

$$\frac{1}{\sqrt{4\tilde{\psi}_+^{(n)}\tilde{\psi}_-^{(n)}}} = 2\left[\frac{1}{\sqrt{4\tilde{\psi}_+^{(n-1)}\tilde{\psi}_-^{(n-1)}}}\right]^2 - 1 = T_2\left(\frac{1}{\sqrt{4\tilde{\psi}_+^{(n-1)}\tilde{\psi}_-^{(n-1)}}}\right) \tag{2.6b}$$

where $T_2(z) = 2z^2 - 1$, is the Chebyshev polynomial of order 2.

The solution of Eq. (2.6a) is obvious:

$$\frac{\tilde{\psi}_+^{(n)}}{\tilde{\psi}_-^{(n)}} = \left[\frac{\tilde{\psi}_+^{(0)}}{\tilde{\psi}_-^{(0)}}\right]^{2^n} \tag{2.7}$$

On the other hand, Eq. (2.6b) is, in fact, identical to the logistic map at fully developed chaos. Its solution goes back to Von Neumann and Ulam. This solution is easily obtained using the following definition and property of the Chebyshev polynomials:

$$T_n(z) = \cosh(n\cosh^{-1}z) \tag{2.8}$$

$$T_n(T_m(z)) = T_{nm}(z)\,. \tag{2.9}$$

Hence

$$\frac{1}{\sqrt{4\tilde{\psi}_+^{(n)}\tilde{\psi}_-^{(n)}}} = T_{2^n}\left(\frac{1}{\sqrt{4\tilde{\psi}_+^{(0)}\tilde{\psi}_-^{(0)}}}\right) = \cosh\left(2^n\cosh^{-1}\frac{1}{\sqrt{4\tilde{\psi}_+^{(0)}\tilde{\psi}_-^{(0)}}}\right) \tag{2.10}$$

where $\cosh^{-1}$ denotes the inverse hyperbolic cosine. Combining Eqs. (2.7) and (2.10), we conclude that

$$\tilde{\psi}_+^{(n)} = \frac{[\sqrt{\tilde{\psi}_+^{(0)}/\tilde{\psi}_-^{(0)}}]^{2^n}}{2\cosh(2^n\xi)} \tag{2.11a}$$

and

$$\tilde{\psi}_-^{(n)} = \frac{[\sqrt{\tilde{\psi}_-^{(0)}/\tilde{\psi}_+^{(0)}}]^{2^n}}{2\cosh(2^n\xi)} \tag{2.11b}$$

where ξ is defined by

$$\cosh\xi = 1/\sqrt{4\tilde{\psi}_+^{(0)}\tilde{\psi}_-^{(0)}}\,. \tag{2.11c}$$

For the case of a Markovian walk with jump rate k, namely,

$$\tilde{\psi}_+^{(0)}(s) = p^{(0)}\frac{k}{k+s} \tag{2.12a}$$

$$\tilde{\psi}_-^{(0)}(s) = q^{(0)}\frac{k}{k+s} \tag{2.12b}$$

one finds:

$$\tilde{\psi}_+^{(n)}(s) = \left(\sqrt{\frac{p^{(0)}}{q^{(0)}}}\right)^{2^n}\frac{1}{2\cosh(2^n\xi)} \tag{2.13a}$$

$$\tilde{\psi}_-^{(n)}(s) = \left(\sqrt{\frac{q^{(0)}}{p^{(0)}}}\right)^{2^n}\frac{1}{2\cosh(2^n\xi)} \tag{2.13b}$$

with

$$\cosh\xi = \frac{k+s}{2k\sqrt{p^{(0)}q^{(0)}}}\,. \tag{2.13c}$$

These results can also be obtained using the known results for the Green function of a biased random walk [6, 7], and the renewal equation (with appropriate boundary conditions) linking the above first passage time densities to this Green function.

Let us now turn to the solution of Eq. (2.5c). This equation is linear in $1/\tilde{\psi}_*$ and can be rewritten as follows:

$$\gamma_n\frac{1}{\tilde{\psi}_-^{(n)}\tilde{\psi}_*^{(n)}} = \frac{1}{\tilde{\psi}_-^{(n-1)}\tilde{\psi}_*^{(n-1)}} - 1 \tag{2.14}$$

where γ_n is given by (cf. Eqs. (2.11)):

$$\gamma_n = \frac{\tilde{\psi}_-^{(n)}\tilde{\psi}_+^{(n-1)}}{\tilde{\psi}_-^{(n-1)}} = \frac{1}{2\cosh(2^n\xi)}\,. \tag{2.15}$$

Eq. (2.14) can easily be solved recursively, and one obtains:

$$\gamma_1\gamma_2\cdots\gamma_n\frac{1}{\tilde{\psi}_-^{(n)}\tilde{\psi}_*^{(n)}} = \frac{1}{\tilde{\psi}_-^{(0)}\tilde{\psi}_*^{(0)}} - (1+\gamma_1+\gamma_1\gamma_2+\ldots+\gamma_1\gamma_2\cdots\gamma_{n-1})\,. \tag{2.16}$$

From the identity

$$\sinh(2\xi) = 2\sinh\xi\cosh\xi \tag{2.17}$$

it follows that

$$\frac{1}{\gamma_1\gamma_2\cdots\gamma_n} = \prod_{i=1}^{n}2\cosh(2^i\xi) = \frac{\sinh(2^{n+1}\xi)}{\sinh(2\xi)}\,. \tag{2.18}$$

On the other, the identity

$$\coth(2\xi) = \coth\xi - \frac{1}{\sinh(2\xi)} \tag{2.19}$$

yields

$$1+\gamma_1+\gamma_1\gamma_2+\ldots+\gamma_1\ldots\gamma_{n-1} = \sinh(2\xi)\sum_{i=1}^{n}\frac{1}{\sinh(2^i\xi)} = [\coth\xi - \coth(2^n\xi)]\sinh(2\xi)\,. \tag{2.20}$$

Hence

$$\tilde{\psi}_{*}^{(n)} = \frac{(\sqrt{\tilde{\psi}_{+}^{(0)}/\tilde{\psi}_{-}^{(0)}})^{2^n}}{\sinh(2^n\xi)\left[\dfrac{1}{\tilde{\psi}_{-}^{(0)}\tilde{\psi}_{*}^{(0)}\sinh(2\xi)} + \coth(2^n\xi) - \coth\xi\right]} \tag{2.21}$$

where ξ has been defined in Eq. (2.11c). The results (2.11) and (2.21) are the exact solutions of the renormalization Eqs. (2.5), for general "initial conditions" $\tilde{\psi}_{+}^{(0)}$, $\tilde{\psi}_{-}^{(0)}$ and $\tilde{\psi}_{*}^{(0)}$. In case of Markovian dynamics (cf. Eqs. (2.12)), with

$$\tilde{\psi}_{*}^{(0)} = \frac{kp^{(0)}}{kp^{(0)}+s}. \tag{2.22}$$

Eq. (2.21) reduces to

$$\tilde{\psi}_{*}^{(n)} = \frac{(\sqrt{p^{(0)}/q^{(0)}})^{2^n}\sinh\xi}{\sinh(2^n+1)\,\xi - \sqrt{q^{(0)}/p^{(0)}}\sinh 2^n\xi} \tag{2.23}$$

again a result which can be obtained from the renewal equation linking the first passage time $\tilde{\psi}_{*}^{(n)}$ to the known Green function of a random walk with a reflecting boundary condition at the origin [6, 7].

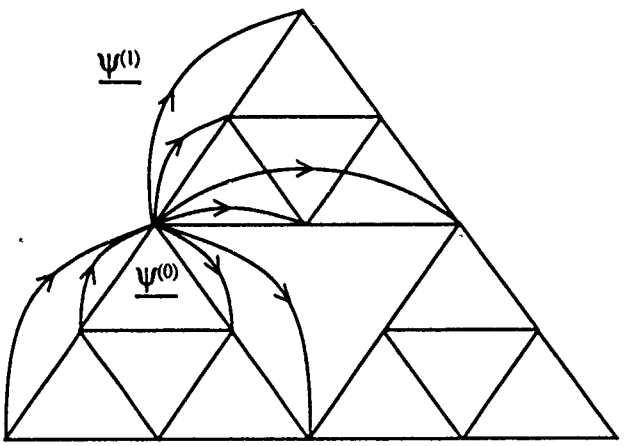


Fig. 2
Renormalization of a continuous time random walk on a Sierpinski gasket

3. Random Walks on Deterministic Fractals

The renomalization procedure that we have discussed in the preceding section can also be applied to simple deterministic fractals, such as the Sierpinski gasket (cf. Fig. 2). At each stage of the decimation, the smallest triangles are removed, and the first passage time density to the four new nearest neighbours is calculated. The renormalization equation has the following form (compare with Eqs. (2.5)) [8], see also [9]:

$$\tilde{\psi}^{(n)} = \frac{[\tilde{\psi}^{(n-1)}]^2}{4-3\tilde{\psi}^{(n-1)}}. \tag{3.1}$$

Note again that this equation preserves the normalization ($\tilde{\psi}^{(n-1)}(s=0) = 1$ implies that $\tilde{\psi}^{(n)}(s=0) = 1$). The mean first passage time $\langle\tau^{(n)}\rangle$ to reach one of the four nearest neighbours on the n-times decimated lattice is given by:

$$\langle\tau^{(n)}\rangle = -\left.\frac{d\tilde{\psi}^{(n)}}{ds}\right|_{s=0}. \tag{3.2}$$

Eq. (3.1) then implies the following simple recursion relation:

$$\langle\tau^{(n)}\rangle = 5\langle\tau^{(n-1)}\rangle. \tag{3.3}$$

Hence it takes (on the average) five times as long to go twice as far (since the distance under consideration doubles after each decimation). This is in agreement with the well-known subdiffusive behavior on this fractal. Higher order moments can be obtained recursively by calculating successively higher order derivatives of both sides of Eq. (3.1). It is, however, possible to write the explicit solution of Eq. (3.1), by introducing the analytic function $f(x)$ that is a solution of the following nonlinear scaling equation [8]:

$$4f^2(x) - 3f(x) = f(5x),\ f(0) = f'(0) = 1. \tag{3.4}$$

One can show that such a solution exists and that it is unique. The solution of Eq. (3.1) can then be written as (compare with Eq. (2.10)):

$$1/\tilde{\psi}^{(n)}(s) = f[5^n f^{-1}(1/\tilde{\psi}^{(0)}(s))] \tag{3.5}$$

where f^{-1} is the inverse function of f. A number of properties of f can be derived from Eq. (3.4). Moreover, it represents the solution to the quadratic map $x_n = 4x_{n-1}^2 - 3x_{n-1}$ (obtained from Eq. (3.1) by setting $x_n = 1/\tilde{\psi}^{(n)}$), and is therefore related to the study of (transient) chaos in such discrete maps [8, 10].

4. Escape and Field-Induced Trapping on a Random Comb

An interesting feature of an external bias on a system with disorder is that it can have a dual effect: on the hand, it induces a drift in the direction of the field; on the other hand, it can create traps, if the network possesses dead-end branches. To participate in the convection, particles have to escape from these dead-ends. This becomes increasingly difficult as the amplitude of the field increases. The question arises as to whether there exists a threshold value of the field, above which the drift velocity vanishes.

A model for which this question can be investigated in full detail is the random comb (see Fig. 3) [11]. A particle performs a random walk on an infinitely long linear lattice (the backbone) with branches of random length emanating at random from the sites of the backbone. We define the following probabilities (see Fig. 3): q is the probability to make a step in the "backward" direction, while p and $p - p_1$ respectively, are the probabilities for a "forward" step on the backbone at a non-vertex point (i.e., no side branches), and at a vertex point. In the last case p_1 is the probability

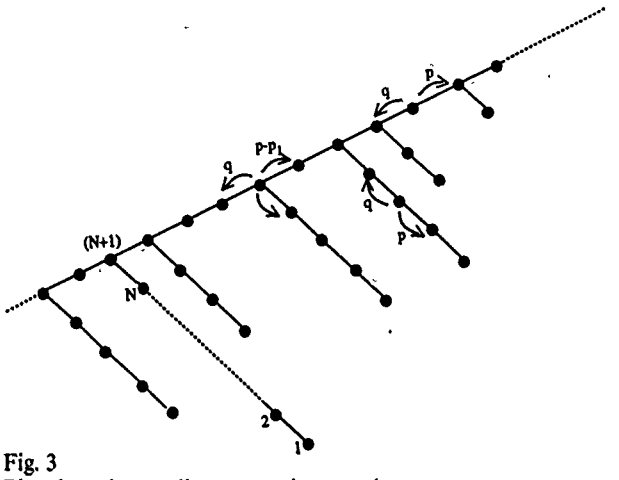


Fig. 3
Biased random walk on a random comb

to move into the side branch. σ_N is the probability that a side branch has a length $N(N=1,2,\ldots)$, and

$$\sigma = \sum_{N=1}^{\infty} \sigma_N \tag{4.1}$$

is the probability that a site is a vertex. An explicit mean field calculation [11] leads to the following value of the drift velocity along the backbone (for $p \neq q$, and choosing the unit of time to be equal to the mean waiting time between jumps):

$$\lim_{t\to\infty} \frac{\langle m(t)\rangle}{t} = v_d = \frac{p-q}{1+\dfrac{p_1}{(1-p_1)(p-q)}\left(\displaystyle\sum_{N=1}^{\infty}\sigma_N(p/q)^N - 2q\sigma\right)}. \tag{4..2}$$

Note that v_d will vanish in the limit of a symmetric walk $p\to q$, as expected, but also in the case when

$$\sum_{N=1}^{\infty} \sigma_N (p/q)^N \tag{4.3}$$

diverges. An interesting situation displaying a non-trivial "critical" behaviour is that of an exponential probability distribution for the branch length $N(N=1,2,\ldots)$:

$$\sigma_N = \sigma \exp(-\varepsilon N)\,(e^{\varepsilon}-1) \quad (\varepsilon > 0)\,. \tag{4.4}$$

Such a distribution has the form of a Boltzmann factor with ε representing the "cost" in energy per site. (If the branches are imagined to represent – albeit crudely – finite clusters attached to the backbone, such an exponential distribution of cluster sizes is not unrealistic, with ε^{-1} standing for the cluster size lengthscale). For this model, a finite drift velocity is obtained for values $1/2 < p < p_c$, with the critical value p_c given by

$$e^{-\varepsilon}\frac{p_c}{1-p_c} = 1\,, \quad \text{or} \quad p_c = \frac{1}{1+e^{-\varepsilon}}. \tag{4.5}$$

As ε, the energy cost per site in the side branches, increases from 0 to ∞, p_c goes from 1/2 to 1. We note that v_d goes to zero linearly with $(p_c - p)$ in the vicinity of p_c:

$$v_d \sim (p_c - p)\frac{(2p_c-1)(1-p_1)}{\sigma p_1 p_c}. \tag{4.6}$$

Beyond p_c, it can be shown that sub-convective behaviour sets in, with [11]

$$\langle m(t)\rangle \sim t^{\varepsilon/\ln\frac{p}{1-p}} \quad p > p_c > \frac{1}{2}. \tag{4.7}$$

5. Random Random Walks

Consider a random walk on the set of integers, such that a walker can move to the left or right at each site $i \in Z$ with transition rates equal to k_i^- and k_i^+ respectively. Furthermore, suppose these rates are themselves random variables, identically distributed but independent from site to site, while the rates at the same site are possibly correlated. To obtain some insight into the transport properties of such a random random walk, we investigate the analogue of the problem discussed in Section 2. A particle starts at the origin of a semi-infinite lattice with disorder (of the kind just described). How long will it take to escape to a certain distance i from the origin? To calculate this time, we will use the following exact result for the moments $T_n = \langle \tau^n \rangle$ of the first passage time τ to go from a site i_0 to i (where $i > i_0$) in a nearest neighbour random walk with general transition rates [7]

$$T_n(i|i_0) = n\sum_{r=i_0}^{i-1}\sum_{s=-\infty}^{n}\frac{T_{n-1}(i|s)\,P(s)}{k_r^+\,P(r)}. \tag{5.1}$$

Here $T_0 \equiv 0$, and the lattice extends to $-\infty$. $P(s)$ is the steady-state probability distribution for the same random walk with a reflecting boundary condition at $s=i$ (i.e. $k_{i-1}^+ = 0$), namely,

$$P(s) = \frac{k_{s+1}^-}{k_s^+}\,\frac{k_{s+2}^-}{k_{s+1}^+}\cdots\frac{k_{i-1}^-}{k_{i-2}^+}\,P(i-1). \tag{5.2}$$

$P(i-1)$ can be found from the normalization condition (we are assuming that this normalization factor is finite, i.e. that $P(s)$ exists). In particular, the mean first passage time $T_1(i|0)$ to go from zero to i, when there is a reflecting boundary at the left of zero, may be obtained from the foregoing general result by setting $k_0^- = 0$ and $P(0) = 0$. We get

$$T_1(i|0) = \sum_{r=0}^{i-1}\left[\frac{1}{k_r^+} + \sum_{s=0}^{r-1}\frac{k_{s+1}^-\cdots k_{r-1}^- k_r^-}{k_s^+ k_{s+1}^+\cdots k_{r-1}^+ k_r^+}\right]. \tag{5.3}$$

In the Appendix, we show how this result can be derived in a simple way using ideas similar to those of the renormalization procedure discussed above. The rates at a given site are possibly correlated, but those at different sites are not.

The average over the disorder can thus easily be carried out, and one finds [7], see also [12]:

$$\overline{T_i(i|0)} = \frac{1}{(1-g)^2}\overline{\left(\frac{1}{k^+}\right)}[g^i - 1 + i(1-g)] \tag{5.4}$$

where we have defined

$$g = \overline{\left(\frac{k^-}{k^+}\right)}. \tag{5.5}$$

We emphasize that two kinds of averages are involved, an average over the statistics of the random walk (T_i is the mean first passage time for a given realization of the quenched disorder), and one over the disorder (denoted by the overbar). The foregoing calculation also applies to the case of non-random constant rates k^+ and k^-, and the result is identical to Eqs. (5.4) and (5.5), with the overhead bars removed. In the calculation above, we have introduced a reflecting boundary at 0 to guarantee that a finite mean first passage time exists. In the case of a disordered system, with a mean bias pointing away from 0, i.e. $g < 1$, we expect that this boundary condition becomes irrelevant for the behavior of the first passage time in the limit $i \to \infty$. In this case, Eq. (5.4) reduces to

$$\overline{T_i(i|0)} = \frac{1}{1-g}\overline{\left(\frac{1}{k^+}\right)}i \tag{5.6}$$

which is identical to the result for an ordinary random walk with the drift velocity

$$v_d = \frac{1}{1-g}\overline{\left(\frac{1}{k^+}\right)}. \tag{5.7}$$

This straightforward calculation thus leads quite easily to the evaluation of the effective drift velocity of the random random walk. Eq. (5.7) is identical to the result obtained by Derrida [13] using a much more complicated procedure. In a similar way, the calculation of the second moment T_2 leads to the correct value of the effective diffusion coefficient [7]. One should, however, be careful in extrapolating results from configuration-averaged first passage time properties directly to actual transport properties of the disordered system. To illustrate the sort of problem that can arise, we discuss the case of so-called Sinai disorder [14].

A random random walk with Sinai disorder is characterized by the following additional properties:

$$\overline{\ln\left(\frac{k_i^+}{k_i^-}\right)} = 0 \qquad \overline{\ln^2\left(\frac{k_i^+}{k_i^-}\right)} < 0. \tag{5.8}$$

The first condition indicates that the disorder is "symmetric on the average", i.e. a bias to the left and to the right are equally probable at any site. The second condition puts a limit on the strength of the disorder. Under these conditions, Sinai [14] showed that while the position of a walker does not change on the average, its root mean square displacement grows extremely slowly with time, namely:

$$\overline{\langle i^2(t)\rangle} \sim \ln^4 t. \tag{5.9}$$

The result (5.9) can be easily understood as follows [15]. One can view the presence of a local bias $k_i^+ > k_i^-$ as a small increase of an effective potential in which the particle is moving. An opposite bias $k_i^+ < k_i^-$ corresponds to a decrease of the potential. Since the rates at different sites are independent, the potential U which one thus obtains in function of i is itself like a realization of an (uncorrelated) random walk (in the variable i); hence the amplitude of the fluctuations of the potential $\sqrt{\langle \Delta U^2\rangle}$ over a region of length i, will be typically of the order of $\sqrt{i}$. In order to cover such a distance, the particle has to overcome a barrier of typical height $\sqrt{\langle \Delta U^2\rangle}$, and the time needed to do so is:

$$\tau \sim e^{\sqrt{\langle \Delta U^2\rangle}} \sim e^{\sqrt{i}}. \tag{5.10}$$

This explains, heuristically, why the length scales as the square of the logarithm of the time in this problem. The foregoing behavior of τ is surprising, for the following reason. We have seen that the disorder-averaged mean first passage time must in fact be essentially the same as that of a particle trapped at the origin by a certain constant effective field biased towards the origin, in a random walk without any disorder. The latter mean first passage time has been found in Eq. (5.4). Now, using Jensen's inequality, we find that

$$\overline{\ln\frac{k^-}{k^+}} \le \ln\overline{\left(\frac{k^-}{k^+}\right)} = \ln g. \tag{5.11}$$

The Sinai condition (5.8) therefore implies that the effective bias is directed towards the origin ($g > 1$). For large distances i, one then gets (employing the standard Arrhenius form for the escape over a barrier)

$$\overline{T_i(i|0)} \sim e^{i\ln g}. \tag{5.12}$$

This is in sharp contrast to the results of the heuristic scaling arguments given above, cf. Eq. (5.10). This discrepancy was first noticed and explained by Noskowicz and Goldhirsch [16]. The explanation is in fact quite obvious: the average over the disorder in Eq. (5.12) is dominated by the configurations in which the effective potential, that the particle has to overcome, is of order i rather than the typical value $\sqrt{i}$. These configurations have an exponentially small probability; but the corresponding first passage times are exponentially large, and they dominate in the calculation of the average. Eq. (5.12), even though an exact result, is atypical for Sinai disorder and does not describe the typical first passage time dynamics that one observes in this case.

We acknowledge support from the N.F.W.O. Belgium and from the Program on Inter University Attraction Poles of the Belgian

Government. C.V.d.B. also acknowledges support from U.S. Department of Energy Grant No. DEFG03-86ER 13606.

Appendix.
First Passage Times for Inhomogeneous Continuous-Time Random Walks in One Dimension

We consider a continuous-time random walk on the set of integers, characterized by the site-dependent waiting time densities $\tilde{\psi}_i^+(\tau)$ and $\tilde{\psi}_i^-(\tau)$ to jump from i to $i+1$ and $i-1$ respectively at time τ (without first jumping to the other neighbour). To calculate first passage times on this lattice, we first consider the first passage time to go from i to $i+1$ (involving any type of excursion to the left of i). Clearly such a first passage can be realized by n jumps to $i-1$ (where $n = 0,1,2,\ldots$), each followed by a first passage back from $i-1$ to i, and a final jump from i to $i+1$. Hence, one obtains the following exact recursion relation for the Laplace transform of the first passage time density $F_i^+(t)$ to go from i to $i+1$:

$$\tilde{F}_i^+(s) = \frac{\tilde{\psi}_i^+(s)}{1-\tilde{\psi}_i^-(s)\,\tilde{F}_{i-1}^+(s)}. \tag{A.1}$$

By setting $s=0$ in this equation one gets the following recursion relation for the probability P_i^+ for a first passage to take place (at any time) from i to $i+1$:

$$P_i^+ = \frac{p_i}{1-q_i P_{i-1}^+}, \tag{A.2}$$

Here $p_i = \tilde{\psi}_i^+(0)$ and $q_i = \tilde{\psi}_i^-(0)$, and we have of course $p_i + q_i = 1$. Note that $P_i^+ \equiv 1$ is a fixed point of this equation. We will assume that this is correct solution for the case under consideration, i.e., first passage occurs with certainty. By differentiating both sides of Eq. (A.1) with respect to s and setting $s=0$, we obtain the following recursion relation for the mean first passage time $T_1(i+1|i)$ to go from i to $i+1$:

$$T_1(i+1|i) = \frac{\langle\tau_i\rangle}{p_i} + \frac{q_i}{p_i}\,T_1(i|i-1) \tag{A.3}$$

where

$$\langle\tau_i\rangle = -\frac{\mathrm{d}}{\mathrm{d}s}\left[\tilde{\psi}_i^+ + \tilde{\psi}_i^-\right]_{s=0} \tag{A.4}$$

is the average residence time at site i. By iteration, one finds (provided the series converges)

$$T_1(i+1|i) = \frac{\langle\tau_i\rangle}{p_i} + \sum_{j=-\infty}^{i} \frac{q_i}{p_i}\cdots\frac{q_j}{p_j}\,\frac{\langle\tau_{j-1}\rangle}{p_{j-1}}. \tag{A.5}$$

Since

$$T_1(i+n|i) = T_1(i+1|i) + T_1(i+2|i+1) \ldots + T_1(i+n|i+n-1) \tag{A.6}$$

one has

$$T_1(m|m_0) = \sum_{r=m_0}^{m-1}\left[\frac{\langle\tau_r\rangle}{p_r} + \sum_{j=-\infty}^{r}\frac{q_r}{p_r}\cdots\frac{q_j}{p_j}\,\frac{\langle\tau_{j-1}\rangle}{p_{j-1}}\right]. \tag{A.7}$$

Note that the above derivation is independent of whether the time variable is a discrete or continuous variable, so that Eq. (A.7) also gives the mean first passage time for discrete time dynamics. For the case of a Markovian walk, with site-dependent jump rates k_j^+ and k_j^- for jumps from j to $j+1$ and $j-1$ respectively, one has

$$\frac{q_j}{p_j} = \frac{k_j^-}{k_j^+} \qquad \frac{\langle\tau_r\rangle}{p_r} = \frac{1}{k_r^+}. \tag{A.8}$$

We thus recover the familar result

$$T_1(m|m_0) = \sum_{r=m_0}^{m-1}\left[\frac{1}{k_r^+} + \sum_{j=-\infty}^{r}\frac{k_r^-}{k_r^+}\cdots\frac{k_j^-}{k_j^+\,k_{j-1}^+}\right] \tag{A.9}$$

in this instance.

References

[1] H. A. Kramers, Physica *7*, 284 (1940).

[2] P. Hanggi, P. Talkner, and M. Borkovec, Rev. Mod. Phys. *62*, 251 (1990).

[3] L. A. Pontryagin, A. Andronov, and A. Vitt, Teor. Fiz. *3*, 165 (1933), D. A. Darling and A. J. F. Siegert, Ann. Math. Stat. *24*, 624 (1953), B. Widom, J. Chem. Phys. *30*, 238; *31*, 1387 (1957), G. H. Weiss, Adv. Chem. Phys. *13*, 1 (1967), R. L. Stratonovich, Topics in the Theory of Random Noise I and II, Gordon and Breach, New York 1963; M. Kac, SIAM Rev. *4*, 1 (1962).

[4] S. Alexander, J. Bernasconi, W. R. Schneider, and R. Orbach, Rev. Mod. Phys. *53*, 175 (1981); J. W. Haus and K. W. Kehr, Phys. Rep. *150*, 263 (1987); J. P. Bouchaud and A. Georges, Paris Preyprint LPTENS 98/5 (August 1989), S. Havlin and D. Ben-Avraham, Adv. Phys. *36*, 695 (1987).

[5] H. Scher and Montroll, Phys. Rev. *B12*, 2455 (1975).

[6] V. Balakrishnan and M. Khantha, Pramana *21*, 187 (1983); M. Khantha and V. Balakrishnan, J. Stat. Phys. *41*, 811 (1985).

[7] C. Van den Broeck, *A Glimpse into the World of Random Walks*, in: "*Noise and Nonlinear Phenomena in Nuclear System*", eds. J. L. Munoz-Cobo and F. C. Difilippo, Plenum, New York 1989.

[8] C. Van den Broeck, Phys. Rev. Lett. *62*, 1421 (1989); Phys. Rev. *A40*, 7334 (1989); C. Van den Broeck, *Random Walks on Fractals* ed. W. Ebeling, in: Teubner Texte für Physik, IPSO-A Conference, Rostock, 1989.

[9] J. Machta, Phys. Rev. *B24*, 5260 (1981); J. M. Parrondo, H. L. Martinez, R. Kawai, and K. Lindenberg, Phys. Rev. *A42*, 723 (1990); B. Khang and S. Redner, J. Phys. *A22*, 887 (1989).

[10] T. Tel, *Transient Chaos*, to be published in "*Directions in Chaos*", Vol 3, ed. Hao Bai-Lin, World Scientific 1990.

[11] V. Balakrishnan and C. Van den Broeck, *Transport Properties on a Random Comb*, preprint, and references cited therein.

[12] See also: A. Engel and F. Moss, Phys. Rev. *A38*, 571 (1988); K. P. N. Murthy and K. W. Kehr, Phys. Rev. *A40*, 2080 (1989); K. W. Kehr and K. P. N. Murthy, Phys. Rev. *A41*, 5728 (1990).

[13] B. Derrida, J. Stat. Phys. *31*, 433 (1983).

[14] Ya G. Sinai, Theory Probab. Appl. *27*, 247 (1982).

[15] E. Marinari, G. Parisi, D. Ruelle, and P. Windey, Phys. Rev. Lett. *50*, 1223 (1983).

[16] S. H. Noskowicz and I. Goldhirsch, Phys. Rev. Lett. *61*, 500 (1988), see also: P. Le Doussal, Phys. Rev. Lett. *62*, 3097 (1989); S. H. Noskowicz and I. Goldhirsch, Phys. Rev. Lett. *62*, 3098 (1989).

Presented at the Discussion Meeting of the Deutsche Bunsen Gesellschaft für Physikalische Chemie "Rate Processes in Dissipative Systems. 50 Years after Kramers" in Tutzing, September 10 – 13, 1990 F 7505

Harmonic Noise Driven Bistable Dynamics

L. Schimansky-Geier, J. J. Hesse, and Ch. Zülicke

Institut für Theoretische Physik, Fachbereich Physik der Humboldt-Universität zu Berlin, Invalidenstr. 42, O-1040 Berlin, Germany

Colored Noise / Inversion States / Nonequilibrium Phenomena / Nonlinear Phenomena

We consider bistable dynamics driven externally by a noisy harmonic oscillator. For small damping we derive a Markovian approximation for the energy dynamics. In conclusion we discuss the possibility of the inversion of bistable oscillators induced by colored noise.

1. Introduction

The coordinate of a white noise driven harmonic oscillator is used as a stochastic source term in bistable dynamics. This simple picture on the one hand side generalizes the concept of colored noise where usually the Ornstein-Uhlenbeck-process is applied to nonlinear dynamics [1]. On the other hand our picture gives rise to resonance phenomena as they are studied in the case of Duffing oscillators [2]. In that case a phase- and amplitude-stabilized periodic function is applied as a driving force on the bistable dynamics. This requires generally a nonlinear driving element to generate the phase and amplitude locking.

Contrary, we think that our situation is simpler since it implies only linear elements in the generation of the noisy periodic force. Also we will assume mean energies of the driving oscillators much smaller than the energy barrier of the bistable oscillator and the resonance phenomena will be of stochastic origin due to amplitude and phase fluctuations.

We see many similarities to the investigations which nowadays are discussed in the framework of "stochastic resonance" [3]. We want to point out that this resonance corresponds more to a modulation since the harmonics of the process are determined by the frequency of the driving function. In contrast to this we will obtain transition frequencies between the two attractors of the bistable dynamics quite different from that of the driving force. This is due to resonance effects between the noisy driving oscillator and the bistable dynamics (comp. [4]).

The model we studied consists in a four-dimensional Markovian dynamics [5,6] (similar proposals were made in Refs. [7], our model describes situations which are related to the microwave modulated Josephson-junctions [8])

$$\begin{aligned} \dot{x} &= v; \quad \dot{v} = -\gamma v + f(x) + y(t) \\ \dot{y} &= s; \quad \dot{s} = -\Gamma s - \Omega_0^2 y + \Omega_0^2 \sqrt{2\varepsilon}\, \xi(t) \end{aligned} \tag{1.1}$$

where $\xi(t)$ is white noise and this stochastic source term is scaled in such a way that ε is the intensity of the noise $y(t)$ in the white noise limit if (i) $\Gamma \to \infty$; $\Omega_0 \to \infty$; $\Gamma/\Omega_0^2 = \tau =$ const; $\varepsilon =$ const and (ii) $\tau \to 0$; $\varepsilon =$ const. We suppose bistable forces $f(x)$.

Let us shortly characterize the dynamics of the driving system [9]. Under the condition $\Omega_0^2 > \Gamma^2/2$ the spectrum

$$S_{yy}(\omega) = \frac{2\varepsilon\Omega_0^4}{(\omega^2\Gamma^2 + (\omega^2 - \Omega_0^2)^2)} \tag{1.2}$$

possesses a peak at $\omega_p = (\Omega_0^2 - \Gamma^2/2)^{1/2}$ corresponding to an oscillating correlation function. The stationary probablity distribution density (p.d.d.) is a Gaussian one and an effective temperature of the noise can be introduced by

$$T_{\mathrm{HN}} = \frac{1}{2}\langle(\Delta s)^2\rangle + \frac{\Omega_0^2}{2}\langle(\Delta y)^2\rangle = \langle e\rangle = \varepsilon\frac{\Omega_0^4}{\Gamma}. \tag{1.3}$$

We see that the quality factor $Q = \Omega_0/\Gamma$ influences strongly the effective temperature.

For fixed temperatures T_{HN} and fixed ε by changing Γ we distinguish three typical regimes of transitions between the two stable attractors [6]:

(i) For small Γ (Ω_0 small as well) it yields a modulation of the bistable oscillator. Once the harmonic oscillator reaches high energy it is slowly damped out. In this situation the bistable oscillator is forced by the noise to move with the frequency of the applied force;

(ii) For large Γ the oscillatory character is suppressed and the noise is effectively white. Transitions are very rare;

(iii) If for medium Γ the effective frequency of the harmonic noise equals to the frequencies of the bistable dynamics in the attractor region transitions occur rapidly due to resonance. The mean transition time is of several magnitudes smaller than in the white noise case.

The maximal number of transitions occurs in the resonance regime. For this case we draw in Fig. 1 the waiting time distribution for an escape. It shows an exponential decay with small peaks at the subharmonics (comp. [4]). The transitions, therefore, are mainly of stochastic origin.

Some properties of the resonant regime can be understood by investigating the effect of the harmonic noise on linear systems (i.e. $f(x) = -\omega_0^2 x$ in Eq. (1.1)). Then the corresponding stationary Fokker-Planck-equation for the four-dimensional dynamics can be solved exactly. It is a Gaussian distribution and the mean energy of the driven oscillator

$$\langle E\rangle = \frac{1}{2}\langle(\Delta v)^2\rangle + \frac{\omega_0^2}{2}\langle(\Delta x)^2\rangle \tag{1.4}$$

 © VCH Verlagsgesellschaft mbH, W-6940 Weinheim, 1991 0005-9021/91/0303-0349 $ 3.50+.25/0

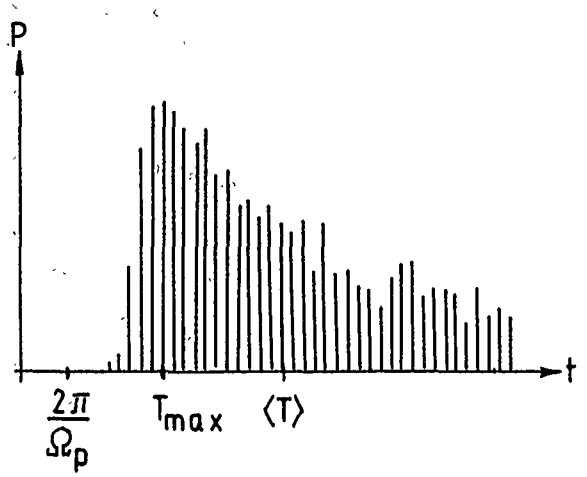


Fig. 1
Waiting time distribution for transitions in the Duffing oscillator. The characteristic times of transitions (the most probable T_{max} as well as the mean time $\langle T\rangle$) are quite different from the characteristic time of the driving force $2\pi/\Omega_p$

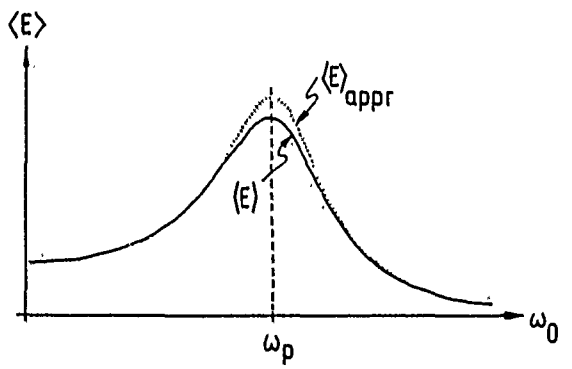


Fig. 2
Mean energy $\langle E\rangle$ in dependence on the frequency of the driven oscillator ω_0 for the linear system. The effective frequency of the driving oscillator is ω_p. The full line is the result for the exact solution; the dotted line is the result from Eq. (2.13)

with the standard deviations

$$\langle(\Delta v)^2\rangle = \frac{\varepsilon}{\gamma\left(\frac{\Gamma}{\Omega_0^2}\left(\gamma+\frac{\Gamma\omega_0^2}{\Omega_0^2}\right)+\frac{(1-\omega_0^2/\Omega_0^2)^2}{1+\gamma/\Gamma}\right)} \tag{1.5}$$

and

$$\langle(\Delta x)^2\rangle = \frac{\varepsilon}{\omega_0^2\left(\gamma+\frac{\Gamma}{\Omega_0^2}\omega_0^2\left(1-\frac{(1+\gamma/\Gamma)^2}{1+\gamma\Gamma(1+\gamma/\Gamma)/\Omega_0^2+\gamma\omega_0^2/(\Gamma\Omega_0^2)}\right)\right)} \tag{1.6}$$

shows resonance (Fig. 2).

In reference [6] we derived a Markovian approximation for the dynamics of the bistable oscillator in the phase space (x, v) and for the overdamped bistable system following the ideas of the unified colored noise approximation [10]. Unfortunately the resulting Fokker-Planck equation for the p.d.d. has been solved for the overdamped limit only $(\gamma \to \infty)$, but not for the general case. In the next section we propose a Markovian approximation for the dynamics of the energy of a harmonic noise driven bistable oscillator, which will be valid for sufficiently small γ.

2. Markovian Approximation for the Energy Dynamics in the low Friction Limit

We consider the damped oscillator driven by harmonic noise and introduce the potential $V(x)$ $(f(x) = -V'(x))$

$$\dot{x} = v; \quad \dot{v} = -\gamma v - \frac{\mathrm{d}V}{\mathrm{d}x} + y(t). \tag{2.1}$$

The energy $E = v^2/2 + V(x)$ of this system will be a slow variable in the low friction regime if

$$\gamma \ll \tau_{cor}^{-1} \ll \omega, \tag{2.2}$$

where ω is the frequency for the motion in the potential and τ_{cor} is the correlation time of the noise. The relation (2.2) implies a Markovian approximation for the energy dynamics. To obtain this Markovian description we use in the following a modification of a method which has been worked out by Carmeli and Nitzan [11].

In a single potential well it is possible to introduce the action angle variables (I, ϕ) defined by the canonical equations

$$\dot{I} = 0 = -\frac{\partial H}{\partial \phi}; \quad \dot{\phi} = \omega(I) = \frac{\partial H}{\partial I} \tag{2.3}$$

where H is the Hamiltonian of the deterministic system without friction. For these new variables we obtain from Eq. (2.1) the Langevin equations

$$\dot{I} = \frac{\partial x}{\partial \phi}(-\gamma v + y(t)); \quad \dot{\phi} = \omega(I) - \frac{\partial x}{\partial I}(-\gamma v + y(t)). \tag{2.4}$$

Expanding the coordinate x and the velocity v in Fourier series

$$x(I,\phi) = \sum_{n=-\infty}^{+\infty} x_n \mathrm{e}^{\mathrm{i}n\phi}; \quad v(I,\phi) = \sum_{n=-\infty}^{+\infty} v_n \mathrm{e}^{\mathrm{i}n\phi} \tag{2.5}$$

the Langevin equations result

$$\dot{I} = -\mathrm{i}\gamma \sum_{n,m=-\infty}^{n,m=+\infty} n x_n v_m \mathrm{e}^{\mathrm{i}(n+m)\phi} + \mathrm{i}y(t) \sum_{n=-\infty}^{+\infty} n x_n \mathrm{e}^{\mathrm{i}n\phi}$$

$$\dot{\phi} = \omega(I) + \gamma \sum_{n,\,m=-\infty}^{+\infty\;+\infty} \frac{\mathrm{d}x_n}{\mathrm{d}I} v_m \mathrm{e}^{\mathrm{i}(n+m)\phi} - y(t) \sum_{n=-\infty}^{+\infty} \frac{\mathrm{d}x_n}{\mathrm{d}I} \mathrm{e}^{\mathrm{i}n\phi}. \tag{2.6}$$

Then the time evolution of the p.d.d. for the action angle dynamics $P(I, \phi, t)$ is given by the Kramers-Moyal expansion

$$\frac{\partial P}{\partial t} = \lim_{\tau\to 0}\left\{\frac{1}{\tau}\sum_{n=1}^{\infty}\frac{(-1)^n}{n!}\sum_{\substack{m,k=0\\ m+k=n}}^{\infty}\left(\frac{\partial}{\partial I}\right)^m\left(\frac{\partial}{\partial\phi}\right)^k \cdot\langle\Delta I_t^m(\tau)\Delta\phi_t^k(\tau)\rangle P\right\}. \tag{2.7}$$

It reduces to the knowledge of the moments $\langle(\Delta I)^m\,(\Delta\phi^k)\rangle$. Their computation can be realized by using the iteration

$$\Delta I_t^{(l)}(\tau) = \int_0^\tau \mathrm{d}s\dot{I}(I(t)+\Delta I_t^{(l-1)}(s), \phi(t)+\Delta\phi_t^{(l-1)}(s), t+s), \tag{2.8}$$

where the starting point $\Delta I_t^{(0)}(s) = 0$; $\Delta\phi_t^{(0)}(s) = \omega(I)s$ follows from (2.3) and $\dot{I}$ is given by (2.6) (similarily for $\Delta\phi_t$).

Corresponding to (2.2) we neglect terms of order $(\gamma/\omega)^n$ and also $(Z_k(\omega)/\omega)^n$ with $n \geq 1$ where $Z_k(\omega)$ are the Fourier expansion coefficients of the stationary correlation function of the harmonic noise. Terms of order τ^n $(n \geq 1)$ vanish in the limit $\tau \to 0$ and so we obtain as in the white noise case that all moments with $m + k > 2$ vanish in (2.7). Because of the periodicity of $P(I, \phi, t)$ in ϕ we get after ϕ-integration and by transition to the energy variable $(\mathrm{d}I = \mathrm{d}E/\omega)$ the Fokker-Planck equation for the dynamics of the energy p.d.d. $P(E, t)$

$$\frac{\partial P}{\partial t} = \frac{\partial}{\partial E}\left(\omega(E)\left(\varepsilon_1(E)+\varepsilon_2(E)\frac{\partial}{\partial E}\right)\omega(E)\right)P \tag{2.9}$$

with

$$\varepsilon_1(E) = 2\gamma\sum_{n=1}^{\infty} n^2 x_n^2(E) \tag{2.10}$$

and

$$\varepsilon_2(E) = \sum_{n=1}^{\infty} n^2 x_n^2(E)\, S_{yy}(n\omega(E)). \tag{2.11}$$

where S_{yy} is the defined spectrum in (1.2). The stationary p.d.d. becomes

$$P^{(\mathrm{ss})}(E) = N^{-1}\omega^{-1}(E)\exp\left(-\int^E \mathrm{d}E'\frac{\varepsilon_1(E')}{\varepsilon_2(E')}\right). \tag{2.12}$$

Generally the $\varepsilon_1(E)$ and $\varepsilon_2(E)$ have to be computed numerically for nonlinear problems. To understand the mechanism we reduce the description onto harmonic potentials $V(x) = \omega_0^2 x^2/2$. In this case all terms in the sums (2.10) and (2.11) with $n > 1$ vanish and we obtain the stationary p.d.d.

$$P^{(\mathrm{ss})}(E) = N^{-1}\omega_0^{-1}\exp\left(-\frac{2\gamma E}{S_{yy}(\omega_0)}\right). \tag{2.13}$$

We see the effect of the noise results in an effective temperature which is determined by the spectrum. For the mean value of the energy $\langle E\rangle = S_{yy}(\omega_0)/2\gamma$ follows a resonance at $\omega_0 = \omega_p$ due to the peak in the spectrum of the harmonic noise at ω_p. For nonlinear potentials we get resonance phenomena as well which result from $\varepsilon_2(E)$ in (2.12). But the resonance frequency will differs from ω_p (cf. [8]). For harmonic potentials an averaging over rapid oscillations in the Langevin Eq. (2.4) leads in the low friction limit [12] to the same stationary p.d.d. $P^{(\mathrm{ss})}(E)$ as the approach described above. This implies that this approach can be interpreted as an averaging over the generalized phase ϕ in the basic Eq. (2.6) for a nonlinear potential $V(x)$.

3. Inversion by Harmonic Noise

For a white noise driven bistable oscillator the probability to be in one of the two stable states is determined by its energy value only. In this chapter we will show the possibility of generating an inversion of bistable oscillators due to the action of the harmonic noise. In detail this means that due to the resonant activation we force the oscillator to be in the state with higher energy with more probability than in the low energy state. For this purpose the high energy state is detuned whereas the low energy state will be in resonance with the harmonic noise. What follows is that the oscillator will leave quickly the low energy state due to resonance and otherwise will stay long times in the detuned state.

To demonstrate this effect we consider the simple model

$$\dot{x} = v; \quad \dot{v} = -\gamma v - \frac{\mathrm{d}V}{\mathrm{d}x} + y(t) \tag{3.1}$$

$$V(x) = \begin{cases} E_{\mathrm{L}0} + \dfrac{\omega_{\mathrm{L}}^2}{2}(x_{\mathrm{L}} - x)^2; & x < 0 \\ E_{\mathrm{R}0} + \dfrac{\omega_{\mathrm{R}}^2}{2}(x_{\mathrm{R}} - x)^2; & x > 0 \end{cases}$$

of a bistable oscillator driven by harmonic noise (cf. Fig. (3)). The essence of this model is the different energy levels of the minima of the potential (which results in different activation energies as well) and the difference of the frequencies in the bottom of the wells.

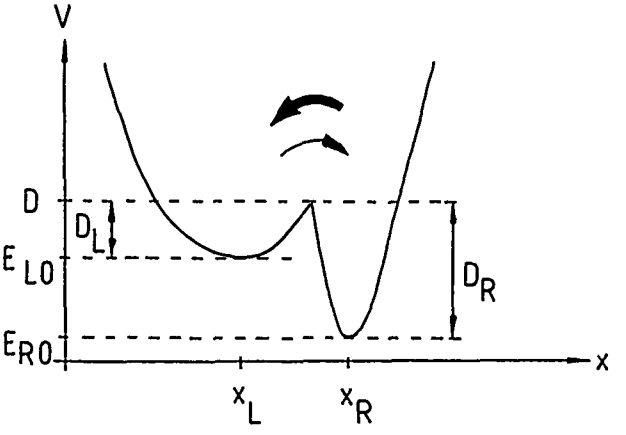


Fig. 3
Bistable oscillator under harmonic noise Here is shown a nonsymmetric bistable oscillator, where the frequency of the harmonic noise is just about the frequency of the right well ($\omega_0 \approx \omega_p$). Hence the transition rates are asymmetrically due to resonace like it is depicted with the arrows

If the barrier energies D_L and D_R are sufficiently large

$$D_i \gg S_{yy}(\omega_i)/2\gamma;\ i = L, R \tag{3.3}$$

than we reduce the p.d.d. in both wells to the canonic-like distribution (2.13), i.e. we put in every well as an first estimate

$$P_i(E) = N_i^{-1}\,\omega_i^{-1} \exp\left(-\frac{2\gamma E}{S_{yy}(\omega_i)}\right);\ 0 \le E \le D_i. \tag{3.4}$$

L and R correspond to the left and right well and the energies E_i are measured from the bottom of each well. The probabilities of the local states in the wells are

$$\bar{P}_i = \int_0^{D_i} dE\, P_i(E). \tag{3.5}$$

Then the ratio

$$s = \bar{P}_L/\bar{P}_R \tag{3.6}$$

is the measure of the inversion. For our case, where we have assumed $D_L < D_R$, the bistable oscillator will be inverted if $s > 1$. The p.d.d. (3.5) to be in the right or in the left state we obtain from the reduced dynamics

$$\dot{\bar{P}}_L = -r_{LR}\,\bar{P}_L + r_{RL}\,\bar{P}_R \tag{3.7}$$

where the r_{LR} and r_{RL} are the rates to leave the left state or the right state correspondingly. These rates can be calculated using the concept of the mean first passage time averaged over the initial condition [13]

$$r_{LR} = \left(\int_0^{D_L} dE\, P_L^{(ss)} \int_0^{D_L} dx \frac{1}{\omega^2(x)\,\varepsilon_2(x)\,P_L(x)} \int_0^{x} dy\, P_L(y)\right)^{-1} \tag{3.8}$$

where $P_L^{(ss)}(E)$ is the steady state distribution in the left well

$$P_L^{(ss)}(E) = \left(1 - \exp\left(-\frac{2\gamma D_L}{S_{yy}(\omega_L)}\right)\right)^{-1} \exp\left(-\frac{2\gamma E}{S_{yy}(\omega_L)}\right). \tag{3.9}$$

Because of the validity of (3.3) we obtain for r_{LR} the approximation

$$r_{LR} = \frac{2\gamma^2 D_L}{S_{yy}(\omega_L)} \exp\left(-\frac{2\gamma D_L}{S_{yy}(\omega_L)}\right) \tag{3.10}$$

(respectively for r_{RL} by a change of L and R). Insertion of (3.10) in Eq. (3.7) yields in the stationary case for the ratio s

$$s = \frac{S_{yy}(\omega_L) D_R}{S_{yy}(\omega_R) D_L} \exp\left(2\gamma\left(\frac{D_L}{S_{yy}(\omega_L)} - \frac{D_R}{S_{yy}(\omega_R)}\right)\right). \tag{3.11}$$

A resonance in the deeper right well ($\omega_R \approx \omega_p$) and a detuning in the left well can lead to a inversion with $s > 1$, the resonance pumps the population in the state with the higher energy. The problem is more complicated in the case of more realistic bistable potentials with a continuous first derivative dV/dx at the barrier. The frequencies vanish $\omega_i \to 0$ as $E_i \to D_i$ ($i = L, R$) and the low friction limit is not valid. Therefore the properties in the wells and at the barrier must be considered separately with some continuity conditions [14,15]. By generalization of the result for our simple model it follows the possiblity of inversion in such bistable systems due to resonance phenomena in the single wells.

References

[1] F. Moss and P. V. E. McClintock, eds.: "Noise in Nonlinear Dynamical Systems", vol. 1–3, Cambridge, Cambridge University Press 1989.

[2] J. Guckenheimer and P. J. Holmes: "Nonlinear Oscillations, Dynamical Systems and Bifurcation of Vector Fields", New York, Springer-Verlag 1983; P. Jung and P. Hänggi, Europhys. Lett. *8*, 505 (1989).

[3] B. McNamara, and K. Wiesenfeld, R. Phys. Rev. Lett. *60*, 1616 (1988).

[4] P. Jung and P. Hänggi, Phys. Rev. *A41*, 2977 (1990); G. Debnath, T. Zhou, and F. Moss, Phys. Rev. *A39*, 4323 (1989).

[5] W. Ebeling and L. Schimansky-Geier, in Ref. 1, vol. 1, p. 279.

[6] L. Schimansky-Geier and Ch. Zülicke, Z. Phys. *B79*, 451 (1990).

[7] Yu. L. Klimontovitch: "The Kinetic Theory of Electromagnetic Processes", pp. 338–342, Berlin, Heidelberg, New York, Springer 1983; T. Munakata and K. Kawakatsu, Prog. Theor. Phys. *74*, 262, (1985); T. Munakata, in Ref. 1, vol. 2, p. 24; S. Faetti and P. Grigolini, Z. Phys. *B47*, 353 (1982); F. Marchesoni and P. Grigolini, Physica *A121*, 269 (1983); T. Fonseca and P. Grigolini, Phys. Rev. *A33*, 1122 (1986); P. Grigolini, in Ref. 1, vol. 1, p. 161.

[8] M. H. Devoret, J. M. Martinis, D. Esteve, and J. Clarke, Phys. Rev. Lett, *53*, 1260 (1984); M. H. Devoret, D. Esteve, J. M. Martinis, A. Cleland, and J. Clarke, Phys. Rev. *B36*, 58 (1987).

[9] S. Chandrasekhar, Rev. Mod. Phys. *15*, 1 (1943); M. C. Wang and G. Uhlenbeck, Rev. Mod. Phys. *17*, 323 (1945).

[10] P. Jung and P. Hänggi, Phys. Rev. *A35*, 4464 (1987); P. Hänggi, in Ref. 1, vol. 1, p. 307; L. H'walisz, P. Jung, P. Hänggi, P. Talkner, and L. Schimansky-Geier, Z. Phys. *B77*, 471 (1989).

[11] B. Carmeli and A. Nitzan, J. Chem. Phys. *79*, 393 (1983).

[12] R. L. Stratonovich, "Topics in the Theory of Random Noise", vol. 2, New York, Gordon and Breach 1967.

[13] C. W. Gardiner, "Handbook of Stochastic Methods", Berlin, Heidelberg, New York, Springer 1983.

[14] B. Carmeli and A. Nitzan, J. Chem. Phys. *80*, 3596 (1984).

[15] P. Hänggi and F. Mojtabai, Phys. Rev. *A26*, 1168 (1982); P. Hänggi, J. Stat. Phys. *30*, 401 (1983).

Presented at the Discussion Meeting of the Deutsche Bunsen-Gesellschaft für Physikalische Chemie "Rate Processes in Dissipative Systems. 50 Years after Kramers" in Tutzing, September 10–13, 1990

E 7506

Pair Nucleation Rate in a Driven Sine-Gordon Chain

F. Marchesoni

Dipartimento di Fisica, Universitá di Perugia, I-06100 Perugia, Italy

Nonlinear Phenomena / Nucleation / Statistical Mechanics / Transport Properties

Thermal production of soliton-antisoliton pairs in an overdamped driven sine-Gordon chain occurs through the activation of a critical nucleus. The relevant pair nucleation rate is calculated explicitly by extending Kramers' theory to the case of an infinite dimensional, multistable system with one neutral equilibrium mode.

1. Introduction

The perturbed sine-Gordon (SG) equation [1]

$$\phi_{tt} - c_o^2 \phi_{xx} + \omega_o^2 \sin\phi = -\gamma\phi_t - F + \zeta(x,t) \tag{1}$$

provides an ideal model to study the nucleation processes of a variety of physical systems at thermal equilibrium [2–4]. For instance, in plasma physics ω_o and c_o model the plasma frequency and the sound speed, respectively. In Eq. (1) the ordinary SG equation has been coupled with a heat bath at temperature T through a damping term, $-\gamma\phi_t$, with γ a constant, and a gaussian noise $\zeta(x,t)$ with zero mean and correlation function

$$\langle\zeta(x,t)\zeta(x',t')\rangle = 2\frac{\gamma}{\beta}\delta(t-t')\delta(x-x') \tag{2}$$

($\beta = 1/kT$). The constant force F is meant to represent an external physical bias which breaks the $\phi \to -\phi$ symmetry, thus making the pair nucleation process possible [5, 6], but preserves the multistable nature of the SG potential $V[\phi] = \omega_o^2(1-\cos\phi)$, i.e. $F \leq \omega_o^2$.

The unperturbed SG equation (i.e. Eq. (1) with the r.h.s. set to zero) has been derived from the relativistically covariant Hamiltonian density

$$H[\phi] = \frac{1}{2}(\phi_t^2 + c_o^2\phi_x^2) + V[\phi] \tag{3}$$

and bears both extended (phonons) and localized solutions. Localized solutions can be well approximated as an appropriate linear superposition of solitons, ϕ_K, and antisolitons, $\phi_{\bar{K}}$, in the limit when the separation among their centres is very large compared with their size (*dilute gas approximation*). For later convenience, we write explicitly the single soliton (antisoliton) solution (mod 2π)

$$\phi_{K(\bar{K})}(x,u) = 4\,\mathrm{tg}^{-1}\exp\left[\pm\frac{\omega_o}{c_o}\frac{x-X(t)}{\sqrt{1-u^2/c_o^2}}\right]. \tag{4}$$

Here, $X(t) = x_o + ut$ denotes the centre of mass of the solution (4), which moves with constant speed u. $\phi_{K(\bar{K})}$ represents a dislocation of the SG chain between the potential minimum at $\phi(-\infty) = 0$ and the adjacent minimum at $\phi(\infty) = \pm 2\pi$, respectively, occuring at $X(t)$ within a length comparable with the $\phi_{K(\bar{K})}$ size c_o/ω_o. The energy required for the SG chain to bridge two adjacent potential minima is $E_o = \int dx\, H[\phi_{K(\bar{K})}(x,0)] = 8\omega_o c_o$ (soliton rest mass). A statistical approach to the SG theory leads to the following prediction for the equilibrium soliton (antisoliton) density ($F = 0$)

$$n_0 = \left(\frac{2}{\pi}\right)^{1/2}\frac{\omega_o}{c_o}(\beta E_o)^{1/2}\,e^{-\beta E_o}. \tag{5}$$

The dilute gas approximation is thus legimate in the low temperature limit $\beta E_o \ll 1$, where $n_o^{-1} \gg c_o/\omega_o$. The soliton and antisoliton solutions (4) carry opposite topological charge and, therefore, they may only be created by the pair. Furthermore, $\phi_{K(\bar{K})}$ are stable under the perturbation considered in Eq. (1), apart from a rigid translation, against which they are in neutral equilibrium (Goldstone mode).

At this stage, the question arises as how a soliton-antisoliton pair may be nucleated starting from a vacuum configuration, e.g. $\phi = 0$. Thermal fluctuations are expected to trigger the process by activating a critical nucleus, the size of which may be shown to increase with decreasing F [2–6]. Provided that the critical nucleus size is small enough to ignore the many-body effects due to the thermalized gas of solitons and antisolitons with density (5), we can describe the nucleation process as a local two-body mechanism. This picture is tenable only for low temperatures and relatively strong external biases. A two-body nucleation mechanism can be treated as an extension of Kramers' theory [7] to multidimensional systems with neutral equilibrium (or zero) modes [2]. In the present paper we investigate this mechanism in the classical limit. Some results reported below have been anticipated in Ref. [6]. The quantum mechanical contributions to the two-body nucleation mechanism at temperatures higher than the thermal activation temperature have been addressed in Ref. [8]. The extension of our approach to other soliton bearing theories is also possible [9].

2. Procedure

It has been shown that in the presence of fluctuation-dissipation terms a single soliton (antisoliton) undergoes

 © VCH Verlagsgesellschaft mbH, W-6940 Weinheim, 1991 0005-9021/91/0303-0353 $ 3.50+.25/0

brownian motion, whereas the bias term pulls ϕ_K and $\phi_{\bar{K}}$ in opposite directions, according to the driven Langevin equation [10]

$$\dot{p} = -\gamma p \pm 2\pi F + E_0 \eta(t) \tag{6}$$

where $\eta(t)$ is a zero-mean valued, gaussian noise with correlation function $\langle \eta(t)\eta(0)\rangle = 2D\delta(t)$, $D \equiv \gamma/\beta E_0$, and p is the boosted momentum of $\phi_{K(\bar{K})}$, $p = E_0 u/\sqrt{1-u^2}$. From now on, we simplify our notation by adopting dimensionless units, i.e.

$$\frac{\omega_0}{c_0} x \to x, \quad \omega_0 t \to t \tag{7}$$

and, consequently, $\gamma/\omega_0 \to \gamma$, $F/\omega_0^2 \to F$ and $\omega_0 c_0/kT \to \beta$. This amounts to setting $\omega_0 = c_0 = 1$ and, in particular, $E_0 = 8$.

The two-body nucleation mechanism is well defined under the supplementary condition that the SG chain is overdamped, i.e. $\gamma \gg 1$. Such a limitation affords three major simplifications: (i) oscillatory solutions of Eq. (1), like breathers and phonon radiation, are damped out and, therefore, do not play any significant role in the statistics of the problem; (ii) the non-relativistic limit, $p = E_0 u$, is a good approximation. Accordingly, the Langevin equation (6) reads

$$\dot{u} = -\gamma u \pm \frac{2\pi F}{E_0} + \eta(t), \tag{8}$$

whence the mean, $u_F = \pm 2\pi F/\gamma E_0$, and the variance of the $\phi_{K(\bar{K})}$ speed, $\langle (u-u_F)^2\rangle = (\beta E_0)^{-1}$; (iii) soliton-antisoliton collisions are always destructive. In fact, the condition for a soliton and an antisoliton to go through each other in the presence of damping [11], $F \geq 2\gamma^{3/2}$, cannot be achieved in the overdamped regime (remember that $F \leq 1$). In the following, we carry out our analysis under the condition $\gamma \gg 1$, even though such an assumption is not always tenable when modelling real physical systems. This point will be discussed further in the last Section.

On deriving the Langevin Eq. (6) we have assumed that the $\phi_{K(\bar{K})}$ shape is stable under perturbation. This is not true when the soliton (antisoliton) is driven by an external constant bias, which tilts the SG potential $V[\phi]$, thus changing the effective plasma frequency [4]: $1 \to \sqrt{1-F^2}$ (in dimensionless units). In order to ignore such corrections we restricted our calculations to the case of small biases $F \ll 1$. Actually, in deriving our results for the pair nucleation rate (Section 3), we shall neglect corrections at the first order in F.

Let us go back, now, to the pair nucleation mechanism. Thermal fluctuations may activate, with finite probability, a nucleus $\phi_N(x,X)$ of length $2X$ about the vacuum configuration, $\phi = 0$. For $X \gg 1$, $\phi_N(x,X)$ is well described by the linear superposition of a soliton and an antisoliton centered in $\mp X$, respectively,

$$\phi_N(x,X) = \phi_K(x+X,0) + \phi_{\bar{K}}(x-X,0) = 4\,\mathrm{tg}^{-1}\left(\frac{\mathrm{sh}\,X}{\mathrm{ch}\,x}\right). \tag{9}$$

The centre of the nucleus has been set at the origin without loss of generality. The components of a large nucleus experience two contrasting forces: an attractive force due to the vicinity of the nucleating partner, the potential of interaction being a function of the distance $2X$ between their centres of mass

$$V_N(X) = -2E_0\, e^{-2X}, \quad X \gg 1, \tag{10}$$

and a repulsive force due to the constant bias F, which pulls ϕ_K and $\phi_{\bar{K}}$ apart, with effective potential $\mp 2\pi F X$, respectively. The critical nucleus configuration, $\phi_N(x,R)$ is attained at the distance between ϕ_K and $\phi_{\bar{K}}$, $2R(F)$, where the two competing forces compensate each other. $\phi_N(x,R)$ is thus the saddle point configuration to overcome for the pair nucleation to take place. The critical nucleus admits of only one unstable mode with negative eigenvalue, λ_0^N, which in the overdamped limit can be safely associated with the relative coordinate $X(t)$ [3].

The nucleation rate Γ (i.e. the number of pairs generated per unit of time and length) can be related to the imaginary part of the free energy of the critical nucleus, $\mathrm{Im}\Im$, by means of Langer's formula [2]

$$\Gamma = \frac{|\lambda_0^N|}{\pi} \beta \mathrm{Im}\Im. \tag{11}$$

In the foregoing Section we compute Γ explicitly applying the Langevin equation approach developed to derive Eq. (6).

3. Results

The rate in Eq. (11) may be re-written in a more suggestive form [2]:

$$\Gamma = \frac{|\lambda_0^N|}{\pi} \frac{Z_N}{Z_0} e^{-\beta \Delta E_N} \tag{12}$$

where Z_0 and Z_N denote the partition function for the vacuum field configuration and the critical nucleus, respectively. $\Delta E_N(F)$ is the energy of the saddle point configuration $\phi_N(x,R)$, which acts as the potential barrier between the relevant stable configurations, the vacuum, with zero energy, and the nucleated pair driven infinitely apart, with energy $2E_0/\sqrt{1-u_F^2} \simeq 2E_0$.

The quantities $\Delta E_N(F)$ and $\lambda_0^N(F)$ can be calculated within the Langevin equation approach. The interacting pair $\phi_K(x+X)$ and $\phi_{\bar{K}}(x-X)$ at large distance obeys the equation of motion

$$\ddot{X} = -\gamma \dot{X} + \frac{2\pi F}{E_0} - 4e^{-2X} + \eta(t) \tag{13}$$

obtained from Eq. (8) by inserting explicitly the attractive drift term corresponding to the potential in Eq. (10). The barrier of the total interaction potential $V_{K(\bar{K})}(X) = -2\pi F X - 2E_0 \exp(-2X)$ is located at

$$R(F) = -\frac{1}{2} \ln\left(\frac{\pi F}{2E_0}\right) \tag{14}$$

with curvature $|V_{K(\bar{K})}(R)| = 4\pi F$. Moreover, the Smoluchowski limit to Eq. (13) yields our estimate for the negative eigenvalue associated with the unstable coordinate $X(t)$:

$$\lambda_0^N(F) = \frac{4\pi F}{\gamma E_0}. \tag{15}$$

We remark, here, that the linearization around the top of the potential barrier implicit in Eq. (11) [2] holds good only under the further restriction that $D/\gamma \ll [V'_{KR}(R)]^2/V''_{KR}(R)$, i.e.

$$2\pi\beta F \gg 1 \tag{16}$$

being $V_{KR}(X)$ a soft potential [12].

Our best estimate for $\Delta E_N(F)$ has been obtained by calculating $\int dx\, H[\phi_N(x,R)]$ with $\phi_N(x,R)$ given in Eq. (9) and $R(F)$ in Eq. (14),

$$\Delta E_N(F) = 2E_0\left[1 - \frac{1}{\mathrm{ch}2R(F)+1}\left(1 + \frac{2R(F)}{\mathrm{sh}2R(F)}\right)\right]. \tag{17}$$

This is an improvement with respect to the estimate reported in Ref. [6]. Our predictions (15) and (17) agree very closely with the results of numerical integration [4].

To accomplish our calculation of Γ we determine, finally, the ratio Z_N/Z_O in Eq. (12). For this purpose, we have recourse to the linear stability analysis [1], whence

$$\frac{Z_N}{Z_O} = \frac{1}{2}\left|\frac{\det(\beta\Upsilon_O/2\pi)}{\det'(\beta\Upsilon_N/2\pi)}\right|^{1/2}[\Delta E_N(F)]^{1/2}. \tag{18}$$

The linear stability operators

$$\Upsilon_O = -\partial_{tt}^2 - \gamma\partial_t + \partial_{xx}^2 - V_{\phi\phi}[0] \tag{19a}$$

and

$$\Upsilon_N = -\partial_{tt}^2 - \gamma\partial_t + \partial_{xx}^2 - V_{\phi\phi}[\phi_N(x,R)] \tag{19b}$$

have been obtained from the unperturbed SG equation by expanding the field $\phi(x,t)$ at the first order around the vacuum configuration $\phi(x,t) = 0$ and the critical nucleus $\phi_N(x,R)$, respectively. The Goldstone mode of the operator Υ_N has been subtracted from $\det(\beta\Upsilon_N/2\pi)$, as denoted by the prime sign, and its contribution calculated explicitly [2,4]. For a full treatment of Eq. (18) the reader is referred to more detailed reports [6,8].

In the overdamped regime we approximate the operators in Eq. (19) as follows

$$\begin{aligned}\Upsilon_O &= -\gamma\partial_t + \partial_{xx}^2 - V_{\phi\phi}[0]\\ \Upsilon_N &= -\gamma\partial_t + \partial_{xx}^2 - V_{\phi\phi}[\phi_N(x,R)]\,.\end{aligned} \tag{20}$$

The eigenvalue spectrum of Υ_O is [1]

$$\gamma\lambda^O(k) = k^2 + 1\,, \quad k \geq 0\,. \tag{21}$$

The eigenvalue spectrum of Υ_N, instead, consists of a negative eigenvalue $\gamma\lambda_0^N(F)$, with $\lambda_0^N(F)$ given in Eq. (15), a zero eigenvalue corresponding to the Goldstone mode, $\gamma\lambda_1^N(F) = 0$, a discrete eigenvalue $\gamma\lambda_2^N(F)$ and a continuum

$$\gamma\lambda^N(k) = k^2 + 1\,, \quad k \geq 0\,. \tag{22}$$

The discrete eigenvalue $\gamma\lambda_2^N(F)$ represents an internal oscillating mode of the critical nucleus and follows the removal of the degeneracy at the continuum threshold, $\gamma\lambda^N(0)$, due to the finiteness of the nucleus size. Of course, $0 < \gamma\lambda_2^N(F) \leq 1$. For small values of F we retain the F-dependence of $\lambda_0^N(F)$, only, whereas $\gamma\lambda_2^N(F)$ is set to one and, thus, incorporated in the continuum. This amounts to approximating the continuous branch of the eigenvalue spectrum of Υ_N with twice the eigenvalue spectrum for the simple soliton (antisoliton) stability operator, which is analytically solvable [1]. In particular, the difference of the continuum state density for Υ_O and Υ_N at $F = 0$ is

$$\Delta(k) \equiv \varrho_O(k) - \varrho_N(k) = \frac{4}{\pi}\,\frac{1}{k^2+1} \tag{23}$$

whence, being $\lambda^O(k) = \lambda^N(k) \equiv \lambda(k)$,

$$\left|\frac{\det(\beta\Upsilon_O/2\pi)}{\det'(\beta\Upsilon_N/2\pi)}\right|^{1/2} \simeq \left(\frac{\beta}{2\pi\gamma|\lambda_0^N|}\right)^{1/2} \cdot \exp\left[\frac{1}{2}\int_0^\infty dk\,\Delta(k)\ln\gamma\lambda(k)\right] = 4\left(\frac{\beta}{2\pi\gamma|\lambda_0^N|}\right)^{1/2}. \tag{24}$$

Substituting Eq. (24) into Eq. (18) and Eq. (18) into Eq. (12) leads to our final result [6]

$$\Gamma(F) = \frac{2}{\pi}\left|\frac{\lambda_0^N(F)}{2\pi\gamma}\right|^{1/2}[\beta\Delta E_N(F)]^{1/2}\,e^{-\beta\Delta E_N(F)}, \tag{25}$$

where $\lambda_0^N(F)$ and $\Delta E_N(F)$ are known from Eqs. (15) and (17), respectively.

4. Discussion

We comment, now, on the applicability of our estimate (25) for the nucleation rate.

i) Eq. (25) applies only for small, finite values of the external bias, i.e. $\beta^{-1} \ll F \ll 1$. The upper bound, $F \ll 1$, allows us to neglect effects $O(F^2)$ due to the relativistic boost and the rescaling of the plasma frequency. The lower bound, $\beta F \gg 1$, instead, has been introduced in Eq. (16) to justify the linear approximation implicit in Langer's formula (11). This restriction amounts to requiring that the mechanical energy needed to pull an isolated soliton (antisoliton) through a distance of the order of its size is larger than the thermal energy, β^{-1}, stored in the critical nucleus [6]. Under such a condition pair nucleation is not described by the linear response theory, as confirmed by the fact that $\Gamma(F)$ is proportional to $\sqrt{F}$ for $F \to 0$. A realistic analysis of the nucleation process at thermal equilibrium for vanishingly small values of the bias cannot ignore the presence of many-body effects as pointed out in Refs. [5,6].

(ii) Corrections to $\Gamma(F)$ are expected at the first order in F. For instance, in Eq. (18) the discrete eigenvalue of Υ_N, $\gamma\lambda_2^N(F)$, has been set to one. In fact, we can give an upper bound to $\gamma\lambda_2^N(F)$, on substituting the potential $V_{\phi\phi}[\phi_N(x,R)]$ in Eq. (20) with the square well potential

$$\begin{aligned}\bar{V}(X) &= 1 && \text{for } |x| > R(F)\\ &= V_{\phi\phi}[\phi_N(0,R)] && \text{for } |x| < R(F)\end{aligned} \tag{26}$$

where $V_{\phi\phi}[\phi_N(0,R)] = 2[2/\mathrm{ch}R - 1]^2 - 1$. For large values of $R(F)$, i.e. small values of F, $\bar{V}(X)$ admits of one discrete eigenvalue, which can be approximated by $1 - 2\pi F$. Since $\bar{V}(X) \geq V_{\phi\phi}[\phi_N(x,R)]$ for any value of x, it follows that

$$\gamma\lambda_2^N(F) \leq 1 - 2\pi F\,. \tag{27}$$

A preliminary estimate of the F-corrections to Eq. (24) can be obtained by noting that expression (9) for $\phi_N(x,R)$ coincides, formally, with the constrained (maximum amplitude) breather solution [1] of the unperturbed SG equation,

$$\phi_B(x,v) = 4\,\mathrm{tg}^{-1}\left\{\left[v\,\mathrm{ch}\left(\frac{x}{\sqrt{1+v^2}}\right)\right]^{-1}\right\} \tag{28}$$

where $(1+v^2)^{1/2}\ln(2/v) = R(F)$ or, equivalently,

$$v^2 \simeq \frac{\pi F}{4}. \tag{29}$$

The eigenvalue spectrum associated with the time-dependent stability equation for the breather solution is known analytically [1]. After rotating $\phi_B(x,v)$ back to the soliton-antisoliton superposition $\phi_N(x,R)$ of Eq. (9) by setting $v = -iu$, the relevant changes in our calculations boil down to substituting the quantity $\Delta(k)$ defined in Eq. (23) with

$$\Delta(k) = \frac{4}{\pi}\,\frac{(1-u^2)^{1/2}}{1+(1-u^2)k^2}. \tag{30}$$

As a result the r.h.s. of the Eq. (24) must be multiplied times the correction factor $[1+(1-u^2)^{-1/2}]^2/4$, which, in view of Eq. (28), implies a correction to $\Gamma(F)$ at the first order in F. The procedure sketched here will be developed rigorously in a future publication.

(iii) Eq. (25) can be improved to account for intermediate to large values of the damping constant γ. A detailed calculation of the determinantal ratio in Eq. (18) is straightforward [8] and leads to the same result for $\Gamma(F)$ as in Eq. (25), with the only condition of rescaling

$$|\lambda_0^N|^{1/2} \to \frac{2|\lambda_0^N|^{1/2}}{(1+4|\lambda_0^N|/\gamma)^{1/2}+1}. \tag{31}$$

Of course, such a rescaling does not provide the correct answer in the limit of vanishingly small damping constant (transition state theory approximation [7]). The extension of Kramers' theory to the underdamped limit of the problem of pair nucleation in thermalized SG chains is still an open problem.

Research supported in part by the Istituto Nazionale di Fisica Nucleare (INFN). Prof. P. Hänggi and Prof. P. Riseborough are thanked for encouragement.

References

[1] R. Rajaraman, Solitons and Instantons, North-Holland, Amsterdam 1982.
[2] J. S. Langer, Ann. Phys. *54*, 258 (1969); for a review see P. Hänggi, P. Talkner, and M. Borkovec, Rev. Mod. Phys. *62*, 251 (1990).
[3] B. V. Petukhov and V. L. Pokrovskii, Zh. Eksp. Teor. Fiz. *63*, 634 (1972); Sov. Phys. JETP *36*, 336 (1973).
[4] M. Büttiker and R. Landauer, Phys. Rev. *A23*, 1397 (1981) and references therein.
[5] F. Marchesoni, Phys. Rev. *B34*, 6536 (1986).
[6] P. Hänggi, F. Marchesoni, and P. Sodano, Phys. Rev. Lett. *60*, 2563 (1988).
[7] H. A. Kramers, Physica *7*, 284 (1940).
[8] P. Hänggi, F. Marchesoni, and P. Riseborough, Europhys. Lett. *13*, 217 (1990); B. I. Ivlev and V. I. Mel'nikov, Phys. Rev. *36*, 6889 (1987).
[9] F. Marchesoni, Phys. Rev. Lett. *64*, 2212 (1990).
[10] F. Marchesoni, Phys. Lett. *115A*, 29 (1986).
[11] N. F. Pedersen, M. R. Samuelson, and D. Welner, Phys. Rev. *B30*, 4057 (1984).
[12] F. Marchesoni, P. Sodano, and M. Zannetti, Phys. Rev. Lett. *61*, 1143 (1988).

Presented at the Discussion Meeting of the Deutsche Bunsen-Gesellschaft für Physikalische Chemie "Rate Processes in Dissipative Systems: 50 Years after Kramers" in Tutzing, September 10–13, 1990 E 7507

Soliton – Assisted Activation Processes

Werner Ebeling and Martin Jenssen*)

Fachbereich Physik, Humboldt-Universität zu Berlin, Invalidenstraße 42, O-1040 Berlin, Federal Republic of Germany

Activation / Chemical Kinetics / Nonequilibrium Phenomena / Nonlinear Phenomena / Solutions

This paper deals with the problem of energetic activation of one or few degrees of freedom of a spatially extended system. The fusion of soliton-like excitations is an efficient nonlinear mechanism to generate high-energy events at soft springs which are embedded in a one-dimensional chain of hard springs. In equilibrium there exists an optimum temperature where thermal energy is mainly partitioned to the soft springs due to the superposition of thermally generated solitons. Some of the features obtained for the one-dimensional system also apply to a solution of soft spheres in a hard-sphere solvent.

1. Introduction

Energetic activation proves to be an essential precondition for a multitude of processes to take place. Obvious examples are chemical reactions or the cracking of materials. In the following we will define activation processes as high energy events appearing at one or a few degress of freedom of a spatially distributed system. The energy gained by the activation coordinates has to be provided by the surrounding system. The first complete theoretical treatment of an activation process is contained in the famous paper of Kramers [1].

Let us start with an elementary consideration of classical activation processes in one degree of freedom The energy corresponding to the motion along the activation coordinate r_0 is assumed to be

$$E_0 = \frac{p_0^2}{2m} + U(r_0), \qquad p_0 = m\dot{r}_0.$$

*) Current address: Forschungsanstalt für Forst- und Holzwirtschaft Eberswalde, Alfred-Möller-Straße, O-1300 Eberswalde, Federal Republic of Germany.

As special models for the shape of the potential-energy function we will use the linear oscillator potential and the nonlinear Toda potential [2], the latter one modelling a wide class of empirical molecular potentials consisting of a steep repulsive and a long-range attractive part:

$$U^{(1)}(r_0) = \frac{1}{2} m\omega_0^2 r_0, \tag{1.1}$$

$$U^{(2)}(r_0) = \frac{m\omega_0^2}{b_0^2}(\exp(-b_0 r_0) - 1 + b_0 r_0). \tag{1.2}$$

The parabolic approximation (1.1) can be obtained from (1.2) for a vanishing stiffness parameter b_0. Now we are going to consider an activation coordinate embedded in a canonical heat bath. Within the classical approach we find from (1.1) and (1.2) for the mean energies

$$\langle p_0^2/2m\rangle = \frac{1}{2}kT, \quad \langle U^{(1)}(r_0)\rangle = \frac{1}{2}kT,$$

$$\langle U^{(2)}(r_0)\rangle = \frac{m\omega_0^2}{b_0^2}\left[\ln\left(\frac{m\omega_0^2}{kTb_0^2}\right) - \Psi\left(\frac{m\omega_0^2}{kTb_0^2}\right)\right],$$

where

$$\Psi(x) = \frac{\mathrm{d}}{\mathrm{d}x}\ln\Gamma(x)$$

denotes the so-called Digamma function. From the above expressions we find

$$\langle U^{(1)}(r_0)\rangle > \langle U^{(2)}(r_0)\rangle .$$

Hence there is no way to get an average energy exceeding $k\,T$ at a single degree of freedom for Toda-like potentials.

In this paper we present a contribution towards a theory of nonlinear energy localization mechanisms thereby restricting ourselves to the investigation of simple classical models. The following part of the paper is dedicated to a brief description of a dynamical effect – the soliton fusion – allowing energy localization at a defined site of a nonlinear molecular chain. This effect could be involved in the catalytic processes occuring in complex reaction systems under nonequilibrium conditions. In the subsequent section we will show that the superposition of thermal solitons may lead to an activation enhancement even in equilibrium. Going beyond the special one-dimensional system presented so far, we will argue finally that the phenomenon of thermal energy localization could be of a more general relevance to the theory of activation processes.

2. Soliton Fusion as a Mechanism of Energy Accumulation

Now we are going to consider the dynamics of a nonuniform chain of masses at position y_n which are connected to their nearest neighbors by Toda springs with the nonlinear spring constant b_n. The Hamiltonian reads

$$H = \sum_n \left\{\frac{p_n^2}{2m} + \frac{a}{b_n}[\exp(-b_n(y_{n+1} - y_n)) - 1] + a(y_{n+1} - y_n)\right\}. \tag{2.1}$$

Here the notation is related to that one used in (1.2) by $ab_n = m\omega_n^2$. For an infinite uniform chain ($b_n = b\,\forall n \varepsilon(-\infty, +\infty)$) Toda found the soliton solution [2]

$$\exp(-b(y_{n+1} - y_n)) - 1 = \sinh^2\varkappa \cdot \operatorname{sech}^2\left(\varkappa n - \sqrt{\frac{ab}{m}}\sinh\varkappa t\right), \tag{2.2}$$

with energy

$$E^s = \frac{2a}{b}(\sinh\varkappa\cosh\varkappa - \varkappa). \tag{2.3}$$

The soliton corresponds to a local compression of the lattice with spatial "width" $\varkappa^{-1}$. The quantity

$$\tau = \left(\sqrt{\frac{ab}{m}}\sinh\varkappa\right)^{-1} \tag{2.4}$$

defines a characteristic excitation time of a spring during soliton passage. The energy of a much energy containing and, therefore extremely localized soliton satisfying the condition

$$\frac{\sinh^2\varkappa}{\varkappa} \gg 1 \tag{2.5}$$

reads according to (2.3) and (2.5):

$$E^s \approx \frac{2a}{b}\sinh^2\varkappa. \tag{2.6}$$

Now we consider a system consisting of two semiinfinite Toda chains of different spring parameters, $b_n = b\;\forall\; n < 0$ and $b_n = b_0\;\forall\; n \geq 0$ with $b_0 < b$. Although this nonuniform chain does not admit exact soliton solutions, the solution [2.2] can be conceived as a right running solution on the hard part with b far to the left of the interface where it behaves as in a uniform chain. In the vicinity of the interface however it will be scattered and evolve into reflected and transmitted waves including both solitons and radiation [3,4]. In particular we observe sufficiently far to the right on the soft part the formation of a transmitted soliton that was evaluated in a previous paper [3].

$$\exp(-b_0(y_{n+1} - y_n)) - 1 = \sinh^2\varkappa_0 \cdot \operatorname{sech}^2\left(\varkappa_0 n - \sqrt{\frac{ab_0}{m}}\sinh\varkappa_0 t + \delta\right), \tag{2.7}$$

$$\sinh^2\varkappa_0 = \frac{b_0}{b}\sinh^2\varkappa .$$

The last expression relates the transmitted soliton to the incident one. δ denotes a constant phase shift that occurs due to the scattering process. In case of strong localization of both incident and transmitted soliton we find from (2.7) and (2.6) for the energy E_0^s of the latter

$$E_0^s \approx \frac{2a}{b}\sinh^2\varkappa \approx E^s .$$

Hence the energy of the incident soliton is almost completely transferred to the transmitted one, i.e., scattering losses are less important for energetic solitons. From (2.2) and (2.7) we find according to (2.4) for the characteristic times τ and τ_0 of the incident and the transmitted soliton, respectively, the simple relationship

$$\frac{\tau_0}{\tau} = \frac{b}{b_0}. \tag{2.8}$$

The existence of different time scales of soliton motion can be used to generate high energy events by soliton fusion which was demonstrated numerically [3]. The energy of two strongly localized solitons of equal magnitudes impinging on the interface will be contained afterwards mainly in one soliton transmitted to the soft chain provided the incident solitons were separated from each other by a time less than τ_0 on the hard chain.

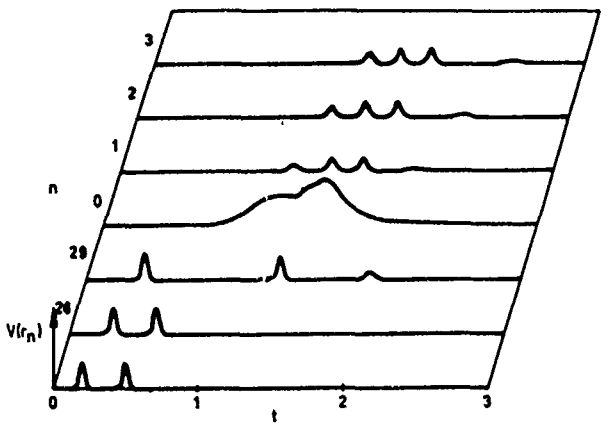


Fig. 1
Superposition of two solitons in a single soft spring ($n = 0$) embedded in a hard Toda lattice ($n = 1, \ldots, 29$) with parameters $m = 2$, $a = 10^{-2}$, $b = 10^2$, $b/b_0 = 10$. The solitons (each of energy $E = 1$) are separated from each other by a time 8.4 τ on the hard lattice initially (τ is the characteristic time (2.4)). the potential energy of springs is plotted vs. time t and spring number n

Now we consider a single soft spring embedded in a surrounding, otherwise uniform hard chain ((2.1) with $b_n = b\,\forall\, n \neq 0$ and $b_0 < b$) instead of the interface between two extended chains of different stiffness. It turns out that this only soft spring is able to trap and superpose narrow solitons impinging from both directions within characteristic excitation time τ_0 which is demonstrated in Fig. 1. We only note that this kind of soliton fusion leads to considerable concentrations of potential energy at the soft spring [3]. Interpreting a compression of this spring up to a certain critical value as activation process we have got a novel mechanism to accumulate the energy of nonequilibrium excitations at a selected degree of freedom to be activated. In a previous work [5] a simple model of global enzyme structure was investigated in order to demonstrate the maintenance of the main features of the effect for a chain of inhomogeneous molecular units interacting via Morse potentials even in the presence of frictional forces and realistic potential parameters. A soft Morse spring was used to model the linkage between catalytically relevant molecular groups of the enzyme.

3. Statistical Thermodynamics of the Nonuniform Toda Chain

In the last section the fusion of solitons was introduced as a special nonequilibrium effect which is suited to support local activation processes. Now we will give a brief summary of some recent findings [6] proving that an activation enhancement occurs even in thermal equilibrium due to the fusion of thermally generated solitons.

We consider a nonuniform Toda chain (2.1) of N particles which is fixed at the left hand side ($y_0 = 0$) and introduce a pressure P acting on the right end particle (y_N). Among the N springs may be N_0 soft springs with spring constant b_0. After changing to spring coordinates, $r_n = y_n - y_{n-1}$, the exact classical partition function can be calculated as for the uniform Toda chain [2]. Using the notations $\beta = 1/kT$, $\gamma = P/kT$, we obtain

$$\begin{aligned} Z(\beta,\gamma) &= \prod_{n=1}^{N}\int_{-\infty}^{+\infty}\int_{-\infty}^{-\infty} \mathrm{d}p_n \mathrm{d}r_n \\ &\quad\cdot\exp\left\{-\frac{\beta p_n^2}{2m} - \frac{\beta a}{b_n}[\exp(-b_n r_n) - 1] - (\beta a + \gamma) r_n\right\} \\ &= \left(\frac{2\pi m}{\beta}\right)^{N/2}\left[\frac{1}{b}\exp\left(\frac{\beta a}{b}\right)\left(\frac{\beta a}{b}\right)^{-\left(\frac{\beta a+\gamma}{b}\right)}\Gamma\left(\frac{\beta a+\gamma}{b}\right)\right]^{N-N_0} \\ &\quad\cdot\left[\frac{1}{b_0}\exp\left(\frac{\beta a}{b_0}\right)\left(\frac{\beta a}{b_0}\right)^{-\left(\frac{\beta a+\gamma}{b_0}\right)}\Gamma\left(\frac{\beta a+\gamma}{b_0}\right)\right]^{N_0}. \end{aligned} \tag{3.1}$$

The partition function splits into separate factors corresponding to hard and soft springs. The internal energy of the chain reads

$$E = -\frac{\partial}{\partial\beta}\ln Z(\beta,\gamma) = \frac{N}{2\beta} + (N - N_0)\langle u\rangle + N_0\langle u_0\rangle ,$$

with

$$\langle u\rangle = \frac{a}{b}\left[\ln\left(\beta\frac{a}{b}\right) - \Psi\left(\beta\frac{a+P}{b}\right)\right] + \frac{P}{b}$$

and (3.2)

$$\langle u_0\rangle = \frac{a}{b_0}\left[\ln\left(\beta\frac{a}{b_0}\right) - \Psi\left(\beta\frac{a+P}{b_0}\right)\right] + \frac{P}{b_0}$$

expressing the average potential energies of a hard and a soft spring, respectively.

Now we are going to elucidate soliton-induced effects in the thermal behaviour of nonuniform Toda chain. Because solitons are destroyed at open ends, we are led to fix the total length of the chain, which can be calculated from the partition functions (3.1). Assuming further a vanishing number of soft springs embedded in a chain of hard springs, i.e. a strongly "diluted solution" $\eta = N_0/N \doteq 0$, whereas $N \to \infty$ and $N_0 \to \infty$, one obtains for the pressure [6]

$$P = \frac{b}{\beta} \Psi^{-1}\left[\ln\left(\beta \frac{a}{b}\right)\right] - a\,. \tag{3.3}$$

By the help of (3.2) and (3.3) we can now calculate the average potential energies of the springs. Especially in the high-temperature limit the ratio of the average potential energies of a soft and a hard spring yields

$$\frac{\langle u_0\rangle}{\langle u\rangle} \underset{\beta\to 0}{\approx} \frac{b}{b_0}\,. \tag{3.4}$$

The ratio of spring energies as well as their absolute values in units of thermal energy are presented in Fig. 2 in dependence on temperature. In the high-temperature limit thermal energy is partitioned mainly to the kinetic degrees of freedom. Whereas the ratio of potential energies of soft and hard springs tends up to the maximum value defined by (3.4), the ratio of potential and kinetic energy tends to zero. Hence only a vanishing part of thermal energy is located at soft springs. At low temperatures equipartition theorem is valid and thermal energy is shared equally among all microscopic degrees of freedom. Between these limits there is an optimum temperature where the potential energy of soft springs amounts to a multiple of $kT/2$ and localization of thermal energy takes place.

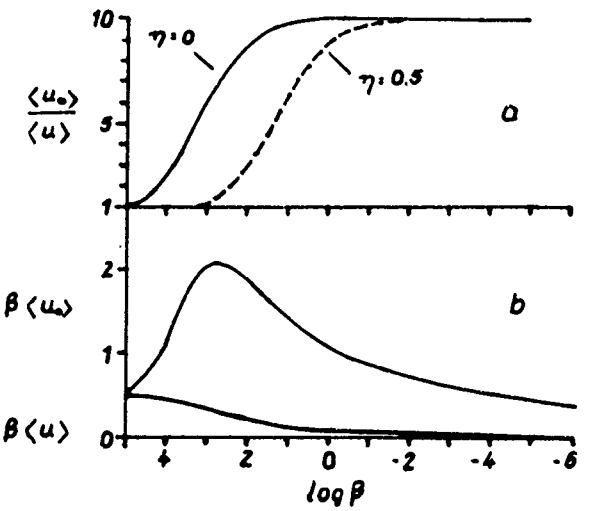


Fig. 2
Average spring energies of soft and hard springs in a nonuniform Toda lattice with fixed average length (cf. Fig. 1) in dependence on $\beta = 1/kT$.
a) The mutual ration of spring energies for two different concentrations $\eta = N_0/N$ of soft springs. Maximum deviation from equipartition of potential energies is obtained in the high-temperature limit for a vanishing number of soft springs.
b) Spring energies in units of thermal energy for a vanishing number of soft springs ($\eta = 0$). In an intermediate temperature range beyond both the harmonic and the hard-core limit a localization of thermal energy takes place at the soft springs

The peculiarities in thermal behaviour of a nonuniform Toda chain can be attributed to the properties of solitons which are the nonlinear modes of motion. Bolterauer and Opper [7] reconstructed the free energy for a uniform Toda chain from a gas of noninteracting solitons. This approach yields reasonable results in case of a fixed total length as temperature T tends to infinity. On these conditions N strongly localized solitons – each of average energy $kT/2$ – are excited on a lattice of N springs. Hence each soliton possesses an average potential energy $\langle u_s\rangle$ equal to the spring energy $\langle u\rangle$. The average distance in time between adjacent solitons can be obtained from (2.2),

$$T = \tau\varkappa \sqrt{\frac{m}{ab}}\, \frac{\varkappa}{\sinh\varkappa}\,. \tag{3.5}$$

Using (2.5) we can approximate the average potential energy of a hard spring by

$$\langle u\rangle \approx \langle u_s\rangle \approx \frac{1}{T}\int_{-T/2}^{+T/2} \mathrm{d}t\, \frac{a}{b} \sinh^2\varkappa\, \mathrm{sech}^2\left(\sqrt{\frac{ab}{m}}\sinh\varkappa t\right)$$
$$\approx \frac{2a}{b}\,\frac{\sinh^2\varkappa}{\varkappa}\,.$$

On the other hand the average energy of one soliton equals $1/2\beta$ if $\beta \to 0$. With (2.6) we find

$$\frac{2a}{b}\sinh^2\varkappa \approx \frac{1}{2\beta}\,,$$

hence

$$\beta\langle u\rangle \approx \left(2\,\mathrm{arcsinh}\sqrt{\frac{b}{4a\beta}}\right)^{-1} \to 0\,.$$

Due to the perfect repulsion between particles the extremely narrow and fast solitons dominating the dynamics at high temperatures do not contribute to the average potential energy of springs but to the kinetic energy of particles.

Now we are going to consider the average potential energy $\langle u_0\rangle$ of the soft spring. Solitons are transmitted to it with an average period $1/T$ given by (3.5). In the high-temperature limit every excitation of the soft spring can be described by a strongly localized transmitted soliton (2.7) and we get

$$\langle u_0\rangle \approx \frac{1}{T}\int_{-T/2}^{+T/2} \mathrm{d}t\, \frac{a}{b_0} \sinh^2\varkappa_0\, \mathrm{sech}^2\left(\sqrt{\frac{ab_0}{m}}\sinh\varkappa_0 t\right)$$
$$\approx 2\frac{a\sinh^2\varkappa}{b_0\,\varkappa} \approx \frac{b}{b_0}\langle u\rangle\,.$$

This is the result (3.4) derived above. So the twofold deviation from equipartition of energy can be explained by non-interacting solitons in the limit of infinite temperatures.

In the intermediate temperature range that is characterized by a localization of thermal energy at the soft spring non-soliton modes participate in the dynamics too. But obviously solitons are responsible for the transfer of thermal energy to the soft springs. This can be understood intuitively. In the high-temperature limit discussed above the mean time T between incident solitons was much greater than the time τ_0 describing the duration of incidence, i.e. $T \gg \tau_0 > \tau$. With decreasing temperature thermal solitons become less localized and both times will be comparably. Thus a substantial superposition of incident solitons as presented in Fig. 1 takes place in the soft spring giving rise to the elevation of average potential energy for intermediate temperatures. At low temperatures however strong interaction is no more confined to the soft spring and individual solitons are destroyed.

At the end of this section we shall discuss the possible relevance of thermal energy localization to reaction theory within the frame of simple transition state theory. We consider an ensemble of particles moving in an initial well with an adjacent barrier of height ΔU forming the boundary of the well. TST assumes all states in the well and around the barrier being populated according to equilibrium distribution. If $U(r_0)$ models the shape of the potential inside the well and $\beta\Delta U \gg 1$ we obtain for the rate of transitions over the barrier [1]

$$k_{\mathrm{TST}} = \frac{\int_0^{+\infty} \mathrm{d}p_0 \frac{p_0}{m} \exp(-\beta H(p_0, r_0^{\mathrm{B}}))}{\int_{-\infty}^{+\infty} \mathrm{d}r_0 \int_{-\infty}^{+\infty} \mathrm{d}p_0 \exp(-\beta H(p_0, r_0)}, \tag{3.6}$$

r_0^{B} denotes the top of the barrier and $U(r_0^{\mathrm{B}}) = \Delta U$. Approximating $U(r_0)$ by a harmonic potential (1.1) we get the well known formula [1]

$$k_{\mathrm{TST}} = \frac{\omega_0}{2\pi} \exp(-\beta\Delta U). \tag{3.7}$$

Now we consider a reaction oscillator coupled to a nonlinear molecular chain. The shape of the well may be described by a Toda potential (1.2). According to the assumption of TST the reaction oscillator is in thermal equilibrium with its surroundings, which is here represented as canonical ensemble by the effective Hamiltonian

$$H(p_0, r_0) = \frac{p_0^2}{2m} + U(r_0) + Pr_0.$$

Physically this result can be interpreted in the following way. The soft reaction oscillator behaves as subsystem in an isobaric-isothermal ensemble [10]. In other words the action of the hard springs may be reduced to the pressure they produce in the system.

The transition rate for the coupled nonlinear reaction oscillator follows from (3.6):

$$k^*_{\mathrm{TST}} = \frac{n_0 \left(\frac{\beta m\omega_0^2}{b_0^2}\right)^{\beta\left(\frac{m\omega_0^2}{b_0^2} + \frac{P}{b_0}\right)}}{\sqrt{2\pi m}\,\Gamma\left[\beta\left(\frac{m\omega_0^2}{b_0^2} + \frac{P}{b_0}\right)\right]} \cdot \exp\left[-\beta\left(\Delta U + Pr_0^{\mathrm{B}} + \frac{m\omega_0^2}{b_0^2}\right)\right]. \tag{3.8}$$

Here the condition $\beta(\Delta U + Pr_0^{\mathrm{B}}) \gg 1$ has to be fulfilled in order to applicate (3.6). The reaction oscillator may be enclosed by a sufficiently large Toda ring with parameters a, b and m. Then formula (3.3) defines the force P in (3.8). At low temperatures the rate (3.8) reduces to the result (3.7). The top of the barrier may be located at a negative reaction coordinate, $r_0^{\mathrm{B}} = -|r_0^{\mathrm{B}}|$, corresponding to a critical mutual distance between reactive molecular groups. Then with increasing temperature a considerable rate enhancement is attained (Fig. 3). The arbitrarily chosen reaction coordinates in Fig. 3, e.g., could be related to catalytically relevant slow-frequency motions observed in enzyme macromolecules [5]. Recently Muto et al. [8] calculated a significant number of solitons generated at physiological temperature in a Toda lattice model of DNA with similar spring parameters as used in Fig. 3. If thermal solitons are present in biomolecular strings they are likely to support energetic activation of functional processes.

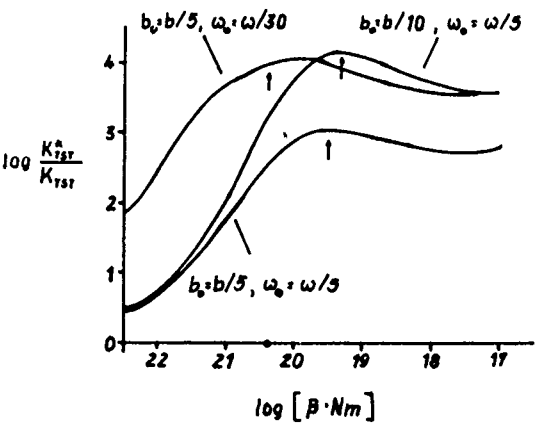


Fig. 3
Enhancement of a hypothetical slow-frequency transition process ($m\omega_0^2 = a_0 b_0$) by coupling to a hydrogen-bonded molecular chain with bond parameters fitted to a Toda potential, $a = 5.6 \cdot 10^{-10} N$, $b = 9 \cdot 10^{10} m^{-1}$ ($m\omega^2 = ab$) according to transition state theory. The relative barrier height $\beta\Delta U = 20$ was chosen to be constant all over the temperature range. The dot on the abscissa marks physiological temperature (310 K) and the arrows indicate the maxima of relative potential energy $\beta\langle u_0\rangle$

4. Activation Processes in Solutions of Soft Spheres in a Hard-Sphere Solvent

Let us first consider a linear chain of hard balls in contact. As everybody knows from popular experiments at school or the basic course in physics, a kicking of the first ball leads

to an excitation running through the chain thereby leaving the intermediate balls essentially at rest. When the excitation arrives at the opposite end of the chain the outer ball is elongated. This experiment is a simple demonstration of a soliton-like excitation. If we put a soft ball into the chain the excitation will be kept there for some time performing an elastic deformation. It should be possible to demonstrate also fusion effects of the type described briefly in the second paragraph and in more detail in a previous paper [3] with such a simple device (there are however no experiments known to the authors). The soft ball serves as a kind of buffer accumulating collisional energy. The result of the activation could be, e.g., a destruction of the soft ball after a critical compression. The theory developed in the previous section applies qualitatively for the prediction of the destruction rate.

Conclusively we want to illustrate that the feature of a soft volume part to get activated by accumulation of collisional energy is not restricted to quasi-one-dimensional systems, even if the interpretation of such an effect by solitons or solitary-like excitations will not be applicable to three-dimensional systems generally. Let us consider a solution of soft spheres in a hard-sphere solvent as simple model for a binary mixture of "soft" and "rigid" molecules. We do not start with a microscopic description as for the Toda chain but simply assume the validity of the compression law (1.2), where now the quantity r_0 denotes the deviation of the volume v_0 of the spheres with radius R_0 from its value $v_0^{(0)}$ at zero pressure and zero temperature:

$$r_0 = v_0 - v_0^{(0)}, \qquad v_0 = \frac{4\pi}{3} R_0^3. \tag{4.1}$$

The parameter b_0 describes the stiffness of the soft-sphere volume now. The soft spheres may be embedded in a solvent of (absolutely) hard spheres. Then in the limit of infinite dilution the pressure P in the solution equals the hard-sphere pressure which reads in the Carnahan-Starling approximation [9]:

$$P = \frac{\varrho}{\beta} \frac{1+f+f^2}{(1-f)^3} = C(\varrho)\,\beta^{-1}. \tag{4.2}$$

Here

$$f = \frac{4\pi}{3} \varrho R^3$$

denotes the packing factor of the hard spheres with radius R and ϱ is the density. Considering an ensemble with constant density the pressure P proves to be a linear increasing function of temperature β^{-1}. Following now the analogy explained in the previous section the soft spheres may be considered as subsystems embedded into an isobaric-isothermal ensemble. Then the average potential energy of an embedded soft sphere can be calculated according to

$$\langle u_0 \rangle = \frac{\int_{-\infty}^{+\infty} dr_0\, U(r_0) \exp[-\beta(U(r_0) + Pv_0)]}{\int_{-\infty}^{+\infty} dr_0 \exp[-\beta(U(r_0) + Pv_0)]}.$$

Inserting (1.2), (4.1) and (4.2) we obtain

$$\langle u_0 \rangle = \frac{m\omega_0^2}{b_0^2}\left[\ln\left(\frac{\beta m\omega_0^2}{b_0^2}\right) - \Psi\left(\frac{\beta m\omega_0^2}{b_0^2} + \frac{C(\varrho)}{b_0}\right)\right] + \frac{C(\varrho)}{b_0\beta}. \tag{4.3}$$

Now we are going to consider the part of thermal energy partitioned to the soft spheres, $\beta\langle u_0\rangle$, in dependence on temperature. Especially for high temperatures we find from (4.3)

$$\beta\langle u_0\rangle \underset{\beta\to 0}{\approx} \frac{C(\varrho)}{b_0}.$$

Depending on this value we find qualitatively different behaviour, as can be seen from Fig. 4. For $C(\varrho)/b_0 > 0.5$ the relative potential energy is increasing monotonously with temperature, in the idealized case of a Hooke's compression law even unbounded (see curve 1 in Fig. 4, a vanishing stiffness $b_0 = 0$ corresponds to the potential-energy function (1.1)). For $C(\varrho)/b_0 < 0.5$ however the curves display a maximum corresponding to a localization of thermal energy at a finite temperature. A comparison of the curves 3 and 4 shows, that these maxima are raised and shifted towards zero temperature for increasing stiffness of the soft spheres. This behaviour is due to the somewhat artificial assumption of an infinite stiff hard-sphere potential even for vanishing temperatures. A more comprehensive discussion on solutions of soft spheres in stiff solvents will be given elsewhere. However already this present short analysis indicates that some of the main results abtained for the Toda chain persist in three-dimensional systems.

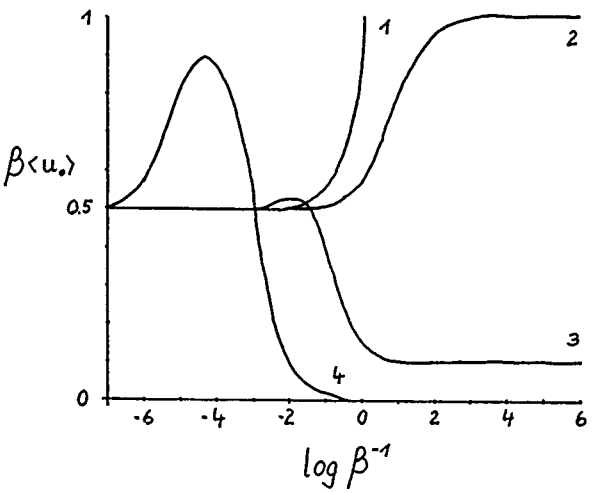


Fig. 4
Average potential energy (in units of thermal energy) of a soft Toda sphere which is surrounded by a constant-density ensemble of hard spheres ($C(\varrho) = 1$) according to formula (4.3) vs. temperature β^{-1}. The eigenfrequency of the soft sphere is given by $m\omega_0^2 = 1$ and the stiffness parameter b_0 varies for the different curves. 1 – $b_0 = 0$, 2 – $b_0 = 1$, 3 – $b_0 = 10$, 4 – $b_0 = 1000$

5. Conclusions

The dynamical effect of soliton fusion provides an efficient mechanism for localization of as well thermal as nonthermal energy at activation sites that are part of a nonlinear molecular chain. We proved the existence of an optimum temperature, where thermal energy is preferably partitioned to few soft springs embedded into a nonuniform Toda chain consisting mainly of hard springs. Here we restricted ourselves to the investigation of the energetic activation of the soft springs. For application to transition processes, e.g. chemical reaction, the simple TST developed in the third paragraph has to be replaced by a theory starting from a nonequilibrium population of particles localized near the bottom of the well. This implies corrections of the TST reaction rate in dependence on the shape of the barrier.

In the last section we intended to demonstrate that the effect of thermal energy localization persists for solutions of soft spheres in hard-sphere solvents. The presented theory is based on pure thermodynamical grounds since a statistical description of the underlying dynamics of the three-dimensional many-body system by nonlinear elementary excitations seems to be impossible. Obviously the soft spheres serve as a kind of buffer accumulating collisional energy from the surroundings. A further investigation of thermal energy localization for three-dimensional systems could be of a principal interest to reaction theory.

References

[1] H. A. Kramers, Physica *7*, 284 (1940); for a review see: P. Hänggi, P. Talkner, and M. Borkovec, Rev. Mod. Phys. *62* 251 (1990).
[2] M. Toda, Theory of nonlinear lattices, Springer, Berlin 1981.
[3] W. Ebeling and M. Jenssen, Physica D *32*, 183 (1988).
[4] C. Camacho and F. Lund, Physica D *26*, 379 (1987).
[5] W. Ebeling, M. Jenssen, and Yu. M. Romanovskii, in: Irreversible Processes and Selforganization, eds. W. Ebeling and H. Ulbricht, pp. 7–24, Teubner, Leipzig 1989.
[6] M. Jenssen, Sharing of Thermal Energy in a Nonuniform Toda Lattice, submitted to Phys. Lett. A (1990).
[7] H. Bolterauer and M. Opper, Z. Phys. B *42*, 155 (1981).
[8] V. Muto, A. C. Scott, and P. L. Christiansen, Phys. Lett. A *136*, 33 (1989).
[9] R. Becker, Theorie der Wärme, Springer, Berlin, 1955.
[10] N. F. Carnahan and K. E. Starling, J. Chem. Phys. *51*, 632, (1969).

Presented at the Discussion Meeting of the Deutsche Bunsen-Gesellschaft für Physikalische Chemie "Rate Processes in Dissipative Systems: 50 Years after Kramers" in Tutzing, September 10–13, 1990 E 7508

Hopping of Quantum Particles on Crystals with Energy Disorder: Influence on Spin Resonance

P. Reineker and J. Köhler

Abteilung Theoretische Physik, Universität Ulm, Albert-Einstein-Allee 11, 7900 Ulm, Germany

Diffusion / Disorder / Energy Transfer / Spectroscopy, Electron Spin Resonance / Transport Properties

For spin 1/2 quantum particles hopping on energetically disordered lattices paramagnetic lineshapes and free induction decay (FID) signals are calculated as a function of the hopping rate γ between nearest neighbours. The energy disorder is modeled by local magnetic fields chosen from a Gaussian or dichotomic distribution. For motion on a linear chain it is derived – using a continued fraction method – that the FID signal shows a cross over from an $\exp(-t^{3/2})$ law to an asymptotic $\exp(-t)$ behaviour. Preliminary investigations for 2- and 3-dimensional lattices have been performed using algebraic multigrid methods.

1. Introduction

In recent years organic metals [1] have been the subject of many experimental and theoretical investigations. One of the aims of these investigations was to understand the transport properties of charge carriers. In these materials, e.g. the fluoranthene radical cation salt $(FA)_2PF_6$, the organic ions (donors) are frequently arranged in stacks with the inorganic counterions (acceptors) sitting between the stacks [2]. The charge transport is assumed to occur in a quasi-one-dimensional manner along the organic stack.

One way of getting more detailed information on the transport of charge carriers is from the investigation of spin resonance. On account of the interaction between the spins of the charge carrier and the protons localized in the fluoranthene units, electron spin resonance (ESR) properties, e.g. the electron spin echo (ESE) decay, are influenced by the motion of the charge carrier. ESE decay measurements for $(FA)_2^+ [(SbF_6)_{1-x} (PF_6)_x]^-$, $x \approx 0.5$ [3] show that the ESE signal decays according to $\exp(-t^{3/2})$ for small times and purely exponentially for large times. In [3] this was interpreted as a transition from 1- to 3-dimensional motion of the particle. On the other hand the ESE in $(FA)_2PF_6$ [4] decays in a purely exponential manner. Thus, from experimental results the question arises whether and why the ESE decay occurs according to $\exp(-(\gamma t)^{3/2})$ or as $\exp(-\gamma t)$.

A similar question comes up also from theoretical investigations of the free induction decay (FID) which for homogeneous systems contains the same information as the

 © VCH Verlagsgesellschaft mbH, W-6940 Weinheim, 1991 0005-9021/91/0303-0362 $ 3.50+.25/0

ESE decay for inhomogeneous ones. Analytical investigations in [5] arrived at the conclusion that the FID decay occurs as $\exp(-(\gamma t)^{3/2})$, Monte-Carlo simulations carried out in [6] led to the conclusion that at least asymptotically the decay follows an exponential law. One of the purposes of this paper is to show that there is a crossover between the two decay laws.

2. Theory of ESR Line Shape and Free Induction Decay

2.1. ESR Line Shape and Free Induction Decay

From linear response theory the ESR line shape is given by the imaginary part of the magnetic susceptibility

$$\chi''(\omega) = \frac{1}{2N}\left(\frac{e}{m}\right)^2 (1-e^{-\beta\omega})\,\mathrm{Re}\int_0^\infty dt\, e^{-i\omega t}\underbrace{\langle S^- S^+(t)\rangle}_{F(t)}. \tag{1}$$

N is the number of unit cells, e and m charge and mass of the charge carrier, $\beta = (kT)^{-1}$, and $F(t) = \langle S^- S^+(t)\rangle$ is the two time correlation function which describes the FID:

$$F(t) = \langle S^- S^+(t)\rangle = \int_{-\infty}^{\infty} dt\, e^{i\omega t} F(\omega). \tag{2}$$

The comparison with (1) shows that – apart from constant factors – the ESR line shape is given by

$$F(\omega) = I(\omega) = \frac{1}{2\pi}\int_{-\infty}^{\infty} dt\, e^{-i\omega t} F(t) = \mathrm{Re}\frac{1}{\pi}\int_0^\infty dt\, e^{-i\omega t} F(t). \tag{3}$$

2.2. Model Hamiltonian

The Hamiltonian of our model is given by

$$H = \underbrace{\sum_{n,n'} h_{n,n'}(t)\, a_n^+ a_{n'}}_{\text{incoherent electron transport}} + \underbrace{\omega_0 S^z}_{\text{Zeeman}} + \underbrace{H'}_{\text{interaction}} \tag{4}$$

The first part describes the hopping motion of the charge carrier. The $h_{n,n}(t)$ are the fluctuations of the transfer matrix element (in the sense of the Haken-Strobl model [7 – 9]) and mathematically described by a δ-correlated Gaussian process with correlation functions

$$\langle h_{n,n\pm1}(t)\, h_{n,n\pm1}(t')\rangle = \langle h_{n,n\pm1}(t)\, h_{n\pm1,n}(t')\rangle = 2\gamma\delta(t-t'). \tag{5}$$

The next term is the Zeemann energy of the charge carrier spin in an external magnetic field. The last term finally describes the hyperfine structure interaction between the electron and proton spins. Explicitely, this term is given by

$$H' = A\sum_n \boldsymbol{S}\boldsymbol{I}_n a_n^+ a_n = A\sum_n (S^z I_n^z + S^+ I_n^- + S^- I_n^+)\, a_n^+ a_n, \tag{6}$$

which means that in our model calculation we have taken into account only the contact interaction (A is the hyperfine coupling constant). To complete the model description, we mention that lateron in the numerical evaluation we shall replace the quantum mechanical hyperfine structure interaction Hamiltonian by a simpler Hamiltonian with frozen proton spins, whose orientation along the z-direction is random. For this simplified model the Hamiltonian becomes

$$H' \to \sum_n \omega_n a_n^+ a_n S^z. \tag{7}$$

2.3. Analytical Evaluation

In the framework of the Mori-formalism [10] the equation of motion for the FID decay function is given by

$$\dot F(t) = i\Omega F(t) - \int_0^t dt'\, M(t-t')F(t') \tag{8}$$

$$\Omega = (S^+, LS^+)\cdot(S^+, S^+)^{-1} \tag{9}$$

$$M(t) = (i\Omega L' S^+, \vec T e^{i\int_0^t d\tau QL(\tau)} iQL' S^+)\cdot(S^+, S^+)^{-1}. \tag{10}$$

In this equation Ω is the frequency, $M(t)$ the memory function, and L the Liouville operator. τ_M is the decay constant for the memory function, and τ_c the one for the free induction signal.

If the memory function is evaluated in Born-approximation, we arrive at

$$M(t) = e^{i\Omega t}\frac{A^2}{4}\langle a_0^+ a_0 \vec T \exp\left(i\int_0^t dt'\, L_M(t'))\, a_0^+ a_0\right\rangle = e^{i\Omega t}\frac{A^2}{4}P(t). \tag{11}$$

The inspection of this result shows that $P(t)$ is the conditional probability of finding the particle at the origin at time t, if it was there at the initial time: $P(t) = P(r=0, t; r=0, t=0)$. The analytical results [5, 11, 12] are summarized in the following.

If the decay time of the memory function is much larger than the decay time of the correlation function, i.e.

$$\tau_M \gg \tau_c, \quad \text{or} \quad \gamma/A \ll 1, \tag{12}$$

which describes the case of slow particle motion, the ESR line is inhomogeneously broadened with the inhomogeneous width determined by the hyperfine structure interaction. The homogeneous width of one component is determined by the life time of the charge carrier at a particular site, i.e. by the hopping rate γ.

In the opposite limit when the decay time of the memory function is much smaller than the decay time of the correlation function, i.e.

$$\tau_M \ll \tau_c, \quad \text{i.e} \quad \gamma/A \gg 1, \tag{13}$$

describing the case of fast particle motion, the FID decay function can be taken out of the integral in [8]. In the interaction representation we finally arrive at

$$\dot{\tilde{F}}(t) = -\int_0^t \mathrm{d}t' \tilde{M}(t')\tilde{F}(t) \rightarrow \tilde{F}(t) = \exp\left(-\int_0^t \mathrm{d}t'(t-t')\tilde{M}(t')\right), \tag{14}$$

where the expression on the righthand side is the solution of the differential equation on the left. For sufficiently long times and taking into account that in the case considered the memory function decays fast, the second term in the exponent can be neglected and asymptotically we arrive at an exponential decay of the correlation function:

$$\tilde{F}(t) = \exp\left(-t\int_0^\infty \mathrm{d}t' \tilde{M}(t')\right). \tag{15}$$

After this rather general consideration, let us investigate the influence of the dimensionality of the motion on the FID decay. In the case of the purely incoherent motion the probability of finding the particle at lattice site n is given by the modified Bessel function of order n [13], if the particle was at the origin at the initial time. Therefore $P(t)$ from above is given by the modified Bessel function of order 0. We therefore have

$$\tilde{M}(t) = \frac{A^2}{3}\mathrm{e}^{-\gamma t} I_0(4\gamma t) \xrightarrow{\text{continuum}} (8\pi\gamma t)^{-1/2} \text{ (algebraic decay)} \tag{16}$$

where the expression in the righthand side describes the behaviour in the continuum limit. If this is inserted into [14], we get for the FID decay

$$\tilde{F}(t) = \exp(-(\Delta\omega_\mathrm{d} t)^{3/2}) \quad \text{dimension } d\text{: } 1\,. \tag{17}$$

In the case of independent random motion in the various space directions, the probability is given by the product of Bessel functions with a corresponding behaviour in the continuum limit. The calculation of the FID then gives

$$\tilde{F}(t) = \exp(-(\Delta\omega_\mathrm{d} t) \quad \text{dimension } d\text{: 2 and 3}\,. \tag{18}$$

Eq. (17) is just the result obtained in [5]. The evaluation of the ESR linewidth in dependence of the dimension results in

$$\Delta\omega_\mathrm{d} = \frac{1}{\tau_\mathrm{c}} = (\langle\omega_n^2\rangle^2/\gamma)^{1/3} \quad \text{dimension } d\text{: } 1 \tag{19}$$

$$\Delta\omega_\mathrm{d} = \frac{1}{\tau_\mathrm{c}} = \langle\omega_n^2\rangle^2/\gamma \qquad \text{dimension } d\text{: 2 and 3}\,. \tag{20}$$

3. Numerical Evaluation of Spin Resonance Properties

Writing out explicitly [2] we get

$$F(t) = \sum_n \sum_{s=\uparrow\downarrow} \langle ns|S^-\left\langle \tilde{T}\exp\left\{\mathrm{i}\int_0^t \mathrm{d}\tau L(\tau)\right\} S^+\right\rangle_{\mathrm{RW}} \varrho_0 |ns\rangle. \tag{21}$$

The states $|ns\rangle$ describe a quantum particle at site n with spin s, ϱ_0 is the density operator at the initial time and the index RW means averaging over the random walk. Assuming as initial condition equal occupation probabilities at each lattice site, (21) may be written as follows:

$$F(t) = \frac{1}{N}\sum_n \langle\downarrow n|\left\langle \tilde{T}\exp\left\{-\mathrm{i}\int_0^t \mathrm{d}\tau L(\tau)\right\} S^-\right\rangle_{\mathrm{RW}} |n\uparrow\rangle \tag{22}$$

$$= \frac{1}{N}\sum_n c_n(t). \tag{23}$$

The functions $c_n(t)$ are defined by the last equality, and are to be determined from the following set of differential equations:

$$\dot{c}_n(t) = (\mathrm{i}\omega_n - 4\gamma)\, c_n + 2\gamma(c_{n+1} + c_{n-1})\,. \tag{24}$$

In matrix form this equation reads

$$\dot{\boldsymbol{c}} = \boldsymbol{A}\boldsymbol{c}\,. \tag{25}$$

In this equation A is a matrix with random diagonal elements ω_n. After a Laplace transformation this set of differential equations is transformed into a set of algebraic ones. For motion of the particle in one dimension, this equation is tridiagonal and can easily be solved with the help of continued fractions. For 2- and 3-dimensional motion we have used multigrid methods [14].

Fig. 1 shows line shapes calculated for motion of the particle on a linear chain with 10^7 sites for dichotomic disorder of the local magnetic fields and various hopping rates, normalized to the strength of the local magnetic fields (strengths ± 1, i.e. $\sigma = 1$). For very small hopping rates as compared to the strength of the local magnetic field, i.e. $\gamma = 0.1$, we have two ESR lines with positions determined by the two values of the local magnetic fields. The width of the lines is given by the life time at the site and thus determined by the hopping rate γ. When γ becomes comparable to the distance in the line positions ($\gamma = 0.5$), the two lines merge into a single line. With increasing hopping rate ($\gamma = 10$, 100) the line narrows; the narrowing, however, is not $\propto \gamma^{-1}$ but given by (19). Furthermore, the comparison with the dashed Lorentzian line in the figure for $\gamma = 100$ shows that in this range of the hopping rates the line shape is not Lorentzian. Increasing γ further, the ESR line becomes structured. The origin of these structures are clusters in the dichotomic distribution of the spins [12]. Increasing the hopping rate further to $\gamma = 10^{10}$, these structures are finally averaged out and we arrive at a Lorentzian line, whose width is $\propto \gamma^{-1}$.

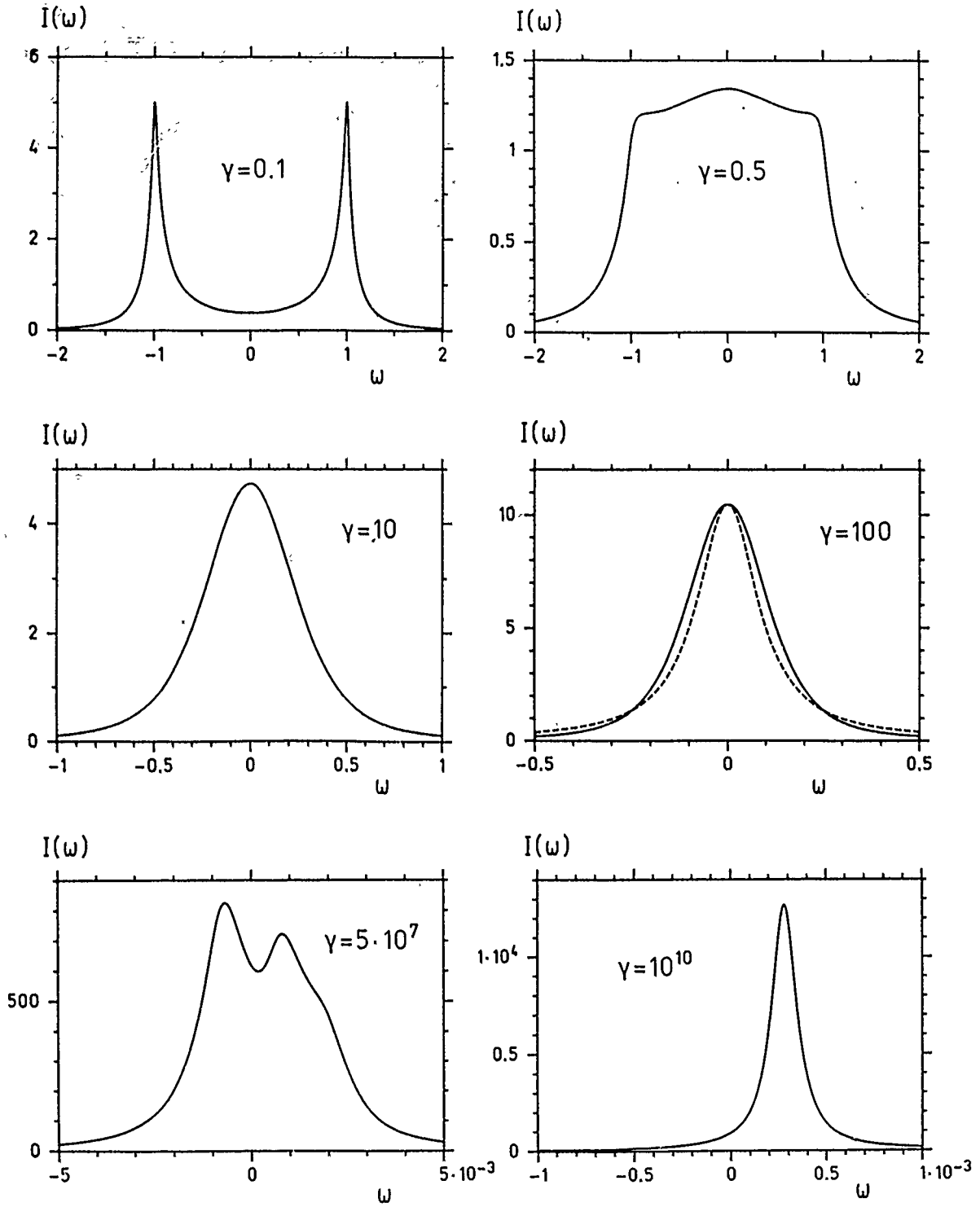


Fig. 1
Line shape as a function of the hopping rate γ for a 1-dimensional motion and dichotomic disorder ($\sigma = 1$, $N = 10^7$)

Fig. 2 shows the FID signal for a chain with $N = 10^7$ sites (to avoid finite size effects), a hopping rate $\gamma = 1000$, and a Gaussian random distribution of the local magnetic fields. The curves are obtained by Fourier transforming line shapes obtained as described in connection with Fig. 1. In the left figure in the upper row, $F(t)$ as a function of t is represented and shows the decay of the FID signal. The figure on the right hand side shows $(-\ln F(t))/t^{3/2}$ as a function of t. In the lower row we have represented $F(t)$ in a logarithmic scale as a function of $t^{3/2}$ in the left figure, and as a function of t on the right hand side. The comparison with the dashed straight line shows that for short times the FID signal decays according to an $\exp(-(\gamma t)^{3/2})$ law and for large times as $\exp(-\gamma t)$. Therefore our calculations show that we have a crossover between the two decay laws, and that the analytical result of [5] holds for short times whereas

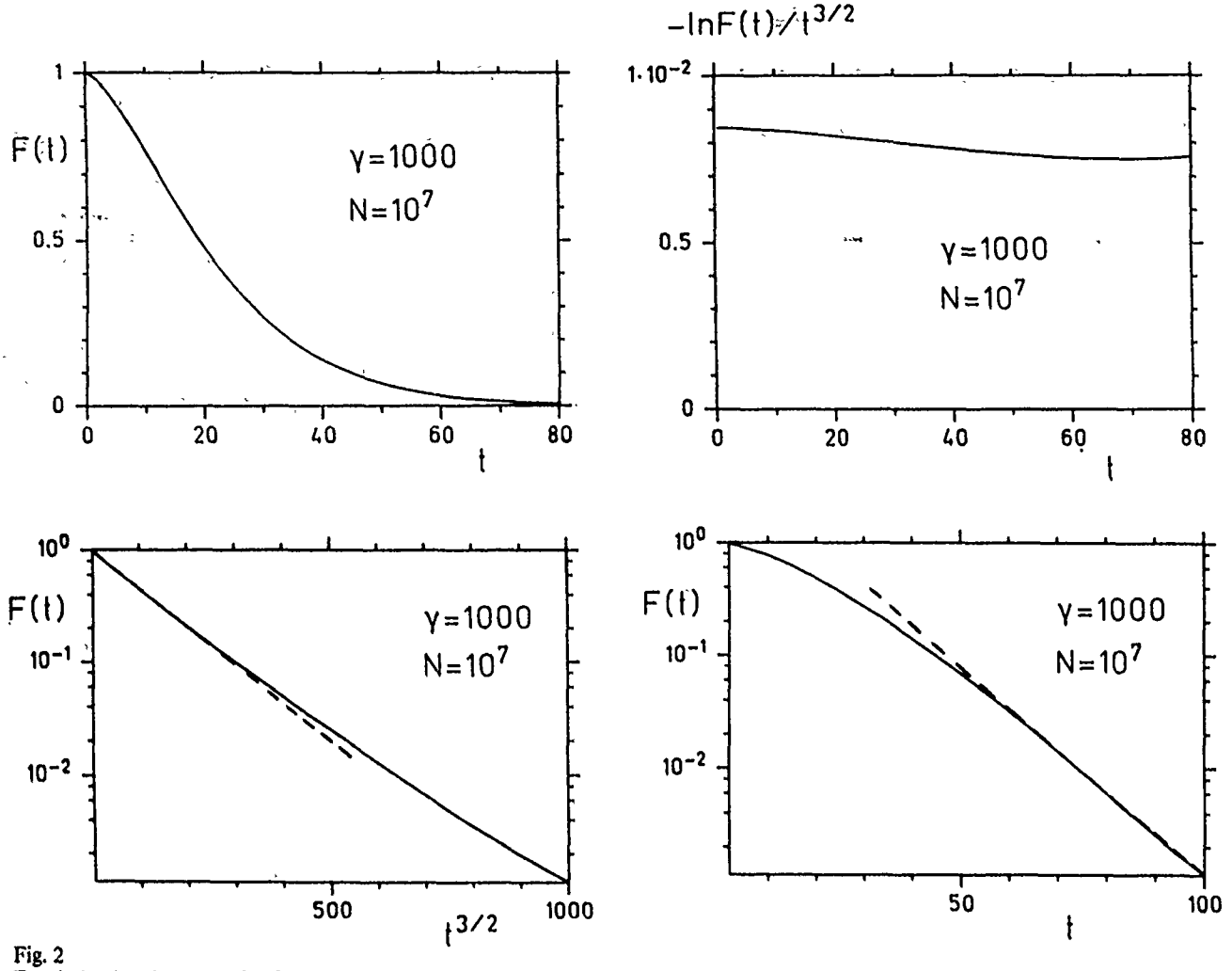


Fig. 2
Free induction decay $F(t)$ for Gaussian distributed local fields and 1-dimensional motion of the particle on a chain with 10^7 sites. Hopping rate $\gamma = 1000$ in units of the standard deviation of the local magnetic fields

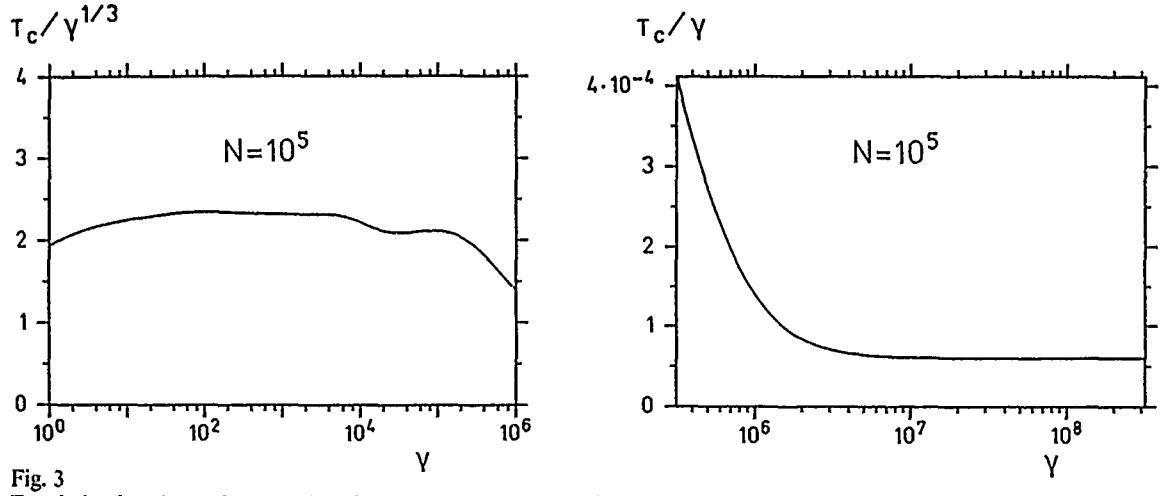


Fig. 3
Free induction decay time as a function of the hopping rate γ in 1 dimension

the simulation result of [6] is valid asymptotically. Furthermore our results also shows that the transition between the two decay laws can also occur for purely 1-dimensional hopping and does not necessarily allow the conclusion that there is a transition from 1- to 3-dimensional motion.

From the analysis of the numerical line shapes we have derived the free induction decay time (maximum of the normalized line shape curve) as a function of the hopping rate for a chain with $N = 10^5$ sites. The plot of $\tau_c/\gamma^{1/3}$ as a function of γ in Fig. 3 on the lefthand side shows that for

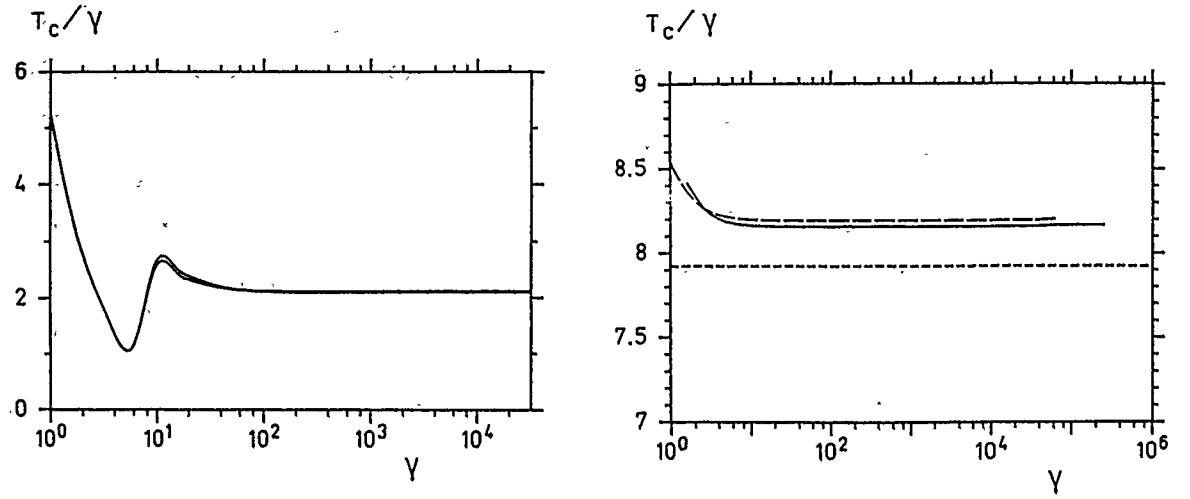


Fig. 4
τ_c/γ as a function of the hopping rate γ for a 300 × 300 lattice (left figure). The two curves correspond to two realizations of a Gaussian process. The figure on the righthand side shows the same quantity for a 28 × 28 × 28 lattice. The full curve represents a Gaussian distribution, short dashes a dichotomic process, long dashes an analytical calculation in the framework of the Mori-formalism

small values of γ the correlation time is proportional to $\gamma^{1/3}$ and thus the linewidth is proportional to $\gamma^{-1/3}$. On the other hand from the figure on the righthand side we see that for large values of γ the correlation time is proportional to γ and the linewidth therefore proportional to γ^{-1}.

Fig. 4 shows preliminary numerical results for the normalized correlation time τ_c/γ for 2- and 3-dimensional lattices obtained [11] with the help of multigrid methods [14]. From the figure for the 2-dimensional 300 × 300 lattice we see that for $\gamma > 100$ (the hopping rates are normalized to the standard deviation of the local field) $\tau_c \propto \gamma$, i.e. the line is motionally narrowed and Lorentzian. The two curves in the figure on the lefthand side correspond to two realizations of a Gaussian stochastic process. The figure on the right shows also τ_c/γ, however now for a 28 × 28 × 28 lattice. In this case $\tau_c \propto \gamma$ as soon as $\gamma > 10$. The full and long-dashed curves correspond to a Gaussian and a dichotomic process, respectively. The short dashed curves are analytical results obtained from the Mori-formalism.

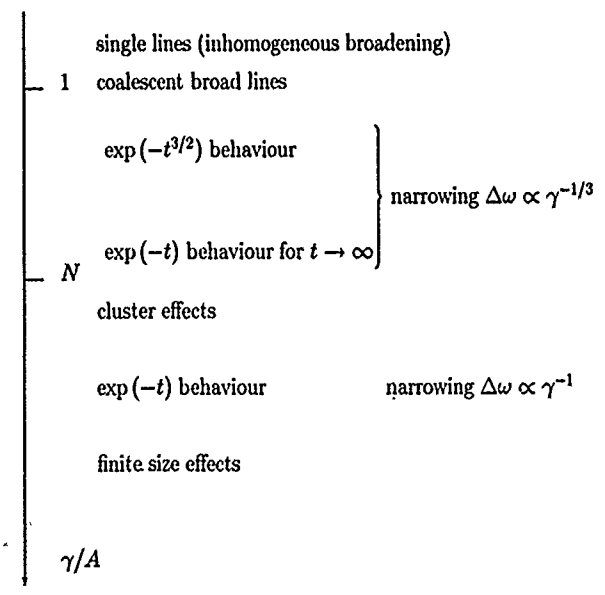


Fig. 5
Summary of spin dynamics for a particle hopping on a linear chain

4. Discussion

Fig. 5 gives a summary of the paper. For small values of γ/A we have inhomogeneously broadened ESR lines, whose width is determined by the distribution of local magnetic fields modeling the hyperfine structure interaction. The width of a single component in the inhomogeneous distribution is determined by the time interval the particle spends at a specific lattice site, i.e. by the hopping rate. For $\gamma/A \approx 1$ we have a coalescent broad line. In the following range of the hopping rate the FID is described by an $\exp(-t^{3/2})$ law, and asymptotically by an exponential function. The width of the ESR line is proportional to $\gamma^{-1/3}$. In the range $\gamma/A \approx N$, where N is the number of sites in the chain, we observe cluster effects. For still larger values of the normalized hopping rate, for which the particle probes the whole chain, the FID is described by an exponential function. The line shape is now Lorentzian because of finite size effects. Finally, it should be mentioned that the transition from 1- to 2- and 3-dimensional motion also results in an exponentially decaying FID.

This work has been supported by the Volkswagenwerk Foundation. The authors are grateful to H. Däubler and G. Glatting for discussions.

References

[1] D. Jérome and L. G. Caron, "Low-Dimensional Conductors and Superconductors", NATO ASI Series B *155*, Plenum, New York, London 1986.
[2] V. Enkelmann, B. S. Mora, Ch. Kröhnke, and G. Wegner, Chem. Phys. *66*, 303 (1982).
[3] J. Sigg, Th. Prisner, K. P. Dinse, H. Brunner, D. Schweitzer, and K. H. Hausser, Phys. Rev. B *27*, 5366 (1983).
[4] W. Stöcklein, B. Bail, M. Schwoerer, D. Singel, and J. Schmidt, "Spin Resonance and Conductivity of Fluoranthenyl Radical

Cation Salts", in: Organic Molecular Aggregates, eds. P. Reineker, H. Haken, and H. C. Wolf, Springer, Berlin, Heidelberg, New York, Tokyo 1983.
[5] M. J. Hennessy, C. D. McElwee, and P. M. Richards, Phys. Rev. B *7*, 930 (1973).
[6] R. Czech and K. Kehr, Phys. Rev. Lett *59*, 1783 (1984); Phys. Rev. B *34*, 261 (1986).
[7] H. Haken and G. Strobl, "Exact Treatment of Coherent and Incoherent Triplet Exciton Migration", in: The Triplet State, ed. A. Zahlan, Cambridge University Press, London 1967.
[8] H. Haken and P. Reineker, Z. Phys. *249*, 253 (1972).
[9] H. Haken and G. Strobl, Z. Phys. *262*, 135 (1973).
[10] H. Mori, Prog. Theor. Phys. *34*, 423 (1965).
[11] J. Köhler, Thesis, University of Ulm (1989).
[12] J. Köhler and P. Reineker, Chem. Phys. *146*, 415 (1990).
[13] P. Reineker, "Exciton Dynamics in Molecular Crystals and Aggregates; Stochastic Liouville Equation Approach: Coupled Coherent and Incoherent Motion, Optical Line shapes, Magnetic Resonance Phenomena", in: Springer Tracts in Modern Physics, Vol. *94*, ed. G. Höhler, Springer, Berlin, Heidelberg, New York 1982.
[14] W. Hackbusch, "Multi-Grid Methods and Applications", Springer, Berlin, Heidelberg, New York 1985.

Presented at the Discussion Meeting of the Deutsche Bunsen-Gesellschaft für Physikalische Chemie "Rate Processes in Dissipative Systems: 50 Years after Kramers" in Tutzing, September 10–13, 1990 E 7509

Anomalous Diffusion in Disordered Systems: An Effective Medium Description

Walter Schirmacher

Physik-Department E13, Technische Universität München, D-8046 Garching, Germany

Amorphous Materials / Diffusion / Electrical Properties / Glasses / Transport Properties

The effective medium theory of diffusion in topologically disordered systems is reviewed with emphasis on the description of disorder induced anomalous diffusion. The effective medium approximation (EMA), for which a new derivation is given, is shown to provide a reliable and simple scheme to discuss the diffusive motion of particles in disordered systems such as electrons in the localized energy region of disordered semiconductors or ions in amorphous solids. Explicit calculations for some pertinent models are presented and the consequences of anomalous diffusion to a.c. conductivity, transient photoconductivity, neutron scattering and NMR data are discussed.

1. Introduction

In many disordered systems as metallic and nonmetallic glasses or disordered polymer materials the diffusive motion of ions or electrons cannot be described by Fick's law which states that a current instantaneously arises if a concentration gradient is present. This is because the disorder leads to retardation effects which can extend into the millisecond time scale. The most striking and simple evidence for such an anomalous diffusive motion comes from conductivity measurements. In many disordered materials the a.c. conductivity is strongly frequency dependent and typically obeys an $\sigma(\omega) \propto \omega^{1-\alpha}$ law over many decades of frequency with $0 < \alpha < 1$ [1,2]. This corresponds to a time dependence of the mean square distance walked by a particle $\langle r^2(t)\rangle \propto t^{\alpha}$, i.e. it increases sublinearly with time instead of linearly.

Further evidence for anomalous diffusion of ions in disordered solids comes from dielectric loss [1–3], NMR [2,4,5], neutron scattering [5], and time dependent electronic density of states data [6]. Further evidence for anomalous diffusion of electrons is obtained from transient photoconductivity data ("dispersive transport") [7]. This anomalous behaviour arises from strong fluctuations of the microscopic kinetic coefficient which govern the transport process.

Anomalous diffusion can also arise as a concequence of fractal topology [8,9], can be caused by critical fluctuations near a glass transition [10], or can be a consequence of Coulomb interactions [11]. These possibilities will not be addressed in the present paper.

For describing ionic or electronic hopping transport or jump diffusion in disordered solids [12] one can start from a set of master Eqs. [13,14], one can use a random walk description [6,15] or an random network model [16,17]. All three approaches are equivalent: the microscopic master and random walk equations are equivalent to Kirchoff's equations for the network. The existing approaches for performing the configuration average and solving for the dynamic diffusivity and conductivity can be divided into three groups: (a) averaging over the kinetic coefficients, which corresponds to an equivalent circuit of parallel impedances [18,19,20–22]; (b) averaging over the unrenormalized single site propagator (single site approximation, SSA) corresponding to a serial equivalent circuit [15,16] and (c) effective medium approaches (EMA) [14,23–30]. It is well known that both (a) and (b) can lead to grossly wrong results, especially in the dc limit. In two and three (or higher) dimensional systems with strongly fluctuating kinetic coefficients one encounters an intrinsic percolation problem [17,33,34]. This behaviour is accounted for by the EMA description although only in a mean field way but not by approximations (a) and (b).

In the present contribution an effective medium theory of hopping transport in disordered systems is reviewed with emphasis on the EMA description of anomalous diffusion.

 © VCH Verlagsgesellschaft mbH, W-6940 Weinheim, 1991 0005-9021/91/0303-0368 $ 3.50+.25/0

The present EMA version is suitable for noncrystalline materials i.e. systems without translational symmetry. In the next section the hopping model is formulated and a new derivation of the EMA is presented. The third section comprises results of model calculations for several systems of interest and the fourth section gives a description of experimental manifestations of anomalous diffusion.

2. Effective Medium Approximation

2.1 Rate Equation

Let us consider the motion of noninteracting particles which can perform instantaneous jumps between sites distributed randomly in space. Such a process can be described by the following set of Markovian master equations

$$\frac{\mathrm{d}}{\mathrm{d}t} n_i = -\sum_j W_{ij} n_i + \sum_j W_{ji} n_j \tag{1}$$

$n_i(t)$ is the occupation probability of site i and W_{ij} are the transition rates between site i and j (kinetic coefficients). In the present contribution only the case of symmetric rates $W_{ij} = W_{ji}$ is considered[1]. Specifically the quantities W_{ij} are assumed to depend on the intersite separation r_{ij} only: $W_{ij} = W(r_{ij}, E_{ij})$. r_{ij} and E_{ij} are random variables with distribution $g(r_{ij})$ (radial pair distribution of sites) and $\varrho(E_{ij})$.

The nontrivial problem consists in obtaining a reliable scheme for evaluating the configurational average in order to obtain quantities like the single particle propagator or the frequency dependent diffusivity. The EMA is such a scheme. Since the derivation of the EMA versions which include disorder in the hopping distances [23,24,26] is somewhat involved a new derivation is presented in the remaining part of this section which follows the spirit of the standard CPA/EMA technique [28–31,35].

2.2 Averaged Propagator and Frequency Dependent Diffusivity

The linear set of Eq. (1) can be solved formally by Laplace transformation (convention $f(p) = \int_0^\infty \mathrm{d}t\, f(t) \exp\{-pt\}$, $p = \mathrm{i}\omega + \varepsilon$, $\varepsilon \gtrsim 0$). The averaged propagator which is the central quantity in the subsequent analysis is given by

$$G(k,p) = \langle \sum_{ij} \exp\{\mathrm{i}k r_{ij}\} [p\hat{1} - \hat{K}]^{-1}_{ij} \rangle . \tag{2}$$

Here $\langle\rangle$ denotes a configurational average, and $\hat{K}$ is a matrix with diagonal elements $K_{ii} = \sum_j W_{ij}$ and off diagonal elements $K_{ij} = W_{ij}$. $\hat{1}$ is the unit matrix. The averaged propagator $G(k,p)$ is the Fourier and Laplace transform of the self density-density correlation function [36] which describes the single particle motion. The corresponding spectrum is the incoherent neutron scattering law

$$S(k,\omega) = \frac{1}{\pi} \mathrm{Re}\{G(k,p)\} . \tag{3}$$

$G(r,t)$ is the conditional probability to find the particle at r and t if it started initially at the origin. Particle number conservation leads to the Green Kubo identity [36]

$$\lim_{k\to 0} G(k,p) = [p + D(p)k^2]^{-1} . \tag{4}$$

$D(p)$ is the dynamic diffusivity which is the Laplace transform of the velocity autocorrelation function $\phi(t)$. $D(p=0) = D$ is the usual diffusivity. As stated in the beginning in disordered systems $D(p)$ is strongly frequency dependent up to the experimental time range so that one has to generalize the diffusion equation in the following way:

$$\frac{\mathrm{d}}{\mathrm{d}t} \varrho(r,t) = \int_0^t \mathrm{d}\tau\, \phi(t-\tau)\, \nabla^2 \varrho(r,\tau) . \tag{5}$$

Here $\varrho(r,t)$ is the particle concentration.

In cases where $\mathrm{Re}\{D(p)\} = D(\omega)$ behaves as $\omega^{1-\alpha}$ we have $\phi(t) \propto t^{-(2-\alpha)}$. The dynamic conductivity is related to the dynamic diffusivity by the generalized Nernst-Einstein relation

$$\sigma(p) = \frac{ne^2}{k_B T} D(p) \tag{6}$$

$\mathrm{Re}\{\sigma(p)\} = \sigma(\omega)$ is the ac conductivity.

2.3 Mean Square Displacement and Anomalous Diffusion

The mean square distance walked by the particle (mean square displacement)

$$\langle r^2(t)\rangle \equiv \langle |r(t) - r(0)|^2 \rangle \tag{7}$$

is connected via its Laplace transform $\langle r^2(p)\rangle$ to $D(p)$ by [36]

$$\langle r^2(p)\rangle = \frac{D(p)}{p^2} . \tag{8}$$

In the case of normal diffusion one has

$$\langle r^2(t)\rangle = 6Dt .$$

Anomalous diffusion is present if $\langle r^2(t)\rangle$ increases *sublinearly* with time. If, for example, $D(\omega) \propto \omega^{1-\alpha}$ we have from (8) and the Tauberian theorems $\langle r^2(t)\rangle \propto t^\alpha$. If the diffusion process is strictly anomalous the sublinear increase of $\langle r^2(t)\rangle$ extends for ever. In many systems of experimental relevance, however, there can be a crossover from anoma-

[1] In systems with energetical disorder the detailed balance leads to $W_{ij} \neq W_{ji}$ and one must use a more general treatment [26]. However, as shown in Ref. 26 in cases where one is only interested in diffusion and not in thermoelectric effects or energy relaxation it is sufficient to use symmetric rates with effective energy barriers leading from i to j.

lous to normal diffusion at a certain time t_0. This corresponds to a change in $D(\omega)$ from being frequency independent for $\omega < \omega_0 = t_0^{-1}$ to being frequency dependent for $\omega > \omega_0$.

2.4 Generalized Master Equation

As a consequence of (4) $G(k,p)$ can be represented in terms of a density relaxation kernel (memory function) in the following way [37]:

$$G(k,p) = [p - m(k,p) + m(\vec{o},p)]^{-1} \tag{9}$$

where $m(k,p)$ has the following Taylor expansion

$$m(k,p) = m(\vec{o},p) - D(p)k^2\,, \tag{10}$$

so that

$$D(p) = -\frac{1}{2}\left(\frac{\partial}{\partial k_x}\right)^2 m(k,p)\Big|_{k=\vec{o}}\,. \tag{11}$$

If one introduces the inverse Fourier and Laplace transform of $m(\vec{k},p)$, the memory function $m(r,t)$ one has from (7) the generalized master equation for $G(r,t)$

$$\frac{\mathrm{d}}{\mathrm{d}t}G(r,t) = \int_0^t \mathrm{d}\tau\left[-\int_{-\infty}^{+\infty}\mathrm{d}^3 r_1 m(r-r_1, t-\tau)\,G(r,\tau) + \int_{-\infty}^{+\infty}\mathrm{d}^3 r_1 m(r-r_1, t-\tau)\,G(r_1,\tau)\right] \tag{12}$$

(12) is so to speak a continuum version of (1): the discrete sites are replaced by the continous space variable and the fluctuating hopping rates by the memory function.

The task is now to calculate $m(\vec{k},p)$ from the microscopic quantities W_{ij}. It is helpful for formulating the EMA to make the following ansatz for the memory function

$$m(r,p) = \int_0^\infty \mathrm{d}t\,\mathrm{e}^{-pt}\,m(r,t) = g(r)\,\gamma(r,p)\,. \tag{13}$$

Here $g(r)$ is the radial distribution function and $\gamma(r,p)$ has the meaning of a frequency dependent hopping rate that corresponds to a hopping distance r.

2.5 Effective Medium

We consider now a fictive plane which divides the disordered system of total volume Ω into two adjacent regions B_1 and B_2 of the volume $\frac{1}{2}\Omega$. If the starting point of the motion lies directly on the plane one obtains from (12) the following set of equations of motions for the propagators G_1 and G_2 which are integrated over the regions B_1 and B_2, respectively:

$$\begin{aligned} pG_1(p) - G_1(t=0) &= \frac{1}{2}m(p)\,[G_2(p) - G_1(p)] \\ pG_2(p) - G_2(t=0) &= \frac{1}{2}m(p)\,[G_1(p) - G_2(p)] \end{aligned} \tag{14}$$

here $m(p) = m(k=0,p)$. $\frac{1}{2}m(p)$ is the relaxation kernel which controls the density relaxation between the two regions.

We now create a "perturbation" by considering a real pair of sites i and j which are supposed to be situated on opposite sides of the plane. Around this pair the real rate equation is supposed to be valid inside a volume $\frac{1}{2}\Omega_s = \frac{1}{2}n_s = \Omega/2N_s$ on each side of the plane. N_S is the total number of sites and n_s is the site density. The perturbing "Hamiltonian matrix" is given by

$$\hat{V} = \begin{bmatrix} \frac{m(p)}{2N_s} - W_{ij} & W_{ij} - \frac{m(p)}{2N_s} \\ W_{ij} - \frac{m(p)}{2N_s} & \frac{m(p)}{2N_s} - W_{ij} \end{bmatrix} \tag{15}$$

The CPA/EMA prescription for calculating $m(p)$ now consists in postulating that on the average the T-matrix that corresponds to $\hat{V}$ should vanish [28–31]. This leads to the following self consistent equation

$$\left\langle \frac{[m(p)/2N_s] - W_{ij}}{1 - 2\,(G_1 - G_2)\,\{[m(p)/2N_s] - W_{ij}\}} \right\rangle = 0 \tag{16}$$

Eq. (16) is very similar to the conventional EMA/CPA Eq. [28–31]. The difference lies in the effective medium. The latter is in the conventional theories a regular lattice of sites with effective frequency dependent hopping rates. Here we did not make any assumption about the structure of the effective medium (except for homogeneity and isotropy). By using (14) one can cast (16) into the form

$$m(p) = N_s\left\langle \frac{2W_{ij}}{1 + 2\left(\frac{2W_{ij}}{m(p)} - \frac{1}{N_s}\right)(1 - pG_1)} \right\rangle. \tag{17}$$

For performing the configurational average we assume that the energy barriers E_{ij} and the distances r_{ij} are distributed independently so that we have for the distribution of the W_{ij}:

$$P(W_{ij})\,\mathrm{d}W_{ij} = \frac{1}{\Omega}\,g(r_{ij})\,\varrho(E_{ij})\,\mathrm{d}^3 r_{ij}\mathrm{d}E_{ij}\,, \tag{18}$$

If we now insert the explicit solution of (14) for the case that the particle was initially in B_1

$$G_1 = \frac{1}{p}\left(p + \frac{m(p)}{2}\right)\Big/\,(p + m(p))\,, \tag{19}$$

we obtain in the limit $N_s, \Omega \to \infty$ (keeping $n_s = N_s/\Omega$ finite)

$$m(p) = n_s \int_{-\infty}^{+\infty}\mathrm{d}^3 r_{ij}\,g(r_{ij}) \int_0^\infty \mathrm{d}E_{ij}\,\varrho(E_{ij})\,\frac{1}{\frac{1}{p + m(p)} + \frac{1}{2W_{ij}}}\,. \tag{20}$$

Since we want (20) to hold for any distribution $g(r_{ij})$ (20) together with (13) implies

$$\gamma(r,p) = n_s \int_0^\infty \mathrm{d}E_{ij}\, \varrho(E_{ij}) \frac{1}{\dfrac{1}{p+m(p)} + \dfrac{1}{2W(r_{ij},E_{ij})}} \tag{21}$$

so that

$$m(k,p) = n_s \int_{-\infty}^{+\infty} \mathrm{d}^3 r_{ij}\, g(r_{ij}) \int_0^\infty \mathrm{d}E_{ij}\, \varrho(E_{ij}) \frac{\exp\{\mathrm{i}kr_{ij}\}}{\dfrac{1}{p+m(p)} + \dfrac{1}{2W_{ij}}}. \tag{22}$$

From (11) and (22) the diffusivity is obtained as

$$D(p) = \frac{n_s}{6} \int_{-\infty}^{+\infty} \mathrm{d}^3 r\, r^2 g(r) \int_0^\infty \mathrm{d}E\, \varrho(E) \frac{1}{\dfrac{1}{p+m(p)} + \dfrac{1}{2W(r,E)}}. \tag{23}$$

In the original derivation of the self consistent EMA Eq. [26] it had been noticed that one encounters a double counting problem which is typical for self consistent mean field theories It was shown that one can compensate this error by multiplying the density that appears in the self consistent equation by a factor $a_p = \lim_{N_s\to\infty} (N_s!/N_s^{N_s})^{1/N_s} = \exp\{-1\}$.

In the dc limit this produces nearly the same results as that provided by a percolation analysis [17, 33, 34]. Butcher and Summerfield [38] have suggested to use instead the inverse percolation number [17]. Incorporating this correction the EMA equation now takes the form

$$m(p) = a_p n_s \int_{-\infty}^{+\infty} \mathrm{d}^3 r\, g(r) \int_0^\infty \mathrm{d}E\, \varrho(E) \frac{1}{\dfrac{1}{p+m(p)} + \dfrac{1}{2W(r,E)}}, \tag{24}$$

this version of the EMA compares well to numerical simulations of hopping models [25, 39].

3. Examples

3.1 Variable-Range Hopping

For phonon-assisted tunneling of electrons in the localized energy region of disordered semiconductors (variable-range hopping [12]) we use the symmetrized expression [26]

$$2W(r,E) = \nu_0 \mathrm{e}^{-2r/a} \mathrm{e}^{-\beta E} \tag{25}$$

where a is the radius of the localized wave function and $\beta = 1/k_B T$. Introducing the effective density of states $N(E) = n_s \varrho(E)$ and setting $g(r) \equiv 1$ we obtain the following EMA equation

$$m(p) = a_p \int_{-\infty}^{+\infty} \mathrm{d}^3 r \int_0^\infty \mathrm{d}E\, N(E) \frac{1}{\dfrac{1}{m(p)+p} + \dfrac{\mathrm{e}^{\beta E}\, \mathrm{e}^{2r/a}}{\nu_0}}. \tag{26}$$

If $N(E)$ does not change appreciably in the range $k_B T$ around the Fermi level E_F one can take $N(E) \approx N(E_F) = N_F$ outside the integral and obtains by a partial integration [25]

$$m_0(p) = \frac{4T}{T_0} \int_0^\infty \mathrm{d}x\, x^3 \frac{1}{\dfrac{1}{m(p)+p} + \dfrac{\mathrm{e}^x}{\nu_0}} \tag{27}$$

with

$$T_0 = \frac{24}{\pi a_p N_F k_B a^3}. \tag{28}$$

The dynamic diffusivity is then given by

$$D(p) = \frac{a^2}{10\, a_p} \frac{T}{T_0} \int_0^\infty \mathrm{d}x\, x^5 \frac{1}{\dfrac{1}{m(p)+p} + \dfrac{\mathrm{e}^x}{\nu_0}}. \tag{29}$$

In Fig. 1 the real parts of $m(p)$ and $D(p)$ as calculated from Eqs. (27) to (29) are plotted against ω for different values of T_0/T. It can be seen that a large frequency range of anomalous diffusion appears which becomes the more extended the larger T_0/T is.

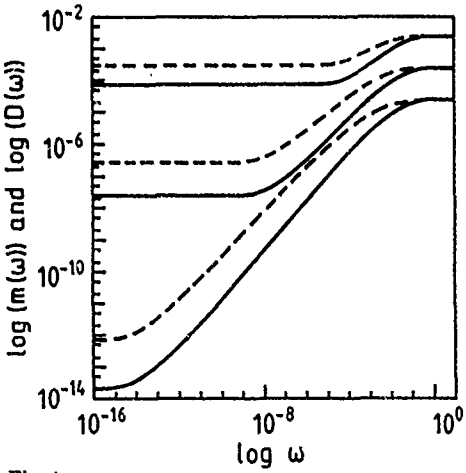


Fig. 1
$m(\omega)/\nu_0$ (——) and $D(\omega)m(\infty)/\nu_0 D(\infty)$ (– – –) for the variable-range hopping model as calculated from Eqs. (27) and (29), resp. for $T/T_0 = 10^{-6}$, 10^{-5}, and 10^{-4}

In the d.c. limit $\omega \to 0$ we have from (29)

$$1 = \frac{4T}{T_0} \int_0^\infty \mathrm{d}x\, x^3 \frac{1}{1+\mathrm{e}^{x-\xi}} \tag{30}$$

with $\xi = -\ln(m(0)/\nu_0)$. For $\xi \gg 1$ the Fermi function in the integrand of (30) can be replaced by a step function with the result

$$1 = \frac{T}{T_0} \xi^4. \tag{31}$$

From this follows Mott's [12] $T^{1/4}$ law:

$$D(0) = \frac{a^2}{60 a_p}\left(\frac{T_0}{T}\right)^{1/2} m(0)$$
$$m(0) = \nu_0 \exp\{-(T_0/T)^{1/4}\}. \tag{32}$$

3.2 Classical Hopping

For classical over-the-barrier hopping of ions in disordered materials we use the following form of $W(r,E)$:

$$2W(r,E) = \theta(r_{\max} - r)\,\nu_0\,e^{-\beta E}. \tag{33}$$

The dynamic diffusivity is given by:

$$D(p) = \frac{1}{6} R^2 m(p) \tag{34}$$

with

$$R^2 = \int_0^{r_{\max}} dr\, r^4 g(r) \Big/ \int_0^{r_{\max}} dr\, r^2 g(r) \tag{35}$$

and the EMA equation for m(p)

$$m(p) = Z a_p \int_0^\infty dE\, \varrho(E) \frac{1}{\dfrac{1}{m(p)+p} + \dfrac{e^{\beta E}}{\nu_0}} \tag{36}$$

where

$$Z = n_s \int_0^{r_{\max}} dr\, 4\pi r^2 g(r)$$

is the coordination number of sites.

As can be seen from Fig. 2 where the self consistent solution of (36) is plotted for a model with $\varrho(E) = \text{const.}$ against frequency the behaviour is quite similar to that of the variable-range model.

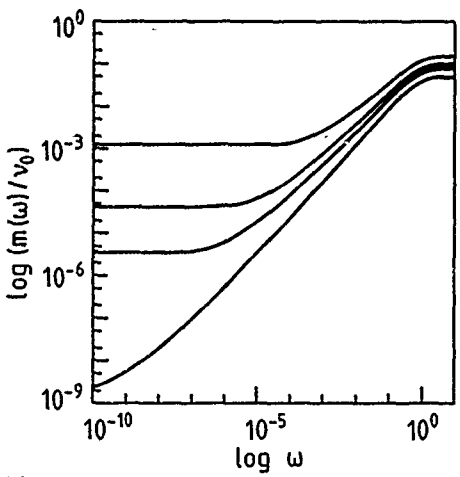


Fig. 2
$m(\omega)/\nu_0$ for the classical barrier hopping model Eq. (30) for a constant barrier distribution $\varrho(E) = P/Za_p k_B T$ with $P = 0.15$, 0.1, 0.08, and 0.05

An important qualitative difference lies in the dc behaviour of $m(p)$. Setting $\omega = 0$ and defining again $\xi = -\ln(m(0)/\nu_0)$, the EMA equation becomes

$$1 = Z a_p \int_0^\infty dE\, \varrho(E) \frac{1}{1 + e^{\beta E - \xi}}. \tag{37}$$

Setting $\xi = \beta\mu$ the problem becomes equivalent to that for finding the chemical potential in a disordered semiconductor for a given number of carriers. For temperature $T \ll \mu$ the Fermi function can, again, be replaced by a step function and we obtain

$$1 = Z a_p \int_0^\mu dE\, \varrho(E) \tag{38}$$

This yields an Arrhenius law for the d.c. diffusivity *independent of the details of the barrier distribution* $\varrho(E)$ [40].

Eqs. (31) and (38) for the d.c. jump rate deserve a further comment. Let us consider the classical hopping model (33). For finding the conductivity in this model one can use the following percolation construction [17, 33, 34]: Let us connect all sites which have a distance less than $r_{\max}$ and a barrier between each other less than E^*. If the level E^* is chosen to be very low there will be only small clusters of connected sites. The size of these clusters will increase if E^* is increased until at $E^* = \mu$ there exists a percolation path through the system Eq. (38) is just the equation which mathematically describes this construction [17, 33, 34]. The same applies to Eq. (30) in the case of variable range hopping. Here, the level which is shifted is defined by $\xi^* = 2\alpha r^* + \beta E^*$ until percolation is achieved at $\xi^* = \xi$. In the limit of low temperature and/or density where the Fermi functions in Eqs. (30) and (37) become step functions, therefore, the d.c. version of the EMA becomes equivalent to the percolation constructions of Refs. [17, 33, 34].

3.3 Percolation

In contrast to the "fictitious" percolation model discussed at the end of the last paragraph let us study now the following "real" percolation model: We consider a disordered system of sites in which there is a bond between neighbouring sites with probability x (concentration of bonds). Two sites are defined to be neighbours if their distance is less than $r_{\max}$. Such a model can be described within the present formalism by the rates

$$2W(r,E) = \begin{cases} W_0 \theta(r_{\max} - r)\,\delta(E) & \text{connected} \\ 0 & \text{disconnected} \end{cases} \tag{39}$$

The EMA Eq. (24) for this case becomes particularly simple

$$m(p) = Z a_p x \frac{1}{\dfrac{1}{m(p)+p} + \dfrac{1}{W_0}}. \tag{40}$$

This is a quadratic equation[2] for $m(p)$ with the solution

$$m(p) = \frac{1}{2}(\varepsilon W_0 - p) \pm \left[\frac{1}{4}(\varepsilon W_0 - p)^2 + (\varepsilon + 1) W_0 p\right]^{1/2} \quad (41)$$

where $\varepsilon = Z a_p x - 1 \equiv \frac{x - x_0}{x_0}$ is the difference from the percolation threshold $x_0 = 1/Z a_p$. One has to choose that solution which renders $\mathrm{Re}\{m(p)\} > 0$. For $\omega = 0$ we obtain

$$m(0) = \begin{cases} \varepsilon W_0 & \varepsilon > 0 \\ 0 & \varepsilon < 0 \end{cases}. \quad (42)$$

For demonstrating the similarities but also the dissimilarities between the models of the preceding paragraphs and the percolation model $m(p)$ as given by Eq. (41) is plotted in Fig. 3. The common feature is that if the control parameter x takes values which approach x_0 from above there exists an increasing frequency range of anomalous diffusion. However, while in the other models $m(0)$ is always finite (albeit exponentially small for low temperatures and/or densities) in the percolation model $m(0)$ becomes 0 for a finite value of x. (For $x < x_0$ the particles become localized inside the percolation clusters rendering the system non-ergodic [41, 42]).

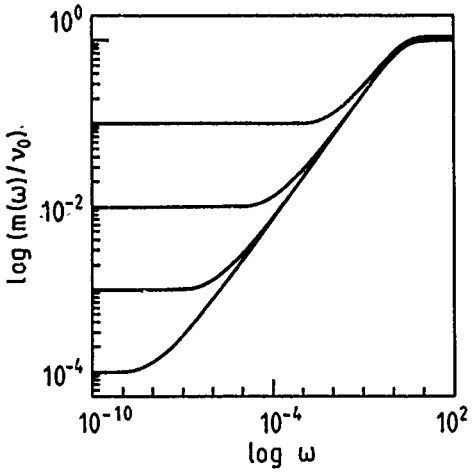


Fig 3
$m(\omega)/W_0$ for the percolation model Eq. (41) with $\varepsilon = 10^{-1}$, 10^{-2}, 10^{-3}, and 10^{-4}

Also the frequency dependence of $m(p)$ is quite different from that of the previous models. While the frequency exponent is 1/2 (mean field exponent) in the percolation model the frequency dependence of $m(p)$ in the other models only *resembles* an $\omega^{1-\alpha}$ behaviour in a certain frequency window, but, as can be seen clearly from Figs. 1 and 2, the $\omega^{1-\alpha}$ law is not obeyed exactly.

[2] This equation is very similar to the mode coupling equation for the Lorentz model [41]. The critical exponents near the percolation threshold are the same.

3.4 Crossover from Normal to Anomalous Diffusion

An important advantage of the EMA description of anomalous diffusion in disordered systems as compared, for example, with the phenomenological CRTW model [7] or the single-site approximation [15, 16, 20–22] is that a possible crossover from anomalous to normal diffusion is accounted for correctly, i.e. that in calculating the d.c. diffusivity the percolative aspects are treated properly. It is not difficult to be convinced from the EMA Eq. (24) and Figs. 1 to 3 that the frequency ω_0 in the neighbourhood of which the transition from normal to anomalous diffusion occurs, is just given by the d.c. value of the generalized jump frequency:

$$\omega_0 = m(p = 0) \quad (43)$$

The value of this parameter decides whether or not one has anomalous diffusion in a time region of interest: anomalous diffusion occurs for $t < t_0 = \omega_0^{-1}$.

4. Description of Different Experimental Manifestations of Anomalous Diffusion

4.1 a.c. Conductivity and Related Data

As emphasized in the beginning the most direct evidence for anomalous diffusion in disordered systems comes from a.c. conductivity data. As an example we reproduce the combined $\sigma(\omega)$ data extracted from several different types of measurement [3] in Fig. 4 and compare it with the EMA result (36) for classical hopping with constant $\varrho(E)$. The anomalous frequency dependence predicted by the EMA (only the activation energy of $\sigma(0)$ was adjusted to the measured value $\mu = 70$ kJ/mol) follows the experimental one remarkably well.

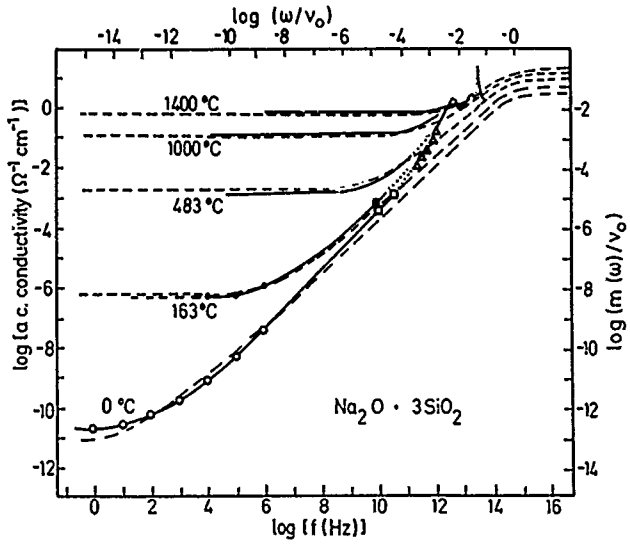


Fig. 4
a.c. conductivity data of $Na_2O \cdot 3SiO_2$ glass as compiled by Wong and Angell [3] (——, △, ■, □, ○) compared with the EMA calculation for classical hopping Eq. (30) with constant $\varrho(E)$, adjusted to the activation energy of the d.c. conductivity, $\mu = 70$ kJ/mol (– – –) from Ref. [40]

4.2 Anomalous Transient Photocurrents in Disordered Semiconductors

In transient photoconduction ("time-of-flight") measurements carriers are created by a light flash on one side of a semiconducting sample which subsequently are drawn towards an electrode by a bias field. In ordered systems one expects a constant current which suddenly drops if the carriers hit the electrode. If L is the sample thickness the mobility $\mu = (e/k_B T) D$ can be calculated from the drift velocity

$$v = \mu F = L/t_T \tag{44}$$

where F is the field and t_T is the transit time. In disordered materials, however, one observes a continously descreasing current [6, 7] which can be described by

$$j(t) \propto \begin{cases} t^{-(1-\alpha)} & t < t_T \\ t^{-(1+\alpha)} & t > t_T \end{cases} \tag{45}$$

with $0 < \alpha < 1$. Scher and Montroll [7] described such a behaviour ("dispersive transport") phenomenologically in terms of a continous-time random walk (CTRW) on a lattice with a waiting time distribution $\Psi(\tau) \propto \tau^{-(1+\alpha)}$. In such a model one has $\langle r^2(t)\rangle \propto t^\alpha$. Obviously the anomalous transients are due to anomalous diffusion. For a microscopic description one can use random trapping [27, 43–49] or hopping models [7, 15, 27]. As shown in Ref. [27] both can be incorporated into a hydrodynamic description [27, 50, 51] with frequency dependent mobility and diffusivity $\mu(p) = (e/k_B T) D(p)$, where the latter behaves as $D(\omega) \propto \omega^{1-\alpha}$. The corresponding propagator is given by

$$G(\boldsymbol{k}, p) = (p - \mathrm{i}k_x \mu(p) F + D(p) k^2)^{-1} \tag{46}$$

Inserting this into a planar geometry with reflecting boundary at the front and absorbing ones at the back electrode one obtains [52] for the Laplace transform $j(p)$ of $j(t)$

$$j(p) = \frac{1}{(\gamma - \eta) L} \left[1 - \frac{\frac{4\gamma\eta}{(\gamma+\eta)^2} \exp[-(\gamma-\eta)L] \left(1 + \frac{\gamma-\eta}{2\eta} \exp[-(\gamma+\eta)L]\right)}{1 + (\gamma-\eta)/(\gamma+\eta) \exp[-2\gamma L]} \right] \tag{47}$$

where $\eta = eF/2k_B T$ and

$$\gamma = [\eta^2 + p/D(p)]^{0.5}. \tag{48}$$

It has been shown in Ref. [27] that for times larger than $t_R = p_R^{-1}$ (where p_R is the solution of $p_R = D(p_R)\eta^2$) the diffusion term in Eq. (46) can be neglected and Eq (47) reduces to the expression given by Leal Ferrera [50].

$$j(p) = \frac{2\eta D(p)}{pL} \left\{ 1 - \exp\left[-\frac{pL}{2\eta D(p)} \right] \right\} \tag{49}$$

$j(t)$ has to be calculated from (47) (or in the case $t \gg t_R$ from (49)) for a given form of $D(p)$ or $\mu(p)$ by numerical Laplace inversion.

The advantage of using the $D(p)$ formalism is that one can easily incorporate dispersive-non-dispersive crossover effects [49] by using a model in which t_0 falls into the experimental time window. For observing a "plateau" in the transient current pulse one has the condition [27, 52, 53] $t_R < t_0 < t_T$.

4.3 Neutron Scattering

The incoherent neutron scattering law corresponding to the particle's motion in the disordered environment is given by Eq. (3). In particular for the classical hopping model (33) it is given by

$$S(k, \omega) = \frac{1}{\pi} \mathrm{Re}\{(p + f(k) m(p))^{-1}\} \tag{50}$$

with the generalized Chudley-Elliott-function

$$f(k) = (4\pi n_s / Z) \int_0^{r_{max}} \mathrm{d}r\, r^2 g(r) [1 - \sin(kr)/kr], \tag{51}$$

for $k \to 0$ we have, of course (cf. Eq. (4))

$$f(k) = \frac{1}{6} k^2 R^2 \tag{52}$$

Neutron quasielastic scattering is an ideal tool to probe anomalous diffusion in a case where this cannot be done via

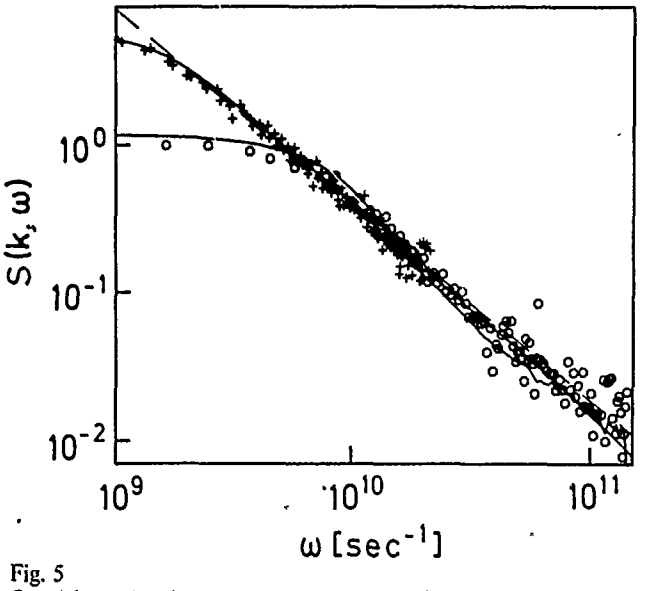


Fig. 5
Quasielastic incoherent neutron scattering data from H in amorphous $Ni_{24}Zr_{76}$, compared with the EMA prediction (Eqs. (36) and (50)) for the classical hopping model with a Gaussian $g(E)$ [56] from Ref. (5b)

an ac conductivity measurement, namely in the case of hydrogen diffusion in amorphous metals. If $m(p)$ has a disorder-induced frequency dependence the spectrum should be non-Lorentzian. This is, in fact, observed [5, 54, 55]. In particular if $m(p) \propto \omega^{1-\alpha}$ one expects $S(k,\omega) \propto \omega^{(1-\alpha)}$. In Fig. 5 quasielastic incoherent neutron scattering data [5] from H in amorphous $Ni_{24}Zr_{76}$ are shown. It can be seen that the data exhibit such a behaviour.

They can be well fitted by a classical hopping model with a Gaussian $\varrho(E)$ as calculated by Richards [56] with the maximum adjusted to be compatible with the experimentally measured [57] activation energy of the diffusion coefficient $D(0)$ [58].

4.4 Nuclear Spin-Lattice Relaxation

A useful method for obtaining information on diffusive motion in disordered solids is the observation of nuclear spin-lattice relaxation as deduced from NMR [59, 60] or nuclear radiation anisotropy which follows a nuclear β decay (β-NMR) [61].

In crystalline solids the temperature dependence of the nuclear spin-lattice relaxation rate can be well described by the BPP formula [62, 63]

$$T_1^{-1} \propto \mathrm{Re}\,\{(p_L + W(T))^{-1}\} \tag{53}$$

where $W(T) \propto \exp\{-\mu/k_B T\}$ is the jump rate that corresponds to the (frequency independent) diffusivity D; $p_L = i\omega_L + \varepsilon$ where ω_L is Larmor frequency. In an Arrhenius plot ln T_1^{-1} against $1/T$ one expects from (53) a symmetric maximum with equal slopes of the wings being equal to the activation energy μ of the diffusivity. On the left side of the maximum T_1^{-1} is independent of ω_L (motional narrowing), on the right it is proportional to ω_L^{-2}. In amorphous materials there are strong deviations from BPP behaviour [2, 59–61, 64–66]. This is not surprising since (53) is based on regular diffusion with a single activation energy. If one averages now expression (53) — as frequently done in the literature [1, 3, 59–61] — over a distribution of activation energies one makes the same mistake as in the approximation schemes labelled a and b in the introduction. A generalization of (53) which is consistent with the EMA analysis is [4, 11]

$$T_1^{-1} \propto \mathrm{Re}\,([p_L + f(k_0)\, m(p_L,T)]^{-1})\,. \tag{54}$$

Here, k_0 is a wavenumber characterizing the spatial fluctuations of electric field gradients or the distance dependence of the magnetic coupling [4]. In Fig. 6 β-NMR relaxation data [67] are compared with the temperature dependence predicted by (54) where $m(p,T)$ has been calculated from (36) (classical diffusion) with constant $\varrho(E)$. The value of the latter was adjusted to give the measured activation energy of the d.c. conductivity. The frequency and temperature dependence of the data is not followed in detail by the model but the strong asymmetry and the deviation from $T_1^{-1} \propto \omega_L^{-2}$ is explained.

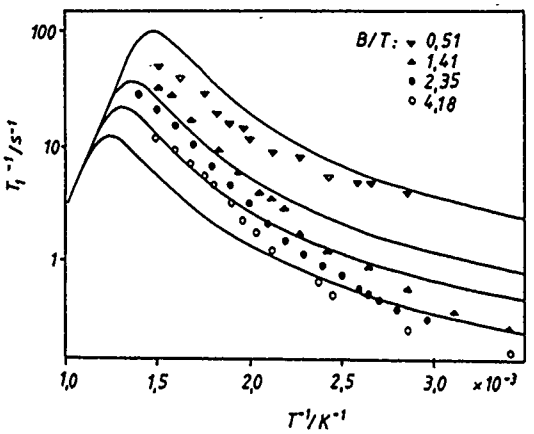


Fig. 6
BPP plot of the spin-lattice relaxation rate of $^7LiO \cdot B_2O_3$ glass [67] compared with the approximate formula (54) where $m(p_L, T)$ has been calculated from Eq. (30) with a constant $\varrho(E)$ adjusted to the measured activation energy of the d.c. conductivity (from Ref. [4])

Conclusion

The effective medium approximation comprises a simple and reliable tool to describe jump diffusion in disordered systems. Anomalous diffusion which is ubiquitous in disordered materials is explained as the result of strong fluctuations of the microscopic transition rates which govern the random walk of the particles. For models which can be characterized by randomly fluctuating distances r_{ij} and energy barriers E_{ij} simple formulae are given for calculating the d.c. and frequency dependent diffusivity $D(\omega)$ and conductivity $\sigma(\omega)$. The only input information is the functional form of the transition rates $W(r,E)$ and the distribution functions $g(r)$ and $\varrho(E)$. The results of such calculations compare well to numerical simulations of the same model. The frequency dependence of $D(\omega)$ and $\sigma(\omega)$ is given by a generalized frequency dependent jump frequency $m(p)$ for which the EMA equation is solved. In cases where $m(0) \neq 0$ a transition from normal to anomalous diffusion occurs at a frequency $\omega_0 = t_0^{-1} = m(0)$. In models with a broad distribution of energy barriers this frequency can be exponentially small at low temperatures giving rise to a region of anomalous diffusion which extends over many orders of magnitude. In this range $D(\omega)$ resembles a $\omega^{1-\alpha}$ behaviour with $0 < \alpha < 1$ but this law is not obeyed exactly. A large class of experimental observations caused by anomalous particle diffusion can be described by the present formalism ranging from ac conductivity and dispersive transient photocurrents to anomalous quasielastic neutron scattering and NMR data.

I am grateful to M. Wagener for many helpful discussions and for producing Figs. 1–3.

References

[1] A. K. Jonscher, Nature *267*, 673 (1979).
[2] K. L. Ngai, Comm. Solid State Phys. *9*, 127 (1979).
[3] J. Wong and C. A. Angell, Glass, structure by spectroscopy, Dekker, New York 1976.
[4] W. Schirmacher and A. Schirmer, Solid State Ionics *28–30*, 134 (1988).

[5] J. B. Suck, H. Rudin, H. U. Künzi, and A. Heidemann, in: "Rapidly Quenched Metals", p. 1545, S. Steeb, H. Warlimont, eds., Elsevier, Amsterdam 1985; W. Schirmacher, M. Prem, J. Suck, and A. Heidemann, Europhys. Lett. 1990, in press.
[6] R. A. Street, C. C. Tsai, J. Kakalios, and W. B. Jackson, Philos. Mag. *B56*, 305 (1987); J. Kakalios, R. A. Street, and W. B. Jackson, Phys. Rev. Lett. *59*, 1037 (1987).
[7] H. Scher and E. W. Montroll, Phys. Rev. *B12*, 2455 (1975); G. Pfister and H. Scher, Adv. Phys. *27*, 747 (1987).
[8] S. Alexander and R. Orbach, J. Phys. (Paris) Lett. *43*, L625 (1982).
[9] R. Rammal and G. Toulouse, J. Phys. (Paris) Lett. *44*, L13 (1983).
[10] W. Götze, in: Amorphous and Liquid Materials, p. 34, eds. by E. Lüscher, G. Fritsch, and G. Jacucci, M. Nijhoff, Dordrecht 1987.
[11] K. Funke and I. Riess, Z. Phys. Chem. Neue Folge *140*, 217 (1984); K. Funke, "Solid State Ionics", *18 & 19*, 183 (1986); K. Funke, Z. Phys. Chem. Neue Folge *154*, 251 (1987).
[12] N. F. Mott and E. A. Davis, Electronic Processes in non-crystalline materials Clarendon Press, Oxford 1971.
[13] H. Böttger and V. V. Bryksin, Hopping conduction in solids, Akademie-Verlag Berlin 1985.
[14] S. Alexander, J. Bernasconi, W. R. Schneider, and R. Orbach, Rev. Mod. Phys. *53*, 175 (1981).
[15] H. Scher and M. Lax, Phys. Rev. *B10*, 4491 and 4502 (1973).
[16] A. Miller and E. Abrahams, Phys. Rev. *120*, 745 (1960).
[17] B. I. Shklovskii and A. L. Efros, Electronic Properties of Doped Semiconductors, Springer-Verlag, Heidelberg 1984.
[18] S. E. Shelby, J. C. Kecton, J. Appl. Phys. *45*, 1458 (1974).
[19] J. Jain, J. Non-Cryst. Solids *66*, 517 (1984).
[20] D. Ravaine and J. L. Souquet, J. Chim. Phys. *5*, 693 (1974).
[21] P. B. Macedo, C. T. Moynihan, and R. Bose, Phys. Chem. Glasses *13*, 171 (1972).
[21] J. C. Dyre, Phys. Lett. *A108*, 457 (1985).
[23] C. R. Gochanour, H. C. Andersen, and D. M. Fayer, J. Chem. Phys. *70*, 4254 (1979).
[24] B. Movaghar, B. Pohlmann, and W. Schirmacher, Solid State Commun. *34*, 451 (1980).
[25] B. Movaghar, B. Pohlmann, and G. Sauer, Phys. Status Solidi (b) *97*, 533 (1980).
[26] B. Movaghar and W. Schirmacher, J. Phys. *C14*, 859 (1981); B. Movaghar, M. Grünewald, B. Pohlmann, D. Würtz, and W. Schirmacher, J. Stat. Phys. *30*, 315 (1983).
[27] W. Schirmacher, Solid State Commun. *39*, 893 (1981).
[28] T. Odagaki and M. Lax, Phys. Rev. *B24*, 5284 (1981).
[29] S. Summerfield, Solid State Commun. *39*, 401 (1981).
[30] I. Webman, Phys. Rev. Letters *47*, 1496 (1981).
[31] S. Kirkpatrick, Rev. Mod. Phys. *45*, 547 (1973).
[32] J. A. McInnes, P. N. Butcher, and J. D. Clark, Philos. Mag. *B41*, 1 (1980).
[33] V. Ambegaokar, B. F. Halperin, and J. S. Langer, Phys. Rev. *B4*, 2612 (1971).
[34] M. Pollak, J. Noncryst. Sol. *11*, 1 (1972).
[35] D. A. G. Bruggeman, Ann. Phys. (Leipzig) *24*, 636 (1935).
[36] J. P. Hansen and I. R. McDonald, Theory of simple liquids, Academic Press London 1976.
[37] J. Klafter and R. Silbey, Phys. Rev. Lett. *44*, 55 (1980).
[38] S. Summerfield and P. N. Butcher, J. Phys. *C15*, 7003 (1982).
[39] B. Ries and H. Bässler, Phys. Rev. *B35*, 2295 (1987).
[40] W. Schirmacher, Solid State Ionics *28–30*, 129 (1988).
[41] W. Götze, E. Leutheusser, and S. Yip, Phys. Rev. *A23*, 2634 (1981).
[42] W. Götze, Solid State Commun. *27*, 1393 (1978).
[43] J. E. Haus and K. W. Kehr, Phys. Rep. *150*, 263 (1987).
[44] J. Noolandi, Phys. Rev. *B16*, 4466 (1977).
[45] F. W. Schmidlin, Phys. Rev. *B16*, 2362 (1977).
[46] V. I. Arkhipov and A. I. Rudenko, Phys. Lett. A 61, 55; Philos. Mag. *B45*, 189 (1982).
[47] T. Tiedje and A. Rose, Solid State Commun. *37*, 49 (1980).
[48] V. N. Prigodin, Sol. State Commun. *50*, 607 (1984); Solid State Commun. *51*, 371 (1984); Sov. Phys. Solid State *26*, 2154 (1984).
[49] H. Schnörer, D. Haarer, and A. Blumen, Phys. Rev. *B38*, 8097 (1988).
[50] G. F. Leal-Ferrera, Phys. Rev. *B16*, 4719 (1977).
[51] P. N. Butcher and J. D. Clark, Philos. Mag. *B42* 191 (1980).
[52] W. Schirmacher, B. Pohlmann, and D. Würtz, IEEE Transactions on Electrical Insulation *EI22*, 195 (1987).
[53] K. Godzik and W. Schirmacher, J. Phys. Paris *10*, Suppl. C4–127 (1981).
[54] J. B. Suck, H. Rudin, H. U. Künzi, and A. Heidemann in: Rapidly quenched metals, p. 1545, S. Steeb, H. Warlimont, eds., Elsevier, Amsterdam 1985.
[55] D. Richter, G. Driesen, R. Hempelmann, and I. S. Anderson, Phys. Rev. Lett. *57*, 731 (1986).
[56] P. M. Richards, Phys. Rev. *B27*, 2059 (1983).
[57] W. Kieniger, Thesis, Max-Planck-Institut für Metallforschung, Institut für Werkstoffwissenschaften, Stuttgart 1989.
[58] R. Kirchheim, F. Sommer, G. Schluckebier, Acta Metall. *30*, 1059 (1982).
[59] W. Müller-Warmuth and H. Eckert, Phys. Rep. *88*, 91 (1982).
[60] O. Kanert, Phys. Rep. *91*, 183 (1982).
[61] P. Heitjans, Solid State Ionics *18 & 19*, 50 (1986).
[62] N. Bloembergen, E. M. Purcell, and R. V. Pound, Phys. Rev. *73*, 679 (1948).
[63] A. Abragam, The Principles of Nuclear Magnetism, Clarendon, Oxford 1961.
[64] R. C. Bowman, Jr., A. J. Maeland, W. K. Rhim, Phys. Rev. *B26*, 6362 (1982).
[65] R. C. Bowman, Jr., A. Attala, A. J. Maeland, W. C. Johnson, Solid State Commun. *47*, 779 (1983).
[66] H. E. Schone, E. F. W. Seymour, G. A. Styles, J. Phys. Paris *12*, Suppl. C8–675 (1985).
[67] A. Schirmer, P. Heitjans, H. Ackermann, B. Bader, P. Freiländer, and H.-J. Stöckmann, Solid State Ionics, *28–30*, 717 (1988).

Presented at the Discussion Meeting of the Deutsche Bunsen-Gesellschaft für Physikalische Chemie "Rate Processes in Dissipative Systems: 50 Years after Kramers" in Tutzing, September 10–13, 1990 E 7510

Proton Quantum Tunneling in Hydrated Protein Surface

G. Careri and G. Consolini

Dipartimento di Fisica, Universita' di Roma "La Sapienza", Piazzale Aldo Moro, 2-00185, Rome, Italy

Dielectrics / Hydration / Tunneling / Protein / Proton Transfer

We measure the protonic conductivity in water clusters adsorbed on lysozyme powders, below room temperature. In the low temperature region the conductivity increases with temperature as $\exp T^{-6}$, in agreement with prediction by the theory of dissipative quantum tunneling. We detect the onset of this effect near 180 K, where a glass transition in the protein matrix is known to take place. Quantum tunneling matches smoothly with thermal hopping near 271 K.

Previous work from this laboratory has shown that hydrated lysozyme powders exhibit dielectric behavior due to proton conductivity [1], and that this behavior can be described in the frame of percolation theory [2, 3]. Long range proton displacement appears only above the critical hydration for percolation h_c (g water/g dry weight), when the 2-dimensional motion takes place on fluctuating clusters of hydrogen-bonded water molecules adsorbed on the protein surface. A similar 2-dimensional protonic percolation has been detected in powdered smaples of purple membrane of *Halobacteriums Halobium* [4]. In both cases the emergence of biological function, respectively enzyme catalysis and photoresponse, has been found to coincide with the critial hydration for percolation h_c. More recently the above room temperature studies have been extended towards other viable systems [5]. Here we report results on the low temperature protonic conductivity of hydrated lysozyme powders, to investigate the possible occurence of proton quantum tunneling in hydrogen bonded water molecules adsorbed on protein.

The dielectric tecnique has been already described [1] as well as the procedure to evaluate the d.c. conductivity σ of the sample [4, 5]. In this work the insulated electrode-capacitor is reduced to a two layer composite capacitor, one layer being the 1.8 mm teflon sheets and the other one the 4.5 mm lysozyme powder at constant water content h. This capacitor was cooled to 170 K by cryogenic apparatus at a rate of 3 K min^{-1}. Dielectric data from 10 KHz to 1 MHz have been recorded while raising the temperature at a rate of about 1 K min^{-1}. A typical run lasted about 6 hours and included about 300 conductivity vs temperature data. Native lysozyme, prepared by Professor John A. Rupley (University of Arizona, Tucson) was at pH 7 [3]. The same preparation, of about 0.3 g, was used in all runs, and it was hydrated by the isopiestic method with either H_2O or D_2O. Several H_2O and D_2O-hydrated samples have been studied, and the pertinent parameters of each sample are shown in Table 1. At the lowest temperatures here investigated the conductivity is found temperature independend, and it is of uncertain origin [6]. This limiting low value of σ_0 varies around $\sigma_0 = (6.3 \pm 0.6) \times 10^{-9}$ mho m^{-1} because of lack of reproducibility of capacitor geometry in different runs. Above Tg1 the conductivity increases with increasing temperatures, and at Tg2 it displays a slight break. Both Tg1 and Tg2 can be associated with protein glass transitions, as it will be discussed elsewhere.

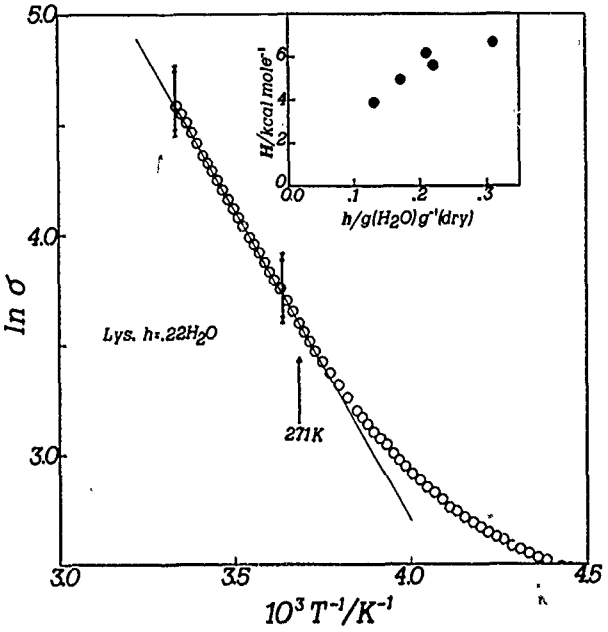


Fig. 1
Natural logaritm of part of conductivity data plotted vs reciprocal absolute temperature $1/T$ in the high temperature region. In the upper inset the activation energy H, defined as the limiting slope reached by the data, is plotted vs hydration level for H_2O-hydrated samples

As shown in Fig. 1, in the high temperature region the Arrhenius law is accurately followed, with an activation energy H slightly increasing with hydration level. Our values of H are close to 29.4 KJ/mol, the activation energy detected by NMR for water reorientation correlation time [7], suggesting that the mobility of the adsorbed water molecules must be the major controlling factor for proton transport, if the proton number density is assumed to be temperature independent. This last assumption is frequently made to describe the electric conductivity of biopolymers [8] and of ice [9], where extrinsic charge carriers are believed to be produced with an energy lower than the dissociation energy of a water molecule. Thus at temperatures above about 260 K the rate process is controlled by a thermally activated hopping of charged defects over an energy barrier which is

Table 1
Parameters of investigated samples, defined and discussed in text

Sample	hydr.	h (g/g)	σ_0 (10^{-9} mho·m^{-1})	$\delta\sigma_0$	H (Kcal/mol)	tgα (10^{-15} K^{-6})	tgβ
1	H_2O	0.07	5.5 ± 0.2	–	–	–	–
2	H_2O	0.13	6.0 ± 0.2	+0.55	3.89 ± 0.06	16.34 ± 0.25	1.73 ± 0.02
3	H_2O	0.17	6.0 ± 0.2	−0.03	4.95 ± 0.08	20.79 ± 0.34	2.76 ± 0.01
4	H_2O	0.21	7.3 ± 0.3	−0.40	6.16 ± 0.06	25.87 ± 0.25	3.90 ± 0.10
5	H_2O	0.22	6.3 ± 0.3	−0.28	5.61 ± 0.01	25.56 ± 0.04	4.32 ± 0.01
6	H_2O	0.31	6.1 ± 0.2	+1.48	6.67 ± 0.06	28.01 ± 0.25	7.00 ± 0.02
7	D_2O	0.22	6.9 ± 0.3	–	5.89 ± 0.06	24.74 ± 0.25	3.75 ± 0.04
8	D_2O	0.06	6.0 ± 0.2	–	–	–	–

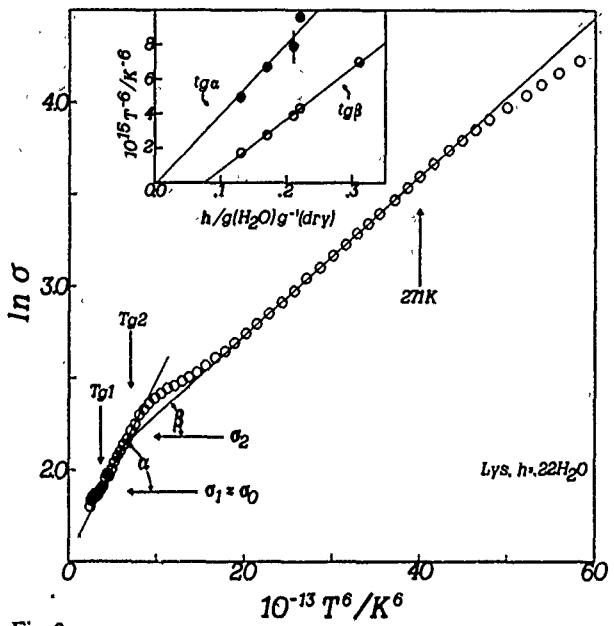


Fig. 2
Natural logaritm of part of conductivity data plotted vs the sixth power of the absolute temperature T^6 in the low temperature range. In the upper inset the slope tgα and tgβ of the straight lines (see Fig. 3) focussing respectively on (Tg_1, σ_1) and (Tg_2, σ_2) are reported vs hydration level h. Solid line is best fit through data included between vertical bars

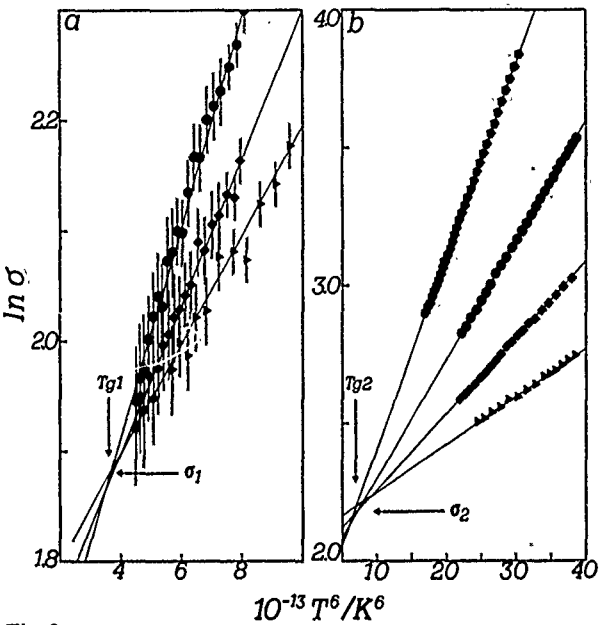


Fig. 3
The same as Fig. 2 including H_2O-hydrated samples at hydration level $h = 0.31$ (pentagons), 0.22 (circles), 0.17 (squares), 0.13 (triangles). Solid lines are best fit through data. Conductivity data shown in (a) have been corrected by an arbitrary $\Delta\sigma_0$ reported in Table 1 and discussed in text. Sample at $h = 31$ has not been included in (a) because affected by large hysteresis at Tg1. From these plots we have evaluated Tg1 = 182 ± 2 K and $\sigma_1 = 6.6 \pm 1 \times 10^{-9}$ mho m^{-1}, and Tg2 = 203 ± 5 K and $\sigma_2 = 8.8 \pm 4 \times 10^{-9}$ mho m^{-1}

temperature independent, in agreement with current models [10] for proton transfer in H_2O networks.

In the following we shall consider the temperature region where tunneling may prevail. A general theory of quantum tunnel out of a metastable state interacting with an environment at temperature T has been produced by Grabert, Weiss and Hänggi (GWH) [11], with the finding that for damping of arbitrary strenght, the tunneling decay rate always matches smoothly with the Arrhenius factor at a crossover temperature and that heat enhances the tunneling probability at $T = 0$ K by a factor exp $[A(T)]$. For undamped system $A(T)$ is exponentially small, whereas for a dissipative system $A(T)$ grows algebrically with temperature. Of particular interest here is the case of tunneling centers in solids, where $A(T)$ increases proportional to T^n at low temperature, with $n = 4$ or 6. In order to test the GWH theory, in Fig. 2 we have plotted the log (conductivity) data versus T^6, and we find that a remarkably simple description can be offered as follows. In this T^6 plot, the conductivity data $\ln\sigma(h,T)$ can be fitted by straight lines originated near Tg1 and $\sigma_1 \sim \sigma_0$, and after a break can be fitted by straight lines originating at Tg2 and $\sigma_2 > \sigma_1$. Fig. 3a shows the procedure followed to detect the focuss by linear extrapolation of the data, imposing a small but arbitrary displacements $\Delta\sigma_0$ to all conductivtity data of each sample, to take into account the above mentioned difficulty to reproduce the capacitor geometry. The focussing on Tg2 is insensitive to this correction because here $\sigma \gg \sigma_0$. As shown in Fig. 4, even the linear T^4 plot is accurately followed up to a crossover temperature range of about 10 K, where it merges with the lower temperature side of the Arrhenius law shown in Fig. 1, as required by GWH theory [11]. Finally, we have fitted

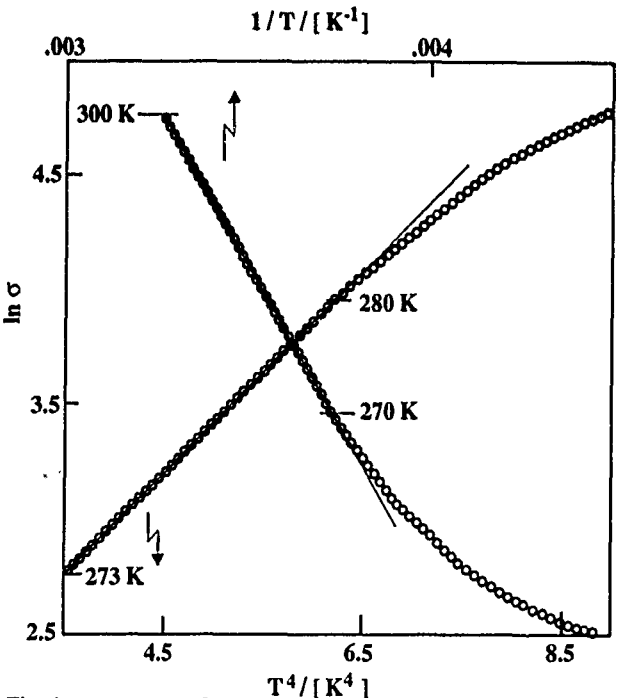


Fig. 4
Natural logaritm of all conductivity data near the crossover region, plotted vs reciprocal absolute temperature (upper scale) and vs the fourth power of the absolute temperature (lower scale) Solid lines are best fit through data included between orizontal bars

our data with different values of n, but Fig. 5 shows that only $n = 4$ gave results comparable with $n = 6$, as predicted by GWH theory [11].

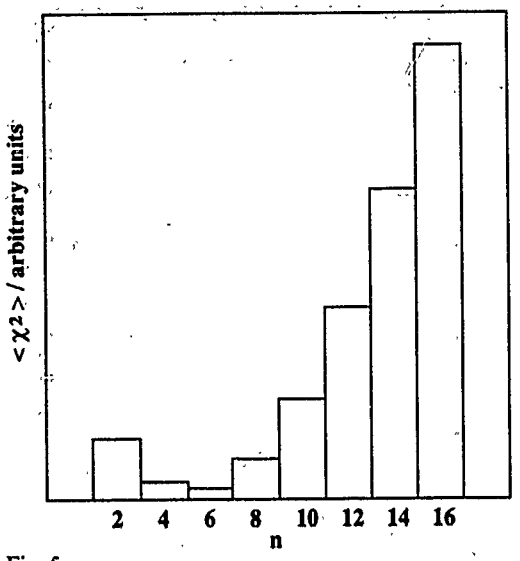


Fig. 5
Statistical best fit $\langle \chi^2 \rangle$ of all conductivity data plotted versus n, the exponent used in GWH theory, defined in Text

Although the linear dependence of $\ln\sigma$ on T^4 or T^6 requested by GWH is certainly fullfilled, this theory requires that proton tunneling start at $T = 0$ K and that it depends on the mass of the carrier. We believe that this apparent contraddiction between GWH theory and our data can be easily overcome by suggesting that charged defects are free to tunnel across an energy barrier only above the protein glass transition temperature Tg1, when the adsorbed water cluster behaves as a supercooled fluid.

In conclusion, our data show that theory can be used as a guide to describe dissipative quantum tunneling in a molecular process. Proton tunneling displayed by hydrated biological systems below room temperature has been reported elsewhere [12].

Several discussions with Prof Peter Hänggi (Augsburg) are gratefully aknowledged. This work was supported in part by I.N.F.M. and by EEC projects SCI000229.

References

[1] G. Careri, M. Geraci, A. Giansanti, and J. A. Rupley, Proc. Natl. Acad. Sci. USA *82*, 5342 (1985).
[2] G. Careri, A. Giansanti, and J. A. Rupley, Proc. Natl. Acad. Sci. USA *83*, 6810 (1986).
[3] G. Careri, A. Giansanti, and J. A. Rupley, Phys. Rev. A *37*, 2703 (1988).
[4] J. A. Rupley, L. Siemankowski, G. Careri, and F. Bruni, Proc. Natl. Acad. Sci. USA *85*, 9022 (1988).
[5] F. Bruni, G. Careri, and J. S. Clegg, Biophys. J. *55*, 331, (1989). F. Bruni, G. Careri, and A. C. Leopold, Phys. Rev. A *40*, 2803 (1989).
[6] R. Pethig, Dielectric and Electronic Properties of Biological Materials, Wiley; New York, 1979.
[7] E. R. Andrew, D. J. Bryant, and T. Z. Rizvi, Chem. Phys. Lett. *95*, 463 (1983).
[8] E. J. Murphy, J. Phys. Chem. Solids *16*, 115 (1960).
[9] P. V. Hobbs, *Ice Physics*, p. 100. Clarendon Press, Oxford, 1974.
[10] St. Pnevmatikos, Phys. Rev. Lett. *60*, 1534 (1988). A. Zolotaryuk and St. Pnevmatikos, Phys. Lett. A *143*, 223 (1990).
[11] H. G. Grabert, U. Weiss, and P. Hänggi, Phys. Rev. Lett. *52*, 2193 (1984); Z. Phys. B, *56*, 171 (1984).
[12] G. Careri and G. Consolini, Biol. Chem. *37*, 165 (1990).

Presented at the Discussion Meeting of the Deutsche Bunsen-Gesellschaft für Physikalische Chemie "Rate Processes in Dissipative Systems: 50 Years after Kramers" in Tutzing, September 10–13, 1990 E 7511

Periodic Orbit Approach to the Quantum-Kramers-Rate

Peter Hänggi and Waldemar Hontscha

Lehrstuhl für Theoretische Physik, Universität Augsburg, Memminger Str. 6, D-8900 Augsburg

Chemical Kinetics / Multidimensional WKB / Quantum Mechanics / Reaction Rate Theory

The quantum analog of Kramers reaction rate for a dissipative environment is derived on the basis of a periodic orbit approach for multidimensional tunneling. The resulting reaction rate expression holds at all temperatures, thus covering [in contrast to the imaginary free energy method ("bounce-"method)] the classical and the quantum regime on the same basis.

Introduction

Quantum reaction rate theory underwent profound developments within the last decade. In particular, the recent progress in the quantum theory in presence of dissipation [1, 2, 3, 4] enables one to generalize the classical theory of Kramers for the rate coefficient in a dissipative environment to the quantum regime [3, 5–9]. Our focus will be on the semiclassical limit of the quantum-transition-state-theory (QTST) in presence of an infinite number of bath degrees of freedom which model the dissipation, i.e. we shall elaborate on a unified approach to the dissipative quantum Kramers rate in a metastable potential $V(x)$ in which the reaction coordinate x of a reactive particle of mass M is coupled to a continuum of bath degrees of freedom.

Conventional quantum-TST represents a rather patchwork affair. In doing quantum calculations one replaces classical partition functions by their quantum counterparts, assuming separability of the various vibrations and/or rotations near the saddle point, and then corrects for multiple crossings near the barrier top by the multiplication of a temperature-

 © VCH Verlagsgesellschaft mbH, W-6940 Weinheim, 1991 0005-9021/91/0303-0379 $ 3.50+.25/0

dependent Wigner-like transmission factor [10, 11]. Therefore, this approach essentially restricts the quantum treatment to the high temperature limit. It was only until recently that the case of dissipation (continuum of bath degrees of freedom) has been discussed within this approach in a beautiful paper by Pollak [12].

Within the last decade, the quantum-Kramers rate has originally been studied over the whole temperature regime by the Augsburg-Essen-Polytechnic-Stuttgart school [5, 7, 8, 9, 13, 14] and the Moscow school [6] which all made use of the imaginary-free-energy methodology [15]. The primary object of this latter method is the dissipative bounce (instanton/anti-instanton) solution. This periodic solution – in absence of the influence of dissipation – has been introduced in Miller's semiclassical quantum-TST for non-separable systems [16], see also Refs. [17–20]. Following the original reasoning of Miller [16], we shall re-evaluate the quantum-Kramers rate results [3, 5–9] by use of the multidimensional WKB-approach for the quantum-TST rate in terms of periodic orbit theory [21, 22]. In doing so, we cover the whole temperature regime from $T = 0$ up to room temperature on a unified basis. In a previous item [23], see also Refs. [8b, 9], we have already reported the results of the continuum limit of this multidimensional WKB quantum rate approach. In this paper, we present a more extended discussion of the various approximations used in arriving at the quantum-Kramer's rate expressions, and give additional new results.

Quantum Reaction Rate Theory

Throughout the following we shall assume that there exists a true time-scale separation for the dynamics within the locally stable state at $x = x_0$, i.e. $V(x_0) = 0$, and the dynamics characterizing the passage through the bottleneck of the metastable potential, $V(x)$ (e.g. a cubic potential) separating products from reactants. Then, an initial nonequilibrium population decays exponentially for times longer than the typical time-scale for nonactivated molecular processes within the well. Thus, the rate coefficient k becomes truely time-independent; it can formally be expressed as the flux integral [24, 25]

$$k = Z_0^{-1}\ \mathrm{Re}[\mathrm{Tr}\{\exp(-\beta H)\,\delta(x)\,(p/M)\,\mathscr{P}\}]. \tag{1}$$

Here, Tr denotes the trace, β denotes the inverse temperature and Z_0 is the partition function of the metastable state at $x_0 < 0$, $x = 0$ indicates the transition state, and $\mathscr{P}$ is the operator that projects onto positive momentum states p in the infinite future ($t \to \infty$). H denotes the total (system plus bath) Hamiltonian operator. The reaction coordinate x of the escaping particle ranges from $x = -\infty$ to $x = +\infty$. With a few manipulations this formally exact rate expression can be cast as an integral over a flux-flux autocorrelation $C(t)$, i.e. [26]

$$k = Z_0^{-1} \int_0^\infty C(t)\,\mathrm{d}t \tag{2}$$

where with $t_c = t - i\hbar\beta/2$

$$C(t) = \mathrm{Tr}\,[\hat{F}\exp(iHt_c^*/\hbar)\,\hat{F}\exp(-iHt_c/\hbar)]\,, \tag{3}$$

wherein $\hat{F} = \frac{1}{2}\,[\delta(x)\,(p/M) + (p/M)\,\delta(x)]$ is the symmetrized flux operator.

Semiclassical Quantum-Transition-State-Theory

Following Miller [16] the quantum – TST approximation to the rate k consists in the replacement in (1):

$$\delta(x)\,(p/M)\,\mathscr{P} \to \frac{1}{2}\,\delta(x)|\dot{x}|\,, \tag{4}$$

and then proceeds by use of the *semiclassical* approximation for the Boltzmann propagator. Thus, one obtains [16]

$$k \to k_{\mathrm{TST}} = Z_0^{-1}\,\mathrm{Re}\left\{\int \mathrm{d}q\,\langle q|\exp(-\beta H)|q\rangle\,\delta(x)\frac{1}{2}|\dot{x}|\right\}. \tag{5}$$

Here, $q \equiv (q_0 = x, q_1, \ldots, q_N)$ are the coordinates of all the degrees of freedom of the system, (x) and bath, $(q_1, \ldots, q_N)$. In going from (1) to (5) we made use of a Weyl ordering for the operator $\delta(x)\,|\dot{x}|$, [16], i.e. we can replace the trace in (1) by the phase-space average over the Wigner function. By use of the semiclassical expression for the propagator $\exp(-\beta H)$ the corresponding phase space [16] integration has – in consistency with the use of the semiclassical result – been evaluated within the stationary phase approximation (SPA). This procedure then yields (5). Continuing in this vein and evaluating the trace in (5) also in SPA yields a continuum of stationary phase points. This continuum of SPA-points just defines the unstable periodic orbit, or the bounce solution [16]. In view of the Boltzmann propagator, however, this periodic orbit exists for pure negative imaginary times only, i.e. the Wick rotated time $t \to \tau = it$, is real and positive. We now measure distance along this periodic orbit, $q_0 \equiv x$, with all other coordinates being orthogonal displacements away from it. Therefore, all the integrations over the orthogonal displacements can again be evaluated within SPA. In terms of the Green's function

$$\frac{1}{E + i\varepsilon - H} = \frac{-i}{\hbar}\int_0^\infty \mathrm{d}t\,\exp\left\{\frac{i}{\hbar}\,(E + i\varepsilon - H)\,t\right\} \equiv G(E + i\varepsilon) \tag{6}$$

we have with

$$\exp(-iHt/\hbar) = \frac{1}{2\pi}\int \mathrm{d}E\,\exp(-iEt/\hbar)\,G(E)\,, \tag{7a}$$

and $\beta = it/\hbar$ the formal identiy

$$\exp(-\beta H) = \lim_{\varepsilon \to 0^+}\frac{1}{2\pi}\int_{-\infty}^{\infty}\mathrm{d}E\,\exp(-\beta E)\,G(E + i0^+)\,. \tag{7b}$$

Inserting (7) into (5) yields the rate coefficient k_{TST} as a *Boltzmann average*

$$k_{TST} = Z_o^{-1} \operatorname{Re}\left\{\frac{i}{2\pi}\int_0^\infty dE \exp(-\beta E) \cdot \int dq\, \delta(q_o)\frac{1}{2}|\dot{q}_o|\langle q|G(E+i0^+)|q\rangle\right\}. \tag{8}$$

In virtue of this expression involving the Green's function one never has to construct a multidimensional wave function. This feature represents a great advantage when treating the effects of dissipation.

The trace in (8) can now be evaluated by use of unstable periodic orbit theory [22]. Integrating within SPA over the orthogonal fluctuations, with $q = q_o$ fixed, and then integrating over q_0 (which is trivially accomplished due to the δ-function in (8)) yields Miller's central result [16]

$$k_{TST} = Z_o^{-1}\frac{1}{2\pi\hbar}\int_0^\infty dE \exp(-\beta E)\, k(E), \tag{9a}$$

where the cumulative reaction probability reads

$$k(E) = \sum_{n=1}^{\infty}(-1)^{n-1}\exp[-n\,\phi(E)/\hbar] \cdot \prod_{i=1}^{N}\left\{2\sinh\left[\frac{1}{2}n\,T(E)\,\omega_i(E)\right]\right\}^{-1}. \tag{9b}$$

Here, $\phi(E)$ is the abbreviated (Euclidean) action integral along the unstable periodic orbit of period $T(E) = -\phi'(E)$ on the inverted potential landscape (Wick rotation of time $t = -iT(E)$). The set $\{\omega_i(E), i = 1, ..., N\}$ are the stability (angular) frequencies of the unstable periodic orbit. If, $\phi(E)$ is positive (low temperatures) we note that only the $n = 1$ term contributes significantly to (9a).

Next we use the selfconsistent solution of

$$E_T = E - \sum_{i=1}^{N}\left(n_i + \frac{1}{2}\right)\hbar\omega_i(E_T) \tag{10}$$

as the energy E_T which is left in the reaction coordinate while the system is crossing the saddle point with the bath being excited $\{n_i\}$ in corresponding modes. Following the reasoning of Miller [27] which he put forward to obtain the improved quantum condition for the eigenvalues of an ergodic system, we now construct an improved, and rather appealing expression for $k(E)$, i.e. following Hänggi and Hontscha [23] we use the tunneling energy in (10) and set [9, 23]

$$k(E) = \sum_{(n_1,\ldots,n_N)=0}^{\infty}\left\{1+\exp[\phi(E_T)/\hbar]\right\}^{-1}. \tag{11}$$

In doing so, we have "unexpanded" the corresponding expression in (9b) which results if the sinh-fcts are expanded into geometric series (for more details, see Refs. 9, 28). Eq. (11) represents a uniform WKB-approximation to $k(E)$, which becomes exact in multidimensional, separable parabolic-like potential landscapes. We stress that (11) accounts for the anharmonic nonlinearities in the reaction coordinate x; but neglects the influence of anharmonicities for the "transverse" bath degrees of freedom.

With $k(E)$ given in (11), the quantum-TST rate is obtained by insertion of (11) into (9a) and then performing the remaining summations and the integration over the range of total energy E of system plus bath. It also should be noticed that this procedure yields a closed expression for the multidimensional quantum TST-rate that holds true for all temperature [23]. Further, with the density of states for a harmonic oscillator, i.e. $\varrho(E) = (2\pi\,\hbar/T(E))^{-1}$ it follows on inspection of (9a) that the quantity

$$\Gamma(E) = k(E)/T(E) \tag{12}$$

denotes a *semiclassical expression for the microcanonical rate coefficient at total conserved energy E.*

Periodic Orbits: A Useful Identity

Before we proceed to evaluate more explicitly the dissipative quantum-Kramers rate in the continuum limit we shall reconcile the various approximations leading to (9). First the trace operation in (5) naturally leads within the semiclassical limit to the consideration of periodic orbits which give the dominant contributions to (5). In view of the Boltzmann propagator $\exp(-\beta H)$, such periodic orbits, which pass through the transition state location (see (8)), *do not exist in real time* but only in (negative) imaginary time $t = -i\tau$, i.e. $\tau = it$. Therefore, it is advantageous to consider the Euclidean version of the propagator. In original time t, such negative imaginary time periods imply for the SPA-evaluation of (6) a distortion of the integration path into the lower complex half-plane. In other words, we analytically continue the semiclassical propagator $\langle q|\exp(-iH\,t/\hbar)|q\rangle$ to complex times $t = -i\tau$. The analytically continued Green's function then formally reads [28]

$$\langle q|G(E)|q\rangle \rightarrow \langle q|G_\varepsilon(E)|q\rangle \equiv \frac{-1}{\hbar} \cdot \int_0^\infty d\tau \exp(E\tau/\hbar)\langle q|\exp(-\tau H/\hbar)|q\rangle. \tag{13}$$

The time integration inherent in (13) must be understood to be performed in SPA with the integration path deformed so as to go through the stationary points in the direction of steepest descent. This procedure is consistent with the use of the semiclassical approximation. Such an approach generally requires some care near conjugate points [focal surfaces], see [29]. This SPA integration fixes the period of the periodic orbit $\tau_{period} = T(E)$, such that the corresponding classical energy of the periodic orbit equals the value $E = E_{periodic\ orbit}$. The final trace over q in (8) is then calculated following the recipe of Gutzwiller [22], i e all the transverse displacements along the periodic orbit are again evaluated

in SPA, while the final integration over q_0 would simply yield the period $T(E)$. By accounting for multiple transversals of the periodic orbit, $T(E) \to n\,T(E)$, and keeping track of the phase changes of the periodic orbit at conjugate points yielding the phase $(-1)\cdot(-1)^{n-1}$, one obtains for the trace of the analytically continued Green's function $G_e(E+i0^+) \equiv \frac{-1}{\hbar}\int_0^\infty d\tau \exp(E\tau/\hbar)\exp(-\tau H/\hbar)$ by use of the Refs. [16, 22] the result [28]

$$\int dq \langle q|G_e(E+i0^+)|q\rangle = \frac{(-i)}{\hbar}[iT(E)] \cdot \sum_{n=1}^{\infty}(-1)^{n-1}\exp(-n\phi(E)/\hbar) \cdot \prod_{i=1}^{N}\left\{2\sinh\left[\frac{1}{2}nT(E)\,\omega_i(E)\right]\right\}^{-1}. \tag{14}$$

Note that in (13) the fundamental period $T(E)$ is obtained independent of the number of periods. This is so because $T(E)$ stems from an integration over q_0, and not over time τ. The multiple traversals must be accounted for because to obtain the SPA result we must sum over all solutions for the period $T(E) \equiv T_e(E)$ yielding a fixed energy E [30, 31]. Thus, we deal with an infinite sequence of stationary points along the (negative) – imaginary time axis, $t_n = -inT(E)$; i.e. $\tau_n = nT(E)$. More generally, the result in (13) would be improved further along the line of reasoning of Hänggi, Weiss and Riseborough [32] by including not only real times τ, but also complex-valued time periods $\tau_{nk} \ldots = nT_e(E) + ik\,T_m(E) + \ldots$, yielding a fixed energy E. Here, the index e stands for "Euclidean" and m for "Minkowskian", in reference to the corresponding regions of the non-inverted, original potential landscape such as the barrier region (e), or the reactant and/or product region (m). In particular, *apart* from the normalization factor Z_0^{-1} the rate expression in (9a) is observed to include information about the classically forbidden region (transition-state region) only. Thus, just as with the imaginary free energy bounce formalism – any interference effects to the decay rate stemming from the classically allowed quantum dynamics in the non-inverted potential landscape is not accounted for. Such effects, for example, include backscattering from reactant regions [32], and/or curvature effects of the classically allowed reaction paths.

In Gutzwiller's procedure, the trace is calculated keeping the fluctuations zero at a fixed point on the periodic orbit, and integrating over these fixed points at the end (yielding the period $T(E)$). Likewise, the trace can be evaluated by considering all closed orbits and allowing both for longitudinal and transversal fluctuations around a fixed periodic orbit $\bar{q}(\tau)$. For the trace of the Wick-rotated Green's function

$$\int dq\,\langle q|G_e(E)|q\rangle = \frac{-1}{\hbar}\int_0^\infty d\tau \exp(\tau E/\hbar)\,\mathrm{Tr}[\exp(-\tau H/\hbar)] \tag{15}$$

one alternatively can evaluate the semiclassical limit following the reasoning of Callan and Coleman [20]. Use of the SPA (in function space) for the trace in (15) yields stationary solutions obeying $\bar{q}(0) = \bar{q}(\tau)$. Among those are two constant solutions $\bar{q}(\tau') = x_0$ characterizing the stable state dynamics (i.e. it yields Z_0, see below), and $\bar{q}(\tau) = 0$, characterizing the barrier motion. In view of (8) we consider now only periodic paths passing forth and back the transition state. We shall restrict the following discussion to low temperatures; i.e. the rate controlling relevant energies E in the expression (9a) all are lying below the barrier energy $E = E_b$. With this in mind, we consider for (15) such τ-values for which the nontrivial periodic solution $\bar{q}(0) = \bar{q}(\tau)$ is real-valued. Setting for a general periodic path

$$q(\tau') = \bar{q}(\tau') + \sum_n c_n x_n(\tau'), \tag{16}$$

with $x_n(\tau')$ obeying periodic boundary conditions $x_n(0) = x_n(\tau)$, one considers – for small $\hbar$ – terms in the action up to quadratic order only. In our case, we consider the Euclidean Lagrangian for a harmonic bath coupled bilineary to the nonlinear reaction coordinate x.

$$L_e = \frac{M}{2}\dot{x}^2 + V(x) + \sum_{i=1}^{N}\frac{1}{2}m_i\left\{\dot{q}_i^2 + \left(\Omega_i q_i + \frac{C_i}{m_i\Omega_i}x\right)^2\right\}. \tag{17}$$

Following the standard procedure, one finds after integrating first over the harmonic bath degrees of freedom in terms of the dissipative bounce trajectory $\bar{q}(\tau')$ and the well-known non-local (Euclidean) Lagrangian L_{eff} [5–9, 13, 14] for the trace the result [28]

$$\mathrm{Tr}[\exp(-\tau H/\hbar)] = iA\tau\left(\frac{S_0}{2\pi\hbar}\right)^{1/2}\prod_{i=1}^{N}\left[2\sinh\left(\frac{1}{2}\tau\Omega_i\right)\right]^{-1} \cdot |\det'\delta^2 S_e|_{\bar{q}}^{-1/2}\exp[-S_e(\bar{q},\tau)/\hbar], \tag{18a}$$

where

$$S_0 = M\int_{-\tau/2}^{\tau/2} du\,(\dot{\bar{q}}(u))^2,\; S_e = \int_0^\tau L_e(\bar{q},\dot{\bar{q}})\,du = \int_0^\tau L_{\mathrm{eff}}[\bar{q},\dot{\bar{q}}]\,du. \tag{18b}$$

det' indicates that the Goldstone mode contribution of the eigenvalue zero must be omitted. A is a normalization constant to be determined below. The τ-integration in (15) is again calculated in SPA. This yields the condition $E = \partial S_e/\partial\tau$, i.e. this fixes the period $\tau_{\mathrm{SPA}} \equiv T(E)_{\mathrm{SPA}}$ to equal the total energy E, i.e. $S_e = \phi(\bar{q}) + T(E)E$. With E in the classically forbidden regime we need to consider the primitive orbit only of period $T(E)$, i.e. $G_e \cong G_e^{(1)}$. Insertion of (18) into (15) yields

$$\int dq\,\langle q|G_e^{(1)}(E+i0^+)|q\rangle) = \frac{A}{\hbar}S_0^{1/2}\,T(E) \cdot [\det'\delta^2 S_e|_{\bar{q}}(-\partial^2 S_e/\partial\tau^2)_{T(E)}]^{-1/2} \cdot \left\{\prod_{i=1}^{N}\left[2\sinh\left(\frac{1}{2}T(E)\,\Omega_i\right)\right]^{-1}\right\}\exp[-\phi(E)/\hbar]. \tag{19}$$

Hereby we observe that the SPA yields a phase $i = \exp(i\pi/2)$, which with $(-1)\,iA(i) = A$ yields a real quantity for the analytically continued object (14, 15). The normalization constant, A, stemming from the measure over $\{c_n\}$, can be obtained if we evaluate Z_o, i.e. we use $\bar{q}(0) = \bar{q}(\tau = T(E)) x_o$. This yields [28]

$$Z_o = A|\det \delta^2 S_c|_{\bar{q}=x_o}^{-1/2} \prod_{i=1}^{N} \left[2\sinh\left(\frac{1}{2}T(E)\Omega_i\right)\right]^{-1} \tag{20a}$$

$$= \prod_{i=0}^{N} \left[2\sinh\left(\frac{1}{2}T(E)\lambda_i^o\right)\right]^{-1}. \tag{20b}$$

Here, the set $\{\lambda_i^o\}$, $i = 0, 1, 2, \ldots, N$, are the normal mode (angular) frequencies at the metastable state $\bar{q} = x_o$. Upon expressing A by use of (20b), one finds with n set equal to one upon the comparison of (19) with (14) the important identity:

$$S_o^{1/2}\left(\frac{|\det \delta^2 S_c|_{\bar{q}=x_o}}{|\det' \delta^2 S_c|_{\bar{q}(\tau)}}\right)^{1/2} = Z_o^{-1}\left(-\frac{\partial^2 S_c}{\partial \tau^2}\right)_{\tau=T(E)}^{1/2} \cdot \prod_{i=1}^{N}\left[2\sinh\left(\frac{1}{2}T(E)\omega_i(E)\right)\right]^{-1}. \tag{21}$$

This relation is of use for the explicit evaluation of determinants. Note also, that in contrast to (14), the SPA in the time integration for (19) is performed here at the end, while for (14) it defines the first step in the approximation scheme, thereby fixing the period $\tau = T(E)$.

The Quantum Kramers Rate

Following Hänggi and Hontscha [23], we now present explicit results for the Kramers rate of a particle that interacts with a continuum ($N \to \infty$) of bath modes, cf. (17). In terms of the spectral function

$$J(\omega) = \frac{\pi}{2M}\sum_{i=1}^{\infty}\frac{C_i^2}{m_i\Omega_i}\delta(\omega - \Omega_i), \tag{22}$$

the Laplace transform the memory-friction kernel $\gamma(t)$ can be expressed as

$$\hat{\gamma}(z) = \frac{2}{\pi}\int_0^{\infty} d\omega \frac{J(\omega)z}{\omega(z^2+\omega^2)}. \tag{23}$$

First, we shall consider high temperatures T above the crossover temperature T_o [5], i.e. with k_B the Boltzmann constant

$$T > T_o = \frac{\hbar}{2\pi k_B}\mu \tag{24}$$

where μ denotes the positive root of

$$\mu = \left[\frac{\hat{\gamma}^2(\mu)}{4} + \omega_b^2\right]^{1/2} - \frac{1}{2}\hat{\gamma}(\mu) \tag{25}$$

and $\omega_b = |M^{-1}V''(q_o = 0)|^{1/2}$. In other words, μ denotes the dissipation-modified normal mode barrier frequency $\omega_b \to \mu(\hat{\gamma})$. With $E_T > E_b$, the effective abbreviated action $\phi(\bar{q})$ is negative. Thus the cumulative reaction probability is not exponentially sensitive, and with $k_BT/E_b \ll 1$, anharmonic corrections are negligible. Thus we can use a harmonic approximation, i.e. the period $T(E)$ assumes a constant value $T(E) = 2\pi/\mu$ and the stability frequencies can be approximated by the normal modes in the saddle point region, i.e. $\omega_i(E) \to \lambda_i^b$. The abbreviated action thus reads

$$\phi(E_T) = (E_b - E_T)\,2\pi/\mu < 0\,. \tag{26}$$

Upon an interchange of the integration in (9a) with the summations we find

$$k_{TST} = Z_o^{-1}\frac{1}{2\pi\hbar}\sum_{n_1,\ldots,n_N=0}^{\infty}\exp\left\{-\beta\left[E_b + \sum\left(n_i + \frac{1}{2}\right)\hbar\lambda_i^b\right]\right\} \cdot \int_0^{\infty} dE \frac{\exp\left\{\beta\left[E_b + \sum_i\left(n_i+\frac{1}{2}\right)\hbar\lambda_i^b - E\right]\right\}}{1+\exp\left\{\beta_o\left[E_b+\sum_i\left(n_i+\frac{1}{2}\right)\hbar\lambda_i^b - E\right]\right\}}, \tag{27}$$

where $\beta_o \equiv 2\pi(\hbar\mu)^{-1}$. Setting

$$x = \exp\left\{\beta\left[E_b + \sum_i\left(n_i+\frac{1}{2}\right)\hbar\lambda_i^b - E\right]\right\},$$

the integral in (27) becomes with $x_o = x(E \equiv 0)$

$$\beta^{-1}\int_0^{x_o} dx \frac{1}{1+x^{\beta\omega/\beta}} = \beta^{-1}\left[\int_0^{\infty}\frac{dx}{1+x^{\beta\omega/\beta}} - \int_{x_o}^{\infty}\frac{dx}{1+x^{\beta\omega/\beta}}\right] = \frac{\pi}{\beta_o}[\sin(\pi\beta/\beta_o)]^{-1} - \frac{x_o^{-(\beta_o-\beta)/\beta}}{(\beta_o-\beta)}\varepsilon, \tag{28}$$

where $\frac{1}{2} < \varepsilon < 1$. With $\beta E_b \gg 1$, this correction can be neglected to give after corresponding summations

$$k_{TST} = \frac{\mu}{2\pi}\frac{2\sinh(\hbar\beta\lambda_o^o/2)}{2\sin(\hbar\beta\mu/2)}\left\{\prod_{i=1}^{N}\frac{2\sinh(\hbar\beta\lambda_i^o/2)}{2\sinh(\hbar\beta\lambda_i^b/2)}\right\}\exp(-\beta E_b), \tag{29}$$

By use of the Pollak identities [12], the products in (29) can be related directly to the dissipation $\hat{\gamma}$, i.e.

$$k_{TST}(T > T_o) = \left(\frac{\mu\omega_o}{\omega_b 2\pi}\right)\exp(-\beta E_b) \cdot \prod_{n=1}^{\infty}\frac{\omega_o^2 + n^2v^2 + nv\hat{\gamma}(nv)}{-\omega_b^2 + n^2v^2 + nv\hat{\gamma}(nv)} \tag{30}$$

where $v = 2\pi/\hbar\beta$, $\omega_o^2 = M^{-1}V''(x = x_{well})$.

At temperatures $T \cong T_o$, the above approximation diverges at $T = T_o$ proportional to $(T - T_o)^{-1}$. Thus, near $T \cong T_o$ we must account for the nonlinearities of the potential landscape. Setting more accurately [23]

$$\phi(E_T) = (E_b - E_T)\frac{2\pi}{\mu} + \frac{1}{2}(E_b - E_T)^2 |T'(E_b)|\,, \tag{31}$$

and proceeding as above we arrive at

$$k_{TST}(T \sim T_o) = \frac{\omega_o}{\omega_b}\frac{\sin(\hbar\beta\mu/2)}{(2\pi\hbar\,|T'|)^{1/2}} \cdot \prod_{n=1}^{\infty} \frac{\omega_o^2 + n^2v^2 + nv\,\hat{\gamma}(nv)}{-\omega_b^2 + n^2v^2 + nv\,\hat{\gamma}(nv)} \cdot \exp\left[-\beta E_b + \frac{\hbar(\beta_o - \beta)^2}{2|T'|}\right] \mathrm{Erfc}\left[\left(\frac{\hbar}{2|T'|}\right)^{1/2}(\beta - \beta_o)\right] + O\left[\exp(-\beta_o E_b)/(\beta_o E_b)^{1/2}\right], \tag{32}$$

where $\mathrm{Erfc}(x) = 2\pi^{-1/2}\int_{-\infty}^{x} dy \exp(-y^2) = \mathrm{erfc}(-x)$. With $v^2 - \omega_b^2 + v\hat{\gamma}(v) \equiv a(T - T_o)/T$ we recover the known result of the imaginary free energy method [6, 7, 8, 9, 14, 23, 33].

At low temperatures $T < T_o$, the cumulative reaction probability becomes with $\phi(E_T) > 0$ exponentially small and we must treat the full nonlinearity of the potential. The integration in (9a) can then be approximated by keeping only the term with $n = 1$.

This integration can be performed within SPA to yield [8b, 9]

$$k_{TST}(T < T_o) = Z_o^{-1}(2\pi\hbar|T'(E_\beta)|)^{-1/2}\exp(-S_b/\hbar) \cdot \prod_{l=1}^{N}\left[2\sinh\left(\frac{1}{2}\hbar\beta\omega_l(E_\beta)\right)\right]^{-1} \tag{33}$$

where $T' = \partial T/\partial E$. The SPA condition yields $T(E) = \hbar\beta$, and $E_\beta \equiv E[T(E) = \hbar\beta]$ denotes the corresponding stationary phase energy. S_b is the dissipative bounce action of the periodic orbit with period $\hbar\beta$, i.e.

$$S_b = \int_0^{\hbar\beta} L_{\mathrm{eff}}(\tau)\,d\tau\,. \tag{34}$$

Upon noticing that

$$\left(\frac{-\partial^2 S_c}{\partial\tau^2}\right)_{\tau=\hbar\beta}^{-1} = \frac{\partial^2\phi(E)}{\partial E^2}\Big|_{E=E_\beta} = |T'(E_\beta)| > 0 \tag{35}$$

we find by use of the identity in (21) the alternative expression, i.e.

$$k_{TST}(T < T_o) = \left(\frac{S_o}{2\pi\hbar}\right)^{1/2}\left(\frac{\det\delta^2 S_c|_{\vec{q}=\vec{x}_o}}{|\det'\delta^2 S_c|_{\vec{q}(0)=\vec{q}(\hbar\beta)}}\right)^{1/2}\exp(-S_b/\hbar)\,. \tag{36}$$

This latter form precisely equals the imaginary free energy result [3, 5–9, 14].

Conclusions

By use of the semiclassical TST of Miller [24] and the periodic orbit theory we managed to obtain from (9a, 9b, 11) all the previously derived results for the quantum-Kramers rate. This approach has for all temperatures the same common basis, i.e. the rate expression in (9a). We have thus demonstrated that the continuum limit of this quantum TST precisely equals the dissipative quantum-Kramers theory. At high temperatures $T \gg T_o$, the results approach up to quantum corrections (see Ref. [34]), the classical Kramers rate derived fifty years ago [9, 35], i.e.

$$k_{TST}(T \gg T_o, N \to \infty) \to k_{\mathrm{Kramers}} = \frac{\mu}{\omega_b}\frac{\omega_o}{2\pi}\exp(-\beta E_b)\,, \tag{37}$$

where for zero memory friction [35], $\gamma(t) \to 2\gamma\,\delta(t)$, i.e. $\hat{\gamma}(\mu) = \gamma$

$$\mu = \left(\frac{\gamma^2}{4} + \omega_b^2\right)^{1/2} - \frac{1}{2}\gamma\,. \tag{38}$$

The above given results therefore generalize the classical treatment of Kramer's dissipative rate to the full (dissipative) quantum regime which extends from $T = 0$ up to room temperatures.

This work has been supported by the Deutsche Forschungsgemeinschaft through Grant No. Ha. 1517/3–1.

References

[1] R. P. Feynman and F. L. Vernon, Ann. Phys. (N.Y.) *24*, 118 (1963).
[2] K. Möhring and U. Smilansky, Nucl. Phys. *A338*, 227 (1980).
[3] A. O. Caldeira and A. J. Leggett, Phys. Rev. Lett. *46*, 211 (1981); Ann. Phys. (N.Y.) *149*, 374 (1983); *153*, 445 (1984).
[4] A. B. Balantekin and N. Takigawa, Ann. Phys. (N.Y.) *160*, 441 (1983).
[5] H. Grabert, U. Weiss, and P. Hänggi, Phys. Rev. Lett. *52*, 2193 (1984).
[6] A. I. Larkin and Yu. N. Ovchinnikov, Sov. Phys. JETP *59*, 420 (1984).
[7] P. S. Riseborough, P. Hänggi, and E. Freidkin, Phys. Rev. *A32*, 489 (1985).
[8] P. Hänggi, Ann. N. Y. Acad. Sci *480*, 51 (1986); Z. Phys. *B68*, 181 (1987).
[9] P. Hänggi, P. Talkner, and M. Borkovec, Rev. Mod. Phys. *62*, 251 (1990).
[10] H. Eyring, J. Chem. Phys. *B*, 107 (1935).
[11] P. Pechukas, in: Dynamics of Molecular Collisions, part B, chapter 6, 269–332 ed. by W. H. Miller (Plenum, N. Y.).
[12] E. Pollak, Chem. Phys. Lett. *127*, 178 (1986).
[13] U. Weiss, H. Grabert, P. Hanggi, and P. Riseborough, Phys. Rev. *B35*, 9535 (1987).
[14] H. Grabert, P. Olschowski, and U. Weiss, Phys. Rev. *B36*, 1931 (1987).
[15] J. S. Langer, Ann. Phys. (N. Y.) *41*, 108 (1967).
[16] W. H. Miller, J. Chem. Phys. *62*, 1899 (1975).
[17] A. M. Polyakov, Phys. Lett. *B59*, 82 (1975).

[18] R. Jackiw and C. Rebbi, Phys. Rev. Lett. *37*, 172 (1976).
[19] S. Coleman, Phys. Rev. *D15*, 2929 (1977).
[20] C. G. Callan and S. Coleman, Phys. Rev. *D16*, 1762 (1977).
[21] M. C. Gutzwiller, J. Math. Phys. *8*, 1979 (1967).
[22] M. C. Gutzwiller, J. Math. Phys. *12*, 343 (1971).
[23] P. Hänggi and W. Hontscha, J. Chem. Phys. *88*, 4094 (1988).
[24] W. H. Miller, J. Chem. Phys. *61*, 1823 (1974).
[25] F. J. McLafferty and P. Pechukas, Chem. Phys. Lett. *27*, 511 (1974).
[26] W. H. Miller, S. D. Schwartz, and J. W. Tromp, J. Chem. Phys. *70*, 4889 (1983).
[27] W. H. Miller, J. Chem. Phys. *63*, 996 (1975).
[28] W. Hontscha, "Semiclassical Approach to Quantum-TST and Numerical Study of Dissipative Tunneling", chapt 2, Ph. D.-thesis, University of Augsburg, July 1990.
[29] K. Möhring, S. Levit, and U. Smilansky, Ann. Phys. *127*, 198 (1980).
[30] R. F. Dashen, B. Hasslacher, and A. Neveu, Phys. Rev. *D10*, 4114 (1974).
[31] S. Levit, J. W. Negele, and Z. Paltiel, Phys. Rev. *C22*, 1979 (1980).
[32] P. Hänggi, U. Weiss, and P. S. Riseborough, Phys. Rev. *A34*, 4558 (1986).
[33] H. Grabert and U. Weiss, Phys. Rev. Lett. *53*, 1787 (1984).
[34] P. Hänggi, H. Grabert, G. L. Ingold, and U. Weiss, Phys. Rev. Lett. *55*, 761 (1985).
[35] H. A. Kramers, Physica (Utrecht) *7*, 284 (1940).

Presented at the Discussion Meeting of the Deutsche Bunsen-Gesellschaft für Physikalische Chemie "Rate Processes in Dissipative Systems: 50 Years after Kramers" in Tutzing, September 10–13, 1990 E 7512

Influence of Non-Linear Dissipation on Quantum Tunneling

Peter S. Riseborough

Department of Physics, Polytechnic University, 333 Jay Street, Brooklyn, New York 11201

Nonequilibrium Phenomena / Nonlinear Phenomena / Quantum Mechanics / Statistical Mechanics

The influence of a non-linear dissipation mechanism on the dynamics of a particle, which performs tunneling through a potential barrier, is investigated. The particular dissipation mechanism considered contains terms quadratic in the normal modes of the heat bath, in addition to linear couplings. The non-linear terms are shown to affect the incoherent tunneling rate.

1. Introduction

Quantum tunneling is an important physical phenomenon which occurs in an enormous variety of different physical system [1–11]. It is therefore not surprising that this phenomenon has been studied extensively [1–14]. Quite early on in the study of tunneling processes, it has been realized that the coupling to a heat bath plays a crucial role in the tunneling dynamics [2]. The coupling's action is two fold: Firstly, it allows the tunneling particle to absorb and emit the elementary excitations of the heat bath, thereby establishing a thermal distribution in the particles energy. Secondly, the coupling also has the effect of renormalizing the dynamical properties of the tunneling particle.

With only a few notable exceptions [5,6], most of the studies of tunneling dynamics have been restricted to consideration of a particle coupled to a harmonic heat bath, in which the coupling is restricted to be linear in the normal modes of the heat bath [1–14]. In such systems, the effect of the linear coupling is to coherently distort the thermal reservoir in the vicinity of the particle, thereby causing the effective potential experienced by the particle to be lowered. At low temperatures, conservation of energy considerations result in tunneling motion being forbidden, unless the distortion of the thermal reservoir also moves and accompanies the particle. The dressing of the particle by the coherent distortion of the thermal reservoir results in the tunneling rate being suppressed, at low temperatures [2,3,11,12]. As the temperature is raised, thermal excitations wash out the coherent distortion of the thermal reservoir thereby increasing the tunneling rate [2,12]. Moreover, the particle may (infrequently) absorb sufficiently large numbers of thermal excitations of the reservoir's normal modes that thermally assisted or activated hopping may occur [2,12].

In this manuscript, we consider the effect of including the lowest order non-linear terms in the coupling of the particle to the heat bath on the tunneling dynamics. In section 2, we describe the model system and in section 3 we review the general formulation for the tunneling rate. In section 4, we calculate the tunneling rate, and in section 5 we discuss the results.

2. The Model System

The system is modeled by a Hamiltonian containing three terms

$$H = H_p + H_r + H_{p\text{-}r}\,, \tag{1}$$

where H_p describes the one dimensional motion of the particle in a potential $V(q)$, and H_r describes the dynamics of the thermal reservoir and $H_{p\text{-}r}$ describes the coupling between the particle and the thermal reservoir. The Hamiltonian governing the particle, H_p, is given

$$H_p = p^2/2M + V(q)\,, \tag{2}$$

 © VCH Verlagsgesellschaft mbH, W-6940 Weinheim, 1991 0005-9021/91/0303-0385 $ 3.50+.25/0

where p and q are the canonically conjugate momentum and coordinate of the particle. The Hamiltonian describing the thermal reservoir, H_r, can be written as

$$H_r = \sum_i [-\hbar^2/2m(\mathrm{d}/\mathrm{d}x_i)^2 + m\omega_i^2/2x_i^2] . \quad (3)$$

This describes a set of Einstein oscillators with frequencies ω_i. The term that couples the particle with the thermal reservoir is written as $H_{p\text{-}r}$, where

$$H_{p\text{-}r} = \sum_i (A_i q x_i + B_i q^2 x_i^2) . \quad (4)$$

This coupling contains the usual bi-linear coupling between the particles coordinate q and the coordinate of the i-th Einstein oscillator, as well as the bi-quadratic coupling in the oscillators coordinates. The latter terms are also quadratic in q, so that in the absence of asymmetry in the potential $V(q)$, the total system of particle and heat bath remains invariant under spatial inversions. As we shall describe later, the above choice of non-linearity in the coupling to the thermal reservoir is the only type which yields relevant modifications to the exponential part of the tunneling rate. The interaction terms which couple the particle to the thermal reservoir also modify the potential $V(q)$ experienced by the particle, leading to an effective potential $V_{\mathrm{eff}}(q)$ given by

$$V_{\mathrm{eff}}(q) = V(q) - \sum_i 1/2(A_i q)^2/(m\omega_i^2 + 2B_i q^2) + \sum_i \hbar\omega_i/2\{[1+2B_i q^2/m\omega_i^2]^{1/2} - 1\} . \quad (5)$$

The first correction term to $V_{\mathrm{eff}}(q)$ can be considered the result of displacing the i-th Einstein oscillator through the distance a, where

$$a = A_i q/(m\omega_i^2 + 2B_i q^2) ,$$

and the second correction term is the shift in zero point energy of the oscillators due to the change of frequency from ω_i to a new position dependent frequency $\omega_{q,i}$, where

$$\omega_{q,i}^2 = \omega_i^2 + 2B_i q^2/m .$$

Stability of the heat bath, in the presence of a particle at a fixed position q, requires that B be positive and in addition the non-linear coupling term is an even function of q, if no cutoff on the range of q is to be imposed. It is seen that the effect of the non-linear coupling term is to reduce the change in potential produced by the linear term, whereas the change of potential due to the zero point motion is already of order h and is irrelevant in the calculation of the exponential terms of the W.K.B. tunneling rate.

In the next section we shall consider the effect that the coupling to the heat bath, has on the tunneling dynamics of the particle. In particular, we shall consider the case which $V_{\mathrm{eff}}(q)$ represents an asymmetric potential with a single metastable local minimum located at $q = 0$, of the type shown in Fig. 1. The local curvature at the origin will be denoted by $M\omega_0^2$, and the point at which the particle escapes from the potential barrier, at zero damping, will be denoted by q_0.

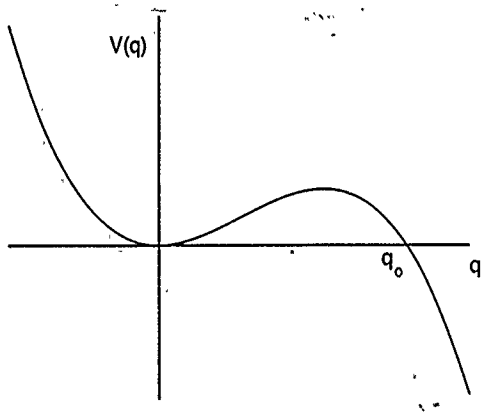


Fig. 1
The effective potential $V_{\mathrm{eff}}(q)$ has a metastable minimum located at $q = 0$ which defines the zero of energy, the potential at the local minimum has curvature of $M\omega_0^2$. The zero damping escape point is denoted by q_0

3. The General Formulation

The tunneling rate can be expressed in terms of the Feynman Functional Integral Formulation of quantum mechanics [7]. The Trace over the normal mode coordinates of the heat bath is performed, leading to an effective action which contains terms non-local in time, that represents the effect of the dissipative coupling to the thermal reservoir [7, 8]. Unlike the case of linear coupling, the dissipative term is not merely a quadratic form in q. After analytically continuing from real to imaginary times the Green's function evaluated in the metastable minimum, transforms into the partition function for the metastable state. The partition function is evaluated by expanding about the extremal trajectories, as in the W. K.B. or semi-classical approximation [9, 10]. The tunneling rate is then expressed in terms of the imaginary part of the free energy [9]. If one further assumes that only the lowest action trajectories make significant contributions to the partition function then, one immediately obtains the lifetime of the metastable state in terms of the single bounce trajectory [9, 10].

We shall first derive the effective action, including the leading relevant terms appropriate for the non-linear dissipation, in addition to the well-studied linear terms [11 - 14]. Only, the leading exponential terms in the rate of decay of the metastable state will be evaluated, as they dominate the properties of the tunneling rate. The exponential terms can be expressed as the difference between two smallest extremal values of the action, and therefore can be evaluated variationally [13].

The coupling to the set of Einstein oscillators which comprises the thermal reservoir, yields terms in the action of the type

$$
\begin{aligned}
&-A_i^2/(4m\omega_i)\int_{-T/2}^{T/2} dt \int_{-T/2}^{T/2} dt' q(t)q(t') \\
&\quad \cdot \cosh[\omega_i(T/2-|t-t'|)]/\sinh \omega_i T/2 \\
&\quad + B_i\hbar/(2m\omega_i)\cdot \int_{-T/2}^{T/2} dt\, q^2(t)\coth \omega_i T/2 \\
&\quad + B_i A_i^2/(4m^2\omega_i^2)\int_{-T/2}^{T/2} dt \int_{-T/2}^{T/2} dt' \int_{-T/2}^{T/2} dt'' q^2(t)q(t')q(t'') \\
&\quad \cdot \cosh[\omega_i(T/2-|t-t'|)\cosh[\omega_i(T/2-|t-t''|)]/\sinh^2\omega_i T/2 \\
&\quad - B_i^2(\hbar/4m^2\omega_i^2)\int_{-T/2}^{T/2} dt \int_{-T/2}^{T/2} dt' q^2(t)q^2(t') \\
&\quad \cdot \cosh^2[\omega_i(T/2-|t-t'|)]/\sinh^2\omega_i T/2 \\
&\quad + \ldots . \qquad (6)
\end{aligned}
$$

The first term, can be recognized as the effect of the linear coupling at finite temperatures [11–14], when evaluated as an integral over the finite range of $-T/2$ to $T/2$, where T is related to the inverse temperature via $T = \hbar\beta$. It is usual to separate out the static term, which renormalizes the effective potential, and the time dependent dissipative terms. The static terms are then canceled by appropriate counter terms in $V(q)$, so that the $T = 0$ value of the effective potential $V_{\rm eff}(q)$ remains of a specific form [11]. The second term in Eq. (6), represents the effect of the zero point motion of the Einstein oscillators on the bi-linear coupling term, it merely produces a static renormalization of the effective potential quadratic in q. This can be recognized as the second term in the expansion of the second correction term in Eq. (5), and in accordance with our previous remarks can be neglected since it is explicitly of order h. The third term in Eq. (6) actually represents the leading relevant correction to the action due to B_i, the relevant higher order terms are generally of the form $B_i^n A_i^2$. The last term displayed represents both the dissipative and static term of order B_i^2. This term is negligible as it is proportional to h. Similarly, the dissipative and static terms of order B_i^n are all negligible, since they are explicitly of order h.

Following Ref. [11], we shall assume the distribution of the thermal reservoirs normal modes and coupling appropriate for ohmic (linear) dissipation, we shall also assume that B_i scales with ω_i^2, as suggested by the form of Eq. (5). The dimensionless ratio $B_i q_0^2/m\omega_i^2$ will be denoted by γ. In the following, we shall investigate the effect of the dissipative part of the action which is of leading order in γ.

4. The Tunneling Rate

We shall evaluate the tunneling rate out of the metastable minimum of the temperature independent effective potential, Fig. 1, i.e.

$$V(q) \equiv V_{\rm eff}(q) = M/2\,\omega_0^2 q^2(1-q/q_0). \qquad (7)$$

The calculation proceeds by utilizing the ansatz

$$q(t) = a/(1-b\cos(2\pi t/T)) \qquad (8)$$

for the bounce trajectory [13], and the parameters a and b are to be evaluated variationally. The physically acceptable values are those where both a and b are real and b lies in the range $-1 < b < 1$. The variational procedure follows along the lines of Ref. [13]. We find that the leading effect of γ is to produce a term in the exponent of

$$-\pi\alpha\gamma M\omega_0 q_0^2 (a/q_0)^4/(1-b^2)^2 4F[(1-b^2)^{-1/2}], \qquad (9a)$$

where $F(x)$ is a positive definite function given by

$$
\begin{aligned}
F(x) = &\sum_{n_1,n_2=-\infty}^{\infty} [(x-1)/(x+1)]^{1/2(|n|+|n|+|n+n|)} \\
&\cdot \{|n_1+n_2|+x\}\cdot\{|n_1|+|n_2|-|n_1 n_2|/(|n_1|+|n_2|)\}.
\end{aligned} \qquad (9b)
$$

For small values of b, the function $F[(1-b^2)^{-1/2}]$ tends to zero as $11/4\,b^2$. Furthermore as b tends to unity, $F[(1-b^2)^{-1/2}]$ diverges to positive infinity as $(1-b^2)^{-2}$. An analytic expression for $F(x)$ is given in the Appendix. In the above expression $\alpha = \eta/(2\omega_0)$ is the usual dimensionless coupling strength characterizing the linear ohmic damping mechanism [11–14]. The non-linear dissipative term given in Eq. (9), can be compared to the usual dissipative contribution

$$+\pi\alpha M\omega_0 q_0^2 (a/q_0)^2 b^2/(1-b^2)^2. \qquad (10)$$

Clearly, for physically acceptable values of a and b, the term proportional to γ shown in Eq. (9) has the effect of reducing the exponential suppression of the tunneling rate due to the bilinear coupling, given by Eq. (10). Simultaneous extremalization of the total action, with respect to a and b, yields a set of coupled algebraic equations which simplify when written in terms of the natural occurring variables [13],

$$y = (a/q_0)\cdot(1-b^2)^{-1/2}, \qquad (11a)$$

and

$$x = (1-b^2)^{-1/2}. \qquad (11b)$$

The equations take the form

$$
\begin{aligned}
&(2\pi k_B T/\hbar\omega_0)^2 1/2(3x^2-1) \\
&\quad + \alpha(2\pi k_B T/\hbar\omega_0)2x - \alpha\gamma y^2(2\pi k_B T/\hbar\omega_0)4F'(x) \qquad (12a) \\
&\quad + 1 - 3yx = 0,
\end{aligned}
$$

and

$$
\begin{aligned}
&(2\pi k_B T/\hbar\omega_0)^2 x(x^2-1) \\
&\quad + 2\alpha(2\pi k_B T/\hbar\omega_0)(x^2-1) \\
&\quad - 4\alpha\gamma y^2(2\pi k_B T/\hbar\omega_0)4F(x) \qquad (12b) \\
&\quad + 2x - 3/2y(3x^2-1) = 0.
\end{aligned}
$$

The simultaneous algebraic equations posses a non-trivial solution for $T < T_0$, where T_0 is the cross-over temperature that does depend on γ. The corresponding action is analogous to Eq. (5) with $n = 1$ in Ref. [13]. (Nota bene: A factor

Table 1
The value of the action S in units of $(\pi M\omega_0 q_0^2)$, for increasing values of α and γ

γ \ α	0	1	2	3	4	5
0.00	0.1799	0.5287	0.9395	1.3687	1.8048	2.2440
0.05	0.1799	0.441	0.732	1.035	1.346	1.661
0.10	0.1799	0.368	0.560	0.754	0.950	1.149

of π is missing from the denominator of the left hand side.) At zero temperature the simultaneous equations can be reduced to the fifth order polynomial equation,

$$5/2u^2+2\alpha u-16/9\alpha\gamma\delta u(2-u^2)^2-1=0\,, \tag{13}$$

where $\delta=4\ln 2+7/24$. The corresponding action, at zero temperature, is given by substituting the solution for u into the expression

$$S/(\pi M\omega_0 q_0^2) = 1/9(2-u^2)^2 \cdot[u+\alpha-4/9\alpha\gamma\delta(2-u^2)^2]\,. \tag{14}$$

This process yields the values of the action shown in Table 1. For zero strength of the non-linear damping coupling constant γ, the action can be expressed as

$$S/(\pi M\omega_0 q_0^2) = (4/75)^2\{10+\alpha\sqrt{4\alpha^2+10}-2\alpha^2\}^2 \cdot[3\alpha+\sqrt{4\alpha^2+10}]/5\,. \tag{15}$$

As shown in Ref. [13], the variational approximation given by Eq. (15) differs by less than 6% from the exact numerical value for the action [14]. This expression also shows that the action increases monotonically with increasing strength of the linear dissipation mechanism. Table 1 shows that the presence of a finite value for γ yields a reduction of the exponential suppression of the tunneling due to the linear dissipation α. This result is in agreement with the physical picture that, at low temperatures, the exponential suppression occurs because the particle tunneling must be associated with a corresponding coherent motion of the distortions in the thermal reservoir. The discussion following Eq. (5) makes it transparent that the non-linear coupling reduces the size of the distortion and hence reduces the size of the exponential suppression. At higher temperatures the action is reduced until, at T_0, the bounce collapses onto the constant value $q(t)=2/3\,q_0$ corresponding to the maximum of the potential $V_{\rm eff}(q)$. At this temperature the solution for x tends to unity and y tends to 2/3. The cross-over temperature is given by the expression

$$(2\pi k_B T_0/\hbar\omega_0)=\sqrt{\alpha^2(1-44/9\gamma)^2+1}-\alpha(1-44/9\gamma). \tag{16}$$

The cross-over temperature is increased for increasing γ, in accordance with our finding that the lowest order non-linear dissipation mechanism under consideration leads to a reduction of the effective value of the linear dissipation strength α.

5. Conclusions

The bi-quadratic coupling between the particle and the thermal reservoir, has been shown to effect an increase in the tunneling rate, through a reduction of the suppression produced by the bi-linear particle-thermal reservoir coupling. In the absence of the bi-linear coupling term, the bi-quadratic term has no effect on the leading exponential terms of the W.K.B. tunneling rate. This is in agreement with earlier studies [5, 6], which show that in such cases the suppression of the tunneling rate still occurs, but only in the form of pre-exponential factors. In fact, dimensional analysis shows that any perturbative non-linearity in the heat bath normal coordinates, whether in the description of anharmonic normal modes by themselves or in the coupling to the particle, are irrelevant as far as the calculation of the exponential term of the W.K.B. tunneling rate.

The authors would like to acknowledge the support of the U.S. Department of Energy, Office of Basic Energy Science, through grant DE FG02-84ER-45127. We would also like to thank Professor Doctors H. Grabert, P. Hanggi and U. Weiss for many stimulating discussions.

Appendix

The function $F(x)$ expressed in Eq. (9.b) as a summation can be evaluated analytically. The result is given by the expression,

$$\begin{aligned}F(x) = {} & 1/24(x-1)(7x^3+343x^2+181x-15)\\ & \pm 1/2(4x^2-1)(x^2-1)\ln(2x/(x+1))\\ & + 1/2(4x^2-3)x\sqrt{x^2-1}\{\ln((x+1)/2)\\ & + 2\ln(1+\sqrt{(x-1)/(x+1)})\}\\ & - 1/4(8x^2+8x+1)(x+1)^2\ln(x)\,.\end{aligned}$$

As x tends to unity, $F(x)$ tends to zero as $11/2\,(x-1)$, while as x tends to infinity $F(x)$ diverges as $x^4\,(4\ln 2+7/24)$.

References

[1] P. Hänggi, P. Talkner, and M. Borkovec, Rev. Mod. Phys. *62*, 251 (1990).
[2] T. Holstein, Ann. Phys. (New York) *8*, 325, 343 (1959).
[3] J. Appel, "Solid State Physics", eds. Seitz and Turnbull, Academic Press, London 1963.
[4] L. B. Schein, C. B. Duke, and A. R. McGhie, Phys. Rev. Lett. *40* (1978).
[5] R. W. Munn and R. Silbey, J. Chem. Phys. *68*, 2439 (1978).
[6] P. S. Riseborough, Ann. Phys. (New York) *153*, 1 (1984).
[7] R. P. Feynman, Statistical Mechanics, Seventh Edition, Benjamin Cummings, Reading Mass. (1982).
[8] R. P. Feynman and Vernon, Ann. Phys. (New York) *24*, 118 (1963).
[9] J. S. Langer, Ann. Phys. (New York) *41*, 108 (1967).
[10] C. G. Callan and S. Coleman, Phys. Rev. D *16*, 1762 (1977).
[11] A. O. Caldeira and A. J. Leggett, Ann. Phys. (New York) *149*, 374 (1983).
[12] H. Grabert, U. Weiss, and P. Hänggi. Phys. Rev. Lett. *52*, 2193 (1984).
[13] E. Freidkin, P. S. Riseborough, and P. Hänggi, Phys. Rev. B *34*, 1952 (1986).
[14] H. Grabert, P. Olschowski, and U. Weiss, Phys. Rev. B *32*, 3348 (1985).

Presented at the Discussion Meeting of the Deutsche Bunsen-Gesellschaft für Physikalische Chemie "Rate Processes in Dissipative Systems. 50 Years after Kramers" in Tutzing, September 10–13, 1990

E 7513

Some New Approaches to Semiclassical and Quantum Transition State Theory

William H. Miller

Department of Chemistry, University of California, and Materials and Chemical Sciences Division, Lawrence Berkeley Laboratory, Berkeley, California 94720

Chemical Kinetics / Quantum Mechanics / Rate Constants / Transition State Theory

Semiclassical and quantum mechanical transition state theory is reviewed and two new approaches described. One is a general implementation of a semiclassical rate expression [Miller, Faraday Discuss. Chem. Soc. *62*, 40 (1977)] that involves the "good" action-angle variables associated with the saddle point (i.e., transition state) of a potential energy surface. The other is an evaluation of a formally exact quantum expression for the rate [Miller, Schwartz, and Tromp, J. Chem. Phys. *79*, 4889 (1983)] in terms of Siegert eigenvalues associated with the transition state. Siegert eigenvalues are usually associated with *scattering resonances*, so their identification with the saddle point of a potential surface, and the expression for the reaction rate in terms of them, is quite an unexpected and novel development.

I. Introduction

Transition state theory [1] is without a doubt the most commonly used theory for describing chemical reaction rates (and also rate processes in many other fields), for both unimolecular and bimolecular reactions. The purpose of this paper is to suggest two new transition state-like theoretical approaches for determining such rates, the first a semiclassical one and the second fully quantum mechanical. In order to focus on the basic theoretical ideas which are the subject of the paper, all expressions below will be written explicitly for total angular momentum $J = 0$; for applications to real molecular systems it is of course necessary to carry out the transition state calculation for each value of J separately and then combine them appropriately. The remainder of the Introduction summarizes the basic notions of transition state theory and earlier related work.

The microcanonical and canonical rate constants are both conveniently expressed in terms of the *cumulative reaction probability* $N(E)$,

$$k(E) = [2\pi\hbar\varrho(E)]^{-1} N(E) \tag{1.1a}$$

$$k(T) = [2\pi\hbar Q_r(T)]^{-1} \int_0^\infty \mathrm{d}E\, \mathrm{e}^{-\beta E} N(E), \tag{1.1b}$$

where E is the total energy of the molecular system, T the temperature [$\beta = (kT)^{-1}$], ϱ is the density of reactant states per unit energy, and Q_r is the reactant partition function. ($k(E)$ is usually of more interest for *unimolecular* reactions, where it is known as RRKM theory, and $k(T)$ typically of more interest for *bimolecular* reactions.) The cumulative reaction probability is in turn given by the sum of *tunneling, or transmission probabilities* over all states $\boldsymbol{n} = (n_1, \ldots, n_{F-1})$ of the "activated complex"

$$N(E) = \sum_{\boldsymbol{n}} P_{\boldsymbol{n}}(E). \tag{1.2}$$

The *activated complex* is the system of F-1 degrees of freedom (F is the total number of degrees of freedom of the molecular system) for motion in the *dividing surface* normal to the reaction coordinate (the Fth degree of freedom) which separates reactants from products. If for some states $\boldsymbol{n}$, $P_{\boldsymbol{n}}$ were to equal 1, and for all other states equal to zero, then $N(E)$ would simply be the number of states for which the transmission probability is unity. In general, therefore, one may think qualitatively of $N(E)$ as the "number of quantum states that react", as a function of the total energy of the system. In the limit of classical mechanics $N(E)$ is also proportional to the microcanonical average of the one-way flux through the dividing surface [2].

The transmission probabilities $\{P_{\boldsymbol{n}}(E)\}$ are thus the primary objects which must be calculated, and then Eqs. (1.2) and (1.1) give the reaction rates [3]. The *simplest* approximation for them is obtained by assuming that the reaction coordinate (mode F) is separable from the (F-1) modes of the activated complex. In this limit

$$P_{\boldsymbol{n}}(E) = P_{1d}(E - \varepsilon_{\boldsymbol{n}}^{\ddagger}), \tag{1.3a}$$

where $\varepsilon_{\boldsymbol{n}}^{\ddagger}$ is the energy eigenvalue for state $\boldsymbol{n}$ of the activated complex, often approximated as harmonic,

$$\varepsilon_{\boldsymbol{n}}^{\ddagger} \cong \sum_{k=1}^{F-1} \hbar\omega_k^{\ddagger}(n_k + 1/2), \tag{1.3b}$$

and $P_{1d}(E_F)$ is a one-dimensional tunneling probability, often approximated by the uniform semiclassical expression

$$P_{1d}(E_F) \cong [1 + \mathrm{e}^{2\theta(E_F)}]^{-1}, \tag{1.3c}$$

where $\theta(E_F)$ is the one-dimensional WKB barrier penetrating integral

$$\theta(E_F) = \int_{\text{barrier}} \mathrm{d}q_F \sqrt{2m[V(q_F) - E_F]/\hbar^2}. \tag{1.3d}$$

If the barrier potential $V(q_F)$ is furthermore assumed to be harmonic (i.e., a parabolic barrier), then

$$\theta(E_F) = \frac{\pi(V_0 - E_F)}{\hbar|\omega_F|}, \tag{1.3e}$$

 © VCH Verlagsgesellschaft mbH, W-6940 Weinheim, 1991 0005-9021/91/0303-0389 $ 3.50+.25/0

where $\omega_F = -i|\omega_F|$ is the imaginary barrier frequency. (From Eqs. (1.3) one can readily see the general characteristic $P_n(E) \to 1$ for $E_F \equiv E - \varepsilon_n^{\ddagger} \gg V_0$.) The totally harmonic limit of the theory thus requires only a normal mode analysis at the transition state (saddle point of the potential surface) in order to determine the frequencies $\{\omega_k\}$, $k = 1,\ldots,F$, and also, of course, the barrier height V_0. As simple as this totally harmonic result is, it is the general basis for describing the effects of dissipation on reaction rates (i.e., Kramers' theory) [4].

A more rigorous expression for the transmission probabilities is given by the "instanton" model [5], i.e., a semiclassical theory that involves a periodic classical trajectory on the upside-down potential surface. In this case, $2\theta(E)$ is the classical action integral (in pure imaginary time) for a complete cycle about the periodic orbit, and $\{\omega_k(E)\}$, $k = 1,\ldots,F\text{-}1$ are the stability frequencies for an infinitesimal perturbation about the periodic orbit. The major advantage of this theory is that one need not choose the reaction path, or even the dividing surface, in some *ad hoc* manner, but rather the full F-dimensional (classical) dynamics selects the reaction path (i.e., the periodic orbit). The transmission probabilities are given in this theory by

$$P_n(E) = \left\{1 + \exp\left[2\theta(E) - 2\theta'(E)\sum_{k=1}^{F-1} \hbar\omega_k(E)(n_k + 1/2)\right]\right\}^{-1}, \tag{1.4}$$

which one sees is very similar in structure to the separable result given by Eqs. (1.3a)–(1.3d), i.e.,

$$P_n^{\text{separable}}(E) = \left\{1 + \exp\left[2\theta\left(E - \sum_{k=1}^{F-1} \hbar\omega_k^{\ddagger}(n_k + 1/2)\right)\right]\right\}^{-1}. \tag{1.5}$$

The primary differences are, first of all, that $\theta(E)$ in Eq. (1.4) is computed along the periodic orbit and not along a separable one dimensional path as in Eq. (1.5). Also, the constant frequencies $\{\omega_k^{\ddagger}\}$ in Eq. (1.5) are replaced in (1.4) by the energy-dependent stability frequencies of the periodic orbit. And finally, the periodic orbit result, Eq. (1.4), inherently assumes that the energy in the activated complex is small compared to the total energy, and the exponent in Eq. (1.4) is expanded to first order in this energy. If the action integral $\theta(E)$ were a *linear* function of E – i.e., if the barrier were assumed to be parabolic, as in Eq. (1.3e) – then this would not be an approximation, but in general it is. Thus the periodic orbit result, though clearly better in many ways than the separable approximation, has the defect that it is not correct in the separable limit if the barrier is anharmonic.

II. Semiclassical Transmission Probabilities Including Anharmonicity

A more rigorous way of including anharmonicity into the transition state transmission probabilities is based on the set of "good" action-angle variables associated with the saddle point on the potential surface [6]. The good action variables about a saddle point are in complete analogy with those associated with a minimum on a potential surface. In the latter case one can compute classical trajectories, determine the invariant tori, calculate the topologically independent action integrals, etc., in order to determine them [7], but this is not possible for the case of a saddle point because the trajectories will "run away". It is necessary to express the classical Hamiltonian in terms of the good action variables by some analytic prescription [8].

The general result of this approach [6] begins with the classical Hamiltonian expressed as a function of its "good" (i.e., conserved) action variables, $E(I_1,\ldots,\ldots,I_F)$. One of these actions is identified with the reaction coordinate, I_F say, and realized to be imaginary,

$$I_F \equiv -i\hbar\theta/\pi \tag{2.1a}$$

while the other (F-1) actions are quantized in the usual semiclassical fashion,

$$I_k = (n_k + 1/2)\hbar\,, \tag{2.1b}$$

$k = 1,\ldots,F\text{-}1$. The equation

$$E = E(n_1,\ldots,n_{F-1},0) \equiv E(n,0)\,, \tag{2.2}$$

is then solved to express $\theta \equiv \theta(n,E)$ as a function of E and the F-1 quantum number n. The transmission probability then has the semiclassical form

$$P_n(E) = [1 + e^{2\theta_n(E)}]^{-1}. \tag{2.3}$$

As an elementary example of this general prescription, consider a harmonic saddle point, for which

$$E(I_1,\ldots,I_F) = V_0 + \sum_{k=1}^{F} \omega_k I_k\,. \tag{2.4a}$$

Making the replacements in Eq. (2.1), with $\omega_F = -i|\omega_F|$, and solving Eq. (2.2) leads to

$$\theta(n,E) = \frac{\pi}{\hbar|\omega_F|}\left(V_0 + \sum_{k=1}^{F-1} \hbar\omega_k(n_k + 1/2) - E\right), \tag{2.4b}$$

i.e., Eq. (1.3e), the harmonic result discussed above.

A less trivial application of this general prescription Eqs. (2.1)–(2.3) was given recently [9] by using perturbation theory to include the effects of cubic and quartic anharmonicities about a saddle point. If $\{q_K\}$, $k = 1,\ldots,F$ denote the usual mass-weighted normal mode coordinates at the saddle point (i.e., the harmonic potential is $V_0 + \sum_k 1/2\,\omega_k^2 q_k^2$), and

$$f_{kjl} = \left(\frac{\partial^3 V}{\partial q_k\,\partial q_j\,\partial q_l}\right)_{q=0} \tag{2.5a}$$

$$f_{kjlm} = \left(\frac{\partial^4 V}{\partial q_k\,\partial q_j\,\partial q_l\,\partial q_m}\right)_{q=0} \tag{2.5b}$$

are the cubic and quartic force constants, then the classical energy is given in terms of the good actions $\{I_k\}$ by

$$E(I_1,\ldots,I_F) = V_0 + \sum_{k=1}^{F} \omega_k I_k + \sum_{k\le k'=1}^{F} x_{kk'} I_k I_{k'}, \tag{2.6}$$

where the anharmonic constants $\{x_{k,k'}\}$ are given in terms of the cubic and quartic force constants,

$$x_{kk} = \frac{1}{16\omega_k^2}\left[f_{kkkk} - \sum_{l=1}^{F} \frac{f_{kkl}^2(8\omega_k^2 - 3\omega_l^2)}{\omega_l^2(4\omega_k^2 - \omega_l^2)}\right] \tag{2.7a}$$

$$x_{kl} = \frac{1}{4\omega_k\omega_l}\left[f_{kkll} - \sum_{m=1}^{F} \frac{f_{kkm} f_{llm}}{\omega_m^2} + \sum_{m=1}^{F} \frac{2f_{klm}^2(\omega_k^2+\omega_l^2-3\omega_l^2)}{[(\omega_k+\omega_l)^2-\omega_m^2][(\omega_k-\omega_l)^2-\omega_m^2]}\right], \tag{2.7b}$$

for $k \neq l$. With the replacements indicated by Eq. (2.1), Eq. (2.2) is a quadratic equation for θ which is readily solved to give

$$\theta(n,E) = \frac{\pi\Delta E}{\hbar\Omega_F}\left(\frac{2}{1+\sqrt{1+4x_{FF}\,\Delta E/(\hbar\Omega_F)^2}}\right), \tag{2.8}$$

where

$$\Delta E = V_0 + \varepsilon_n^{+} - E \tag{2.9a}$$

with

$$\varepsilon_n^{+} = \sum_{k=1}^{F-1} \hbar\omega_k(n_k+1/2) + \sum_{k\le k'=1}^{F-1} \hbar^2 x_{kk'}(n_k+1/2)(n_{k'}+1/2), \tag{2.9b}$$

and

$$\hbar\Omega_F = \hbar\tilde{\omega}_F - \sum_{k=1}^{F-1} \hbar^2 \tilde{x}_{kF}(n_k+1/2), \tag{2.10a}$$

with

$$\tilde{\omega}_F = i\omega_F = |\omega_F|, \tag{2.10b}$$

$$\tilde{x}_{kF} = -ix_{kF}, \tag{2.10c}$$

($\tilde{x}_{kF}$ is real). Eqs. (2.8)–(2.10) incorporate anharmonicity in the energy levels of the activated complex (cf. Eq. (2.9b)), anharmonicity in the reaction coordinate itself (via x_{FF}), and coupling between the reaction coordinate and modes of the activated complex (i.e., reaction path curvature) through the anharmonic constants $\tilde{x}_{kF}$ in Eq. (2.10a).

It is useful to note that having the energy to quadratic order in the actions, Eq. (2.6), can describe anharmonic effects quite realistically. Morse oscillator vibrational eigenvalues, for example, are given exactly through second order in $(n+1/2)$. Also, consider the popular Eckart potential barrier

$$V(x) = V_0\,\mathrm{sech}^2(\alpha x), \tag{2.11a}$$

which is often used to model anharmonic barriers. The one-dimensional WKB action integral for it is given by

$$\theta(E) = \pi\sqrt{\frac{2m}{\hbar^2\alpha^2}}\,(\sqrt{V_0}-\sqrt{E}), \tag{2.11b}$$

so that the energy as a function of θ is

$$E(\theta) = V_0 - \frac{\theta}{\pi}\hbar\alpha\sqrt{\frac{2V_0}{m}} + \left(\frac{\theta}{\pi}\right)^2\frac{\hbar^2\alpha^2}{2m}; \tag{2.11c}$$

i.e., the energy is given exactly as a quadratic function of the action. One thus feels that Eq. (2.6), and the transmission probability that results from it, can have a useful range of validity for including the effects of anharmonicity of the transition state.

Is it possible to apply the general semiclassical theory of Eqs. (2.1)–(2.3) *non-perturbatively*? The following procedure is one scenario. The idea is to use *quantum mechanics* to obtain the energy in terms of the quantum numbers (i.e., action variables) by diagonalizing a Hamiltonian matrix.

Thus suppose that the potential is harmonic plus cubic and quartic anharmonic terms. One first imagines that *all* the frequencies $\{\omega_k\}\,k=1,\ldots,F$ are real and writes out the simple (analytic) matrix representation of the Hamiltonian, $H_{n,n'}$, in the harmonic oscillator basis (where here n and n' denote F quantum numbers). After the matrix elements are calculated, one makes the replacement

$$\omega_F \longrightarrow -i|\omega_F|,$$

whereby the matrix $H_{n,n'}$ becomes *complex symmetric*. Diagonalizing it thus gives *complex eigenvalues*, i.e., the complex energies that would result in the perturbation expression Eq. (2.6) if *all* the actions were replaced by $I_k = (n_k + 1/2)\hbar, k=1,\ldots,F$. That is, when diagonalizing a Hamiltonian matrix to obtain eigenvalues — the non-perturbative quantum mechanical procedure — *all* the actions have "automatically" been set to their quantum values, i.e., (half-integers)x$\hbar$. To apply Eqs. (2.1)–(2.3), therefore, it is necessary to *fit* these numerically obtained eigenvalues to an analytic function of the quantum numbers, such as Eq. (2.6) or possibly a more general function, e.g., a Pade approximant. Once the analytic function $E(n)$ is determined, one can then make the replacement Eq. (2.1a), solve Eq. (2.2) and obtain the transmission probability via Eq. (2.3).

III. A Fully Quantum Rate Expression

The discussion at the end of the previous section describes a *quantum mechanical* calculational procedure (diagonalizing a particular complex symmetric Hamiltonian matrix), the result of which is then used in a *semiclassical* theory. This seems wasteful; i.e., after one has done a quantum

calculation, one would like to be able to determine the rate fully quantum mechanically.

This is possible by realizing that the complex eigenvalues discussed at the end of Section II are the *Siegert eigenvalues* [10] of the system. This is clear when one considers the boundary conditions satisfied by the corresponding eigenfunctions. For modes $k = 1,\ldots,F\text{-}1$ the harmonic oscillator functions have real frequencies so that the eigenfunctions will decay in these coordinates in the usual fashion. For mode F, though, with $\omega_F = -i|\omega_F|$, the harmonic oscillator functions have the form

$$\phi_{n_F}(q_F) \sim \exp(i|\omega_F| q_F^2/2\hbar) \cdot H(q_F), \tag{3.1}$$

where H is a polynomial in q_F. This function is an *outgoing* wave in both directions $q_F \to \pm\infty$ i.e., the Siegert boundary condition.

As has been used recently in quantum reactive scattering theory [11], though, an outgoing wave basis set is what is necessary to construct a finite basis set representation of the Green's function $G^+(E)$ (provided one is interested in matrix elements of G^+ between short-range states). Thus if $\{E_l\}$, $\{\psi_l(q)\}$, $l = 1,\ldots$ are the complex eigenvalues ($\mathrm{Im}\, E_l < 0$) and corresponding eigenfunctions that result from the calculation described at the send of Section II, then one has the approximation [11]

$$G^+(E) = \sum_{l=1} \frac{|\psi_l\rangle\langle\psi_l|}{E - E_l}, \tag{3.2}$$

which becomes exact in the limit of a complete basis. (Note that there is no complex conjugation of the wavefunction in the bra symbol.) The microcanonical density operator is then given by [12]

$$\begin{aligned}\delta(E-H) &= -\frac{1}{\pi}\mathrm{Im}\, G^+(E) \\ &= -\frac{1}{2\pi i}(G^+(E) - G^-(E)) \\ &= -\frac{1}{2\pi i}\left[\sum_l \frac{|\psi_l\rangle\langle\psi_l|}{E-E_l} - \frac{|\psi_l^*\rangle\langle\psi_l^*|}{E-E_l^*}\right].\end{aligned} \tag{3.3}$$

Since the time evolution operator can be expressed as

$$e^{-iHt/\hbar} = \int_{-\infty}^{\infty} dE\, e^{-iEt/\hbar}\, \delta(E-H), \tag{3.4a}$$

use of Eq. (3.3) in (3.4a) – and noting that $\mathrm{Im}\, E_l < 0$, $\mathrm{Im}\, E_l^* > 0$ – and evaluating the integral over E by closing the contour in the lower half plane, gives (for $t > 0$)

$$e^{-iHt/\hbar} = \sum_l e^{-iE_l t/\hbar} |\psi_l\rangle\langle\psi_l|. \tag{3.4b}$$

Eqs. (3.3) and (3.4) make it possible to carry out a direct evaluation of the exact quantum rate expressions given by Miller, Schwartz, and Tromp [13]. Thus the canonical rate constant is given by

$$k(T) = Q_r^{-1} \int_0^{\infty} dt\, C_f(t), \tag{3.5a}$$

where the flux correlation function is

$$C_f(t) = \mathrm{tr}[e^{iHt/\hbar} e^{-\beta H/2} F e^{-\beta H/2} e^{-iHt/\hbar} F], \tag{3.5b}$$

where F is the flux-through-the-surface operator. Use of Eq. (3.4) in (3.5b) (and some straightforward manipulation) give the flux correlation function as

$$C_f(t) = -\sum_{l,l'} \langle\psi_l^*|F|\psi_l\rangle^2 e^{-\beta(E_l+E_l^*)/2} e^{it(E_l^*-E_l)/\hbar}. \tag{3.6}$$

Since $\mathrm{Im}(E_l^* - E_l) > 0$, this correlation function decays exponentially as $t \to \infty$, the correct behavior (which has *not* been obtained in previous basis set calculations of this correlation function [13, 14]). With Eq. (3.6), the time integral in Eq. (3.5a) can be readily carried out, giving

$$k(T) = \frac{\hbar}{Q_r}\mathrm{Im}\sum_{l,l'} (\langle\psi_l^*|F|\psi_l\rangle)^2 e^{-\beta(E_l^*+E_l)/2}/(E_l^* - E_l). \tag{3.7}$$

One can similarly use Eq. (3.3) to evaluate the flux expression for the cumulative reaction probability $N(E)$,

$$N(E) = \frac{1}{2}(2\pi\hbar)^2 \mathrm{tr}[F\delta(E-H)F\delta(E-H)]. \tag{3.8}$$

The result of this calculation is

$$N(E) = \hbar^2\, \mathrm{Re}\sum_{l,l'} \frac{\langle\psi_l^*|F|\psi_l\rangle^2}{(E-E_l^*)(E-E_l)} - \frac{\langle\psi_{l'}|F|\psi_l\rangle^2}{(E-E_{l'})(E-E_l)}. \tag{3.9}$$

It remains to apply Eqs. (3.7) and (3.9) and test their ease of use, generality, and efficiency (i.e., how rapidly convergence is achieved with increasing size of basis set). It is nevertheless interesting to see how these formally exact quantum rate expressions can be written in terms of the Siegert eigenvalues (and eigenfunctions) which are related to the transition state. Siegert eigenvalues usually are discussed only with regard to scattering *resonances* [10], for which the imaginary parts of the eigenvalues are small. Here, on the other hand, the imaginary parts are *large* – e.g., for a parabolic saddle point

$$\mathrm{Im}\, E_n = -\hbar|\omega_F|(n_F + 1/2)$$

$n_F = 0,1,2,\ldots$ – and have nothing to do with resonances. This appears to be a totally new context for these quantities.

This work has been supported by the Director, Office of Energy Research, Office of Basic Energy Sciences, Chemical Sciences Division of the U.S. Department of Energy under Contract No. DE-AC03-76SF00098.

References

[1] (a) P. Pechukas, in: *Dynamics of Molecular Collisions B* (Vol. 2, p. 269 of *Modern Theoretical Chemistry*), ed. W. H. Miller, Plenum 1976; (b) D. G. Truhlar, W. L. Hase, and J. T. Hynes, J. Phys. Chem. *87*, 2664 (1983).

[2] See, for example, W. H. Miller, J. Chem. Phys. *65*, 2216 (1976).

[3] As an aside, it is also interesting to note that the tunneling/transmission probabilities are also central for determining the *probability distribution* of state-specific unimolecular rates. I.e., $k(E)$ is the *average* rate for energy E, but various individual quantum states (all with essentially the same energy E) can have widely disparate rates. This distribution is given by

$$P(k) = (2\pi)^{-1} \int_{-\infty}^{\infty} dt\, e^{ikt} \prod_n [1 + 2it P_n(E)/2\pi\varrho(E)]^{-1/2}.$$

See W. H. Miller, R. Hernandez, C. B. Moore, and W. F. Polik, J. Chem. Phys. *93*, 5657 (1990).

[4] E. Pollak, J. Chem. Phys. *85*, 865 (1986); Phys. Rev. A *33*, 4244 (1986).

[5] (a) W. H. Miller, J. Chem. Phys. *62*, 1899 (1975); (b) C. G. Callan and S. Coleman, Phys. Rev. D *16*, 1762 (1977); (c) P. Hänggi, P. Talkner, and M. Borkovec, Rev. Mod. Phys. *62*, 251 (1990).

[6] W. H. Miller, Faraday Discuss. Chem. Soc. *62*, 40 (1977).

[7] See, for example, I. C. Percival, Adv. Chem. Phys. *36*, 1 (1977).

[8] S. Chapman, B. C. Garett, and W. H. Miller, J. Chem. Phys. *64*, 502 (1976).

[9] W. H. Miller, R. Hernandez, N. C. Handy, D. Jayatilaka, and A. Willetts, Chem. Phys. Lett. *172*, 62 (1990).

[10] (a) A. J. F. Siegert, Phys. Rev. *56*, 750 (1939); (b) See also, A. D. Isaacson, C. W. McCurdy, and W. H. Miller, Chem. Phys. *34*, 311 (1978).

[11] W. H. Miller and B. M. D. D. Jansen op de Haar, J. Chem. Phys. *86*, 6213 (1987).

[12] See, for example, R. G. Newton, *Scattering Theory of Waves and Particles*, p. 176 et seq., Springer-Verlag 1982.

[13] W. H. Miller, S. D. Schwartz, and J. W. Tromp, J. Chem. Phys. *79*, 4889 (1983).

[14] (a) R. E. Wyatt, Chem. Phys. Lett. *121*, 301 (1985); (b) T. J. Park and J. C. Light, J. Chem. Phys. *85*, 5870 (1986); *88*, 4897 (1988); *91*, 974 (1989).

Presented at the Discussion Meeting of the Deutsche Bunsen-Gesellschaft für Physikalische Chemie "Rate Processes in Dissipative Systems: 50 Years after Kramers" in Tutzing, September 10–13, 1990 E 7514

A Feynman Path Integral Approach for Calculating Quantum Rate Constants in Complex Systems

Gregory A. Voth

Department of Chemistry, University of Pennsylvania, Philadelphia, Pennsylvania, 19104-6323, USA

Chemical Kinetics / Methods and Systems / Quantum Mechanics / Statistical Mechanics

A theoretical framework is discussed in which imaginary time Feynman path integration is adapted to define a quantum mechanical free energy for activated rate processes. Recently developed variational theories for the estimation of this factor, as well as the quantum dynamical corrections to the rate constant, are also discussed.

I. Introduction

Voth, Chandler, and Miller [1] (VCM) have presented an analysis of thermally activated rate processes that has extended several aspects of the classical description of such processes into the quantum regime. As an outgrowth of their analysis, VCM have argued [1] that the exact quantum mechanical rate constant k for a general activated process can be sensibly written in a way similar to the classical theory as [1]

$$k = \kappa \frac{k_B T}{h Q_A} \exp(-\beta F_c^*), \tag{1}$$

where β equals $1/k_B T$, Q_A is the quantum reactant partition function, κ is a correction factor of order unity, and the *quantum* free energy of activation is given by

$$F_c^* = -k_B T \ln[Q^*/(m/2\pi\hbar^2\beta)^{1/2}]. \tag{2}$$

In Eq. (2), Q^* is the equilibrium "path centroid density" [1,2], defined as the constrained imaginary time Feynman path integral [3]

$$Q^* = \int\cdots\int Dx(\tau)\, Dq(\tau)\, \delta(q^* - \tilde{q}_0)\, e^{-S[q(\tau),x(\tau)]/\hbar}, \tag{3}$$

where $q(\tau)$ is the reaction coordinate which has a transition state value of q^*, the vector $x(\tau)$ constants the nonreactive "bath" degrees of freedom, and $S[q(\tau),x(\tau)]$ is the imaginary time action functional [1–3]. The quantity $\tilde{q}_0$ in Eq. (3) is the centroid of each reaction coordinate quantum path $q(\tau)$ and is given by [1,2]

$$\tilde{q}_0 = \frac{1}{\hbar\beta} \int_0^{\hbar\beta} d\tau q(\tau). \tag{4}$$

A quantum transition state theory may be readily defined from Eq. (1) by approximating κ to have a value of unity [1]. Such a theory has considerable potential for applications to many different physical problems because, in the spirit of classical transition state theory [4], no explicit quantum dynamical information is required to estimate the rate constant [1]. Additionally, the central quantity Q^* in Eqs. (1) – (3) (the centroid density) can be directly calculated [1] from imaginary time path integral Monte Carlo techniques [5]. In fact, Eq. (1) has been successfully employed

 © VCH Verlagsgesellschaft mbH, W-6940 Weinheim, 1991 0005-9021/91/0303-0393 $ 3.50+.25/0

for a number of problems, [1, 6, 7] and methods to determine the dynamical correction factor to Eq. (1) (either exactly or approximately) have also been proposed [1, 8, 9].

The justification of the quantum rate equation in Eq. (8) may be pursued from three complementary points of view [1]: The first approach relates the centroid density [Eq. (3)] to the expressions for the quantum rate constant for the multidimensional parabolic barrier model [10–12]. In that case, Eq. (1) is *exact* provided κ is taken to be the Grote-Hynes generalization of the Kramers dynamical correction factor [1, 4, 9]. Although the usual quantum parabolic barrier model [10–12] exhibits a pathological divergence for temperatures such that $\hbar\beta\lambda_0^{\ddagger} \geq 2\pi$ (where $\lambda_0^{\ddagger}$ is the magnitude of the true multidimensional parabolic barrier frequency [11, 12]), that model can be extended to calculate the centroid density for realistic potentials at low temperatures via a variational principle [1].

The second justification [1, 2] of Eq. (1) relates the centroid density to the low temperature "instanton" expression [4, 13] for quantum rate processes which are dominated by tunneling. In that case, κ is again close to unity and its explicit derivation is discussed in Ref. [1]. The latter semiclassical analysis, although more general, gives the same result as Gillan's insightful low temperature path integral centroid density analysis of a double well potential coupled linearly to a classical bath of harmonic oscillators [2].

The third, and probably most rigorous, justification of the quantum rate formula in Eq. (1) is closely related to the method for calculating quantum rate constants put forth in Ref. [1]. In that paper, a procedure was outlined which facilitates the efficient sampling of activated quantum dynamics. In the case of such dynamics, the reactive "events" which take the system from reactants to products are quite rare because of the potential energy barrier separating the two stable states. In classical mechanics, of course, the probability of barrier crossing is essentially given by the free energy of activation. The analogous quantum mechanical quantity was argued in Ref. [1] to be the centroid density in Eq. (3) by noting that it is, in fact, the underlying factor in the complex dynamical weighting functional which dominates the overall value of the rate constant. The sampling of the quantum reactive dynamics in thereby greatly facilitated by constraining the centroid of the thermal quantum paths to be in the region of the classical transition state [1]. In a sense, the centroid constraint defines the appropriate quantum "activated complex" in the path integral language, while at the same time allowing for the delocalized nature of the quantum dynamics.

In the present paper, two aspects of the quantum rate constant formula in Eq. (1) will be explored. In Sec. II, a variational theory for the quantum activation factor $\exp(-\beta F_c^{\ddagger})$ will be outlined which maps the realistic problem of a nonlinear reaction coordinate barrier potential coupled to a linearly responding medium into a simple *separable* parabolic barrier reaction coordinate. A particularly useful limiting form of this equation will also be derived. In Sec. III, the problem of the quantum dynamical correction factor will be addressed by virtue of a multidimensional parabolic model and a similar variational technique [9]. This analysis of the dynamical correction is in the same spirit as the classical Kramers/Grote-Hynes theory, [4, 14] particularly as re-formulated by Pollak [11, 12]. Concluding remarks are the given in Sec. IV.

II. A Variational Effective Barrier Model for the Centroid Density

In order to calculate the quantum activation factor in Eq. (1), one must evaluate the constrained Feynman path integral (or centroid density) in Eq. (3). As a complementary and insightful approach to the direct numerical calculation of Eq. (3) [1] by path integral Monte Carlo [5], approximate analytical approaches may also be pursued (see, e.g., Ref. [1] for one possible variational extension of the parabolic barrier model). Most activated rate problems [4] are well described by an imaginary time action in Eq. (3) given by

$$S[q(\tau), x(\tau)] = \int_0^{\hbar\beta} d\tau \left\{ \frac{m}{2}\dot{q}(\tau)^2 + V_r[q(\tau)] + \sum_{i=1}^{N} \frac{m_i}{2}\dot{x}_i(\tau)^2 + V_{qx}[q(\tau), x(\tau)] \right\}, \tag{5}$$

where $V_r[q(\tau)]$ is the nonlinear potential along the reaction coordinate q, and $V_{qx}[q(\tau), x(\tau)]$ is the potential energy term which contains both the potential for the bath coordinates x_i and the couplings between the reaction coordinate and the bath.

For an environment which is well described by linear response theory, it is now well known that the bath can be represented by an *effective* set of harmonic oscillators coupled linearly to the reaction coordinate [4, 15]. Specifically, this physical situation is accounted for in Eq. (5) via the potential term

$$V_{qx}(q, x) = \sum_{i=1}^{N} \frac{1}{2} m_i \omega_i^2 \left(x_i + \frac{c_i}{m_i \omega_i^2} q \right)^2 . \tag{6}$$

In the above equation, m_i and ω_i are, respectively, the mass and frequency of bath oscillator i, while c_i is its coupling constant to the reaction coordinate q. This model is also based on the assumption that the reaction coordinate potential $V_r(q)$ in Eq. (5) is "renormalized" so as to contain the equilibrium averaged contributions from the interactions with the bath [i.e., $V_r(q)$ is a potential of mean force [16]]. The bath potential term contained in Eq. (6) therefore represents a Gaussian model for the fluctuations of the forces on the reaction coordinate about a mean value of zero. The fluctuating external force on the reaction coordinate at q^* in this model has the form

$$\delta F_{\text{ext}} = -\left(\frac{\partial V_{qx}}{\partial q} \right)\Big|_{q=q^*} = -\sum_{i=1}^{N} c_i (x_i - \bar{x}_i), \tag{7}$$

where the quantity $\bar{x}_i$ is the equilibrium value of the coordinate x_i when the effective bath is in equilibrium, but still

coupled to the reaction coordinate with a fixed value of q^*. It has been frequently argued that the influence of most realistic environments on rate processes can be modeled by choosing an effective set of harmonic bath oscillators with an appropriate spectral density [15].

The path integration in Eq. (3) can be simplified by first "integrating out" the bath coordinates in the usual way [3,15,17] to give the expression for the centroid density

$$Q^* = Q_{\text{bath}} \int \cdots \int Dq(\tau)\, \delta(q^* - \tilde{q}_0) \exp\{-S_{\text{eff}}[q(\tau)]/\hbar\}, \quad (8)$$

where Q_{bath} is the partition function for the bath in the absence of coupling to the reaction coordinate, and the effective path integral action functional $S_{\text{eff}}[q(\tau)]$ is given by

$$S_{\text{eff}}[q(\tau)] = \int_0^{\hbar\beta} d\tau \left\{\frac{m}{2}\dot{q}(\tau)^2 + V_r[q(\tau)]\right\} - \int_0^{\hbar\beta} d\tau \int_{-\infty}^{\infty} d\tau' \alpha(|\tau-\tau'|) q(\tau) q(\tau'). \quad (9)$$

In Eq. (9), the potential $V_r(q)$ is the modified potential

$$V_r(q) = V_r(q) + \sum_{i=1}^{N} \frac{c_i^2}{2m_i\omega_i^2} q^2, \quad (10)$$

and $\alpha(|\tau|)$ is the kernel of the imaginary time influence functional [3,15,17], given by

$$\alpha(|\tau|) = \frac{1}{2\pi} \int_0^{\infty} d\omega J(\omega) \exp(-\omega|\tau|). \quad (11)$$

The spectral density of the bath $J(\omega)$ in Eq. (11) is given explicitly in the linear model [Eq. (6)] by the expression [15]

$$J(\omega) = \frac{\pi}{2} \sum_{i=1}^{N} \frac{c_i^2}{m_i\omega_i} \delta(\omega - \omega_i). \quad (12)$$

At this point, the problem of computing the quantum activation factor in Eq. (1) via the centroid density [Eq. (3)] has been greatly simplified by the linear response approximation for the bath. However, the exact analytic evaluation of the effective path integral in Eq. (8) remains a daunting task for a realistic reaction coordinate potential $V_r[q(\tau)]$. It is therefore advantageous from a computational, as well as conceptual, point of view to employ a variational theory. Such a theory is possible because of the rigorous inequality for the centroid density [1,18]

$$Q^* \geq Q_0^* \exp(-\langle \Delta S \rangle_0^*/\hbar), \quad (13)$$

where Q_0^* is the centroid density for some reference action S_0, ΔS is the difference between the actual and reference actions, and $\langle \cdots \rangle_0^*$ denotes path integral averaging in the reference system with the path centroids constrained to be at q^*. A variational theory for the reference system may then be defined by optimizing the parameters of the reference potential to maximize the right-hand-side of Eq. (13). Therefore, the challenge in such as theory is to pick an accurate and conceptually useful reference action. (For one possible approach, see Ref. [1]).

A very simple approach is to first simplify the inequality in Eq. (13) by invoking the linear response approximation for the bath [cf. Eqs. (8)–(12)] and to then employ the *effective* reference action

$$S_{\text{eff},0}[q(\tau)] = \int_0^{\hbar\beta} d\tau \left\{\frac{m}{2}\dot{q}(\tau)^2 + V_0 - \frac{1}{2}m\bar{\omega}_b^2 (q-q^*)^2\right\}. \quad (14)$$

The potential of mean force in the reference action is taken to be simple parabolic barrier with a variationally adjustable parameter $\bar{\omega}_b^2$ (i.e., the square of the unstable barrier frequency). It is important to note that in this simple reference action there is no influence functional [Eqs. (9) and (11)] so that both the nonlinearity of the reaction coordinate potential $V_r[q(\tau)]$ and the influence of the linear dissipation are treated in Eq. (14) by the single variational parameter $\bar{\omega}_b^2$.

The evaluation of the inequality in Eq. (13) and the subsequent derivation of the variational equation for $\bar{\omega}_b^2$ is facilitated by first re-expressing the reaction coordinate potential $V_r[q(\tau)]$ in terms of its Fourier transform $\hat{V}_r(k)$:

$$V_r[q(\tau)] = \frac{1}{2\pi} \int_{-\infty}^{\infty} dk \hat{V}_r(k) \exp[ikq(\tau)]. \quad (15)$$

The average $\langle \Delta S \rangle_0^*$ in Eq. (13) is now readily accomplished by Fourier path integration [1,3,5] wherein the quantum paths $q(\tau)$ are represented by

$$q(\tau) = \sum_{n=-\infty}^{\infty} \tilde{q}_n \exp(i\Omega_n \tau); \quad \tilde{q}_{-n} = q_n^*, \quad (16)$$

and Ω_n equals $2\pi n/\hbar\beta$. The result of this path integration for $Q_0^* \exp(-\langle \Delta S \rangle_0^*/\hbar)$ is

$$Q_0^* \exp(-\langle \Delta S \rangle_0^*/\hbar) = (m/2\pi\hbar^2\beta)^{1/2} Q_{\text{bath}} \cdot \frac{(\hbar\beta\bar{\omega}_b/2)}{\sin(\hbar\beta\bar{\omega}_b/2)} \exp[-\beta V_{\text{eff}}(\bar{\omega}_b, q^*)], \quad (17)$$

where the effective potential $V_{\text{eff}}(\bar{\omega}_b, q^*)$ is given by

$$V_{\text{eff}}(\bar{\omega}_b, q^*) = \frac{1}{\sqrt{2\pi\Delta q^2}} \int_{-\infty}^{\infty} dq V_r(q+q^*) \exp(-q^2/2\Delta q^2) + \sum_{n=1}^{\infty} \frac{\Omega_n \hat{\eta}(\Omega_n)/m + \bar{\omega}_b^2}{\beta(\Omega_n^2 - \bar{\omega}_b^2)}. \quad (18)$$

The width factor Δq^2 in Eq. (18) is also dependent on $\bar{\omega}_b^2$ and is given by

$$\Delta q^2 = \frac{2}{\beta m} \sum_{n=1}^{\infty} \frac{1}{\Omega_n^2 - \bar{\omega}_b^2}. \quad (19)$$

The other important quantity in Eq. (18) is $\hat{\eta}$ which is the Laplace transform of the *classical* autocorrelation function

of the environmental force fluctuations $\delta F_{ext}(t)$ on the reaction coordinate at the transition state. The transform in this case is evaluated at $z = \Omega_n$ and is explicitly given by

$$\tilde{\eta}(z) = \beta \int_0^\infty dt\, e^{-zt} \langle \delta F_{ext}(t)\, \delta F_{ext}(0) \rangle_{q^*} \tag{20}$$

where $\langle \cdots \rangle_{q^*}$ denotes classical Boltzmann averaging over bath variables which are equilibrated with the reaction coordinate fixed at q^*.

The optimal variational parameter $\bar{\omega}_b^2$ for use in Eq. (17) is obtained by maximizing the right-hand-side of Eq. (13) with respect to $\bar{\omega}_b^2$. The resulting transcendental equation is

$$m\bar{\omega}_b^2 = -\frac{\sum_{n=1}^{\infty} \frac{\Omega_n \tilde{\eta}(\Omega_n)}{(\Omega_n^2 - \bar{\omega}_b^2)^2}}{\sum_{n=1}^{\infty} \frac{1}{(\Omega_n^2 - \bar{\omega}_b^2)^2}} - \frac{1}{\sqrt{2\pi\Delta q^2}} \cdot \int_{-\infty}^{\infty} dq\, V_r'''(q+q^*) \exp(-q^2/2\Delta q^2), \tag{21}$$

where $V_r'''(\cdots)$ denotes the second derivative of the nonlinear potential of mean force along the reaction coordinate. The above equation can be efficiently solved by an iterative procedure on a computer. It is also important to note that the classical friction and the potential of mean force along the reaction coordinate are the only quantities required to solve Eq. (21) and hence to estimate the quantum rate constant from Eq. (1). In general, a positive classical friction leads to a lower effective barrier frequency in Eq. (21) than one would obtain in the absence of friction. Stated differently, tunneling dynamics in the presence of dissipation is equivalent in the present theory to the simple tunneling of a particle through a broader potential barrier.

For many realistic physical situations (e.g., intramolecular proton transfer in polar solvents), the timescale t_{cl} of the classical friction $\eta(t)$ is considerably longer than the timescale for the quantum particle along the reaction coordinate. In this case, a considerable simplification of Eqs. (18) and (21) results. This simplification arises due to the limiting expression.

$$\Omega_n \tilde{\eta}(\Omega_n) = \Omega_n \int_0^\infty dt\, e^{-\Omega_n t} \eta(t) \underset{t_{cl}\to\infty}{\approx} \Omega_n \eta(0) \int_0^\infty dt\, e^{-\Omega_n t} = \eta(0), \tag{22}$$

where $\eta(0)$ is the value of the classical friction at $t = 0$. Eq. (18) then simplifies to

$$V_{eff}(\bar{\omega}_b, q^*) \underset{t_{cl}\to\infty}{\approx} \frac{1}{\sqrt{2\pi\Delta q^2}} \int_{-\infty}^{\infty} dq [V_r(q+q^*) - V_r''(q+q^*)\Delta q^2/2] \exp(-q^2/2\Delta q^2). \tag{23}$$

Additionally, the transcendental equation for the variational parameter $\bar{\omega}_b^2$ simplifies to

$$m\bar{\omega}_b^2 \underset{t_{cl}\to\infty}{\approx} -\eta(0) - \frac{1}{\sqrt{2\pi\Delta q^2}} \cdot \int_{-\infty}^{\infty} dq\, V_r'''(q+q^*) \exp(-q^2/2\Delta q^2). \tag{24}$$

The utility of the latter equations lies in the fact that only classical equilibrium properties are required for the evaluation of the quantum rate constant.

The accuracy of these variational equations may be tested on a model problem of an infinite harmonic bath [cf. Eq. (6)] coupled to a reaction coordinate with an Eckart barrier potential [19]. The bath in this model is characterized by a classical friction of the form

$$\eta(t) = \eta(0) \exp(-t/t_{cl}), \tag{25}$$

where the timescale of the classical friction t_{cl} equals $4\omega_{b,cl}^{-1}$. (Here, $\omega_{b,cl}^{-1}$ is roughly the timescale for a classical particle to fall off of the Eckart barrier in the absence of coupling to the bath). The quantity which was calculated is the ratio of the quantum to classical activation factors, given by

$$\Gamma_a = e^{-\beta F^\ddagger}/e^{-\beta V_0}, \tag{26}$$

where V_0 is the height of the potential barrier at the transition state ($q = q^*$). This ratio was determined for various values of $\eta(0)$ (shown in fractions of $m\omega_{b,cl}^2$). In Fig. 1, the results for Γ_a are plotted from a full path integral Monte Carlo calculation of Eq. (2) with the exact action in Eq. (9) (open squares), from the rigorous variational equations

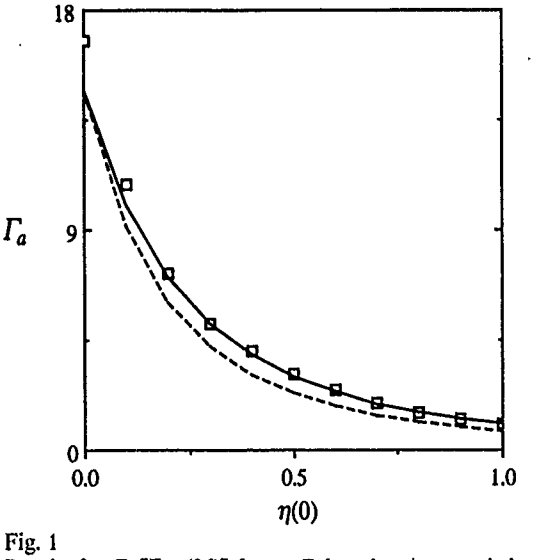


Fig. 1
Results for Γ_a [Eq. (26)] for an Eckart barrier coupled to the bath with a classical friction given by Eq. (25). The open squares are obtained from a full path integral Monte Carlo calculation of Eq. (2) with the exact action in Eq. (9), the solid line is from the rigorous variational equations given in Eqs. (17)–(19), and the dashed line is from the limiting theory based on Eq. (17) with the approximate equations in Eqs. (23) and (24). The height of the Eckart barrier is 2000 cm^{-1}, and the magnitude of the classical unstable barrier frequency is 1047 cm^{-1}. The temperature in the calculation was 188 K

given in Eqs. (17)–(19) (solid line), and from the limiting theory based on Eq. (17) with the approximate equations in Eqs. (23) and (24) (dashed line). The two sets of variational results are clearly in good agreement with the exact Monte Carlo calculation of the quantum activation factor. It is also interesting to note that the disagreement between the exact and variational results diminishes rapidly with increasing strength of the friction.

III. Variational Theory for the Dynamical Correction Factor κ

Although the basic form of the equation for the rate constant in terms of a path integral centroid density has been established [Eq. (1)], an exact analytic solution for the general quantum transmission coefficient κ has not yet been obtained. An accurate desription of κ is, however, desirable because that factor contains additional multidimensional dynamical and tunneling effects which are not already included in the centroid density Q^* [1,9].

The exact quantum mechanical expression for the transmission coefficient is given by [1]

$$\kappa = (2\pi m\beta)^{1/2} \int_{-\infty}^{\infty} dq \frac{Q_c(q)}{Q^*} v(q), \tag{27}$$

where $Q_c(q)$ is the centroid density [Eq. (3)] at a general position q along the reaction coordinate, Q^* equals $Q_c(q^*)$, and $v(q)$ is given by the quantum dynamical expression [1]

$$v(q) = \frac{2}{\hbar\beta} \mathrm{Im} \int dq' \int dq'' h_A(q') h_B(q'') \langle q'|e^{-\beta\hat{H}}|q''\rangle_q^{(c)} \cdot \langle q''|e^{i\hat{H}\Delta t/\hbar} h_B e^{-i\hat{H}\Delta t/\hbar}|q'\rangle / Q_c(q). \tag{28}$$

Here, $h_A(\cdots)$ [$h_B(\cdots)$] is the population operator for the reactant (product), and the imaginary time path integral [3,5] for $\langle q'|e^{-\beta\hat{H}}|q''\rangle_q^{(c)}$ has the centroids of its quantum paths constrained to be at a position q along the reaction coordinate. For notational simplicity, Eq. (28) has been written in terms of the reaction coordinate only, but inclusion of the bath modes is straightforward. Eq. (28) can also be written in a cyclic path integral form as [1]

$$v(q) = \frac{2}{\hbar\beta} \mathrm{Im} \int Dq_a(\tau) \int Dq_b(t) \int Dq_c(t) \cdot \delta(\tilde{q}_{0,a} - q) h_A[q_a(0)] h_B[q_a(\hbar\beta)] \cdot h_B[q_b(\Delta t)] e^{-\{S[q_a(\tau)] - iS_r[q_b(t)] + iS_r[q_c(t)]\}/\hbar} / Q_c(q), \tag{29}$$

where the $S_r[\cdots]$'s denote real time actions [3b], and the limits on the path integrations are

$$q_a(\beta\hbar) = q_b(0), \quad q_b(\Delta t) = q_c(0), \quad q_c(\Delta t) = q_a(0) \tag{30}$$

which are also integrated over. In principle, Eq. (27) facilitates the exact determination of the transmission coefficient from a real time quantum dynamics calculation [8]. Without such an efficient reactive sampling procedure, a "brute force" dynamics calculation for realistic problems would be enormously time consuming and essentially impossible. (Even with the above procedure, a quantum reactive dynamics calculation may still be very computationally demanding!)

As a complementary approach, it is clearly desirable to have simplified theories to estimate the value of κ as well as to provide some physical insight. Theories of this sort are, for example, in the same spirit as the Kramers [4] and Grote-Hynes [4,14] corrections to classical TST. In order to proceed in an analogous fashion to the latter authors, a model for the dynamics may be employed in the evaluation of Eq. (27). For example, the simple choice of free particle dynamics yields the result $\kappa = 1$ (i.e., a quantum TST approximation), while if a multidimensional parabolic model is employed one obtains the result $\kappa = \kappa_{GH}$ (i.e., the Grote-Hynes correction) which accounts for the coupling between a parabolic reaction coordinate and a linearly responding bath. In the latter theory, the transmission coefficient has the well known form [14]

$$\kappa_{GH} = \frac{\lambda_0^*}{\omega_b}; \quad \lambda_0^* = \frac{\omega_b^2}{\lambda_0^* + \hat{\eta}(\lambda_0^*)/m}, \tag{31}$$

where $\hat{\eta}(\lambda_0^*)$ is given from Eq. (20), and ω_b is the magnitude of the parabolic reaction coordinate barrier frequency.

The utility of the parabolic model is derived in part from the fact that the exact dynamical result for the corresponding rate constant [10] can also be obtained directly by statistical mechanical methods. The central feature of the latter analysis is a coordinate transformation to a separable set of normal modes [11,12]. In that procedure, the potential energy function for the fully parabolic model, given by Eq. (6) for $V_{qx}(q,x)$ and

$$V_r(q) \approx V_0 - \frac{1}{2} m\omega_b^2 (q - q^*)^2 \tag{32}$$

for the reaction coordinate, is first transformed into the separable form [11,12]

$$H = \frac{p_\varrho^2}{2} + (V_0 - \frac{1}{2}\lambda_0^{*2}\varrho^2) + \sum_{j=1}^{N} \frac{1}{2}(p_{y,j}^2 + \lambda_j^2 y_j^2), \tag{33}$$

where ϱ is the unstable normal mode with a squared imaginary frequency $-\lambda_0^{*2}$, and the y_j's are the uncoupled stable normal modes with frequencies λ_j. For this multidimensional quadratic Hamiltonian, it is immediately obvious that one should choose the unstable mode ϱ as the *true multidimensional reaction coordinate* since no recrossings of a transition state at $\varrho = \varrho^*$ are possible and transition state theory is therefore exact [11,12]. This choice of reaction coordinate is to be contrasted with that of the "bare" reaction coordinate q (which is obviously the correct choice in the absence of any coupling to a bath).

The *exact* quantum rate constant for multidimensional parabolic model may then be expressed as [9]

$$k_{pb} = \frac{k_B T}{h Q_A} \exp(-\beta F_c^*), \tag{34}$$

where the quantum activation free energy is given in terms of a centroid density by

$$F_c^* = -k_B T \ln[Q^*/(1/2\pi\hbar^2\beta)^{1/2}]. \tag{35}$$

In Eq. (35), Q^* denotes the centroid density in mass scaled coordinates with the centroids of the true multidimensional reaction coordinate paths $\varrho(\tau)$ constrained to be at their transition state value ϱ^*. In other words, the centroid constraint is now on the true multidimensional reaction coordinate ϱ rather than on the bare reaction coordinate q as in Eqs. (1)–(3).

On the other hand, for the parabolic model it is possible to derive a simple relationship between the quantum activation factor along q (at $q = q^*$) and the activation factor along ϱ(at $\varrho = \varrho^*$). This relationship is [9]

$$\exp(-\beta F_c^*) = (\lambda_0^*/\omega_b) \exp(-\beta F_c^*). \tag{36}$$

Thus, for the parabolic barrier/harmonic bath model, a calculation of the centroid density at the transition state of the simple reaction coordinate q is equivalent to a calculation of the centroid density at the transition state of the true multidimensional reaction coordinate ϱ *provided the former result is multiplied by the correction factor* λ_0^*/ω_b [9]. This perspective defines the transmission coefficient as the correction factor one must include in the calculation to compensate for being in the wrong transition state [9, 11, 12].

The perspective on the transmission coefficient outlined above can also be exploited to develop a theory for κ in systems having a *nonlinear* reaction coordinate potential [9]. In particular, the result in Eq. (36) may be combined with the variational principle for $\exp(-\beta F_c^*)$ based on the inequality in Eq. (13). The actual variational methodology in this case, however, differs somewhat from that discussed in Sec. II. Specifically, a reference action is now employed in the form [9]

$$\begin{aligned} \bar{S}_{\text{eff},1}[q(\tau)] = &\int_0^{\hbar\beta} d\tau \left\{ \frac{m}{2}\dot{q}(\tau)^2 + V_0 - \frac{1}{2} m\bar{\omega}_{b,1}^2 (q-q^*)^2 \right\} \\ &- \int_0^{\hbar\beta} d\tau \int_{-\infty}^{\infty} d\tau' \varphi(|\tau-\tau'|) q(\tau) q(\tau'), \end{aligned} \tag{37}$$

where the linear dissipation of the bath is now explicitly included, and there is a new variational parameter $\bar{\omega}_{b,1}^2$ (which generally differs in value from $\bar{\omega}_b^2$ in Sec. II). In Eq. (37), the variational parameter specifically treats the anharmonicity of the actual potential of mean force along the q direction, while the influence of the bath oscillators is described explicitly through $\alpha(|\tau - \tau'|)$ [cf. Eqs. (11) and (12)].

The optimization of the right-hand-side of Eq. (13) for the reference system in Eq. (37) can be performed explicitly [9] and yields the transcendental equation for $\bar{\omega}_{b,1}^2$:

$$m\bar{\omega}_{b,1}^2 = -\frac{1}{\sqrt{2\pi\Delta q_1^2}} \int_{-\infty}^{\infty} dq\, V_r''(q+q^*) \exp(-q^2/2\Delta q_1^2), \tag{38}$$

where $V_r''(\cdots)$ is the second derivative of the potential of mean force along the reaction coordinate, and the width factor Δq_1 is given in this case by

$$\Delta q_1^2 = \frac{2}{\beta m} \sum_{n=1}^{\infty} \frac{1}{\Omega_n^2 - \bar{\omega}_{b,1}^2 + \Omega_n \hat{\eta}(\Omega_n)/m}. \tag{39}$$

Note here that, as in Sec. II, $\hat{\eta}(\Omega_n)$ is given by the classical expression [Eq. (20)] evaluated at $z = \Omega_n$. Therefore, for a realistic problem one might employ *classical* molecular dynamics to evaluate Eq. (39) as input to the transcendental equation for $\bar{\omega}_{b,1}^2$ [Eq. (38)].

After a determination of $\bar{\omega}_{b,1}^2$ for the realistic reaction coordinate potential, one may then employ the relationship in Eq. (36) to relate the variational/parabolic activation factor along $\dot{q}$ to the activation factor along the more realistic variational/parabolic estimate of the multidimensional reaction coordinate ϱ. The resulting expressions are [9]:

$$\exp(-\beta F_c^*) = \frac{\bar{\lambda}_0^*}{\bar{\omega}_{b,1}} \exp(\beta F_c^*); \quad \bar{\lambda}_0^* = \frac{\bar{\omega}_{b,1}^2}{\bar{\lambda}_0^* + \hat{\eta}(\bar{\lambda}_0^*)/m}. \tag{40}$$

The quantum transmission coefficient in Eq. (1) which is appropriate for nonlinear barrier potentials is therefore given by [9]

$$\kappa = \bar{\lambda}_0^*/\bar{\omega}_{b,1}. \tag{41}$$

The transcendental equation in Eq. (40) which defines $\bar{\lambda}_0^*$ clearly has the same from as the classical Grote-Hynes result [Eq. (31)]. However, because the effective barrier frequency $\bar{\omega}_{b,1}$ is optimized through Eq. (38) to characterize a nonlinear barrier potential of mean force, it generally decreases with decreasing temperature in order to capture the anharmonic nature of the potential and the quantum tunneling motion. Thus, for nonlinear barriers at lower temperatures there is effectively a lower variational barrier frequency $\bar{\omega}_{b,1}$ than at higher temperatures. According to the powerful insight provided by the Grote-Hynes relationship [Eq. (31)] [14], a system having a barrier with a low frequency (or curvature) "feels" the entire spectrum of the bath fluctuations much more than one with a higher frequency (or sharper) barrier As a results, the factor $\kappa = \bar{\lambda}_0^*/\bar{\omega}_{b,1}$ in the quantum rate equation [Eq. (1)] should be less than the classical Grote-Hynes value $\kappa_{GH} = \lambda_0^*/\omega_b$ [9].

An example of the temperature dependence of the quantum κ in Eq. (41) is shown in Fig. 2 for the same Eckart barrier, infinite harmonic bath system described at the end of Sec. II. The solid line is the "quantum Grote-Hynes" result calculated from Eqs. (38) – (41), while the dashed line is the

standard classical Grote-Hynes result [Eqs. (31)]. The quantum result begins to deviate significantly from the classical theory at the lower temperatures. Research is in progress in our laboratory to determine rather the small amount of additional tunneling not already included in the centroid density [Eq. (3)] would contribute significantly to the value of the quantum κ at low temperature [1]. Such additional tunneling is expected to add a multiplicative factor Eq. (41) which is slightly larger than unity at low-T, but it is unclear whether that factor will qualitatively alter the behavior of the quantum result in Fig. 2.

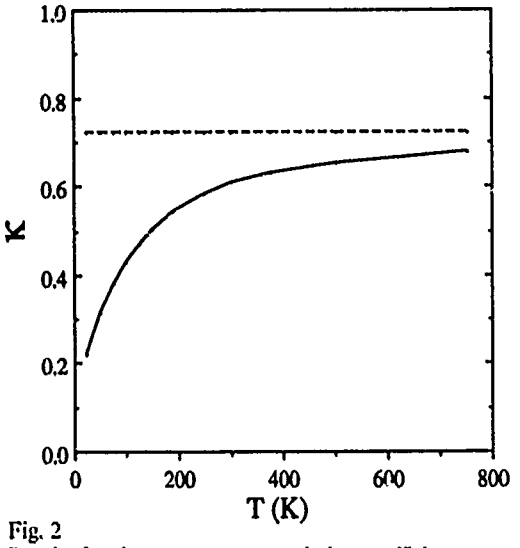


Fig. 2
Results for the quantum transmission coefficient κ as a function of temperature for the Eckart barrier/infinite harmonic bath system employed in the calculations for Fig. 1. The solid line is the "quantum Grote-Hynes" result calculated from Eqs. (38)–(41), while the dashed line is the standard classical Grote-Hynes result [Eq. (31)]

IV. Concluding Remarks

In the present paper, two aspects of the quantum rate constant expression given in Eq. (1) have been explored. In Sec. II a simple, but quite accurate, variational theory for the quantum activation factor was discussed that maps the nonlinearity of the reaction coordinate barrier and the linear dissipation of a Gaussian fluctuating bath into a separable parabolic reference action. A much simplified form of the variational equations was also presented which is valid for cases in which the correlation time of the classical friction is long compared to the timescale for the motion of the quantum particle along the reaction coordinate. In Sec. III, another variational approach was discussed which is the basis for a theory of the dynamical correction factor κ in Eq. (1). The resulting quantum expression for κ was shown to deviate significantly from the classical result at low temperatures. A number of studies of quantum activated rate problems based on Eq. (1) are presently underway, and the results of those studies will be reported in future publications.

G.A.V. is a recipient of a Camille and Henry Dreyfus Foundation New Faculty Award (1989–1994).

References

[1] G. A. Voth, D. Chandler, and W. H. Miller, J. Chem. Phys. *91*, 7749 (1989).
[2] The VCM work (Ref. [1]) draws on the important insights contained in M. J. Gillan, J. Phys. Chem. *20*, 3621 (1987).
[3] (a) R. P. Feynman, Statistical Mechanics, Addison-Wesley, Reading, MA, 1972; (b) R. P. Feynman and A. R. Hibbs, Quantum Mechanics and Path Integrals, McGraw-Hill, New York 1965.
[4] For a review of the classical and quantum theory of activated dynamics, see P. Hänggi, P. Talkner, and M. Borkovec, Rev. Mod. Phys. *62*, 251 (1990).
[5] For reviews, see B. J. Berne and D. Thirumalai, Annu. Rev. Phys. Chem. *37*, 401 (1987); D. L. Freeman and J. D. Doll, Adv. Chem. Phys. *70B*, 139 (1988); J. D. Doll and D. L. Freeman, ibid. *73*, 289 (1989); Quantum Simulations of Condensed Matter Phenomena, eds. D. Doll and J. E. Gubernatis, World Scientific, Singapore 1990; D. Chandler, in: Liquides, Cristallisation et Transition Vitreuse, Les Houches, Session LI, eds. D. Levesque, J. P. Hansen, and J. Zinn-Justin, Elsevier Science Publishers B.V. 1990.
[6] Eq. (1) has been used to study an electron transfer problem in water by J. S. Bader, R. A. Kuharski, and D. Chandler, J. Chem. Phys. *93*, 230 (1990).
[7] Eq. (1) has been applied to H-atom diffusion on metal surfaces by Y.-C. Sun and G. A. Voth (in preparation) and to intromolecular proton transfer by G. A. Voth (in preparation).
[8] C. H. Mak and D. Chandler, Phys. Rev. A *41*, 5709 (1990).
[9] G. A. Voth, Chem. Phys. Lett. *170*, 289 (1990).
[10] P. G. Wolynes, Phys. Rev. Lett. *47*, 968 (1981).
[11] E. Pollak, J. Chem. Phys. *85*, 865 (1986); ibid. *86*, 3944 (1987); see also the earlier discussion in G. van der Zwan and J. T. Hynes, J. Chem. Phys. *78*, 4174 (1983); Chem. Phys. *90*, 21 (1984).
[12] E. Pollak, Chem. Phys. Lett. *127*, 178 (1986); Phys. Rev. A *33*, 4244 (1986).
[13] W. H. Miller, J. Chem. Phys. *62*, 1899 (1975); S. Coleman, in: The Whys of Subnuclear Physics, ed. A. Zichichi, Plenum, New York 1979.
[14] R. F. Grote and J. T. Hynes, J. Chem. Phys. *73*, 2115 (1980); ibid. *74*, 4465 (1981); see also P. Hänggi and F. Mojtabai, Phys. Rev. *A26*, 1168 (1982).
[15] R. Zwanzig, J. Stat. Phys. *9*, 215 (1973); A. O. Calderia and A. J. Leggett, Ann. Phys. (N.Y.) *149*, 374 (1983); *153*, 445(E) (1984); A. J. Leggett, S. Chakravarty, A. T. Dorsey, M. P. A. Fisher, A. Garg, and W. Zwerger, Rev. Mod. Phys. *59*, 1 (1987).
[16] See, e.g., D. Chandler, Introduction to Statistical Mechanics, p. 201, Oxford University Press 1987; D. Chandler and L. R. Pratt, J. Chem. Phys. *65*, 2925 (1976).
[17] R. P. Feynman and F. L. Vernon, Ann. Phys. (N.Y.) *24*, 118 (1963).
[18] The variational principle based on this expression is analogous to the path integral extension proposed by Feynman (Ref. [3a], Sec. 3.4) of the Gibbs-Bogoliubov variational principle. Its further extension to centroid densities was developed in Ref. [1]. See also the related work of J. Cao and B. J. Berne, J. Chem. Phys. *92*, 7531 (1990) on ways to use the centroid density variational principle to improve the convergence of path integral Monte Carlo calculations.
[19] H. S. Johnston, Gas Phase Reaction Rate Theory, pp. 40–44, Ronald Press, New York 1966.

Presented at the Discussion Meeting of the Deutsche Bunsen-Gesellschaft für Physikalische Chemie "Rate Processes in Dissipative Systems. 50 Years after Kramers" in Tutzing, September 10–13, 1990 E 7515

Quantum Brownian Motion and its Classical Limit

Vinay Ambegaokar*)

Institut für Theorie der Kondensierten Materie, Universität Karlsruhe, D-7500 Karlsruhe 1, Germany

Chemical Kinetics / Diffusion / Nonequilibrium Phenomena

The Feynman-Vernon, Caldeira-Leggett model for a quantum dissipative system is used, via a general kinetic equation due to Chow, Browne, and the present author, to cast light on the classical limit of quantum Brownian motion, with special attention paid to the requirement of coarse graining in time.

I. Introduction

In §.2 of Kramers' classic paper [1], which we are here to celebrate, he discusses the conditions under which simple equations govern the diffusion of a classical Brownian particle. Central to his thinking is the existence of a "range of time intervals τ which has the following properties: On the one hand τ must be so short, that the change of velocity suffered in the course of τ may be considered as very small; on the other hand τ must be so large that the chance for X [the "irregular force"] to take a given value at the time $t+\tau$ is independent of the value which X possessed at the time t."

In this contribution I discuss how this requirement emerges in the classical limit of a model of quantum Brownian motion, for which a completely general quantum kinetic equation formulation was given some years ago [2, 3]. The derivation does not make the assumption that the system is weakly damped.

In a certain sense, what follows is an exercise in futility: the model used is known to lead in the appropriate limit to the classical Langevin equation [4] which is Kramers' starting point. On the other hand, the passage to the classical limit via the kinetic equation shows that this equation, which contains memory effects, itself signals the scale on which coarse graining in time is needed if a simple Markoff equation is to be valid, and it is instructive to see how what has to happen does in fact happen.

It is also interesting to note that this procedure cures a "positivity problem," pointed out to me by P. Pechukas [5], thereby casting light on the extensive literature on the so-called Dynamical Semi-groups [6].

II. Procedure

II.1. Kinetic Equation

Consider the Feynman-Vernon [7], Calderia-Leggett [8] model for dissipative quantum mechanics. This is a "system" plus "environment" scheme, in which the environment is a large number of harmonic oscillators equilibrated by fiat in the distant past. The Hamiltonian is

$$H = \frac{p^2}{2m} + V(q) + \sum_l \left[\frac{p_l^2}{2m_l} + \frac{1}{2} m_l \omega_l^2 \left(q_l - \frac{C_l q}{m_l \omega_l^2}\right)^2\right]. \tag{II.1}$$

To keep the length of the present article reasonable, it will be necessary to refer to Ref. [2], in which the notation, with rare exceptions, is identical. There, the thermodynamic field theory for this model was set up. A crucial point is that the *time-relaxed* reduced density matrix for the system described by the variables p, q is the object for which a formal integro-differential equation is always valid. This quantity is defined by the equation

$$\hat{G}(t_1 t_2) = \mathrm{Tr}_B[U(t_1, -\infty)\, \varrho(-\infty)\, U^\dagger(t_2, -\infty)] \tag{II.2}$$

where the trace is over the environment variables, $U(t, -\infty)$ is the time evolution operator corresponding to the full Hamiltonian (II.1), and $\varrho(-\infty)$ is the initial density matrix for the system *and* bath in the distant past, when the oscillators are assumed to be in equilibrium. The reduced density matrix for the system is $\hat{G}(t,t)$, i.e. at equal times, which we shall call $\hat{\varrho}(t)$. This is the quantity (like $\hat{G}$ a matrix in the Hilbert space of the system) which most kinetic theories deal with. While it is true that averages of dynamical variables of the system can be calculated once $\hat{\varrho}$ is known, the time evolution of $\hat{\varrho}$ need not be, and in fact is not, simple on all time scales. On the other hand, the general principles of statistical quantum field theory lead to the following kinetic equation for $\hat{G}$:

$$\mathrm{i}\left(\frac{\partial}{\partial t_1} + \frac{\partial}{\partial t_2}\right)\hat{G}(t_1, t_2) - [H_0 + \mathrm{Re}\sigma, \hat{G}] - [\hat{\sigma}, \mathrm{Re}g] = \frac{\mathrm{i}}{2}\{A, \hat{\sigma}\} - \frac{\mathrm{i}}{2}\{\Gamma, \hat{G}\}. \tag{II.3}$$

There are many symbols needing definition here, of which the simplest is H_0, the system Hamiltonian $(p^2/2m) + V(q)$. Before getting involved in all the other definitions, it may be useful to step back and observe that (II.3) has a standard form for a kinetic equation, with the left hand side describing the drift of excitations, and the right hand side collisions ["scattering in" and "scattering out"] between excitations.

*) On sabbatical leave from. Laboratory for Atomic & Solid State Physics, Cornell University, Ithaca, NY, 14853-2501, USA.

 © VCH Verlagsgesellschaft mbH, W-6940 Weinheim, 1991 0005-9021/91/0303-0400 $ 3.50+.25/0

The complication is that, as in any field theory, the left side includes energy shifts which modify the excitations of the uncoupled system, and the right side describes the scattering of these true excitations. At a formal level, there is no way of avoiding the fact that these renormalizations involve infinite order perturbation theory, which can however be tucked into "self-energy" operators.

Now, for the definitions. There are two auxiliary propagators which enter the time evolution of the two sides of $\varrho(-\infty)$:

$$G^{r}(t_1,t_2) = -i\theta(t_1-t_2)\,\mathrm{Tr}_B[U(t_1,t_2)\,\varrho_{eq}^{bath}]$$
$$G^{a}(t_1,t_2) = i\theta(t_2-t_1)\,\mathrm{Tr}_B[U(t_1,t_2)\,\varrho_{eq}^{bath}]\,. \tag{II.4}$$

Corresponding to each of the propagators $\hat{G}$, G^r, G^a are self energy operators. These are defined by

$$G^{r,a}(t_1,t_2) = G_0^{r,a}(t_1,t_2) + \int_{-\infty}^{\infty} dt_1' \int_{-\infty}^{\infty} dt_2'\, G_0^{r,a}(t_1,t_1')\,\sigma^{r,a}(t_1',t_2')\,G^{r,a}(t_2',t_2)$$
$$\hat{G}(t_1,t_2) = G^{r}(t_1,-\infty)\,\hat{\varrho}(-\infty)\,G^{a}(-\infty,t_2) + \int_{-\infty}^{\infty} dt_1' \int_{-\infty}^{\infty} dt_2'\, G^{r}(t_1,t_1')\,\hat{\sigma}(t_1',t_2')\,G^{a}(t_2',t_2)\,. \tag{II.5}$$

Products on the right of (II.5) and (II.3) are matrix products in the function space of the system, and folded time integrals, as in (II.5), are implied in (II.3). From their definitions (II.4), one sees that G^r and G^a are not independent; the kinetic equation (II.3), obtained by applying time derivatives to the left and right of (II.5), has been rewritten by introducing $G^{r,a} \equiv \mathrm{Re}g \mp \frac{i}{2}A$ and $\varrho^{r,a} = \mathrm{Re}\sigma \mp \frac{i}{2}\Gamma$. The square brackets in (II.3) denote commutators and the curly brackets anticommutators.

The preceding may seem unnecessarily formal. However, this is the nature of quantum kinetic equations; (II.3) is nothing more or less than the Keldysh [9], or equivalently the Baym-Kadanoff [10], scheme applied to the present problem, in which the "system" consists of one particle. The basic point is that "forward" and "backward" time evolution is needed for statistical operators.

The equilibrating nature of the oscillator heat bath is contained in the environment propagator

$$\alpha(t,t') = \sum_i C_i^2\,\mathrm{Tr}_B[x_i(t)\,x_i(t')\,\varrho_{eq}^{bath}] = \int_{-\infty}^{\infty} \frac{d\omega}{\pi} J(\omega)\,[1+n(\omega)]\,e^{-i\omega(t-t')}\,. \tag{II.6}$$

In the last line $n(\omega) = 1/[\exp(\beta\omega)-1]$, and $J(\omega)$ has been defined via

$$J(\omega) = \pi \sum_i \frac{C_i^2}{2m_i\omega_i}\,\delta(\omega-\omega_i)\,, \tag{II.7}$$

Caldeira and Leggett [8], and Leggett [11] have emphasized the fact that details of dissipative mechanisms can be simulated by an appropriate choice of $J(\omega)$. In particular, a friction force linear in the velocity – often called Ohmic dissipation, – to which we restrict ourselves from now on, corresponds to $J(\omega) = m\gamma\omega\theta(\omega_c - |\omega|)$ where $m\gamma$ is the classical coefficient of friction. Here for the first time appears an upper frequency cut-off, ω_c. Its reciprocal is the classical correlation time of the environment, which plays the role here of the duration of a collision, and will be important in what follows.

It is worth nothing already that when t_1 is set equal to t_2, in the first term of (II.3), thereby constructing $\frac{\partial}{\partial t_1}\hat{\varrho}(t_1)$, the remaining terms cannot be written as $M\{\hat{\varrho}(t_1)\}$ where M is a map only in the space of H_0. Thus (II.3) does not lead to an equation of the form studied in Ref. [6]. This feature persists, as well shall see, in the classical limit.

II.2. Classical Limit and The Generalized Born Approximation

Eq. (II.3) needs to be supplemented by equations relating the self-energies back to $\hat{G}$, G^r and G^a to make a closed system. At this point, uncontrolled approximations are hard to avoid except in the case of extremely weak damping. However, in the classical limit, $T > \hbar\omega_c$ (T-temperature in the energy units also favored by Kramers [12]), one can argue that, if the inequality $\omega_c^{-1} \ll \gamma^{-1}$ is satisfied, corrections to a very simple closure are small. The argument is given in the appendix. The following scheme, called the generalized Born approximation in Ref. [2], is then valid:

$$\sigma^{r,a}(t_1,t_2) = \alpha(t_1-t_2)\,qG^{r,a}(t_1,t_2)\,q + \delta(t_1-t_2)\cdot\int_0^{\omega_c}\frac{d\omega}{\pi\omega}J(\omega)\,q^2$$
$$\hat{\sigma}(t_1,t_2) = \alpha(t_2-t_1)\,q\hat{G}(t_1,t_2)\,q\,. \tag{II.8}$$

It may be useful to emphasize that this is not second order pertubation theory because the self-consistent $G^{r,a}$ and $\hat{G}$ occur on the right. The approximation corresponds to the neglect of vertex corrections and is similar to what is called "Migdal's theorem" in the problem of the electron-phonon interaction in metals [13]. Within this approximation, it is straigth forward to work out the kinetic equation. First, note that for $T > \hbar\omega_c$ the Bose factor $[1+n(\omega)]$ in (II.6) may be approximated by $(T/\hbar\omega)+(1/2)$. Then for Ohmic dissipation one sees that

$$\alpha(t_1-t_2) = 2m\gamma T\delta_c(t_1-t_2) + im\gamma\frac{\partial}{\partial t_1}\delta_c(t_1-t_2)\,. \tag{II.9}$$

Where δ_c is a δ-function spread out on a time scale ω_c^{-1}. For the steps that follow, it is convenient to write (II.3) in the equivalent form

$$i\left(\frac{\partial}{\partial t_1}+\frac{\partial}{\partial t_2}\right)\hat{G} - [H_0,\hat{G}] = \sigma^r\hat{G} - \hat{G}\sigma^a + \hat{\sigma}G^a - G^r\hat{\sigma}\,. \tag{II.10}$$

Look at the first term on the right of (II.10). Using (II.9), (II.8), and (II.4) we have

$$\sigma^r \hat{G} = -i2m\gamma T \cdot \frac{1}{2} \cdot q^2 \hat{G}(t_1 t_2) + im\gamma \int d\bar{t} \left[\frac{\partial}{\partial t_1} \delta_c(t_1 - \bar{t}) \right] q G^r(t_1 \bar{t})\, q \hat{G}(\bar{t} t_2) + \int d\bar{t} m\gamma \delta(t_1 - \bar{t}) \frac{\omega_c}{\pi} q^2 \hat{G}(\bar{t}, t_2). \quad \text{(II.11)}$$

In doing a partial integration in the second term, it is important to recognize that G^r has a sharp step function in time. Then, identifying $\delta_c(0)$ with (ω_c/π), a cancellation occurs and one obtains

$$[\sigma^r \hat{G}](t_1 t_2) = -im\gamma T q^2 \hat{G}(t_1 t_2) + \frac{im\gamma}{2} \left\{ q \frac{\partial}{\partial t_1'} G^r(t_1, t_1')\, q \hat{G}(t_1, t_2) - i q^2 \frac{\partial}{\partial t_1} \hat{G}(t_1, t_2) \right\}_{t_1' = t_1 - 0}. \quad \text{(II.12)}$$

The reduced density matrix $\hat{\varrho}$ is constructed on the left of (II.10) by setting $t_1 = t_2$. Note, again, that on the right side of (II.12) the time derivatives do not enter symmetrically, as on the left. From the definition of G^r and $\hat{G}$, (II.4) and (II.2), one identifies

$$\frac{\partial}{\partial t'} G^r(t_1, t_1')|_{t_1' = t_1 - 0} = \mathrm{Tr}_B[H \varrho_{eq}^{bath}] \quad \text{(II.13)}$$

and

$$\frac{\partial}{\partial t'} \hat{G}(t_1, t_1')|_{t_1' = t_1} = -i\, \mathrm{Tr}_B[H \varrho(t_1)] \quad \text{(II.14)}$$

where $\varrho(t_1)$ is the *full* density matrix of system and bath evolved to time t_1. In a similar way, one can work out all the terms on the right of (II.10). Further algebra will not be given here. A perhaps useful hint for someone who wishes to check it is that the answer has been tidied up by noting that the only part of H, given in (II.1), that does not commute with the system coordinate q is $(p^2/2m)$, and that the commutator of this term can be worked out explicitly as needed. Finally, one obtains

$$\frac{\partial \hat{\varrho}}{\partial t} = \frac{-i}{\hbar} [H_0, \hat{\varrho}] - \frac{m\gamma T}{\hbar^2} [q, [q, \hat{\varrho}]] - i \frac{\gamma}{2\hbar} [q, \{p, \hat{\varrho}\}] + \hat{C} \quad \text{(II.15)}$$

where

$$\hat{C} = \frac{im\gamma}{2\hbar^2} \{ q^2 (\langle H \rangle_B \hat{\varrho}(t) - \mathrm{Tr}_B[H \varrho(t)]) + (\hat{\varrho}(t) \langle H \rangle_B - Tr_B[\varrho(t) H]) q^2 + q (Tr_B[\varrho(t) H] - \hat{\varrho}(t) \langle H \rangle_B) q + q (Tr_B[H \varrho(t)] - \langle H \rangle_B \hat{\varrho}(t)) q \}. \quad \text{(II.16)}$$

In the last equation $\langle H \rangle_B \equiv \mathrm{Tr}_B[H \varrho_{eq}^{bath}]$. With the exception of the term $\hat{C}$, Eq. (II.15) is an equation that may be familiar to some readers. It has the feature that in the Wigner representation [14,15] it looks exactly like the classical Fokker-Planck equation. It would have been surprising if this equation could have been derived without further approximiation, since the existence of the "range of time intervals" mentioned by Kramers has nowhere been used. In the next section we examine the physics contained in Eq. (II.16).

II.3. Physics of the New Terms

Eqs. (II.15) and (II.16) are the central results of this paper. To the best of my knowledge, the terms called $\hat{C}$ have not been previously captured in a form as general as here given. It will be instructive to examine these terms – which evidently describe energy transfers between system and bath – more generally.

Note, first, that all parts of the Hamiltonian (II.1) involving *only* the system variables q, p, drop out of (II.16). Call the remainder H'. Evidently

$$H' = \sum_i \left(\frac{p_i^2}{2m_i} + \frac{1}{2} m_i \omega_i^2 q_i^2 \right) - \sum_i C_i q_i q. \quad \text{(II.17)}$$

Consider the contribution of H' to the second term in the bracket of (II.16). This can be written as a double functional integral.

$$\mathrm{Tr}_B[H' \varrho(t)] = \int \mathcal{D}q' \mathcal{D}q''\, e^{iS_0(q')} e^{-iS_0(q'')} \cdot Tr_B \{ H'[q'(t)]\, U'([q'], t, -\infty) \cdot \varrho_B^{eq} U'([q''], -\infty, t) \}\, \varrho_s(-\infty) \quad \text{(II.18)}$$

where $S_0(q)$ is the classical action associated with H_0, and the U''s are time evolution operators corresponding to H' for the Feynman paths q' and q''. Now the trace in curly brackets on the right of (II.18), called $\langle H' \rangle$ below, can be explicitly evaluated, the calculation being only slightly more complicated than that for the Feynman-Vernon influence functional, and I have worked it out in general. However, in the classical limit it suffices to assume that the forward, q', and backward, q'', paths are identical. Then, the general result simplifies to a form, the time derivative of which can be obtained directly in the following way:

$$\frac{d}{dt} \langle H' \rangle = \left\langle \frac{\partial H'}{\partial t} \right\rangle = -\sum_i C_i \dot{q}(t) \cdot \left[\int^t \frac{du}{m_i \omega_i} \sin \omega_i (t-u) C_i q(u) \right] = -m\gamma \int_{-\omega_c}^{\omega_c} \frac{d\omega}{\pi} \omega \int_{-\infty}^{t} du \sin \omega (t-u) \dot{q}(t) q(u) = m\gamma \dot{q}^2(t). \quad \text{(II.19)}$$

In (II.19) the response of the oscillator i to the classical force $C_i q(t)$ has been used to eliminate $q_i(t)$. This equation shows

that $\hat{C}$ in (II.15) describes aperiodic energy transfers – and an associated loss of quantum coherence – between the Brownian particle and its environment due to collisions.

III. Results

III.1. Positivity Disease and its Cure

When $\hat{C}$ is neglected, Eq. (II.15) suffers from a disease that was pointed out to me by P. Pechukas [5]. Here, I summarize his formulation of the problem and show how it is cured by the new terms.

Since $\hat{\varrho}$ is a density matrix it must obey $\langle\psi|\hat{\varrho}|\psi\rangle \geq 0$ for any system state $|\psi\rangle$. Suppose that at $t = 0$ $\hat{\varrho}(0)$ describes a pure state, i.e. let $\hat{\varrho}(0) = |\phi\rangle\langle\phi|$. Let the wavefunction $\phi(q)$ be even in q and choose $\psi(q) = \mathrm{d}\phi/\mathrm{d}q$. Evidently, $\langle\psi|\hat{\varrho}(0)|\psi\rangle = 0$. Now consider the average in $|\psi\rangle$ of the time derivative of $\hat{\varrho}$ at $t = 0$. From (II.15), ignoring $\hat{C}$, it follows that

$$\langle\psi|\frac{\mathrm{d}\hat{\varrho}}{\mathrm{d}t}|\psi\rangle\Big|_{t=0} = \gamma\left(\int \mathrm{d}q\,\psi(q)q\phi(q)\right)\cdot\left(\int \mathrm{d}q\,\psi(q)\frac{\mathrm{d}}{\mathrm{d}q}\phi(q)\right) + \frac{2mT\gamma}{\hbar^2}\left(\int \mathrm{d}q\,\psi q\phi\right)^2. \tag{III.1}$$

Now, the first bracket on the right of (III.1) is negative and can be made as negative as one wishes by choosing $\phi(q)$ to be more and more peaked around $q = 0$. This means that the right hand side of (III.1) can be made negative, so that at a small positive time $\hat{\varrho}$ violates the positivity requirement.

It is instructive to make the criterion for positivity violation more quantitive. Choose $\phi(q)$ to be a Gaussian centered at the origin with width l. Then, the criterion for (III.1) to change sign is seen to be

$$l^2 < \frac{\hbar^2}{4mT} \tag{III.2}$$

i.e. that the initial state be concentrated within a thermal de Broglie wavelength.

The analysis in (II.3) immediately provides a cure for this problem, along the lines suggested in the quotation from Kramers with which the present paper opened: "coarse-graining" in time over a few collisions. We have required that ω_c^{-1}, the duration of collision, be much less than γ^{-1}, the relaxation time. Let $\Delta t = K\omega_c^{-1}$ with K a moderately large number but such that $\gamma\Delta t \ll 1$. Then since quantum coherence will, via $\hat{C}$, be totally lost on the time scale Δt, an uncontrollable indefiniteness in the energy, momentum, and position of the Brownian particle will ensue. The uncertainty in momentum is given by $\Delta p \approx \sqrt{2m\hbar/\Delta t}$. Correspondingly, the uncertainty in x obeys

$$\Delta x \sim \sqrt{\frac{\hbar\Delta t}{m}} \gg \sqrt{\frac{\hbar}{m\omega_c}} \gg \sqrt{\frac{\hbar^2}{mT}}. \tag{III.3}$$

When (II.15) is coarse grained on the time scale Δt, the terms in $\hat{C}$ will average to zero via (II.19). This, as (III.3) shows, has as a corollary the condition that $\hat{C}$ can only be neglected in (II.15) when lengths on the scale of the positivity disease are forbidden.

III.2. Concluding Remarks

In this brief article, I have attempted to show that in the passage to the classical limit of quantum dissipation, as in the purely classical treatment of dissipation, times corresponding to the duration of several collisions must be averaged over before a simple theoretical scheme emerges. Since this is obvious from a physical point of view, a natural question is: has a sledgehammer been used to crack a peanut? Yes, but the following is new, to the best of my knowledge, about the exercise as here presented:

(i) Weak dissipation, in the sense of the relaxation time of the system being long compared to its characteristic frequencies, has nowhere been assumed.

ii) The general kinetic equation, containing all memory effects and renormalizations due to coupling with the environment, has been shown to *contain* the requirement of coarse graining. Unless some such procedure is followed, the equation remembers the stochastic transfer of energy between system and environment.

The weak damping limit of the problem has been previously treated in an explicitly quantum mechanical way [3, 16]. In particular, in Ref. [3], the resulting Redfield equations [17] were shown, in the classical limit to lead to Kramers' low damping, i.e. energy diffusion, limit of the Fokker-Planck equation. By contrast, Eq. (II.15) when coarse grained gives the full Fokker-Planck equation which is the basis for §3 and the rest of Kramers' paper.

For arbitrary damping, the implementation in real, as opposed to imaginary, time of the kind of quantum mechanical scheme used here remains a largely open question.

Dana A. Browne suggested that the generalized Born approximation might capture all of the relevant physics in the classical limit, and the arguments of Sec. III.1 are due to Mark Oxborrow. I am very grateful to these kind souls for telling me how this work should start and end, but they should not be held in any way responsible for the intermediate steps.

It is a pleasure to thank the Alexander von Humboldt-Stiftung for a. U. S. Senior scientist award, and Albert Schmid for the hospitality of his institute. I express my gratitude to the organisers of this meeting for their invitation. This work is supported in part by the U.S. National Science Foundation under grant Nr. DMR-88 15828.

Appendix

Here the neglect of Feynman graphs with overlapping environment propagators is justified when $\gamma \ll \omega_c$. The connection between perturbation theory and Feynman graphs in the present context is described in Appendix A of Ref. [2]. Consider first the contributions to $\hat{\sigma}$ of the graphs shown in Figs. 1(a) and 1(b). Call these the direct

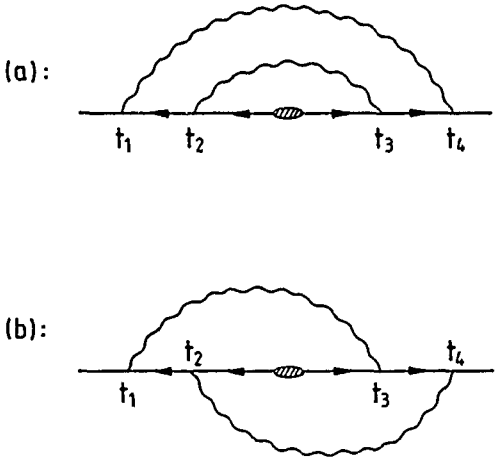


Fig. 1
Direct (a), and Overlap (b) Feynman graphs for $\hat{\sigma}$. The wavy lines denote environment propagators, the solid lines directed to the left (right) $G_0^<$, and the lines with two opposed arrows $\hat{G}_0$

and overlap graphs, respectively. Corresponding to 1(a) belongs the contribution

$$\hat{\sigma}_{\text{direct}}(t_1,t_4) = \int_{-\infty}^{\infty} dt_2 \int_{-\infty}^{\infty} dt_3\, q G_0^{\delta}(t_1 t_2) q \hat{G}_0(t_2 t_3) q G_0^{a}(t_3 t_4) q \cdot \alpha(t_4 - t_1)\alpha(t_3 - t_2)\,, \tag{A.1}$$

whereas Fig 1(b) contributes

$$\hat{\sigma}_{\text{direct}}(t_1,t_4) = \int_{-\infty}^{\infty} dt_2 \int_{-\infty}^{\infty} dt_3\, q G_0^{\delta}(t_1 t_2) q \hat{G}_0(t_2 t_3) q G_0^{a}(t_3 t_4) q \cdot \alpha(t_4 - t_2)\alpha(t_3 - t_1)\,. \tag{A.2}$$

The regions of time integration in (A.1) and (A.2) are different. In (A.1) one has strictly $t_1 \geq t_2$, $t_3 \leq t_4$, and, through (II.9), $t_4 \simeq t_1$, $t_3 \simeq t_2$, where the symbol $\simeq$ means an approximate equality controlled by ω_c^{-1}. By contrast, in (A.2) one has the same strict inequalities, but $t_4 \simeq t_2$, $t_3 \simeq t_1$. The latter region of time integration is thus of order ω_c^{-2}, whereas the former is over a strip in the t_2, t_3 plane of width ω_c^{-1} and length the range of $\hat{G}_0(t_2 t_3)$. To estimate the latter one has to recognize that in higher order $\hat{G}_0$ will be replaced by $\hat{G}$, whereupon it becomes clear that γ^{-1} is the relevant time scale. It thus follows that

$$\hat{\sigma}_{\text{overlap}} \approx \frac{\gamma}{\omega_c}\,\sigma_{\text{direct}}\,. \tag{A.3}$$

The same reduction, whenever an overlap occurs, can be seen to happen in an arbitrary order of perturbation theory.

For σ^{r} and σ^{a} one may argue as follows. As shown in Appendix A of Ref. [2], to preserve detailed balance, i.e. for the left and right hand sides of the kinetic equation to vanish separately in equilibrium, topologically similar graphs for $\hat{\sigma}$, σ^{r}, and σ^{a} have to be treated together. Thus, consistency requires that overlapping graphs for σ^{r} and σ^{a} also be dropped.

References

[1] H. A. Kramers, Physica *VII*, 284 (1940).
[2] K. S. Chow, D. A. Browne, and V. Ambegaokar, Phys. Rev. *B37*, 1624 (1988).
[3] K. S. Chow and V. Ambegaokar, Phys. Rev. *B38*, 11, 168 (1988).
[4] A. Schmid, J. Low Temp. Phys. *49*, 609 (1982).
[5] P. Pechukas, private communication, and to appear in Proc. NATO ASI "Lange - Scale Molecular Systems" (Manatea, Italy, Spring 1990 meeting).
[6] H. Spohn, Rev. Mod. Phys. *52*, 569 (1980).
[7] R. P. Feynman and F. L. Vernon, Ann. Phys. (N.Y.) *24*, 118 (1963).
[8] A. O. Caldeira and A. J. Leggett, Ann. Phys. (N.Y.) *149*, 374 (1983).
[9] L. V. Keldysh, Zh. Eksp. Teor. Fiz. *47*, 1515 (1964) [Sov. Phys. JETP *20*, 1018 (1965).]
[10] L. P. Kadanoff and G. Baym, Quantum Statistical Mechanics, W. A. Benjamin, New York, 1962.
[11] A. J. Leggett, Phys. Rev. *B30*, 1208 (1984).
[12] Perhaps this is an appropriate occasion to wonder why time is wasted writing the anachronism k_B, when it is so much more natural to express temperature in units of energy, and correspondingly to make entropy dimensionless. If Boltzmann needs to be honored, why not call 10^{-16} erg 1 Boltzmann?
[13] A. B. Migdal, Zh. Eksp. Teor. Fiz. *34*, 1438 (1958). [Sov. Phys. JETP *7*, 996 (1958).]
[14] H. Dekker, Phys. Rev *A 16*, 2116 (1977).
[15] A. O. Caldeira and A. J. Leggett Physica *121A*, 587 (1983).
[16] E. B. Davies, Commun. Math. Phys. *49*, 113 (1976).
[17] A. J. Redfield, IBM J. Res. Develop. *1*, 19 (1957).

Presented at the Discussion Meeting of the Deutsche Bunsen-Gesellschaft für Physikalische Chemie "Rate Processes in Dissipative Systems: 50 Years after Kramers" in Tutzing, September 10—13, 1990 E 7527

Traversal Time in Tunneling

Rolf Landauer

IBM Research Division, T. J. Watson Research Center, Yorktown Heights, New York 10598, USA

Quantum Mechanics / Transport Properties / Traversal Time / Tunneling

Traversal time in tunneling has become a somewhat controversial subject, and this note presents a personal perspective on some of these discussions. There is a widely invoked linear relationship yielding dwell time as a weighted average of traversal time and reflection time. I assert that it is totally without basis. Many authors follow wave packets through barriers. The results of such calculations are hard to correlate with experiment. Stevens has provided a wave packet approach which avoids some of the problems typically faced by such analyses; nevertheless its analytical details are questioned. The significance of complex traversal times, favored by some investigators, is questioned. The relative merit of various possible "clocks" in the analysis of traversal time is discussed, but without definitive conclusions.

1. Introduction

How long does a particle tunneling through a barrier interact with that barrier? This question was investigated by MacColl [1], and on many occasions since then. The work by Büttiker and Landauer [2] triggered a more intensive and systematic concern with the question. For a number of years following Ref. [2] the papers on the subject expressed a diversity of opinions, but generally some degree of overlap with Ref. [2]. More recently the spectrum of available views has widened, and experimental results have appeared [3]. This is not a settled and mature field, there are genuinely murky aspects and unsettled questions. Unfortunately, the highly visible controversies and the areas of real difficulty have little relation, in my opinion. An example of a real difficulty, which we will not take up in detail here, was cited in Ref. [4]. There it was pointed out that the approach of Ref. [2], applied to tunneling in the midst of a forbidden gap in a periodic potential, leads to anomalously

 © VCH Verlagsgesellschaft mbH, W-6940 Weinheim, 1991 0005-9021/91/0303-0404 $ 3.50+.25/0

large velocities. There are other physical situations which exhibit the same problem, e.g. frustrated internal reflection of electromagnetic waves.

This is not a systematic review; rather it is an informal commentary. It represents a personal viewpoint, and is bound to appear controversial to some readers. Systematic reviews have been provided by Hauge and Støvneng [5], Büttiker [6], Jonson [7], and by Leavens and Aers [8]. We refer the reader to these for a more extensive listing of the literature. Some disagreement with Ref. [5] has already been registered in response [9] to another publication by Støvneng and Hauge [10]. Other disagreements with Refs. [5] and [10] were recorded in Ref. [6].

Ref. [2] invoked a time-dependent, sinusoidally modulated, barrier potential with a very small modulation amplitude. If the modulation period is long compared to a presumed traversal time then the tunneling particle will see a barrier potential which is characteristic of the time of incidence for the particle. If the modulation frequency is increased sufficiently, the particle will no longer see a small part of the cycle, and we can expect a serious deviation from the adiabatic approximation valid at low modulation frequencies. This change in behavior can be interpreted as an approximate indication of what we have called the traversal time, τ_T. This traversal time is not the eigenvalue of a Hermitean operator, and is not necessarily a precisely measurable quantity. Indeed the traversal time of Ref. [2] may represent an average over a distribution of possible times [11, 12], rather than a single crisp value. In complete analogy to the traversal time for transmitted particles we can also evaluate a time, τ_R, for the barrier interaction of the reflected particles [13]. Our approach to τ_R (and τ_T) is intended to answer: How long have the reflected (transmitted) particles spent in the barrier? It is not necessarily an increase in particle delay caused by the insertion of the barrier, when measured far from the barrier (assuming, for the moment, that such measurements are possible). We return to that particular question in Sec. 6.

The literature on this subject frequently invokes a dwell time τ_D, defined in a variety of ways. (See Refs. [2] and [13], as well as the cited review papers for detailed discussion). The simplest approach is to invoke a stationary state with a time independent flux j incident on the barrier. The dwell time is taken to be

$$\tau_D = \frac{1}{j}\int_B |\psi^2|\,dx\,, \tag{1.1}$$

with the density of particles integrated over the extent B of the barrier. τ_D is, thus, the time required for the incident flux to supply the integrated particle density under the barrier. Consider a classical situation in which a particle stream is incident on a region which can reflect or transmit carriers, perhaps through a series of successive walls with holes, possibly oscillating or rotating in the directions perpendicular to the incident beam. In that case $j^{-1}\int_B \varrho\,dx$ with ϱ the linear particle density, clearly represents the average time spent in B.

In a remarkable variation on Eq. (1.1) Ref. [14] divides by the transmitted current, rather than the incident current, to obtain a so-called "traversal time".

2. Relation Between τ_D, τ_T and τ_R

A widely invoked relationship is

$$\tau_D = T\tau_T + R\tau_R\,, \tag{2.1}$$

with T and R representing, respectively, transmission and reflection probability. This is the most widely accepted of several viewpoints with which I take issue. It is a pivotal point in Ref. [5] leading to the conclusion there: "It is not clear that a generally valid answer [to the traversal time question] exists". But Eq. (2.1) is also advocated in Ref. [7], by Leavens and Aers [15, 16], and by Leavens [17]. Remarkably, Eq. (2.1) is treated by some of these investigators as one which is immediately and conspicuously valid, and needs no justification. I find this intensely puzzling. Of course, we can always perform the averaging operation indicated on the r.h.s. of Eq. (2.1). But it is then up to the proponents of Eq. (2.1) to demonstrate that this averaging does indeed yield the same quantity τ_D, defined originally in a totally different way, e.g. as in Eq. (1.1). Note that Eq. (1.1) and Eq. (2.1) together yield

$$\int_B |\psi^2|\,dx = jT\tau_T + jR\tau_R\,, \tag{2.2}$$

suggesting that the integrated density under the barrier consists of two contributions, one associated with transmitted particles and one associated with reflected particles. For a classical beam with reflection and transmission probabilities, as already invoked, that is sensible [18]. In quantum mechanics, however, we typically do not add particle densities, but add wave functions. Thus, we can ask what is the wave function which results in a beam going out to the right, with nothing going out to the left. This will be a wave function with particles incident from both sides of the barrier. We can also find the wave function which only has particles emerging from the barrier, all going to the left. These two wave functions, added with suitable coefficients, do yield our desired state, with particles incident from only one side. But even these two additive wave functions do not correspond to the situation that the proponents of Eq. (2.2) have in mind. As stated these two superposed wave functions will both have particles *incident from both sides.*

Büttiker [6], following a suggestion by Pippard [18], calculated the diminution of transmitted particles in a barrier which absorbs, i.e. has an imaginary component to the barrier potential. The resulting reduction turns out to be proportional to the dwell time, rather than the traversal time. The physical interpretation for this result: The absorption acts on *all* the particles in the barrier, they cannot – within the barrier – be separated into a transmitted component and a reflected component.

Leavens and Aers [15] do justify Eq. (2.1) in a supplemental way by a brief reference to Feynman and Hibbs [19],

and this is echoed by Jonson [7]. Ref. [15] asserts that Eq. (2.1)

> "... must hold because a particle incident on the barrier is either transmitted or reflected (these are exclusive rather than interfering alternatives in the language of Feynman and Hibbs.)"

Now, if we were to evaluate the average z-component of spin, after encounter of a barrier, that reasoning would be applicable. But if τ_D relates to the behavior in *the barrier*, why are the possibilities "... exclusive rather than interfering ..."?

3. Wave Packet Following

A number of investigators like to follow wave packets through barriers and we cite only two recent efforts [20, 21]. As stressed in Ref. [5], we can follow a peak, or else follow a center of gravity. Büttiker and I have, in the past, argued that incoming peaks do not, in any simple physical sense, turn into outgoing peaks. Similarly for the center of gravity.

Are electrons incident on a barrier necessarily in the form of a wave packet? That, of course, depends on the electron source. Electrons released by a shutter, externally controlled, and open for a specified time, are wave packets. Electrons coming out of a typical electron reservoir [22], analogous to a radiative black body, are not that clearly wave packets. Ken Stevens, in correspondence, has argued that the time between successive inelastic events in the reservoir acts much like a shutter. These inelastic events are, however, not externally timed. Wave packets require correlation between nearby energies. Way inside a reservoir one should be able to invoke $\varrho \sim \exp(-\beta H)$, which exhibits no such correlations. It is this view which allowed me to rederive the Nyquist theorem from the viewpoint which calculates conductance from the transmissive behavior of the sample [23]. On the other hand this is a difficult question, not necessarily settled by the brief allusion to $\exp(-\beta H)$. It is really the complete Hamiltonian, including coupling to phonons, that must be invoked in $\exp(-\beta H)$.. Furthermore $\exp(-\beta H)$ applies to a closed system, rather than to "way inside a reservoir."

The wave packet following papers, typically, provide a mathematically correct analysis. It is not illegal to discuss the trajectory of a peak before it reaches the barrier, and after it emerges. It is, however, up to the proponents of such a calculation to demonstrate that this is a physically interesting and significant quantity, and relatable to experiment. Let me indulge, here, in a somewhat exaggerated and playful analogy. A theory can, perhaps, be generated describing the length of time it takes to write the tunneling Hamiltonian on a blackboard. If done carefully, it may be a correct theory. But it is up the proponents of such a theory to demonstrate that this time is interesting. Furthermore, the proponents of this viewpoint have no basis arguing with the authors of our other citations, because their answer differs.

It is incumbent upon those who follow wave packet peaks, or wave packet centers of gravity, to tell us how to relate that to measurement. In that connection we stress the great distinction between photons and electrons. In the case of photons we can put a great many of them into the same incident photon state. We can tap off a small portion of the incident electromagnetic energy and make measurements on it, leaving most of the photons undisturbed to go through some interesting region. We can then do the same after the photons have emerged from the special region of interest. In the case of electrons, of course, we have at most one per quantum state. Timing measurements, on an external clock, are likely to be disruptive events [24]. It is possible, however, that experiments performed on many wave packets, prepared in an identical fashion, can circumvent this problem.

Several recent papers have applied Bohm's approach to quantum mechanics to the study of traversal time [17, 25, 26]. In this approach we follow an ensemble of particles, each following a classical path. The quantum mechanical phase of the wave function is given by the solution of the corresponding Hamilton-Jacobi equation, much as in the case of the WKB approximation. The wave function magnitude is also determined by the spread or convergence of nearby classical paths, again as in the WKB approximation. The classical path, however, is not that due to the actual potential, but due to a potential which supplements that by a "quantum potential", which in turn depends on the actual exact wave function. The classical nature of the motion (but not in the *original* potential) then makes the identification of time spent in a given region a trivial conceptual problem. Ref. [25] demonstrates that for a wave packet approaching a barrier, all the transmitted paths come from the front of the wave packet, all the reflected paths come from the tail. In my opinion that is not a physically meaningful result.

An interesting approach to wave packet following has been developed by Stevens [27 – 29]. It is a little less delicate than the other wave packet discussions because it does not require identification of a peak or center of gravity. Stevens's approach, however, has a more significant advantage. Many authors (for an example, see Sec. II B of Ref. [5]) discussing wave packet propagation, apply the stationary phase approximation uncritically, even when the dependence of transmitted amplitude on energy exhibits a strong exponential variation. Stevens's work escapes that problem, the exponential behavior is taken very explicitly into account. Stevens's first results [27] preceded Ref. [2], and are in agreement with it. Stevens's approach has been criticized by Jauho and Jonson [30], based on numerical calculations. I will not try to evaluate the validity of that criticism. I do discuss some other questions posed by Stevens's work in the Appendix. The critique of Ref. [27 29] has been relegated to an Appendix, because it is presented with less confidence than our other material. Even if my critique is valid, it is possible that a repaired analysis, along the lines originally presented by Stevens, would yield his original results.

4. Can Traversal Time be Complex?

A good many papers in this field advocate a complex traversal time, and we can cite only a sampling [11, 31 35]

(Note, however, that Ref. [35] was subsequently reinterpreted, somewhat, by one of its authors [36]). It is clear that there are a variety of reasonable analytical procedures which lead to a complex time, related to tunneling. We can, after all, take any two characteristics of the tunneling process with the dimension of time, and construct a complex number out of them. I totally agree, however, with Refs. [5] and [7] that the *duration of an event is a real number. It cannot be complex.* Has anyone seen a stop-watch with complex numbers on its dial? If traversal times are best characterized by a statistical distribution [11,12], that distribution may need many numbers for its total characterization. But combining two of these to form a complex number, does not yield a better traversal time. Of course, anyone can give a complex number the label *traversal time*; the authors of Ref.[2] do not possess a trademark for that expression. The real question relates to experiments as discussed in Ref. [3] and to the material in Sec. 5 and Sec. 6 concerned with clocks. How is the traversal time used?

5. Clocks

When and why is traversal time interesting? Basically, because we often oversimplify and treat a many-dimensional or many-particle tunneling problem as a one-dimensional problem. We need to know whether this cheating is reasonable; do the neglected degrees of freedom, coupled to the emphasized direction of motion, have time to adjust to the progress of the tunneling process? For example, for an electron tunneling through a barrier, between electrodes, do the image charges on the electrodes have time to adjust to the motion of the tunneling electron [37–39]? In a Josephson junction circuit under constant current bias, tunneling out of a metastable state, how much of a transmission line, connected across the junction, can respond while the tunneling occurs [3,40]? Such coupled degrees of freedom are not the only possible "clock" for the tunneling. We can also consider tunneling in an intentionally modulated barrier [41,42] much as in Ref. [2], though the proposed experiments of that type have not reached the developed state of those associated with coupled degrees of freedom, adjusting to the progress of tunneling. In any case, we emphasize that all these proposed or completed experiments have little relation to the following of a wave packet peak or center of gravity through a barrier.

The notion of comparing the speed of simultaneous processes, as a clock for one of them, is deeply imbedded in physics. One version [43] seems particularly close to Ref. [2], and served as a model for that. Consider an atom in a crystal lattice which can jump back and forth between two positions. Now apply an oscillatory small stress designed to favor one of the two positions. At frequencies slow compared to the jump rate the atom will, essentially, see a static stress and the thermal equilibrium distribution between the two sites will apply. At frequencies high compared to the jump rate the atom cannot respond to the oscillatory stress. At intermediate stress frequencies the atomic adjustment will lag the stress, and the jump is a source of energy dissipation.

Is the traversal time totally independent of the choice of clock? Very likely not. In the case of an image charge on an electrode surface, adjusting to the motion of an electron through a barrier, it is clear that the adjustment is most important when the electron is near one of the two electrodes. That is not necessarily characteristic of other clocks. That dependency, however, hardly inviolates the general utility of the concept. Consider, as an analogy, the uncertainty principle $\Delta E \Delta t \sim \hbar$. It really needs a great many footnotes to make it precise; that does not make it uninteresting or useless. For example, consider two similar wave packets following each other, but far apart. The applicable Δt is that of the separate packets.

The Larmor clock for tunneling was introduced by Rybachenko [44]. This approach was corrected by Büttiker [13], and widely explored, thereafter, particularly by Leavens and Aers and by Büttiker. In this case we have a field which acts on the spin of the tunneling particle only while it is in the barrier. The extent of the spin changes during barrier traversal are taken as a measure of the time spent in the barrier. Rybachenko originally assumed, incorrectly, that if the spin, the magnetic field, and the direction of tunneling were all perpendicular that only a spin precession would occur, and the precession then would be proportional to the time spent in the barrier. Büttiker realized that the component of the transmitted spin, in the direction of the field, would also change.

Like all the other candidates for a clock, the Larmor clock has some minor blemishes. I do not suggest that they invalidate the validity of the Larmor clock, but only that they deserve further attention. Let me list these blemishes; they are probably of varying seriousness. First of all a spatially variable magnetic field requires apparatus for its generation. Is it clear that this apparatus can be built in such a way as to interact with the tunneling particle only through its magnetic field? The apparatus required for a time-dependent potential is described in Ref. [45]. It is customary in conceptual arguments to invoke arbitrary fields which are physically possible, and the question raised here is, perhaps, unnecessarily demanding.

The magnetic field in the barrier has an affect not only on the spin, but also on the particle's spatial motion. This effect has been measured [46], and analyzed [47]. The recognition that the spin has not only a precession required modification of Rybachenko's original analysis; wouldn't it be equally appropriate to allow for the simultaneous spatial and spin effects? Possibly, as suggested by both C. R. Leavens and M. Büttiker in private communication, the differing dependence on powers of the magnetic field, H, in the spin and spatial effects, permit us to consider them separately. The reduction of transmission, due to the spatial effects is of order H^2. Spin precession is proportional to H, as is the spin polarization in the direction of H (for small H).

Finally, as pointed out by Jonson [7]. Once we go beyond Rybachenko's original erroneous limitation to spin precession, the interpretation is harder. Section D of Ref. [13] invokes an analogy with two level systems to yield a traversal time. Plausible, but not totally definitive.

There are many alternative clocks possible that have not yet been investigated in the literature. We can have a particle beam with a time-varying spin incident on a barrier which transmits all the incident spin directions equally. Does the emerging beam faithfully and instantaneously replicate the incident beam? This version of a clock suffers from some of the same blemishes as the wave packet following proposals. Or, instead of varying the incident spin, we can modulate the incident energy. Instead, Refs. [4, 48] invoke a beam with an oscillatory incident amplitude. Does the emergent beam faithfully and instantaneously replicate the incident beam? As the modulation period is reduced, by increasing the energy separation of the interfering arriving beams, where does the faithful replication cease? Clearly this approach to traversal time yields a result which depends on the energy dependence of the complex transmission coefficient. This approach also, of course, suffers some of the blemishes of wave packet following. The effects of the Lorentz force, due to a magnetic field limited to the barrier, providing a spatial deflection during barrier traversal, offers another possible clock.

6. Energy Dependent Transmission vs. Barrier Height Dependence

The approach of Ref. [2] invoked barrier height modulation; the traversal time depends on the barrier height dependence of the complex transmission coefficient. At incident energies way above a smooth barrier, where the WBK approximation applies, there is complete transmission. There, it is only the dependence of the phase of the transmission coefficient which counts, giving a result which agrees with the usual notion that $\partial\omega/\partial k$, with $\hbar k$ a local momentum, describes the particle's velocity. For incident energies below the barrier peak, and for opaque square barriers, or opaque barriers to which the WKB approximation applies, it is primarily the magnitude of the transmission coefficient that matters. The effective local crossing velocity is then $\partial\omega/\partial\kappa$ with $\hbar\kappa$ the magnitude of a local imaginary momentum. At intermediate values of energy, or for more complicated potentials, e.g. as in resonant tunnelling, both magnitude and phase may have a comparable barrier height dependence. A general result for the traversal time was proposed in Ref. [13]. In terms of the transmission amplitude $T^{1/2}e^{i\Delta\phi}$, where T is the transmission probability and $\Delta\phi$ is the phase change in transmission through the barrier, the traversal time can be expressed in the form [see Eq. (2.18c) of Ref. [13] and Eq. (6.1) of Ref. [16]].

$$\tau_T = \hbar[(\partial \ln T^{1/2}/\partial V)^2 + (\partial\Delta\phi/\partial V)^2]^{1/2} . \tag{6.1}$$

It is the sensitivity of the transmission probability as well as that of the phase, with respect to a small change in the barrier height V, that counts.

Clearly, Eq. (6.1) has the correct limiting behavior when only one of the two r.h.s. terms is present. It gives a traversal time which is real and measures the over-all dependence of the complex transmission coefficient on barrier height. Nevertheless, I agree with Jonson [7] that Eq. (6.1) while reasonable, is not the only possible quantity that meets the expectations that we have listed. If, instead of stressing barrier height dependence, we stress dependence on incident energy, as suggested in Refs. [4], and [48] then the equivalent of Eq. (6.1) (with the $\partial/\partial V$ replaced by $\partial/\partial E$) becomes a natural consequence of the reasoning provided in Refs. [4] and [48].

Earlier we pointed out that the traversal time of Ref. [2] does not necessarily correspond to the delay caused by the insertion of a barrier. Consider the case where we have a long region of uniform potential, with a barrier in its center, and apply Eq. (6.1). The r.h.s. of Eq. (6.1) has the form $(a^2 + b^2)^{1/2}$. For $b \gg a$ this is approximated by $b + a^2/2b$. If the region of uniform potential is made sufficiently long, then the $(\partial\Delta\phi/\partial V)$ term in Eq. (6.1) dominates. The effects of the barrier opacity manifested via $\partial \ln T^{1/2}/\partial V$ become unimportant, and do not give us an additive contribution to the total τ_T of Eq. (6.1). On the other hand any terms due to the barrier, related to wave function phase changes, do simply add to the $\partial\Delta\phi/\partial V$ contribution arising from propagation through the remaining long region. Thus, if we accept Eq. (6.1), it is natural that wave packet followers, concerned with the asymptotic behavior far from the barrier (e.g. Ref. [49]) do not see the results of Ref. [2], but see only a phase related term.

As already stated in Sec. 5, instead of using the dependence of the transmission coefficient on barrier height, we can invoke the energy dependence. If we modulate the potential along the whole axis, then, whether we modulate energy or potential is irrelevant. That, however, was not the intent of Ref. [2], which only invoked a potential change limited to the barrier. Leavens and Aers [16, 50], have emphasized the distinction between energy dependence and barrier height dependence. See, for example, Figs. 3 and 4 in Ref. [16]. This point is echoed by Büttiker [6]. These investigators are, of course, in a literal sense, correct. But the distinction does not really seem as serious as maintained in Refs. [6, 16, 50] which stress the behavior at very low incident energies. At low incident energies, with a long incident wavelength, the matching at the barrier boundaries becomes important; the energy dependence of the transmission coefficient is not dominated by the exponential decay in the barrier. As a result the energy dependence of the transmission coefficient diverges at low energies, whereas the derivative with respect to barrier height decreases monotonically as the incident energy is decreased. That, however, is the behavior for a given value of barrier length. For longer barriers the terms due to the exponential decay in the barrier become, relatively, more important. As a result, the energy range, in which the difference between energy dependence and barrier height dependence is important, becomes smaller.

Which is the more significant measure of traversal time? That resulting from the energy derivative of the transmission coefficient, or that resulting from the barrier height variation? The derivative with respect to incident energy results from arguments closely akin to following wave packets, and

shares some of those problems. It is more sturdy, however, allowing us to avoid the concern with peaks and centers of gravity. Changes in transmission, as we change energy, *are measurable*. In contrast, the barrier height derivative arises from the introduction of a physical "clock". Despite some preference for barrier height modulation, this is not necessarily the most settled question, and it remains a murky corner of the subject. We will discuss it, here, in some more detail, without necessarily settling it.

The variation of transmission coefficient with energy has the advantage that it is clearly defined. By contrast, varying the barrier height is an ambiguous operation, except perhaps for the rectangular barrier. In that case, with a uniform potential in the barrier, the obvious interpretation is to invoke a simple modulation of the barrier height. In the case of a smoothly varying $V(x)$, however, it is not equally clear what modulation $\delta V(x)$ should be chosen. Note, incidentally, that some support for the choice of a δV independent of x, in the region of interest, is provided by the case of a periodic potential. In that case, within an allowed band, $\partial\omega/\partial k$, with k the Floquet wave number, is well established as a physical velocity. We get that result (but complicated by boundary matching effects) if we take δV independent of x. A non-uniform $\delta V(x)$, on the other hand, will produce interband transitions which are hard to relate to the expected result.

The distinction between energy variation and potential height variation is, of course, not all that great. A variation in the barrier height can always be represented (in the small modulation linear approximation limit) as a sum over spatially localized potential oscillations. At each location x, along the barrier, we have a potential modulation limited to the immediate vicinity of x. The overall effect of a smooth potential variation, $\delta V(x)$, all along the barrier, is the sum of such localized effects. At each localized potential oscillation, with an unperturbed wave function at energy E_0, we generate "sidebands" at $E_0 \pm \hbar\omega$. These, then, propagate away from their point of origin according to the unmodulated potential. In the case of a time modulated incident wave function, the terms at different energies are already present in the incident wave; in the modulated barrier case they are generated all along the barrier. In many cases, that will not result in a serious qualitative distinction. In the case of a modulated incident wave, of course, any energy sensitivity in the matching procedure at the turning point will contribute. That is the reason for the distinction between barrier height dependence and energy dependence stressed in Refs. [6, 16] and [50], and already discussed.

I am indebted to stimulating interaction with G. Aers, M. Jonson, and K. W. H. Stevens, even if we did not reach complete agreement. The interactions with M. Büttiker and C. R. Leavens have been totally critical to the development of my views, but once again do not reflect a complete overlap in taste.

Appendix

Stevens presents several related analyses in Refs. [27 - 29], and we will exemplify our difficulties, and not discuss all of Stevens's cases separately. We will use Ref. [28] as the basis for our discussion. In Ref. [28], for example, one of Stevens's cases deals with a pulse which has just arrived at a barrier. We quote from Ref. [28]:

> Then just inside the barrier we assume that ψ has been zero up until $t = 0$ and now it begins to oscillate with a definite frequency ω_0. That is, we require a solution of our equation which describes propagation in the positive x-direction (which is in the barrier) and satisfies
>
> $$\psi(0,t) = \begin{cases} 0 & \text{for } t < 0 \\ e^{-i\omega_0 t} & \text{for } t > 0. \end{cases}$$
>
> The contour integral
>
> $$\frac{1}{2\pi i}\int \frac{e^{i\omega t}}{(\omega - \omega_0)} d\omega$$
>
> taken along the line $\omega = +\infty + i\varepsilon$ to $-\infty + i\varepsilon$ satisfies the initial condition, ...

Stevens then goes on to take a superposition of solutions which at the left end of the barrier correspond to the above contour integral. Note, however, that if the incident wave from the far left, just to the left of the barrier, behaves as described in the above equations for $\psi(0,t)$, then the combination of incident and reflected waves will differ. And it is this combination which has to be matched just to the right of the barrier; it is not just the incident wave which needs to be matched. Stevens, in correspondence, indicates that he is really analyzing the case where the combination of incident and reflected wave vanishes for $t < 0$ and oscillates as $e^{i\omega_0 t}$ for $t > 0$. In that case his analysis is correct, but its relationship to the rest of the papers discussed here becomes more obscure.

In a subsequent example, Stevens has a barrier to the right of $x = 0$, extending to $x = \infty$. As initial condition he assumes that at x_0, where $x_0 < 0$, the disturbance is zero until $t = 0$, when it becomes $e^{-i\omega_0 t}$. Now, Stevens finds a superposition of plane waves, coming from the left, which satisfies this requirement. Let us denote this wave function by $\int A(k)\, e^{i(kx-\omega t)}$. In the presence of the barrier we will have a set of eigenstates, $\psi_k(x)$, which include reflected waves and have an evanescent behavior in the barrier. Let us choose the normalization of $\psi_k(x)$ such that the incident portion of the wave, coming from the left, is $e^{i(kx-\omega t)}$. Now Stevens chooses

$$\psi(x,t) = \int A(k)\psi_k(x) e^{-i\omega t} \tag{A.1}$$

as his total solution, which clearly obeys the Schrödinger equation, along the whole x-axis. But, unfortunately, it is not clear how the total wave function, including incident plus reflected waves, behaves at x_0 with time. Is it clear that Eq. (A.1) gives us a ψ which for $t \leq 0$ vanishes in the barrier and has a vanishing reflected wave contribution?

In a third case Stevens assumes that at $t = 0$ the wave function is given by

$$\psi(x,0) = \begin{cases} \exp(ix\omega_0^{1/2}) & \text{for } x \leq x_0 < 0 \\ 0 & \text{for } x > x_0. \end{cases} \tag{A.2}$$

where x_0 is the left of the barrier. Eq. (A.2) invokes Stevens's notation and units, where the incident wave number is expressed in terms of the square root of the incident energy. Then, once again, Stevens chooses a superposition of exact solutions (in the presence of the barrier) *whose incident wave portions*, considered by themselves at $t = 0$, add up to give (A.2). But does the total superposition of the correct eigenstates also add up to yield (A.2)? Why should they? To continue in a little more detail $\psi(x,0)$ can be represented as a sum over a set of Hamiltonian eigenstates. That holds whether we take $\psi(x,0)$ as in Eq. (A.2), or whether we take $\psi(x,0)$ to be $\exp(ix\omega_0^{1/2})$ only between two points x_1 and x_2, and vanishing outside of that interval. (We may want to take this latter choice, suggested in correspondence by Stevens, to avoid wave functions ex-

tending to infinity). If the basis functions are $\phi_k(x)$ then the relative weight of ϕ_k in the expansion of ψ is given by $\int \phi_k^* \psi(x,0)\,dx$. First of all, let ϕ_k be the plane wave states over the whole x-axis. That leads to the results given by Stevens on pg. 3651 of Ref. [28]. Now consider a potential which is infinite for $x > 0$, then the eigenstates will be

$$u_k = 2i \sin kx = e^{ikx} - e^{-ikx}. \tag{A.3}$$

Now expand $\psi(x,0)$ in terms of the u_k. Stevens asserts that the expansion in terms of the u_k is trivially given by the expansion in terms of the ϕ_k. That requires

$$\int_{-\infty}^{0} \phi_k^* \psi(x,0)\,dx = \int_{-\infty}^{\infty} u_k^* \psi(x,0)\,dx. \tag{A.4}$$

(I ignore possible normalization questions, arising from the fact that the u_k are nonvanishing only in the left half-axis. Any correction due to such questions will be manifested by a factor independent of the value of k). The two integrals in Eq. (A.4) can only be equal if the reflected wave, given by the final r.h.s. term of Eq. (A.3), makes no contribution to the r.h.s. integral in Eq. (A.4). And that is not in agreement with the results of elementary integration, for almost all k. Note that the ratio between the two sides of Eq. (A.4) depends on k, and cannot be offset by any possibly neglected normalization questions. Thus Stevens is using incorrect expansion coefficients, multiplying correct eigenfunctions of the Schrödinger equation.

In correspondence Stevens has countered my objections to his "third case", discussed in the preceding paragraph. Stevens asserts that the contribution of the e^{-ikx} terms in Eq. (A.3), after using his weighting, derived from the l.h.s. of Eq. (A.4), and integrating over all k, vanishes at $t = 0$, and for $x < 0$. Therefore, the initial conditions are satisfied, on the left hand side of the x-axis. And, clearly he has a solution of the Schrödinger equation.

References

[1] L. A. MacColl, Phys. Rev. *40*, 621 (1932).
[2] M. Büttiker and R. Landauer, Phys. Rev. Lett. *49*, 1739 (1982).
[3] R. Landauer, Nature *341*, 567 (1989).
[4] M. Büttiker and R. Landauer, Phys. Scr. *32*, 429 (1985).
[5] E. H. Hauge and J. A. Støvneng, Rev. Mod. Phys. *61*, 917 (1989).
[6] M. Büttiker, in: Electronic Properties of Multilayers and Low Dimensional Semiconductors, p. 297, eds. J. M. Chamberlain, L. Eaves, and J. C. Portal, Plenum Press, New York 1990.
[7] M. Jonson, in: Quantum Transport in Semiconductors, eds. C. Jacoboni and D. K. Ferry, Plenum Press, New York, in press.
[8] C. R. Leavens and G. C. Aers, in: Basic Concepts and Applications of Scanning Tunneling Microscopy and Related Techniques, ed. R. J. Behm, Kluwer Academic Publisher, Dordrecht in press.
[9] M. Büttiker and R. Landauer, J. Stat. Phys. *58*, 371 (1990).
[10] J. A. Støvneng and E. H. Hauge, J. Stat. Phys. *57*, 841 (1989).
[11] C. R. Leavens, Solid State Commun. *68*, 13 (1988).
[12] H. A. Fertig, Phys. Rev. Lett. *65*, 2321 (1990).
[13] M. Büttiker, Phys. Rev. *B27*, 6178 (1983).
[14] M. A. de Moura and D. F. de Albuquerque, Solid State Commun. *74*, 353 (1990).
[15] C. R. Leavens and G. C. Aers, Phys. Rev. *B40*, 5387 (1989).
[16] C. R. Leavens and G. C. Aers, Solid State Commun. *63*, 1101 (1987).
[17] C. R. Leavens, Solid State Commun. *74*, 923 (1990).
[18] R. Landauer and M. Büttiker, Phys. Rev. *B36*, 6255 (1987).
[19] R. P. Feynman and A. R. Hibbs, Quantum Mechanics and Path Integrals, McGraw-Hill, New York 1965.
[20] A. P. Jauho and M. Jonson, J. Phys.: Condens. Matter *1*, 9027 (1989).
[21] H. DeRaedt, N. Garcia, and J. Huyghebaert, Solid State Commun. *76*, 847 (1990).
[22] R. Landauer in: Analogies in Optics and Micro Electronics, p. 243, eds. W. van Haeringen and D. Lenstra, Kluwer Academic, The Netherlands 1990.
[23] R. Landauer, Physica *D 38*, 226 (1989).
[24] A. Peres, Am. J. Phys. *48*, 552 (1980).
[25] C. R. Leavens, Solid State Commun. *76*, 253 (1990).
[26] T. P. Spiller, T. D. Clark, R. J. Prance, and H. Prance, Europhys. Lett. *12*, 1 (1990).
[27] K. W. H. Stevens, Eur. J. Phys. *1*, 98 (1980).
[28] K. W. H. Stevens, J. Phys. C: Solid State Phys. *16*, 3649 (1983).
[29] C. L. Foden, K. W. H. Stevens, J. Phys. Condens. Matter *2*, 5179 (1990).
[30] A. P. Jauho and M. Jonson, Superlattices Microstruct. *6*, 303 (1989).
[31] D. Sokolovski, L. M. Baskin, Phys. Rev. A *36*, 4604 (1987).
[32] D. Sokolovski, P. Hänggi, Europhys. Lett. *7*, 7 (1988).
[33] C. R. Leavens and G. C. Aers, Solid State Commun. *63*, 1107 (1987).
[34] C. R. Leavens and G. C. Aers, Solid State Commun. *67*, 1135 (1988).
[35] E. Pollak and W. H. Miller, Phys. Rev. Lett. *53*, 115 (1984).
[36] E. Pollak, J. Chem. Phys. *83*, 1111 (1985).
[37] M. Jonson, Solid State Commun. *33*, 743 (1980).
[38] P. Guéret, et al. Appl. Phys. Lett. *53*, 1617 (1988).
[39] P. Guéret, et al. Solid State Commun. *68*, 977 (1988).
[40] D. Esteve, J. M. Martinis, C. Urbina, E. Turlot, M. H. Devoret, P. Grabert, and S. Linkwitz, Phys. Scr. *T29*, 121 (1989).
[41] H. Hübner, Optik *64*, 113 (1983).
[42] A. A. Lucas, P. H. Cutler, T. E. Feuchtwang, T. T. Tsong, T. E. Sullivan, Y. Yuk, H. Nguyen, and P. J. Silverman, J. Vac. Sci. Technol. *A6*, 461 (1988).
[43] C. M. Zener, Elasticity and Anelasticity of Metals, University of Chicago Press, 1948.
[44] V. F. Rybachenko, Yad. Fiz. *5*, 895 (1966) [Sov. J. Nucl. Phys. *5*, 635 (1967)].
[45] R. Landauer, in: Der Informationsbegriff in Technik und Wissenschaft, p. 139, eds. O. G. Folberth and C. Hackl, R. Oldenbourg, München 1986.
[46] P. Guéret, A. Baratoff, and E. Marclay, Europhys. Lett. *3*, 367 (1987).
[47] L. Eaves, K. W. H. Stevens, and F. W. Sheard, in: The Physics and Fabrication of Microstructures and Microdevices, p. 343, eds. M. J. Kelly and C. Weisbuch, Springer, Heidelberg 1986.
[48] M. Büttiker and R. Landauer, IBM J. Res. Develop. *30*, 451 (1986).
[49] N. Teranishi, A. M. Kriman, and D. K, Ferry, Superlattices and Microstructures, *3*, 509 (1987).
[50] C. R. Leavens and G. C. Aers, J. Vac. Sci. Techn. *A6*, 305 (1988).

Presented at the Discussion Meeting of the Deutsche Bunsen-Gesellschaft für Physikalische Chemie "Rate Processes in Dissipative Systems. 50 Years after Kramers" in Tutzing, September 10–13, 1990 E 7516

The Role of Barrier Fluctuations in the Tunneling Problem

Yu. Kagan

I. V. Kurchatov Institute of Atomic Energy, 123182 Moscow, USSR

Barrier Fluctuations / Quantum Mechanics / Tunneling

Interaction of a tunneling particle with fluctuations of the barrier induced by phonon or electron excitations is analyzed. Special role of nonadiabatic excitations with the energy smaller than the reciprocal time a particle spends under the barrier is discussed. In an insulator the interaction with barrier fluctuations can play a dominant role leading to qualitatively alteration of the pattern of the quantum diffusion. At that, the increase of the tunneling transition amplitude (coherent bandwidth) instead of the polaronic narrowing and significant change of the temperature dependence of incoherent tunneling motion take place. Analysis of recent experimental results on the quantum diffusion of muonium in KCl crystal revealing the decisive role of the barrier fluctuations is given. – The infrared divergence accompanying the rescattering of the electron-hole excitations near the Fermi-surface causes the increase of the interaction with the barrier fluctuations in a metal. Rigorous analysis for a two-well system with a completely arbitrary interaction of the electrons with a tunneling particle is carried out. It shows that there are no parameter values for which the interaction with barrier fluctuations overweight the intrawell interaction though the inelastic transition rate sharply enhances. The general problem of the validity of substitution of a phonon heat bath for an electron one is discussed.

1. Introduction

In an analysis of the tunneling of particles in a two-well potential or in a regular crystal, there are typically two mechanisms for interaction with excitations of the medium. The first is intrawell interaction which leads to a polaron effect and which predetermines disruption of the coherent coupling between wells or dynamic destruction of a band. At higher temperatures this mechanism leads to incoherent transitions with "shaking" of the polaron "cloud". The intrawell interaction does not depend on the overlap integral.

The second mechanism involves fluctuations of the barrier resulting from the interaction with electron or phonon excitations. The majority of works treating the tunneling motion of particles in the medium do not take into consideration this mechanism. However, there are no grounds for that in the general case. As long as in the early work [1] it was shown that the interaction with the barrier fluctuations can qualitatively change the pattern of quantum diffusion in the medium. First of all, this is due to the so called effect of fluctuational barrier preparation. In an insulator, with taking into account the interaction with phonons, an effective reduction of the barrier for extreme path of the particle under-barrier motion corresponds to this effect. As a result, there arises a considerable increase of the tunneling transition amplitude and, instead of the polaron narrowing, the interaction with phonons may cause an increase in the coherent bandwidth. Simultaneously, the temperature dependence of the quantum diffusion coefficient is also changed, including the region of exponential increase of $D(T)$ with rising T.

Below we shall follow a vivid manifestation of the role played by the interaction with the barrier fluctuations in the insulator, by using experiments on the quantum diffusion of muonium in KCl crystal [2], [3] as example.

In considering the barrier fluctuations relevant to the interaction with the conduction electrons in a metal, we face a specific situation. As it has been established earlier [4], the tunneling particle is actually scattered only by nonadiabatic electron excitations lying within the energy interval with the width ω_0 in the vicinity of the Fermi level (ω_0 being the inverse time of the particle passage under the barrier). The small phase volume of these excitations results in a limited scale of the barrier fluctuations. If we neglect the electron rescattering by the particle, the probability W_B of the tunneling transition induced by the barrier fluctuations at low $T \ll \omega_0$ is small over the parameter

$$\left[\frac{(T, \xi)_{\max}}{\omega_0}\right]^2 \ll 1 \tag{1.1}$$

as compared with the transition probability in conservation of only the intrawell interaction. Here ξ is the asymmetry of the neighboring wells. (It is assumed that $\xi \ll \omega_0$).

However, in taking into account the rescattering of electrons, the well-known infrared divergence sharply enhances W_B. This circumstance was originally pointed out by Kondo [5]. Zawadowski et al. [6 – 8] undertook a detailed analysis of this problem, using a multicomponent renormalization-group method for the partition function of the system. They found a significant increase in the role played by this mechanism during tunneling in a metal. However the question of whether the second mechanism can become more important than the first one in an actual tunneling problem remained open.

In addition to everything else, this problem has one important aspect: The overwhelming majority of the studies of the tunneling of a heavy particle in a metal have used the concept that the electronic and phonon thermal baths are equivalent and phonon bath has been used in the calculations (see, e.g., the review [9]). In the case of phonons, however, there is no infrared enhancement during the rescattering of excitations, so the inequality (1.1) makes it possible

 © VCH Verlagsgesellschaft mbH, W-6940 Weinheim, 1991 0005-9021/91/0303-0411 $ 3.50+.25/0

to ignore fluctuations of the barrier. In terms of the widely used spin Hamiltonian, the implication here is that there is no term representing an interaction with excitations of the medium which is proportional to the matrix σ_x. The question of the role of the inelastic processes associated with fluctuations of the barrier is thus related to the general questions of whether it is valid to replace the electron bath by the phonon bath.

This paper contains the results [10] of the direct solution of the kinetic problem while incorporating the interaction with barrier fluctuations, for a completely arbitrary interaction of the electrons with the tunneling particle. It turns out to be possible to find the explicit relationship between the renormalized amplitude for a tunneling transition and the probability for hopping between wells, on the one hand, and the scattering phase shifts, on the other. These phase shifts are actual physical parameters which characterize the interaction. The primary of the analysis below is the rigorous proof that there are no parameter values for which the second mechanism outweighs the first. The proof is presented for a two-well Hamiltonian of a general type.

The approach used in this paper is based on a direct determination of the overlap integral of the many-particle intrawell wave functions. This method allows one to take into consideration the barrier fluctuations in a natural way and to single out coherent and incoherent tunneling independently. This makes it possible to proceed simply from the results for the two-well system to a crystal in order to solve the quantum diffusion problem.

2. Adiabatic Problem

In analyzing the tunneling motion of heavy particles in the crystal, only the under-barrier motion between two equivalent positions in the nearest unit cells practically always turns out to be significant. In this case, the problem of particle motion in the two-well potential at an arbitrary interaction with excitations of the medium is isomorphic for the description of the elementary act. The solution of the two-well problem is sufficient both for the description of the coherent motion of particles in the crystal and for the incoherent motion, when the phase memory is lost at each translational step.

Let's consider the tunneling between two wells, the lower levels of which are separated by an amount ξ, and assume that the tunneling amplitude Δ_0, temperature T and ξ are small in comparison with the distance ω between energy levels in an individual well

$$\Delta_0, \xi, T \ll \omega . \tag{2.1}$$

At the same time, the ratio between Δ_0, ξ and T can be arbitrary. The condition (2.1) allows us to ignore activation processes and to assume that the transitions occurs only through the lowest level.

Two time scale are characteristic of the problem. the lifetime of the particle in a well τ and the time ω_0^{-1} spent by the particle under the barrier. For a common non-exotic potential relief in a crystal the frequencies ω_0 and ω are close by the magnitude and further we will not distinguish between them.

Taking into account (2.1) and the evident relation $\tau^{-1} > \Delta_0$, one immediately obtains the inequality

$$\omega_0 \tau \gg 1 \tag{2.2}$$

During the long lifetime τ a many-particle wave function $\psi_\alpha^{(i)}(r, R)$ in a well i, incorporating all virtual excitations with $\varepsilon > \tau^{-1}$, is formed. The solution of the adiabatic problem has a crucial meaning for the structure of this wa function and it's evolution in a process of tunneling. As was shown in Ref. [4] in this case the correct results could be obtained only if one takes into consideration the intrawell virtual excitations of a particle. The analysis leads to a natural distinction between "fast" and "slow" excitations of the medium. The fast excitations with frequencies $\varepsilon > \omega_0$ adjust adiabatically to the position of the moving particle both in the well and under the barrier. They form the screening and thereby, give rise to a renormalization of the potential relief, $U(R)$, and to a slight extent the particle mass. On the contrary, the slow excitations with $\varepsilon < \omega_0$ do not follow the particle and the modified wave function of the medium which corresponds to these excitations turns out to be oriented toward the center of the potential well. These excitations have the decisive effect on the tunneling. The interaction with them predetermines the appearance of the polaron effect and due to (2.1) the entire diffusion kinetics at low temperatures. In forming this nonadiabatic part of the wave function, the energy interval of slow excitations turns out to be truncated not only at the top but also at the bottom on the scale of τ^{-1}. This is connected with the finiteness of the particle lifetime in an individual well. In virtue of this, the admixture of states with $\varepsilon < \tau^{-1}$ fails to be formed.

In a metal the spectrum of electronic excitations extends up to the energy ε_0 which, in the order of magnitude, is equal to the Fermi energy ε_F or the bandwidth. The following inequality is always characteristic of the heavy particle tunneling

$$\omega_0 \ll \varepsilon_0 \tag{2.3}$$

This means that the small phase volume corresponds to the nonadibatic electronic excitations. In spite of the above, the part played by these excitations turns out to be very significant in virtue of the well-known infrared divergence specified by the electron-hole pairs with the energy close to zero (see, e.g., Ref. [11, 12]).

During interaction with phonon a different pattern takes place. If the mass of a tunneling particle is relatively small, then $\omega_0 > \omega_0$, where ω_0 is now of the order of the Debye temperature Θ_D. In this case the whole phonon spectrum turns out to be nonadiabatic. In the opposite limiting case of a heavy particle tunneling in a light matrix, the (τ^{-1}, ω_0) interval turns out to be nonadiabatic, as in the case of electron. However, in actual crystals the density of phonon ex-

citations goes to 0 as $\varepsilon \to 0$, which removes the infrared divergence and the phase volume smallness is not compensated for.

In a sense, the particle and adiabatic excitations which have adjusted to it form a real physical entity the under-barrier motion of which as a whole one has to study. Therefore, in general, the problem reduces to one of studing a Hamiltonian which describes the motion of such a "particle" in a renormalized potential $U(R)$ with a slightly renormalized mass M. The interaction with the medium contains only slow excitations $V(r,R)$ with energies $\varepsilon < \omega_0$.

In the renormalized potential relief we single out nondecaying individual well $U^{(i)}(R)$, extending its edges in the usual way. If the Hamiltonian of a particle in such a well is denoted by $H_p^{(i)}$, the genral Hamiltonian of the one-well problem can be written in the form

$$H^{(i)} = H_p^{(i)} + H_{ex}(r) + V(r,R),\ H_p^{(i)} = -\frac{\nabla_R^2}{2M} + U^{(i)}(R), \qquad (2.4)$$

where $H_{ex}(r)$ is the Hamiltonian of the excitation subsystem. Let us use $H'(R)$ to denote the difference between the true potential relief and the chosen non-decaying well $U^{(i)}(R)$. Then, for the matrix element of the transition from one well to the other we have

$$M_{\alpha\beta} = \langle \psi_\alpha^{(1)}(r,R) | H'(R) | \psi_\beta^{(2)}(r,R) \rangle, \qquad (2.5)$$

where $\psi_\alpha^{(i)}(r,R)$ are the eigenfunctions of the Hamiltonian (2.4).

Under the condition (2.1) the knowledge of the matrix elements (2.5), both nondiagonal and diagonal in the state of the medium α, fully determines the problem of tunneling with interaction with the medium. This also applies to the problem of a coherent transition with the formation of band ($\alpha = \beta$), if we are dealing with a crystal.

The fact that only the interaction with slow excitations appears in (2.4) predetermines the possibility of seeking the eigenstates of this Hamiltonian in the frame of reciprocal adiabatic approximation

$$\psi_\alpha^{(i)}(r,R) = \varphi_0^{(i)}(R,r)\Phi_\alpha^{(i)}(r), \qquad (2.6)$$

where the wave functions $\varphi_0^{(i)}$ and $\Phi_\alpha^{(i)}$ are solution of the equations

$$\begin{aligned} &[H_p^{(i)} + V(r,R)]\varphi_0^{(i)}(R,r) = \varepsilon_0^{(i)}(r)\varphi_0^{(i)}(R,r) \\ &[H_{ex}^{(i)} + \varepsilon_0^{(i)}(r)]\Phi_\alpha^{(i)}(r) = E_\alpha^{(i)}\Phi_\alpha^{(i)}(r). \end{aligned} \qquad (2.7)$$

Now the particle is moving in the distorted potential relief, created by slow excitations.

The scale of displacement of the particle located at the lowest level in the well from the equilibrium position R_i is small as compared with the inter atomic distance "a". Therefore,

$$\begin{aligned} \varepsilon_0^{(i)}(r) &= \frac{\omega^{(i)}}{2} + \langle \varphi_0^{(i)}(R,r) | V(r,R) | \varphi_0^{(i)}(R,r) \rangle \\ &\approx \frac{\omega^{(i)}}{2} + V(r,R_i). \end{aligned} \qquad (2.8)$$

It follows from (2.8) and the second equation in (2.7) that in shaping the wave function $\Phi_\alpha^{(i)}$ the excitations effectively see the particle positioned at the center of the potential well:

$$\Phi_\alpha^{(i)}(r) = \Phi_\alpha(r,R_i).$$

Substituting (2.6) into (2.5) we find

$$\begin{aligned} &M_{\alpha\beta} = \langle \Phi_\alpha^{(1)}(r) | J(r) | \Phi_\beta^{(2)}(r) \rangle; \\ &J(r) = \langle \varphi_0^{(1)}(R,r) | H'(R) | \varphi_0^{(2)}(R,r) \rangle. \end{aligned} \qquad (2.9)$$

The expression for $J(r)$ reflects the dependence of the transition tunneling amplitude on the distortions of the barrier which result from the interaction with fluctuations in the slow excitations subsystem. Interestingly, the situation which arises is precisely the opposite of the conventional adiabatic case; during the time it takes the particle to pass through the barrier the electron or phonon fluctuations remain static.

The expression for $J(r)$ can be written in the form

$$J(r) = \Delta_0 e^{-B(r)}, \qquad (2.10)$$

where $B(r)$ is given by

$$B = \int [2M(U+V)]^{1/2} dR - \int [2MU]^{1/2} dR.$$

Noting that the scale of the changes in the barrier are small in comparison with its height, one can expand this expression

$$B = \int \frac{dR}{\vartheta(R)} V(r,R) \approx \frac{V(r,R_0)}{\omega_0}. \qquad (2.11)$$

Here $\vartheta(R)$ is the velocity of the particle in the upturn barrier Substituting (2.10) into (2.9), we finally find

$$M_{\alpha\beta} = \Delta_0 \langle \Phi_\alpha^{(1)}(r) | e^{-B(r)} | \Phi_\beta^{(2)}(r) \rangle. \qquad (2.12)$$

The structure of expressions (2.9), (2.10), (2.12) reflects the fact that the effective reduction of the barrier due to the fluctuations corresponds to the optimal path of tunneling. This effect called "fluctuational barrier preparation" was considered for the first in Ref. [1] for the tunneling problem in interaction with phonons.

In the case of interaction with electrons the small phase volume of the energy interval of nonadiabatic excitations, which determines B (2.11), results in the estimate $B \lesssim 1$. In interaction with phonons, if $\omega_0 > \Theta_D$, there are no principal limitations on the magnitude of the B value.

The matrix element (2.12) is defined in terms of wave functions which are eigenfunctions of different Hamiltonians. As always in such situations, it is thus convenient to introduce a unitary operator A, which relates the representations of the functions $\Phi_\beta^{(1)}$ and $\Phi_\beta^{(2)}$. We make use of the circumstance that the translational symmetry of the problem

makes it possible to retain the same classification at the displacement of a particle. We can then write

$$\Phi_\beta^{(2)} = \Lambda \Phi_\beta^{(1)} \equiv \Lambda|\beta\rangle; \tag{2.13}$$

and, correspondingly,

$$M_{\alpha\beta} = \Delta_0 \langle\alpha|e^{-B}\Lambda|\beta\rangle. \tag{2.14}$$

Here the α and β subscripts belong to the eigenstates which are the solutions of the second equation in (2.7) for i = 1 with allowance for (2.8), or to the eigenfunctions of the Hamiltonian

$$H_1 = H_{ex} + V(\hat{r}, \hat{R}_1).$$

The amplitude Δ_C of the coherent transition between the wells, which is responsible for the formation of a band in a crystal, is determined by the relation

$$\Delta_C = \Delta_0 \langle\alpha|e^{-B}\Lambda|\alpha\rangle = \mathrm{Sp}\{\varrho e^{-B}\Lambda\}, \tag{2.15}$$

where ϱ is the equilibrium density matrix of the excitations. After the dynamic destruction of the coherent band with increasing temperature [13, 14], the tunneling motion of the particle acquires an incoherent character. In this case the site representation is adequate for the problem and the probability of a transition to the next well can be represented in the following form

$$W_{12} = \Delta_0^2 \int_{-\infty}^{\infty} dt e^{i\xi t} \mathrm{Sp}\{\varrho \Lambda^+(t) e^{-B(t)} e^{-B(0)} \Lambda(0)\}. \tag{2.16}$$

3. Electron Polaron Operator

To study the role of the barrier fluctuations, we begin from the case of interaction with electrons.

The Hamiltonian of the system for the case in which the particle is in well 2 can be written in the form

$$H_2 = H_1 + \Delta V = \sum_{k\sigma} \varepsilon_k a_{k\sigma}^+ a_{k\sigma}^+ \sum_{kk'\sigma} \Delta V_{kk'} a_{k\sigma}^+ a_{k'\sigma};$$
$$\Delta V_{kk'} = V_{kk'}(1 - \exp(i(k-k')(R_1 - R_2))). \tag{3.1}$$

We seek the wave function $\Phi_\beta^{(2)}$ in (2.13) as an expansion in states of the Hamiltonian H_1. $\Phi_\beta^{(2)}$ differs from $\Phi_\beta^{(1)}$ in an arbitrary number of electron-hole pairs. We make use of the fact that the amplitude for the creation of two pairs breaks up into a product of amplitudes with a macroscopic accuracy. The operator Λ can then be written as

$$\Lambda = S \exp\left\{-\sum_{ss'}^{a} C_{ss} a_s^+ a_s\right\} = S \prod_{ss'}^{a} (1 - C_{ss'} a_s^+ a_s), \tag{3.2}$$

where S is the normalization factor; $s \equiv k, \sigma$. The index s in the product (3.2) specifies exclusively vacant single-particle states in $|\alpha\rangle$, while s' specifies exclusively occupied states (the α on the summation and product signs is intended to flag this circumstance). It is this circumstance which allows us to go to the latter equality in (3.2), since the spaces $\{s\}$ and $\{s'\}$ do not overlap, and all the terms in the exponential function commute with each other.

We substitute expansion (3.2) into the Schrödinger equation

$$[H_1 + \Delta V]\Phi_\beta^{(2)} = E_\beta \Phi_\beta^{(2)},$$
$$[\Lambda^{-1}(H_1 + \Delta V)\Lambda]_{\beta\beta'} = E_\beta \delta_{\beta\beta'}. \tag{3.3}$$

Since the effect of the operator Λ (and Λ^{-1}) reduces to one of simply creating independent electron-hole pairs, there is no difficulty in finding an explicit form of Eq. (3.3). A solution can be written in the form

$$E_\alpha = E_\alpha^0 - \sum_{ss'} \Delta V_{ss'} C_{ss'}, \tag{3.4}$$

$$C_{ss'} = \frac{1}{\varepsilon_s - \varepsilon_{s'}} \cdot \left\{\Delta V_{ss'} - \sum_p (1 - n_p)\Delta V_{sp} \cdot C_{ps'} + \sum_{p'} n_{p'} \Delta V_{p's'} \cdot C_{sp'} - \sum_{pp'} (1 - n_p) n_{p'} \Delta V_{pp'} \cdot C_{sp} C_{ps'}\right\}. \tag{3.5}$$

It can be concluded from the form of (3.2) that the coefficients $C_{ss'}$ mean the probability amplitude for finding in $\Phi_\beta^{(2)}$ state with a single electron-hole pair, $a_s^+ a_{s'}|\alpha\rangle$. It is thus no accident that relations (3.5), (3.4) are the usual equations of the perturbation theory. A state with a single pair can be obtained through direct creation from state $|\alpha\rangle$, through rescattering of an electron or a hole, or through annihilation of an extraneous pair from a state with two electron-hole pairs. These possibilities correspond to the order of the terms in (3.5).

Let us expand $\Delta V_{kk'}$ in some complete system of function defined on a unit sphere, separately for the argument k/k and k'/k'. One can easily show that th Hamiltonian (3.1) can be put in a diagonal form in the general case for k and k' near the Fermi surface. Then

$$\Delta V_{kk'} = \sum_j \Delta V_j(\varepsilon, \varepsilon') \cdot \Omega_j(k) \cdot \Omega_j^*(k'); \tag{3.6}$$

To make the exposition more transparent we assume separability of $\Delta V_j(\varepsilon, \varepsilon')$

$$\Delta V_j(\varepsilon, \varepsilon') = \Delta V_j \alpha_j(\varepsilon) \alpha_j^*(\varepsilon'), \tag{3.7}$$

where $\alpha_j(\varepsilon)$ is a smooth function of the energy, and $\alpha_j(0) = 1$.

The solution of Eq. (3.5) can then be sought in the form

$$C_{kk'} = \sum_j \Omega_j(k) \cdot \Omega_j^*(k') \cdot C_j(\varepsilon, \varepsilon');$$
$$C_j(\varepsilon, \varepsilon') = \frac{\Delta V_j(\varepsilon, \varepsilon')}{\varepsilon - \varepsilon'} \cdot \xi_j(\varepsilon)\eta_j(\varepsilon'). \tag{3.8}$$

After averaging over angles, the terms with different j split up, and we find equations for ξ_j and η_j.

$$\xi(\varepsilon) = 1 - \Delta V_j \int d\varepsilon' \varrho(\varepsilon') \frac{n_{\varepsilon'} |\alpha_j(\varepsilon')|^2}{\varepsilon' - \varepsilon} \eta_j(\varepsilon') \xi_j(\varepsilon)$$
$$\eta_j(\varepsilon) = 1 - \Delta V_j \int d\varepsilon' \varrho(\varepsilon') \frac{(1 - n_{\varepsilon'}) |\alpha_j(\varepsilon')|^2}{\varepsilon' - \varepsilon} \xi_j(\varepsilon') \eta_j(\varepsilon) \tag{3.9}$$

(3.9) is a system of nonlinear integral equations which entangle the mechanisms of electron and hole scattering. The system has a latent symmetry, however, which allows us to convert it into a linear system of equations.

$$\xi_j(\varepsilon) = 1 - \xi_j(\varepsilon) \Delta V_j \int \frac{|\alpha_j(x)|^2}{x - \varepsilon} \varrho(x) dx + \Delta V_j \int \frac{|\alpha_j(y)|^2 (1 - n(y))}{y - \varepsilon} \xi_j(y) \varrho(y) dy . \tag{3.10}$$

Here $\varrho(\varepsilon)$ is the electron density of states, and $n(\varepsilon)$ is the occupation number. It turns out that η_j and ξ_j are connected by the simple relation

$$\eta_j(\varepsilon') = \frac{G_j(\varepsilon')}{\pi g_j \xi_j(\varepsilon')},$$
$$G_j(\varepsilon) = \pi g_j \left(1 + \Delta V_j \int \frac{|\alpha_j(x)|^2}{x - \varepsilon} \varrho(x) dx\right)^{-1}, \tag{3.11}$$

where $g_j = \varrho(\varepsilon_F) \Delta V_j$ is a dimensionless interaction constant.

This kind of equations is well-known in the theory of singular integral equations and has an exact solution [15]. The equation of this type has been used extensively by Nozieres and de Dominicis [12] for the problem of X-ray absorption in a metal, accompanied by the creation of an electron near ε_F.

We are interested in the solution of (3.10) at $\varepsilon \approx 0$. It acquires a particularly simple form at $T = 0$

$$\xi_j(\varepsilon) \approx A_j \left|\frac{\omega_0}{\varepsilon}\right|^{\delta_j/\pi}, \quad \delta = \tan^{-1} G_j(0) \tag{3.12}$$

($A_j \sim 1$). And, consequently,

$$C_j(\varepsilon, \varepsilon') = \frac{\Delta V_j(\varepsilon, \varepsilon')}{\varepsilon - \varepsilon'} \cdot \left|\frac{\varepsilon'}{\varepsilon}\right|^{\frac{\delta_j}{\pi}} \frac{\sin \delta_j}{\pi g_j}. \tag{3.13}$$

In these expressions δ_j is the phase shift in scattering of an electron at the Fermi surface in the potential ΔV_j.

At finite temperature, approximate expressions sufficient for all physical applications can be written in the form

$$\xi_j(\varepsilon) \approx A_j \left|\frac{\omega_0}{(\varepsilon, T)_{\max}}\right|^{\delta_j/\pi}$$
$$C_j(\varepsilon, \varepsilon') = \frac{\Delta V_j(\varepsilon, \varepsilon')}{\varepsilon - \varepsilon'} \cdot \left|\frac{(\varepsilon', T)_{\max}}{(\varepsilon, T)_{\max}}\right|^{\delta_j/\pi} \frac{\sin \delta_j}{\pi g_j}. \tag{3.14}$$

The normalization factor S in (3.2) is equal to the overlap integral $\langle \phi_\alpha^{(1)} | \phi_\alpha^{(2)} \rangle$. Its value can be calculated from the relation $\langle \alpha | \Lambda^+ \Lambda | \alpha \rangle = 1$. At $T = 0$

$$S = \exp\left\{ - b \cdot \int_{\varepsilon_{\min}}^{\omega_0} \frac{d\varepsilon}{\varepsilon} \right\}, \quad b = \sum_j \left(\frac{\delta_j}{\pi}\right)^2. \tag{3.15}$$

This result was known from the previous studies [12], [16]. In the tunneling problem the cutoff of the logarithmic divergence in (3.15) is connected with a finite lifetime of the particle in a well and $\varepsilon_{\min} \sim \tau^{-1}$.

4. Effect of Barrier Fluctuations on a Tunneling in a Metal

The results of the preceding section allow us to determine the effect of the barrier fluctuations on coherent and incoherent tunneling processes. Retaining the first two terms in the expansion of the exponential function in (2.15), we find

$$\Delta_c = \Delta_c^{(0)} + \Delta_0 \operatorname{Sp}(\varrho B \Lambda)$$
$$\Delta_c^{(0)} = \Delta_0 \cdot S . \tag{4.1}$$

Taking into account that $\varepsilon_{\min} = \gamma \Delta_c$, the self-consistent value of $\Delta_c^{(0)}$ is equal to (see, e.g., [9])

$$\Delta_c^{(0)} \approx \Delta_0 \left(\frac{\gamma \Delta_0}{\omega_0}\right)^{b/(1-b)}; \tag{4.2}$$

γ is a known numerical factor for lattices of different types.

According to (2.11) the expression for B can be written in the form

$$B = \sum_{kk'\sigma} \frac{B_{kk'}}{\omega_0} a^+_{k\sigma} a_{k'\sigma} . \tag{4.3}$$

Let us expand $B_{kk'}$ with $|\varepsilon_k|, |\varepsilon_{k'}| < \omega_0 \ll \varepsilon_F$ in the same system of functions Ω_j:

$$B_{kk'} = \sum_{jj'} B_{jj'} \cdot \Omega_j(k) \cdot \Omega^*_{j'}(k') . \tag{4.4}$$

The fact that all the terms in the argument of the exponential function in the definition of the operator Λ in (3.2) commute (this circumstance is the basic distinctive feature of the method which was selected for constructing this operator) means that the evaluation of the matrix elements will be a simple process. In the case at hand, using (4.4), we immediately find the following expression for the second term in expression (4.1) at $T = 0$

$$\Delta_c^{(0)} 2 \sum_j \frac{B_{jj} \Delta V_j \sin \delta_j}{\omega_0 \pi g_j} \varrho^2(\varepsilon_F) \int_{-\omega_0}^{+\omega_0} \int \frac{(1 - n_\varepsilon) n_{\varepsilon'} d\varepsilon d\varepsilon'}{\varepsilon - \varepsilon'} \left|\frac{\varepsilon'}{\varepsilon}\right|^{\delta_j/\pi}. \tag{4.5}$$

The value of this integral is determined at the upper limits of the integration, so the simple estimate with allowance for (2.11) can be obtained

$$\Delta_0 \mathrm{Sp}(\varrho B \Lambda) \approx \Delta_c^{(0)} \varrho(\varepsilon_F) \Delta V \sin\delta. \tag{4.6}$$

Using $\varrho \Delta V \lesssim 1$, we see that the renormalization of Δ_c is not of fundamental importance. This result continues to hold at nonzero temperature $T \ll \omega_0$, since $\varepsilon, \varepsilon' \sim \omega_0$ are important in integral (4.5). It is easy to show that the corrections from higher-order terms in the expansion of e^{-B} do not alter this result.

Thus, the infrared catastrophe near the Fermi surface has no essential effect on the fluctuational preparation of the barrier in the formation of Δ_c.

As shown in Ref. [13], the amplitude for a coherent transition begins to decay exponentially even at temperature $bT \gtrsim \Delta_c$. The under-barrier motion of the particle is now accompanied by an excitation of the electron subsystem, and it thereby becomes incoherent. Under these conditions the transition probability is determined by (2.16). Ignoring first the fluctuations of the barrier, one can transform (2.16) to (see, e.g., Ref. [17, 18, 4])

$$W' = \Delta_0^2 \int_{-\infty}^{\infty} dt\, e^{i\xi t} e^{-\chi(t)} \tag{4.7}$$

$$\chi(t) = 2b \int_0^{\omega_0} \frac{dy}{y} \left[(1 - \cos(yt)) \coth\left(\frac{y}{2T}\right) + i \sin(yt) \right].$$

An evalution of this integral leads to the expression [19, 20, 4]

$$W'(\xi) = \frac{2\tilde{\Delta}_0^2(T)\Omega_T}{\xi^2 + \Omega_T^2} \pi^{1/2} \frac{|\Gamma(1 + b + i\xi/2\pi T)|^2}{\Gamma(1+b)\Gamma(1/2+b)} e^{\xi/2T}, \tag{4.8}$$

$$\tilde{\Delta}_0(T) = \Delta_0 (\pi T/\omega_0)^b, \quad \Omega_T = 2\pi b T. \tag{4.9}$$

Consider the probability for the process in which the excitation of the electron system is coupled specifically with fluctuations of the barrier, and begin with a perturbation theory in B. We first ignore the rescattering of the electron-hole pair created by the operator B. In this case the transition probability is given by

$$W'' = \Delta_0^2 \sum_{ss'} |B_{ss'}/\omega_0|^2 (1 - n_s) n_{s'} \cdot \int_{-\infty}^{\infty} dt \exp\left[i(\xi + \varepsilon_{s'} - \varepsilon_s) t - \chi(t) \right] = \sum_{ss'} |B_{ss'}/\omega_0|^2 (1 - n_s) n_s, W'(\xi + \varepsilon_{s'} - \varepsilon_s). \tag{4.10}$$

The integral over dt in (4.10) is determined over time scales $1/(T, \xi)_{\max}$. We single out the constant part of $\xi(t)$, which leads to renormalization of Δ_0 by $\tilde{\Delta}_0(T)$; the remainder leads to a δ-function which is smeared over a scale Ω_T. As a result we find the simple estimate ($\zeta = 0$)

$$W'' \approx (\tilde{\Delta}_0/\omega_0)^2 \Omega_T. \tag{4.11}$$

Comparison of this expression with (4.8) leads to the ratio

$$W''/W' \sim (\Omega_T/\omega_0)^2 \ll 1. \tag{4.12}$$

In the general case it is required to evaluate the effective matrix element $\tilde{B}_{ss'}$ which corresponds to a transition from well 2 to well 1, in a process accompanied by the creation of a single electron-hole pair:

$$\tilde{B}_{\alpha\beta} = S^{-1} \langle \alpha | B \Lambda | \beta \rangle. \tag{4.13}$$

From the definition of the operator Λ, one can easily collect possible matrix elements which lead to the state $|\alpha\rangle = a_s^+ a_{s'} |\beta\rangle$:

$$\tilde{B}_{ss'} = B_{ss'} - \sum_k (1 - n_k) B_{sk} C_{ks'} + \sum_{k'} n_{k'} B_{k's'} C_{sk'} - \sum_{kk'} (1 - n_k) n_{k'} B_{k'k} C_{ks'} C_{sk'}. \tag{4.14}$$

Substituting expressions (3.8) and (4.4) into this equation, we find

$$\tilde{B}_{jj'}(\varepsilon, \varepsilon') = B_{jj'} \xi_j(\varepsilon) \eta_{j'}(\varepsilon'). \tag{4.15}$$

Using (3.14) and (3.11), we have finally

$$\tilde{B}_{jj'}(\varepsilon, \varepsilon') \approx B_{jj'} \left(\frac{\omega_0}{(\varepsilon, T)_{\max}} \right)^{\frac{\delta_j}{\pi}} \left(\frac{\omega_0}{(\varepsilon', T)_{\max}} \right)^{-\frac{\delta_{j'}}{\pi}}. \tag{4.16}$$

This expression demonstrates that there can be an appreciable increase in the amplitude for an incoherent transition due to the fluctuations of the barrier when the rescattering of the electron and hole is taken into account. This circumstance was first pointed out by Kondo [5]. Zawadowski et al. [6, 7, 8] undertook a detailed analysis of the renormalization of this amplitude. A result similar to (4.16) was first derived by a multicomponent renormalization-group method [8] for the model with commutator

$$[V(r, R_1), V(r, R_2)] = 0.$$

The transition probability determined by the amplitude $\tilde{B}$ is obviously given by expression (4.10), with B replaced by $\tilde{B}$

$$W''' = \sum_{jj'} f_{jj'} \int_{-\infty}^{\infty} W'(\xi + \varepsilon' - \varepsilon)(1 - n_\varepsilon) n_{\varepsilon'} \cdot \left[\frac{\omega_0}{(\varepsilon, T)_{\max}} \right]^{\frac{2\delta_j}{\pi}} \cdot \left[\frac{\omega_0}{(\varepsilon', T)_{\max}} \right]^{-\frac{2\delta_{j'}}{\pi}} \frac{d\varepsilon d\varepsilon'}{\omega_0^2}, \tag{4.17}$$

where $f_{jj'} = \varrho^2(\varepsilon_F) B_{jj'}^2$. We can estimate the relative order of magnitude of W''' even without writing an explicit expression

for W'. The integral over $d\varepsilon$ and $d\varepsilon'$ is determined at energies of the electron-hole pairs of the order $\varepsilon - \varepsilon' \sim (\xi, T)_{\max}$ (at energy transfer $E > T$, the probability W' falls exponentially, $\sim e^{-E/T}$). Then immediately

$$W'' \sim W' \left| \frac{(\xi, T)_{\max}}{\omega_0} \right|^{2(1-\theta)} \tag{4.18}$$

$$\theta = (\theta_{jj'})_{\max}, \quad \theta_{jj'} = (\delta_j - \delta_{j'})/\pi \tag{4.19}$$

Thus, the problem of whether the barrier fluctuations in a metal can become a leading channel of scattering depends on the possibility for the parameter θ to become larger than 1. However, it will be shown below that θ is, nevertheless, always smaller than 1 and the intrawell scattering remains to be the leading process. In this case, one should bear in mind that, taking into account the rescattering, the transition probability also contains a correction being linear in B. However, this correction is determined only by j-diagonal of the B operator, which display no enhancement (4.16). At the same time, the small parameter appearing in this case contains the ratio $(\xi, T)_{\max}/\omega_0$ only to the first power.

The δ_j phases which occur in expression (4.19) characterize the scattering in the nonspherical potential created by the difference $V(\boldsymbol{r}, \boldsymbol{R}_2) - V(\boldsymbol{r}, \boldsymbol{R}_1)$. The scattering matrix S corresponding to these phases can be expressed in terms of the S-matrices relevant to the scattering by the particle in an individual well. Indeed, the outcoming wave $\phi_{R_2}^{\text{out}}$ being the solution of the Schrödinger equation for the Hamiltonian $H^{(2)}$ is, on the one hand, conventionally connected with the outcoming part of the plane wave φ_0^{out}

$$\phi_{R_2}^{\text{out}} = S_2 \, \varphi_0^{\text{out}},$$

while, on the other hand, through the $\tilde{S}$ matrix it is related to the wave outcoming from the center at the point $\boldsymbol{R}_1$

$$\phi_{R_2}^{\text{out}} = \tilde{S} \, \phi_{R_1}^{\text{out}} = \tilde{S} \, S_1 \, \varphi_0^{\text{out}}$$

Hence, it immediately follows that

$$\tilde{S} = S_2 \, S_1^{-1} = e^{i\boldsymbol{p}\boldsymbol{R}} \, S_1 \, e^{-i\boldsymbol{p}\boldsymbol{R}} \, S_1^{-1}, (\boldsymbol{R} = \boldsymbol{R}_2 - \boldsymbol{R}_1), \tag{4.20}$$

(cf. [16]). In the latter equality we made use of the translational symmetry, $\boldsymbol{p}$ is the momentum operator.

The eigenvalues of the $\tilde{S}$ operator equal to $e^{2i\delta}$. The difficulty in their finding is attributed to the noncommutative character of the S_1 and S_2 matrices, since $[V_1, V_2] \neq 0$. Within the representation of standard spherical functions $Y_\alpha(k/k)$, $\alpha \equiv (l, m)$, where the S_1 matrix is diagonal, the eigenvalues are determined from the condition

$$\det \left| \sum_\gamma \mathbb{E}_{\alpha\gamma} e^{-2i\delta_{(0)}^{\gamma}} \mathbb{E}_{\gamma\beta}^{+} e^{-2i\delta_{(0)}^{\beta}} - e^{2i\delta} \delta_{\alpha\beta} \right| = 0, \tag{4.21}$$

where

$$\mathbb{E}_{\alpha\beta} = \int \frac{d\sigma_k}{4\pi} Y_\alpha^*(k) \, e^{ikR} \, Y_\beta(k); \quad \mathbb{E}^{+} = \mathbb{E}^{-1}. \tag{4.22}$$

At the finite number of the $\delta_\alpha^{(0)}$ phases, it is convenient to transform the elements of the determinant (4.21) to the form which would contain phases only in the combination $(e^{\mp 2i\delta^{(0)}} - 1)$. After that, the determinant rank becomes finite. Direct algebraic transformations of (4.21) make it possible to reduce it to the form

$$\det \left| \sum_\gamma \mathbb{E}_{\alpha\gamma} \frac{G_\gamma}{G_\gamma - z} \mathbb{E}_{\gamma\beta}^{\nabla +} \, G_\beta - \frac{G_\alpha + z}{1 + z^2} \delta_{\alpha\beta} \right| = 0. \tag{4.23}$$

Here

$$G_\alpha = \tan \delta_\alpha^{(0)}, \quad z = \tan \delta. \tag{4.24}$$

The symmetry specified by the shift operator $e^{i\boldsymbol{p}\boldsymbol{R}}$, if we choose $\boldsymbol{R}$ as a polar axis, predetermines the decay of the determinant (4.21) into the product of determinants, each of which is characterized by its own azimuthal quantum number m.

If the potential V_1 is characterized by only one scattering phase $\delta_{l_0}^{(0)}$, and, consequently, $G_{(l,m)} = G_{l_0} \, \delta_{ll_0}$, then (4.23) is reduced to a trivial equation

$$\frac{G_{l_0}^2 - z^2}{1 + z^2} = \mathbb{E}_{l_0 m}^2 \, G_{l_0}^2; \quad \mathbb{E}_{l_0 m} \equiv \mathbb{E}_{(l_0, m)(l_0, m)}. \tag{4.25}$$

Its solution has the form

$$z = \tan \delta = \pm \frac{\sqrt{1 - \mathbb{E}_{l_0 m}^2} \, \operatorname{tg} \delta_{l_0}^{(0)}}{\sqrt{1 + \mathbb{E}_{l_0 m}^2 \operatorname{tg}^2 \delta_{l_0}^{(0)}}}. \tag{4.26}$$

Now, if the b parameter (3.15) is calculated, we immediately have the result which was for the first time obtained by Yamada [18, 21].

At $\boldsymbol{R} \to 0$ the ΔV interaction (3.1) and, at the same time, δ, tend to zero (the overlapping integral (3.15) should reduce to 1). Hence, it is possible to conclude that at small $\boldsymbol{R}$'s the phase values should be determined by the $\tan^{-1}$ branch between $-\pi/2$ and $\pi/2$. From the viewpoint of the θ parameter, the crucial problem is whether the solution (4.26) would be able to intersect the boundary $|\delta| = \pi/2$ at a continuous variation of the $\boldsymbol{R}$, $\delta^{(0)}$ quantities. This would mean that at a certain point z would go to ∞. It follows from the form of Eq. (4.26) that this could take place only under a simultaneous condition of $\tan \delta_{l_0}^{(0)} = \pm \infty$; $\mathbb{E}_{l_0 m} = 0$. But these singular points are only the point of contact of the solution δ to $\pm \pi/2$ values. This immediately follows from the continuity of δ as a function of $\delta^{(0)}$ and $\boldsymbol{R}$.

Thus, we come to an important conclusion that, in the case of one scattering phase, $|\delta| \leq \pi/2$ (cf. [21, 22]). From this the restriction $\theta \leq 1$ directly follows.

Let us now consider the case of an arbitrary number of phases $\delta_\alpha^{(0)}$ and find out the conditions under which the solution for z goes to ∞. To this aim, we rewrite (4.23) for the case of $z = \infty$

$$\det \left| \sum_\gamma \mathbb{E}_{\alpha\gamma} \, G_\gamma \, \mathbb{E}_{\gamma\beta}^{+} \, G_\beta + \delta_{\alpha\beta} \right| = 0. \tag{4.27}$$

We make use the representation of the spherical functions in the form

$$Y_{lm} = \mathrm{i}^l \Theta_{lm}\, \mathrm{e}^{\mathrm{i}m\varphi}/\sqrt{2\pi}.$$

One can easily follow that the relations

$$\mathbb{E}_{\alpha\beta} = \mathbb{E}^*_{\alpha\beta}; \quad \mathbb{E}_{\alpha\beta} = (-1)^{l_\alpha - l_\beta}\, \mathbb{E}_{\beta\alpha}$$

take place. Let's introduce two complex matrices

$$\mathbb{A}_{\alpha\beta} = (-1)^{l_\alpha}\delta_{\alpha\beta} + \mathrm{i}\mathbb{E}_{\alpha\beta}G_\beta; \quad \mathbb{B}_{\alpha\beta} = (-1)^{l_\alpha}\delta_{\alpha\beta} - \mathrm{i}\mathbb{E}^+_{\alpha\beta}G_\beta$$

Their product is equal to the matrix, the determinant D of which coincides with (4.27). Hence,

$$D = \det|\mathbb{A}_{\alpha\beta}| \cdot \det|\mathbb{B}_{\alpha\beta}|\,.$$

It follows from the complexity of the matrices $\mathbb{A}$ and $\mathbb{B}$ that in the general case it is required to satisfy at least two independent conditions in order to have zero D.

As a result, in the space of the $\{\delta_\alpha^{(0)}\}$, R parameters of dimension d the singular points $z = \infty$ form hypersurfaces of the dimension $d - 2$. In the same way as in the case with one scattering phase, this means that at the continuous variation of the parameters the solutions δ_l do not cross the $|\delta_l| = \pi/2$ value, and always remain on the $\tan^{-1}$ branch $(-\pi/2, \pi/2)$. It is particularly evident in the space of three parameters $\{\delta_1^{(0)}, \delta_2^{(0)}, R\}$. In this case the singular points form lines and all the phase space points may be connected to the origin without crossing the singular lines.

Thus, we arrive at a general statement that, in the case of the tunneling motion of the particle, the interaction with barrier fluctuations always remains weak as compared with the intrawell interaction, in spite of the enhancement due to the infrared singularity.

From the consideration presented, it is clear that the fermion and boson heat baths are, strictly speaking, not equivalent. It is possible to ignore this fact only to the extent to which all the contributions connected with the barrier fluctuations can be omitted.

5. Effect of Barrier Fluctuations on a Tunneling Transition in an Insulator

Consider now the role of barrier fluctuations during tunneling motion in an insulator, when the interaction with phonons plays decisive role. Naturally, all the results of Sect. 2, in particular, expressions (2.15) and (2.16) are presented in this case. The polaron operator Λ (2.13) is constructed now on the interaction

$$\Delta V = \sum_\alpha C_\alpha(b_\alpha + b^+_{-\alpha}) + \frac{1}{2}\sum_{\alpha\beta} C_{\alpha\beta}(b_\alpha + b^+_{-\alpha})(b_\beta + b^+_{-\beta})$$

$$C_\alpha = C_\alpha(R_2) - C_\alpha(R_1),\ C_{\alpha\beta} = C_{\alpha\beta}(R_2) - C_{\alpha\beta}(R_1)\,. \tag{5.1}$$

Here the subscript $\mp\alpha \equiv \mp q,\lambda$, where q is the wave vector; λ is the phonon branch number. At $\omega_\alpha, \omega_\beta \to 0$

$$C_\alpha(R_i) \sim \sqrt{\omega_\alpha}, \quad C_{\alpha\beta}(R_i) \sim \sqrt{\omega_\alpha\omega_\beta} \tag{5.2}$$

Usually, in analyzing the tunneling in the medium, only the one-phonon interaction in (5.1) is considered. However, the allowance for the two-phonon interaction has quite a principal character. As shown in Ref. [14], only in this case the tunneling motion in a crystal acquires a "viscous" or "ohmic" character of behavior. It is not accidental that the quantum diffusion in a regular crystal at low T is determined precisely by the two-phonon interaction [23, 24]. We preserve only the two-phonon interaction in (5.1), since by taking into account the terms of a higher order we do not introduce any qualitative changes. The results presented below were obtained on the assumption that the two-phonon interaction was a weak one and it is treated within the perturbation theory.

Bearing this in mind, it becomes possible to represent the polaron operator in the form [14]

$$\Lambda = \Lambda_2\,\Lambda_1\,. \tag{5.3}$$

Here Λ_1 is the conventional shift operator of normal oscillators

$$\Lambda_1 = \exp\left\{\sum_\alpha\left(\frac{C_\alpha}{\omega_\alpha}b_\alpha - \frac{C_{-\alpha}}{\omega_\alpha}b^+_\alpha\right)\right\}. \tag{5.4}$$

In constructing Λ_2 related to the two-phonon interaction, in (5.1) only the terms of the scattering type $b^+_{-\alpha}b_\beta$ and $b^+_{-\beta}b_\alpha$ turns out to be significant.

$$\Lambda_2 = \exp\left\{-\frac{1}{2}\sum_{\alpha\beta}\left[\frac{C_{\alpha\beta}}{\omega_\alpha - \omega_\beta + \mathrm{i}/\tau}b^+_{-\alpha}b_\beta - \frac{C^*_{\alpha\beta}}{\omega_\alpha - \omega_\beta - \mathrm{i}/\tau}b^+_\beta b_{-\alpha}\right]\right\}. \tag{5.5}$$

It should be reminded that in (5.1), (5.4), (5.5) the summation is taken over the nonadiabatic interval of phonon excitations $\omega_\alpha < \omega_0$. In determining B (2.11), we preserve only the barrier fluctuations stipulated by the one-phonon interaction

$$B = \frac{1}{\omega_0}\sum_\alpha\left(B_\alpha b^0_\alpha + B_{-\alpha}b^{0+}_\alpha\right). \tag{5.6}$$

Here, b^0_α, b^{0+}_α are the operators of the secondary quantization, which correspond to the phonons of the lattice nonperturbed by the particle. They are connected with the operators b_α, b^+_α in (5.4), which are determined at the phonon states with the displaced centers of oscillators when the particle is in well 1, by the relations

$$b^0_\alpha = b_\alpha - \frac{C^{(1)}_{-\alpha}}{\omega_\alpha}; \quad b^{0+}_\alpha = b^+_\alpha - \frac{C^{(1)}_\alpha}{\omega_\alpha}$$

We shall now calculate the coherent transition amplitude (2.15). By neglecting the rescattering due to the two-phonon processes, we have

$$\Delta^c = \Delta_0 \langle e^B \Lambda_1 \rangle \langle \Lambda_2 \rangle . \tag{5.7}$$

Here, $\langle \ldots \rangle \equiv \mathrm{Sp}\{\varrho \ldots\}$.

The calculation of the first average value is performed directly [1].

$$\Delta_c = \tilde{\Delta}_0 \langle \Lambda_2 \rangle . \quad \tilde{\Delta}_0(T) = \Delta_0 e^{B_0} e^{-\varphi(T)+G(T)} . \tag{5.8}$$

In this expression:

$$\varphi(T) = \frac{1}{2}\sum_\alpha \frac{|C_\alpha|^2}{\omega_\alpha^2} \coth\left(\frac{\omega_\alpha}{2T}\right); \tag{5.9}$$

is the conventional polaron factor;

$$G(T) = \frac{1}{2}\sum_\alpha \frac{|B_\alpha|^2}{\omega_0^2} \coth\left(\frac{\omega_\alpha}{2T}\right) \tag{5.10}$$

is an exponent stipulated by the barrier fluctuations.

The B_0 determines the barrier variation connected with atoms shifts to the positions equal to a half-sum of the static shifts appearing when the particle is in wells 1 and 2

$$B_0 = \sum_\alpha \frac{B_{-\alpha}(C_\alpha^{(1)} + C_\alpha^{(2)})}{\omega_0 \omega_\alpha} . \tag{5.11}$$

The B_0 value is temperature-independent.

At $T \to 0$ the average $\langle \Lambda_2 \rangle \to 1$ and the coherent amplitude and, correspondingly, the coherent bandwidth in the crystal is determined by the $\tilde{\Delta}_0(0)$ value. As seen from the expression (5.8), there takes place a competition between the polaron effect and the fluctuational barrier preparation. The ratio between φ and G is arbitrary in the general case, since the basic contributions made to (5.9) and (5.10) may be connected with the shifts of different groups of atoms. If the barrier fluctuations prevail, then, instead of the decrease, the one-phonon interaction causes the increase of Δ_c and, instead of the polaron narrowing, the bandwidth will grow with rising temperature. It should be stressed that at $\omega_0 > \Theta_D$ the whole phonon spectrum takes part in the formation of G (or φ), and the scale of these quantities may be appreciable. On the contrary, in the case of a heavy particle tunneling, when $\omega_0 \ll \Theta_D$, the part played by both the factors may be rather small.

The $\langle \Lambda_2 \rangle$ value starts to drop drastically with rising temperature. Already at $\Theta_D \gg T \gg \tau^{-1}$ the calculation of this value, taking into account the explicit form of (5.5), brings about the result [14]

$$\langle \Lambda_2 \rangle = e^{-\Omega\tau/2} . \tag{5.12}$$

The $\Omega(T)$ frequency connected with the phase relaxation rate in the tunneling transition is determined by the expression [24, 14]

$$\begin{aligned} \Omega(T) &= \pi \sum_{\alpha\beta} |C_{\alpha\beta}|^2 N_\alpha (1+N_\beta)\, \delta(\omega_\alpha - \omega_\beta) \\ &= \pi \int_0^{\omega_0} d\omega\, g^2(\omega)\, \lambda(\omega) \frac{\exp(\omega/T)}{(\exp(\omega/T)-1)^2} , \end{aligned} \tag{5.13}$$

where $g(\omega)$ is the phonon density of states. The function $\lambda(\omega)$ is the average at $\omega_\alpha = \omega_\beta = \omega$ over the phase volume and branches of the phonon spectrum from $|C_{\alpha\beta}|^2$.

The condition $\Omega\tau \gg 1$, under which the coherent band break-down takes place, occurs in the region of low temperatures $T \ll \Theta_D$, where $\tilde{\Delta}_0$ differs still slightly from its value at $T = 0$. At that, there takes place a transition to the incoherent regime, which is described by the general expression for the transition probability (2.16) with allowance for (5.3)–(5.6). The straightforward calculation of (2.16) results in the relation [14] (see also [1])

$$\begin{aligned} W = \tilde{\Delta}_0^2 e^{\xi/2T} \int_{-\infty}^{\infty} dt \exp\left\{ i\xi t - \frac{\Omega}{\pi T} \ln(\cosh(\pi T t)) \right\} \\ \cdot \exp\left(\Psi(t) + i\tilde{\Psi}(t) \right) . \end{aligned} \tag{5.14}$$

Here

$$\begin{aligned} \Psi(t) &= \sum_\alpha \left[\frac{|C_\alpha|^2}{\omega_\alpha^2} + \frac{|B_\alpha|^2}{\omega_0^2} \right] \frac{\cos(\omega_\alpha t)}{\sinh\left(\frac{\omega_\alpha}{2T}\right)} ; \\ \tilde{\Psi}(t) &= 2\sum_\alpha \frac{C_\alpha B_{-\alpha}}{\omega_\alpha \omega_0} \frac{\sin(\omega_\alpha t)}{\sinh\left(\frac{\omega_\alpha}{2T}\right)} . \end{aligned} \tag{5.15}$$

At $T \ll \Theta_D$ and restricted ξ this expression is strongly simplified and results in the form [25]

$$W \approx \frac{2\tilde{\Delta}_0^2 \Omega}{\xi^2 + \Omega^2} \frac{\xi/T}{1 - e^{-\xi/2T}} . \tag{5.16}$$

At $\xi = 0$, proceeding from this expression to the diffusion coefficient, we have [24]

$$D(T) = \frac{za^2}{3} \frac{\tilde{\Delta}_0^2}{\Omega(T)} ; \tag{5.17}$$

z is the number of equivalent wells with the same energy in the nearest coordination sphere. This expression hold true in a broader interval of temperatures and only the $T \gg \tau^{-1}$ condition [24] is required. Thus, at low temperatures the quantum diffusion is determined by the two-phonon processes. The one-phonon interaction, in particular that the barrier fluctuations, is introduced through the renormalized amplitude $\tilde{\Delta}_0$ (5.8). The transitions induced by this interaction constitute just a negligible correction to (5.17).

However, the picture changes, when the condition $T \ll \Theta_D$ ceases to hold true. In this case, the inelastic processes related to the barrier fluctuations and "shaking" of the polaron "cloud" start to play a decisive role. In (5.14) the $\Psi(t)$ and $\tilde{\Psi}(t)$ functions are responsible for these processes. It follows from the form of expressions (5.15) that the under-barrier and intrawell interactions can, to an equal extent, be dominant. At that, the character of the temperature dependence will differ appreciably in both the cases.

Here we present the expression for W (5.14), which corresponds to the region of high temperature, when it is possible to assume that $\Psi \gg 1$. At a large scale of the barrier fluctuations or a large polaron effect such an inequality takes place already at relatively moderate temperature

$$W \approx \Delta_0^2 e^{2B_0} \sqrt{\frac{\pi}{4(E+\gamma)T}} \exp\left\{-\frac{E}{T}+\frac{T}{E_B}-\frac{(\xi_B)^2 T}{16(E+\gamma)}\right\}. \tag{5.18}$$

Here

$$E = \frac{1}{4}\sum_\alpha \frac{|C_\alpha|^2}{\omega_\alpha}; \quad E_B^{-1} = 4\sum_\alpha \frac{|B_\alpha|^2}{\omega_0^2 \omega_\alpha};$$
$$\gamma = \frac{1}{4}\sum_\alpha \frac{\omega_\alpha |B_\alpha|^2}{\omega_0^2}; \quad \xi_B = 4\sum_\alpha \frac{C_\alpha B_{-\alpha}}{\omega_\alpha \omega_0}. \tag{5.19}$$

The sum of two linear in T terms in the exponent has a positive coefficient. Thus, the transition probability rises exponentially both due to the polaron effect and due to the barrier fluctuations. However, the temperature dependence is different in these two cases. If the polaron effect is decisive, we obtain the activation dependence which is well-known within the small-radius polaron theory (see [26,27]). If the interaction with the barrier fluctuations prevails, the law changes. Now the exponent rises with temperature, following the linear law. From the formal point of view, at a sufficiently large value of the T/Θ_D ratio the fluctuation mechanism will always play the key role.

Thus, we see that in the case of an insulator the interaction of the tunneling particle with the barrier fluctuations can be of cardinal importance.

6. Quantum Diffusion of Muonium in KCl Crystal

The recently published very interesting works [2,3] present the results of investigation of the quantum diffusion of muonium in KCl and NaCl crystals. The discovery of the diffusion coefficient increase by $2.5 \div 3$ orders of magnitude with decreasing T, which supersede the exponential drop of $D(T)$ is, surely, most impressive. It was for the first time that within one experiment the low-temperature increase of $D(T)$ was observed on such a scale, as well as the passage through the minimum and the under-barrier character of the motion at the high-temperature branch of the dependence at $T > T_{min}$. The appearance of a small preexponential factor, as compared with the oscillation frequency of a particle in a well $\omega \sim 10^{13}\ s^{-1}$, is a clear manifestation of the latter. All that allows us to analyze the role of the interaction with the barrier fluctuations by comparing the theoretical and experimental results. Here we shall confine ourselves to the results of the analysis for KCl (for details, see Ref. [28]).

At low temperature $T < T_{min}$ the diffusion coefficient is determined by the expression (5.17), while the corresponding lifetime in a cell has the value ($\hbar = 1$)

$$\tau^{-1} \approx 4D(T)/a^2 = \frac{8\tilde{\Delta}_0^2}{\Omega}; \tag{6.1}$$

(coefficient 4 is a result of a numerical calculation for a simple cubic structure). It is precisely τ^{-1} that was determined in Refs. [2,3]. Within the limit $T \to 0$ in (5.13) the function $\lambda(\omega) \sim \omega^{2+(2)}$ and, correspondingly,

$$\Omega(T) \sim T^{7+(2)}. \tag{6.2}$$

Two additional powers of T appear in the case of particle tunneling between the absolutely equivalent sites. In the NaCl structure the neighboring sites are not equivalent as far as the interaction with phonons is considered and the (2) factor must be omitted.

In Refs [2,3] an appreciably weaker dependence was observed, as compared with (6.2). As it has been found out [28], that is not a consequence of violation of the decisive role played by the two-phonon interaction but is due to the necessity of taking into account the actual phonon spectrum of the crystal in (5.13). The calculations performed for KCl, allowing for the experimentally determined $g(\omega)$ function [29] and the simplest form the vertex of the two-phonon interaction

$$|C_{\alpha\beta}|^2 = \lambda_{2ph}\, \omega_\alpha \omega_\beta \tag{6.3}$$

are shown in Fig. 1. At that, it was assumed that $\tilde{\Delta}_0 \approx$ const. At $T \to 0$ the inverse lifetime goes out into a constant value

$$\tau_0^{-1} = 2\sqrt{2}\,\tilde{\Delta}_0. \tag{6.4}$$

The transition from coherent regime (6.4) to incoherent one (6.1) could be described by the interpolation formula

$$\tau_c^{-1} = \frac{\tau_0^{-1}}{1+\Omega\tau_0}. \tag{6.5}$$

The limiting behavior of the experimental curves at low T allowed $\tilde{\Delta}_0$ to be determined independently. It was obtained

$$\tilde{\Delta}_0 \approx 0.13\ \text{K (KCl)}. \tag{6.6}$$

Thus, only one fitting parameter λ_{2ph} was used which controls the scale rather than temperature dependence of $\Omega(T)$.

It is clear from Fig. 1 that just after the minimum point the experimental and theoretical results are rather close. The latter correspond to the dependence $D(T) \sim T^{-5}$, in experiment [2] $D \sim T^{-7}$. An analogous result was obtained for NaCl.

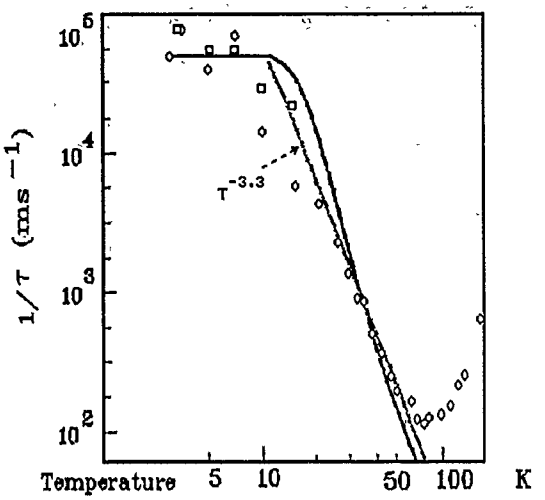


Fig. 1
Low temperature behavior of the inverse lifetime in KCl. Experimental point are from Refs. [2,3]. Fitting parameters for the theoretical curves are: $\tilde{\Delta}_0 = 0.13$ K, $\lambda_{2ph} = 0.11$

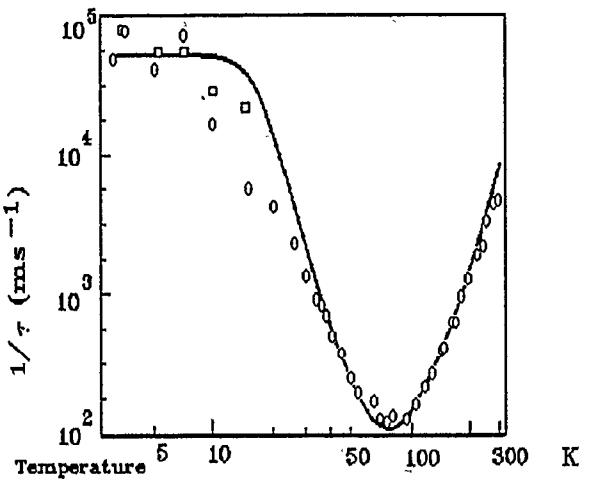


Fig. 2
Temperature dependence of the inverse lifetime in KCl. Experimental point are from Refs. [2,3]. Fitting parameters for the theoretical curve are: $\tilde{\Delta}_0 = 0.13$ K, $\lambda_{2ph} = 0.11$, $\lambda_B = 0.25$

Considering the temperature region $T \gtrsim T_{min}$ we conserve in (5.14) the one-phonon interaction only. After singling out from (5.14) the two-phonon part (5.16), (5.17), (6.1) the expression for τ^{-1} can be written in the form ($\xi = 0$)

$$\tau^{-1} \approx 4W = 4\tilde{\Delta}_0^2 \int_{-\infty}^{\infty} dt\,(e^{\Psi(t)+i\Psi(t)} - 1) \tag{6.7}$$

The sum of (6.5) and (6.7) describe the actual lifetime in a unit cell.

To start with, we assume that the barrier fluctuations do not play any role and we take $B_\alpha \approx 0$. The one-phonon interaction vertex can be presented in the form.

$$|C_\alpha|^2 = \lambda_{1ph}\omega_\alpha\,\omega_m\,, \tag{6.8}$$

where ω_m is the maximum frequency of the phonon spectrum.

If we make use of the activation energy value $E \approx 390$ K, found in Ref. [2], then, taking into account the actual phonon spectrum for KCl [29], we immediately determine the λ_{1ph} value from (5.19). This also allows us to find the polaron exponent $\varphi(T)$ (5.9). As a result, all the values in (6.5) and (6.7) turn out to be determined unambiguously. Now, if we find τ^{-1} for the whole temperature range, we make sure that there takes place a complete discrepancy between the experimental and calculated results for $T \approx T_{min}$. The preexponent in the activation dependence turns out to be three orders of magnitude larger than the experimental value and T_{min} falls within the range of considerably lower T. Such a sharp discrepancy cannot be compensared for by a simple redistribution of the parameters.

Let us now treat the opposite case when the barrier fluctuations play the decisive role, and assume $C_\alpha \approx 0$. We shall again make use of the simplest form for B_α

$$\frac{|B_\alpha|^2}{\omega_0^2} = \lambda_B \frac{\omega_\alpha}{\omega_m} \tag{6.9}$$

and, using the same $g(\omega)$ function determine the value of $G(T)$ (5.10) and $\Psi(t)$ (5.15). The results of the calculation, making use of only one fitting parameters λ_b, are presented in Fig. 2. One can see that remarkable agreement takes place between the experimental and theoretical results, including the position of the minimum, the scale of τ at $T \sim T_{min}$ and the whole high-temperature behavior of $\tau^{-1}(T)$. The contrast between the both limiting cases is so pronounced that there remains no doubt about the decisive role of the barrier fluctuations for the quantum diffusion of muonium in KCl.

References

[1] Yu. Kagan and M. I. Klinger, Zh. Eksp. Teor. Phys. *70* (1976) 256 [Sov. Phys. JETP *43*, 132 (1976)].
[2] R. F. Kiefl, R. Kadono, J. H. Brever, G. M. Luke, H. K. Yen, M. Celio, and E. J. Ansaldo, Phys. Rev. Lett. *62*, 792 (1989).
[3] R. Kadono, R. F. Kiefl, E. J. Ansaldo, J. H. Brewer, M. Celio, S. R. Kreitzman, and C. M. Luke, Phys. Rev. Lett. *64*, 665 (1990).
[4] Yu. Kagan and N. V. Prokofev, Zh. Eksp. Teor. Phys. *90*, 2176 (1986), [Sov. Phys.-JETP *63*, 1276 (1986)].
[5] J. Kondo, Physica (B+C) *84*, 207 (1976).
[6] K. Vladar and A. Zawadowski, Phys. Rev. B *28*, 1564, 1582, 1596 (1983).
[7] K. Vladar, G. T. Zimani, and A. Zawadowski, Phys. Rev. Lett. *56*, 286 (1986).
[8] K. Vladar, A. Zawadowski, and G. T. Zimani, Phys. Rev. B *38*, 2001, 2015 (1988).
[9] A. J. Leggett, S. Chakravarty, A. T. Dorsey, M. P. A. Fisher, A. Garg, and W. Zwerger, Rev. Mod. Phys. *59*, 1 (1987).
[10] Yu. Kagan and N. V. Prokofev, Zh. Eksp. Teor. Phys. *96*, 1473 (1989); [Sov. Phys.-JETP *69*, 836 (1989)].
[11] P. W. Anderson, Phys. Rev. Lett. *18*, 1049 (1967); Phys. Rev. *164*, 552 (1967).
[12] P. Nozieres and C. T. deDominicis, Phys. Rev. *178*, 1097 (1969).
[13] Yu Kagan and N. V. Prokofev, Zh. Eksp. Teor Phys. Pis'ma *45*, 91 (1987); [Sov. Phys.-JETP Lett. *45*, 114 (1987)].
[14] Yu. Kagan and N. V. Prokofev, Zh. Eksp. Teor. Phys. *96*, 2209 (1989); [Sov. Phys.-JETP *69*, 1250 (1989)].
[15] N. I. Muskhelishvili, Singular Integral Equations, P. Noordhoff Ltd., Groningen, The Netherlands 1953.

[16] K. Yamada and K. Yosida, Progr. Theor. Phys. *68*, 1504 (1982).
[17] J. Kondo, Physica (B+C) *126*, 377 (1984).
[18] K. Yamada, Progr. Theor. Phys. *72*, 195 (1984).
[19] H. Grabert and U. Weiss, Phys. Rev. Lett. *54*, 1605 (1985).
[20] M. P. A. Fisher and A. T. Dorsey, Phys. Rev. Lett. *54*, 1609 (1985).
[21] K. Yamada, A. Sakurai, S. Miyazima, and H. S. Hwang, Progr. Theor. Phys. *75*, 1030 (1986).
[22] Y. Tanabe and K. Ohtaka, Phys. Rev. *B 34*, 3763 (1986).
[23] Yu. Kagan and L. A. Maksimov, Zh. Eksp. Teor. Phys. *65*, 622 (1973); [Sov. Phys.-JETP *38*, 307 (1974)].
[24] Yu. Kagan and M. I. Klinger, J. Phys. *C 7*, 2791 (1974).
[25] Yu. Kagan and L. M. Maksimov, Zh. Eksp. Theor. Phys. *79*, 1363 (1980); [Sov. Phys.-JETP *52*, 688 (1980)]; Zh. Eksp. Theor. Phys. *84*, 792 (1983); [Sov. Phys.-JETP *57*, 459 (1983)].
[26] J. Appel, Solid State Phys. *21*, 193 (1968).
[27] C. P. Flynn and A. M. Stoneham, Phys. Rev. *B 1*, 3966 (1970).
[28] Yu. Kagan and N. V. Prokofev, Phys. Lett. A. 150, 320 (1990).
[29] H. Bilz and W. Kress, "Phonon. Dispersion Relations in Insulators", Springer-Verlag, Berlin, Heidelberg, New York 1979.

Presented at the Discussion Meeting of the Deutsche Bunsen-Gesellschaft für Physikalische Chemie "Rate Processes in Dissipative Systems: 50 Years after Kramers" in Tutzing, September 10–13, 1990 E 7525

Tunneling in Metals as a Dissipative Quantum Process

J. Kondo

Physics Department, Toho University, Funabashi, Chiba, Japan

Diffusion / Metals / Transport Properties / Tunneling

There are two characteristic energies for the proton in metals: the orbiting frequency within a site ($\hbar\omega_0$) and the tunneling integral between neighbouring sites (Δ). Since typically $\hbar\omega_0$ is 1000 K and Δ less than 10 K, the temperature range defined by $\hbar\omega_0 \gg kT \gg \Delta$ is experimentally accessible. This is peculiar to the proton and proton isotopes. – Low-energy excitations of the metal electrons cannot follow instantaneously the orbiting motion of the proton in a single well. They are equal to those when the proton potential is averaged over the proton wave function representing the orbiting motion. When the proton tunnels to another site, the low-energy excitations must be rearranged to correspond to the new proton position. Then the tunneling integral of the proton acquires a factor of the overlap integral between two electronic wave functions corresponding to two proton positions. This integral turns out to be much smaller than unity and depends on a power of the temperature when $\hbar\omega_0 \gg kT \gg \Delta$. This power law is a result of the non-adiabatic response of the metal electrons to proton motion. Such a power law will manifest itself in diffusion constant of the proton or proton isotopes.

1. Introduction

My talk is concerned with protons or positive muons tunneling between interstitial sites in metals [1]. This is a typical example of quantum processes in dissipative media. In this case, the metal electrons constitute a dissipative system. But my approach to this subject was motivated by an observation of peculiar properties of metal electrons. As you know, the characteristic energy scale for metal electrons is the Fermi energy, which is order of electron volts. But in this system electron-hole pair excitations can have an arbitrarily small energy. It is known that excitations with such a small energy give rise to two important effects.

The first is dissipation. An example of this is the Korringa relaxation of a spin placed in a metal. Its rate is proportional to kT, which is a direct manifestation of dissipative nature of the metal electrons. The second is infrared divergence. In some cases, perturbation theory for problems of metals breaks down due to vanishing excitation energy. A typical example of this is the electrical resistivity due to spin scattering, which is proportional to $\log kT$. So, our concern is what these effects result in for proton-tunneling in metals.

2. Protons in Metals [2]

We consider protons or positive muons in metals. These particles occupy interstitial sites in metals. In general, there are several energy levels for them in each site. Inelastic neutron scattering experiments tell us that the level separation in a single well is about 1000 K for the proton. These particles jump among interstitial sites and diffuse in metals. The jump rate depends strongly on the temperature. At high temperatures lattice vibration is important to understand the jump rate. At low temperatures, however, the effect of lattice vibration can be renormalized. So we will not consider its effect explicitly. At low temperatures, the jump may take place via tunneling between lowest levels of neighbouring sites. We will study the effect of metal electrons on such a tunneling.

Here, there are three relevant energies. The first is the level separation for the proton in a single well, which is denoted by $\hbar\omega_0$. The second is the splitting of the lowest levels due to tunneling, denoted by Δ. The third is the Fermi energy of the electrons, denoted by ε_F. These are generally related by

$$\varepsilon_F \gg \hbar\omega_0 \gg \Delta\,. \tag{1}$$

3. Single-Well Problem

First we consider the proton moving within a single well. The proton wave function will be denoted by $\chi_n(R - R_A)$ ($n = 0,1,2,\ldots$), where R is the proton coordinate and R_A

 © VCH Verlagsgesellschaft mbH, W-6940 Weinheim, 1991 0005-9021/91/0303-0422 $ 3.50+.25/0

the center coordinate of the well. We expect that χ_n is close to the harmonic wave function at least for small n.

We take a jellium model for the electrons. The electron wave function is denoted by $\Phi_\alpha(r_1, r_2, \ldots)$, where $r_1, r_2, \ldots$ are the electron coordinates. In particular, Φ_0 is the Fermi sphere state, where all the states within the Fermi sphere are occupied. $\Phi_{k\to k'}$ is the state obtained from Φ_0 by exciting the electron k to an empty state k'.

If the interaction between the proton and the electrons were absent, the total wave function would be the product $\chi_n \cdot \Phi_\alpha$. As an interaction we take a short-range potential, which is denoted by

$$\sum_i V(r_i - R) . \tag{2}$$

We consider two extreme approximations for this single-well problem [3].

3.1. Adiabatic Approximation

In this approximation we take the total wave functions as

$$\Psi = \chi_0(R - R_A) \cdot \Phi_R(r_1, r_2, \ldots) , \tag{3}$$

where Φ_R is the electron wave function which is obtained when the proton is fixed at R. Eq. (3) implies that the electrons follow the proton instantaneously.

Perturbation theory tells us that Φ_R is written in the first-order of V as

$$\Phi_R = \Phi_0 - \sum \frac{V_0 \, e^{i(k-k')\cdot R}}{\varepsilon' - \varepsilon} \Phi_{k\to k'} , \tag{4}$$

where the summation is over k and k' with the restriction that k is inside of the Fermi sphere and k' outside of it. V_0 is the Fourier transform of $V(r)$, which we assume is independent of the wave number. ε and ε' stand for ε_k and $\varepsilon_{k'}$. These abbreviations will also be used in later parts of this paper. The phase factor in (4) takes accounts of the fact that the proton is fixed at R.

This wave function would be valid, if the electrons moved much faster than the proton does. This is not the case, however. If one takes the average of the total energy with Ψ, one finds that it is logarithmically divergent. This divergence comes from excitations with vanishing energy. The electrons are slow due to the presence of such excitations and cannot follow the proton instantaneously. In order to remove such a divergence I used an anti-adiabatic scheme. On the other hand Kagan and Prokof'ev took account of higher-order terms of the adiabatic scheme [4]. Their approach is more systematic. However, it turned out that the essential physics had already been involved in our scheme.

3.2. Anti-Adiabatic Approximation

We then consider the other extreme case, where the electrons feel a potential which is averaged over the proton wave function:

$$\sum_i \bar{V}(r_i - R) = \sum_i \int V(r_i - R) \, |\chi_0(R - R_A)|^2 \, d^3R . \tag{5}$$

The electron wave function in this potential will be written as

$$\Phi_{R_A} = \Phi_0 - \sum \frac{\bar{V}_0 \, e^{i(k-k')\cdot R_A}}{\varepsilon' - \varepsilon} \Phi_{k\to k'} + \ldots , \tag{6}$$

where $\bar{V}_0$ is the Fourier transform of $\bar{V}(r)$ whose wave number dependence is also neglected. The total wave function is written as

$$\Psi = \chi_0(R - R_A) \, \Phi_{R_A}(r_1, r_2, \ldots) . \tag{7}$$

This wave function no longer involves an infrared divergence. Instead it turned out that it involved a large non-adiabatic effect.

4. Two-Well Problem

In order to see what effect Eq. (7) involves, we will now consider a two-well problem, where there are two total wave functions corresponding to the proton in the left well (centered at R_A) and in the right well (centered at R_B).

4.1. Adiabatic Approximation

In this approximation, the two wave functions are

$$\Psi_A = \chi_0(R - R_A) \cdot \Phi_R , \tag{8}$$

$$\Psi_B = \chi_0(R - R_B) \cdot \Phi_R . \tag{9}$$

The effective tunneling integral in this case will be written as

$$\Delta_{\text{eff}} = \int \Psi_B^* H_{\text{tunnel}}(R) \, \Psi_A \, d^3R \, d^3r_1 \, d^3r_2 \ldots , \tag{10}$$

where $H_{\text{tunnel}}(R)$ is some Hamiltonian which causes proton-tunneling from $\chi_0(R - R_A)$ to $\chi_0(R - R_B)$ or vice versa. With the use of (8) and (9) in (10), one finds that the integration over the electron coordinates gives us unity, because of the normalization of Φ_R. So, one finds that Δ_{eff} is equal to the bare tunneling integral Δ:

$$\begin{aligned} \Delta_{\text{eff}} &= \int \chi_0^*(R - R_B) \, H_{\text{tunnel}}(R) \, \chi_0(R - R_A) \, d^3R \\ &\equiv \Delta . \end{aligned} \tag{11}$$

In this case the electrons have no effect on tunneling of the proton.

4.2. Anti-Adiabatic Approximation

In this case, the two wave functions are

$$\Psi_A = \chi_0(R - R_A) \cdot \Phi_{R_A}(r_1, r_2 \ldots) , \tag{12}$$

$$\Psi_B = \chi_0(R - R_B) \cdot \Phi_{R_B}(r_1, r_2 \ldots) . \tag{13}$$

The effective tunneling integral is now written as

$$\Delta_{\text{eff}} = \Delta \int \Phi^*_{R_B} \Phi_{R_A} \, d^3r_1 \, d^3r_2 \ldots . \tag{14}$$

The overlap integral in the above expression is calculated from (6) with proper normalization as

$$1 - \sum \frac{|\bar{V}_0|^2 [1 - e^{i(k-k')\cdot(R_A - R_B)}]}{(\varepsilon' - \varepsilon)^2} + \ldots . \tag{15}$$

One finds that the second term is logarithmically divergent because of excitations with vanishing denominators. This means that the non-adiabatic effect implied by (12) and (13) is quite large.

This logarithmic divergence is replaced by a $\log T$ term at finite temperatures. A finite-temperature version of Eq. (15) is calculated as [5]

$$1 - 2|\bar{V}_0|^2 \varrho^2 \left(1 - \frac{\sin^2 k_F a}{k_F^2 a^2}\right) \log \frac{D}{kT} + \ldots , \tag{16}$$

where ϱ is the density of electron states at ε_F, a the distance between R_A and R_B, D the cut-off energy for the electron which is of the order of ε_F. This is logarithmically divergent as $T \to 0$. Calculation of higher-order terms tells us that [5]

$$\Delta_{\text{eff}} = \Delta \left(\frac{kT}{D}\right)^K , \tag{17}$$

where K is defined by

$$K = 2|\bar{V}_0|^2 \varrho^2 \left(1 - \frac{\sin^2 k_F a}{k_F^2 a^2}\right). \tag{18}$$

Since $kT/D \ll 1$ in general, the non-adiabatic effect incorporated in this anti-adiabatic scheme is large, whereas the adiabatic scheme had no effect on proton-tunneling.

The correct answer will be in between. We will see, however, that this non-adiabatic effect does exist in a correct theory. Eq. (17) is still valid only with replacement of D by $\hbar\omega_0$ as Kagan and Prokof'ev first pointed out [4].

5. Systematic Perturbation Theory for Single-Well Problem

To find a correct answer, we write the wave function for the single well problem as

$$\Psi_A = c_{00} \chi_0(R) \Phi_0 + \sum_{n\alpha} c_{n\alpha} \chi_n(R) \Phi_\alpha , \tag{19}$$

where we set $R_A = 0$ for simplicity. In the first term both the electrons and the proton are in the ground states. In the second term, both or one of them may be excited. A perturbation theory tells us that the first-order term is written as

$$-\sum \sum_{n=0}^{\infty} \frac{V_0 \int \chi_n^*(R') \chi_0(R') e^{i\kappa\cdot R'} \, d^3R'}{E_n - E_0 + \varepsilon' - \varepsilon} \chi_n(R) \Phi_{k\to k'} \tag{20}$$

with $\kappa = k - k'$, where the first summation is over k and k' with the restriction mentioned before.

We first fix k and k' and consider the n summation. We set $\varepsilon' - \varepsilon \cong Nh\omega_0$. We first consider the case where N is a large integer. Then the terms with n larger than $N(E_n - E_0 > Nh\omega_0)$ may be neglected because the denominators of those terms are large. (Here we assume harmonic functions for the proton states.) But for the terms with $n < N$, the proton energy may be neglected. Then the n summation of (20) may be approximated by

$$\sum_{n=0}^{N} \frac{V_0}{\varepsilon' - \varepsilon} \int \chi_n^*(R') \chi_0(R') e^{i\kappa \cdot R'} \, d^3R' \cdot \chi_n(R) , \tag{21}$$

We now expand the exponential as

$$e^{i\kappa\cdot R'} \cong \sum_{m=0}^{M} \frac{(i\kappa \cdot R')^m}{m!} .$$

If one takes M as an integer much larger than $\kappa \cdot R'$, the exponential can be approximated by the right hand side. Using this expansion in (21), one finds that the integral over R' will vanish for $n > m$, when χ_n's are harmonic wave functions. This fact enables us to distinguish two cases.

Case 1. $N > M$

The summation over n in (21) can be extended to ∞, because the added terms vanish. Then one can make use of the completeness theorem

$$\sum_{n=0}^{\infty} \chi_n^*(R') \chi_n(R) = \delta^3(R - R') ,$$

and find that (21) becomes

$$\frac{V_0}{\varepsilon' - \varepsilon} \chi_0(R) \sum_{m=0}^{M} \frac{(i\kappa \cdot R)^m}{m!}$$

$$\cong \frac{V_0}{\varepsilon' - \varepsilon} \chi_0(R) e^{i\kappa\cdot R} .$$

From the above derivation one sees this result is valid when

$$\frac{\varepsilon_{k'} - \varepsilon_k}{\hbar\omega_0} \gg \kappa \cdot R . \tag{22}$$

Case 2. $N < M$

In this case, among the terms with $n = 0$ to N, only the term with $n = 0$ will be important:

$$\frac{V_0 \int |\chi_0|^2 e^{i\kappa \cdot R'} \, d^3R'}{\varepsilon' - \varepsilon} \chi_0(R)$$

$$= \frac{\bar{V}_0 e^{i(k-k')\cdot R_A}}{\varepsilon' - \varepsilon} \chi_0(R) .$$

This result also applies to the case where $\varepsilon' - \varepsilon \lesssim \hbar\omega_0$.

Putting all these together, one can write the correct wave function for the single-well problem to the first-order of V as

$$\Psi_A = (\Phi^L_{R_A} + \Phi^H_R) \cdot \chi_0(R - R_A) . \tag{23}$$

where

$$\Phi^L_{R_A} = \Phi_0 - \Sigma^L \frac{\bar{V}_0 e^{i(k-k')\cdot R_A}}{\varepsilon' - \varepsilon} \Phi_{k \to k'} + \dots , \tag{24}$$

$$\Phi^H_R = - \Sigma^H \frac{V_0 e^{i(k-k')\cdot R}}{\varepsilon' - \varepsilon} \Phi_{k \to k'} + \dots . \tag{25}$$

In the low frequency part $\Phi^L_{R_A}$ the summation is over k and k' with the restriction

$$N\hbar\omega_0 > \varepsilon_{k'} - \varepsilon_k > 0 .$$

In the high frequency part Φ^H_R, the restriction is

$$\varepsilon_{k'} - \varepsilon_k > N\hbar\omega_0 .$$

N is given by

$$N = \begin{cases} 1 & \kappa \cdot R \ll 1 \\ \kappa \cdot R & \kappa \cdot R \gg 1 \end{cases} . \tag{26}$$

A typical magnitude of κ is k_F: the Fermi wave number, whereas R may be of the order of the radius of the proton wave function. Thus we see that the correct wave function is a hybrid of the adiabatic and anti-adiabatic wave functions. This was first pointed out by Kagan and Prokof'ev [4].

6. Effective Tunneling Integral

Having found a correct wave function for the single-well problem, we now consider the effective tunneling integral (10), where

$$\Psi_A = (\Phi^L_{R_A} + \Phi^H_R) \cdot \chi_0(R - R_A) , \tag{27}$$

$$\Psi_B = (\Phi^L_{R_B} + \Phi^H_R) \cdot \chi_0(R - R_B) . \tag{28}$$

The renormalization factor is solely contributed by the low frequency parts:

$$\Delta_{\text{eff}} = \Delta \int \Phi^{L*}_{R_B} \Phi^L_{R_A} \, d^3 r_1 \, d^3 r_2 \dots . \tag{29}$$

The high frequency parts follow the proton instantaneously and do not contribute to renormalization. The above overlap integral is calculated as

$$1 - \Sigma^L \frac{|\bar{V}_0|^2 [1 - e^{i(k-k')\cdot(R_A - R_B)}]}{(\varepsilon' - \varepsilon + \Delta)^2} + \dots . \tag{30}$$

Here, we have put Δ in the denominator. We note that Δ should be included in the unperturbed energy, because we are doing perturbation expansion in terms of V.

We note that the integration over R in (10) is mainly contributed from the region where $\chi_0(R - R_A)$ and $\chi_0(R - R_B)$ overlap. In this region $|R - R_A| \cong a/2$, where a is the jump distance. Then (26) may be replaced by

$$N = \begin{cases} 1 & k_F a/2 \ll 1 \\ k_F a/2 & k_F a/2 \gg 1 \end{cases} . \tag{31}$$

Since $k_F a$ is usually larger than unity (~ 3.5 for Cu metal), we take the second case of (31). The restriction L in (30) is now expressed by [6]

$$(k_F a/2)\hbar\omega_0 > \varepsilon_{k'} - \varepsilon_k > 0 , \tag{32}$$

so the cut-off B is now defined by

$$B = (k_F a/2)\hbar\omega_0 . \tag{33}$$

With the cut-off thus defined, we find that (30) is calculated as

$$1 - K \log \frac{B}{\Delta} + \dots = \left(\frac{\Delta}{B}\right)^K .$$

Finally we have

$$\Delta_{\text{eff}} = \Delta \cdot \left(\frac{\Delta}{B}\right)^K . \tag{34}$$

Now I will explain what (34) implies. When the proton is in the left well, the electrons are pushed to it and an electron cloud will be formed around it. When it tunnels to the right well, the electron wave function must be rearranged so as to correspond to the new proton position. Excitations with energy larger than B can follow the proton instantaneously, so they do not contribute to the non-adiabatic effect. Now the proton goes back to the left well within a time $\sim \hbar/\Delta$. So excitations with energy less than Δ do not have enough time to rearrange the wave function, so they do not contribute to the non-adiabatic effect either. Only those excitations with energy between Δ and B contribute to it. This is what (34) implies.

I will mention two corrections to (34). The first is self-consistency correction due to Yamada et al. [7]. Actually the proton goes back to the original site within a time $\sim \hbar/\Delta_{\text{eff}}$, because Δ_{eff} represents the real speed of tunneling. So we must have

$$\Delta_{\text{eff}} = \Delta \cdot \left(\frac{\Delta_{\text{eff}}}{B}\right)^K$$

instead of (34). Solving this equation for Δ_{eff}, one has

$$\Delta_{\text{eff}} = \bar{\Delta} \equiv \Delta \cdot \left(\frac{\Delta}{B}\right)^{\frac{K}{1-K}} , \tag{35}$$

where $\bar{\Delta}$ is the characteristic energy of our problem. A sum rule tells us that $K < 1/2$ for a singly charged particle in metals [8]. Thus there is no possibility of self-trapping in this case.

The second correction is due to a finite temperature. The above result is for the ground state or for $kT \ll \bar{\Delta}$. When $B \gg kT \gg \bar{\Delta}$, excitations with energy up to kT are not like those of a degenerate Fermi system, and so do not contribute to the non-adiabatic effect. Thus the low-frequency cut-off must be kT:

$$\Delta_{\text{eff}} = \Delta \cdot \left(\frac{kT}{B}\right)^K \qquad B \gg kT \gg \bar{\Delta}. \tag{36}$$

Our main result is this power law of the effective tunneling integral.

7. Connection with Experiments

I will discuss the possibility of observing this power law. For this purpose the temperature range defined by the inequality in (36) must be experimentally accessible. For the proton $\hbar\omega_0$ is about 1000 K and B is of the same order, still $\bar{\Delta}$ may be as small as less than 10 K. In this case the above criterion is satisfied. This is also the case for the positive muon and the other isotopes of the proton. For the positron, on the other hand, both $\hbar\omega_0$ and $\bar{\Delta}$ may be more than electron volts. For heavier atoms, on the contrary, $\hbar\omega_0$ may be less than 1 K and $\bar{\Delta}$ may be much smaller. In this sense the proton and its isotopes are peculier.

Up to this point I have considered the effective tunneling integral, which gives the level splitting. The non-adiabatic effect involved in it is a manifestation of infrared divergence associated with metal electrons. If the effect of the electrons is only to renormalize the tunneling integral, the proton energy level would have a vanishing width. Actually the electrons cause dissipation and give rise to the level broadening. The mechanism of the broadening is essentially equal to that of the Korringa relaxation. It is shown that the broadening is given by [9]

$$\Gamma = \pi K k T. \tag{37}$$

When $\Gamma \ll \Delta_{\text{eff}}$, the proton will go back and forth many times between the two sites before the motion is damped (coherent case). When $\Gamma \gg \Delta_{\text{eff}}$, the proton will sit in a site for a long time before it tunnels to the other site (overdamped case). The cross-over occurs when $\Gamma = \Delta_{\text{eff}}$. The cross-over temperature is given by

$$kT_c \approx \bar{\Delta}, \tag{38}$$

with the assumption $\pi K \sim 1$.

In the overdamped case ($kT > \bar{\Delta}$), the jump rate to the neighbouring site is given by

$$W = \frac{\Delta_{\text{eff}}^2}{\Gamma}, \tag{39}$$

which is proportional to T^{2K-1}. Such a power law of the diffusion constant was observed for the positive muon in Cu and Al [10]. A cross-over from the overdamped to coherent case was observed for the proton in the $Nb-O_x$ system, as the temperature is lowered from 10 K to 1 K [11].

In conclusion we have shown that tunneling of light particles in metals is influenced by the metal electrons very much. This is due to the fact that excitations of the electrons in metals can have an arbitrarily small energy.

References

[1] See for example, J. Kondo, in: Fermi Surface Effects, eds. J. Kondo and A. Yoshimori, Springer Series in Solid-State Sciences 77, p. 1, Springer 1987.
[2] Y. Fukai and H. Sugimoto, Adv. Phys. *34*, 263 (1985).
[3] J. Kondo, Physica *124B*, 25 (1984).
[4] Yu. Kagan and N. V. Prokof'ev, Sov. Phys.-J.E.T.P. *63*, 1276 (1986).
[5] J. Kondo, Physica *84B*, 40 (1976).
[6] J. Kondo, J. Phys. Soc. Jpn. *56*, 1638 (1987).
[7] K. Yamada, A. Sakurai, and M. Takeshige, Progr. Theor. Phys. *70*, 73 (1983).
[8] K. Yamada, A. Sakurai, and S. Miyazima, Progr. Theor. Phys. *73*, 1342 (1985).
[9] J. Kondo, Physica *125B*, 279 (1984); ibid. *126B*, 377 (1984).
[10] R. Kadono, T. Matsuzaki, K. Nagamine, T. Yamazaki, D. Richter, and J.-M. Welter, Hyperfine Interactions *31*, 205 (1986); J. H. Brewer, M. Celio, D. R. Harshman, R. Keitel, S. R. Kreitzman, G. M. Luke, D. R. Noakes, R. E. Turner, E. J. Ansaldo, C. W. Clawson, K. M. Crowe, and C. Y. Huang, Hyperfine Interactions *31*, 191 (1986); O. Hartmann, E. Karlsson, E. Wäcklegard, R. Wäppling, D. Richter, R. Hempelmann, and T. O. Niinikoski, Phys. Rev. B *37*, 4425 (1988).
[11] H. Wipf, D. Steinbinder, K. Neumaier, P. Gutsmiedl, A. Margerl, and A. J. Dianoux, Europhys. Lett. *4*, 1379 (1987).

Presented at the Discussion Meeting of the Deutsche Bunsen-Gesellschaft für Physikalische Chemie "Rate Processes in Dissipative Systems: 50 Years after Kramers" in Tutzing, September 10–13, 1990

E 7528

Quantum Coherence in Rate Processes

Ulrich Weiss and Maura Sassetti*)

Institut für Theoretische Physik, Universität Stuttgart, D-7000 Stuttgart 80, Germany

Correlation Functions / Neutron Scattering / Nonequilibrium Phenomena / Quantum Dissipation / Statistical Mechanics

The quantum dissipative dynamics of a particle which tunnels through the barrier of a double well potential and is coupled to an Ohmic heat bath is studied. Exact formal expressions for correlation functions are presented and examined. Attention is focused on the region in which coherence effects are important, and on the algebraic long-time tails at zero temperature. Coherence effects in the dissipative quantum transport of a particle in a tight-binding lattice are also investigated.

1. Introduction

The decay of metastable state is a very common phenomenon and plays a central role in physical and chemical sciences. At high temperatures the decay is thermally activated, and the rate of classical escape over the potential barrier follows the Arrhenius law [1]. As the temperature is lowered, thermal fluctuations die out exponentially fast so that at very low temperatures the metastable state can only decay via quantum tunneling. In recent years, it has become clear both on the experimental and theoretical side that quantum tunneling is strongly affected by the frictional influence of the environment, this being the impetus behind the intense increase in activity in this field. Dissipation was found to cause novel features such as dissipative phase transitions [2], exponential suppression of tunneling rates at zero temperatures [3], and qualitative change of their behavior at finite temperatures [4]. The theoretical predictions for the temperature and damping dependence of tunneling rates in macroscopic quantum tunneling (MQT) have been verified precisely, e.g., in experiments on the decay of the zero-voltage state of a Josephson junction [5].

It has been pointed out by Kondo that the dynamics of tunneling systems in metals are strongly affected by the interaction with conduction electrons [6]. The nonadiabatic effect of the electronic screening cloud causes anomalous temperature dependence, such as the increase of the diffusion coefficient with decreasing temperature, a behavior first observed for muon diffusion in aluminum and copper. In this region, the defect tunnels incoherently to a neighboring site. As the temperature is decreased quantum coherence between many sites becomes increasingly important. The defect becomes delocalized with a wave function extending over several interstitial sites. In this contribution we focus our attention to the transition from incoherent to coherent tunneling in the presence of a fermionic environment.

The simplest situation for quantum coherence is the delocalization of a particle in a double well potential. At sufficiently low temperatures, excitations in the two wells can be neglected, and the double well can be truncated to a two-state system formed by two energetically split tunneling eigenstates. In the following we provide a unified view of the two-state dynamics under the influence of conduction electrons. Special attention is given to the crossover from incoherent to coherent tunneling and to the behavior at very low temperatures where the presence or absence of system-bath correlations in the initial state gives qualitative differences in the evolution of the system at long times. The equilibrium correlation function shows algebraic long-time tails at zero temperature, and the system approaches thermal equilibrium always faster for a factorizing initial state. Correspondingly, the spectral properties of the system at low frequencies are qualitatively influenced by correlations in the initial state. The important influence of conduction electrons on defect tunneling has been verified in neutron-spectroscopy experiments on hydrogen trapped by oxygen in niobium [7]. We also consider the crossover from incoherent to coherent quantum transport of light interstitials in a one-dimensional tight-binding lattice in the presence of conduction electrons.

The functional integral method provides a unified approach to the dynamics of two-state and multi-state systems in the presence of dissipative influences. In Section 2 we briefly review this method and present exact formal expressions for the two-state system. Section 3 is devoted to the discussion of the dynamics both in the region of incoherence and coherence. In Section 4 we study coherence effects in the quantum transport of a particle in a multi-state system.

2. Exact Formal Expressions For The Two-state Dynamics

We consider a quantum particle interacting with conduction electrons and tunneling in a double well with bias energy $\hbar\varepsilon$ and with tunneling matrix element $\hbar\Delta_0$. We consider the case where the characteristic energy scales of the problem are such that

$$V_0 \gg \hbar\omega_0 \gg \hbar\Delta_0, \hbar\varepsilon, k_B T. \tag{2.1}$$

Here, V_0 is the barrier height and $\hbar\omega_0$ is the energy of excitation in a single well. The dynamics of the isolated system is then simply described by the pseudospin Hamiltonian

$$H_0 = -\frac{\hbar}{2}(\Delta_0\sigma_x + \varepsilon\sigma_z), \tag{2.2}$$

where the σ's are the Pauli matrices.

*) On leave from Dipertimento di Fisica, CISM, Università di Genova, Italy.

 © VCH Verlagsgesellschaft mbH, W-6940 Weinheim, 1991 0005-9021/91/0303-0427 $ 3.50+.25/0

In the temperature region of interest the influence of the conduction electrons is governed by gross features such as the density of low energy excitations off the Fermi surface. The fermionic bath can be mapped onto a bosonic bath with an appropriately chosen spectral density of the coupling strength. The simpler spin-boson Hamiltonian is

$$H = H_0 + \sum_l \left[\frac{p_l^2}{2m_l} + \frac{1}{2} m_l \omega_l^2 x_l^2 - \frac{1}{2} c_l x_l q_0 \sigma_z \right], \quad (2.3)$$

where the parameter q_0 represents the distance between the two wells of the original problem. The effects of the bosons are in the spectral function [8]

$$J(\omega) = \frac{\pi}{2} \sum_l \frac{c_l^2}{m_l \omega_l} \delta(\omega - \omega_l), \quad (2.4)$$

and the equivalence with a fermionic bath holds for the specific form

$$J(\omega) = \eta \omega \, e^{-\omega/\omega_c} = (2\pi\hbar K/q_0^2)\omega \, e^{-\omega/\omega_c}, \quad (2.5)$$

where we have chosen an exponential cut-off. The spectral density (2.5) is known to cause Ohmic dissipation in the classical limit [3]. Here, η is the phenomenological friction coefficient, while K is a characteristic dimensionless damping strength introduced by Kondo [6]. The parameter K is identical to the parameter α introduced by Leggett et al. [8]. The cut-off frequency of the fermions is of the order of the Fermi energy $\varepsilon_F \gg \hbar\omega_0$. However, since we have truncated here the original potential problem to a two-state problem, the spectral density of the environment is effectively cut off at a frequency ω_c which is of the order of ω_0 [8,9]. The high-frequency modes ($\omega > \omega_c$) affect the tunneling process only by a dressing factor [8]. In the following, Δ denotes the matrix element renormalized by this factor. The damping strength K can be expressed in terms of the original parameters characterizing the Fermi bath and the coupling [10]. There follows from a sum rule that K is restricted to the range $0 \leq K \leq 1/2$.

The dynamic quantities of interest are the functions ($\beta = 1/k_B T$)

$$P(t) = \langle \sigma_z(t) \rangle, \quad (2.6)$$
$$C(t) = \frac{1}{2} \langle \sigma_z(t)\sigma_z(0) + \sigma_z(0)\sigma_z(t) \rangle_\beta .$$

The function $P(t)$ describes the expectation value of σ_z at time $t > 0$ supposing that at all times $t < 0$ the system has been held in (say) the state $\sigma_z = +1$, and the environment is assumed to have come into thermal equilibrium with it. The system is let go at $t = 0$, and the system plus environment is allowed to evolve according to the full Hamiltonian (2.3). The conditional expectation value $P(t)$ is the relevant quantity in the macroscopic quantum coherence (MQC) problem. The exact formal solution for $P(t)$ based on the Feynman-Vernon influence functional method [11] has been given Refs. [12] and [8]. The other dynamical quantity is the symmetrized thermal equilibrium correlation function. The Fourier transform of $C(t)$ is directly related to the dynamic structure factor for neutron scattering [13,14]. Within the real-time path integral approach the exact formal solution of $C(t)$ has been discussed in Ref. [15]. Let us briefly sketch the derivation. The functions $C(t)$ and $P(t)$ are related to the joint probability $P(\sigma,t;\sigma,0;\sigma',t_0)$ according to

$$C(t) = \lim_{t_0 \to -\infty} \sum_{\sigma = \pm 1} [P(\sigma,t;\sigma,0;\sigma,t_0) + P(-\sigma,t;-\sigma,0;\sigma,t_0)] - 1, \quad (2.7)$$
$$P(t) = 2 \lim_{t_0 \to -\infty} P(+1,t;\sigma = +1, t_0 \leq \tau \leq 0) - 1,$$

where in the latter relation the system is constrained to the state $\sigma = +1$ of σ_z for negative times τ in the region $t_0 \leq \tau \leq 0$. As the heat bath modes are represented by Gaussian integrals in the functional integral approach, they can be evaluated exactly. One finds that the environmental influences are described by a complex interaction $S(\tau) + iR(\tau)$ between each pair of tunneling transitions. The pair potential depends on the spectral density and on temperature through the relations

$$S(\tau) = \frac{q_0^2}{\pi\hbar} \int_0^\infty d\omega \frac{J(\omega)}{\omega^2} (1 - \cos\omega\tau) \coth\left(\frac{\hbar\beta\omega}{2}\right),$$
$$R(\tau) = \frac{q_0^2}{\pi\hbar} \int_0^\infty d\omega \frac{J(\omega)}{\omega^2} \sin\omega\tau, \quad (2.8)$$

which for the special choice (2.5) and for $\omega_c\tau \gg 1$ assume the form

$$S(\tau) + iR(\tau) = K\left[2\ln\left[\frac{\hbar\beta\omega_c}{\pi} \sinh\left(\frac{\pi\tau}{\hbar\beta}\right)\right] + i\pi \right]. \quad (2.9)$$

The equivalence of the bosonic bath with the special choice (2.5) with a fermionic bath follows from the fact that the influence of conduction electrons indeed leads to a pair interaction of the form (2.9). (See, e.g., Ref. [6]).

Following Ref. [8] it is convenient to formulate the expression for the joint probability in terms of a single path integral over the four states of the reduced density matrix. The periods $t_{2j} < \tau < t_{2j+1}$, in which the system is in a diagonal state, are called *sojourns*, and the periods $t_{2j-1} < \tau < t_{2j}$, in which the system is in a nondiagonal state, are called *blips*. There are two kinds of sojourns, and the j'th sojourn will be labelled by $\chi_j = +1$ ($\chi_j = -1$) if the system is in the $RR(LL)$ diagonal state. Similarly, there are two kinds of blips, and we shall assign the label $\xi_j = +1$ ($\xi_j = -1$) to the j'th blip, if the system is in the nondiagonal state $RL(LR)$. For later convenience we introduce the blip lengths $\tau_j = t_{2j} - t_{2j-1}$ and sojourn lengths $s_j = t_{2j+1} - t_{2j}$.

It is straightforward to write down the various factors constituting the path integral expression. The amplitude per unit time to switch from a diagonal to a nondiagonal state

(or vice versa) is $\pm i\Delta/2$. The amplitude to stay in a sojourn is unity, while the amplitude to stay in the j'th blip with label ξ_j and length τ_j is $\exp(i\varepsilon\xi_j\tau_j)$. It is convenient to include this factor into the phase of the influence functional. If we define:

$$\begin{aligned} S_{jk} &= \tilde{S}(t_j - t_k)\,; \\ \Lambda_{jk} &= S_{2j,2k-1} + S_{2j-1,2k} - S_{2j,2k} - S_{2j-1,2k-1}\,, \end{aligned} \tag{2.10}$$

the influence functional for n blips at negative times and m blips at positive times (modified by the bias factors) may be written $F_{m,n} = G_{m,n} H_{m,n}$, where

$$\begin{aligned} G_{m,n} &= \exp\left\{ -\sum_{j=1}^{m+n} S_{2j,2j-1} - \sum_{j=2}^{m+n} \sum_{k=1}^{j-1} \xi_j \xi_k \Lambda_{jk} \right\}, \\ H_{m,n} &= \exp\left\{ i \sum_{j=1}^{m+n} \xi_j [\varepsilon\tau_j + \pi K \chi_{j-1}] \right\}. \end{aligned} \tag{2.11}$$

It is obvious from (2.11) with (2.10) that the blips may be viewed as neutral pairs of *charges* ± 1 (dipoles). The term Λ_{jk} represents the interaction energy of two blips, and because it is multiplit by the factor $\xi_j \xi_k$ in (2.11) blips can both attract and repel one another. For the time ordered integrations over the flip times t_j we introduce the compact notation

$$\int_{t_0}^{t} D_{m,n}\{t_j\} \equiv \int_0^t \mathrm{d}t_{2n+2m} \cdots \int_0^{t_{2n+2}} \mathrm{d}t_{2n+1} \int_{t_0}^{0} \mathrm{d}t_{2n} \cdots \int_{t_0}^{t_2} \mathrm{d}t_1 \,. \tag{2.12}$$

Summing over all possible arrangements of blips and sojourns we find for the joint probability the expression

$$\begin{aligned} P(\sigma,t;\sigma,0;\sigma',t_0) = \sum_{m=0}^{\infty} \sum_{n=0}^{\infty} \left(-\frac{\Delta^2}{4}\right)^{m+n} \\ \cdot \int_{t_0}^{t} D_{m,n}\{t_j\} \sum_{\{\xi_j\}} G_{m,n} \sum_{\{\chi_j\}''} H_{m,n} \,. \end{aligned} \tag{2.13}$$

The sum over arrangements $\{\xi_j\}$ and $\{\chi_j\}$ extends over the possible values ± 1 of the ξ_j and χ_j, $(j = 1,2,\ldots,m+n)$. The double prime in $\{\chi_j\}''$ is to indicate the constraint $\chi_0 = \sigma'$, $\chi_n = \chi_{m+n} = \sigma$. Next, the χ_j-sum in (2.13) can be carried out straightforwardly. In the end we find from (2.7) with (2.13) the result

$$\begin{aligned} P(t) &= P_s(t) + P_-(t)\,, \\ C(t) &= P_s(t) + Q(t)\,, \end{aligned} \tag{2.14}$$

where $P_s(t) = 1 + P_+(t)$ and

$$P_\pm(t) = \sum_{m=1}^{\infty} \int_0^t D_{m,0}\{t_j\} \sum_{\{\xi_j\}} A_m^{(\pm)} G_{m,0}\,, \tag{2.15}$$

$$\begin{aligned} Q(t) = -\lim_{t_0 \to -\infty} \sum_{m=1}^{\infty} \sum_{n=1}^{\infty} (\tan(\pi K))^2 \\ \cdot \int_{t_0}^{t} D_{m,n}\{t_j\} \sum_{\{\xi_j\}} \xi_1 \xi_{n+1} A_{m+n}^{(+)} G_{m,n}\,, \end{aligned} \tag{2.16}$$

with

$$\begin{aligned} A_m^{(+)} &= \left(\frac{-\Delta^2 \cos\pi K}{2}\right)^m \cos\left(\varepsilon \sum_{j=1}^{m} \xi_j \tau_j\right), \\ A_m^{(-)} &= \left(\frac{-\Delta^2 \cos\pi K}{2}\right)^m \sin\left(\varepsilon \sum_{j=1}^{m} \xi_j \tau_j\right). \end{aligned} \tag{2.17}$$

The expressions (2.14)–(2.16) represent the exact formal solution in the form of a series in Δ^2 for $P(t)$ and $C(t)$. The function $P_s(t)$ ($P_-(t)$) is the symmetric (antisymmetric) contribution of $P(t)$ under the inversion of the bias $\varepsilon \to -\varepsilon$.

The assumption of a factorizing system-bath initial condition at $t = 0$ corresponds to the neglect of interactions between the positive and negative time parts in (2.16). In this approximation we have $C(t) = C^{(0)}(t)$, where

$$C^{(0)}(t) = P_s(t) + P_\infty P_-(t)\,, \tag{2.18}$$

and where $P_\infty = P_-(t \to \infty)$ is the equilibrium value of $P(t)$. Hence in this approximation $C(t)$ is completely determined by the components of $P(t)$.

In recent theoretical studies [13, 14, 16] the structure factor for neutron scattering has been calculated from the Fourier transform of $C^{(0)}(t)$. Below it will be discussed that the low-frequency behavior of the structure factor is modified drastically at low temperatures, when system-bath correlations in the initial state are taken into account. Correspondingly, the long-time behavior of $C(t)$ at $T = 0$ changes qualitatively in the presence of the correlations in the initial state.

3. Dynamic Properties

Despite its formidable appearance, the above formal expressions for $P(t)$ and $C(t)$ can be summed in certain limits by analytic methods. This is the subject of this Section. It is important to note that much progress has been made also very recently in the numerical path integral simulation of similar expressions by Monte Carlo methods in conjunction with a stationary phase filtering method [17].

3.1. Noninteracting-blip Approximation

When the interblip correlations Λ_{jk} are neglected, the terms of the series (2.15) and (2.16) are in the form of a convolution and the Laplace transforms $\tilde{P}(\lambda)$ and $\tilde{C}(\lambda)$ can be summed to [12, 18, 8, 19]

$$\begin{aligned} \tilde{P}(\lambda) &= \tilde{P}_s(\lambda) + \tilde{P}_-(\lambda)\,, \\ \tilde{C}(\lambda) &= \tilde{P}_s(\lambda) + \tilde{P}_\infty \tilde{P}_-(\lambda)\,, \end{aligned} \tag{3.1}$$

where $P_\infty = \tanh(h\beta\varepsilon/2)$, and

$$\begin{aligned} \tilde{P}_s(\lambda) &= \frac{1}{\lambda + [\Sigma(\lambda_+) + \Sigma(\lambda_-)]/2}\,, \\ \tilde{P}_-(\lambda) &= -\tan(\pi K)\,[\Sigma(\lambda_+) - \Sigma(\lambda_-)]\,\tilde{P}_s(\lambda)/(2i\lambda)\,. \end{aligned} \tag{3.2}$$

Here, $\lambda_\pm = \lambda \pm i\varepsilon$. The self-energy $\Sigma(\lambda)$ is given by the expression

$$\Sigma(\lambda) = \Delta_c \left(\frac{\hbar\beta\Delta_c}{2\pi}\right)^{1-2K} \frac{1}{K+\hbar\beta\lambda/2\pi}\, g(\lambda), \tag{3.3}$$

where $g(\lambda) = \Gamma(1+K+\hbar\beta\lambda/2\pi)/\Gamma(1-K+\hbar\beta\lambda/2\pi)$ and where $\Gamma(z)$ is the gamma function. Here, we have introduced the effective zero temperature tunneling splitting [12]

$$\Delta_c = \Delta \left(\frac{\Delta}{\omega_c}\right)^{K/(1-K)} [\cos(\pi K)\Gamma(1-2K)]^{1/(2-2K)}. \tag{3.4}$$

The behavior of $P(t)$ based on these expressions has been studied in Refs. [12], [18], [8], and [19]. The corresponding properties of the neutron scattering function

$$j(\omega) = \mathrm{Re}\tilde{C}(\lambda = i\omega) \tag{3.5}$$

are discussed in Refs. [13], [14] and [16].

Let us examine the self-consistency of the noninteracting-blip approximation (NIBA). It is obvious that for fairly high temperatures the pair interaction $S(\tau)$ in (2.9) may be approximated by

$$S(\tau) = 2K \ln(\hbar\beta\omega_c/2\pi) + 2\pi K\tau/\hbar\beta. \tag{3.6}$$

With this choice the interblip interactions Λ_{jk} cancel out, and we end up with the expressions (3.1) with (3.2) where the self-energy $\Sigma(\lambda)$ is in the form (3.3) with the factor $g(\lambda) = g(\lambda = 0)$. Thus, the self-consistency condition of the NIBA is $\hbar\beta|\lambda_\pm| \ll 2\pi$, which in the relevant frequency range corresponds to temperatures $T > T_0$, where $k_B T_0 = \hbar(\Delta_c^2 + \varepsilon^2)^{1/2}$. In the limit $g(\lambda) \to g(\lambda = 0)$, the functions $\tilde{P}(\lambda)$ and $\tilde{C}(\lambda)$ have apart from a *static* pole at $\lambda = 0$ three *dynamic* poles determined by a cubic equation with real coefficients. The trajectories of these poles and the corresponding behavior of $P(t)$ have been discussed in Ref. [19].

For a symmetric system ($\varepsilon = 0$), the functions $P(t)$ and $C(t)$ are the same in the NIBA, and, for $k_B T > \hbar\Delta_c$, the Laplace transform $\tilde{P}(\lambda)$ has two poles which are determined by a quadratic equation, as follows from (3.2) with (3.3) and $g(\lambda) \to g(\lambda = 0)$. For $K < 1/2$ the poles are complex conjugate to each other for $T < T^*(K)$, and real for $T > T^*(K)$. The crossover temperature $T^*(K)$ separates the coherence region in which the system shows damped oscillations from incoherence. The corresponding phase diagram has been discussed in Refs. [20, 19, 8]. A slightly different definition of the phase separation line, namely that the scattering function $j(\omega)$ is double peaked below $T^*(K)$ and single peaked above $T^*(K)$ has been considered in Ref. [13]. For the limiting value $K = 1/2$ one finds $T^* = \hbar\Delta_c/(k_B\pi)$, while for $K \ll 1$ there holds $T^* = \hbar\Delta_c/(Kk_B\pi)$. At temperatures $T \gg T^*(K)$ one finds incoherent relaxation $P(t) = \exp(-\gamma t)$ with a rate

$$\gamma = \Delta_c \frac{\Gamma(K)}{\Gamma(1-K)} \left(\frac{2\pi k_B T}{\hbar\Delta_c}\right)^{2K-1} = \frac{\sqrt{\pi}}{2} \frac{\Gamma(K)}{\Gamma(K+1/2)} \left(\frac{\pi k_B T}{\hbar\omega_c}\right)^{2K-1} \frac{\Delta^2}{\omega_c}, \tag{3.7}$$

which for $K < 1/2$ increases with decreasing temperature. The high temperature behavior T^{2K-1} was discussed first by Kondo [21, 6].

3.2. Weak Damping Case

The case $K \ll 1$ is especially interesting, since for defect tunneling in metals K was found to be very small, namely near $K = 0.05$ [7]. Since the blips can both attract and repel one another, one finds that for a *symmetric* system ($\varepsilon = 0$), the effect of the interblip interactions is of order K^2, while the intrablip interactions give nontrivial effects of order K. Hence, the NIBA is a systematic weak-coupling approximation for a *symmetric* system down to $T = 0$ (except for extremely long times, as discussed below). For *asymmetric* two-state systems the effect of the interblip interactions contributes to the order K at temperatures $T < T_0$, so that the NIBA is inadequate in this case. A systematic study of the effect of the interblip correlations in linear order in K is given in Ref. [16]. In the remainder of this Section we restrict our attention to the symmetric case ($\varepsilon = 0$).

In the region $T < T^*(K)$ the system shows damped oscillations with frequency Ω and damping rate γ. At very low temperatures, $T \ll T^*(K)$, they are given by

$$\Omega(T) = \hbar\Delta_c\{1 + K[\mathrm{Re}\psi(i\hbar\Delta_c/2\pi k_B T) - \ln(\hbar\Delta_c/2\pi k_B T)]\}, \tag{3.8}$$

$$\gamma(T) = (\pi K/2)\hbar\Delta_c \coth(\hbar\Delta_c/2k_B T),$$

where $\psi(z)$ is the digamma function. Correspondingly, the scattering function has two Lorentzians centered at $\omega = \pm\Omega(T)$ with linewidth $2\gamma(T)$.

At temperatures in the range $T_0 \ll T \ll T^*$ the formulas (3.8) smoothly map onto the solutions of the quadratic equation discussed above. Near $T = T^*$ the two Lorentzians merge into another, while at temperature $T \gg T^*$ there is only a single quasielastic peak centered at $\omega = 0$ with linewidth $2\gamma(T)$ where γ is given by (3.7).

3.3. Long-time Behavior of $P(t)$ and $C(t)$

The NIBA gives the asymptotic behavior both of $P(t)$ and $C(t)$ qualitatively wrong at low temperatures. In the absence of a bias the functions $P(t)$ and $C^{(n)}(t)$ are the same, and within the NIBA at $T = 0$, they are given in terms of a Mittag-Leffler function [18], which decays asymptotically with the power law $t^{-2(1-K)}$. The asymptotic behavior of $P(t)$ and of $C(t)$ is changed qualitatively by the interblip correlations. Regarding $P(t)$, the quantitative calculation of the effect of the interblip interactions is very difficult since all frequency scales are coupled together, as is well-known

from the Kondo problem. In the first step, the correlations lead to irreducible sojourns which are effectively narrow. In the next step an irreducible blip which has inside an arbitrary number of irreducible sojourns is considered. By iterating this procedure we then go to longer and longer time scales. In the end we find that $\tilde{P}(\lambda)$ is regular at the origin [22]. Hence, $P(t)$ shows in fact at $T=0$ not algebraic, but exponential decay, as $t\to\infty$.

On the other hand, the equilibrium correlation function decays algebraically at zero temperature. The algebraic long-time tails of $C(t)$ arise from the correlations between the positive and negative time parts in the function $G^{(0)}_{m,n} = G_{m,n}(T=0)$ defined in (2.11). As $t\to\infty$, the leading contribution under the integral in (2.16) is

$$A^{(+)}_{m+n} G_{m,n} \approx G^{(0)}_m G^{(0)}_n A^{(+)}_m A^{(+)}_n \cdot\left(1 - \sum_{j=1}^{n} \sum_{k=n+1}^{m+m} \xi_j \xi_k \tau_j \tau_k \ddot{S}_0(t)\right), \tag{3.9}$$

where $S_0(t) = 2K\ln(\omega_c t)$ and where $G^{(0)}_m A^{(+)}_m$ and $G^{(0)}_n A^{(+)}_n$ are the interaction factors at zero temperature in the positive and negative time parts, respectively. With the use of (3.9) one finds in the end

$$C(t) = (2\hbar\chi_0)^2 \ddot{S}_0(t), \tag{3.10}$$

where we have identified $(\partial P_\infty/\partial\hbar\varepsilon)|_{\varepsilon=0}$ with twice the static susceptibility χ_0 at $T=0$.

Inserting the above zero temperature expression $S_0(t)$ for the pair interaction we finally get the algebraic long time behavior [23]

$$C(t\to\infty) = -2K(2\hbar\chi_0)^2 \frac{1}{t^2}. \tag{3.11}$$

The behavior (3.11) is exact for $K<1$. From (3.11) we may also infer the behavior in frequency space near $\omega=0$. We find for the scattering function (3.5)

$$j(\omega\to 0) = 2\pi K(2\hbar\chi_0)^2|\omega|. \tag{3.12}$$

This relation is analogous to a relation that has been proven by Shiba [24] for the general Anderson model. It is interesting to note that the formula (3.12) holds also in the presence of a bias, if we identify χ_0 with the nonlinear susceptibility at zero temperature.

We conclude this Section with the remark that recently the functions $C(t)$ and $P(t)$ have been determined exactly in the entire (t,ε,T)-parameter space for the special value $K = 1/2$ [15].

4. Quantum Coherence in the Dissipative Multi-state System

In this Section we deal with coherence effects in the quantum transport of a particle in a onedimensional tight-binding lattice with spacing q_0. This may be looked upon as a somewhat crude model for diffusion of interstitials like positive muons or protons in metals [25], and for the dynamics of the phase of a resistively shunted single Josephson junction in the extreme quantum limit [26,27]. The diagonal elements of the reduced density matrix are the occupation probabilities $P_n(t)$ of the n'th well with the initial condition $P_n(t=0) = \delta_{n,0}$. In the tight binding limit each transition between system states is associated with an amplitude $\pm i\Delta/2$ per unit time. We shall assume that the environmental coupling is of the form (2.3)–(2.5) so that the complex interaction between any pair of transitions is again given by (2.9). An exact formal expression for $P_n(t)$ which is in the form of a power series in Δ^2 has been derived in Ref. [28]. It may be written in the form

$$P_n(t) = \sum_{m=|n|} (-1)^{m-n} (\Delta/2)^{2m} \cdot \int_0^t D_{m,0}\{t_j\} \sum_{\{\xi_j\}}{}' G_m \sum_{\{\chi_j\}}{}' H_m, \tag{4.1}$$

where

$$G_m = \exp\left[\sum_{j=2}^{2m}\sum_{l=1}^{j-1} \xi_j\xi_l S(t_j - t_l) - i\varepsilon \sum_{j=2}^{2m} \xi_j t_j\right],$$
$$H_m = \exp\left[i\pi K \sum_{k=1}^{2m-1} \chi_k \sum_{j=k+1}^{2m} \xi_j\right]. \tag{4.2}$$

The sum over arrangements $\{\xi_j\}$ and $\{\chi_j\}$ extends over the possible values ± 1 of the ξ_j and $\chi_j (j = 1,2,\ldots,2m)$, and the prime denotes that each arrangement obeys the constraints

$$\sum_{j=1}^{2m} \chi_j = 2n, \quad \sum_{j=1}^{2m} \xi_j = 0. \tag{4.3}$$

Further, $\hbar\varepsilon$ is the potential drop between neighboring wells provided by the external force $F = \hbar\varepsilon/q_0$. It is convenient to introduce the generating functional

$$Z(\lambda,t) = \sum_{n=-\infty}^{+\infty} e^{\lambda q_0 n} P_n(t). \tag{4.4}$$

Now, the $\{\chi_j\}'$-sum can be done explicitly, and moments $\langle q^N(t)\rangle$ of $P_n(t)$ are obtained by differentiating N times the function $Z(\lambda,t)$ with respect to λ at $\lambda=0$. One then finds

$$\langle q^N(t)\rangle = q_0^N \sum_{m=1}^{\infty} (-1)^{m-1} \Delta^{2m} \cdot \int_0^t D_{m,0}\{t_j\} \sum_{\{\xi_j\}}{}' a^{(N)}_m G_m. \tag{4.5}$$

The coefficients of the first and second moment are

$$a^{(1)}_m = \frac{i}{2} \prod_{j=1}^{2m-1} \sin(\pi K g_{j,m}),$$
$$a^{(2)}_m = \frac{1}{2} \sum_{l=1}^{2m-1} \cos(\pi K g_{l\,m}) \prod_{j=1,\, j\neq l}^{2m-1} \sin(\pi K g_{j\,m}), \tag{4.6}$$

where we have introduced the off-diagonal measure

$$g_{j,m} = -\sum_{l=1}^{j} \xi_l = \sum_{l=j+1}^{2m} \xi_l . \tag{4.7}$$

Eq. (4.5) is the exact formal expression for the time evolution of a particle in a tilted tight-binding lattice in the presence of Ohmic dissipation.

At high temperatures, the particle tunnels incoherently from well to well. This particular case of the dynamics can be described by master equations for the probabilities $P_n(t)$ [29, 30]. It is the case, where the density matrix after each pair of transitions is again in a diagonal state. In the above it formally corresponds to restricting the sum over paths by the condition $|g_{j,m}| \leq 1$ for all j and m. In this limit the nonlinear mobility

$$\mu = \lim_{t\to\infty} \langle q(t)\rangle / Ft \tag{4.8}$$

is found to be $\mu = \tanh(\hbar\beta\varepsilon/2) q_0^2 \gamma/\hbar\varepsilon$ where γ is the rate of incoherent relaxation in the biased two-state system [18]. The linear mobility μ_l is related to the diffusion coefficient

$$D = \lim_{t\to\infty} \langle q^2(t)\rangle / t \tag{4.9}$$

of the untilted system ($\varepsilon = 0$) by the Einstein relation

$$\mu_l = D/2k_B T . \tag{4.10}$$

In the high temperature limit one finds $D = D_0$, where $D_0 = q_0^2\gamma$, and where γ is the rate (3.7) describing incoherent relaxation in a symmetric two-state system. Note that in this limit both the mobility and the diffusion coefficient are of order Δ^2.

As the temperature decreases, quantum coherence effects leading to contributions to the mobility of higher order in Δ^2 become increasingly important. Such contributions are partly taken into account within a self-energy approach in Refs. [31] and [32].

The formidable expression (4.5) can be summed if we insert the high temperature formula (3.6) for the pair interaction $S(\tau)$ [28]. The result for the linear mobility is

$$\mu_l = \mu_0 [1 - 1/I_0^2(y)] , \tag{4.11}$$

where $\mu_0 = q_0^2/(2\pi\hbar K)$. The function $I_0(y)$ is a modified Bessel function, and

$$y = (2\pi K\hbar\gamma/k_B T)^{1/2} , \tag{4.12}$$

and γ is given by (3.7). The formula (4.11) is a consistent result for temperatures for which y is order of unity or smaller. Astonishingly, it also reproduces the correct zero temperature result for the linear mobility $\mu_l(T=0) = \mu_0$, a value obtained from a duality transformation between the tight-binding limit and the weak corrugation case [33, 30]. Thus, (4.11) is exact at $T = 0$ and at high temperatures, and reasonably interpolates between these cases in the intermediate regime. However, it does not decribe the algebraic low temperature corrections to the zero temperature mobility.

The low temperature expansion of the mobility is determined by the low temperature expansion of the pair interaction $S(\tau)$. We may write $S(\tau) = S_0(\tau) + S_1(\tau)$, where $S_0(\tau)$ is the zero temperature expression of (2.9) and where $S_1(\tau)$ represents the contributions at finite T. The leading low temperature correction is given by

$$S_1(\tau) = K\frac{\pi^2}{3}\left(\frac{\tau}{\hbar\beta}\right)^2 + 0\left(\left(\frac{\tau}{\hbar\beta}\right)^4\right). \tag{4.13}$$

Thus we obtain from (4.2)

$$G_m = G_m^0 \left\{1 - K\frac{\pi^2}{3}\left(\frac{k_B T}{\hbar}\right)^2 \left[\sum_{j=1}^{2m} \xi_j t_j\right]^2 + 0(T^4)\right\}. \tag{4.14}$$

Substituting (4.14) in (4.5) we see that the second term in the curly bracket of (4.14) can be generated by differentiation with respect to the bias. In the end we find for the mobility in the region $K < 1$ the asymptotic expansion

$$\mu(T) = \mu(T=0) + K\frac{\pi^2}{3}\left(\frac{k_B T}{\hbar}\right)^2 \frac{1}{\varepsilon}\frac{\partial^2}{\partial\varepsilon^2} \cdot (\varepsilon\mu(T=0)) + 0(T^4) . \tag{4.15}$$

The leading temperature dependence is given by a T^2-power law and the numerical factor in (4.15) is exact for arbitrary bias and for all $K < 1$.

It is interesting to note that if one evaluates the second moment $\langle q^2(t)\rangle$ with the pair interaction (3.6) one finds for the diffusion coefficient (4.9)

$$D = q_0^2 \frac{k_B T}{\pi\hbar K}[1 - 1/I_0^2(y)] . \tag{4.16}$$

Comparing (4.16) with (4.11) we see that the Einstein relation (4.10) is satisfied in all orders in Δ^2. As the temperature decreases the diffusion coefficient goes through a maximum [26], and it approaches zero as $T \to 0$. Thus, the system shows subdiffusive behavior at $T = 0$. It can be shown quite generally that for $K < 1$ and $T = 0$ the second moment behaves as $\langle q^2(t)\rangle \approx \ln t$ as $t \to \infty$.

For the special case $K = 1/2$ the formal expression (4.5) can be evaluated exactly for arbitrary T, t and ε [28]. The result for the nonlinear mobility is

$$\mu(T) = \mu_0 \frac{2\gamma}{\varepsilon} \operatorname{Im}\psi(1/2 + h\gamma/\pi k_B T + i\hbar\varepsilon/2\pi k_B T) , \tag{4.17}$$

where $\gamma = \gamma(K = 1/2) = \pi\Delta^2/(2\omega_c)$. At high temperatures, (4.17) simplifies to the form discussed previously,

$$\mu = \mu_0 \pi \frac{\gamma}{\varepsilon} \tanh(\hbar\beta\varepsilon/2) , \tag{4.18}$$

and at zero temperature

$$\mu(T=0)=\mu_0\frac{2\gamma}{\varepsilon}\arctan\left(\frac{\varepsilon}{2\gamma}\right). \tag{4.19}$$

Thus, indeed, $\mu_l(T=0)=\mu_0$. Also, it is easy to show that the asymptotic low temperature behavior of $\mu(T)$ in (4.17) is exactly in the form (4.15). Further, the diffusion coefficient is given by

$$D=\frac{2}{\pi^2}q_0^2\gamma\psi'(1/2+\hbar\gamma/\pi k_B T), \tag{4.20}$$

which again vanishes at $T=0$, and reduces to the previous result $D=q_0^2\gamma$ at high temperatures. At zero temperature, the second moment is found to increase logarithmically only, $\langle q^2(t)\rangle=(2/\pi^2)q_0^2\ln(2\gamma t)$, as $t\to\infty$. Thus, the specific case $K=1/2$ reflects all of the general features discussed above.

We are grateful to S. Dattagupta, H. Grabert, P. Hänggi, S. Linkwitz, M. Milch, Th. Negele, H. Wipf, and M. Wollensak for many enjoyable and enlightening discussions. It is a pleasure to thank the organizers of this meeting for their invitation. Partial financial support was provided by the C.N.R. (Italy).

References

[1] For a general review of classical rate theory, see P. Hänggi, P. Talkner, and M. Borkovec, Rev. Mod. Phys. *62*, 251 (1990).
[2] S. Chakravarty, Phys. Rev. Lett. *49*, 681 (1982); A. J. Bray and M. A. Moore, ibid. *49*, 1545 (1982).
[3] A. O. Caldeira and A. J. Leggett, Ann. Phys. (N.Y.) *149*, 374 (1983).
[4] H. Grabert, P. Olschowski, and U. Weiss, Phys. Rev. *B36*, 1931 (1987).
[5] A. N. Cleland, J. M. Martinis, and J. Clarke, Phys. Rev. *B37*, 5950 (1988), and references therein.
[6] For a review of the fermionic effects, see J. Kondo, in: Fermi Surface Effects, Vol. *77* of Springer Series in Solid-State Sciences, eds. J. Kondo and A. Yoshimori, Springer-Verlag, Berlin 1988. See also J. Kondo, this volume.
[7] H. Wipf, D. Steinbinder, K. Neumaier, P. Gutsmiedl, A. Magerl, and A. J. Dianoux, Europhys. Lett. *4*, 1379 (1987); D. Steinbinder, H. Wipf, A. Magerl, A. J. Dianoux, and K. Neumaier, ibid. *6*, 535 (1988). For a review see H. Grabert and H. Wipf, in: Festkörperprobleme/Advances in Solid State Physics, Vol. *30*, p. 1, ed. U. Rössler, Vieweg, Braunschweig 1990.
[8] A. J. Leggett, S. Chakravarty, A. T. Dorsey, M. P. A. Fisher, A. Garg, and W. Zwerger, Rev. Mod. Phys. *59*, 1 (1987).
[9] Yu. Kagan and N. V. Prokof'ev, Zh. Eksp. & Teor. Fiz. *90*, 2176 (1986) [Sov. Phys. JETP *63*, 1276 (1986)]; Yu. Kagan, this volume.
[10] K. Yamada, A. Sakurai, and S. Miyazima, Progr. Theor. Phys. *73*, 1342 (1985).
[11] R. P. Feynman and F. L. Vernon, Ann. Phys. (N.Y.) *24*, 118 (1963).
[12] S. Chakravarty and A. J. Leggett, Phys. Rev. Lett. *53*, 5 (1984).
[13] H. Grabert, S. Linkwitz, S. Dattagupta, and U. Weiss, Europhys. Lett. *2*, 631 (1986).
[14] S. Dattagupta, H. Grabert, and R. Jung, J. Phys. Cond. Mat. *1*, 1405 (1989).
[15] M. Sassetti and U. Weiss, Phys. Rev. *A41*, 5383 (1990).
[16] U. Weiss and M. Wollensak, Phys. Rev. Lett. *62*, 1663 (1989).
[17] C. H. Mak and D. Chandler, Phys. Rev. *A41*, 5709 (1990); D. Chandler, this volume.
[18] H. Grabert and U. Weiss, Phys. Rev. Lett. *54*, 1605 (1985).
[19] U. Weiss, H. Grabert, and S. Linkwitz, J. Low Temp. Phys. *68*, 213 (1987).
[20] A. Garg, Phys. Rev. *B32*, 4746 (1985).
[21] J. Kondo, Physica *84B*, 40 (1976).
[22] U. Weiss and M. Sassetti, in: Microscopic Aspects of Nonlinearity in Condensed Matter, NATO ASI, ed. V. Tognetti, Plenum, New York 1991.
[23] M. Sassetti and U. Weiss, Phys. Rev. Lett. *65*, 2262 (1990).
[24] H. Shiba, Progr. Theor. Phys. *54*, 967 (1975).
[25] For a review see Proceedings of the Fourth Conference on Muon Spin Rotations, Uppsala 1986 [Hyperfine Interactions *31* (1986)].
[26] U. Weiss and M. Wollensak, Physica *B152*, 154 (1988).
[27] G. Schön and A. D. Zaikin, preprint (1990).
[28] U. Weiss and M. Wollensak, Phys. Rev. *B37*, 2729 (1988).
[29] U. Weiss and H. Grabert, Phys. Lett. *108A*, 63 (1985).
[30] M. P. A. Fisher and W. Zwerger, Phys. Rev. *B32*, 6190 (1985).
[31] U. Eckern and F. Pelzer, Europhys. Lett. *3*, 131 (1987).
[32] M. Sassetti, P. Saracco, E. Galleani d'Agliano, and F. Napoli, Z. Phys. *77*, 491 (1989).
[33] A. Schmid, Phys. Rev. Lett. *51*, 1506 (1983).

Presented at the Discussion Meeting of the Deutsche Bunsen-Gesellschaft für Physikalische Chemie "Rate Processes in Dissipative Systems: 50 Years after Kramers" in Tutzing, September 10–13, 1990 E 7524

Dynamics of an Impurity Spin Coupled to a Spin-Boson Dissipative System

Sushanta Dattagupta and Tabish Qureshi

School of Physical Sciences, Jawaharlal Nehru University, New Delhi, 110067, India

Diffusion / Nonequilibrium Phenomena / Quantum Mechanics / Spectroscopy, Nuclear Magnetic Resonance / Statistical Mechanics

The dynamics of an impurity spin coupled to a spin-boson dissipative system is studied using the resolvent expansion technique. In one particular physical realization the model simulates a highly anisotropic Kondo system. The transverse correlation function of the impurity spin is calculated and the result obtained is analyzed in various limiting cases. NMR lineshapes are also calculated for various temperatures which are relevant in another physical realization of the model. Motional narrowing is observed at high temperature.

1. Introduction

An example of current research interest in rate processes in dissipative systems is found in the physics of a defect, such as positive muon or hydrogen, tunneling between two trap sites in a metal [1]. This example concerns the study of a quantum two-state system in contact with a thermal bath

Although the latter is made up of fermions, the low temperature behaviour is dominated by low-lying excitations off the Fermi surface which are approximately described by bosons. This has motivated the introduction of the spin-boson Hamiltonian that has been the focus of much attention in recent years [2]. The Hamiltonian, written as

$$\mathscr{H} = -\frac{1}{2}\hbar\Delta_0\sigma_x + \sigma_z\sum_j G_j(b_j + b_j^+) + \sum_j \hbar\omega_j b_j^+ b_j, \tag{1.1}$$

accompanied by the spectral function:

$$J(\omega) = (2/\hbar^2)\sum_j G_j^2\,\delta(\omega-\omega_j) = K\omega\,\mathrm{e}^{-\omega/D}, \tag{1.2}$$

provide a mapping of the two-state system in a fermionic bath to a two-state system in contact with a bosonic bath. In the above equations σ's are Pauli spin operators representing the two-state system, Δ_0 is the tunneling frequency, b_j (b_j^+) is the annihilation (creation) operator for the jth boson of frequency ω_j and G_j is the coupling constant. The assumed form of the spectral density given by the right most term of (1.2) describes what is known as Ohmic dissipation parameterized by the dimensionless coupling constant K, and the high frequency cut-off D.

The object of the present investigation is **not** tunneling states in metals but the spin dynamics of an impurity spin I coupled to a spin-boson Hamiltonian. What we study is therefore a variant of the problem posed in (1.1) in that the σ's now represent a real spin-half entity which in turn is in interaction with another spin I. The chosen Hamiltonian is written as

$$\mathscr{H} = \frac{1}{2}aI_z\sigma_z - \frac{1}{2}\hbar\Delta_0\sigma_x + \sigma_z\sum_j G_j(b_j + b_j^+) + \sum_j \hbar\omega_j b_j^+ b_j + \sum_j \frac{G_j^2}{\hbar\omega_j}, \tag{1.3}$$

where a is a coupling parameter and the last term is a counter-term that disappears upon a unitary transformation on $\mathscr{H}$ (see below). We are interested in enquiring what should be the influence of the dissipative dynamics of σ's on the spin dynamics of I. In particular, we are interested in calculating the transverse correlation function

$$C_{xx}(t) = \langle I_x(0) I_x(t)\rangle, \tag{1.4}$$

where $\langle \ldots \rangle$ denote statistical average.

A motivating factor behind formulating the Hamiltonian in (1.3) is the interest in studying a highly anisotropic Kondo system which is approximately described by (1.3) sans the first term [2]. In this context σ represents the electronic spin of the localized Kondo impurity whereas the spin-boson part is taken to model the interaction between the localized spin and the conduction electrons. The additional interaction, represented by the first term of our model Hamiltonian, is viewed to describe a uniaxial hyperfine interaction with coupling constant a between the nuclear spin I and the electronic spin σ of the impurity. A quantity such as $C_{xx}(t)$ would be relevant in interpreting resonance experiments e.g. nuclear magnetic resonance in Kondo like systems [3]. A related quantity is also useful for analyzing other hyperfine line shapes as can be measured by the Mössbauer and angular correlation techniques [4]. It may be further mentioned that a stochastic version of (1.3) has been looked at by Kehr and Kitahara in which the authors consider the depolarization of a positive muon tunneling between two sites which have oppositely directed magnetic fields [5].

The plan of the paper is as follows. In §2 we set up the method of calculating $C_{xx}(t)$ based on the Hamiltonian given in (1.3). The method, which goes under the name of "relaxation theory", is only briefly sketched here as most of the details are already given in our earlier paper on structure factor calculation for the spin boson model [6]. As shown in [6], our approach is entirely equivalent to the dilute bounce gas approximation within a functional integral formulation of the problem [2, 7]. In §3 we analyze the result for the correlation function calculated in §2.

2. The Transverse Correlation Function

2.1 The Preliminaries

We have argued earlier [6] that a convenient perturbative treatment of the spin-bath coupling (i.e. the second term in (1.3)) ensues upon making a unitary transformation of the Hamiltonian:

$$\tilde{\mathscr{H}} = S\,\mathscr{H}\,S^{-1} \tag{2.1}$$

where S is a unitary operator defined by

$$S \equiv \exp\left(-\sigma_z\sum_j (G_j/\hbar\omega_j)(b_j - b_j^+)\right). \tag{2.2}$$

We obtain

$$\tilde{\mathscr{H}} = \frac{1}{2}a\,I_z\sigma_z - \frac{1}{2}\hbar\Delta_0(B_+\sigma_- + B_-\sigma_+) + \sum_j \hbar\omega_j b_j^+ b_j \tag{2.3}$$

where $\sigma_\pm = \sigma_x \pm \mathrm{i}\sigma_y$ and

$$B^\pm = \exp\left(\pm 2\sum_j (G_j/\hbar\omega_j)(b_j - b_j^+)\right). \tag{2.4}$$

In terms of $\tilde{\mathscr{H}}$ the transverse correlation function in (1.4) may be written as

$$C_{xx}(t) = \mathrm{Tr}\left(\tilde{\varrho}\,I_x(0)\,\tilde{I}_x(t)\right) \tag{2.5}$$

where

$$\tilde{\varrho} = \frac{\exp(-\beta\tilde{\mathscr{H}})}{\mathrm{Tr}\,[\exp(-\beta\tilde{\mathscr{H}})]}, \tag{2.6}$$

and

$$\tilde{I}_x(t) = \exp(\mathrm{i}\tilde{\mathscr{H}}\,t)\,I_x(0)\exp(-\mathrm{i}\tilde{\mathscr{H}}\,t). \tag{2.7}$$

We may further write

$$\tilde{I}_x(t) = U(t)\, I_x(0) \tag{2.8}$$

where

$$U(t) \equiv \exp(\mathrm{i}\tilde{L}t), \tag{2.9}$$

$\tilde{L}$ being the Liouvillian associated with $\tilde{\mathscr{H}}$. (The notations used here are the same as in [6]). Making the customary factorization approximation the density matrix $\tilde{\varrho}$ can be expressed as

$$\tilde{\varrho} \approx \varrho_S \cdot \varrho_B, \tag{2.10}$$

where ϱ_S is the density operator for the spin system denoted by the first term in (2.3) and ϱ_B is the density matrix for the bath the Hamiltonian of which is given by the third term in (2.3). This approximation is very good unless either the coupling constant K or the temperature is very small. With this the Laplace transform of $C_{xx}(t)$ is given by

$$\tilde{C}_{xx}(z) = \mathrm{Tr}_S\left(\varrho_S I_x\, [\mathrm{Tr}_B(\varrho_B \hat{U}(z)]\, I_x\right), \tag{2.11}$$

where

$$\hat{U}(z) = \frac{1}{z - \mathrm{i}\tilde{L}}, \tag{2.12}$$

and Tr_S and Tr_B represent the traces over the quantum states of the coupled spin system (of I and σ) and the bath respectively. Denoting the states of I by the latin indices m_0 and m_1 and those of σ by the Greek indices μ and ν, (2.11) may be reexpressed as

$$\tilde{C}_{xx}(z) = \sum_{m_0 m_1} |\langle m_1|I_x|m_0\rangle|^2 \frac{1}{Z_S} \sum_{\nu\nu'} \exp(-\frac{1}{2}\beta a_1 m_1 \nu) \cdot (m_0\nu, m_1\nu|(\mathrm{Tr}_B\{\varrho_B \hat{U}(z)\})|m_0\nu', m_1\nu'), \tag{2.13}$$

where Z_S is the partition function associated with ϱ_S. In writing (2.13) we have used the fact that $\mathscr{H}_I$ is diagonal amongst the states of I.

2.2 Resolvent Expansion

Our strategy is to first evaluate the trace over the bath states. Formally,

$$\mathrm{Tr}_B[\varrho_B \hat{U}(z)] \equiv [\hat{U}(z)]_{\mathrm{av}} = \sum_{n,n'} \langle n|\varrho_B|n\rangle\, (nn|\,\hat{U}(z)|n'n') \tag{2.14}$$

where $|n\rangle$ denotes the occupation number states for the boson operators and $|mn)$ the "states" for the corresponding Liouvillian (see [6]). Developing the interaction term, i.e. the one associated with the second term in (2.3), as perturbation and suitably rearranging terms up to the second order, we have

$$[\hat{U}(z)]_{\mathrm{av}} = \frac{1}{z - \mathrm{i}L_S + [L_I(z - \mathrm{i}L_S - \mathrm{i}L_B)^{-1} L_I]_{\alpha\nu}}, \tag{2.15}$$

where L_I is the Liouvillian associated with the interaction Hamiltonian:

$$\mathscr{H}_I = -\frac{1}{2}\hbar\Delta_0(B_+\sigma_- + B_-\sigma_+), \tag{2.16}$$

and L_B is the Liouvillian associated with the bath Hamiltonian:

$$\mathscr{H}_B = \sum_j \hbar\omega_j b_j^+ b_j. \tag{2.17}$$

As we require the matrix elements of $[U(z)]_{\mathrm{av}}$ amongst the combined spin states of I and σ it is convenient first to tabulate the matrix elements of the self-energy given in (2.15). Applying the properties of the Liouvillian, we find

$$(m_0\mu, m_1\nu|[L_I(z - \mathrm{i}L_S - \mathrm{i}L_B)^{-1} L_I]_{\mathrm{av}}|m_0\mu', m_1\nu') = (1/\hbar^2) \sum_{n,n'} \cdot \langle n|\varrho_B|n\rangle \left(\delta_{\nu\nu'} \sum_\eta \frac{\langle\mu n|\mathscr{H}_I|\eta n'\rangle\langle\eta n'|\mathscr{H}_I|\mu' n\rangle}{z - \mathrm{i}(E_n - E_{n'})/\hbar - \mathrm{i}(\eta a_0 m_0 - \nu a_1 m_1)/2}\right.$$

$$+ \delta_{\mu\mu'} \sum_\eta \frac{\langle\nu' n|\mathscr{H}_I|\eta n'\rangle\langle\eta n'|\mathscr{H}_I|\nu n\rangle}{z - \mathrm{i}(E_{n'} - E_n)/\hbar - \mathrm{i}(\mu a_0 m_0 - \eta a_1 m_1)/2}$$

$$- \frac{\langle\mu n|\mathscr{H}_I|\mu' n'\rangle\langle\nu' n'|\mathscr{H}_I|\nu n\rangle}{z - \mathrm{i}(E_{n'} - E_n)/\hbar - \mathrm{i}(\mu' a_0 m_0 - \nu a_1 m_1)/2}$$

$$\left. - \frac{\langle\mu n|\mathscr{H}_I|\mu' n'\rangle\langle\nu' n'|\mathscr{H}_I|\nu n\rangle}{z - \mathrm{i}(E^n - E^{n'})/\hbar - \mathrm{i}(\mu a^0 m^0 - \nu' a^1 m^1)/2}\right) \tag{2.18}$$

where E_n is the eigenvalue of the bath Hamiltonian $\mathscr{H}_B$. The next step is to plug in the explicit form of $\mathscr{H}_I$ (cf. (2.16)), rewrite the denominators back in the form of integrals over t and express the sum over the bath states (n,n', etc.) as correlation functions for bath operators. We find that the matrix for $z - \mathrm{i}L_S + [L_I(z - \mathrm{i}L_S - \mathrm{i}L_B)^{-1} L_I]_{\mathrm{av}}$, for a fixed set of m_0 and m_1 and within the sub space of σ, is block diagonal with 2×2 blocks at the diagonal. This simplifies the inversion that is required in order to obtain the matrix elements for $[\hat{U}(z)]_{\mathrm{av}}$. However, as is evident from (2.13), we need focus on the upper left block in (2.18), and thus we find (displaying only the upper left block) for the matrix of $[U(z)]_{\mathrm{av}}$:

$$\frac{1}{\mathrm{Det}(m_0, m_1)} \begin{bmatrix} z + \frac{\mathrm{i}}{2}(a_0 m_0 - a_1 m_1) + \hat{\phi}_{+-}(z_-) + \hat{\phi}'_{+-}(z_+) & \hat{\phi}_{+-}(z_-) + \hat{\phi}'_{+-}(z_+) \\ \hat{\phi}_{-+}(z_+) + \hat{\phi}'_{-+}(z_-) & z - \frac{\mathrm{i}}{2}(a_0 m_0 - a_1 m_1) + \hat{\phi}_{-+}(z_+) + \hat{\phi}'_{-+}(z_-) \end{bmatrix} \tag{2.19}$$

where the $\mathrm{Det}(m_0, m_1)$ is given by

$$\mathrm{Det}(m_0, m_1) = z^2 + z\,[\hat{\phi}_{+-}(z_-) + \hat{\phi}_{-+}(z_+) + \hat{\phi}'_{+-}(z_+) + \hat{\phi}'_{-+}(z_-)] + \frac{1}{4}(a_0 m_0 - a_1 m_1)^2 + \frac{\mathrm{i}}{2}(a_0 m_0 - a_1 m_1) \{[\hat{\phi}_{-+}(z_+) + \hat{\phi}'_{-+}(z_-)] - [\hat{\phi}_{+-}(z_-) + \hat{\phi}'_{+-}(z_+)]\}. \tag{2.20}$$

Here the rows and columns are labelled by $++$, $--$, $+-$ and $-+$ respectively, and

$$\Phi_{\pm\pm}(t) = \frac{\hbar^2}{4}\langle B_{\pm}(0)\, B_{\pm}(t)\rangle . \tag{2.21}$$

Further, all primed quantities are obtained by replacing the argument t by $-t$, and the hat denotes the Laplace transform. It may be stressed that the angular brackets in (2.21) denote thermal averages governed by ϱ_B and the time development of $B_{\pm}(t)$ is dictated by $\mathscr{H}_B$ alone. It may also be noted that in writing the elements in (2.19) we have kept in mind the possibility of the hyperfine constant taking two distinct values a_0 and a_1 depending on whether the state is m_0 or m_1. This is particularly relevant in an experiment involving the Mössbauer effect wherein the states m_0 and m_1 refer to the ground and excited states of the nucleus. On the other hand, in the case of magnetic resonance or angular correlation experiments, $a_0 = a_1 = a$ [4].

Using the correlation function for the bath variables within the Ohmic dissipation model we have shown earlier that [6]

$$\begin{aligned}\hat{\phi}_{+-}(z) = \hat{\phi}_{-+}(z) \equiv \hat{\phi}(z) = F(z)\exp(i\pi K),\\ \hat{\phi}'_{+-}(z) = \hat{\phi}'_{-+}(z) \equiv \hat{\phi}'(z) = F(z)\exp(-i\pi K),\end{aligned} \tag{2.22}$$

where

$$F(z) = \frac{\Delta_0^2}{4D}\left(\frac{2\pi}{\hbar\beta D}\right)^{2K-1}\frac{\Gamma(1-2K)\,\Gamma(K+z\hbar\beta/2\pi)}{\Gamma(1-K+z\hbar\beta/2\pi)}. \tag{2.23}$$

Γ in (2.23) denotes Euler's gamma function.

2.3 Results for the Correlation Function

It is evident from (2.13) that the quantity of central importance is the matrix elements of the averaged time-development operator that may be denoted as

$$\begin{aligned}G_{m_0m_1}(z) \equiv \sum_{\nu\nu'}\frac{1}{Z_S}\exp\left(\frac{1}{2}\beta a_1 m_1\right)(m_0\nu, m_1\nu\\ \cdot|(\mathrm{Tr}_B[\varrho_B\hat{U}(z)])|m_0\nu', m_1\nu').\end{aligned} \tag{2.24}$$

A knowledge of $G_{m_0m_1}(z)$ is adequate for evaluating the line shapes for different kinds of hyperfine spectra [4]. After a bit of algebra we obtain

$$\begin{aligned}G_{m_0m_1}(z) = \frac{1}{2}\Bigg(z + \frac{(a_0m_0 - a_1m_1)^2/2 - (a_0m_0 - a_1m_1)(F(z_+) - F(z_-))\sin(\pi K)}{z + 2(F(z_+) + F(z_-))\cos(\pi K)}\Bigg)^{-1}\\ + \frac{i\tanh(\frac{1}{2}\beta a_1 m_1)(a_0m_0 - a_1m_1)^2/4}{z^2 + 2z(F(z_+) + F(z_-))\cos(\pi K) + \frac{1}{4}(a_0m_0 - a_1m_1)^2 - (a_0m_0 - a_1m_1)(F(z_+) - F(z_-))\sin(\pi K)}.\end{aligned} \tag{2.25}$$

Specializing for the moment to NMR, and also for the sake of simplicity to the case $I = 1/2$, we find

$$\tilde{C}_{xx}(z) = \frac{1}{4}\left(z + \frac{a^2/4}{z + 4F(z)\cos(\pi K)}\right)^{-1}. \tag{2.26}$$

3. Discussion of Results

In order to have a more physical appreciation of the results given in (2.32) and (2.33) it is useful to consider first certain limiting cases as enumerated below.

(i) The Case of Zero Damping: $K = 0$

Eq. (2.26) now yields (cf. (2.23))

$$\tilde{C}_{xx}(z) = \frac{1}{4}\frac{z^2 + \Delta_0^2}{z(z^2 + \Delta_0^2 + \frac{1}{4}a^2)}. \tag{3.1}$$

On the other hand, zero damping implies also that the spin system is totally decoupled from its surroundings, in which case the Hamiltonian in (1.3) is reduced to

$$\mathscr{H} = \frac{1}{2}a\, I_z\sigma_z - \frac{\hbar}{2}\Delta_0\sigma_x . \tag{3.2}$$

Eq. (3.2) allows for a direct calculation of the correlation function in (1.4), which, after some straightforward algebra, leads to (3.1).

(ii) The Overdamped and High Temperature Case

In this limit it is expected that the effect of coherence (contained in the tunneling term in (2.3)) would be completely washed out, leading to total incoherence. Another way of saying the same thing is to look at (1.3) and argue that in the present situation, the system-bath coupling would move the spin in the x-direction, i.e., σ_x, so rapidly that its effect would be averaged out. This phenomenon is, therefore, very similar to "motional narrowing" in magnetic resonance [3].

If the effect of the tunneling term disappears from (1.3) one is left with just a "static" Hamiltonian:

$$\mathscr{H} = \frac{1}{2}a\, I_z\sigma_z + \sum_j \hbar\omega_j b_j^+ b_j . \tag{3.3}$$

It is now rather trivial to calculate directly the correlation function of (1.4) and one obtains

$$\tilde{C}_{xx}(z) = \frac{1}{8\cosh(a\beta/2)}\left(\frac{\exp(-a\beta/4)}{z + ia/2\hbar} + \frac{\exp(a\beta/4}{z - ia/2\hbar}\right). \tag{3.4}$$

It is not so easy to show how the general expression of (2.26) reduces to (3.4) analytically, but it is certainly possible to demonstrate this fact numerically, as exhibited in Fig. 1.

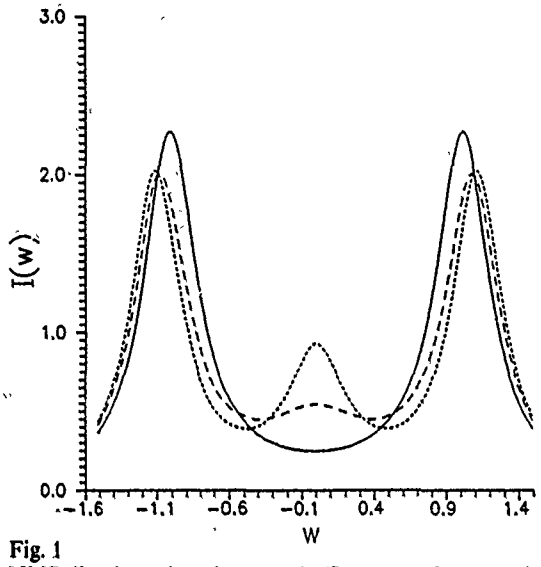


Fig. 1
NMR lineshape based on (2.26). For convenience we have introduced a new temperature $\tau = 2\pi/\hbar\beta$. The Laplace transform variable z is set equal to $i\omega + \Gamma/2$ where Γ has been fixed at 0.4 in order to account for a possible instrumental width. The temperature τ is fixed at 5, Δ_0 at 0.25, a at 1.0 and the cutoff D at 100. We plot the lineshape $I(\omega) = \tilde{C}(z)$. The solid line corresponds to $K = 0.2$, the dashed line to $K = 0.05$ and the dotted line to $K = 0.01$

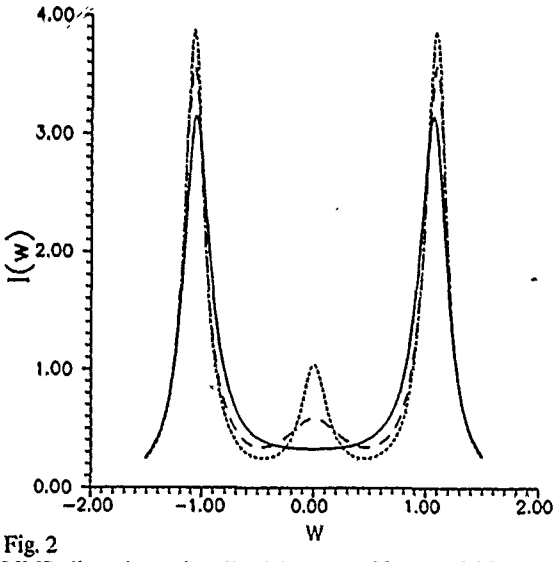


Fig. 2
NMR line shape for $K = 0.05$, $D = 100$, $\Delta_0 = 0.25$, $a = 1.0$ and $\Gamma = 0.2$ for various values of the temperature τ (1 for the dotted line, 5 for the dashed line and 15 for the solid line)

(iii) The Case of High Temperature

An increase in temperature also leads to incoherence but not to that large an extent as discussed under case (ii). Here one may neglect the β-dependent terms in the argument of the gamma functions appearing in (2.23), and show that

$$\tilde{C}_{xx}(z) = \frac{1}{4}\,\frac{z + \gamma(K,\beta)}{z^2 + z\,\gamma(K,\beta) + \frac{1}{4}a^2}\,, \tag{3.5}$$

where

$$\gamma(K,\beta) = \frac{\Delta_0^2}{D}\left(\frac{2\pi}{\hbar\beta D}\right)^{2K-1}\frac{\Gamma(1-2K)\,\Gamma(K)}{\Gamma(1-K)}\cos(\pi K)\,. \tag{3.6}$$

In this limit it is reasonable to argue that the physics of the problem is equivalent to that described by an effective stochastic model Hamiltonian:

$$\mathscr{H}(t) = I_z\,h(t)\,, \tag{3.7}$$

where $h(t)$ is a two-state jump process having two possible values $+a/2$ and $-a/2$. Such a process is a special class of Markov processes and leads to a lineshape expression that agrees completely with (3.5) [4].

(iv) Numerical Plots

Finally we present, in Figs. 1 and 2, a series of plots based on numerical computations of (2.26) in various domains of interest, most of which have been covered already under (i)–(iii) above. As one can see, very weak damping leads to three resonance lines, the central peak corresponding to an effective field component the nuclear spin I "sees" in the x-direction. When the temperature increases this component disappears because of incoherence. Finally, as damping also gets to be large the two reasonance lines get completely "motionally narrowed".

We would like to thank the Department of Science and Technology, and the University Grants Commission, Government of India, for supporting this research.

References

[1] J. Kondo, Fermi Surface Effects, Springer Ser. Solid State Sci., Vol. 77, Springer Heidelberg 1988.
[2] A. J. Legett, S. Chakravarty, M. P. A. Fisher, A. T. Dorsey, A. Garg, and W. Zwerger, Rev. Mod. Phys. *59*, 1 (1987).
[3] C. P. Slichter, Principles of Magnetic Resonance, Harper and Row, New York 1963.
[4] S. Dattagupta, Relaxation Phenomena in Condensed Matter Physics, Academic, New York 1987.
[5] K. W. Kehr and K. Kitahara, J. Phys. Soc. Jpn. *57*, 2819 (1988).
[6] S. Dattagupta, H. Grabert, and R. Jung, J. Phys.: Condensed Matter *1*, 1405 (1989).
[7] H. Grabert, S. Linkwitz, S. Dattagupta, and U. Weiss, Europhys. Lett. *2*, 631 (1986).

Presented at the Discussion Meeting of the Deutsche Bunsen-Gesellschaft für Physikalische Chemie "Rate Processes in Dissipative Systems: 50 Years after Kramers" in Tutzing, September 10–13, 1990 E 7523

Low-Temperature Tunneling of Hydrogen in $Nb(OH)_x$ and $Nb(NH)_x$

H. Wipf

Institut für Festkörperphysik, Technische Hochschule Darmstadt, Hochschulstraße 6, D-6100 Darmstadt

Diffusion / Neutron Scattering / Quantum Mechanics / Tunneling

Hydrogen interstitials in Nb are trapped by O or N impurity atoms below ~160 K. The trapped hydrogen occupies two nearest-neighbor tetrahedral sites. It represents, therefore, a model system for experimental studies of the tunneling dynamics of a particle in a double-well potential. The tunneling dynamics of the trapped hydrogen was investigated by neutron spectroscopy in the temperature range between 0.05 and 160 K. The experiments demonstrate the transition from a low-temperature coherent tunneling ($T \leq 10$ K) to an incoherent jump diffusion at elevated temperatures ($T \geq 10$ K). Up to ~60 K, both coherent tunneling and jump diffusion is controlled by a nonadiabatic coupling of the hydrogen to conduction electrons (Kondo's coupling constant $K = 0.055 \pm 0.005$). Above ~60 K, the jump diffusion of the hydrogen is increasingly dominated by an interaction with phonons.

1. Introduction

The decisive role of tunneling in low-temperature diffusion processes of hydrogen interstitials in metals is well established since more than two decades [1,2]. This holds especially for hydrogen diffusion in bcc metals such as V, Nb and Ta where the distances between the (tetrahedral) interstitial sites occupied by the hydrogen are smaller (about 1.1 Å) than in most of the other metal-hydrogen systems. The tunneling matrix elements of the hydrogen are, therefore, particularly large. An important progress in our understanding of the tunneling dynamics of the hydrogen was the recent observation that this dynamics is strongly affected by a nonadiabatic interaction with the conduction electrons of the host metal. This nonadiabatic effect, which is ignored within the conventional adiabatic or Born-Oppenheimer approximation, means specifically that the tunneling dynamics of the hydrogen interstitials in a metal cannot be explained by solely considering interatomic lattice potentials. The nonadiabatic influence of conduction electrons on the motion of the interstitial hydrogen was first demonstrated 1984 in low-temperature ultrasonic experiments on hydrogen in Nb by Wang et. al. [3]. In the same year, nonadiabatic electronic effects were also proposed by Kondo and Yamada [4,5] as a mechanism to understand the previously unexplained temperature dependence observed for the diffusion rate of muons in Al and Cu (the muon can be considered to represent a light hydrogen isotope).

This paper summarizes the results of recent neutron spectroscopic measurements which investigated the tunneling of hydrogen interstitials in Nb which were trapped below ~160 K by (immobile) O or N impurity atoms under formation of O–H or N–H pairs [6–10]. In this case, the trapped hydrogen occupies a double-well potential which consists of two neighboring tetrahedral interstitial sites whith a distance of ~1.17 Å. The tunneling of the trapped hydrogen in Nb represents, therefore, the simplest situation possible for a quantum transport, namely that in a double well potential. It is, at the same time, the situation for which the influence of nonadiabatic effects was intensively investigated in recent years (see [4,5,9,11–18], and references therein). The experiments were performed in the temperature range between 0.05 and 160 K, and on Nb samples with O–H or N–H pair concentrations up to 1.1 at%. They demonstrate, at ~10 K, the transition from a low-temperature coherent tunneling with two well-defined and energetically splitted eigenstates (inelastic neutron spectra) to an incoherent high-temperature jump diffusion of the trapped hydrogen (quasielastic spectra). The observed tunneling dynamics is, up to ~60 K, consistently and quantitatively described solely by a nonadiabatic interaction between the conduction electrons and the hydrogen (the adiabatic interaction with phonon modes effects only a temperature-independent renormalization of the tunnel splitting). The dimensionless Kondo parameter, which characterizes the strengh of the nonadiabatic interaction, was determined to be $K = 0.055 \pm 0.005$. Above ~60 K, finally, the adiabatic influence of the phonons becomes important and dominates, in fact, the tunneling dynamics of the hydrogen.

The trapping of H in Nb by O or N impurities – and thus the formation of O–H or N–H pairs – provides a unique possibility of investigating transport processes of hydrogen interstitials in metals even at low temperatures where, in the absence of traps, the hydrogen is immobile because of precipitation [19,20]. The transport process in this case is a coherent tunneling or an incoherent (local) jump diffusion of the hydrogen between two neighboring tetrahedral interstitial sites that form the double-well potential in which the trapped hydrogen is located. It is worth pointing out that such a locally restricted transport process is described by the same theoretical concepts as ordinary long-range diffusion. Further, the fact that Nb is a superconductor with the (relatively) high transition temperature of 9.2 K will be found of great advantage for the present experimental investigation.

An important aspect of the tunneling behavior of the trapped hydrogen is the occurrence of an asymmetry energy between the two interstitial sites of a given hydrogen interstitial due to random (static) lattice strains induced by sur-

 © VCH Verlagsgesellschaft mbH, W-6940 Weinheim, 1991 0005-9021/91/0303-0438 $ 3.50+.25/0

rounding O–H or N–H pairs [21,22]. The asymmetry energies increase with rising pair concentration, and they reach typical values of several meV for concentrations in the at% range [22]. The influence of the asymmetry energies will explicitly be considered within the discussion of the neutron spectroscopic results.

2. Samples and Experimental Details

The measurements were carried out on three $Nb(OH)_x$ samples with $x = 0.0002$, 0.002 and 0.011, and on three $Nb(NH)_x$ samples with $x = 0.0005$ and 0.004 (two samples). The techniques applied for sample preparation and analysis are described in [6,7,10,22]. The neutron spectra were taken with the time-of-flight spectrometer IN 6 at the Institute Laue-Langevin in Grenoble.

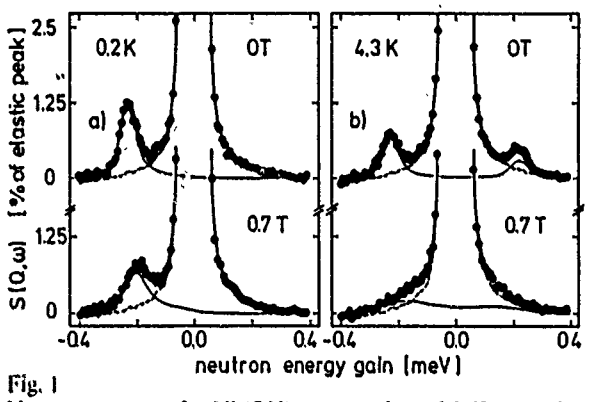


Fig. 1
Neutron spectra of a $Nb(OH)_{0.0002}$ sample at 0.2 K (a) and 4.3 K (b) [6,9]. For both temperatures, the spectra were taken in the superconducting (0T) and normal conducting (0.7T) electronic state. The thick and the thin solid lines represent fit curves for the total and the inelastic scattering intensity, respectively. The broken lines are for the elastic intensity

3. Experimental Results and Discussion

3.1. Coherent Tunneling Regime Below ~10 K

Fig. 1 presents four neutron spectra measured from the $Nb(OH)_{0.0002}$ sample at 0.2 K (Fig.1a) and 4.3 K (Fig.1b) [6]. Both temperatures are well below the superconducting transition temperature of 9.2 K for the investigated sample. For this reason, spectra could be taken in both the superconducting and the normal conducting electronic state where the latter state was achieved by application of a magnetic field of 0.7 T. The top and bottom spectra in Fig. 1 represent the results for superconductivity (0T) and normal conductivity (0.7T), respectively. It can be seen that both spectra taken in the superconducting state show a clearly identifiable inelastic line at ~0.2 meV. This demonstrates a coherent tunneling behavior with two well-defined eigenstates due to a delocalization of the hydrogen between two interstitial sites, and a value of $J_s \simeq 0.2$ meV for the (renormalized) tunnel splitting between the two states. In the normal conducting state, the inelastic lines show a center shift and a broadening at 0.2 K, and a transition to an almost quasi-elastic behavior at 4.3 K. These distinct differences between superconductivity and normal conductivity demonstrate the influence of nonadiabatic electronic effects since phononic effects are not expected to depend noticeably on the electronic state.

For a quantitative discussion of the results, the measured spectra were fitted to a scattering law that presupposes a coherent tunneling of the hydrogen because of a delocalization between its two interstitial sites [6,9,13–18]. The two relevant fit parameters were the temperature-dependent tunnel splitting $J(T)$ between the two eigenstates of the hydrogen and a (temperature-dependent) relaxation rate $\gamma(T)$ which describes the (reciprocal) lifetimes of these states. The damping characterizes also the broadening of the inelastic lines of the spectra.

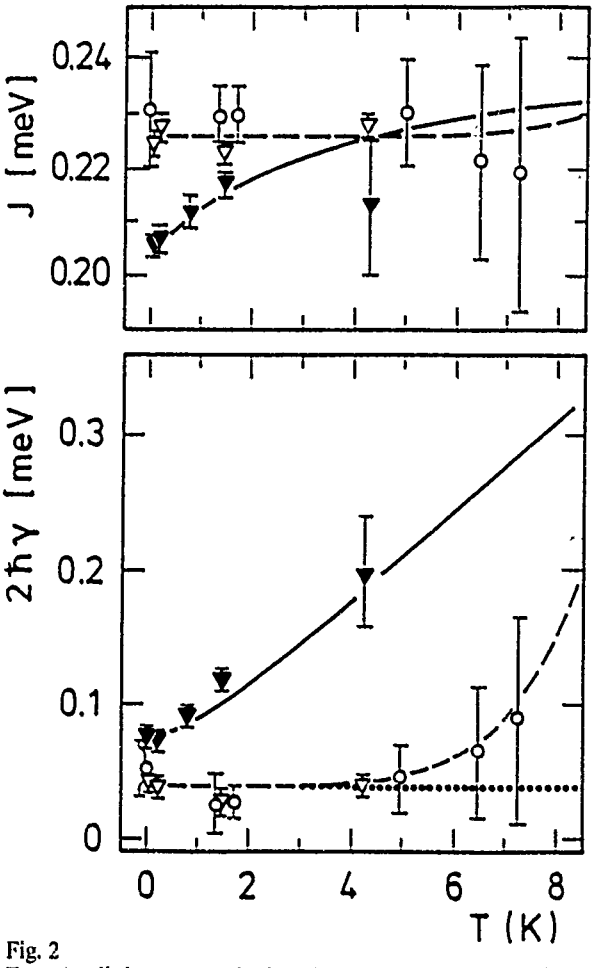


Fig. 2
Tunnel splitting J (a) and relaxation rate γ (or damping $2\hbar\gamma$) (b) in a plot versus temperature [6,9]. Triangles and circles are the results for the $Nb(OH)_x$ samples with $x = 0.0002$ and 0.002, respectively. Full data points indicate normal conductivity, and open data points are for superconductivity. The solid and broken curves are explained in the text The dotted curve represents an inhomogeneous contribution to the relaxation rate [6]

Fig. 2 compiles the fit results for $J(T)$ and $\gamma(T)$ as obtained in the temperature range below 10 K for two $Nb(OH)_x$ samples with $x = 0.0002$ and 0.002 [6] in a plot versus temperature. The open and full data points discriminate between results derived in the superconducting and normal conducting state, respectively. In the low-temperature limit $T \to 0$ K, the tunnel splitting is found to be

$J_s(0) = (0.226 \pm 0.004)$ meV for the superconducting and $J_n(0) = (0.206 \pm 0.003)$ meV for the normal conducting state. The latter quantity shows an additional renormalization (reduction) by 9% due to the presence of the normal conducting electrons. The relaxation rate $\gamma(T)$, on the other hand, is distinctly larger in the normal conducting than in the superconducting state.

It is demonstrated in [6,9] that the dependence of both $J(T)$ and $\gamma(T)$ on the temperature and the electronic state can quantitatively be described by the theories developed in [9,13–18] for a nonadiabatic interaction with the conduction electrons. The interaction with phonons is considered to cause only a temperature-independent renormalization of the tunnel splitting which is identical for both electronic states. A quantitative description requires further the knowledge of the temperature-dependent electronic energy gap $\Delta_g(T)$ which was assumed to behave according to BCS theory (for Nb, the zero temperature energy gap is $\Delta_g(0) = 1.53$ meV). The results of the above theories are indicated in Fig. 2 by broken and full lines for the superconducting and normal conducting state, respectively. Particularly at low temperatures, where the experimental accuracy is high, the theories can be seen to provide a good description of the experimental data.

The Kondo parameter derived from the data in Fig. 2 is $K = 0.055 \pm 0.005$. We point out that the complete theoretical description as shown in this figure requires only one additional parameter, for instance the tunnel splitting $J_n(0) = (0.202 \pm 0.003)$ meV for $T \to 0$ K in the normal conducting state.

The experimental results presented so far applied to hydrogen tunneling in $Nb(OH)_x$ samples in which the hydrogen was trapped by O impurities. Fig. 3 shows a comparison of neutron spectra obtained at 1.5 K from the $Nb(NH)_{0.0005}$ and the $Nb(OH)_{0.0002}$ sample (both samples were in the superconducting state) [10]. The data show that the tunnel splitting of the hydrogen which is trapped by N is significantly smaller than that of hydrogen trapped by O. This indicates – similarly as a previous study on C traps [23] – that the respective trapping impurity influences noticeably the lattice potential and, therefore, the tunnel splitting of the hydrogen interstitials.

The thick solid lines in Fig. 3 are fit curves to the data which allowed the determination of the tunnel splitting $J_s(0)$ for $T \to 0$ K in the superconducting state [10]. The results for this quantity were $J_s(0) = (0.165 \pm 0.004)$ meV and $J_s(0) = (0.2222 \pm 0.004)$ meV for hydrogen trapped by N or O impurities, respectively [10]. The result for the O traps agrees excellently with that of the previous studies [6,9] discussed above whereas, for the N traps, the tunnel splitting is found to be about 30% smaller. The value of $J_s(0)$ in the case of the N traps is, however, very close to that one reported recently for hydrogen in Nb that is trapped by C

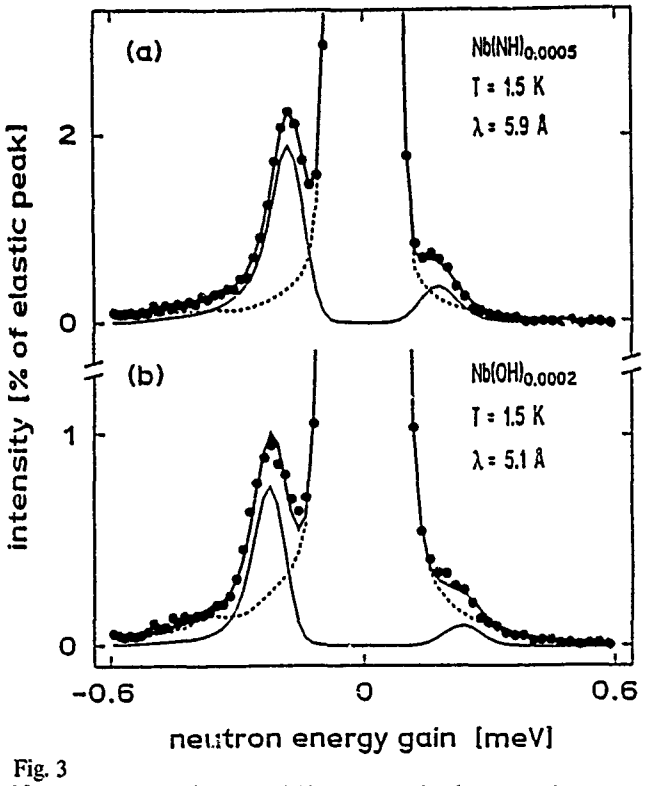


Fig. 3
Neutron spectra taken at 1.5 K (superconducting state) from the $Nb(NH)_{0.0005}$ (a) and the $Nb(OH)_{0.0002}$ (b) sample [10]. The thick and the thin solid lines represent fit curves for the total and the inelastic scattering intensity, respectively. The broken lines are for the elastic intensity

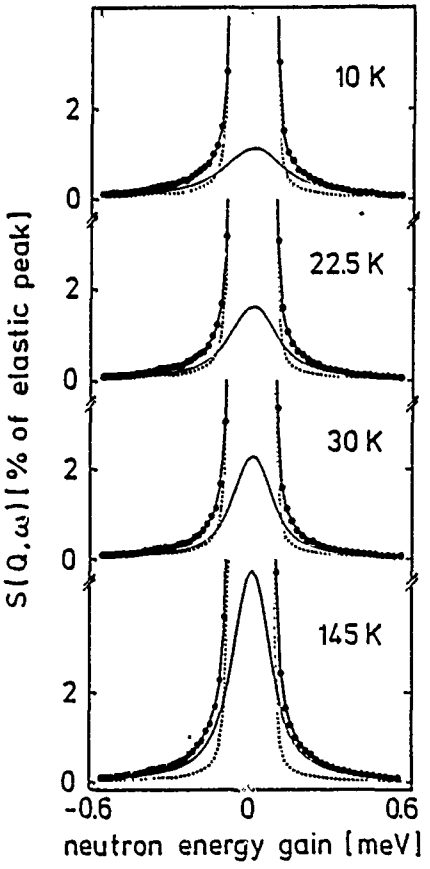


Fig. 4
Quasielastic neutron spectra of the $Nb(OH)_{0.002}$ sample [7,9] The thick and the thin solid lines represent fit curves for the total and the inelastic scattering intensity, respectively The broken lines are for the elastic intensity as given by the measured V resolution

impurities [23]. We shall see later that a smaller tunnel splitting will be reflected, at higher temperatures, by a correspondingly lower jump rate of the trapped hydrogen.

3.2. Incoherent Jump Diffusion above ~10 K

Fig. 4 presents four neutron spectra obtained from a $Nb(OH)_{0.002}$ sample in the temperature range between 10 and 145 K [7,9]. The spectra demonstrate clearly a quasielastic behavior as expected for an incoherent jump diffusion process of the trapped hydrogen. Since the temperature range discussed in this Section is above the superconducting transition temperature of 9.2 K, experiments could only be carried out in the normal conducting electronic state.

The transition from a low-temperature coherent tunneling behavior to an incoherent jump diffusion process at higher temperatures is theoretically expected. The transition temperature defined in [13] is the temperature at which the curvature of the scattering law changes, at zero energy gain of the neutrons, from a positive to a negative value. According to the experimental results for the Kondo parameter K and and the tunnel splitting J as described in the previous section, the transition temperature is theoretically calculated to be ~11 K [7,13].

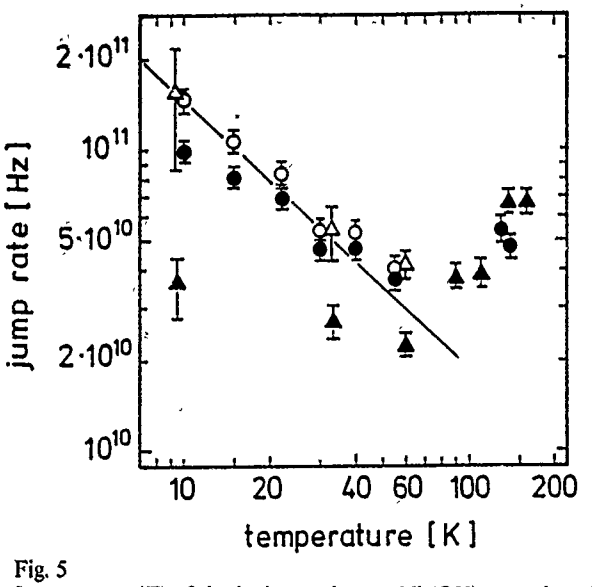


Fig. 5
Jump rates $\nu(T)$ of the hydrogen in two $Nb(OH)_x$ samples with x = 0.002 (circles) and 0.011 (triangles) [7,9]. For further details, see text

The jump rates $\nu(T)$ extracted in the temperature range above 10 K from measurements on two $Nb(OH)_x$ samples with x = 0.002 and 0.011 are compiled in Fig. 5 [7,9]. Fig. 6 shows jump rates accordingly determined for the three $Nb(NH)_x$ samples [10]. The analysis yielding the data in Fig. 5 and 6 is described in detail in [7]. It will, therefore, be discussed only briefly within this paper. However, it is pointed out that the explicit consideration of the asymmetry energies ε is important for the data analysis.

The results in Fig. 5 and 6 are summarized as follows. The solid lines are the theoretical prediction for the jump

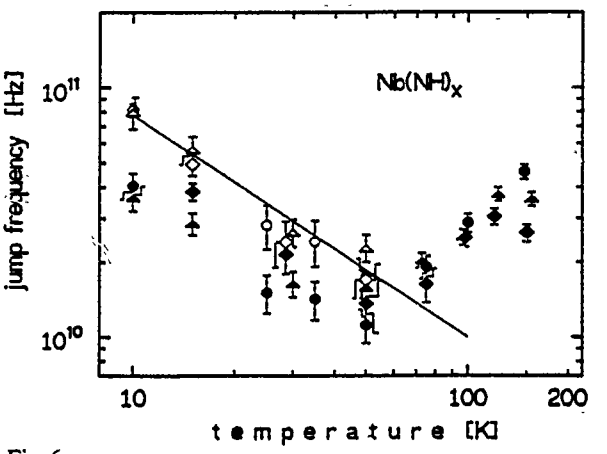


Fig. 6
Jump rates $\nu(T)$ of the hydrogen in three $Nb(NH)_x$ samples with x = 0.0005 (squares) and 0.004 (circles and triangles) [10]. For further details, see text

rate $\nu(T, \varepsilon = 0)$ derived under the assumption (i) of a (sole) nonadiabatic coupling between the hydrogen and the conduction electrons and (ii) of a vanishing asymmetry energy ε between the two interstitial sites of the hydrogen (i.e. for $\varepsilon = 0$). In thise case, the jump rate $\nu(T, \varepsilon = 0)$ is given by [7,9,11–13,16–18]

$$\nu(T, \varepsilon = 0) = \frac{1}{2} \frac{\Gamma(K)}{\Gamma(1-K)} \frac{J_n(0)}{\hbar} \left(\frac{2\pi k_B T}{J_n(0)} \right)^{2K-1} \qquad (1)$$

where $\Gamma(x)$ denotes the gamma-function. For hydrogen that is trapped by O impurities, the foregoing discussion yielded a Kondo parameter $K = (0.055 \pm 0.005)$ [6,9]. Since this quantity is not expected to vary significantly with the type of the trapping atom, it was assumed that this result is also valid in the case of N traps.

The quantity $J_n(0)$ in (1) describes the tunnel splitting in the limit $T \to 0$ for a *normal conducting* sample. For the samples in which the hydrogen was trapped by O, the corresponding result $J_n(0) = (0.206 \pm 0.003)$ meV was directly obtained from measurements in which these samples were normal conducting because of the application of a magnetic field. The measurements in which the hydrogen was trapped by N, on the other hand, were carried out on a *superconducting* sample (Fig. 3). However, we can calculate the tunnel splitting for normal conductivity from its value in the superconducting state and from the Kondo parameter K [6,15,17,18]. Using the value $J_s(0) = (0.165 \pm 0.004)$ meV for the superconducting state, we find from such a calculation an about 10% smaller tunnel splitting $J_n(0) = 0.148$ meV for normal conductivity in the case of hydrogen that is trapped by N impurities.

The above values for K and the tunnel splittings $J_n(0)$ allow the calculation of the jump rate $\nu(T, \varepsilon = 0)$ according to (1) without any further adjustable parameter. The results of this calculation are shown by the solid lines in Fig. 5 and 6. The jump rate $\nu(T, \varepsilon = 0)$ is, according to (1), proportional to T^{2K-1}, it decreases, therefore, with rising temperature.

The full data points in Fig. 5 and 6 indicate jump rates $\bar{\nu}$ that were obtained from the neutron spectra under the invalid (see later) assumption that the random asymmetry energies ε between the two interstitial sites of a hydrogen interstitial can entirely be neglected [7]. Below ~ 60 K, these jump rates decrease in both Fig. 5 and 6 with rising temperature as theoretically expected. Their absolute value is, however, smaller than that of the theoretical predictoin for $\nu(T, \varepsilon = 0)$ (solid lines in Fig. 5 and 6). The jump rates $\bar{\nu}$ exceed, on the other hand, the theoretical prediction for temperatures above ~ 60 K, increasing, at the same time, with rising temperature.

Up to now, we did not consider the influence of the asymmetry energies ε in our analysis. A consideration of these energies is possible since the (actually measured) jump rates in the presence of an asymmetry energy ε are theoretically completely determined by the value of ε and the jump rate $\nu(T, \varepsilon = 0)$ for a zero energy shift as long as we presuppose a sole nonadiabatic interaction with conduction electrons [7, 11, 12, 17, 18]. This fact allows the determination of $\nu(T, \varepsilon = 0)$ even from data which are taken from samples that exhibit asymmetry energies ε provided that we know these energies or their distribution function $Z(\varepsilon)$. The open data points in Fig. 5 and 6 are the jump rates $\nu(T, \varepsilon = 0)$ that were, in the temperature range below 60 K, accordingly derived from the spectra of the investigated samples (the procedure how $\nu(T, \varepsilon = 0)$ is determined is described in detail in [7]). The jump rates $\nu(T, \varepsilon = 0)$ were derived under the assumption of a Lorentzian distribution function $Z(\varepsilon)$ and with widths (HWHM) ε_0 for this function that were 0.2 meV ($x = 0.002$) and 8 meV ($x = 0.011$) for the $Nb(OH)_x$ samples in Fig. 5 and 0.20 meV ($x = 0.0005$), 2.2 meV ($x = 0.004$) and 3 meV ($x = 0.004$) for the $Nb(NH)_x$ samples in Fig. 6, respectively. We point out that the width of 0.20 meV for the $Nb(NH)_x$ sample with $x = 0.0005$ was directly obtained from the 1.5 K spectrum in Fig. 3 [10]; it was, therefore, not an adjustable parameter. The above widths increase further – as expected – with rising O–H or N–H pair concentration, and they agree with a quantitative estimate reported in previous specific heat measurements [22].

The jump rates $\nu(T, \varepsilon = 0)$ derived below 60 K under consideration of the asymmetry energies agree in both Fig. 5 and 6 excellently with the theoretical prediction. This agreement supports our assumption of a dominant nonadiabatic interaction with conduction electrons up to ~ 60 K, and it demonstrates the validity of Kondo's T^{2K-1} power law up to this temperature. It is worth mentioning that the jump rates $\nu(T, \varepsilon = 0)$ for hydrogen which is trapped by O (Fig. 5) are about 60% larger than those found for hydrogen trapped by N (Fig. 6). This difference reflects, according to (1), mainly the fact that the tunnel splitting $J_n(0)$ is about 30% larger in the case of the O traps.

In the case of a sole nonadiabatic interaction, the jump rate $\nu(T, \varepsilon = 0)$ for a zero asymmetry energy exceeds always the jump rate $\bar{\nu}$ derived under the (invalid) assumption of negligible asymmetry energies if an asymmetry actually does exist [7, 11, 12, 17, 18]. This means that the data above 60 K in Fig. 5 and 6 cannot be explained by a (sole) nonadiabatic interaction with conduction electrons since the differences between experimental data and theoretical prediction there would actually even increase if we would account for asymmetry energies. We conclude, therefore, that phonons begin to dominate the jump rate of the hydrogen in the temperature range above ~ 60 K. The phonons are, then, also responsible for the fact that, above ~ 60 K, the jump rates $\bar{\nu}$ in Figs. 5 and 6 increase with rising temperature.

The present work was financially supported by the Bundesministerium für Forschung und Technologie.

References

[1] J. Völkl and G. Alefeld, in: Topics in Applied Physics, Vol. 28, Hydrogen in Metals I, p. 321, eds. G. Alefeld and J. Völkl, Springer-Verlag, Berlin 1978.
[2] Y. Fukai and H. Sugimoto, Adv. Phys. *34*, 263 (1985).
[3] J. L. Wang, G. Weiss, H. Wipf, and A. Magerl, in: Springer Series in Solid State Sciences, Vol. 51, p. 401, eds. W. Eisenmenger, K. Laßmann, and S. Döttinger, Springer-Verlag, Berlin 1984.
[4] J. Kondo, Physica *125B*, 279 (1984) and *126B*, 377 (1984).
[5] K. Yamada, Progr. Theor. Phys. *72*, 195 (1984).
[6] H. Wipf, D. Steinbinder, K. Neumaier, P. Gutsmiedl, A. Magerl, and A.-J. Dianoux, Europhys. Lett. *4*, 1379 (1987).
[7] D. Steinbinder, H. Wipf, A. Magerl, D. Richter, A.-J. Dianoux, and K. Neumaier, Europhys. Lett. *6*, 535 (1988).
[8] H. Wipf and K. Neumaier, Z. Phys. Chem. Neue Folge *164*, 953 (1989).
[9] H. Grabert and H. Wipf, in: Festkörperprobleme/Advances in Solid State Physics, Vol. 30, p. 1, ed. U. Rössler, Fried. Vieweg & Sohn, Braunschweig 1990.
[10] D. Steinbinder, H. Wipf, A.-J. Dianoux, A. Magerl, D. Richter, K. Neumaier, and R. Hempelmann, J. Less-Common Metals., in print
[11] H. Grabert and U. Weiss, Phys. Rev. Lett. *54*, 1605 (1985).
[12] M. P. A. Fisher and A. T. Dorsey, Phys. Rev. Lett. *54*, 1609 (1985).
[13] H. Grabert, S. Linkwitz, S. Dattagupta, and U. Weiss, Europhys. Lett. *2*, 631 (1986).
[14] Yu. Kagan and N. V. Prokof'ev, Sov. Phys. JETP *63*, 1276 (1986).
[15] H. Teichler, Proc. Phys. (Springer-Verlag, Berlin) *17*, 167 (1987) and private communication.
[16] S. Dattagupta, H. Grabert, and R. Jung, J. Phys.: Condensed Matter *1*, 1405 (1989).
[17] U. Weiss and M. Wollensack, Phys. Rev. Lett. *62*, 1663 (1989).
[18] R. Görlich, M. Sassetti, and U. Weiss, Europhys. Lett. *10*, 507 (1989).
[19] G. Pfeiffer and H. Wipf, J. Phys. F Met. Phys. *6*, 167 (1976).
[20] A. Magerl, J. J. Rush, J. M. Rowe, D. Richter, and H. Wipf, Phys. Rev. B *27*, 927 (1983).
[21] H. Wipf, A. Magerl, S. M. Shapiro, S. K. Satija, and W. Thomlinson, Phys. Rev. Lett. *46*, 947 (1981).
[22] H. Wipf and K. Neumaier, Phys. Rev Lett *52*, 1308 (1984).
[23] K. Neumaier, D. Steinbinder, H. Wipf, H. Blank, and G. Kearley, Z. Phys. B – Condensed Matter *76*, 359 (1989).

Presented at the Discussion Meeting of the Deutsche Bunsen-Gesellschaft für Physikalische Chemie "Rate Processes in Dissipative Systems. 50 Years after Kramers" in Tutzing, September 10 – 13, 1990 E 7522

Accepted Papers

Non-Equilibrium Water Dissociation Effects in Ion Transport Through Anion Exchange Membranes with Thin Cation Exchange Surface Films

P. RAMÍREZ

Dpto. Física Aplicada, E. U. Politécnica A. Univ. Castilla-La Mancha, 02071 Albacete, Spain

(Received on September 18th, 1990; final version on January 24th, 1991)

J. A. MANZANARES, S. MAFÉ

Dpto. Termodinámica Fac. Física. Univ. Valencia, 46100 Burjassot, Spain

Gas Liquid Critical Temperatures of Binary Mixtures of Polar Compounds + Hydrocarbons or + Other Polar Compounds

G. CHRISTOU

University of Melbourne, Department of Chemistry, Parkville, Victoria 3052, Australia

C. L. YOUNG, and *P. SVEJDA*

Ruhr-Universität Bochum, Institut für Thermo- und Fluiddynamik, Postfach 102148, W-4630 Bochum 1, Germany

(Received on September 26th, 1990)

Thermodynamic Study of the Gaseous Heterocomplexes $NaSnCl_3$ and $NaSnBr_3$

K. HILPERT, M. MILLER, and *V. VENUGOPAL*

Institute for Reactor Materials Research Centre Jülich (KFA) P. O. Box 1913, W-5170 Jülich, Germany

(Received on November 20th, 1990)

Coherence in Disordered Condensed Matter. V: Thermally Activated Quantum Correlations in High-T_c Superconductivity

E. J. BRÄNDAS

Quantum Chemistry Group for Research in Atomic, Molecular and Solid State Physics, Uppsala University, Box 518, S-751 20 Uppsala, Sweden

C. A. CHATZIDIMITRIOU-DREISMANN

Iwan N. Stranski-Institute for Physical and Theoretical Chemistry, Technical University of Berlin, Straße des 17. Juni 112, W-1000 Berlin 12, Federal Republic of Germany

(Received on November 23rd, 1990)

Temperature Dependence of the Electric Conductivity of a Triethylamine/Water Mixture of Critical Composition

F. HÖHN and *D. WOERMANN*

Institut für Physikalische Chemie, Universität Köln

(Received on October 17th, 1990)

Electric Field Induced Structure Changes in Nonionic Water-in-Oil Microemulsions: Field Dependence of the Electric Conductivity

F. RUNGE, W. RÖHL, and *G. ILGENFRITZ*

Institut für Physikalische Chemie, Universität Köln, Luxemburger Straße 116, W-5000 Köln 41

(Received on January 2nd, 1991)

Thermodynamic Studies on Beta-Silver Sulfide

S. N. MOSTAFA

Chemistry Department, Faculty of Science, Al-Azhar University, Nasr City, Cairo, Egypt

(Received on September 4th, 1990, final version on January 28th, 1991)

Integration of Stiff Differential Equations Including Sensitivity Analysis by Laplace-Transformation

T. BERNDT, R. PICHT, and *K. SCHERZER*

Technische Hochschule Merseburg, Institut für Physikalische Chemie, Otto-Nuschke-Straße O-4200 Merseburg, Germany

(Received on October 22nd, 1990, final version on February 18th, 1991)

Determination of the Structure of Fluid Deuterium Chloride by Neutron Diffraction

T. BAUSENWEIN, H. BERTAGNOLLI
Institut für Physikalische Chemie der Universität Würzburg, Marcusstr. 9–11, W-8700 Würzburg
K. TÖDHEIDE
Institut für Physikalische Chemie und Elektrochemie, Universität Karlsruhe, W-7500 Karlsruhe
P. CHIEUX
Institut Laue Langevin, F-38042 Grenoble, France
(Received on October 10th, 1990, final version on January 10th, 1991)

The Influence of Unimolecular Fall-off Behaviour on Pyrolysis Systems. A Case Study

M. OLZMANN, K. SCHERZER, and *M. SCHWEDE*
Institut für Physikalische Chemie der Technischen Hochschule Merseburg, Otto-Nuschke-Straße O-4200 Merseburg, Germany
(Received on November 12th, 1990, final version on February 13th, 1991)

Precise Measurements of Second Virial Coefficients of Simple Gases and Gas Mixtures in the Temperature Range Below 300 K

B. SCHRAMM, L. KERN, GH. NATOUR, and *CH. WEBER*
Physikalisch-Chemisches Institut, Universität Heidelberg, Im Neuenheimer Feld 253, W-6900 Heidelberg, Germany
(Received on November 30th, 1990, final version on February 19th, 1991)

Osmotic Properties of Crystalline Inorganic Precipitation Membranes: Study of Barium Sulfate Membranes

M. MILZ, R. FORKE, D. WOERMANN
Institut für Physikalische Chemie, Universität Köln
U. SUNN
Department of Chemistry, Rangoon University, Burma
(Received on November 30th, 1990)

The Dielectric Properties of tert.-Butanol/Water Mixtures as a Function of Composition

U. KAATZE, A. SCHUMACHER, and *R. POTTEL*
Drittes Physikalisches Institut, Universität Göttingen, Bürgerstraße 42–44, W-3400 Göttingen
(Received on December 5th, 1990)

Zusammensetzung, Eigenschaften und Anwendungen Mesomorpher Tensidphasen

RUDOLF HEUSCH
Leverkusen, Paul-Klee-Straße 85
(Received on December 19th, 1990)

Site Specific Surface Interaction of Electron Donors and Acceptors on FeS_2 (100) Cleavage Planes

C. PETTENKOFER, W. JAEGERMANN, and *M. BRONOLD*
Hahn-Meitner-Institut, Abteilung Solare Energetik Glienicker Straße 100, W-1000 Berlin 39, Germany
(Received on December 21st, 1990, final version on February 13th, 1991)

Photochromic Characteristics of Mixded WO_3–MoO_3 Thin Films in Alcohol Vapors

J. N. YAO, B. H. LOO, K. HASHIMOTO, and *A. FUJISHIMA*
Department of Synthetic Chemistry, Faculty of Energineering, University of Tokyo, Hongo, Tokyo 113, Japan
(Received on January 15th, 1991)

Photo-Enhancement of Electrochromism in MoO_3 Thin Films

J. N. YAO[1], *B. H. LOO*[1,2], *K. HASHIMOTO*[1], and *A. FUJISHIMA*[1]
[1] Department of Synthetic Chemistry, Faculty of Engineering, The University of Tokyo, Hongo, Tokyo 113, Japan
[2] Department of Chemistry, The University of Alabama in Huntsville, Huntsville, AL 35899, USA
(Received on January 17th, 1990)

Electrostatic Interactions of Bodies Bearing Thin Double-Layers III Dissimilar Double-Layers

Z. ADAMCZYK, P. BELOUSCHEK, and *D. LORENZ*

Institute of Physical Chemstry of the University Essen, Universitätsstraße 5–7, W-4300 Essen FRG

Institut of Catalysis and Surface Chemistry Polish Academy of Sciences 30–239 Krakow, ul. Niezapominajek 1, Poland

(Received on January 25th, 1991)

The Absorption Spectrum of the Nitrate (NO_3) Radical in Aqueous Solution

H. HERRMANN and *M. EXNER*

Institut für Physikalische Chemie, Universität Göttingen, Tammannstraße 6, W-3400 Göttingen, West Germany

R. ZELLNER

Institut für Physikalische Chemie und Elektrochemie Universität Hannover, W-3000 Hannover

(Received on January 2nd, 1991)

Dynamics of 18-Crown-6 Ether in Aqueous Solution Studied by Quasielastic Neutron Scattering

H. W. PELC[1,2], *R. HEMPELMANN*[2,1], *M. PRAGER*[2], and *M. D. ZEIDLER*[1]

[1] Institut für Physikalische Chemie, Rheinisch-Westfälische Technische Hochschule Aachen, Templergraben 59, W-5100 Aachen

[2] Institut für Festkörperforschung, Forschungszentrum Jülich, Postfach 1913, W-5170 Jülich

(Received on February 1st, 1991)

Electromagnetic Response of an Electrically Small Bianisotropic Ellipsoid Immersed in a Chiral Fluid

AKHLESH LAKHTAKIA

Department of Engineering Science and Mechanics, Pennsylvania State University, University Park, PA 16802 USA

(Received on February 13th, 1991)

Vorstand der Bunsen-Gesellschaft:
Prof. Dr. F. Hensel
Erster Vorsitzender
Dr. K. Schuhmann
Zweiter Vorsitzender
Dr. K. von Kessel
Schatzmeister

Geschäftsführer:
Dr. H. Behret

Personalia

Ehrungen

Prof. Dr. Joachim Maier, Max-Planck-Institut für Festkörperforschung, Stuttgart, Mitglied der Bunsen-Gesellschaft, hat den Ruf auf eine C4-Professur für Werkstoffwissenschaft an der Universität des Saarlandes erhalten.

Dr. Roland Rubner, Fachgebietsleiter in der Zentralen Forschung und Entwicklung der Siemens AG, Erlangen, Mitglied der Bunsen-Gesellschaft, wurde zum Honorarprofessor an der Universität Erlangen ernannt.

Prof. Dr. Horst T. Witt, Institut für Biophysikalische und Physikalische Chemie der Technischen Universität Berlin, Mitglied der Bunsen-Gesellschaft, wurde mit der "Otto-Warburg-Medaille" ausgezeichnet.

Geburtstage

Prof. Dr. Fritz Beck, FB 6/Elektrochemie der GHS Duisburg, Lotharstraße 63, 4100 Duisburg, beging am 5. März seinen 60. Geburtstag.

Prof. Dr.-Ing. Bernhard Schrader, Soniusweg 20, 4300 Essen 15, beging am 15. März seinen 60. Geburtstag.

Prof. Dr. Konrad Heusler, Einersberger Blick 21, 3392 Clausthal-Zellerfeld, beging am 22. März seinen 60. Geburtstag.

Prof. Dr. Frigyes Solymosi, Institute of Solid State and Radiochemistry, University of Szeged, P.O. Box 105, H-6710 Szeged, beging am 30. März seinen 60. Geburtstag.

Prof. Dr. Ernst Schumacher, Institut für Anorganische Chemie der Universität Bern, Freie Straße 3, CH-3000 Bern, beging am 12. März seinen 65. Geburtstag.

Prof. Dr. Dr. Heinz A. Staab, Schloß-Wolfsbrunnenweg 43, 6900 Heidelberg, beging am 26. März seinen 65. Geburtstag.

Prof. Dr. Josef Brandmüller, Hubertusstraße 61, 8035 Gauting, beging am 28. März seinen 70. Geburtstag.

Todesfall

Prof. Dr. D. Nakamura, Daiman-cho 2-57, Meito-hu, 465 Nagoya, Japan, ist am 27. Februar 1991 im Alter von 56 Jahren verstorben.

Neuanmeldungen zur Mitgliedschaft

Nr. 77038 Heuchel, Matthias, Dr. (Fachbereich Chemie, Universität Leipzig) Josephinenstraße 31, O-7050 Leipzig
(durch G. Geiseler)

Nr. 77039 Wiemhöfer, Hans-Dieter, Dr. (Institut für Physikalische und Theoretische Chemie der Universität Tübingen, Auf der Morgenstelle 8, W-7400 Tübingen) (durch W. Göpel)

Nr. 77040 Geipel, Gerhard, Dr. (Zentralinstitut für Kernforschung, Rossendorf) Am Pfeiferberg 9, O-8101 Schullwitz
(durch G. Kreysa)

Nr. 77041 Rex, Sibylle (Universität Leipzig) Scheffelstraße 50c, O-7030 Leipzig (durch G. Geiseler)

Nr. 77042 Keller, Michael, Dipl.-Chem. (RWTH Aachen, Institut für Physikalische Chemie, Templergraben 59, W-5100 Aachen) (durch H. Versmold)

Nr. 77043 Beuermann, Sabine, Dipl.-Chem. (Institut für Physikalische Chemie der Universität Göttingen) Stumpfe Eiche 13, W-3400 Göttingen
(durch M. Buback)

Nr. 77044 Jäger, Martin (Institut für Physikalische Chemie der Universität Frankfurt am Main, Niederurseler Hang, W-6000 Frankfurt/Main 50)
(durch K. Dehe)

Nr. 77045 Richter, Manfred Dr. (Zentralinstitut Physikalische Chemie, Berlin) Rosa-Luxemburg-Straße 9, O-1600 Königs Wusterhausen
(durch H. Behret)

Nr. 77046 Sauer, Joachim, Dr. (Zentralinstitut für Physikalische Chemie, Rudower Chaussee 5, O-1199 Berlin-Adlershof)
(durch R. Ahlrichs)

Nr. 77047 Dähne, Siegfried, Prof. Dr. (Analytisches Zentrum Berlin, Rudower Chaussee 5, O-1199 Berlin-Adlershof)
(durch W. A. P. Luck)

Nr. 77048 Fiedler, Klaus, Dr. (Zentralinstitut für Physikalische Chemie, Rudower Chaussee 5, O-1199 Berlin) Babeufstraße 45, O-1017 Berlin
(durch H. R. von Hirschhausen)

Nr. 77049 Marian, Christel, Dr. (Institut für Physikalische und Theoretische Chemie der Universität Bonn, Wegelerstraße 12, W-5300 Bonn 1)
(durch S. Peyerimhoff)

Nr. 77050 Bockhorn, Henning, Prof. Dr. (Physikalisch-chemisches Institut, Universität Heidelberg, Im Neuenheimer Feld 253, W-6900 Heidelberg)
(durch J. Wolfrum)

Nr. 77051 Hoang, Dang Lanh Dr. (AdW, Zentralinstitut für Physikalische Chemie, Rudower Chaussee 5, O-1199 Berlin) Kremmener Straße 14, O-1058 Berlin (durch H. Behret)

Nr. 77052 Patz, Rainer, Dr. (TH Merseburg, Postfach, O-4200 Merseburg) Weinberg 2, O-4200 Merseburg (durch H. Behret)

Nr. 77053 Brand, Paul, Prof. Dr. (Bergakademie Freiberg, Fachbereich Chemie, Institut für Physikalische Chemie) Maxim-Gorki-Straße 18, O-9200 Freiberg (durch F. Hensel)

Nr. 77054 Pelzl, Gerhard, Dr. (Sektion Chemie, WB Physikalische Chemie, Martin-Luther-Universität Halle, Mühlpforte 1, O-4020 Halle/S)
(durch D. Demus)

Nr. 77055 Struve, Peter, Dr. (Zentralinstitut für Physikalische Chemie Berlin, Rudower Chaussee 5) Markomannenstraße 28, O-1185 Berlin (durch H. Behret)

Nr. 77056 Dombrowski, Dieter, Dr. (Karl-Marx-Universität Leipzig, Sektion Chemie) Michaelisstraße 5, O-7010 Leipzig
(durch H. Behret)

Nr. 77057 Mögel, Hans-Jörg, Doz. Dr. (Bergakademie Freiberg, Institut für Physikalische Chemie) P. v. Ladenbergstraße 23, O-4070 Halle/S
(durch G. Brezesinski)

Nr. 77058 Janietz, Peter-Johannes, Dr. (Humboldt-Universität, Fachbereich Chemie) Lienhardtweg 33, O-1178 Berlin
(durch W. Gründler)

Nr. 77059 Hartung, Helmut, Prof. Dr. (Universität Halle, Institut für Physikalische Chemie) Rudolf-Haym-Straße 17, O-4200 Halle/S. (durch H. Sackmann)

Nr. 77060 Voigt, Wolfgang, Prof. Dr. (Institut für Physikalische Chemie, Bergakademie Freiberg) Friedmar-Brendel-Weg 13, O-9200 Freiberg
(durch H. Behret)

Nr. 77061 Millat, Jürgen, Doz. Dr. (Universität Rostock, Fachbereich Chemie, WB Physikalische Chemie) Schiffbauerring 5, O-2520 Rostock 27
(durch H. Behret)

Nr. 77062 Näfe, Helfried, Dr. (Max-Planck-Institut für Festkörperforschung, Stuttgart) Postfach 204-14, Bautzner Landstraße 90, O-8051 Dresden
(durch W. Weppner)

Nr. 77063 Schmelzer, Jürgen, Dr. (Karl-Marx-Universität Leipzig, Sektion Chemie) Möbiusstraße 11, O-7050 Leipzig
(durch U. Messow)

Nr. 77064 Kosslick, Hendrik, Dr. (Zentralinstitut für Physikalische Chemie, Berlin 1199) Schönhauser Allee 42, W-1000 Berlin 58 (durch H. Behret)

Nr. 77065 Heidrich, Dietmar, Doz. Dr. (Sektion Chemie, Universität Leipzig) Augustusplatz/HG, O-7010 Leipzig
(durch H. Behret)

Nr. 77066 Guth, Ulrich, Dr. (Ernst-Moritz-Arndt-Universität Greifswald, Fachbereich Chemie, Soldtmannstraße 16, O-2200 Greifswald) Kräpeliner Wende 8, O-2200 Greifswald
(durch D. Möbius)

Nr. 77067 Quitzsch, Konrad, Prof. Dr. (Universität Leipzig, Fachbereich Chemie/WB Physikalische Chemie) Maurice-Thorez-Straße 24, O-7031 Leipzig
(durch U. Messow)

Nr. 77068 Müller, Thomas S. (Institut für Physikalische Chemie der Universität Saarbrücken, Bau 9.2) - Im Stadtwald - W-6600 Saarbrücken
(durch H. D. Breuer)

Nr. 77069 Schuh, Jörg, Dipl.-Chem. (Institut für Physikalische Chemie der Universität Saarbrücken) Kirchhofstraße 2, W-6670 St. Ingbert (durch H. D. Breuer)

Veranstaltungen

Tagungen der Deutschen Bunsen-Gesellschaft

Hauptversammlung 1991 – Thema. „Physikalisch-chem. Aspekte dünner Schichten"
Vom 9. bis 11. Mai 1991 in Bochum.
Wissenschaftliche Vorbereitung: H Cherdron, Frankfurt am Main, G. Ertl, Berlin, H. Oechsner, Kaiserslautern und K. G. Weil, Darmstadt.
(Siehe auch Programm in Heft 2/91).

Hauptversammlung 1992 – Thema. „Festkörper: Thermodynamik, Struktur und Bindung"
Vom 28. bis 30. Mai 1992 in Wien.
Wissenschaftliche Vorbereitung. R. Hoppe, Gießen, K. L. Komarek, Wien, A. Neckel, Wien und H. Schmalzried, Hannover.

Hauptversammlung 1993 – Thema: „Flüssigkristalle" (Arbeitstitel)
Vom 20. bis 22. Mai 1993.
Wissenschaftliche Vorbereitung: H. Finkelmann, Freiburg i. Br., R. Rubner, Erlangen und H. Stegemeyer, Paderborn.

Hauptversammlung 1994 mit 100-Jahr-Feier der Gesellschaft
Vom 12. bis 14. Mai 1994 in Berlin.

Hauptversammlung 1995
Vom 25. bis 27. Mai 1995.

Bunsen-Diskussionstagung Herbst 1991, 169th Event of the FECS – Thema: „Physikalische Chemie der Atmosphäre"
Vom 7. bis 9. Oktober 1991 in Schliersee.
Wissenschaftliche Vorbereitung: H. Baumgärtel, Berlin, R. Zellner, Göttingen und C. Zetzsch, Hannover.
(Siehe auch Ankündigung in Heft 2/91)

Bunsen-Diskussionstagung Frühjahr 1992 – Thema: „Reaktivität von Clustern"
Frühjahr 1992.
Wissenschaftliche Vorbereitung: H. Baumgärtel, Berlin, F. Hensel, Marburg und E. W. Schlag, München.

Bunsen-Diskussionstagung Herbst 1992 – Thema: „In-situ-Untersuchungen physikalisch-chemischer Prozesse an Grenzflächen"
Herbst 1992.
Wissenschaftliche Vorbereitung: G. Ertl, Berlin, W. Göpel, Tübingen, H. Knözinger, München und W. Schultze, Düsseldorf.

Bunsen-Diskussionstagung Frühjahr 1993 – Thema: „Laserdiagnostik für industrielle Prozesse"
Frühjahr 1993.
Wissenschaftliche Vorbereitung: J. Wolfrum, Heidelberg.

48. Bunsen-Kolloquium – Thema: „Nichtlineare Prozesse in Oxiden unter hohen elektrischen Feldern"
Vom 29. bis 30. August 1991 in Aachen.
Wissenschaftliche Vorbereitung: M. Martin, Hannover und R. Waser, Aachen.
(Siehe auch Ankündigung in Heft 2/91)

49. Bunsen-Kolloquium – Thema: „Die Anwendung von Synchrotronstrahlung zur Lösung chemischer Probleme"
Erste Jahreshälfte 1991 in Berlin.
Wissenschaftliche Vorbereitung: H. Baumgärtel, Berlin und F. Hensel, Marburg.

50. Bunsen-Kolloquium – Thema. „Physikalisch-chemische Grundlagen der Protein-Immobilisierung bei Biokatalyse und Biosensoren" (Arbeitstitel)
Wissenschaftliche Vorbereitung: K. Schügerl, Hannover.

"8th International Conference on Fourier Transform Spectroscopy" des Deutschen Arbeitskreises für Angewandte Spektroskopie in der Fachgruppe Analytische Chemie der Gesellschaft Deutscher Chemiker unter der Schirmherrschaft der Deutschen Bunsen-Gesellschaft für Physikalische Chemie, Deutschen Physikalischen Gesellschaft, Working Party on Analytical Chemistry (WPAC) of the Federation of European Chemical Societies (FECS)
Vom 1. bis 6. September 1991 in Lübeck-Travemünde.
Auskunft: Gesellschaft Deutscher Chemiker, Abteilung Tagungen, Postfach 900440, D-6000 Frankfurt am Main 90.

Joint Meeting Herbst 1991 – Société Française de Chimie, Division de Chimie Physique, gemeinsam mit: Associazione Italiana di Chimica Fisica. Deutsche Bunsen-Gesellschaft für Physikalische Chemie, Faraday Division of the Royal Society of Chemistry – Thema: "Synchrotron Radiation and Dynamic Phenomena"
Vom 9. bis 13. September 1991 in Grenoble/Frankreich.
Wissenschaftliche Vorbereitung: H. Baumgärtel, Berlin; J. A. Beswick, Orsay; C. R. A. Catlow, London; P. Decleva, Triest; H. Dexpert, Orsay; E. Geissler, Grenoble; J. Goulon, Grenoble; J. Lajzerowicz, Grenoble; I. Nenner, Orsay; J. Pannetier, Grenoble; C. Troyanowsky, Paris.
Auskunft: Dr. C. Troyanowsky, Société de Chimie Physique, 10, Rue Vauquelin, F-75231 Paris Cedex 05, Tel.: Paris 47075448.
(Siehe auch Ankündigung in Heft 7/90).

Joint Meeting Herbst 1992 – Associazione Italiana di Chimica Fisica, Divissione di Chimica Fisica Della Società Chimica Italiana, gemeinsam mit: Deutsche Bunsen-Gesellschaft für Physikalische Chemie, Faraday Division of the Royal Society of Chemistry, Société Française de Chimie, Division de Chimie Physique, – Thema: "European Conference on Molecular Electronics"
Vom 24. bis 28. August 1992 in Padua.
Wissenschaftliche Vorbereitung: G. Giacometti, Padua, F. Hensel, Marburg, C. Pecile, Padua, R. Bozio, Padua.
Auskunft: Prof. R. Bozio, ECME '92, Department of Physical Chemistry, 2 Via Loredan 2, I-35131 Padova, Italy.

Faraday Division of The Royal Society of Chemistry with Polymer Physics Group and Macro Group UK – "Polymer Surfaces and Interfaces II"
Vom 21.–26. Juli 1991, University of Durham.
Auskunft: Dr. M. J. Richardson, National Physical Laboratory, Teddington, Middlesex TW11 0LW.

Faraday Division of The Royal Society of Chemistry with Polymer Physics Group – "Biennial Meeting"
Vom 9.– 11. September 1991, University of Leeds
Auskunft: Dr. M. J. Richardson, National Physical Laboratory, Teddington, Middlesex TW11 0LW.

Faraday Division of The Royal Society of Chemistry with Colloid and Interface Science Group – "Adsorption of Surfactants and Polymers"

Vom 10. – 12. September 1991, University of Bath.

Auskunft: Dr. W. D. Cooper, Shell Research Ltd., Thornton Research Centre, P. O. Box 1, Chester CH1 3SH.

Faraday Division of The Royal Society of Chemistry with Polymer Physics Group and the Institute of Marine Engineers – "Polymers in a Marine Environment"

Vom 23. – 25. Oktober 1991, London

Auskunft: Rhian Bufton, Conference Organiser, Institute of Marine Engineers, The Memorial Biulding, 76 Mark Lane, London EC3R 7JN.

Versammlungen und Veranstaltungen

„Energieversorgung – Dienstleistung für rationelle Energienutzung"

Vom 2.–3. Mai 1991, Schliersee.

Auskunft: VDE-Zentralstelle Tagungen und Seminare, Stresemannallee 15, 6000 Frankfurt/Main 70.

33. IUPAC Congress of Pure and Applied Chemistry

Vom 17.–22. August 1991, Budapest, Ungarn.

Auskunft: Hungarian Academy of Sciences, attn.: E. Pungor, ter 4, Gellert, H-1111 Budapest.

8. International Conference on Fourier Transform Spectroscopy

Vom 1.–6. September 1991, Travemünde.

Auskunft: Gesellschaft Deutscher Chemiker, Abteilung Tagungen, Postfach 90 04 40, 6000 Frankfurt/Main 90.

6. European Electromagnetic Structures Conference

Vom 4.–6. September 1991, Friedrichshafen.

Auskunft: Dornier Luftfahrt GmbH, Dep. SN 10, z.H. Dr. J. Wiedmann, P. O. Box 13 03, 7990 Friedrichshafen 1.

1st European Metals Conference on "Nonferrous Metallurgy"

Vom 15.–20. September 1991, Brüssel/B.

Auskunft: Gesellschaft Deutscher Metallhütten- und Bergleute, Postfach 10 54, 3392 Clausthal-Zellerfeld.

Conference on Speciality Polymers (SP): Supermolecular Aspects of Polymer Synthesis and Polymer Structure

Vom 30. September–2. Oktober 1991, Mainz.

Auskunft: Butterworth Scientific Ltd., Conference Organizer, P. O. Box 63, Westbury House, Bury St., Buildford, Surrey GU2 5BH, UK.

Energy Efficiency Measures

Oktober 1991, Ljubljana, Yugoslavia.

Auskunft: United Nations, Energy Div. Economic Commission for Europe, attn.: F. Romig, Palais des Nations, CH-1211 Geneva 10.

Third European Forum Eurospore 91

Vom 6.–8. November 1991, Hyeres, France.

Auskunft: Eurospore 91, Association Bernard Gregory, Université de Toulon et du Var, BP 132, F-83957 La Garde Cedex.

3rd International Symposium on Trends and New Applications in Thin Films

Vom 25.–29. November 1991, Straßburg.

46. Bunsen-Kolloquium

„Kinetik von Elektronentransferreaktionen in Lösung"

Das 46. Bunsen-Kolloquium, vom 26. bis 28. September 1990 in Erlangen, hat großen Anklang gefunden. Die Vorbereitung lag in den Händen von Priv.-Doz. Dr. G. Grampp. Besonders haben wir uns über die Teilnahme russischer Wissenschaftler gefreut, die einen großen Beitrag zu den Diskussionen lieferten. In vielen persönlichen Gesprächen kam die Hoffnung zum Ausdruck, ein solch erfolgreiches Kolloquium in ca. zwei Jahren zu wiederholen. Diesen Wunsch äußerten brieflich auch amerikanische Kollegen, die nicht an dem Kolloquium teilnehmen konnten.

Wissenschaftlich im Vordergrund standen diejenigen Themen, die auch derzeit in der Fachliteratur heftig diskutiert werden. An erster Stelle ist hier die Diskussion des dynamischen Einflusses von Lösungsmitteln auf die Kinetik von Elektronentransferreaktionen zu nennen. Dieser Einfluß wird dadurch vorausgesagt, daß gewisse Lösungsmitteleigenschaften (z.B. die longitudinale Relaxationszeit τ_L) im präexponentiellen Faktor der Geschwindigkeitsgleichung auftreten. Beiträge zu dieser Thematik stammten von L. D. Zusman (Novosibirsk), M. V. Basilevsky (Moskau), W. Nadler (Tübingen) und K. V. Mikkelsen (Kopenhagen). Mit den experimentellen Ergebnissen dieses Lösungseinflusses befaßten sich die Vorträge von P. Suppan (Fribourg), H. Rau (Stuttgart) und S. Farid (Rochester, USA).

Über den Einfluß von Magnetfeldern auf die Kinetik von photoinduzierten Elektronentransferreaktionen referierten A. Weller (Göttingen) und U. E. Steiner (Konstanz). In den Vorträgen von S. Fischer (München) und T. Clark (Erlangen) wurden theoretische Gesichtspunkte des Elektronentransfers abgehandelt.

Mehrere Beiträge befaßten sich mit experimentellen Methoden. So berichtete J. Daub (Regensburg) über spektroelektrochemische Methoden und R. van Eldik (Witten-Herdecke) über druckabhängige Untersuchungen zum Elektronentransfer. Über Untersuchungen zum intramolekularen Elektronentransfer berichten K. H. Drexhage (Siegen) und A. Vogler (Regensburg).

Über die Bedeutung des Elektronentransfers bei der Photosynthese gaben die Vorträge von A. Angerhofer (Stuttgart) und C. C. von Borczyskowski (Berlin) einen Einblick. Berührungspunkte zum Elektronentransfer an Festkörpern klangen in dem Beitrag von D. Faßler (Jena) und D. Meissner (Hannover) an.

Zudem wurden noch Poster zum Thema präsentiert und die Postersession fand ebenfalls großen Anklang.

Auskunft: M. J. Fauvet, S. F. V.-Soc. Francaise du Vide, 19, rue du Renard, F-75004 Paris.

4th Conference Separation of Ionic Solutes SIS' 91

Vom 9.–13. Dezember 1991, Smolenice, Czecho-Slovakia.

Auskunft: Dr. Silvia Cechová, Secretary SIS' 91, Kat. jadrovej chémie PFUK, Mlynská, dolina CH-1, 842 15 Bratislava, Czecho-Slovakia.

Conference on Electrochemical Engineering and the Environment

Vom 7.–9. April 1992, Loughborough, UK

Auskunft: Dr. R. J. Mortimer, Dept. of Chemistry, Univ. of Technology, Loughborough LE11 3TU, UK.

4th International Conference on Molten Slags and Fluxes

Vom 8.–11. Juni 1992, Sendai, Japan.

Auskunft: Secretariat, Molten Slags & Fluxes '92, The Iron and Steel Institute of Japan, Keidanren Kaikan, 3rd Floor, 1-9-4, Otemachi, Chiyoda-ku, Tokyo 100, Japan.

Verschiedenes

Arbeitskreis für Chemosensoren

Im Rahmen der letzten Vorstandssitzung der GDCh-Fachgruppe Analytische Chemie wurde auf Anregung von Prof. Camman, Münster, vereinbart. Vorbereitungen zur Gründung eines Arbeitskreises „Chemosensoren" zu treffen. Wegen des interdisziplinären Charakters, der z.B. bei den Biosensoren als einer der Untergruppen der Chemosensoren besonders ausgeprägt ist, soll dieser Arbeitskreis fachgruppenübergreifend etabliert werden. Gedacht ist neben einer Mitbeteiligung der GDCh-Fachgruppen Biochemie und Wasserchemie auch an die Deutsche Bunsen-Gesellschaft.

Es wurde bemerkt, daß die Chemiker die Entwicklung und Eignungsprüfung von Sensoren zur chemischen Analyse nicht allein den Elektronikern oder ihrem Standardisierungsinstitut überlassen können. Auf der ANAKON '91 von 22. bis 24. April 1991 sowie auf der nächsten Bunsentagung vom 9. bis 11. Mai 1991 in Bochum sollen außerhalb des Programms Treffen durchgeführt werden, auf denen über die Arbeitsfelder dieses neuen Arbeitskreises diskutiert werden soll. Der Arbeitskreis für Chemosensoren soll, ähnlich z.B. der Arbeitsgemeinschaft Massenspektrometrie (AGMS), auch Wissenschaftlern angrenzender Disziplinen offenstehen.

Ausschreibung

An der Fakultät für Chemie der Ruhr-Universität Bochum ist eine

Professur C3 für Physikalische Chemie

kurzfristig wiederzubesetzen.

Von dem Bewerber/der Bewerberin wird erwartet, daß er/sie in der Lage ist, die Physikalische Chemie in der Lehre in voller Breite zu vertreten. In den wissenschaftlichen Aktivitäten soll er/sie die an der Fakultät für Chemie vorhandenen Forschungsrichtungen im Fach Physikalische Chemie sinnvoll ergänzen. Habilitation oder gleichwertige wissenschaftliche Leistungen werden vorausgesetzt. Die Ruhr-Universität Bochum bemüht sich um die Förderung von Frauen in Forschung und Lehre. Die Bewerbung geeigneter Schwerbehinderter ist erwünscht.

Bewerbungen mit Lebenslauf, Publikationsliste und Verzeichnis der abgehaltenen Lehrveranstaltungen sind bis 26. April 1991 an den Dekan der Fakultät für Chemie der Ruhr-Universität Bochum, Postfach 102148, W-4630 Bochum 1, zu richten.

Bücher

R. Carbó and M. Klobukowski (Eds.): **Self-consistent Field – Theory and Applications**, Bd. 70 der Reihe: **Studies in Physical and Theoretical Chemistry**, Elsevier, Amsterdam and New York 1990. ISBN 0-444-88168-9, 920 Seiten, Preis: Dfl. 560.–.

Das vorliegende Buch gibt auf rund 900 Seiten einen sehr vollständigen Überblick über ein wichtiges Gebiet der theoretischen Chemie, nämlich das der selbstkonsistenten Felder. Darunter wird die näherungsweise Behandlung der elektronischen Wechselwirkung mit Hilfe von gemittelten Potentialen verstanden. Diese einschneidende Näherung hat die theoretische Behandlung vieler Moleküle überhaupt erst ermöglicht. Sie dient weiterhin als Ausgangspunkt verbesserter Theorien, welche die Behandlung elektronischer Korrelationen einschließen.

Das Konzept der selbstkonsistenten Felder (SCF) ist heute so gut verstanden, und die Anwendungen sind inzwischen so vielseitig, daß ein umfassender Überblick über das Gebiet wünschenswert ist. Das Buch füllt somit eine Lücke. In 23 Beiträgen werden die verschiedenen Aspekte der Theorie und deren Anwendungen beleuchtet. Ein zentrales Thema ist dabei die Diskussion von Instabilitäten von Hartree-Fock Lösungen. Hier geben die Artikel von Paldus, Cook, Smeyers u.a. eine erschöpfende Übersicht. Das Thema taucht in vielen der Beiträge auf. Nicht immer wird dabei klar unterschieden zwischen Instabilitäten, die artifiziell sind und nur deshalb auftreten, weil in einer Hartree-Fock Rechnung die elektronischen Korrelationen fehlen (Beispiel H_2 Molekül bei großen interatomaren Abständen) und solchen, die „echt", d.h. auch bei Einschluß von Korrelationen vorhanden sind (Beispiel: Dimerisierung in Polyacetylen.)

Neben den normalen SCF Verfahren werden auch solche mit mehreren Ausgangskonfigurationen (MC SCF) ausführlich behandelt. So wird überzeugend gezeigt, daß MC SCF Rechnungen als Standardmethode zum Verständnis von Reaktivitäten dienen können (Robb). Auch die praktische Bestimmung optimaler Orbitale für SCF und MC SCF Rechnungen wird ausführlich diskutiert.

Eine Reihe von Beiträgen befassen sich mit rechentechnischen Fortschritten, die gemacht wurden, um SCF Lösungen zu erhalten. Hier ist der Beitrag von Almlöf und Faegri über „direkte SCF Verfahren" zukunftsweisend, da mit diesem verbesserten Verfahren auch größere Moleküle rechenbar werden. In dieselbe Rubrik fallen Verfahren zur direkten numerischen Berechnung von Wellenfunktionen nach der MC SCF Methode (Hinze und Bieglер-König). Ein Verfahren zur direkten Minimalisierung der Energie in der Hartree-Fock-Näherung, d.h. ohne vorherige Berechnung von Orbitalen, wird ebenfalls beschrieben (Fernández Rico). Relativistische Korrekturen mit vielen Beispielen werden in einem anderen Beitrag behandelt (Malli). Die lokale Spin-Dichtenäherung für den Austausch wird in einem sehr schönen Beitrag ebenfalls diskutiert (Whitehead). Sehr klar beschrieben wird die Propagator Methode unter Benutzung von Superoperatoren (Pickup). Insgesamt sind die Anwendungen der selbstkonsitenten Felder schwächer vertreten als die rein methodischen oder theoretischen Beiträge. Die Schwerpunkte liegen dabei bei den Polymeren (André und Delhalle) sowie bei den elektrischen und magnetischen Eigenschaften (Craw et al.). Festkörper werden nicht diskutiert. Diese Beispiele mögen einen kleinen Überblick über den Themenkreis geben, der im Buch ausführlich behandelt wird.

Wie nicht anders zu erwarten, sind die verschiedenen Beiträge von recht unterschiedlicher Qualität. Einige der besonders wichtigen und klar geschriebenen Abhandlungen wurden bereits erwähnt. Einige der behandelten Themen sind stark spezialisiert, weil die Theorie inzwischen weit entwickelt ist. So sind z.B. die Arbeiten zur „Minimalisierung der elektronischen Energie durch Cayley orthogonale Transformationen der Orbitale" im wesentlichen auf eine Gruppe beschränkt (Polezzo et al.) und unter den 25 Zitaten finden sich nur 5 Fremdzitate. Ein Beitrag, der Verständ-

nisschwierigkeiten bereitet, ist der von Yamaguchi, der übrigens voller Druckfehler ist. Zum Beispiel enthält der Aufsatz die Feststellung, daß HF Rechnungen gezeigt hätten, da die Cu–O Bindungen in den neuen Hochtemperatur-Supraleitern nicht zu den stark, sondern zu den mittelstark korrelierten Systemen zu zählen sind. Hier werden offenbar verschiedene Begriffe vermischt, denn die gemachte Feststellung ist sicher nicht richtig. Zusammenfassend kann man feststellen, daß das vorliegende Buch seinen Zweck erfüllt und regen Anklang bei den Quantenchemikern finden sollte. Es gibt eine absolut kompetente und vollständige Darstellung eines sehr wichtigen Gebiets der theoretischen Chemie.

P. Fulde

C. P. Slichter:
Principles of Magnetic Resonance, 3rd enlarged and updated ed., Vol. 1 aus der Reihe: **Springer Series in Solid State Sciences,** Springer-Verlag, Berlin 1990. ISBN 3-340-50157-6, 655 Seiten, Preis: DM 89,–.

Als Charles P. Slichter 1963 die erste Auflage seines inzwischen weltweit bekannten und geschätzten Buches veröffentlichte, konnte noch niemand erahnen, welche Bedeutung magnetische Resonanzmethoden in der Chemie und Medizin einmal erlangen sollten. Der damalige Untertitel „mit Beispielen aus der Festkörperphysik" kann fast programmatisch gedeutet werden; denn neben den 2 D-FT-NMR-Methoden in Lösung, der EPR-Spektroskopie und der NMR-Tomographie, ist es gerade die NMR-Festkörperspektroskopie, die in den letzten beiden Jahrzehnten durch technische und methodische Fortschritte völlig neue Möglichkeiten zum Studium der kondensierten Materie auf mikroskopischem Niveau erschlossen hat. Um das heute existierende und beeindruckende experimentelle NMR-Potential aber wirklich ausnutzen zu können, bedarf es intimer theoretischer Kenntnisse der auf dem Gebiet der magnetischen Resonanz tätigen Wissenschaftler und einer entsprechenden Ausbildung unserer Mitarbeiter. Slichters Buch wendet sich nach eigener Aussage an fortgeschrittene "Studenten der magnetischen Resonanz" (Physiker, Chemiker, Materialwissenschaftler, Biologen, Mediziner) mit entsprechenden Vorkenntnissen in Quantenmechanik. Anstelle einer erschöpfenden Darstellung einzelner Themen soll der „Student durch das Buch vorbereitet werden, Literatur auf diesem Gebiet lesen zu können".

Schon der Umfang spiegelt zu Recht die dramatische Entwicklung auf dem NMR- und EPR-Gebiet wider. Während die erste Auflage (1963) noch mit 246 Seiten auskam, waren es bei der zweiten Auflage (1980, erstmals in der "Springer Series") 397 und sind es jetzt 655 Seiten. Dabei wurden die ersten vier Kapitel (Elemente der Resonanz, Grundlagentheorie, magnetische Dipolverbreiterung in starren Gittern, magnetische Wechselwirkungen von Kernen und Elektronen) von einigen nützlichen Ergänzungen (quantenmechanische Behandlung von Spinechos, Verschiebungstensoren für Einkristalle) abgesehen im wesentlichen übernommen. Das gleiche gilt für die Behandlung der elektrischen Quadrupoleffekte (Kap. 10). Kapitel 5 (Spin-Gitter-Relaxation und Bewegungsverengung von Resonanzlinien), das auch den Formalismus der Dichtematrixmethode einführt, ist um einige wichtige Abschnitte erweitert worden, welche Anwendungen der Dichtematrix behandeln. Dazu gehört vor allem die Fourier-Transform-NMR. Das Konzept der Spintemperatur (Kap. 6) fand bereits Eingang in die 2. Auflage und wurde nur unwesentlich ergänzt.

Der schnellen Entwicklung verfeinerter NMR-Methoden in den letzten Jahren wurde in den Kapiteln 7 (Doppelresonanz), 8 (moderne Konzepte bei der gepulsten magnetischen Resonanz) und 9 (Mehrquantenkohärenz) Rechnung getragen. In diesem Zusammenhang werden die für die Praxis wichtigen Doppelresonanz- und Kreuzpolarisationsmethoden (Overhauser-Effekt, Festkörpereffekt, ENDOR, Hartmann-Hahn- und Pines-Gibby-Waugh-Methode, Spinentkopplung, Spinecho-Doppelresonanz) diskutiert und eine ausführliche Einführung in die 2 D-FT- und Bildgebungs-Methoden gegeben (Kap. 7). Die Theorie der Impulssequenzen, eine unabdingbare Voraussetzung für das Verständnis der verschiedensten bei der NMR-Spektroskopie auftretenden Probleme – einschließlich Festkörperecho, Erzeugung von dipolarer Ordnung, MAS und Multipulsprogramme zur Ausmittlung bestimmter Spektralanteile – wird formal entwickelt und in einer Weise behandelt, wie sie für die Erschließung weitergehender Anwendungen benötigt wird (Kap. 8). Schließlich erläutert das 9. Kapitel die physikalischen Konzepte zum Verstehen der Mehrquantenphänomene, die heute auf vielen Gebieten der magnetischen Resonanz eine Rolle spielen.

Als eines der wenigen Lehrbücher der magnetischen Resonanz bezog der „Slichter" von Anfang an die paramagnetische Elektronenresonanzspektroskopie (EPR bzw. ESR) in seine hauptsächlich an der NMR-Spektroskopie orientierte Darstellung ein. Das ist von der Sache her vernünftig, weil gerade bei der theoretischen Behandlung viele Analogien bestehen, auch wenn die Symbole verschieden sind. Außer sinnvollen Ergänzungen wurde an dieser Stelle ein Abschnitt über Elektronenspinechos aufgenommen.

Das bestens eingeführte und viel gelobte Buch bedarf eigentlich keiner neuerlichen Empfehlung. Die Kompetenz des Autors als Forscher und Lehrer prägt das Werk und seine Sprache. Die Neuauflage trägt der rapiden Entwicklung auf dem Gebiet der magnetischen Resonanz Rechnung und erhöht den Wert des Buches als Standardwerk für alle, die sich intensiver mit der NMR-Spektroskopie beschäftigen wollen, erheblich. Das sind nicht nur Studenten, sondern auch Experten, die sich zwar laut Vorwort nicht unbedingt angesprochen fühlen sollen, die aber durchaus profitieren können, um ihre theoretischen Kenntnisse bei der Bearbeitung spezieller Probleme aufzufrischen oder zu erweitern. Um keine Mißverständnisse aufkommen zu lassen: Trotz des Vorteils einer ausführlichen Darstellung der grundlegenden Theorie und des Eingehens auf Einzelheiten der Rechnungen (auch der um vier Abschnitte ergänzte Anhang ist hier zu loben), muß der physikalische Chemiker solide Vorkenntnisse in Physik und besonders Quantenmechanik mitbringen, um den vollen Genuß dieses Buches erleben zu können. Er ist dann aber auch gut gerüstet, anspruchsvolle Probleme, z. B. beim Einsatz komplizierter Pulsfolgen oder bei der NMR-Festkörperspektroskopie, anzugehen.

Trotz seiner Erweiterung (auch im Literaturteil) und des hohen Anspruchs bleibt der „Slichter" in dem Sinne Einführung und Lehrbuch, daß er nicht Spezialliteratur ersetzen kann oder einen Überblick über Anwendungen und Stoffuntersuchungen geben möchte. Daher schadet es auch nicht, wenn naturgemäß die meisten der in den einzelnen Kapiteln diskutierten Beispiele der amerikanischen Literatur entnommen sind. Die Chance, bei der neuen Auflage SI-Maßeinheiten einzuführen, wurde (bis auf die von der 2. Auflage übernommene Umrechnungstabelle) leider nicht genutzt.

W. Müller-Warmuth

M. Suzuki:
Adsorption Engineering, Vol. 25 aus der Reihe: **Chemical Engineering Monographs,** Elsevier Science Publishers, Amsterdam and New York 1989. 306 Seiten, Preis: 139.– US$.

Monographien über Auslegungsmethoden für Adsorptionsapparate sind nicht sehr zahlreich. Insofern ist dieses Buch sehr zu begrüßen, in dem der langjährig auf diesem Teilgebiet des Chemieingenieurwesens tätige Autor die Grundlagen und die in neuerer Zeit erzielten Fortschritte systematisch zusammengestellt hat.

Die Kapitel über Adsorbentien, Adsorptionsgleichgewichte, Diffusion in porösen Teilchen und Kinetik einer chargenweise betriebenen Adsorption sind grundlegender Natur. Ihnen folgen Kapitel über kontinuierlich betriebene Chromotographie-Säulen, Berechnung von Durchbruchkurven bei Adsorbern, Wärmeeffekten bei der Adsorption sowie die Regeneration von Adsorbentien und schließlich die Theorie der chromatographischen Trennung, der

Druckwechseladsorption und des Einsatzes der Adsorption zum Energietransport (Wärmepumpen usw.)

Alle Kapitel enthalten viel interessante und gut verständlich dargestellte, qualitative Informationen zur Adsorption, die – wenngleich meist am Beispiel der Aktivkohle demonstriert – für den Praktiker wie den Theoretiker von großem Nutzen sein können.

Leider gibt es zahlreiche Flüchtigkeitsfehler in dem englischen Text, die bei etwas mehr redaktioneller Sorgfalt leicht zu vermeiden gewesen wären. Natürlich wird ein Kontaktwinkel in grd und nicht in °C gemessen, Herr Bosanquet heißt nicht Bosanquit und Herr Chang nicht Chiang! Auch fehlt es manchmal an Detailerläuterungen in Abbildungsunterschriften, was besonders stört, wenn sie aus der japanischen Originalliteratur reproduziert sind, da japanisch sicher nicht so allgemein bekannt ist wie englisch.

Zusammenfassend: Ein nützliches Buch für den Praktiker und den Studierenden des Chemieingenieurwesens, leider aber voller Fußangeln.

H. Hofmann

J. W. T. Spinks, R. J. Woods:
An Introduction to Radiation Chemistry, Third Edition, John-Wiley and Sons, Inc., New York, Toronto 1990. ISBN 0-471-61403-3, 574 Seiten, Preis: DM 91,45.

Die zwei früheren Ausgaben des „Spinks und Wood" erschienen 1963, d.h. zu einer Zeit, in der die Strahlenchemie in einer rasanten Entwicklung begriffen war (nicht zuletzt dank der Methode der Pulsradiolyse), und 1975, d.h. zu einer Zeit, in der diese Entwicklung weitgehend abgeschlossen war und die wesentliche Aufgabe in der Anwendung strahlenchemischer Methoden auf anderen Gebieten der Chemie bestand. Wie würde der „Spinks and Wood 90" aussehen?

Der Rezensent ist ein wenig enttäuscht. Anstatt das Buch weitgehend umzuarbeiten, um die modernen Entwicklungen strahlenchemischer Art in den Vordergrund zu stellen, mit dem Ziel, das Buch hochaktuell zu machen, haben die Autoren die alte Fassung mehr oder weniger belassen und lediglich auf den neuesten Stand gebracht. „The most conspicuous difference between this and earlier editions is the move to SI units", schreiben sie im Vorwort. Der Rezensent hätte sich mehr „moves" gewünscht!

Wie die früheren Ausgaben ist das Buch als Lehrbuch für Studenten zu umfangreich, wenngleich der Lehrende ihm viel Material entnehmen kann. Das Buch enthält viele nützliche Informationen, die es einem Chemiker möglich machen, sich mit den Arbeitsmethoden und Theorien in der Strahlenchemie vertraut zu machen und den Weg in die spezielle Literatur zu finden. Die Auswahl des Stoffs und der Zitate ist weitgehend auf die den Autoren nahestehenden Gebiete und die angelsächsische Literatur beschränkt. Zum Beispiel enthält die Liste der früheren Bücher über Strahlenchemie nur die in englischer Sprache erschienenen oder übersetzten. So kommt es wohl auch, daß Listen an anderen Stellen nicht vollständig sind; z.B. ist in der Übersicht der chemischen Dosimeter das Tetranitromethan-Dosimeter nicht erwähnt, das sich durch die gleichzeitige Dosimetrie von Optik und Leitfähigkeit bei pulsradiolytischen Messungen auszeichnet.

In den ersten Kapiteln werden Strahlenquellen, die Wechselwirkung von Strahlung mit Materie, und Dosimetrie behandelt. Diese Kapitel sind umfangreicher als eine „Einführung" erwarten läßt. Sie sind klar und für den Chemiker leicht verständlich geschrieben. Es folgt dann ein Kapitel über Ionen, angeregte Moleküle und freie Radikale, in dem die wichtigsten Eigenschaften von kurzlebigen Zwischenprodukten der Radiolyse allgemein beschrieben werden. Bei der Aufzählung der verschiedenen Reaktionstypen freier Radikale fällt auf, daß die O^--Übertragung, die sauerstoffreiche Radikale untereinander eingehen können, nicht erwähnt ist, obgleich dieser Reaktionstyp bei strahlenchemischen Versuchen entdeckt worden ist. In dem folgenden Kapitel über Kinetik und experimentelle Methoden werden die einfachsten kinetischen Geschwindigkeitsgesetze bei homogenen Reaktionen beschrieben, auf inhomogene Reaktionskinetik kurz eingegangen, und dann Methoden der Detektion von Zwischenprodukten, nämlich durch ESR, Blitzphotolyse und Pulsradiolyse erwähnt. Die Beschreibung der Pulsradiolyse, immerhin die wichtigste Methode der Strahlenchemie, kommt hierbei zu kurz weg: Die Anwendung von empfindlichen Leitfähigkeitsmessungen, die gleichzeitig mit der optischen Detektion durchgeführt werden können, sowie die Polarographie kurzlebiger Radikale werden nicht beschrieben; man findet nicht einmal Literaturhinweise auf diese Methoden.

In den folgenden Kapiteln wird die Radiolyse spezieller Systeme beschrieben. Zwei Kapitel behandeln die Strahlenchemie des Wassers (Dampf und Flüssigkeit) und wäßriger Lösungen von anorganischen und organischen Substanzen. Die Auswahl des Stoffs ist hier weitgehend auf Systeme beschränkt, deren Untersuchung vor zwei Jahrzehnten im Vordergrund stand. Keine Hinweise auf die Strahlenchemie mizellarer Systeme und anorganischer Kolloide, nichts über die Anwendung von Strahlung zur Herstellung von Kolloiden, nichts über die Wirkung von Kolloiden als Elektronenspeicher bei Mehrelektronen-Übertragungsreaktionen freier Radikale. Der Rezensent wäre ja schon zufrieden gewesen, wenn einige bescheidene Literaturhinweise auf diese seit 15 Jahren intensiv bearbeiteten Gebiete gegeben worden wären.

In einem Kapitel über die Radiolyse organischer Systeme werden verschiedene Verbindungsklassen, wie Kohlenwasserstoffe, organische Halogenverbindungen, Alkohole und Äther, Karbonylverbindungen und stickstoffhaltige Verbindungen beschrieben. Auch hier sprengt der Umfang des Materials bei weitem den Rahmen einer Einführung, wenngleich die Zusammenstellungen durchaus nützlich sind, um eine Übersicht über diese Gebiete, besonders die früheren Arbeiten, zu erhalten. Aber auch hier vermißt man moderne Entwicklungen: Kein Wort über Beweglichkeit, Energiezustände und chemische Reaktionen von quasifreien und solvatisierten Elektronen in dielektrischen Flüssigkeiten. Das Buch schließt mit zwei Kapiteln über Strahleneffekte in Festkörpern und Angewandte Strahlenchemie; auch hier besteht der Eindruck, daß moderne Entwicklungen zu kurz gekommen sind. In Anhang 1 – 3 findet man schließlich nützliche Zusammenstellungen, z.B. über die Umrechnung alter Maßeinheiten in neue des SI-System. In Anhang 4 findet man Aufgabenstellungen und ihre Lösungen.

Abschließend sei gesagt, daß das Buch als eine nützliche Ergänzung zu bestehenden, kürzeren Einführungen in die Strahlenchemie empfohlen werden kann sowie als Informationsquelle über viele Daten in Teilgebieten der Strahlenchemie.

A. Henglein

D. H. Volman, G. S. Hammond, K. Gollnick (eds.):
Advances in Photochemistry, Vol. 15, John Wiley + Sons, New York, Chichester 1990. ISBN 0-471-63289-9, 390 Seiten, Preis: £ 74.35.

Die „Advances" streben keine lückenlosen Literaturberichte an; statt dessen bieten sie Raum für gründliche, auch persönlich gefärbte, Diskussionen ausgewählter Bereiche, auf denen der jeweilige Autor über längere Zeit selbst gearbeitet hat. Die Kapitel eines Bandes sind in sich geschlossen und nicht aufeinander bezogen. Ziel ist immer die Einsicht in molekulare Mechanismen. Was einen photochemischen Mechanismus kennzeichnet, erläutert der Autor des letzten der fünf Beiträge des vorliegenden Bandes. Die Kapitel sind der Reihe nach:

1. Ultrafast Photochemical Intramolecular Charge Transfer and Excited State Solvation, von P. F. Barbara und W. Jarzeba, University of Minnesota, 68 Seiten, 32 Abb., 6 Tab., 150 Referenzen. (Das Wort Transfer fehlt zwar in der Überschrift, aber sonst nicht mehr.) Die Autoren untersuchen den Einfluß der Lösungsmittelrelaxation auf die Dynamik eines photoinduzierten intermolekularen Charge-transfer- (CT-)Übergangs. Probemoleküle sind solche mit „dualer Fluoreszenz", bei denen beide

angeregte Strukturen, vor und nach dem CT-Prozeß, fluoreszieren, noch enger abgegrenzt: bei denen der von Z. R. Grabowski 1979 vorgeschlagene Twist-Mechanismus (TICT = twistet intramolecular CT) angenommen wird, z. B. Bianthryl. Beobachtet wird die zeitliche Entwicklung des Fluoreszenzspektrums nach dem Anregungsimpuls auf ps-Zeitskala, in Abhängigkeit von Lösungsmittel und Temperatur. Die Diskussion geschieht auf der Basis eines (erweiterten) Debye-Onsager-Modells der Solvatation und einer vereinfachten Langevin-Gleichung für die Kopplung an eine „charakteristische" Solvat-Koordinate. Es wird versucht, die Elektronen-Transfer-Zeit von 9,9'-Bianthryl mit der Solvatationsrelaxationszeit von Cumarin im jeweils gleichen (polaren) Lösungsmittel zu korrelieren.

2. Atomspheric Reactions involving Hydrocarbons: FTIR Studies, von H. Niki, York University, Canada, und P. D. Maker, Ford Motor Company, Dearborn, Michigan, USA; 68 Seiten, 25 Abb., 159 Ref.
Der Artikel zeigt an z.T. noch nicht publizierten Beispielen die experimentellen Voraussetzungen und den Nutzen der IR-Spektrometrie bei kinetischen Untersuchungen der Reaktionen von Kohlenwasserstoffen mit Radikalen (HO, HOO, R, RO, ROO u.a.) in einer Modellatmosphäre. Ergebnisse werden vorgelegt für A. Methan (CH_3O_2; HCHO, HO + CO; HO + CH_3OOH); B. Ethan und höhere Alkane ($C_2H_5O_2$; CH_3CHO; $CH_3C(O)O_2$; RO_2, $R \geq C_4$; C. Alkene und Alkine (HO-, O_3-, NO_3-initiierte Reaktionen;
D. Aromaten: Oxidation; ungesättigte 1,4-Dicarbonyle.
Die Ergebnisse der kinetischen Analyse werden z.T. mit solchen aus anderen Untersuchungen verglichen.

3. Excited State Reactivity and Molecular Topology Relationships in Chromophorically Substituted Anthracenes, von H. D. Becker, Chalmers University Gothenburg, Schweden, 88 Seiten, 37 Abb., 30 Tab., 150 Ref.
Der Artikel ist im Stil von J. B. Birks' „Photophysics of Aromatic Molecules" gehalten. Er enthält Absorptions- und Fluoreszenzspektren und Tabellen mit Lumineszenz- und Photoreaktions-Quantenausbeuten in verschiedenen Lösungsmitteln. Es handelt sich um über 100 meist unpublizierte, 9-substituierte Anthracene. Substituenten sind π-Elektronensysteme mit fehlender oder sterisch behinderter oder voller π-Konjugation zum Anthracen. Nicht betrachtet werden Anthracenophane, bisubstituierte Anthracene, Kronenether und intramoleculare Exciplexe. Die auftretenden, z.T. konkurrierenden Reaktionen sind $(4\pi+4\pi)$- bzw. $(4\pi+2\pi)$-Cycloaddition (ca. 40 Verb.), trans-cis- und andere geometrische Photoisomerisierung (ca. 30 Verb.); sensibilisierte Triplett-Reaktionen.
Der Artikel faßt im wesentlichen Arbeiten der Autoren aus den letzten 10 Jahren zusammen; sie beklagen sich etwas, daß ein Referent die frühere Publikation einiger neuer Verbindungen verhindert hat, können dafür aber jetzt mehr davon vorlegen.

4. Photophysics and Photochemistry of Phytochrome, von K. Schaffner, S.E. Braslawsky und A. Holzwarth, MPI für Strahlenchemie, Mülheim a.d. Ruhr, 48 Seiten, 24 Abb., 161 Ref.
Neben der Photosynthese unterliegen Pflanzen und Algen noch einigen anderen lichtgesteuerten Reaktionen; so reagieren Wachstum und morphologische Entwicklung in charakteristischer Weise auf Wechsel der spektralen Verteilung und Intensität des Lichts. Der hierbei wichtigste Rezeptor ist Phytochrom, ein offenkettiges, konjugiertes Tetrapyrrolsystem mit einer exo-Doppelbindung, kovalent an ein bestimmtes Cystein in einer Proteintasche gebunden. Die Umgebung ermöglicht verschiedene Konformationen und protomere Formen mit jeweils charakteristischen Absorptions - und Fluoreszenzspektren. Grundfragen sind die Zuordnung von Spektrum und Molekülzustand und die Mechanismen von photoinduzierten und thermischen Umlagerungen; praktische Probleme sind die Präparation einheitlicher Proben und die Messung schwacher und rasch abklingender Fluoreszenzspektren. Die Autoren haben besonders zur meßtechnischen Seite viele Beiträge geleistet. Deren Ergebnisse sind in diesem Artikel zusammengefaßt und diskutiert. Für einige Reaktionsschritte wird ein konsistentes Modell vorgeschlagen.

5. Photochemical Mechanisms in Single Crystals: FTIR Studies of Diacyl Peroxides, von M. D. Hollingsworth, University of Alberta, Canada, und J. M. McBride, Yale University, New Haven, USA; 100 Seiten, 35 Abb. 99 Ref.
Dieses Kapitel ist als „Review" gedacht, nicht allgemein über alle neueren photochemischen Reaktionen in organischen Kristallen, sondern über eine spezielle Methodik, ihre Leistungsfähigkeit und die damit im Vergleich zu anderen Techniken zu gewinnende Information. Es handelt sich darum, photochemische Reaktionen in organischen Einkristallen anhand der IR-Spektren der beteiligten Spezies mechanistisch aufzuklären. Die Autoren formulieren zunächst ein darauf abgestelltes Konzept des Begriffs „Mechanismus", schildern die Vorteile der Vororientierung im Kristall und die durch die Matrix bedingten Abweichungen von Gas- und Lösungsreaktionen (Streß, Deaktivierung). Es folgt eine Aufzählung der wichtigsten Probenparameter und Meßtechniken, insbesondere der Fourier-Transform IR-Spektroskopie, bis in praktische Details. Fast alles wird mit Beispielen aus der Forschung der Autoren belegt, nämlich der Photolyse von Fettsäure-diazyl-peroxiden. Das freigesetzte CO_2 ist eine ideale IR-Sonde. In Kombination mit ESR-Daten wird zum Schluß ein plausibler Mechanismus formuliert.

Alle fünf Kapitel des Bandes erfüllen, mit verschiedener Gewichtung, die Ansprüche der Serie. Da sie nicht einige brandneue Resultate, sondern den aktuellen Stand eines Bereiches darlegen sollen, frage ich mich aber, ob es nicht doch möglich wäre, in einem solchen Band jeweils einige sich inhaltlich näher stehende Gebiete zu vereinen.

F. Dörr

Zur Besprechung eingegangene Bücher

H. D. Roth, G. J. Kavarnos, F. D. Saeva, E. Krogh, P. Wan, L. Lopez, H.-J. Timpe, D. F. Eaton: *Photoinduced Electron Transfer I*, Vol. 56, aus der Reihe: *Topics in Current Chemistry*, Springer Verlag, Berlin, Heidelberg, New York, ISBN 3-540-52379-0, 1990.

K. Yoshihara, N. Suzuki, G. Harbottle, Y. Ito, J. I. Kim, R. Stumpe, R. Klenze: *Chemical Applications of Nuclear Probes*, Vol. 57, aus der Reihe: *Topics in Current Chemistry*, Springer-Verlag, Berlin, Heidelberg, New York ISBN 3-540-52423-1, 1990.

A. S. Mikhailov: *Foundations of Synergetics I – Distributed Active Systems*, Springer-Verlag, Berlin, Heidelberg, New York, ISBN 3-540-52775-3, 1990.

V. I. Minkin, B. Ya. Simkin, R. M. Minyaev: *Quantum Chemistry of Organic Compounds – Mechanisms of Reactions*, Springer-Verlag, Berlin, Heidelberg, New York, ISBN 3-540-52530-0, 1990.

H. Kaesche: *Die Korrosion der Metalle, 3. Auflage*, Springer-Verlag, Berlin, Heidelberg, New York, ISBN 3-540-51569-0, 1990.

VCH Titles on Spectroscopy

Breitmaier, E. /Voelter, W.

Carbon-13 NMR Spectroscopy

High-Resolution Methods and Applications in Organic Chemistry and Biochemistry
Third, completely revised edition

1990. XVI, 515 pages with 129 figures and 158 tables.
Hardcover. DM 240.00. ISBN 3-527-26466-3

Busch, K.L. /Glish, G.L. /McLuckey, S.A.

Mass Spectrometry/Mass Spectrometry

Techniques and Applications of Tandem Mass Spectrometry

1990. XII, 333 pages with 112 figures and 14 tables.
Hardcover. DM 154.00. ISBN 3-527-26785-9

Friebolin, H.

Basic 1 D and 2 D NMR Spectroscopy

1991. XXI, 344 pages with 144 figures and 42 tables.
Softcover. DM 58.00. ISBN 3-527-28108-8

Foreword by J.D. Roberts

Lucid and information-packed, this book is highlighted by its
- clear and descriptive illustrations
- numerous examples constructed especially for the material presented
- comprehensive treatment of the most important areas of NMR spectroscopy
- excellent didactic approach

It is suitable both as a textbook for students as well as a selfstudy guide for professionals.

Hummel, D.O.

Atlas of Polymer and Plastics Analysis/Atlas der Polymer-und Kunststoffanalyse

Volume 1/Band 1 Defined Polymers/Definierte Polymere
Part a/Teil a Part b/Teil b

1991. Ca LXXX, 1080 pages with 2809 figures.
Hardcover. DM 750.00. Subs. price: DM 620.00.
ISBN 3-527-28034-0

To order please contact your bookseller or:
VCH, P.O. Box 10 11 61, D-6940 Weinheim • VCH, P.O. Box, Hardstrasse 10, CH-4020 Basel • VCH, 8 Wellington Court, Cambridge CB1 1HZ, UK • VCH, Suite 909, 220 East 23rd Street, New York, NY 10010-4606, USA

Michl, J. /Thulstrup, E.W.

Spectroscopy with Polarized Light

Solute Alignment by Photoselection, in Liquid Crystals, Polymers, and Membranes

1987. XVI, 573 pages with 139 figures and 21 tables.
Hardcover. DM 265.00. ISBN 3-527-26516-3

Neuhaus, D. /Williamson, M.P.

The Nuclear Overhauser Effect in Structural and Conformational Analysis

Series: Methods in Stereochemical Analysis

1990. XXII, 522 pages with 198 figures and 17 tables.
Hardcover. DM 194.00. ISBN 3-527-26639-9

Schrader, B.

Raman/Infrared Atlas of Organic Compounds

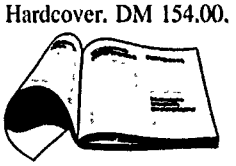
1989. XIV, 1118 pages with 1044 figures.
Hardcover in slip case. DM 680.00.
ISBN 3-527-26969-X

Tonelli, A.E.

NMR Spectroscopy and Polymer Microstructure

The Conformational Connection

1989. X, 252 pages with 150 figures and 24 tables.
Hardcover. DM 154.00. ISBN 3-527-27942-3



JOURNALS

Angewandte Chemie International Edition

Published by the German Chemical Society (GDCh)

Berichte der Bunsen-Gesellschaft für Physikalische Chemie

An International Journal of Physical Chemistry
Published under the auspices of the German Bunsen Society for Physical Chemistry

If you would like more information on these journals or a free sample copy please contact VCH.

VCH